Novel Bisnaphthalimidopropyl Polyamine Derivatives: Their Mode of Action in a Breast Cancer Cell System

Gemma A Barron

School of Pharmacy and Life Sciences,
The Robert Gordon University, Aberdeen

A thesis submitted in partial fulfilment of the requirements of The Robert Gordon University for the degree of Doctor of Philosophy

June 2010

Declaration

I declare that the work presented in this thesis is my own, except where otherwise acknowledged, and has not been submitted in any form for another degree or qualification at any other academic institution.
Information derived from the published or unpublished work of others has been acknowledged in the text and a list of references is given.

Gemma A Barron

Acknowledgements

I would like to acknowledge and thank deeply my supervisors, Professor Paul Kong Thoo Lin (School of Pharmacy and Life Sciences, RGU) and Dr(s) Giovanna Bermano (Centre for Obesity Research and Epidemiology, RGU) and Amanda Gordon (School of Pharmacy and Life Sciences, RGU), for their support, knowledge, kindness and understanding over the past three (and a bit!) years.

I would like to gratefully thank Professor(s) Don Cairns (RGU) for helpful discussions, much needed help and input into the DNA binding studies, in particular, the molecular modelling study, and Wayne Flintoff from University of Western Ontario, Canada for kindly donating the CHO and CHO-MG cell lines used in the polyamine transporter studies.

I would like to thank Dr Susan Duthie (Rowett Institute of Nutrition and Health, University of Aberdeen) for many interesting and helpful discussions, and invaluable technical help with the DNA damage and repair studies; Dr Marie Goua (RGU) for demonstration, input and discussion regarding the apoptosis flow cytometry study and Dr Charles Bestwick (Rowett Institute of Nutrition and Health, University of Aberdeen) for advice, and discussion with cell cycle studies. I would also like to thank Mr Simranjeet Kaur and Dr Nilanjan Roy (National Institute of Pharmaceutical Education and Research, India) for conducting the molecular modelling and docking experiments of BNIPP derivatives in hSIRT1 and hSIRT2 models.

I also thank Mr John Wood for technical advice regarding use of the UV-Vis spectrophotometer, luminescence spectrophotometer and HPLC analysis. I would also like to thank Mrs Emily Hunter and Mr Iain Tough for technical help with the fluorescence microscope used in COMET analysis.

I am very grateful to the financial support and assistance provided by the Robert Gordon University (RDI Funding) throughout the course of my research.

Finally, I would like to thank my family and friends, and in particular, my mum, dad, brother, David and fiancé, Stewart, who were all incredibly patient and supportive (even when they should not have been!), and who have endured the many ups and downs, I have, over the last three years.

Abstract

Novel Bisnaphthalimidopropyl Polyamine Derivatives: Their Mode of Action in a Breast Cancer Cell System

Gemma A Barron, for the degree of Doctor of Philosophy

The synthesis and characterisation of novel bisnaphthalimidopropyl polyamine (BNIPP) derivatives, has gained pace over the last couple of years, as they have enhanced aqueous solubility, without loss of biological activity, in contrast to parent bisnaphthalimide derivatives. Recent work has shown that bisnaphthalimidopropyl spermidine (BNIPSpd) bis-intercalates to DNA, induces oxidative DNA damage, depletes polyamine levels and causes cell death, by apoptosis, in human colon cancer CaCO-2 and HT-29 cells. The aim of this thesis was to synthesise new BNIPP derivatives to highlight the important structural features required for biological activity, particularly, bisnaphthalimidopropyl functionality, and investigate their subsequent modes of action in breast cancer MDA-MB-231 and breast epithelial MCF-10A cells. Initially, work focused on determining the DNA binding affinities and biological activity of BNIPP derivatives. All BNIPP derivatives, except bisphthalimidopropyl diaminodecane (BPHPDadec) and mononaphthalimidopropylamine (NPA) (ΔT_m values of 15.8 and 10.2 °C, respectively, C_{50} values of > 10 µM, IC_{50} values of > 40 µM), exhibited strong DNA binding affinities and cytotoxic properties in both cell lines. Results indicate that BNIPP derivatives interact with DNA by bis-intercalation suggesting, therefore, that BNIPP derivatives target DNA. For the first time, an investigation into the mechanism of cellular entry, via the polyamine transport (PAT) system, was studied. However, none of the BNIPP derivatives utilised the MGBG-specific PAT system, suggesting that BNIPP derivatives utilise other modes of cellular entry. Two BNIPP derivatives, BNIPSpd and BNIPDaCHM, were further investigated, and results show that these derivatives significantly induced a dose dependent increase in DNA strand breaks from ≥ 0.1 µM, after 4 hours. BNIPSpd and BNIPDaCHM (at non toxic concentrations) also inhibited the repair of oxidative (H_2O_2) and methylative (MMS)-induced DNA strand breaks. Based on phosphatidylserine exposure and membrane integrity analyses, early apoptotic cell death was determined as a mode of cell death utilised by both BNIPSpd and BNIPDaCHM (5 µM), after only 0.5 hours treatment in MDA-MB-231 cells. Interestingly, BNIPDaCHM was identified, using HDAC assay kits, as a potent and selective SIRT2 enzyme inhibitor, thus, identifying, a novel structural backbone for the selective inhibition of HDAC enzymes.

Keywords: Bisnaphthalimidopropyl, Bis-intercalation, DNA damage, Apoptosis, HDAC inhibition, Breast cancer

Table of Contents

Chapter 3.

Chapter 4.

List of Figures

Chapter 1.

Chapter 2.

Chapter 3.

Chapter 4.

Chapter 5.

Chapter 6.

Chapter 7.

Chapter 8.

List of Tables

Chapter 7.

List of Schemes

Chapter 2.

Abbreviations

7-AAD	7-amino-actinomycin D
ADP	Adenosince diphosphate
AO/EB	Acridine Orange/Ethidium Bromide
ATCC	American Tissue Culture Collection
ATP	Adenosine triphosphate
Bcl-2	B-cell lymphoma 2 family
BESpm	Bis (ethyl) spermine
BENSpm	N^1, N^{11} Bis (ethyl) norspermine
BER	Base Excision Repair
BMI	Body Mass Index
BNIP	Bisnaphthalimidopropyl derivatives
BNIPP	Bisnaphthalimidopropyl polyamine derivatives
BRCA 1	BReast CAncer 1
BRCA 2	BReast CAncer 2
BrdU	Bromodeoxyuridine
Cad	Cadaverine
CD	Circular Dichroism
CDKs	Cyclin dependent kinases
CHO	Chinese Hamster Ovary cells
CHO-MG	PAT deficient mutant Chinese Hamster Ovary cells
Cip1	CDK-interacting protein 1
CNS	Central Nervous System
CR	Calorie Restriction
CTCL	Cutaneous T-cell lymphoma
CZE	Capillary Zone Electrophoresis
DAPI	4',6-diamidino-2-phenylindole
DBU	1, 8 Diazabicyclo [5.4.0] undec-7-ene
DEPT-135	Distortionless Enhancement of Polarisation Transfer
DFMO	Difluoromethylornithine
DMEM/F12	Dulbecco's Modified Eagle/Nutrient Mixture F12 medium
DMF	Dimethylformamide
DMSO	Dimethylsulfoxide
DNA	Deoxyribonucleic Acid
ds	Doubled Stranded
DSBs	Double Strand Breaks
DTT	Dichlorodiphenyltrichloroethane
ECACC	European Collection of Cell Cultures

EDTA	Ethylenediaminetetraacetic acid
EGF	Epidermal Growth Factor
ER	Estrogen Receptor
ER+	Estrogen Receptor Dependent (positive)
ER-	Estrogen Receptor Independent (negative)
ESI	Electrospray Ionisation
EtBr	Ethidium Bromide
FCS	Foetal Calf Serum
FDA	Food and Drug Administration (U.S.)
FIA	Flow Injection Analysis
FOXO	Forkhead box 0 transcription factor
fs	Frequency steps
5-FU	5-Fluorouracil
G1	Gap phase 1
G2	Gap phase 2
GC	Gas Chromatography
GI_{50}	Growth Inhibition
^{1}H	Hydrogen (proton) nuclei
HAT	Histone Acetyltransferase
HDAC	Histone Deacetylase
HIF-1	Hypoxia-inducible factor-1
HNPCC	Hereditary non polyposis colon cancer
HPLC	High Performance Liquid Chromatography
HR	Homologous Recombination
HRT	Hormone Replacement Therapy
HS	Horse Serum
IBC	Inflammatory Breast Cancer
IC_{50}	Inhibitory Concentration
ID_{50}	Inhibitory Dose
IL-1	Interleukin-1
ITC	Isothermal Titration Calorimetry
LDH	Lactate dehydrogenase
LMP	Low Melting Point
M	Mitosis
MAL	*N*-(4-methyl-7-coumarinyl)-*N*-α-(*tert*-butyloxycarbonyl)-*N*-ε-acetyllysinamide
MAT	Methionine adonosyltransferase
MBC	Metastatic Breast Cancer
MCF-10A	Human breast epithelial cells

MD	Molecular Dynamics
MDA-MB-231	Human metastatic breast cancer cells
MGBG	Methylglyoxalbis(guanylhydrazone)
MGMT	O^6-alkylguanine-DNA-alkyltransferase
MMR	Mismatch Repair
MTT	3-(4, 5-dimethylthiazol-2-yl)-2, 5-diphenyl tetrazolium bromide
MTS	(3-(4,5-dimethylthiazol-2-yl)-5-(3-carboxymethoxyphenyl)-2-(4-sulfophenyl)-2*H*-tetrazolium inner salt
mRNA	Messenger Ribonucleic Acid
MS	Mass Spectrometry
Mts	Mesitylenesulfonyl chloride
m/z	Mass-to-charge
NAD^+	Nicotinamide adenine dinucleotide
NADH	Nicotinamide adenine dinucleotide phosphate
NCI	National Cancer Institute
NER	Nucleotide Excision Repair
NHEJ	Non Homologous End Joining
NMR	Nuclear Magnetic Resonance
NR	Neutral Red
OD	Optical density
ODC	Ornithine decarboxylase
PAO	Polyamine oxidase
PARP	Poly (ADP-ribose) polymerase
PAT	Polyamine Transporter
PBS	Phosphate Buffered Saline
PCBs	Polychlorinated biphenyls
PCD	Programmed Cell Death
Pd/C	Palladium on carbon
PI	Propidium iodide
PS	Phosphatidylserine
Put	Putrescine
RNA	Ribonucleic acid
ROS	Reactive Oxygen Species
RPMI-1640	Roswell Park Memorial Institute 1640 medium
RT-PCR	Reverse transcription polymerase chain reaction
S	DNA synthesis
SAHA	Suberoyl hydroxamic acid; Vorinostat
SAMDC	S-Adenosyl Methionine Decarboxylase
SCGE	Single Cell Gel Electrophoresis

SEM	Scanning electron microscope
Spd	Spermidine
SPE	Solid Phase Extraction
Spm	Spermine
ss	Single stranded
SSAT	Spermidine/Spermine N^1-Acetyl Transferase
SSBs	Single Strand Breaks
SSC	Saline Sodium Citrate
TEM	Transmission electron microscope
TLC	Thin Layer Chromatography
TNFα	Tumour Necrosis Factor alpha
TOPO	Topoisomerase Enzyme
TOPO II	Topoisomerase II
TP53	Tumour Protein p53
TSA	Trichostatin A
Ts-Cl	Toluenesulfonylchloride
TUNEL	Terminal deoxynucleotidyl transferase-mediated dUTP nick-end labelling
UV	Ultraviolet
Waf1	Wild-type p53-activated fragment 1
XTT	Sodium 2, 3-bis(2-methoxy-nitro-5-sulfophenyl)-5-[(phenylamino)-carbonyl]-2H-tetrazolium inner salt

Abbreviations for Bisnaphthalimidopropyl derivatives

BNIPDaCHM	Bisnaphthalimidopropyl diaminodicyclohexylmethane
BNIPDadec	Bisnaphthalimidopropyl diaminodecane
BNIPDadodec	Bisnaphthalimidopropyl diaminododecane
BNIPDahex	Bisnaphthalimidopropyl diaminohexane
BNIPDanon	Bisnaphthalimidopropyl diaminononane
BNIPDaoct	Bisnaphthalimidopropyl diaminooctane
BNIPDaoxoct	Bisnaphthalimidopropyl diaminooxaoctane
BNIPDeta	Bisnaphthalimidopropyldiethyltriamine
BNIPDpta	Bisnaphthalimidopropyldipropyltriamine
BNIPOPut	Bisnaphthalimidopropyl oxaputrescine
BNIPOSpm	Bisnaphthalimidopropyl oxaspermine
BNIPOSpd	Bisnaphthalimidopropyl oxaspermidine
BNIPPut	Bisnaphthalimidopropyl putrescine
BNIPSpd	Bisnaphthalimidopropyl spermidine
BNIPSpm	Bisnaphthalimidopropyl spermine

BPHPDadec	Bisphthalimidopropyl diaminodecane
NPA	Mononaphthalimidopropylamine

Chapter 1

Introduction

1.1. Cancer

For over a century, differences between cancerous (neoplastic) and normal cells have been recognised (Balducci 2007), and, the disease continues to dominate as a present day risk to human life.

A neoplasm or tumour is a build up or 'lump' of abnormal cells, where cells have escaped the normal controls of the cell cycle, resulting in irregular cell proliferation and differentiation. A tumour is benign when neoplastic cells grow slowly in a non aggressive self contained manner without spreading to the surrounding tissues (Stavros *et al*. 1995, Cancer Research UK 2004). A tumour is malignant when neoplastic cells grow in an uncontrolled abnormal manner, invade adjacent tissues and metastasise to distant sites, with the formation of new tumours (Gupta and Massagué 2006, Chiang and Massagué 2008). Cancer can be used to describe both benign and malignant tumours, but only malignant tumours are truly cancerous, and often fatal (Blows 2005). The common hallmarks of malignant cell growth have been recently expanded by Luo *et al.* (2009) to include the stress phenotypes. Therefore, including the stress phenotypes, the hallmarks of malignant cell growth are: self-sufficiency in growth signals, insensitivity to anti-growth signals, evasion of programmed cell death (apoptosis), limitless replicative potential, sustained angiogenesis (Hanahan and Weinburg 2000), together with metabolic stress, proteotoxic stress, mitotic stress, oxidative stress, deoxyribonucleic acid (DNA) damage stress and finally evasion of immune surveillance (Hanahan and Weinburg 2000, Luo *et al.* 2009, Zhivotovsky and Orrenius 2010).

Over 200 different types of cancers have been identified, with 54 % of all newly diagnosed cases worldwide being accounted for by breast, lung, colorectal (large bowel) and prostate cancers (Cancer Research UK 2009a). In 2006, approximately 293,000 people were diagnosed with cancer in the UK (Cancer Research UK 2009a); with the latest statistics indicating that one in three people will be diagnosed with some form of cancer during their lifetime in the UK (Cancer Research UK 2009b).

1.1.1. Breast Anatomy

A woman's breast is composed of adipose tissue, connective tissue and gland (lobes) tissue. In a lactating woman, milk is produced by these lobes, and delivered to the nipple by small tubes, known as milk ducts (NHS Choices UK 2008) (refer to Figure 1.1). The natural development of breast tissue occurs in response to hormones, in particular, during puberty, pregnancy and breast feeding (World Cancer Research Fund-UK, 2010).

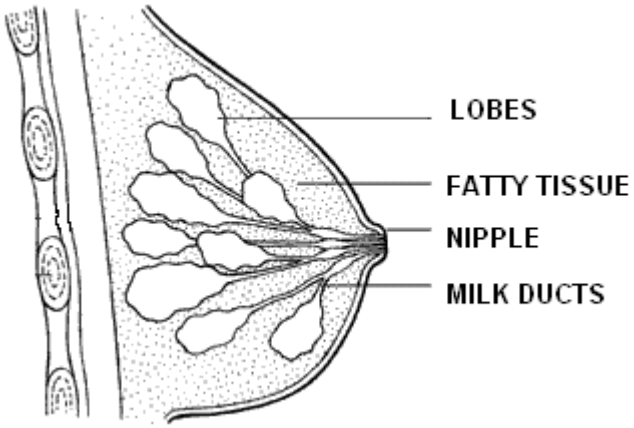

Figure 1.1.: Internal structure of a women's breast (adapted from Cancerbackup, May 2009, available from http://www.cancerbackup.org.uk/Cancertype/Breast/DCISLCIS)

1.1.2. Epidemiology of Breast Cancer

Breast cancer is the most common cancer in the UK (even though it is extremely rare in men), with around 46,000 new cases of breast cancer diagnosed in women and 300 new cases in men, in 2006 (Cancer Research UK 2009c). Latest statistics indicate that breast cancer incidence rates have risen by over 50% in the last 25 years (Cancer Research UK 2009c), with rates higher in more developed countries (e.g., North America and Europe) than in less developed countries (e.g., Africa and Asia) (Cancer Research UK 2009d). Although the survival rates of breast cancer have improved over the last 20 years because of earlier detection and improved treatment; breast cancer remains the third most common cause of death (8 %) after lung (22 %) and colorectal (10 %) cancers in the UK (Cancer Research UK 2009c, Cancer Research UK 2009d).

1.1.3. Aetiology of Breast Cancer

Although the aetiology of breast cancer remains largely unknown (Debruin and Josephy 2002); breast cancer can be associated with three distinct groups of risk factors: reproductive and hormonal factors, environmental (including lifestyle) factors, and hereditary factors.

The age of an individual is highly influential in the aetiology of breast cancer, and has been suggested to be the strongest risk factor; as the risk of breast cancer increases with age, with 8 out of 10 breast cancer cases developing in postmenopausal women, over the age of 50 (Cancerbackup 2008). Therefore, several reproductive factors related to age have been identified that influence the risk of breast cancer. These include (i) age at menarche (i.e., younger age at menarche (before age of 12), higher risk of breast cancer), (ii) age at first birth (i.e., younger age at first birth, lower risk of breast cancer), (iii) breastfeeding (i.e., breastfeeding for longer, lower risk of breast cancer), and (iv) age at menopause (i.e., older age at menopause (over age of 55), higher risk of breast cancer).

Besides reproductive factors, hormonal factors have also been linked to the risk of breast cancer, including (i) endogenous hormones (i.e., higher levels of oestrogen or testosterone, higher risk of breast cancer) or exogenous hormones (i.e., use of oral contraceptives or hormone replacement therapy, higher risk of breast cancer) (Key *et al.* 2001).

Studies into geographic variations related to the incidence of breast cancer have shown that cases of breast cancer are higher in developed countries, suggesting that environmental and lifestyle choices are highly influential in the aetiology of breast cancer. The risk of breast cancer is linked to (i) a high Body Mass Index (BMI[1]; ie, being overweight or obese, particularly after menopause), (ii) drinking alcohol (i.e., drinking more than two units of alcohol per day over several years' increases risk by 7 – 12%) (Cancerbackup 2008, Cancer Research UK 2009d), (iii) a lack of physical activity (i.e., moderate physical activity reduces the risk of breast cancer) (Key *et al.* 2001), or (iv) exposure to ionising radiation or environmental oestrogens (e.g., dichlorodiphenyltrichloroethane (DTT) or polychlorinated biphenyls (PCBs) (Keys *et al.* 2001).

Environmental and lifestyle factors rather than inherited genetic factors are primarily responsible for most cases of breast cancer. However, a small number of breast cancer cases (5 – 10%) are hereditary. For these genetically predisposed cases, occurrence is due to an inherited germline mutation within, for example, the BRCA1 (BReast CAncer 1), BRCA2 (BReast CAncer 2) or TP53 (Tumour Protein p53) genes (Blows 2006, Nelson *et al.* 2005, Balducci 2007). Mutations in BRCA1 and BRCA2 genes result in a high incidence of breast (56 – 84% risk), and in some cases, ovarian (15 – 45% risk) cancers (Key *et al.* 2001, Honrado *et al.* 2006). These genes are involved in transcriptional regulation, induction of apoptosis, control of cell cycle and DNA repair mechanisms (Yang and Lippman 1999, DeBruin and Josephy 2002, Honrado *et al.* 2006). Whilst, mutations in TP53, a tumour suppressor gene, are the most common in human cancers (found in 50% of human cancers) (Bertheau *et al.* 2008); it is also responsible for the regulation of apoptosis, cell cycle and DNA repair mechanisms (DeBruin and Josephy 2002).

1.1.4. Types of Breast Cancer

There are various different types of breast cancer, classified as either non-invasive or invasive. Approximately 80 % of all breast cancer cases, diagnosed in women, develop within the cells which line the milk ducts, known as non-invasive Ductal cancer (NHS Choices UK 2008). Other forms of breast cancer can occur within the cells which line the milk producing lobes (Lobular cancer), below the skin of the breast where the tumour has

[1] BMI is calculated by dividing the weight by height squared. A BMI less than 18.5 is underweight; 18.5 – 24.9 is an ideal weight; 25 – 29.9 is overweight and 30 and over is obese.

blocked the lymph nodes (Inflammatory Breast Cancer, IBC) or around the nipple (Paget's disease of the breast) (NHS Choices 2008, National Cancer Institute 2006, Cancer Research UK 2009e). Breast cancer can also spread or metastasise to other organs within the body, in particular, the lungs, liver, bones and brain (Lacroix 2006, Chiang and Massagué 2008, Hu, Kang and Wang 2009).

Hormones, in particular, oestrogens are important in the development and maintenance of female characteristics, including breast development. Oestrogens bind the estrogen receptors (ER; a protein molecule and member of the transcription factor family), resulting in cell proliferation (Yamaguchi and Hayashi 2009). Consequently, the levels of ER expression can denote the particular type of breast cancer. For example, cells which have ERs, thus oestrogen dependent, are ER-positive breast cancer cells (ER+), whilst cells which do not have ERs, thus oestrogen independent, are ER-negative breast cancer cells (ER-) (Koutsilieris *et al*. 1999, Lacroix and Leclercq 2004). ER+ breast cancer cells exhibit a better prognosis and are more responsive to treatment, whereas ER- breast cancer cells are highly invasive and do not respond well to current treatments (Koutsilieris *et al.* 1999, Rochefort *et al.* 2003, Lacroix and Leclercq 2004).

1.1.5. Treatment of Breast Cancer

Treatment of breast cancer is generally dependent upon an individual's circumstances (i.e., ER expression levels: ER+ or ER-), but commonly involves removal of the tumour by surgical excision. Chemotherapy, radiotherapy and, in some cases, hormone or biological therapy (i.e., treatment working with either hormones or the immune system, respectively) can be used, either before surgery (non-adjuvent therapy) or after surgery (adjuvent therapy). These treatments aim to increase patient survival and prevent the occurrence of metastatic tumour formation (Garibolidi *et al.* 2007, NHS Choices UK 2008).

Adjuvent chemotherapy is the most common approach for the treatment of primary and advanced breast cancers: ER+ breast cancers can be treated with anti-oestrogen (endocrine) therapies, and ER- breast cancers can be treated by chemotherapy. Endocrine therapies block the effect of oestrogen, thus, decreasing the rate of breast cancer cell proliferation (Yamaguchi and Hayashi 2009). Examples of endocrine therapies include tamoxifen (for premenopausal women) or aromatase inhibitors (for postmenopausal women) (Figure 1.2). Chemotherapy instead kills cells with the use of cytotoxic agents, for example, anthracyclines or taxanes, which can be used individually or in combination therapy (Friedrichs, Hölzel and Jänicke 2002) (Figure 1.2).

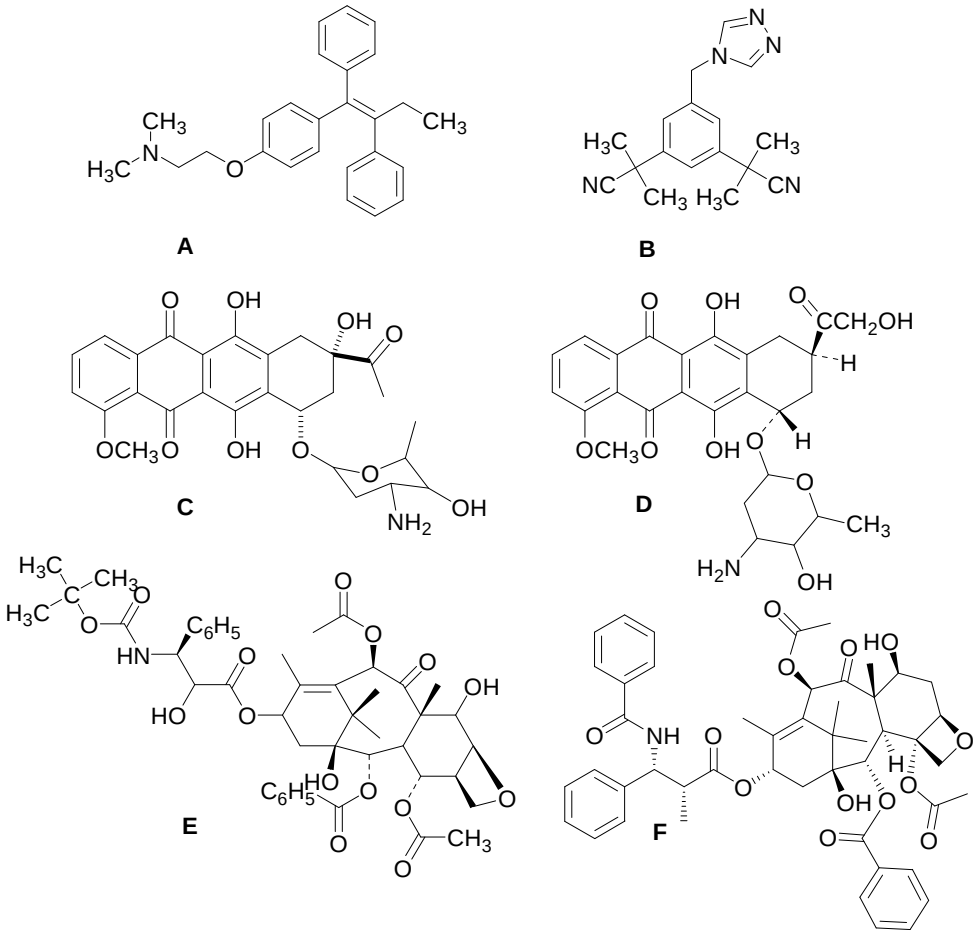

Figure 1.2.: Structure of **A**. Tamoxifen, **B**. Anastrazole, **C**. Daunorubicin (Daunomycin), **D**. Doxorubicin (Adriamycin), **E**. Docetaxal (Taxotere®) and **F**. Paclitaxal (Taxol®)

Over the last 20 years, adjuvent chemotherapy has been the key mode of breast cancer treatment, but response and survival rates remain modest over time (Robson and Verma 2009). The search for novel chemotherapeutics with less toxicity, better sensitivity and greater response rates, and with increased patient survival, therefore, remains critical for the future enhanced treatment of breast cancer (Arcamore 1992, Widakowich *et al*. 2007).

1.2. Cancer Therapeutics and Apoptosis

The treatment of cancer is highly reliant upon cytotoxic chemotherapeutic agents, as discussed in Section 1.1.5. Investigations into the mode of action of chemotherapeutic agents have established that many affect cancer cell death by initiation of apoptosis (or programmed cell death) (Kerr *et al.* 1994, Hannun 1997, Hu and Kavanaugh 2003, D'Agostini *et al*. 2005) (Table 1.1). However, a consequence of this is that the effectiveness of anti cancer agents is limited, since they do not discriminate between cancerous and non cancerous cells (MacFarlane 2009). Identification of novel targets related to apoptotic pathways and, the development of specific anti cancer agents which selectively induce apoptosis in cancer cells alone remains, therefore, of paramount importance (Kaufmann 1989, Hannun 1997, Lowe and Lin 2000).

Table 1.1.: Apoptosis-inducing chemotherapeutic agents used for the treatment of cancer

Chemotherapeutic Agents associated with Apoptosis	***Cancer Types associated with Apoptosis***
Bleomycin	Bladder carcinoma
Camptothecin	Breast carcinoma
Chlorambucil	Colon carcinoma
Cis-platinum	Leukaemia
Cyclophosphamide	Lung Carcinoma
Dexamethasone	Lymphoma
Doxorubicin	Ovarian carcinoma
Etoposide	Testicular carcinoma
5-Flourouracil	
Melphalan	
Methotrexate	
Paclitaxel	
Vincristine	

Note: adapted from Hannun (1997)

1.2.1. Cell Death: Apoptosis and Necrosis

Cell death can occur by multiple mechanisms; however, apoptosis and, to some extent, necrosis remain central to the area of cancer research. Cell death is defined by distinct morphological characteristics that are specific to each mode of cell death.

Apoptosis (or programmed cell death) is an important feature in normal cell development, as it regulates cellular homeostasis by balancing between cell proliferation and cell death (Schwartzman and Cidlowski 1993, Kerr *et al*. 1994, Scovass 2006). Also defined as cellular suicide or physiological cell death; apoptosis occurs when a single cell or small cell population voluntarily inactivate and completely dissemble their own structural components after exposure to external stimuli (Schwartzman and Cidlowski 1993, Holdenrieder and Stieber 2004). The morphological characteristics of apoptosis (Figure 1.3) involve cell shrinkage, cytoplasmic and cell membrane blebbing, chromatin

condensation, DNA fragmentation and the formation of apoptotic bodies, which are rapidly removed by phagocytosis (Kerr *et al.* 1994, Jin and El-Deiry 2005, Scovassi 2006, Burz *et al.* 2009). Removal by phagocytosis eliminates the risk of an inflammatory response in surrounding tissues. Apoptosis is a highly controlled energy dependent process, which is extremely important in the removal of damaged or dysfunctional cells in multi-cellular organisms. If these damaged cells are not efficiently removed, the formation of several pathological conditions, such as, cancer, autoimmune and degenerative diseases, or developmental defects could occur (Jin and El-Deiry 2005, Burz *et al.* 2009).

Necrosis, in contrast, occurs in cell populations or whole tissues, and results in cellular swelling, organelle dissolution and chromatin lysis, where ultimately the plasma membrane ruptures and the cellular contents leaks out (Figure 1.3). This leads to an inflammatory response in the adjacent extracellular space and surrounding tissues (Schwartzman and Cidlowski 1993, Jin and El-Deiry 2005). Also defined as accidental or pathological cell death, necrosis occurs in response to a variety of harmful conditions, including hyperthermia, hypoxia, direct cell trauma or exposure to toxic substances (Schwartzman and Cidlowski 1993, Chamond *et al*. 1999, Holdenrieder and Stieber 2004).

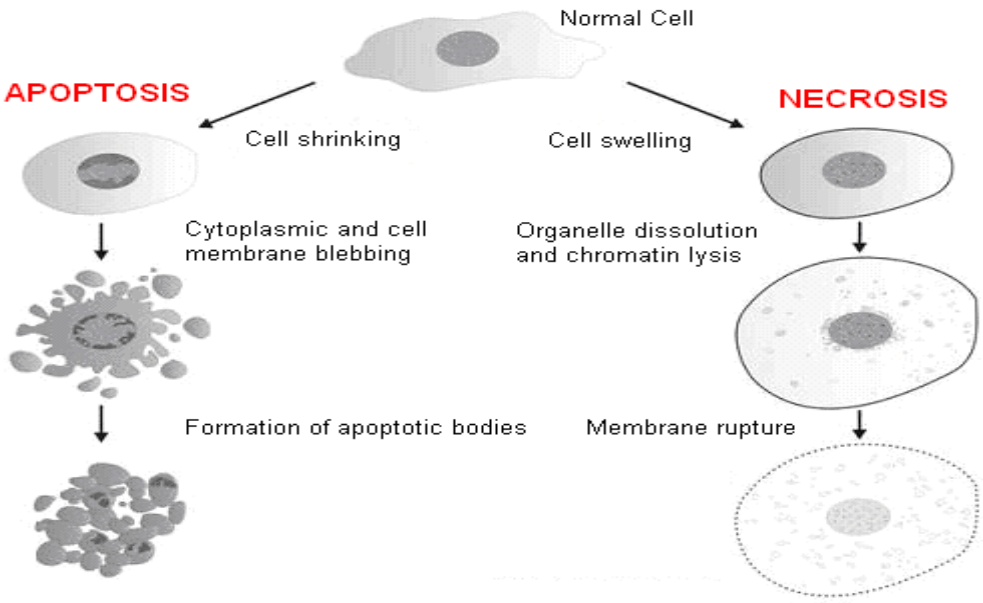

Figure 1.3.: The morphological differences between apoptosis and necrosis (Adapted from Direction maladies infectieuses et transmissibles, Aug 2009, available from http://www.pasteur.be/_en/indexf273.html?page=cellular_microbiology)

1.2.1.1. Cell Death Pathways

Apoptosis can be activated by two distinct, yet linked, signaling pathways: the death receptor (extrinsic) pathway and mitochondrial (intrinsic) pathway (MacFarlane 2009) (Figure 1.4). Both pathways stimulate initiator and effector caspases (cysteine-dependent aspartate-specific proteases), present in cells as pro-caspases, thus, leading

to caspase activation via the 'caspase cascade' (Holdenrieder and Stieber 2004, MacFarlane 2009).

In the extrinsic pathway, activation of the cell surface death receptors CD95 ligand (CD95-L) and tumour necrosis factor (TNF)-related apoptosis-inducing ligand (TRAIL) (members of the TNF receptor superfamily of proteins) results in the formation of a 'death-inducing signaling complex' (DISC), which activates the initiator pro-caspase-8 and -10, whilst in the intrinsic pathway, mitochondrial stress (e.g., DNA damage) disturbs the mitochondria, and results in the release of cytochrome *c*[2] (Holdenrieder and Stieber 2004, MacFarlane 2009). When released into the cytosol, cytochrome *c* binds to the apoptotic protease-activating factor-1 (Apaf-1), resulting in the formation of an apoptosome complex, which activates the initiator pro-caspase-9 (Igney and Krammer 2002, MacFarlane 2009). Activation and cleavage of pro-caspase-8, -9 or -10 leads to activation of effector caspases-3, -6 and -7, which in turn cleave and activate apoptotic cell death (Igney and Krammer 2002).

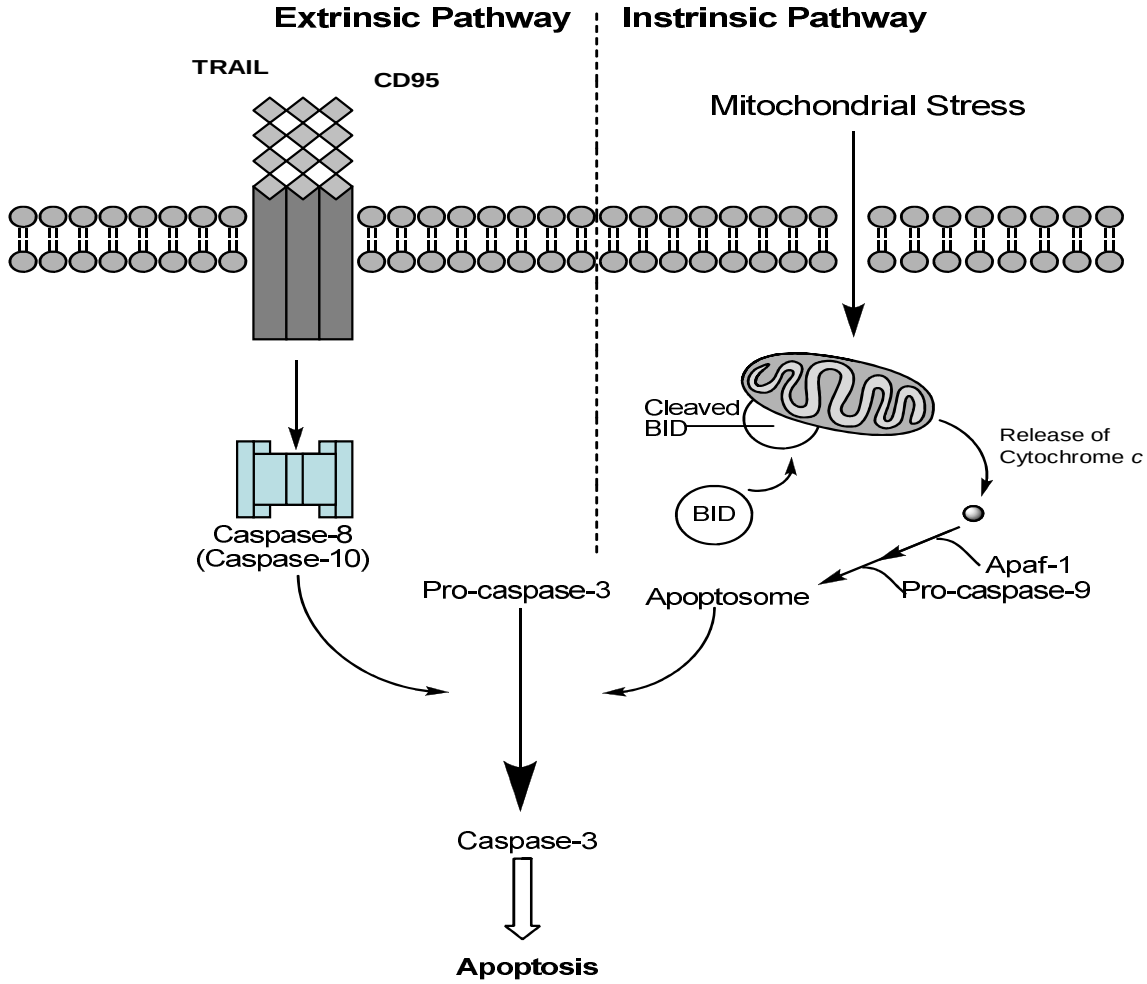

Figure 1.4.: Simplified representation of the key steps in apoptotic signaling pathways. CD95 ligand (CD95-L), tumour necrosis factor (TNF)-related apoptosis-inducing ligand (TRAIL) and apoptotic protease-activating factor-1 (Apaf-1)

[2] Cytochrome *c* is released from the inner membrane space of the mitochondria, and is regulated by members of the Bcl-2 family (anti-apoptotic members; Bcl-2, Bcl-x_L and pro-apoptotic members; Bax, Bak).

1.3. Cancer Therapeutics and Epigenetics

Epigenetics, defined as “heritable changes in gene expression that occur without changes in the DNA sequence” (Schemies *et al.* 2009), can explain the diversity of phenotypes within a population (Esteller 2008). Classical epigenetic modifications, such as, DNA methylation or histone acetylation, play an essential role in normal cell physiology, where modifications can regulate, for example, the development and progression of cancer (Carey and La Thangue 2006, Esteller 2008). Interestingly, histone acetylation, and more so, histone deacetylation have been identified as therapeutic targets (Ropero and Esteller 2007, Paris *et al.* 2008).

The recent development of drugs, which target epigenetic modifications, has created a new class of chemotherapeutic agents: histone deacetylase (HDAC) inhibitors (Carey and La Thangue 2006). Inhibition of HDACs (i.e., histone hyperacetylation via HDAC inhibitors) can cause cell growth arrest, induce cell differentiation, changes in gene expression, cell cycle arrest, and finally, apoptosis (Minucci and Pelicci 2006, Glaser 2007, Bieliauskas and Pflum 2008). However, only one HDAC inhibitor has been approved so far by the U.S. Food and Drug Administration (FDA), suberoyl hydroxamic acid (SAHA; Vorinostat; Figure 1.5), approved for the treatment of cutaneous T-cell lymphoma (CTCL) (Mann *et al.* 2007, Richon *et al.* 2009). Therefore, the discovery of drugs related to HDAC inhibition, and the development of combination strategies (i.e., epigenetic therapy with chemotherapy), remains of high importance, and could make it possible to reduce toxicity, increase sensitivity, and remove resistance to current therapies, which are the main reasons for unsuccessful cancer treatment (Kristensen *et al.* 2009).

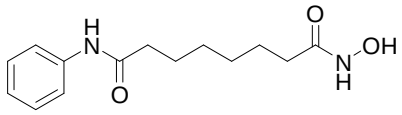

Figure 1.5.: Structure of SAHA

1.3.1. Histone Modifications

Eukaryotic DNA is packaged in core nucleosomes, which are composed of an octamer of proteins called histones (2 copies each of H2A, H2B, H3 and H4) (Kristensen *et al.* 2009). As histones are positively charged; an interaction with the negatively charged phosphate groups allows DNA to wind tightly around the nucleosomes. This interaction between histones and DNA, forms chromatin, which exist in two conformations (i.e., open or closed). Conformational changes in living cells are highly reliant upon the post-translational histone modifications: histone acetylation and histone deacetylation (Figure 1.6). Histone acetylation involves the addition of an acetyl group to the lysine

chains on histones, and is catalysed by histone acetyltransferases (HATs), whilst removal of acetyl groups can be achieved by histone deacetylation, via histone deacetylases (HDACs). Acetylation neutralises the positive charge of histones, thus, loosening their interaction with DNA, and opening the chromatin structure (Kristensen *et al.* 2009). Acetylation is associated with transcriptional activation (Legube and Trouche 2003), and is involved in DNA proliferation, DNA repair and chromosomal organisation (Esteller 2008, Kristensen *et al.* 2009).

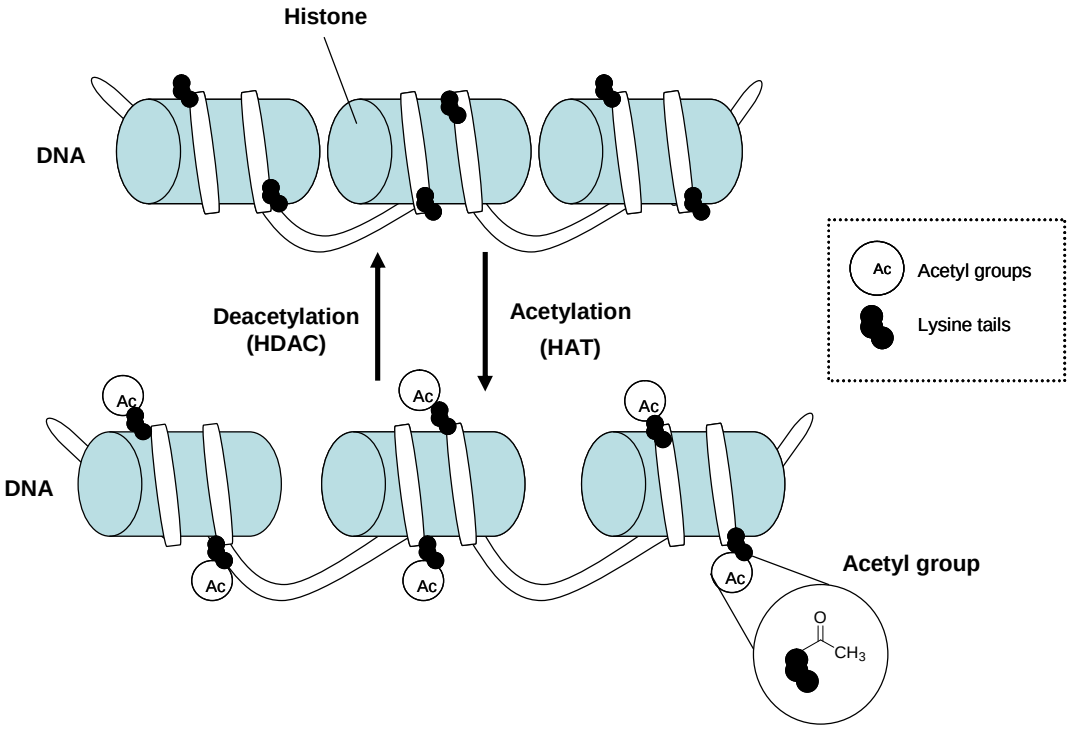

Figure 1.6.: Epigenetic changes: histone acetylation and histone deacetylation

HDAC inhibition causes transcriptional deactivation, where the chromatin structure closes, therefore, altering the overall structure of chromatin (Saunders and Verdin 2006). As polyamines (Section 1.4) are important in altering the structure and conformation of Deoxyribonucleic Acid (DNA), Ribonucleic Acid (RNA) and proteins (Childs *et al.* 2003); they may also aide or hinder HDAC inhibition (Hobbs *et al.* 2002, Saunders and Verdin 2006). Saunders and Verdin (2006) found that polyamine depletion in human colon cancer HCT116 cells blocked apoptotic cell death induced by HDAC inhibitors (the cyclic tetrapeptide trapoxin A and short-chain fatty acid sodium butyrate). Thus, polyamines appear to modulate the cellular response of HDAC inhibitors.

1.4. Cancer Therapeutics and Polyamines

Polyamines play an essential role in normal cell proliferation and differentiation, and their levels are regulated in accordance with the rate of cell growth. Inhibition of cell proliferation and growth has, therefore, been associated with a decrease in polyamine levels (Pegg 1988, Pegg and McCann 1982, Russell 1983, Davidson *et al*. 1999). In addition, polyamines have been suggested to play a vital role in the development of cancer, as it was observed by Wallace *et al.* (2000) and Wallace and Caslake (2001) that breast and colon cancer cells have higher concentrations of polyamines, compared with the equivalent normal cells. Polyamines were, thus, thought to be a biochemical marker for cancer (Criss 2003). However, increased levels of polyamines are not only restricted to individuals with cancer: elevated levels can also be found in individuals with Cystic Fibrosis, Psoriasis, Duchenne Muscular Dystrophy, or even during pregnancy (Russell *et al.* 1978, Wallace and Caslake 2001, Wallace and Fraser 2003, Larqué *et al.* 2007). As a result, polyamines have a limited role as specific biochemical cancer markers. Nevertheless, intracellular polyamine levels have been used as tools to determine the efficiency of several novel polyamine derivatives as anti cancer agents (Porter and Bergeron 1988, Wallace and Fraser 2003).

Over the last twenty years, particular attention was paid to the inhibition of the polyamine biosynthetic and catabolic pathways (Bergeron *et al.* 1988, Casero and Woster 2009). Specific inhibitors have been identified for every enzyme in the polyamine biosynthetic pathway i.e., ornithine decarboxylase (ODC), S-adenosyl methionine decarboxylase (SAMDC), spermidine/spermine N^1-acetyltransferase (SSAT) and polyamine oxidase (PAO) (Casero and Woster 2001), however, their efficacy is limited and none of these inhibitors has ever reached the pharmaceutical market.

Recent efforts have focused on the identification of novel derivatives that produce cellular effects independent of, or in addition to, the inhibition of polyamine biosynthetic enzymes; polyamine linker chains also continue to be used to improve the cellular uptake of potential anti cancer agents (Casero and Woster 2009).

1.4.1. Polyamines

The naturally occurring polyamines, Spermidine (Spd) ($C_7H_{19}N_3$) and Spermine (Spm) ($C_{10}H_{26}N_4$) and, the diamine, Putrescine (Put) ($C_4H_{12}N_2$) (Figure 1.7) are present within all eukaryotic cells (Tabor and Tabor 1985). They are small, water soluble, nitrogen bearing long aliphatic polycation chains, which have multiple functions, particularly, within the normal growth and proliferation of mammalian cells (Thomas and Thomas 2001). Putrescine, spermidine and spermine also have specific roles in embryonic development (i.e., increased polyamine synthesis in the foetus increases cell growth or accumulation of

polyamines aides tooth development), cell cycle (i.e., depletion of polyamines by inhibition of the polyamine biosynthetic pathway alters rate of cell cycle) and cancer (i.e., accumulation of putrescine and spermidine in cells favours malignant transformation) (Gritli-Linde *et al.* 1995, Pegg 1988, Seiler *et al.* 1998, Larqué *et al.* 2007). Polyamines have also been found to have a stimulating effect on DNA, RNA and protein synthesis (Childs *et al.* 2003) and, can protect DNA, proteins and lipids from oxidative damage, as they are scavengers of reactive-oxygen species (ROS) (Khuhawar and Qureshi 2001, Ah Byun *et al.* 2009).

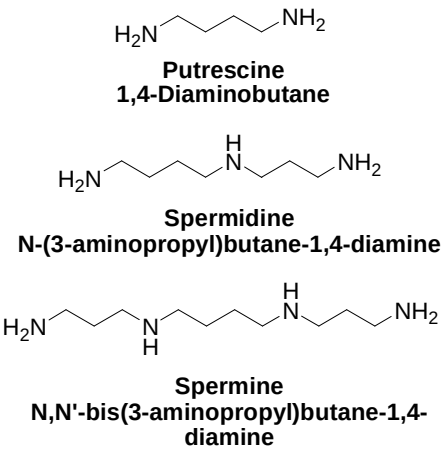

Figure 1.7.: Structures of polyamines putrescine, spermidine and spermine

1.4.1.1. Polyamine Biosynthesis and Catabolism

Polyamines are endogenously synthesised and catabolised by two highly regulated pathways: the biosynthetic pathway and the catabolic pathway (Figure 1.8). Both pathways synthesise polyamines from each other (i.e., biosynthesis occurs in order of putrescine, spermidine and spermine, whilst catabolism occurs in the reverse order), by seven independent enzyme reactions (Seiler *et al.* 1996, Criss 2003, Wallace 2007).

In the biosynthetic pathway, polyamines are firstly synthesised via decarboxylation of L-ornithine, by the enzyme ODC, which produces putrescine (**[1]** Figure 1.8). Secondly, decarboxylation of S-adenosylmethionine (SAM) produces decarboxylated S-adenosylmethionine, catalysed by SAMDC (**[2]** Figure 1.6). Thirdly, spermidine is derived from putrescine by the addition of a propylamine group from SAM, by the action of the enzyme spermidine synthase (**[3]** Figure 1.8). Finally, spermine is derived from spermidine, by the enzyme spermine synthase and the addition of a second propylamine group from SAM (**[4]** Figure 1.8) (Wallace *et al.* 2003, Larqué *et al.* 2007).

In the catabolic pathway, polyamine interconversion is controlled by two coupled reactions: acetylation, controlled by the enzyme SSAT (**[5]** Figure 1.8), and cleavage, via the action of the enzyme POA (**[6]** Figure 1.8) (Larqué *et al.* 2007). Additionally, a new enzyme, spermine oxidase has recently been identified, which oxidises spermine to produce spermidine with exclusion of the N-acetylation step (**[7]** Figure 1.8) (Wallace

2007, Hector *et al.* 2008). Polyamines are also exogenously sourced from the diet by active gut uptake (from cheese, fruit and vegetables), and by adsorption of intestinal and pancreatic secretions (Larqué *et al.* 2007).

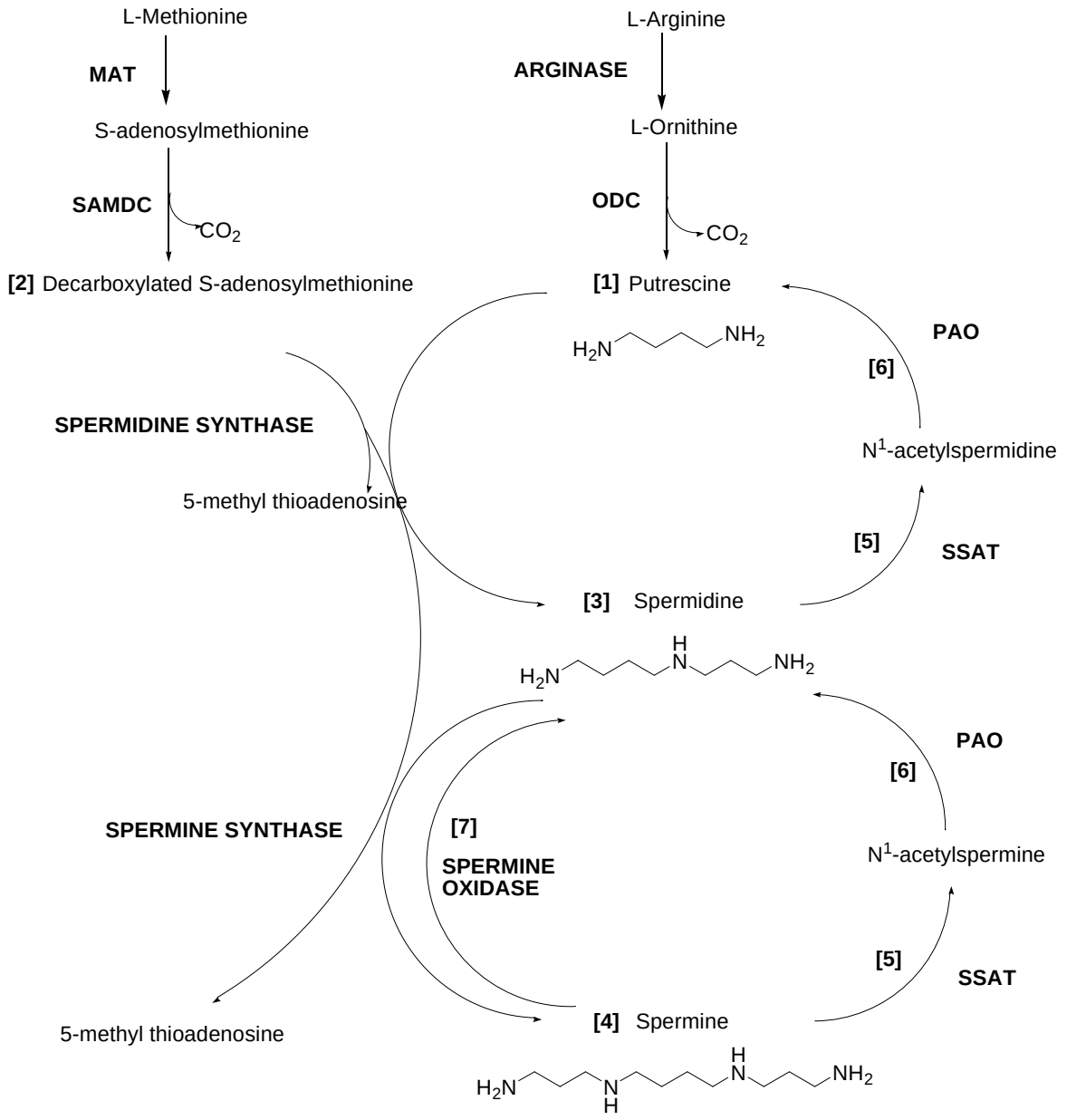

Figure 1.8.: The pathway of polyamine biosynthesis and catabolism. Methionine adenosyltransferase (MAT), ornithine decarboxylase (ODC), S-adenosyl methionine decarboxylase (SAMDC), polyamine oxidase (PAO) and spermidine/spermine N^1-acetyl transferase (SSAT) ([n] indicates each independent enzyme reaction, [n] = [1 - 7])

1.5. Cancer Therapeutics and Polyamine Derivatives

Research within the field of polyamine derivatives was originally focussed upon the synthesis and development of polyamine analogues and derivatives which inhibit specific enzymes of the polyamine biosynthetic (ODC and/or SAMDC) and catabolic (SSAT and/or PAO) pathways, as mentioned previously (Bergeron *et al.* 1988, Casero and Woster 2009) (Section 1.4; Figure 1.8). The shift away from the study of polyamine biosynthetic or catabolic enzymes was due to their limitations as anti cancer agents. Current research now focuses on the development of analogues that contain polyamine linker chains, in order to improve transport into cells, via the polyamine transporter (PAT) (Seiler *et al.* 1996) or to serve as carriers (Casero and Woster 2009).

1.5.1. Symmetrical Bis(alkyl)Polyamine Derivatives as Anti Cancer Agents

The first polyamine derivatives synthesised as anti cancer agents were the symmetrical *N*-alkylated spermidine derivatives, comprising of a series of N^4 spermidine substituted derivatives (N^4-methyl-spermidine, N^4-ethyl-spermidine, N^4-acetyl-spermidine, N^4-hexyl-spermidine, N^4-hexanoyl-spermidine, N^4-benzyl-spermidine and N^4-benzoyl-spermidine) (Porter *et al.* 1982), and N^1, N^8 spermidine derivatives [N^1, N^8-bis(ethyl)-spermidine, N^1, N^8-bis(acetyl)-spermidine, N^1, N^8-bis(propyl)-spermidine and N^1, N^8-bis(propionyl)-spermidine] (Porter *et al*. 1985). These derivatives were synthesised using methodologies described by Bergeron (1986) and were structurally similar to the natural polyamines (i.e., with terminal primary amines and various alkyl linker lengths) (Casero and Woster 2009). Out of the 11 *N*-alkylated spermidine derivatives, only N^4-hexyl-spermidine (HSpd), N^1, N^8-bis (ethyl)-spermidine (BESpd) and, N^1, N^8- bis (propyl)-spermidine (BPSpd) (Porter *et al.* 1985) (Figure 1.9) showed antiproliferative activity against L1210 leukaemia cells (50% inhibition after 48 hours at 30, 40 and 50 µM, respectively). BESpd was most effective at depleting putrescine and spermidine levels and reducing spermine by approximately 50% after 96 hours (Porter *et al.* 1985). BESpd also decreased the activity of ODC (98% decrease) and SAMDC (62% decrease) (Porter *et al.* 1985). BESpd was thought to be acting as a biosynthetic enzyme regulator; however, it could not control the normal functions of polyamines (i.e., cell growth) (Porter *et al.* 1985).

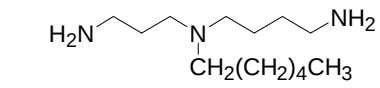

a

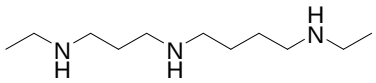

b

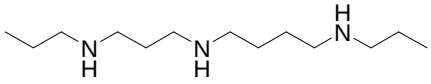

c

Figure 1.9.: Structures of bis (alkyl) spermidine derivatives: **a:** HSpd, **b:** BESpd and **c:** BPSpd

Following the positive results obtained from Porter *et al.* (1985), additional symmetrical *N*-alkylated polyamines were synthesised to determine their structure activity relationships, comprising of the series of N^1, N^{12} dialkylated spermine derivatives (Bergeron *et al.* 1988). The N^1, N^{12} bis (methyl)-spermine (BMSpm), (N^1, N^{12} bis (ethyl)-spermine (BESpm) and N^1, N^{12} bis-propyl spermine (BPSpm), were the most active derivatives, in comparison with N^1, N^1, N^{12}, N^{12} terminally tetra alkylated spermine (TESpm), N^4, N^9 internally alkylated spermine (IDESpm) or 1, 20-bis (*N*-ethylamino) -4,8,13,17-tetraazaeicosane (YANK) (Figure 1.10). The activity order was found to be spermine derivatives (ethyl > propyl > methyl) > YANK > spermidine derivatives (Bergeron *et al.* 1988). BESpm was the most cytotoxic analogue with IC_{50}[3] values of 10 and 0.1 µM after 48 and 96 hours, respectively (Bergeron *et al.* 1988). BESpm also demonstrated a similar cytotoxicity against Daudi human Burkett's lymphoma cells and promyelocytic leukaemia HL-60 cells (IC_{50} values less than 1 µM after 96 and 144 hours in both cell lines) (Bergeron *et al*. 1988). Further investigations by Porter *et al.* (1987) demonstrated that BESpm had the potential to be both an antiproliferative agent (IC_{50} values after 48 hours of 1 µM in L1210 murine leukaemia cells), and also a probe for investigating the regulation of the polyamine pathway (at 10 µM BESpm decreased ODC (99%) and SAMDC (84%) activities (Porter *et al.* 1987).

[3] IC_{50} (Inhibitory Concentration) is defined as the derivative concentration that causes 50% growth inhibition of the cell population compared to that of control cells.

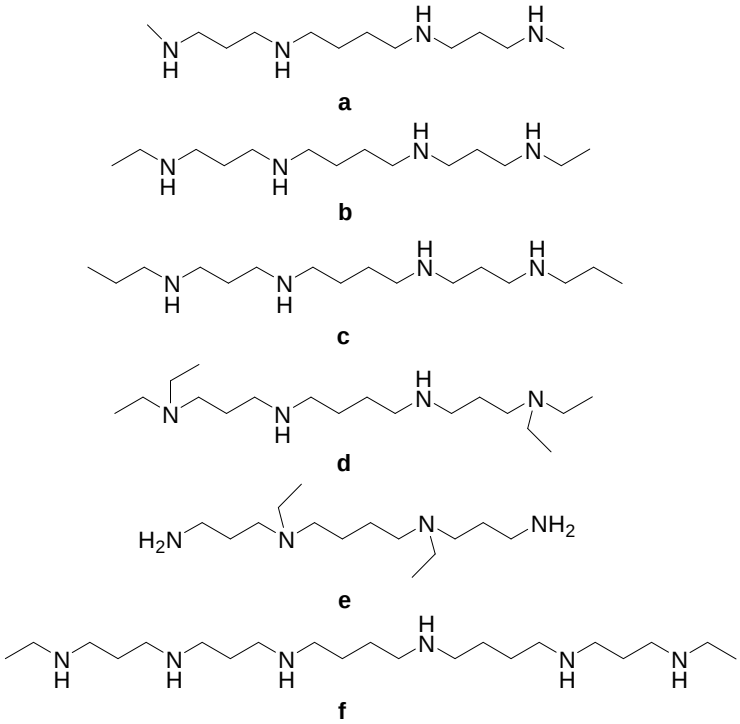

Figure 1.10.: Structures of bis (alkyl) spermine derivatives: **a:** BMSpm, **b:** BESpm, **c:** BPSpm, **d:** TESpm, **e:** IDESSpm and **f:** YANK

Pegg *et al.* (1989) further investigated the work of Bergeron, Porter *et al.* (1985, 1987 and 1988) regarding the symmetrical bis (alkyl) polyamine derivatives: BESpm, N^1, N^{11} Bis (ethyl) norspermine (BENSpm) and N^1, N^{14} Bis (ethyl) homospermine (BEHSpm) (Figure 1.11) on cellular polyamine metabolism in human colon HT-29 cancer cells. All derivatives reduced intracellular polyamine levels (> 90% reduction by all derivatives), with the greatest reduction in spermine levels (BENSpm, 94%; BESpm, 86%, and BEHSpm, 60%). These derivatives also brought about a greater reduction of polyamine levels than a mixture of α-Difluoromethyl ornithine (DFMO, an inhibitor of ODC) and 5'-deoxy-5'-[*N*-methyl-*N*-[2-(aminooxy) ethyl]) amino adenosine (MAOEA, an inhibitor of SAMDC) (Pegg *et al.* 1989). ODC and SAMDC activity was decreased (Pegg *et al*. 1989, Bergeron *et al*. 1988), whilst SSAT activity was increased, thus promoting the degradation of polyamines (Pegg *et al.* 1989, Creaven *et al.* 1997). However, the bis (alkyl) spermine derivatives, like the bis (alkyl) spermidine derivatives, were unable to act as replacements for polyamines and control the normal cell regulatory functions of polyamines.

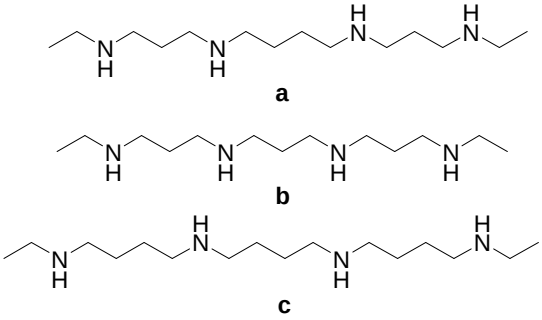

Figure 1.11.: Structures of bis (alkyl) spermine derivatives: **a:** BESpm, **b:** BENSpm and **c:** BEHSpm

The most effective bis (alkyl) polyamine derivatives are BESpm and BENSpm (Figure 1.11). BENSpm has undergone Phase I and II clinical trials (Creaven *et al.* 1997, Streiff and Bender 2001, Hahm *et al.* 2002, Wolff *et al*. 2003). Although, it was found to be safe with minimal toxicity, it did not show any significant clinical effects in the treatment of breast and colon cancer (Streiff and Bender 2001, Hahm *et al.* 2002, Wolff *et al*. 2003, Casero and Woster 2009). However, convincing preclinical data by Hector *et al.* (2008) could allow the facilitation of a clinical trial, which would involve the combination of BENSpm with two standard chemotherapeutic agents, oxaliplatin and 5-fluorouracil (5-FU) to be used in the treatment of colorectal cancer.

1.5.2. Symmetrical Bis(alkyl)Polyamine Derivatives with Modified Linker Chains as Anti Cancer Agents

A second generation of the symmetrical bis (alkyl) spermine derivatives (Figure 1.10 - 11) were synthesised with specific alterations to the flexible polyamine backbone of BESpm. The derivatives consisted of conformational restrictions which were introduced by replacement of the central butane linker region with a *cis*- and *trans*-cyclopropyl, a *cis*- and *trans*-cyclobutyl ring, a *cis*- and *trans*- double bond, a triple bond or a 1, 2-disubstituted aromatic ring (Figure 1.12).

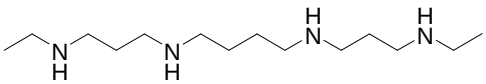

Bis (ethyl) Spermine (BESpm)

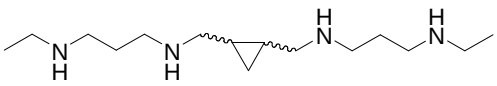

i

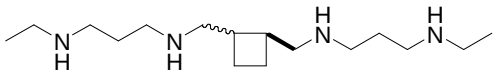

ii

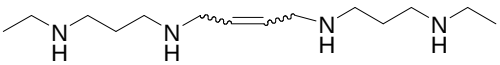

iii

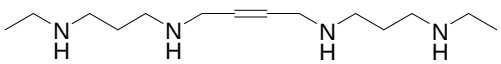

iv

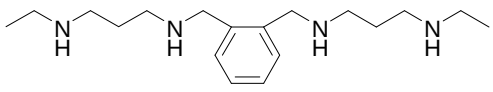

v

Figure 1.12.: Structures of conformationally restricted derivatives of BESpm: **i**, *cis*- and *trans*-cyclopropyl, **ii**, a –cyclobutyl ring, **iii**, a *cis*- and *trans*- double bond, **iv**, a triple bond or **v,** a 1, 2-disubstituted aromatic ring

The *cis*- and *trans*-cyclopropyl (**i**), *cis*- and *trans*-cyclobutyl ring (**ii**) and *cis*- and *trans*-double bond (**iii**) derivatives (Figure 1.12) showed low micromolar toxicity, with ID_{50}[4] values of 0.01 – 2 µM after 6 days, against human lung A549, colon HT-29, prostate DU145 and brain U251MG cancer cells, with less toxicity in prostate PC-3 and breast MCF-7 (ID_{50} values of 0.24 - > 31.25 µM, after 6 days) cancer cells (Reddy *et al.* 1998). No significant difference in toxicity was observed between the *cis*- or *trans*- conformations of these derivatives (**i**, **ii** and **iii**), or the depletion of intracellular polyamine levels in DU145 prostate cancer cells (Reddy *et al*. 1998). Reddy *et al.* (1998) synthesised two further conformationally restricted derivatives of BESpm, **iv** and **v** (Figure 1.12), containing a triple bond or a 1, 2-disubstituted aromatic ring, respectively. These derivatives did not exhibit toxicity against any of the cancer cell lines investigated, except in DU145 cancer cells, where ID_{50} values of 1.33 µM and 12.60 µM, were observed after 6 days, respectively. These derivatives did not deplete intracellular polyamine levels in DU145 cells, however, it should be noted that **iv** and **v** were taken up by DU145 cancer cells just as effectively as the other derivatives investigated (Reddy *et al.* 1998).

The *cis*-double bond derivative, *cis*-**iii** (CGC-11047) (Figure 1.13) is currently in Phase I clinical trials for cancer treatment (Holst *et al.* 2006), and has been found to inhibit the growth of small cell lung cancer H82 and H69, and non small cell lung cancer A549 and H157 cell lines (Hacker *et al.* 2008). Within the non small lung cancer cells, CGC-11047 decreased ODC activity, significantly increased polyamine catabolism and depleted polyamine pools. The same effects were observed to a lesser degree in the small lung cancer cells (Hacker *et al*. 2008, Casero and Woster 2009). CGC-11047 is therefore a promising new conformationally restricted polyamine analogue, although further preclinical and clinical trials need to be undertaken.

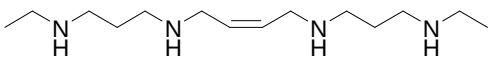

Figure 1.13.: Structure of conformationally restricted BESpm analogue *cis*-**iii** (CGC-11047)

[4] ID_{50} (Infectious Dose) is defined as the drug dose required to reduce the final cell number to 50% of the control (Twentyman and Luscomber 1987).

1.6. Cancer Therapeutics and DNA Intercalating Agents

DNA is an important biochemical target in the design of anti cancer therapeutic compounds. Intercalating anti cancer compounds target DNA by interfering with the processes of DNA replication and transcription (Lerman 1961, Palchaudhari and Hergenrother 2007, Anderson *et al.* 2009), and classically contain planar or heteroaromatic chromophores. DNA intercalating agents work by reversibly binding to DNA, by insertion and stacking between the base pairs of the DNA double helix (Martinez and Chacon-Garcia 2005, Kamel *et al.* 2007), thus resulting in the DNA partially unwinding and lengthening. As a result, DNA replication and transcription is inhibited (Thomas 2000, Palchaudhuri and Hergenrother 2007). Many intercalating anti cancer agents also target topoisomerase II (TOPO II) activity. TOPO II is an essential enzyme that has a critical role in the processes of DNA untangling and unknotting. The inhibition of TOPO II can elevate the number of DNA double strand breaks, therefore, leading to irreparable, permanent strand breaks, which may trigger apoptosis (Burden and Osheroff 1998, Hande 1998, Fortune and Osheroff 2000, Brana *et al.* 2001). Doxorubicin is an example of an intercalating TOPO II poison (Figure 1.2)

Alongside, DNA intercalation compounds can also target DNA by electrostatic interactions (non specific binding along the exterior of the DNA helix), or groove binding interactions (specific binding with the edges of the base pairs in either the major or minor grooves within the DNA double helix) (Brana *et al.* 2001, Martinez and Chacon-Garcia 2005) (refer to Chapter 3).

Several chemotherapeutic agents classically use DNA intercalation, for example anthracyclines (e.g., doxorubicin and daunorubicin; Figure 1.2), and acridine (e.g., proflavin) derivatives (Demeunynck 2004, Ferguson and Denny 2007, Ashley and Poulton 2009). However, the DNA intercalating compounds of interest to this study are naphthalimides and bisnaphthalimides. These derivatives intercalate by the planar aromatic rings inserting between the base pairs of the DNA double helix, which distorts the DNA backbone, and leads to their cytotoxicity against a panel of human cancer cell lines (Brana *et al.* 1980, Brana *et al.* 2001, Brana and Ramos 2001, Kong Thoo Lin *et al.* 2003, Martinez and Chacon-Garcia 2005).

1.6.1. Naphthalimides

Mononaphthalimide compounds were designed and synthesised, in the 1970s. They are comprised of the structural components of several anti tumour agents (the β-nitronaphthalene of the aristolochic acid, the glutarimide rings of cycloheximide, CG-603, and the basic side chain of tilorone) (Figure 1.14) into a single molecule. Napthalimides were easily synthesised by condensation of 3-nitro-1,8-naphthalic anhydride with the

corresponding amine, as described by Brana and Ramos (2001). Subsequently, a larger group of naphthalimides were synthesised by Brana *et al.* (2001) and Brana and Ramos (2001) which consisted of napthalimides with varying side chains, and ring substitutions.

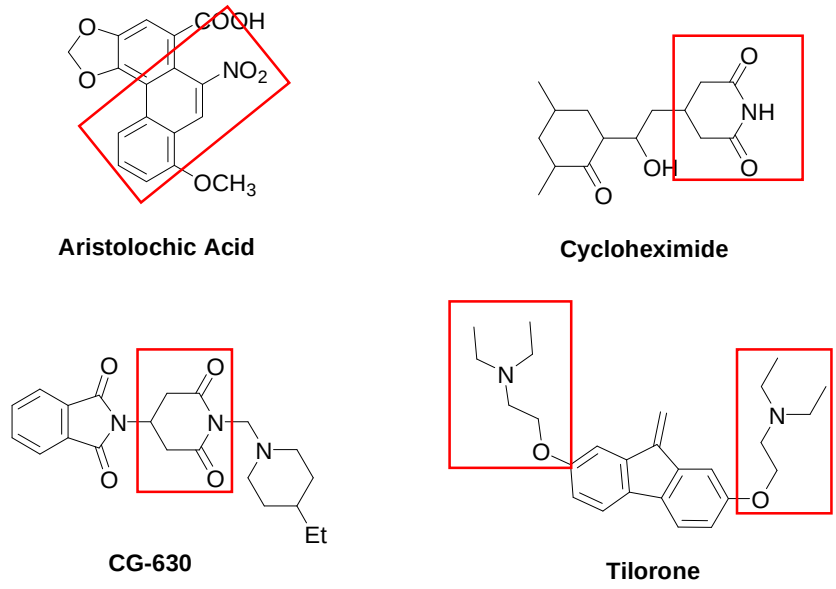

Aristolochic Acid **Cycloheximide**

CG-630 **Tilorone**

Figure 1.14.: Structure of anti tumour agents contributing to the design of naphthalimides (important structural components are boxed in red)

A basic terminal group in the side chain is essential for cytotoxic activity, since substitution of the nitrogen atom with a carbon, sulphur and oxygen atom resulted in inactive compounds (Brana *et al.* 2001, Brana and Ramos 2001). A decrease in basicity of the substitutes on the naphthalimido ring (i.e., at position 5) also reduced their activity (Brana and Ramos 2001). The key structural requirements for optimal activity of naphthalimides are shown in Figure 1.15.

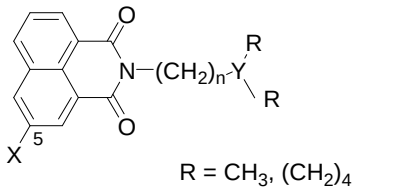

Figure 1.15.: Structure of the key structural requirements for monosubstituted naphthalimides

A quantitative structure activity relationship (QSAR) study was undertaken for compounds substituted at position 5 (Figure 1.15), and the most active derivatives screened and evaluated by the National Cancer Institute (NCI), in the USA (Brana and Ramos 2001). The most active derivatives were named mitonafide (NSC 300288) and amonafide (NSC 308847) (Figure 1.16), which were active in leukaemia (P388 and L1210), and human cervical (HeLa and KB) cancer cells, respectively (Brana and Ramos 2001). Mitonafide and amonafide both bind to double stranded DNA by intercalation of

the chromophore group and inhibit TOPO II action (Waring *et al*. 1979, Hsiang *et al*. 1989, Brana *et al.* 1993, 2001, Chau *et al*. 2008). However, TOPO II inhibition was not observed in naphthalimides, which lack the basic side chain (Brana and Ramos 2001).

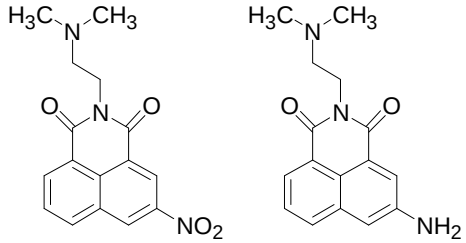

Figure 1.16.: Structures of **a:** Mitonafide and **b:** Amonafide

Mitonafide and amonafide have been extensively studied, and were selected for Phase I and II clinical trials (Saez *et al.* 1989, Brana *et al*. 1993, Asbury *et al*. 1997, Brana *et al.* 2001, 2004). During Phase I clinical trials, mitonafide resulted in inappropriate central nervous system (CNS) toxicity in five patients treated with daily short (1 hour) administration schedules, (doses above 118 mg/m^2 x 5 days), resulting in an irreversible loss of memory in all five patients, and in one case, leading to dementia (Llombart *et al.* 1992, Brana *et al*. 1997, Brana and Ramos 2001). This was considered to be due to a dose-limiting toxicity, which was related to the short administration schedule (Llombart *et al.* 1992). Further Phase I clinical trials which administered mitonafide as a continuous 120 hour infusion, did not result in CNS toxicity (Rosell *et al.* 1992, Casado *et al.* 1996). However, slower administration resulted in a lack of efficacy of mitonafide in the treatment of solid tumours, subsequently leading to the removal of mitonafide from further clinical trials. Amonafide has also been removed from clinical trials (Ott *et al.* 2008), as it is metabolised into an active metabolite *N*-acetyl amonafide, which is responsible for severe myelosupression (Alami *et al.* 2007).

Other naphthalimides that are structurally similar to amonafide have been synthesised to increase the potency of the mononaphthalimide series. One approach involved the modification of the chromophore to include an anthracene moiety rather than the simpler naphthalene (Brana *et al*. 1997, Brana and Ramos 2001). These compounds were tested against human melanoma UAC375, ovarian OVCAR3 cancer and leukaemia L1210 cells for their cytotoxicity (Brana and Ramos 2001). Azonafide (Figure 1.17) was the most cytotoxic compound, with a higher cytotoxicity than Amonafide in all cell lines (IC_{50} values ranged between 0.007 – 0.071 µM for azonafide, and 0.625 – 2.180 µM for amonafide) (Sami *et al.* 1993, Brana *et al*. 1997, 2001, Brana and Ramos 2001). Additional approaches included further substitutions to the chromophore, thus, resulting in new types of phenanthrene and azaphenanthrene analogues of Azonafide (Brana *et al.* 2001).

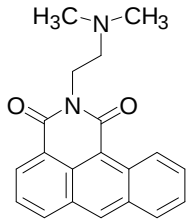

Figure 1.17.: Structure of Azonafide

1.6.2. Bisnaphthalimides

In the 1980s, Brana *et al.* (1993, 2001) designed and synthesised a new series of symmetrical bis-intercalating compounds: the bisnaphthalimides. These compounds comprised of key structural components of parent naphthalimides, and were synthesised using a similar method (i.e., nucleophilic reaction of 1, 8-naphthalic anhydride with the corresponding alkyltetraamine), as described by Brana *et al.* (1993, 1995, 2003). In contrast to naphthalimides, the structure of bisnaphthalimides lead to improvements in the DNA binding capacity, and, thus, the overall therapeutic profile of these compounds as anti cancer agents (Brana and Ramos 2001). Bisnaphthalimides are composed of two chromophore units (naphthalimido rings) linked together by linker chains containing at least one or two amine groups (Figure 1.18), since in the mononaphthalimide series, the amino group was proven to be essential for cytotoxic activity (Brana *et al*. 1993, 2001). Thus, a series of compounds with different substitutions in the chromophore, as well as differences in the length of the linker chain were designed and synthesised (Brana *et al*. 1993, Bailly *et al.* 2003).

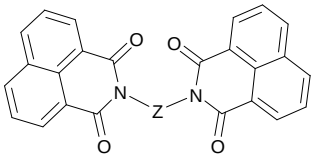

Figure 1.18.: Basic bisnaphthalimide structure (Z indicates the position of the linker chain)

Structural changes were found to improve the biological activity of these compounds by increasing their cytotoxic activity in human colon HT-29 cancer cells, when compared to the parent compounds (Brana *et al.* 1993, 2001). Cytotoxicity increased with certain chromophore substitutions, in the order NO_2 > H > NH_2 > CH_3CONH in compounds with the same linker chain (IC_{50} values of 0.72, 2.70, 39.00 and >100 µM, respectively) (Brana and Ramos 2001) (Figure 1.19). Also, the length and nature of the linker chain was responsible for altered cytotoxicity (Brana *et al*. 1993, Brana and Ramos 2001). However, the bisnaphthalimide compounds failed to provide an accurate structure activity relationship, thus, suggesting different mechanisms of intercalation, even if TOPO II activity had been significantly inhibited (Brana *et al*. 1993, Brana and Ramos 2001).

Although, bisnaphthalimides had an increased cytotoxicity, compared with naphthalimides; many were poorly soluble in aqueous solutions, which renders their testing difficult (Brana *et al*. 1995).

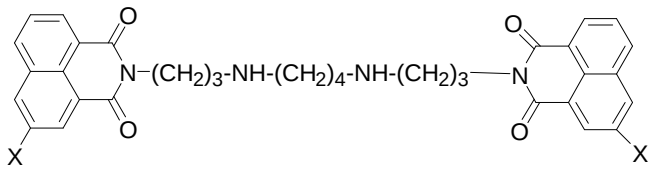

Figure 1.19.: Chromophore substituted bisnaphthalimide structure (X indicates the position of the chromophore substitution; NO_2, H, NH_2 and CH_3CONH)

In 1992, Du Pont Merck Pharmaceuticals synthesised a new series of non-symmetric bisnaphthalimide compounds (Brana *et al*. 1995). These compounds comprised of an acenaphthalimide chromophore to increase aqueous solubility, and a conveniently substituted naphthalimide ring to produce anti tumour activity (Brana *et al*. 1995, Brana and Ramos 2001) (Figure 1.20). These compounds, however, were less cytotoxic and did not drastically improve the aqueous solubility compared with the symmetrical bisnaphthalimides (Brana *et al.* 1995).

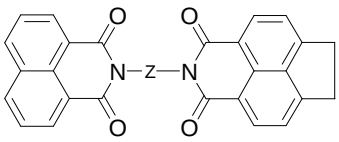

Figure 1.20.: Basic acenaphthalimide bisnaphthalimide structure

Interestingly, a study conducted by Bailly *et al.* (1996) found that bisnaphthalimides could intercalate bifunctionally into the double helix via the major groove. These derivatives were formed by linking two non-substituted naphthalimide groups with a polyamine linker, and the derivatives bearing these structural features were LU79553, (Elinafide), LU 77655 and LU84743 (Bailly *et al.* 1996) (Figure 1.21). The most cytotoxic bisnaphthalimide, Elinafide, (Figure 1.21), had three methylene groups in its linker chain, but lacked any substitutions to the chromophore (Bousquet *et al.* 1995, Brana and Ramos 2001, Ralton *et al.* 2007). Elinafide was selected for Phase I and II clinical trials in Europe and the USA (Bousquet *et al*. 1995, Bailly *et al.* 1996, Brana *et al*. 1993, 2001, 2003, Villalona-Calero *et al*. 2001). However, its future development as an anti cancer agent has been delayed as Denny (2004) found that its dose-limiting toxicity (DLT) was of a cumulative nature.

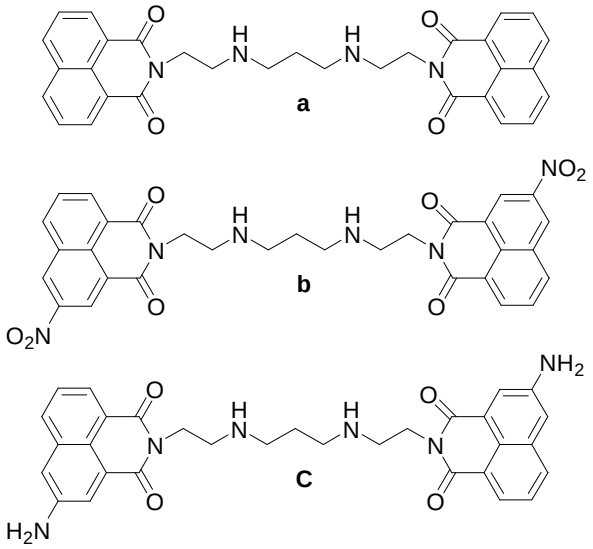

Figure 1.21.: Structure of **a:** LU 79553 (Elinafide), **b:** LU77655 and **c:** LU 84743

Bisnaphthalimides have shown promise as DNA targeted anti cancer agents, which intercalate with DNA and inhibit TOPO II action. To achieve this, the key features required are (i) nitro substitutions in the chromophore rings (Brana *et al.* 1993), (ii) two internal nitrogen atoms (Bailly *et al.* 1996), or (iii) an alkyl linker chain of at least 3 methylene groups (Bailly *et al.* 1996, Brana *et al.* 1997). However, as these compounds are poorly soluble in aqueous solutions (Bailly *et al*. 2003), further studies are required to improve this major obstacle (Brana *et al.* 2004).

1.6.3. Novel Bisnaphthalimidopropyl Polyamine Derivatives

Bisnaphthalimidopropyl polyamine (BNIPP) derivatives were initially designed and synthesised, in 2000, by Kong Thoo Lin and Pavlov (2000), who incorporated natural polyamines into the structure of bisnaphthalimides (e.g., elinafide, Figure 1.21). Kong Thoo Lin and Pavlov (2000) theorised that the addition of more heteroatoms into the linker chain would result in an increased aqueous solubility of bisnaphthalimides, hence, improve their solubility, activity and, thus, their potential as anti cancer agents (Kong Thoo Lin and Pavlov 2000). BNIPP derivatives were synthesised comprising of two naphthalimido rings linked by the natural polyamines: putrescine, spermidine, spermine and an oxa-polyamine (oxa-putrescine), using a three step reaction which incorporated the synthetic strategies for bis (alkyl) polyamines (Bergeron 1986) (Section 1.5.1), and bisnaphthalimide derivatives (Brana *et al.* 1993, Brana *et al.* 1995, Brana *et al.* 2003) (Section 1.6.2), and introducing an *N*-alkylation reaction (Kong Thoo Lin and Pavlov 2000). The newly synthesised bisnaphthalimidopropyl putrescine (BNIPPut), spermidine (BNIPSpd), spermine (BNIPSpm) contain 2, 3, or 4 nitrogen atoms in their linker chain, respectively, whilst oxa-putrescine (BNIPOPut) has 2 nitrogen and 2 oxygen atoms in its linker chain (Kong Thoo Lin and Pavlov 2000, Pavlov *et al.* 2001) (Figure 1.22).

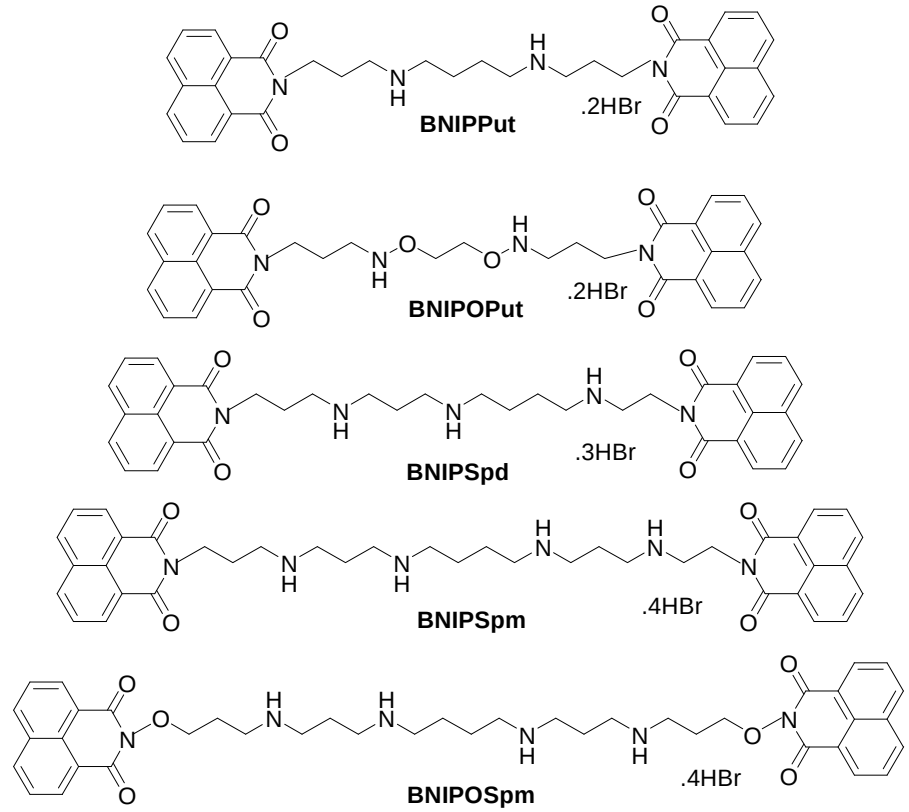

Figure 1.22.: Structures of bisnaphthalimidopropyl polyamine derivatives: BNIPPut, BNIPOPut, BNIPSpd, BNIPSpm and BNIPOSpm

Cytotoxicity of the BNIPP derivatives was initially conducted at the National Cancer Institute (NCI) in the USA, who determined an *in vitro* screen in a variety of human cancer cell lines, including leukaemia, lung, colon, prostrate and breast cancer cells (Kong Thoo Lin and Pavlov 2000). After 48 hours treatment, BNIPOPut (oxa-putrescine) was the least cytotoxic derivative with a mean GI_{50}[5] value of 68.55 μM, whereas BNIPPut, BNIPSpd and BNIPSpm exhibited 0.58, 1.42 and 4.31 μM mean GI_{50} values, respectively (Kong Thoo Lin and Pavlov 2000). Cytotoxicity was in the order of BNIPPut, followed by BNIPSpd, BNIPSpm and then BNIPOPut (Kong Thoo Lin and Pavlov 2000). However, in previous bis (alkyl) polyamine derivative screens, spermine derivatives tended to be more cytotoxic than spermidine derivatives (Section 1.5.1), in contrast with the results obtained for BNIPP derivatives. Results also showed that the cytotoxicity and aqueous solubility of BNIPP derivatives was dependent upon the length of the polyamine linker chain (i.e., shorter polyamine; greater cytotoxicity), and the number of heteroatoms in the compound (i.e., more heteroatoms; greater aqueous solubility, whilst the introduction of oxygen atoms dramatically decreased cytotoxicity) (Kong Thoo Lin and Pavlov 2000, Pavlov *et al.* 2001). BNIPPut and BNIPOPut were not, however, used in further studies, because they were insoluble in both water and 10% DMSO (although soluble in 10% DMSO after heating) (Kong Thoo Lin and Pavlov 2000).

[5] GI_{50} (Growth Inhibition) is defined as the concentration required for 50 % inhibition of cell growth, compared to that of untreated cells (Kong Thoo Lin and Pavlov 2000).

Interestingly, BNIPPut, BNIPSpd and BNIPSpm were found to be highly selective against breast cancer cells. As BNIPPut, BNIPSpd and BNIPSpm were 202-, 443- and 24-fold more active against breast cancer HS 578T cells than NCI/ADR-RES cells, respectively (Kong Thoo Lin and Pavlov 2000).

Pavlov *et al.* (2001) expanded the work of Kong Thoo Lin and Pavlov (2000) by investigating the cytotoxic properties of BNIPSpd, BNIPSpm and BNIPoxa-spermine (BNIPOSpm) (Figure 1.22) in human breast cancer MCF-7 cells. The DNA binding properties and nuclear localisation of these derivatives were also investigated by Pavlov *et al.* (2001). All BNIPP derivatives were capable of significantly inhibiting the growth of MCF-7 cells, with IC_{50} values for BNIPSpd, BNIPSpm and BNIPOSpm of 1.38, 2.91 and 8.45 μM, respectively (Pavlov *et al.* 2001). BNIPOSpm, although the least cytotoxic, had the highest DNA binding affinity, followed by BNIPSpd and BNIPSpm (ΔT_m[6] of 22.0, 20.6 and 18.3 °C compared to *Calf Thymus* DNA without BNIPP derivative, respectively) (Pavlov *et al.* 2001). The fluorescent properties of the BNIPP derivatives were exploited, and all derivatives were located in the cell nuclei of the MCF-7 cells, after 8-hours treatment (Pavlov *et al.* 2001). These results support those of Kong Thoo Lin and Pavlov (2000); as cytotoxicity remains dependent upon the length of the polyamine linker (i.e., shorter polyamine (BNIPSpd); greater cytotoxicity), and the number of heteroatoms (i.e., more heteroatoms (BNIPOSpm); lower cytotoxicity) (Pavlov *et al.* 2001, Pavlov *et al.* 2002). Finally, BNIPP derivatives were found to bind to DNA by intercalation and groove binding (Pavlov *et al.* 2001); a similar mode of action to that of the parent bisnaphthalimides (Brana and Ramos 2001).

A study undertaken by Kong Thoo Lin *et al.* (2003) discovered, for the first time that BNIPSpd and BNIPSpm induced apoptotic cell death in human leukaemia HL-60 cells. HL-60 cells treated for 24 hours with BNIPSpd and BNIPSpm showed characteristics of undergoing apoptotic cell death, in particular, HL-60 cells treated with BNIPSpd (Kong Thoo Lin *et al.* 2003). Again, this study can be compared with the previous studies of Kong Thoo Lin and Pavlov (2000) and Pavlov *et al.* (2001), as cytotoxicity, and also DNA binding affinity of BNIPP derivatives is dependent upon the nature of the polyamine linker chain (Kong Thoo Lin *et al.* 2003).

[6] ΔT_m is defined as the melting temperature difference between drug treated *Calf Thymus* DNA and *Calf Thymus* DNA without drug.

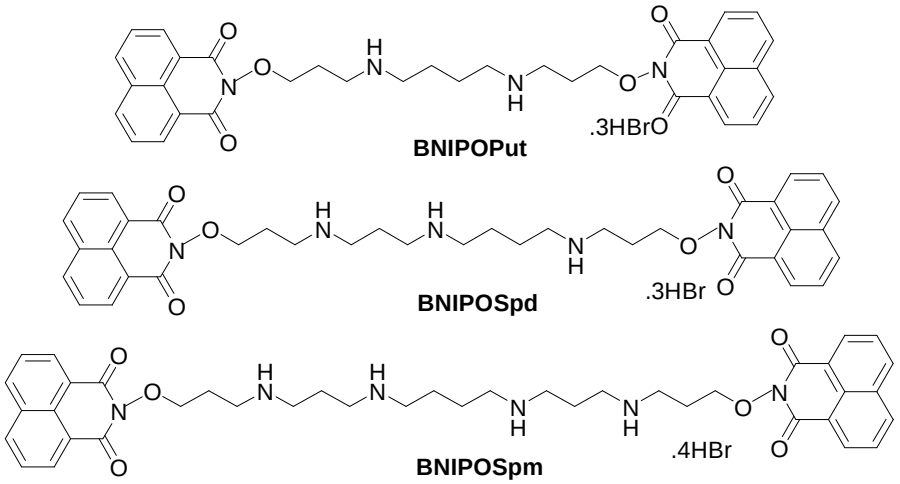

Figure 1.23.: Structures of bisaminooxypropylnaphthalimido polyamine derivatives: BNIPOPut, BNIPOSpd and BNIPOSpm

A further extension of the original work by Kong Thoo Lin and Pavlov (2000), involved the synthesis of three new bisaminooxypropylnaphthalimido polyamine derivatives, BNIPOPut, BNIPOSpd and BNIPOSpm (Figure 1.23), where oxygen atoms were introduced into the α-position of the naphthalimido ring (Dance *et al.* 2005). Dance *et al.* (2005) rationalised that synthesising these new BNIPP derivatives would show an enhancement of aqueous solubility, without affecting cytotoxicity. The results obtained for the new BNIPP derivatives were compared with BNIPSpd and BNIPSpm (Dance *et al.* 2005) and showed that solubility of these new BNIPP derivatives was increased, and all derivatives had good solubility properties in 20% DMSO. However, the presence of oxygen atoms in the α-position caused a decrease in cytotoxicity in MCF-7 cells. After 24 hours, BNIPOPut and BNIPOSpm were the least cytotoxic derivatives with IC_{50} values of > 50 μM, whereas BNIPSpd, BNIPSpm and BNIPOSpd exhibited IC_{50} values of 1.5, 13.3 and 32.1 μM, respectively (Dance *et al.* 2005). This order of cytotoxicity was the same after 48 hours (i.e., BNIPSpd > BNIPSpm > BNIPOSpd > BNIPOSpm > BNIPOPut). Therefore, cytotoxicity was again highly reliant on the nature of the polyamine linker chain between the two napthalimido rings (Kong Thoo Lin and Pavlov 2000, Pavlov *et al.* 2001, Kong Thoo Lin *et al.* 2003, Dance *et al.* 2005). In addition, this study also revealed that bisnaphthalimidopropyl functionality was essential for optimum cytotoxicity, as an oxygen atom in the α-position, reduced cytotoxicity (Dance *et al.* 2005). All BNIPP derivatives, irrespective of the polyamine linker chain, were able to interact with DNA in the order BNIPSpd > BNIPSpm > BNIPOSpd > BNIPOSpm > BNIPOPut (Dance *et al.* 2005), suggesting, therefore, a relationship between DNA binding affinity and cytotoxicity. The most active BNIPP derivatives, BNIPSpd and BNIPSpm, alongside BNIPOSpm were selected for DNA damage studies. After 4 hours, BNIPSpd and BNIPSpm caused significant DNA damage (at 0.1 μM); however, BNIPOSpm did not achieve a similar level of DNA damage to that of BNIPSpm after 12 hours treatment in MCF-7 cells (Dance *et al.*

2005). These results highlight the importance of DNA as a biological target for BNIPP derivatives.

Further syntheses of bisnaphthalimidopropyl di- [diamino-octane (BNIPDaoct), diamino-nonane (BNIPDanon) and diamino-decane (BNIPDadec)], and triamines [dipropyl-triamine (BNIPDpta) and diethyltriamine (BNIPDeta)] (Figure 1.24), based on the parent derivative, BNIPSpd, were synthesised to modify the central linker chain by introducing different alkyl lengths with 2 or 3 nitrogen atoms (Oliveira *et al.* 2007). Oliveira *et al.* (2007) were, thus, modulating the number of positive charges present within each BNIPP derivative, and its effect on cytotoxicity in human colon cancer CaCO-2 cells. After 24 hours, all BNIPP derivatives, except BNIPDeta (IC_{50} value of 21.7 μM) exerted IC_{50} values in the range of 0.47 – 6.20 μM, with the order of cytotoxicity the same after 48 hours (Oliveira *et al.* 2007). The results also demonstrate that removing a nitrogen atom from the linker chain did not affect cytotoxic properties. Interestingly, Oliveira *et al.* (2007) showed that by increasing the length of the linker chain; aqueous solubility increased. Previously, when an alkyl linker was a butyl linker, the BNIPP derivative (BNIPPut) was not soluble in water or 10% DMSO (Kong Thoo Lin and Pavlov 2000). Therefore, aqueous solubility is also highly reliant on the nature of the polyamine linker chain.

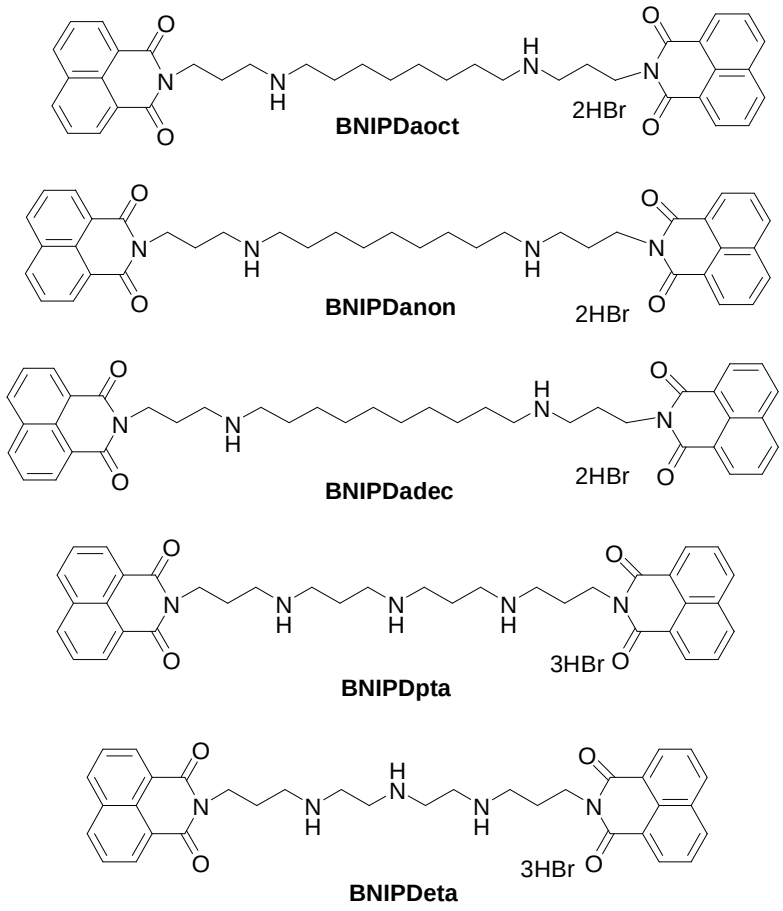

Figure 1.24.: Structures of bisnaphthalimidopropyl polyamine derivatives: BNIPDaoct, BNIPDanon, BNIPDadec, BNIPDpta and BNIPDeta

The most recent study conducted by Ralton *et al*. (2009) focused on BNIPSpd treatment in human colon cancer CaCO-2 and HT-29 cells. After 48 hours, BNIPSpd was more cytotoxic in CaCO-2 cells (IC_{50} 0.15 µM) compared to HT-29 cells (IC_{50} 1.64 µM) (Ralton *et al.* 2009). In both cell lines, BNIPSpd induced significant DNA damage after 4 hours, caused cell death by apoptosis, and depleted intracellular spermidine and spermine levels after 24 hours (Ralton *et al.* 2009), suggesting that BNIPP derivatives primarily induce apoptosis in colon cancer cells (Ralton *et al.* 2009). Bisnaphthalimidopropyl polyamine (BNIPP) derivatives have been shown to enhance solubility and activity, which provides a good basis for their further development as potential anti cancer agents (Ralton *et al.* 2007).

Interestingly a recent publication by Filosa *et al.* (2009) described the synthesis of a series of bisnaphthalimide derivatives containing heterocyclic and other cyclic moieties inserted into the linker chain, for example, piperazine, cis-dimethylpiperazine, diazabicyclo [3.2.1] octane or cyclopropane groups. This group have modified the *N*-alkylation reaction originally developed by Kong Thoo Lin and Pavlov (2000). After 72 hours, N^1, N^1-bis [2-(5-nitro-1, 3-dioxo-2,3-dihydro-1H-benz[*de*]-iso-quinolin-2-yl)]propane-2-ethanediamine (Figure 1.25) was identified as the most active derivative with an IC_{50} value of 0.50 µM, in HT-29 cells (Filosa *et al.* 2009). This derivative was also found to effectively intercalate with DNA, and significantly induce apoptosis (40% at 0.1 µM) in HT-29 cells (Filosa *et al.* 2009).

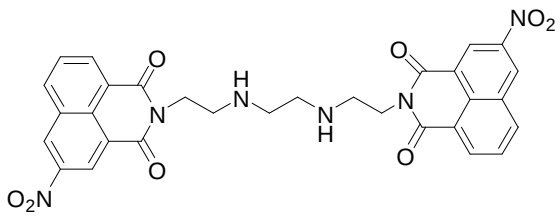

Figure 1.25.: Structure of N^1, N^1-bis [2-(5-nitro-1, 3-dioxo-2,3-dihydro-1H-benz[*de*]-iso-quinolin-2-yl)]propane-2-ethanediamine

1.7. Aims of Project

The aim of this project was to synthesise new BNIPP derivatives and determine their cytotoxicity and mode of action within a breast cancer cell system. This study was undertaken to complement and further previous studies on breast cancer MCF-7 cells, human leukaemia HL-60 cells and, colon cancer CaCO-2 and HT-29 cells (Kong Thoo Lin and Pavlov 2000, Pavlov *et al.* 2001, Dance *et al*. 2005, Ralton 2006, Oliveira *et al*. 2007, Ralton *et al.* 2009).

Four novel BNIPP derivatives were synthesised based on synthetic methods previously described by Kong Thoo Lin and Pavlov (2000), Dance *et al.* (2005) and Oliveira *et al.* (2007). These derivatives were synthesised to highlight and confirm the importance of the common features found within BNIPP derivatives, and demonstrate, in particular, that the bisnaphthalimido moiety was essential for biological activity.

As BNIPP derivatives have been previously shown to bind to DNA by bis-intercalation (Pavlov *et al.* 2001, Dance *et al.* 2005), a selection of BNIPP derivatives were investigated for their DNA binding affinities by examination of DNA binding capacity and competitive displacement, and by molecular modelling.

Human MDA-MB-231 breast adenocarcinoma cells and human MCF-10A breast epithelial cells were used, in order to establish a structure-activity relationship and to determine the biological activity of BNIPP derivatives on cell morphology, and cellular uptake and distribution. BNIPP derivative affinity for the MGBG-specific polyamine transport system and their ability to reduce intracellular polyamine levels were also investigated. Breast cancer MDA-MB-231 cells were chosen in this study to expand and compare work which had been undertaken in breast cancer MCF-7 cells (Pavlov *et al.* 2002, Dance *et al.* 2005). MCF-7 cells are oestrogen receptor dependent (oestrogen positive; ER+), and exhibit a favourable response to chemotherapy, whereas MDA-MB-231 cells are oestrogen receptor independent (oestrogen negative; ER-), highly invasive and do not respond well to current chemotherapy treatments (Koutsilieris *et al.* 1999, Lacroix and Leclercq 2004). For that reason, the MDA-MB-231 cells can provide a reliable model by which to study the effects of BNIPP treatment on breast cancer cells that are highly resistant to chemotherapy.

Furthermore, the effect of BNIPP derivative treatment on MDA-MB-231 cells, in relation to DNA damage and natural DNA repair mechanisms were investigated. BNIPP derivatives have also been shown to induce apoptotic cell death in HL-60, HT-29 and CaCO-2 cells (Kong Thoo Lin *et al.* 2003, Ralton 2006). Further investigations into the mode of cell death were undertaken in this study by examination of early apoptotic cell death and cell cycle distribution. In addition, the effects of BNIPP derivatives on p53 and $p21^{Waf1/Cip1}$ gene expression were investigated. Finally, the effect of BNIPP derivatives on histone deacetylase (HDAC) inhibition was studied after encouraging observations by

colleagues in Portugal (Tavares *et al.* 2010). Tavares *et al.* (2010) identified for the first time that BNIPP derivatives were inhibitors of the human SIRT1 enzyme (e.g., IC_{50} value of 116.5 and 97.4 μM for BNIPDaoct and BNIPDanon, respectively). Recently, HDAC inhibitors (HDACi) have shown promise as anti cancer agents and have, thus, aided the interest of screening BNIPP derivatives as potential HDAC inhibitors (Taylor *et al.* 2008, Cang *et al.* 2009, Casero and Woster 2009, Epping and Bernards 2009).

1.7.1. Layout of Thesis

The results chapters (Chapters 2 – 7) have been arranged, so that each individual chapter has its own specific introduction, material and methods, results, discussion and conclusion sections so to provide an in depth analysis of each area.

Chemical synthesis and characterisation of BNIPP derivatives are fully explained in Chapter 2. DNA binding and molecular modelling studies of BNIPP derivatives are described in Chapter 3. Cell morphology, cytotoxicity, cellular uptake and distribution, polyamine transport and effect on polyamine intracellular levels by BNIPP derivatives are explained in Chapter 4, whilst the extent of DNA damage and the effect on repair mechanisms are explained in Chapter 5. Chapter 6 focuses on the effect of BNIPP derivatives on apoptotic cell death, cell cycle distribution, p53 and $p21^{Waf1/Cip1}$ mRNA levels, whereas Chapter 7 describes HDAC inhibition by BNIPP derivatives.

The final chapter (Chapter 8) combines all the findings from this study into an integrated final summary, which includes concluding and future work sections.

Chapter 2

Synthesis of Novel Bisnaphthalimidopropyl Polyamine Derivatives

2.1. Synthesis of Novel Bisnaphthalimidopropyl Polyamine Derivatives

A number of bis(alkyl)polyamine analogues have previously been published indicating their potential anti cancer properties. These compounds have the ability to inhibit cell growth in a variety of cancer cell lines, for example, in leukaemia (L1210), Burkett's lymphoma (Daudi), colon (HT-29), prostrate (DU145), ovarian (OVCAR3) and breast (MCF-7) cancer cells (Porter *et al.* 1985, Bergeron *et al.* 1988, Pegg *et al*. 1989, Reddy *et al.* 1998, Brana and Ramos 2001, Pavlov *et al.* 2001). Polyamine analogues have been shown to deplete intracellular polyamine levels, and in some cases, have decreased the activity of certain important enzymes within the polyamine biosynthetic pathway (Porter *et al*. 1985, Pegg *et al*. 1989). Furthermore, several analogues including *cis*-**iii** (CGC-11047) are currently undergoing Phase I and II clinical trials (Casero and Woster 2009) (Figure 1.13).

Naphthalimido and bisnaphthalimido derivatives have also revealed potential anti cancer properties. These derivatives bind to DNA by intercalation, where the planar aromatic rings insert between the base pairs of the DNA double helix, thus resulting in cytotoxicity within several cancer cell lines including melanoma (UAC375) and colon (HT-29) cancer cells (Brana *et al.* 2001, Brana and Ramos 2001). The naphthalimide Amonafide and the bisnaphthalimide Elinafide were selected for Phase I and II clinical trials (Brana *et al*. 2003). Following on from these derivatives, Bisnaphthalimidopropyl polyamine (BNIPP) derivatives, linked to the natural polyamines with diamino and triamino alkyl linker chains were synthesised by Kong Thoo Lin and Pavlov (2000). These BNIPP derivatives were synthesised to overcome the biological obstacles faced by bisnaphthalimides with regards to their aqueous insolubility and delivery (Ralton *et al.* 2007). BNIPP derivatives were found to demonstrate enhanced aqueous solubility, and exhibited *in vitro* anti cancer activity (Kong Thoo Lin and Pavlov 2000, Pavlov *et al.* 2001, Dance *et al.* 2005).

The aim of the experimental work presented in this chapter was to synthesise and characterise several new members of the BNIPP derivative series: two bisnaphthalimidopropyl diamino derivatives; a bisphthalimidopropyl diamino derivative and a mononaphthalimidopropyl derivative (Figure 2.1).

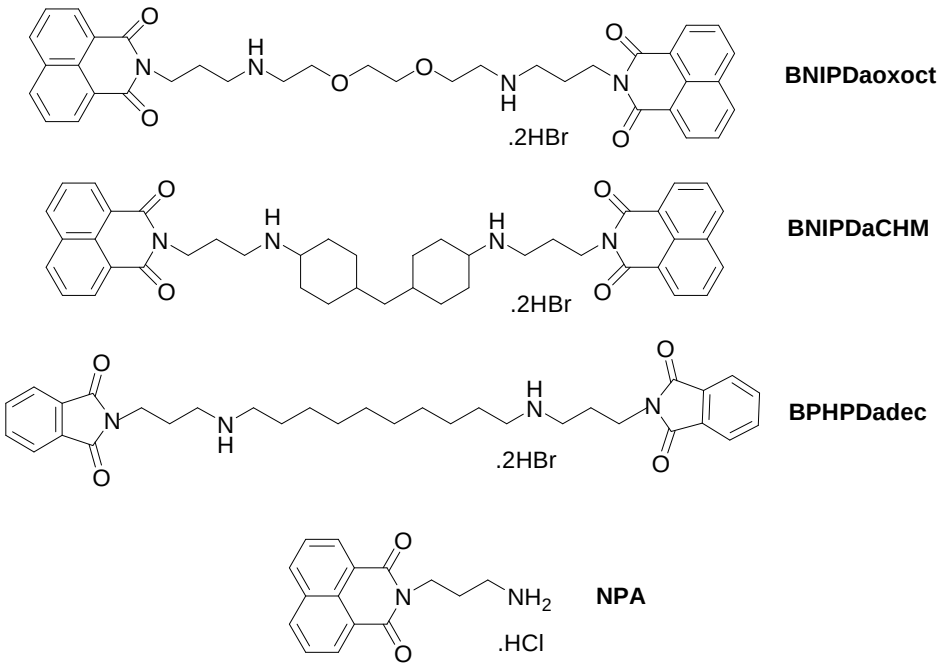

Figure 2.1.: Structures of Bisnaphthalimidopropyl diaminooxaoctane (BNIPDaoxoct), Bisnaphthalimidopropyl diaminodicyclohexylmethane (BNIPDaCHM), Bisphthalimidopropyl diaminodecane (BPHPDadec) and mononaphthalimidopropylamine (NPA)

The general synthetic methods used to synthesise the bis(alkyl)polyamine analogues, naphthalimides, bisnaphthalimides, and BNIPP derivatives relevant to this project are described below (Sections 2.1.1 – 2.1.5).

2.1.1. General Synthetic Method for Symmetrical Bis(alkyl)Polyamine Analogues

The most extensively studied symmetrical bis(alkyl)polyamine analogue, Bis-ethylspermine (BESpm) was synthesised by Bergeron and colleagues in 1988. BESpm and subsequent bis (ethyl) analogues have been synthesised in a three step reaction **[1-3]** (Figure 2.2). The starting material used was the commercially available spermine tetrahydrochloride, which was protected and activated by *p*-toluenesulfonyl chloride (Ts-Cl) in dry dichloromethane, at room temperature, for 48 hours **[1]**. The resulting sulfonamide was treated with sodium hydride in dimethylformamide (DMF), in the presence of excess ethyl iodide which yielded N^1, N^{12} Bis-ethyl – N^1, N^4, N^9, N^{12} tetratosylspermine **[2]**. Deprotection of the sulfonyl protecting groups was carried out by treatment with sodium in liquid ammonia at -78 °C for 4 hours, to give N^1, N^{12} Bis-ethylspermine. N^1, N^{12} Bis-ethylspermine was purified as a hydrochloride salt **[3]** (Bergeron *et al.* 1988). The synthesis of BESpm and its analogues is simple and only dependent upon the availability of the starting material, the parent polyamine backbone. This method is amenable to larger scale synthesis.

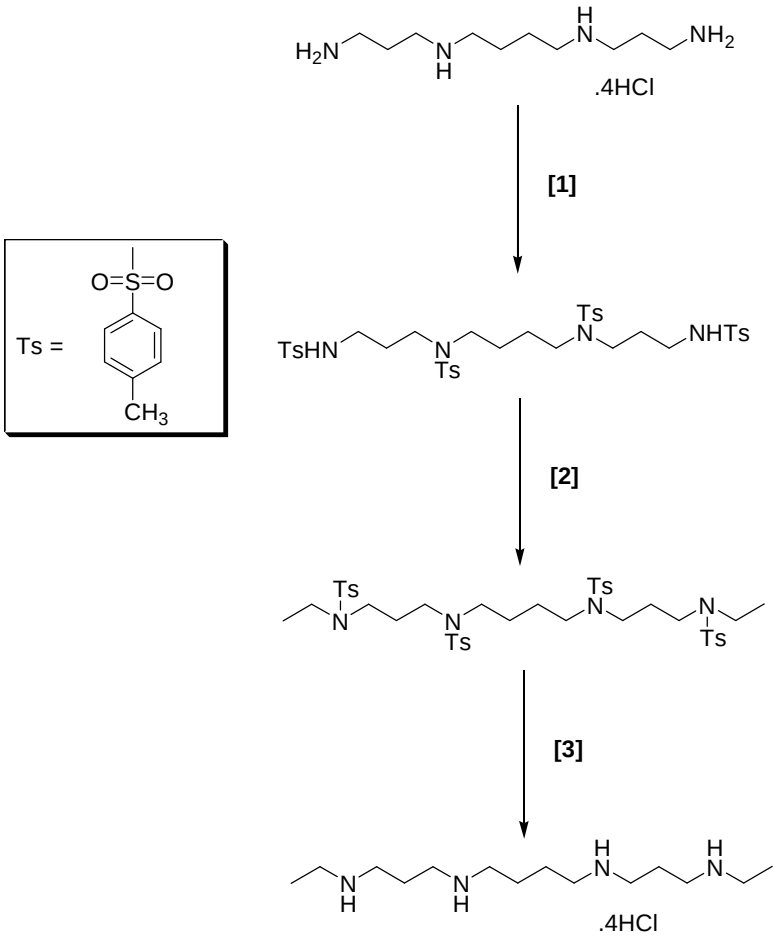

Figure 2.2.: General synthetic method for the synthesis of N^1, N^{12} bis-ethylspermine (BESpm). Reagents and conditions: **[1]** Ts-Cl, CH_2Cl_2, 10% NaOH (aq), RT, 48 h **[2]** NaH, DMF, Ethyl iodide, 0 °C, 1 hr, reflux at 70 – 80 °C, 12 h **[3]** THF, Na spheres in liquid NH_3, -78 °C, 4 h.

2.1.2. General Synthetic Method for Confomationally Restricted Bis(alkyl)Polyamine Analogues

The conformationally restricted bis(alkyl)polyamine analogues of BESpm were synthesised by Reddy and colleagues (1998) by a general synthetic strategy again consisting of a three step reaction **[1-3]** (Figure 2.3). The common starting material was a *cis-trans*-1,2-bis (mesitylenesulfonyloxy)methyl compound, prepared from either the commercially available *cis-trans*-1,2-bis(dihydroxymethyl)cyclopropane, *cis-trans*-1,2-bis(dihydroxymethyl)cyclobutane, *cis-trans*-2-butenediol, butyne-1,4-diol or benzene-1,2-dimethanol molecules by esterification **[1]**. Protection and activation of the N^1-ethylpropane-1, 3-diamine was carried out with mesitylenesulfonyl chloride (Mts) in sodium hydroxide and dioxane at room temperature for 18 hours. For the synthesis of the fully protected conformationally restricted analogues, *N*-alkylation with *N*-Ethyl-*N*-(3-(mesitylenesulfonylamino)propyl)mesitylenesulfonamide, in the presence of sodium hydride and anhydrous DMF, yielded the fully protected analogues **[2]**. Deprotection to release the amino groups was carried out by established procedures using phenol and hydrogen bromide in glacial acetic acid at room temperature for 48 hours, to give 3,7,13,17-tetraaza-9,10-[(*E*)-1,2-cyclopropyl] octadecane, 3,7,13,17-tetraaza-9,10-[(*Z*)-

1,2-cyclopropyl]octadecane, 3,7,13,17-Tetraaza-9,10-[(*E*)-1,2-cyclobutyl]octadecane, 3,7,13,17-Tetraaza-9,10-[(*Z*)-1,2-cyclobutyl]octadecane, (*E*)-3,7,12,16-Tetraazaoctadec-9-ene, (*Z*)-3,7,12,16-Tetraazaoctadec-9-ene, 3,7,12,16-Tetraazaoctadec-9-yne and 9,10-Benzo-3,7,12,16-tetraazaoctadecane, as their corresponding tetrahydrochloride salts **[3]** (Bergeron *et al.* 1994, Roemmele and Rapoport 1988, Reddy *et al.* 1998).

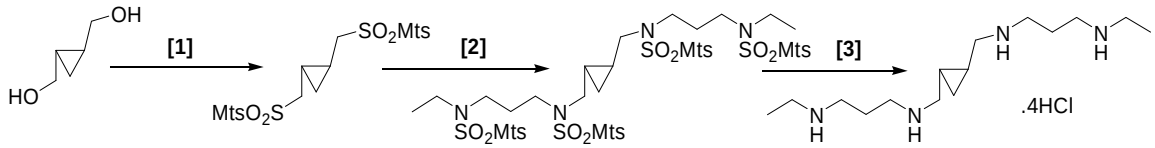

Figure 2.3.: Example of the general synthetic method for the synthesis of conformationally restricted BESpm analogues. Example shown for the synthesis of 3,7,13,17-Tetraaza-9,10-[(*E*)-1,2-cyclopropyl] octadecane. Reagents and Conditions: **[1]** Pyridine, Mts, 25 °C, 3 h **[2]** *N*-Ethyl-*N*-(3-(mesitylenesulfonylamino)propyl) mesitylenesulfonamide, NaH, DMF, 70 °C, 4 h **[3]** HBr/glacial CH_3CO_2H in Phenol, RT, 48 h.

2.1.3. *General Synthetic Method for Naphthalimide Derivatives*

As indicated in Section 1.6, the intercalating compounds relevant to this research project are the naphthalimides and bisnaphthalimides which were first synthesised by Brana and colleagues (2001) (Figure 2.4).

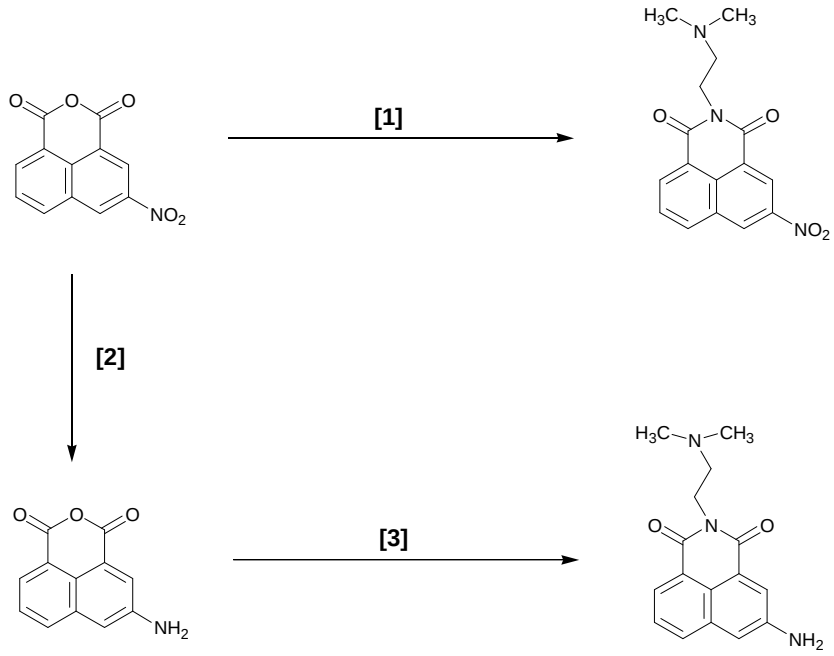

Figure 2.4.: General synthetic method in the synthesis of mitonafide **[1]** and amonafide **[2-3]**. Reagents and conditions: **[1]** $NH_2(CH_2)_2N(CH_3)_2$, C_2H_5OH, reflux, 2 h **[2]** H_2/Pd **[3]** $NH_2(CH_2)_2N(CH_3)_2$, C_2H_5OH, reflux, 2 h

The synthesis of Mitonafide and Amonafide, the most active compounds in the naphthalimide series were synthesised by one step and two step reactions, respectively (Brana *et al.* 1993, 2001). The starting material, 3-nitro-1,8-naphthalic anhydride was

used in the synthesis of both mitonafide and amonafide. 3-nitro-1, 8-naphthalic anhydride and *N*, *N*-dimethylethylenediamine were refluxed in ethanol for 2 hours to produce mitonafide **[1]**. 3-nitro-1, 8-naphthalic anhydride was first hydrogenated over 10 % palladium on carbon (Pd/C) to give 3-amino-1, 8-naphthalic anhydride **[2]** followed by the addition of *N*, *N*-dimethylethylenediamine, which were refluxed in ethanol for 2 hours to produce amonafide **[3]** (Brana *et al.* 2001).

The two step synthesis of amonafide is simple but is highly dependent upon the availability of 3-amino-1, 8-naphthalic anhydride. 3-amino-1, 8-naphthalic anhydride is not readily available in vast quantities, thus making its pharmaceutical preparation exceedingly difficult. Several scaled up variations to the methods described have been approved, therefore, allowing the production of amonafide in acceptable pharmaceutical quantities (Ajami and Barlow 2004, Brown 2005).

2.1.4. General Synthetic Method for Bisnaphthalimide Derivatives

Due to the success of the naphthalimide derivatives, Brana and colleagues (1993, 2001) designed and synthesised bisnaphthalimide derivatives. The derivatives were based on the most active naphthalimides: mitonafide and amonafide.

The general synthesis for the preparation of bisnaphthalimide derivatives was similar to that of naphthalimide derivatives. A nucleophilic reaction of 1, 8-naphthalic anhydride with the corresponding alkyltetraamine in a 2:1 ratio was refluxed in ethanol, until reaction completion (Brana *et al*. 1993, Brana *et al.* 1995, Brana *et al.* 2003) (Figure 2.5).

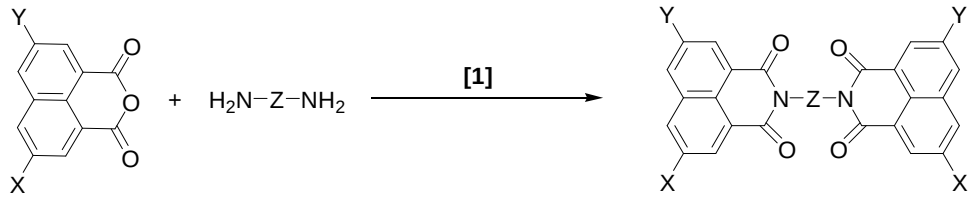

Figure 2.5.: General synthetic method in the synthesis of bisnaphthalimides **[1]** reflux, C_2H_5OH (X and Y indicates the position of the chromophore substitution; NO_2, H, NH_2 and CH_3CONH. Z indicates the position of the linker chain).

2.1.5. General Synthetic Method for Bisnaphthalimidopropyl Polyamine (BNIPP) Derivatives

BNIPP derivatives were synthesised by Kong Thoo Lin and Pavlov in 2000, with the subsequent synthesis of additional BNIPP derivatives in 2005 (Dance *et al.* 2005). The general synthetic strategy used to synthesise the BNIPP derivatives involves a three step reaction **[1-3]**, by combining the synthetic strategies for bis (alkyl) polyamine and bisnaphthalimide analogues (Figure 2.6).

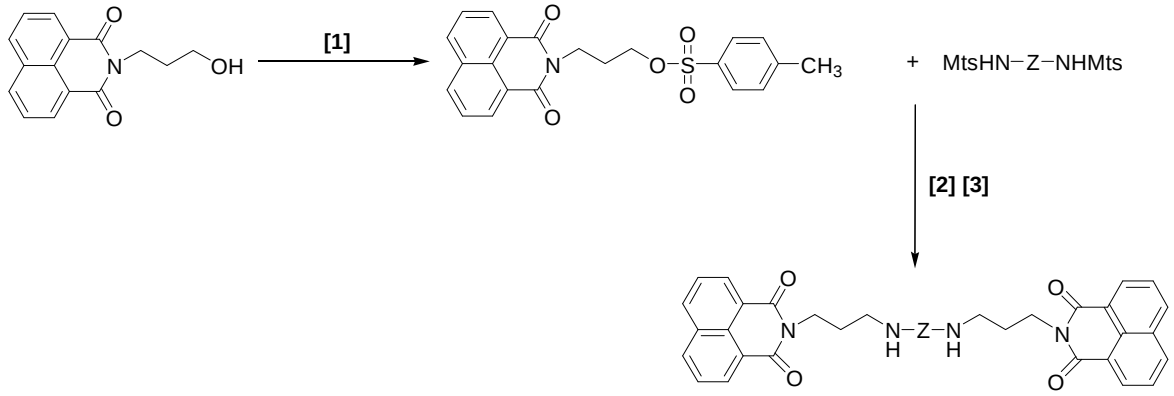

Figure 2.6.: General synthetic method in the synthesis of bisnaphthalimidopropyl polyamine derivatives. **[1]** Ts-Cl, pyridine, 4 °C, 4h **[2]** DMF, Mts, Cs_2CO_3, 85 °C, 12 h **[3]** HBr/glacial CH_3CO_2H in CH_2Cl_2 , RT, 24 h. (Z indicates the position of the linker chain).

The common intermediate was toluenesulfonyloxypropylnaphthalimide, which was prepared from *N*-(3-hydroxypropyl) naphthalimide upon reaction with Ts-Cl, at 4 °C for 12 hours **[1]** (Figure 2.6). Protection and activation of the natural polyamines, diamines and triamines was carried out with mesitylenesulfonyl chloride (Mts) in pyridine at room temperature for 4 hours. Fully protected BNIPP derivatives were obtained by *N*-alkylation of mesitylatediamines with toluenesulfonyloxypropylnaphthalimide, in the presence of caesium carbonate in anhydrous DMF. This reaction successfully yielded fully protected BNIPP derivatives. Deprotection of the Mts groups with hydrobromic acid/glacial acetic acid in CH_2Cl_2, at room temperature, for 24 hours, afforded BNIPP derivatives as their corresponding dihydrobromide salts **[2-3]** (Figure 2.6) (Kong Thoo Lin and Pavlov 2000, Dance *et al*. 2005).

2.1.6. Instrumental Techniques for Identification and Characterisation of Derivatives

The instrumental techniques employed to characterise the products at each reaction stage were Thin Layer Chromatography (TLC), Nuclear Magnetic Resonance (NMR) and Mass Spectrometry (MS). TLC is a straightforward and low-cost separation technique, which is widely used in the rapid identification of several components within a solution (Braithwaite and Smith 1994). TLC was used to determine reaction completion and compound purity at each stage. For TLC determination, a silica gel aluminium plate (adsorbent stationary phase) was spotted with a small drop of the mixture, using a micro pipette. Once dry, the silica gel plate was placed and stood vertically in a solvent (mobile phase) within a TLC development tank. As the solvent travels up the plate by capillary action, the components in the solution travel at different rates, thus separating the mixture into discrete spots. The spots are visualised under UV-light (Figure 2.7).

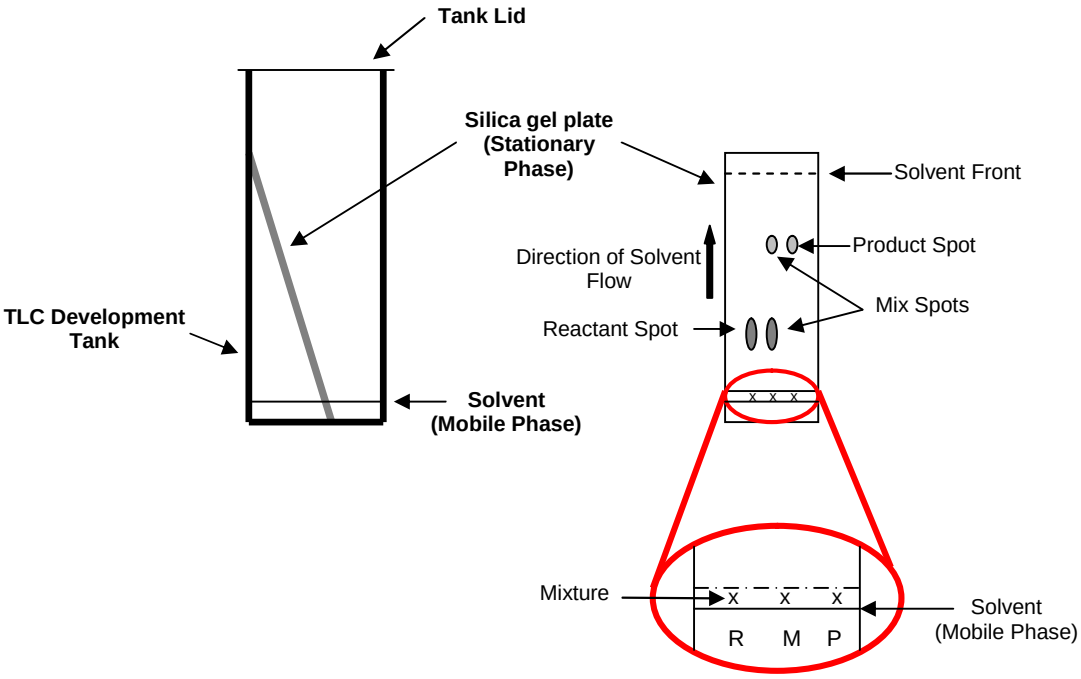

Figure 2.7.: A TLC development tank (Left) and thin-layer chromatogram (Right). (KEY: - R. Reactant Mixture, M. Mix of Reactant and Product and P. Product Mixture)

Nuclear Magnetic Resonance (NMR) is an important and powerful analytical tool, which was used to determine and characterise the complete structure of each intermediate and the final products. NMR samples were prepared by dissolving the sample in a deuterated solvent, for example, Chloroform-D ($CDCl_3$) or Dimethyl Sulfoxide-D6 (DMSO-d_6). This solution was transferred to an NMR tube, capped and introduced into the NMR instrument. The sample was lowered into the NMR probe, rotated, locked, shimmed, then acquired and processed by Bruker Topspin 1.3 software, to give an NMR spectrum.

In essence, NMR spectroscopy relies upon the magnetic properties (nuclear spin) of specific atomic nuclei, in particular, proton (^{1}H or hydrogen) and carbon-13 (^{13}C) nuclei. ^{1}H NMR allows the detection of protons, whereas ^{13}C NMR detects carbon nuclei, both in relation to their immediate environments. Another ^{13}C NMR experiment, Distortionless Enhancement of Polarisation Transfer (DEPT-135), can be used to verify similar information to that of ^{13}C NMR. For DEPT-135 NMR, the -CH_3 and CH signals appear above the baseline but the -CH_2- signals appear inverted (below the baseline). Quaternary carbons are not visible using this ^{13}C NMR technique. Therefore, DEPT-135 can be used to confirm the number of hydrogens attached to carbons within a compound (Figure 2.8). ^{1}H and ^{13}C NMR are observed at different frequencies, 400.1 and 100.6, respectively. Therefore, the complete chemical structure of a compound can be successfully determined by ^{1}H, ^{13}C and DEPT-135 NMR (Loudon 2002b).

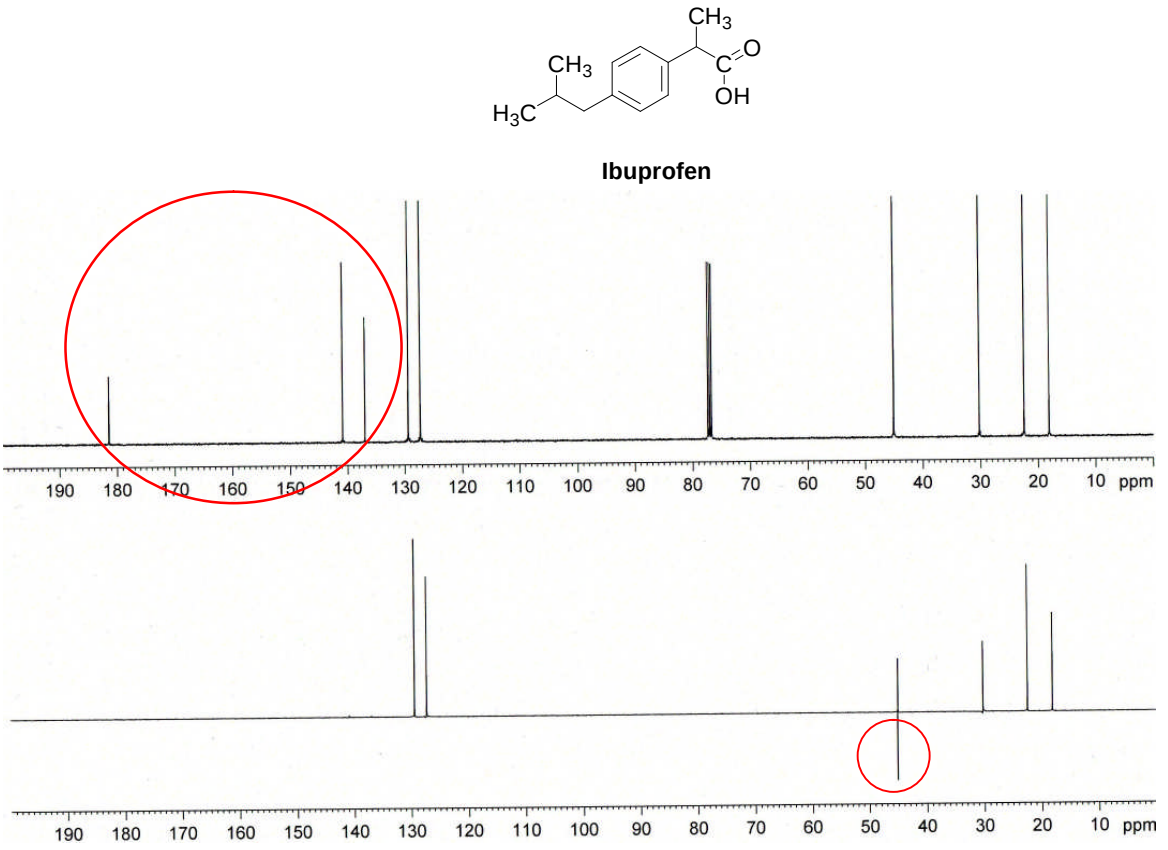

Figure 2.8.: An example of the ^{13}C and DEPT-135 spectra of Ibuprofen (Highlighted signals indicate quaternary carbons which are not visible in DEPT-135 and $-CH_2-$ groups which appear inverted)

Alongside NMR spectroscopy, Mass Spectrometry (MS), was employed to determine the purity and molecular mass of final BNIPP derivatives and their fragments. As a result, MS was used to verify the structure of each new member of the BNIPP derivative series. The basic principle of MS is to generate and separate charged molecules according to their mass-to-charge ratio (*m/z*): the mass of an ion, using an electric and/or magnetic field. Molecules are firstly introduced into the MS, through an inlet and, converted to a charged or ionised form by an ion source. Several ionisation methods exist, but the preferred method used in the analysis of BNIPP, BPHP and NPA derivatives was Electrospray Ionisation (ESI). ESI was used for both low and high resolution MS. The basis of ESI is to atomise a sample solution into highly charged droplets, thus producing negatively charged ions which are accelerated into a mass analyser, amplified and detected, upon which a mass spectrum is produced (Siuzdak 1996, Loudon 2002a).

2.2. Materials

2.2.1. Materials

All reagents were purchased from Fisher Scientific, UK unless otherwise stated, and were used without purification.

3-amino-1-propanol	Sigma-Aldrich, UK
N-(3-Bromopropyl) phthalimide	Lancaster Synthesis, UK
Caesium carbonate	Lancaster Synthesis, UK
Chloroform-D	Cambridge Isotope Laboratories Inc, USA
1, 10 Diaminodecane	Aldrich, UK
4, 4 Diaminodicyclohexylmethane	Aldrich,UK
1, 8 Diamino-3, 6-dioxaoctane	Acros Organics, Belgium
1, 8 Diazabicyclo [5.4.0] undec-7-ene (DBU)	Lancaster Synthesis, UK
Dimethyl Sulfoxide	Aldrich, UK
Dimethyl Sulfoxide-D_6	Cambridge Isotope Laboratories Inc, USA
Hydrazine hydrate	Lancaster Synthesis, UK
Hydrobromic acid/glacial acetic acid	Acros Organics, Belgium
Mesitylenesulphonylchloride (Mts)	Sigma-Aldrich, UK
1, 8-naphthalic anhydride	Aldrich, UK
Potassium phthalimide	Lancaster Synthesis, UK
Silica 60 F_{254} gel	Merck, Germany
Toluenesulphonyl chloride	Lancaster Synthesis, UK

2.2.2. Instrumentation

Thin Layer Chromatography (TLC) was performed on silica gel 60 F_{254} Aluminium plates (2 cm x 5 cm) (Merck, Germany) in a chloroform:methanol (99:1 or 97:3) mobile phase, and spots visualised using UV-light (254 nm).

Nuclear Magnetic Resonance (NMR) spectroscopy was recorded on a Bruker 400 Ultrashield spectrometer operating at 400.1 MHz for proton (^{1}H) and, 100.6 MHz for carbon-13 (^{13}C) and DEPT-135 NMR. Wilmad 5 mm Economy NMR Tubes (N51 glass, WG-1228-8) were purchased from Goss Scientific Ltd, UK. The NMR solvents, Chloroform-D ($CDCl_3$) and Dimethyl Sulfoxide-D_6 (DMSO-d_6) were used for analysis of reaction intermediates and final products as their corresponding dihydrobromide or hydrochloride salts, respectively.

The mass spectral analysis was undertaken at the Engineering and Physical Sciences Research Council's (EPSRC) National Mass Spectrometry Service Centre at

Swansea University, Swansea, UK. ESI spectra were obtained on a ZQ4000 (low resolution) or a MAT95XP instrument (accurate mass).

Dichloromethane was distilled over phosphorus pentoxide (P_2O_5).

2.3. Methods

The strategy adopted to synthesise the bisnapthalimidopropylalkyl diamine analogues, Bisnaphthalimidopropyl diaminooxaoctane (BNIPDaoxoct) and Bisnaphthalimidopropy diaminodicyclohexylmethane (BNIPDaCHM) (Figure 2.1), was based on the synthetic methods previously described (Section 2.1.5) (Scheme A) (Kong Thoo Lin and Pavlov 2000, Dance *et al.* 2005).

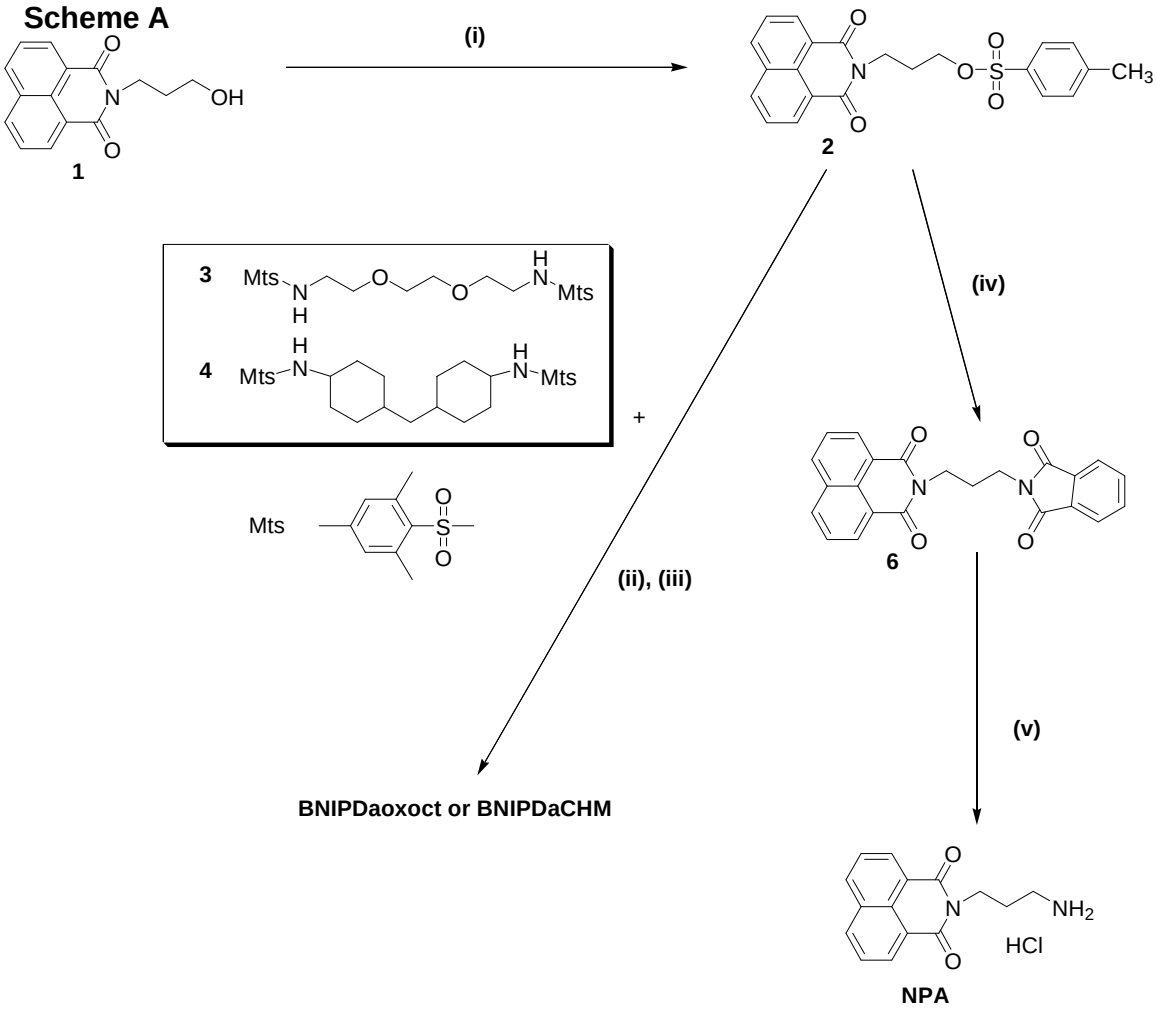

Scheme A.: Strategy for the synthesis of bisnaphthalimidopropylalkyl-diamine derivatives. Reagents and Conditions: (i) ts-Cl, Pyridine, 0-5 °C, 12 hr. (ii) **2**, Mts, Cs_2CO_3, DMF, 50 °C, 96 hr for **3** and **4**. (iii) HBr/glacial CH_3CO_2H, CH_2Cl_2, RT, 24 hr. (iv) ts-Cl, $C_8H_4KNO_2$, DMF, 50 °C, 12 hr. (v) **6**, C_2H_5OH, hydrazine hydrate, 85 °C, 12 hr; Ethanol/conc. HCl

Scheme B.: Strategy for the synthesis of bisphalimidopropyl diaminodecane. Reagents and Conditions: (vi) **7**, *N*-(3-(Bromopropyl)phthalimide, Cs_2CO_3, DMF, 85 °C, 12 hr.

2.3.1. Synthesis of Toluenesulfonyloxypropylnaphthalimide (2)

1, 8-Naphthalic anhydride (6.46 g, 0.03258 mol) was dissolved in dimethylformamide (DMF) (70 mL), followed by the addition of 3-amino-1-propanol (2.45 g, 0.03258 mol) and 1, 8 diazabicyclo [5.4.0] undec-7-ene (DBU) (7.45 mL). The solution was stirred for 4 hours, at 85 °C. The resulting solution was poured into icy water (200 mL) to form a precipitate. The latter was filtered off and washed with water. The product, *N*-(3-hydroxypropyl)naphthalimide, **1** (82.9 %) (Scheme A) was pure enough to be taken to the next step without further purification. ^{1}H NMR ($CDCl_3$): δ 8.6 – 7.7 (aromatic protons), 4.3 (CH_2-O<u>H</u>), 3.6 (N-C<u>H_2</u>), 3.1 (broad, O<u>H</u>), 2.0 (C<u>H_2</u>). ^{13}C NMR ($CDCl_3$): δ 165.0 (<u>C</u>=O), 134.0 – 122.0 (aromatic carbons), 59.0, 37.0, 31.0 (3 x <u>C</u>H_2) (Figure A.1., Appendix 1).

1 (5.10 g, 0.02 mol) was dissolved in anhydrous pyridine (80 mL). The solution was stirred for 15 minutes, at 0 °C. Toluenesulphonyl chloride (Ts-Cl) (5.72 g, 0.03 mol) was added slowly, over 30 minutes and was left overnight, at 4 °C. The solution was poured into icy water (200 mL) to form a precipitate. The latter was filtered off and washed thoroughly with water. Pure toluenesulfonyloxypropylnaphthalimide, **2** (75 %) was obtained by recrystallised from ethanol (Scheme A). ^{1}H NMR ($CDCl_3$): δ 8.6 – 7.7 (aromatic protons), 7.3 (O-Ts aromatic protons), 4.2 (C<u>H_2</u>-O, C<u>H_2</u>-N), 2.3 (C<u>H_3</u>), 2.1 (C<u>H_2</u>) (Figure 2.10). ^{13}C NMR ($CDCl_3$): δ 165.0 (<u>C</u>=O), 138.0 – 125.0 (aromatic carbons), 146.0 - 129.0 (O-Ts aromatic carbons), 70.0, 39.0, 29.0 (3 x <u>C</u>H_2), 23 (<u>C</u>H_3) (Figure A.2., Appendix 1).

2.3.2. General Method for the Synthesis of *N, N*-Dimesitylalkyl diamines (3-5)

The corresponding diamines (0.01145 mol) (1.69 g 1, 8 Diamino-3, 6-dioxaoctane; 2.41 g 4, 4 Diaminodicyclohexylmethane, 1.97 g 1, 10 Diaminodecane) were individually dissolved in anhydrous pyridine (70 mL) followed by the addition of mesitylenesulphonylchloride (Mts) (2.1 M excess) (5.26 g, 0.0240 mol; 5.50 g, 0.0250 mol; 5.26 g, 0.0204 mol respectively). The resulting solution was stirred for 4 hours, at room temperature. Removal of the pyridine followed by the addition of icy water (200 mL), resulted in the formation of a precipitate. The latter was filtered off, washed thoroughly with water and dried under *vacuo*. All the dimesitylalkyldiamines (**3-5**) (61 – 75 %) synthesised showed only one spot on TLC and they were used in the next step without further purification (Scheme A and B).

2.3.2.1. N^1, N^8-Dimesityl-3, 6-dioxaoctane (3) (66 %), ^{1}H NMR ($CDCl_3$): δ 6.9 (aromatic protons), 5.5 (-C<u>H_2</u>-O), 3.4 (-C<u>H_2</u>-O), 3.0 (-C<u>H_2</u>-N), 2.5 (C<u>H_3</u>.Mts), 2.2 (C<u>H_3</u>.Mts).

^{13}C NMR ($CDCl_3$): δ 140 – 127 (aromatic carbons), 70.7 (4 x $\underline{C}H_2$-O), 40.7 (2 x $\underline{C}H_2$-NH), 21.5 ($\underline{C}H_3$.Mts), 13.6 ($\underline{C}H_3$.Mts) (Figure A.3., Appendix 2).

2.3.2.2. N^4, N^4-Dimesityldicyclohexylmethane (4) (61 %), ^{1}H NMR ($CDCl_3$): δ 8.6 (N$\underline{H}$), 7.7 – 6.9 (aromatic protons), 4.7 (-C$\underline{H}$-N), 2.6 (C$\underline{H_3}$.Mts), 2.3 (C$\underline{H_3}$.Mts), 1.8 – 0.8 (-C$\underline{H_2}$- and cyclohexane protons). ^{13}C NMR ($CDCl_3$): δ 140.0 – 127.0 (aromatic carbons), 43.0 (2 x $\underline{C}$H-N.cyclohexane), 39.0 ($\underline{C}H_2$), 30.1 – 27.0 (cyclohexane carbons), 21.5 ($\underline{C}H_3$.Mts), 13.6 ($\underline{C}H_3$.Mts) (Figure 2.12).

2.3.2.3. N^1, N^{10}-Dimesityldecane (5) (75 %), ^{1}H NMR ($CDCl_3$): δ 6.9 (aromatic protons), 4.6 (N$\underline{H}$), 2.9 (-C$\underline{H_2}$-N), 2.7 (-C$\underline{H_2}$-), 2.3 (-C$\underline{H_2}$-), 1.4 (C$\underline{H_3}$.Mts), 1.2 (C$\underline{H_3}$.Mts). ^{13}C NMR ($CDCl_3$): δ 140.0 – 127.0 (aromatic carbons), 40.7 (2 x $\underline{C}H_2$-NH), 30.0 – 26.0 (8 x $\underline{C}H_2$), 21.5 ($\underline{C}H_3$.Mts), 13.6 ($\underline{C}H_3$.Mts) (Figure A.3., Appendix 2).

2.3.3. General N-alkylation Reaction

Dimesitylalkyldiamines (**3-4**) (0.50 g) (0.00098 mol, **3**; 0.00087 mol, **4**) were dissolved in DMF (7 mL) followed by the addition of **2** (2.1 M excess) (0.84 g, 0.00205 mol; 0.75 g, 0.00183 mol, respectively) and caesium carbonate (6 M excess) (1.90 g, 0.00585 mol; 1.69 g, 0.00521 mol, respectively). The solution was left stirring for 96 hours at 50 °C. Reaction completion was monitored by TLC. The solution was poured into icy water (200 mL) to form a precipitate. Hydrochloric Acid (HCl) (20 mL, 2 M) was added to neutralise the solution. The precipitate was collected by filtration and washed thoroughly with water.

2.3.4. General Deprotection Reaction

The fully protected bisnaphthalimidopropylalkyl diamino derivatives were dissolved in anhydrous dichloromethane followed by the addition of hydrobromic acid (33 wt %) solution in glacial acetic acid. Each solution was left stirring for 24 hours at room temperature. The precipitate formed was filtered off and washed with dichloromethane (20 mL), and ether (5 mL) **(BNIPDaCHM)** (75 %) (Scheme A). For **BNIPDaoxoct** (69 %), dichloromethane and hydrobromic acid/glacial acetic acid were removed under *vacuo* and the residue washed with dichloromethane (5 mL). The crude product was recrystallised with absolute ethanol (Scheme A).

2.3.4.1. BNIPDaoxoct, ^{1}H NMR (DMSO-d_6): δ 8.5 (N$\underline{H}$), 8.2 – 7.8 (aromatic protons), 3.5 (O-C$\underline{H_2}$), 3.4 (O-C$\underline{H_2}$), 3.2 (N-C$\underline{H_2}$), 2.7 – 1.7 (-C$\underline{H_2}$-). ^{13}C NMR (DMSO-d_6): δ 161.0 ($\underline{C}$=O), 138.0 – 125.0 (aromatic carbons), 72.0 (O-$\underline{C}H_2$), 70.0 (O-$\underline{C}H_2$), 50.0 – 30.0

(-CH_2-) (Figure A.4., Appendix 3). HRMS (ESI): calculated for $C_{36}H_{40}N_4O_6Br_2$, 702.6134 $[M-2H-Br]^+$, found: 702.2589 $[M-2H-Br]^+$.

2.3.4.2. BNIPDaCHM, ^{1}H NMR (DMSO-d_6): δ 8.5 (NH), 8.0 – 7.5 (aromatic protons), 3.2 (N-CH_2), 2.6 – 1.2 (-CH_2- and cyclohexane protons). ^{13}C NMR (DMSO-d_6): δ 161.0 (C=O), 136.0 – 122.0 (aromatic carbons), 51.0 – 27.0 (-CH_2- and cyclohexane carbons) (Figure 2.14). HRMS (ESI): calculated for $C_{43}H_{50}N_4O_4Br_2$, 685.3753 $[M-H-2Br]^+$, found: 685.3748 $[M-H-2Br]^+$ (Figure A.5., Appendix 4).

2.3.5. Synthesis of Bisphthalimidopropyldiaminodecane (BPHPDadec)

N^1, *N*^{10}-Dimesityldecane, **5** (0.5 g, 0.00093 mol) was dissolved in DMF (7 mL) followed by the addition of *N*-(3-Bromopropyl)phthalimide (2.1 M excess) (0.52 g, 0.01956 mol) and caesium carbonate (6 M excess) (1.81 g, 0.00558 mol) (Scheme B). The solution was left stirring overnight, at 85 °C. Reaction completion was monitored by TLC. The solution was poured into icy water (200 mL) to form a precipitate followed by the addition of HCl (20 mL, 2 M). The precipitate was collected by filtration, washed thoroughly with water and dried under *vacuo*.

The fully protected derivative (0.2 g, 0.00219 mol) was dissolved in anhydrous dichloromethane (5 mL) followed by the addition of hydrobromic acid/glacial acetic acid (0.8 mL). The solution was left stirring for 24 hours at room temperature. The precipitate formed was filtered off and washed with dichloromethane (20 mL), ether (5 mL) and dried under *vacuo* to give **BPHPDadec** (96 %), as its dihydrobromide salt (Scheme B).

2.3.5.1. BPHPDadec, ^{1}H NMR (DMSO-d_6): δ 8.3 (NH), 7.8 (aromatic protons), 3.6 (N-CH_2), 3.2 (NH-CH_2), 2.5 – 1.2 (-CH_2-). ^{13}C NMR (DMSO-d_6): δ 135.0 (C=O), 142.0 – 122.0 (aromatic carbons), 46.0 (NH-CH_2), 39.0 (N-CH_2), 32.0 – 27.0 (-CH_2-) (Figure 2.16). HRMS (ESI): calculated for $C_{32}H_{44}N_4O_4Br_2$, 547.3279 $[M-2HBr+H]^+$, found: 547.3281 $[M-2HBr+H]^+$ (Figure A.6., Appendix 4).

2.3.6. Synthesis of Naphthalimidopropylamine (NPA)

2.3.6.1. Step 1

2 (0.5 g, 0.00122 mol) was dissolved in DMF (7 mL) followed by the addition of Potassium phthalimide (1.95 M excess) (0.44 g, 0.00237 mol). The solution was left stirring for 12 hours, at 50 °C. Reaction completion was monitored by TLC. The solution was poured into icy water (200 mL) to form a precipitate, **6**. The precipitate was collected by filtration, washed thoroughly with water and recrystallised with absolute ethanol. **6**, (65 %) (Scheme A). ^{1}H NMR ($CDCl_3$): δ 8.2 – 7.5 (aromatic protons), 4.3 (CH_2-N), 3.8 (N-

CH_2, naphthalimido), 2.1 (-CH_2). ^{13}C ($CDCl_3$): δ 161.0 (C=O), 140.0 – 123.0 (aromatic carbons), 39.0 (CH_2-N), 38.0 (N-CH_2), 27.0 (-CH_2-).

2.3.6.2. Step 2

6 (0.5g, 0.00130 mol) was dissolved in Ethanol (25 mL) followed by the addition of Hydrazine hydrate (10 M excess) (650 µL, 0.01300 mol). The solution was left stirring for 12 hours, at 85 °C. Reaction completion was monitored by TLC. The ethanol was evaporated off and followed by the addition of dichloromethane (10 mL) giving rise to a precipitate. The latter was filtered off and the filtrate was evaporated to dryness to give thick oil, as naphthalimidopropylamine (NPA) in quantitative yield. The latter was immediately converted to its corresponding hydrochloride salt by dissolving the amine in ethanol (2 mL), followed by the addition of concentrated HCl (3 mL) followed by ether (10 mL). The white precipitate formed was filtered off, recrystallised (95% ethanol) and dried under *vacuo* to give **NPA** (26%) as the hydrochloride salt (Scheme A).

2.3.6.2.a. NPA, ^{1}H NMR (DMSO-d_6): δ 8.5 – 7.9 (aromatic protons), 4.1 (N-CH_2), 3.3 (-NH_2), 2.8 (CH_2-NH_2), 2.0 (-CH_2-). ^{13}C NMR (DMSO-d_6): δ 164.0 (C=O), 134.0 – 122 .0 (aromatic carbons), 38.0 (CH_2-NH_2), 37.0 (N-CH_2), 26.0 (-CH_2-) (Figure 2.18). HRMS (ESI): calculated for $C_{15}H_{14}N_2O_2$ 255.1131 $[M+H]^+$, found: 255.1128 $[M+H]^+$.

2.4. Results and Discussion

The synthesis of a selection of new BNIPP derivatives, two bisnaphthalimidopropylalkyl diamines (BNIPDaoxoct and BNIPDaCHM), bisphthalimidopropyl diaminodecane (BPHPDadec) and mononaphthalimidopropylamine (NPA), has been described above (Section 2.3 and, Schemes A and B). The rationale for synthesising these analogues was to (i) demonstrate that bisnaphthalimido moiety is essential for biological activity, for example, in BPHPDadec, the naphthalimido rings were replaced with phthalimide rings, and in the case of NPA only one naphthalimido ring is present, and (ii) study the effect upon biological activity when the alkyl linker chains are modified with the introduction of oxygen atoms or cyclohexane rings, for example, BNIPDaoxoct and BNIPDaCHM. Earlier work has demonstrated that the length of the alkyl linker chain was extremely important for enhanced solubility, and effective biological activity against colon cancer (CaCO-2) cells (Oliveira *et al*. 2007).

2.4.1. Synthesis of Bisnaphthalimidopropyl diamine Derivatives (BNIPDaoxoct and BNIPDaCHM)

The synthetic strategy adopted to synthesise the bisnapthalimidopropyl diamino analogues, BNIPDaoxoct and BNIPDaCHM, was based on methods previously developed and is outlined in Scheme A (Kong Thoo Lin and Pavlov 2000, Dance *et al*. 2005, Oliveira *et al*. 2007). The common starting material was toluenesulfonyloxypropylnaphthalimide, **2**, which was prepared from *N*-(3-hydroxypropyl) naphthalimide, **1**. Protection and activation of the diamines was carried out with mesitylenesulfonyl chloride (Mts) in pyridine at room temperature to give compounds **3** to **4** in high yield (66 and 61 % respectively). For the synthesis of the fully protected BNIPP derivatives, *N*-alkylation with toluenesulfonyloxypropylnaphthalimide, **2**, in the presence of caesium carbonate in anhydrous DMF yielded fully protected BNIPP derivatives. Deprotection with hydrobromic acid/glacial acetic acid in CH_2Cl_2 gave BNIPDaoxoct and BNIPDaCHM, as their corresponding dihydrobromide salts in high yields of 69 and 75 %, respectively (Scheme A, Reactions **i-iii**).

2.4.1.1. Synthesis of Toluenesulfonyloxypropylnaphthalimide. 2.

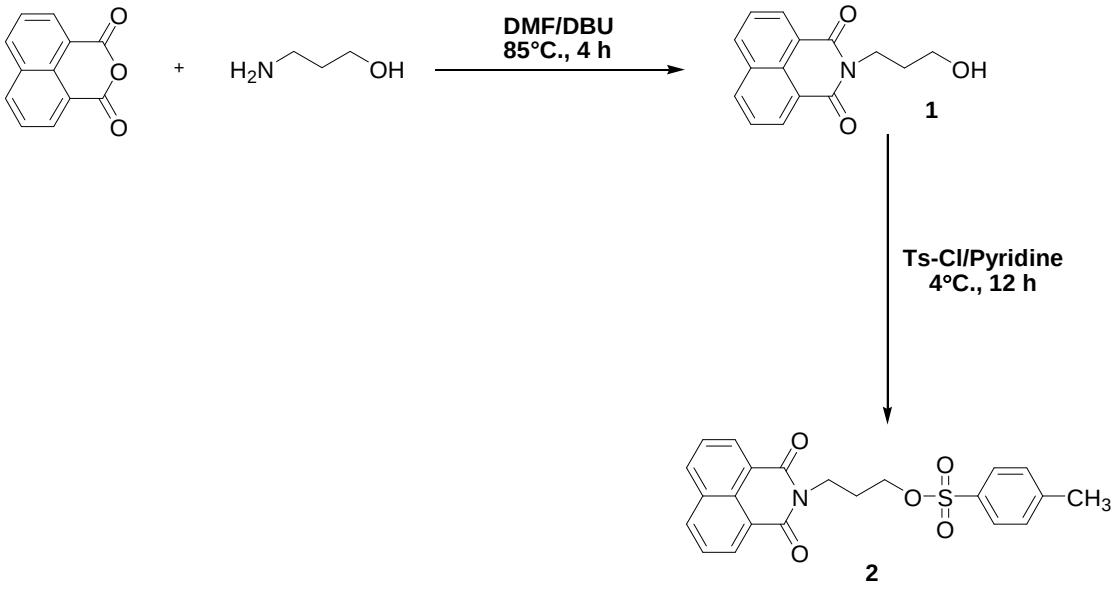

Figure 2.9.: Synthesis of *N*-(3-hydropropyl) naphthalimide, **1**, and toluenesulfonyloxypropylnaphthalimide, **2** (Scheme A, Reaction **i**).

Initially *N*-(3-hydroxypropyl) naphthalimide, **1** (82.9 %), was obtained from the reaction between 1, 8-Naphthalic anhydride in DMF with 3-amino-1-propanol and DBU. Toluenesulfonyloxypropylnaphthalimide, **2** (75 %), was obtained from the reaction with **1** in pyridine with Toluenesulphonyl chloride (Scheme A, Reaction **i**) (Figure 2.9). The products, **1** and **2** were characterised by TLC and NMR analyses (Figures A.1 and A.2., Appendix 1). By using NMR spectroscopy, the important structural features of **2** were confirmed by their chemical shift, expressed in parts per million (ppm). In ^{1}H spectra the chemical shifts for alkyl groups are generally present between 0.8 – 5.0 ppm. Therefore, Figure 2.10 shows the methylene (-CH_2-) and methyl (-CH_3) group (from the tosyl group) at 2.1 and 2.3 ppm, respectively. The methylene groups, C-CH_2- and CH_2-O were found at 4.2 ppm, with the aromatic protons from the naphthalene and benzene groups were observed between 7.7 – 8.6 ppm. The ^{1}H spectrum for **2** is shown in Figure 2.10.

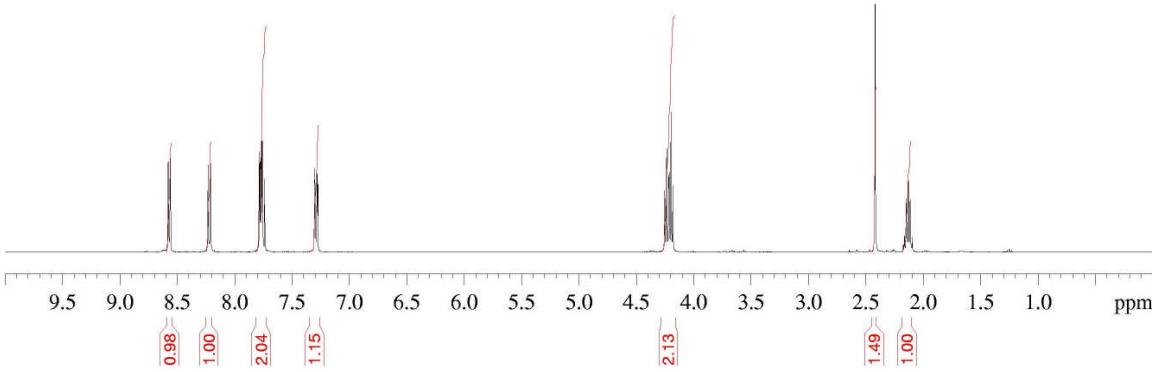

Figure 2.10.: ^{1}H NMR spectra of toluenesulfonyloxypropylnaphthalimide, **2**.

2.4.1.2. General Method for the Synthesis of N, N- Dimesitylalkyl diamines. 3-5.

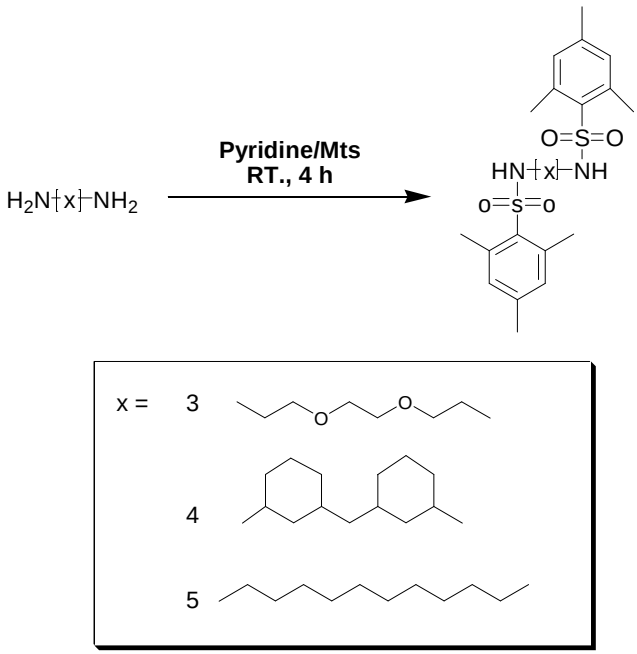

Figure 2.11.: Synthesis of dimesitylalkyldiamines; N^1, N^8 – dimesityl-3,6-dioxaoctane (**3**), N^4, N^4 – dimesityldicyclohexylmethane (**4**), N^1, N^{10}-dimesityldecane (**5**).

Dimesitylalkyldiamines were obtained from the corresponding diamines in pyridine with Mesitylenesulphonylchloride. N^1, N^8 – Dimesityl-3,6-dioxaoctane **3**, N^4, N^4 – Dimesityldicyclohexylmethane **4** and N^1, N^{10}-Dimesityldecane **5**, in yields of 66, 61 and 75 %, respectively (Figure 2.11). **3**, **4** and **5** were characterised by TLC and NMR analyses (Figure A.3., Appendix 2). Figure 2.12 shows the methylene (-CH_2-) groups from the cyclohexane rings between 0.8 – 1.8 ppm. Methyl (-CH_3 groups from Mts) were found between 2.3 – 4.7 ppm and the aromatic protons from the benzene group of Mts were observed between 6.9 - 7.7 ppm. The amino (-NH-) group was present at 8.6 ppm. Since the two cyclohexane rings in **4** and BNIPDaCHM can adopt three interchangeable conformational arrangements, (i) boat, (ii) twisted boat and (iii) chair. As a result, complex multiplets resonance signals between 0.8 – 3.4 ppm and 20 – 56 ppm, in the ^{1}H and ^{13}C NMR spectra of **4** and BNIPDaCHM, respectively (Figures 2.12). The ^{1}H spectrum of **4** is shown in Figure 2.12.

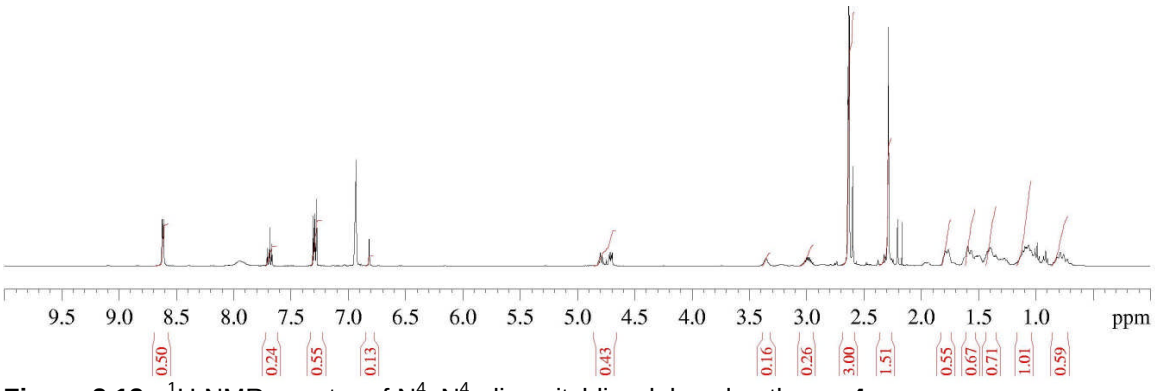

Figure 2.12.: ^{1}H NMR spectra of N^4, N^4–dimesityldicyclohexylmethane, **4**.

2.4.1.3. General N-alkylation Reaction

Fully protected BNIPP derivatives were obtained by *N*-alkylation of the dimesitylalkyldiamines, **3-4** which were reacted with **2** in a 2:1 ratio in DMF, in the presence of caesium carbonate (Scheme A, Reaction **ii**). Completion of the reaction was monitored by TLC. After drying, the fully protected BNIPP derivative products were produced in high yields (83 – 96 %).

2.4.1.4. General Deprotection Reaction

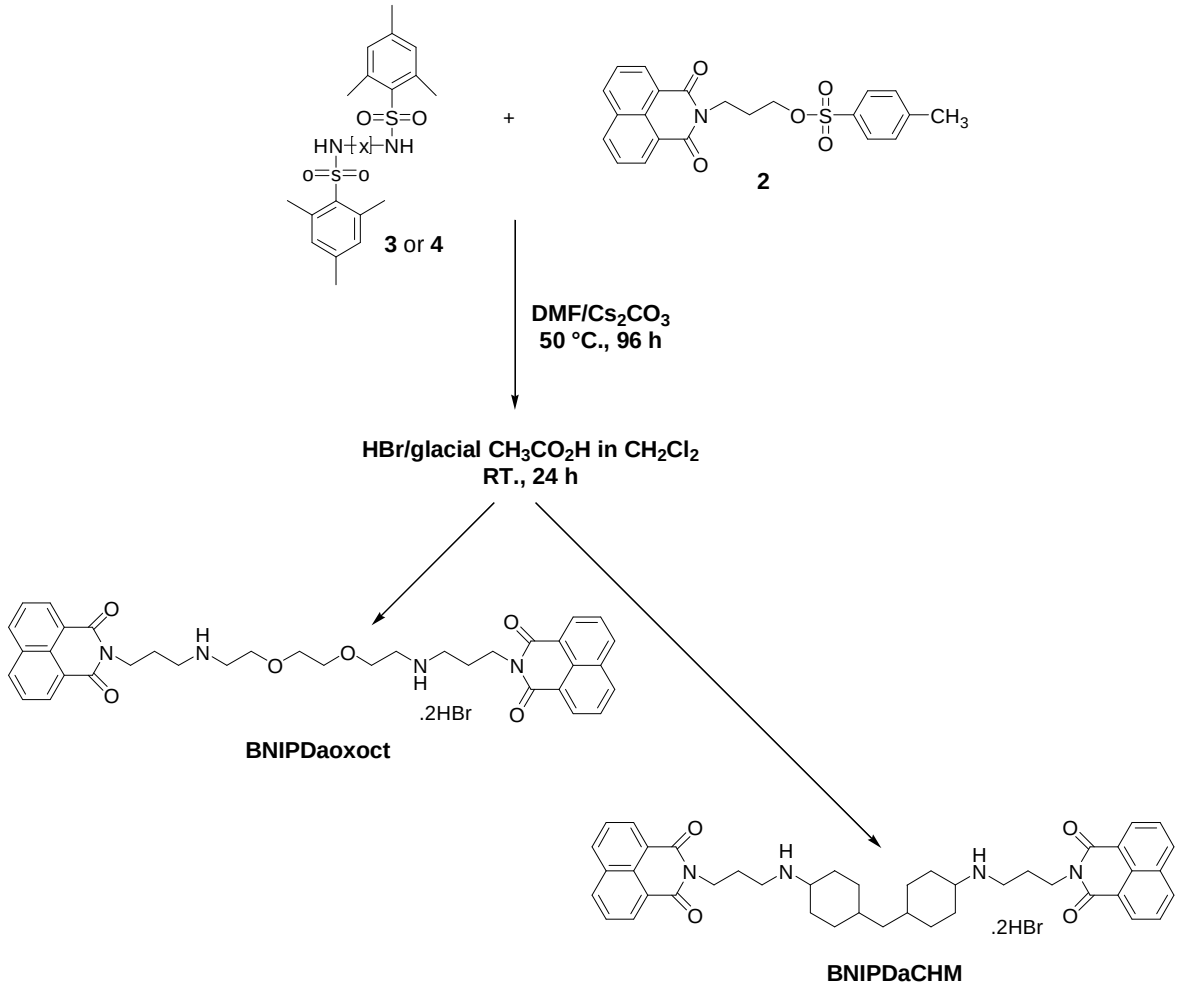

Figure 2.13.: Synthesis of protected and deprotected bisnaphthalimidopropyl diaminooxaoctane (BNIPDaoxoct) and bisnaphthalimidopropyl diaminodicyclohexylmethane (BNIPDaCHM) Derivatives (Scheme A, Reaction **ii** and **iii**).

The deprotected BNIPP analogues; BNIPDaoxoct and BNIPDaCHM were obtained from the reaction between fully protected BNIPP derivatives in anhydrous CH_2Cl_2 with hydrobromic acid/glacial acetic acid (Figure 2.13) (Scheme A, **iii**). BNIPDaoxoct and BNIPDaCHM, as their corresponding dihydrobromide salts were obtained in high yields of 69 and 75 %, respectively. BNIPDaoxoct and BNIPDaCHM were characterised by NMR and MS analyses (Figure A.5., Appendix 4). Generally, for BNIPDaoxoct and BNIPDaCHM, the ^{1}H NMR showed methylene (-CH_2-) groups between 1.2 – 3.5 ppm and

aromatic protons from the naphthalene group between 7.5 -8.2 ppm. The amino (-NH) groups were present at 8.5 ppm. The ^{13}C NMR for BNIPDaoxoct and BNIPDaCHM showed aliphatic hydrocarbons (-CH_2-) between 27 – 72 ppm with aromatic carbons from the naphthalene group between 122 – 138 ppm. The amide (N-C=O) groups were observed at 161 ppm. The DEPT-135 spectra (Figure 2.14 and Figure A.4., Appendix 3) showed that the -CH_2- groups present in the propyl and cyclohexane groups were inverted, between 27 – 70 ppm, and the quaternary carbons, e.g., from the amide had disappeared. An example of the ^{13}C and DEPT-135 NMR spectra of BNIPDaCHM are shown in Figure 2.14.

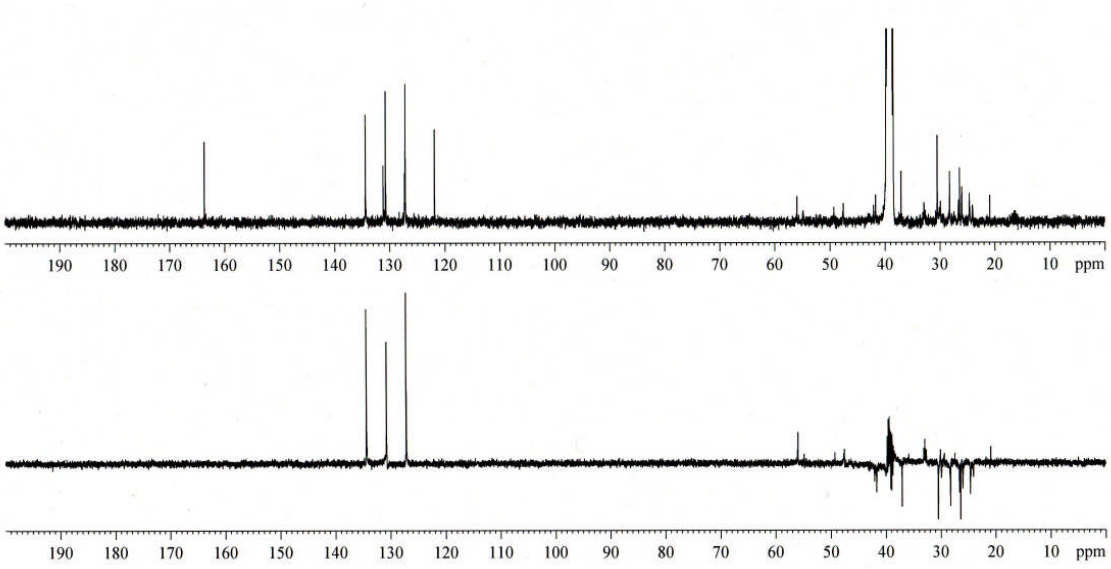

Figure 2.14.: ^{13}C and DEPT-135 NMR spectra of BNIPDaCHM

2.4.2. Synthesis of Bisphthalimidopropyldiaminodecane (BPHPDadec)

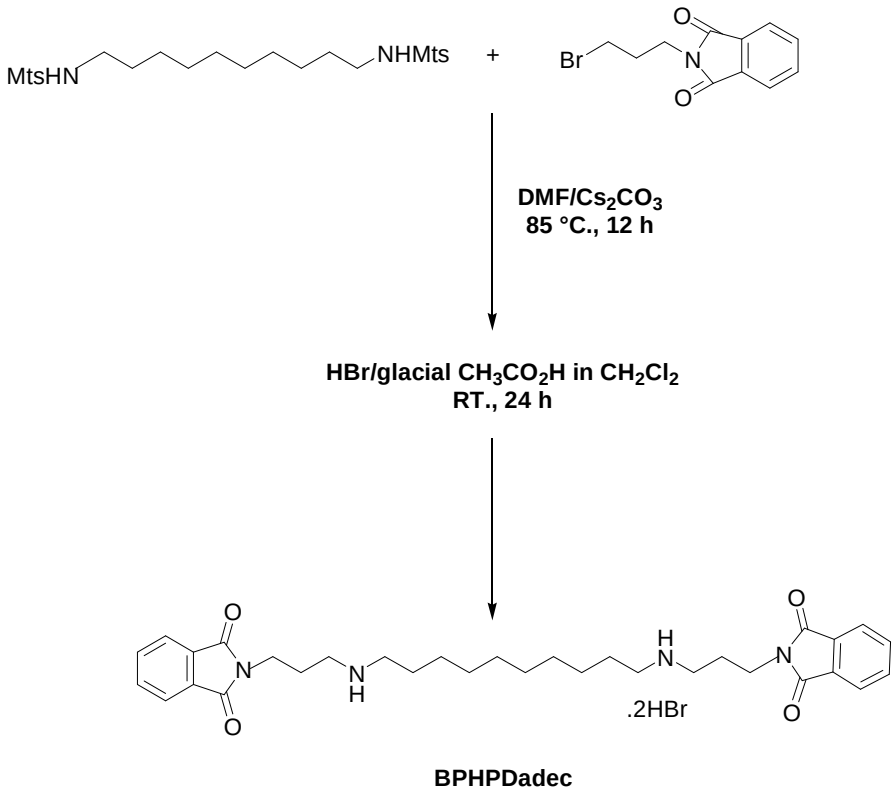

Figure 2.15.: Synthesis of bisphthalimidopropyl diaminodecane (BPHPDadec) (Scheme B, **vi** and **iii**)

BPHPDadec was synthesised by treating dimesitylenediaminodecane, **5**, with *N*-(3-Bromopropyl) phthalimide in DMF in the presence of caesium carbonate (Figure A.3., Appendix 2). Subsequent deprotection with hydrobromic acid/glacial yielded BPHPDadec as its dihydrobromide salt, at 96 % (Scheme B, Reaction **vi** and **iii**) (Figure 2.15). BPHPDadec was characterised by TLC, NMR and MS analyses (Figure A.6., Appendix 4). For BPHPDadec (Figure 2.16), the ^{1}H NMR showed methylene (-CH_2-) groups between 1.2 – 3.6 ppm, in particular, the CH_2-N was observed at 3.6 ppm. The aromatic protons from the naphthalene group and the amine (NH) groups were present at 7.8 ppm and 8.3 ppm, respectively. The ^{13}C NMR for BPHPDadec showed aliphatic hydrocarbons (-CH_2-) between 27 – 46, with aromatic carbons between 122 – 135 ppm and the amide (N-C=O) group at 168 ppm. The DEPT-135 spectra verified the -CH_2- groups, which were inverted, between 27 – 46 ppm, and the quaternary carbons, which had disappeared. The ^{1}H, ^{13}C and DEPT-135 spectra of BPHPDadec are shown in Figure 2.16.

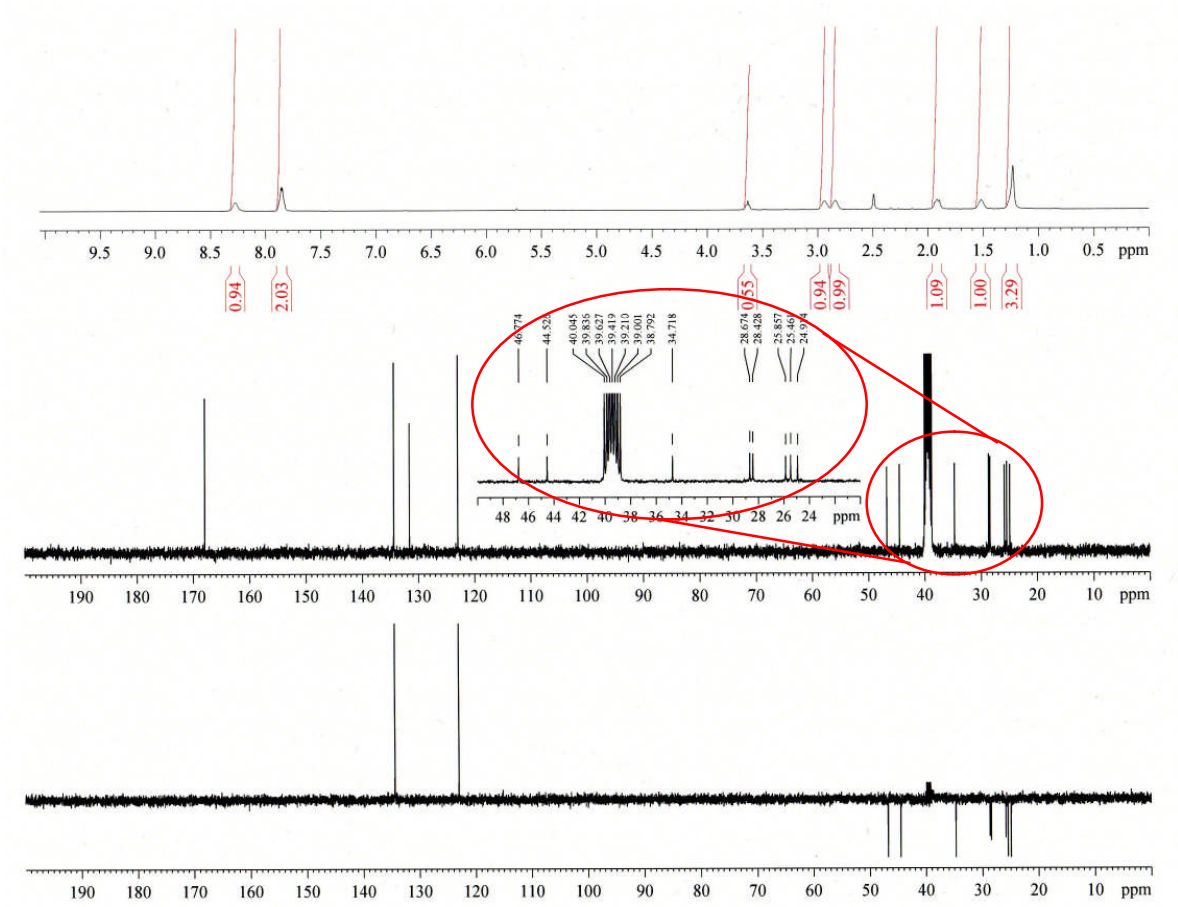

Figure 2.16.: ^{1}H, ^{13}C and DEPT-135 NMR spectra of BPHPDadec

2.4.3. Synthesis of Naphthalimidopropylamine (NPA)

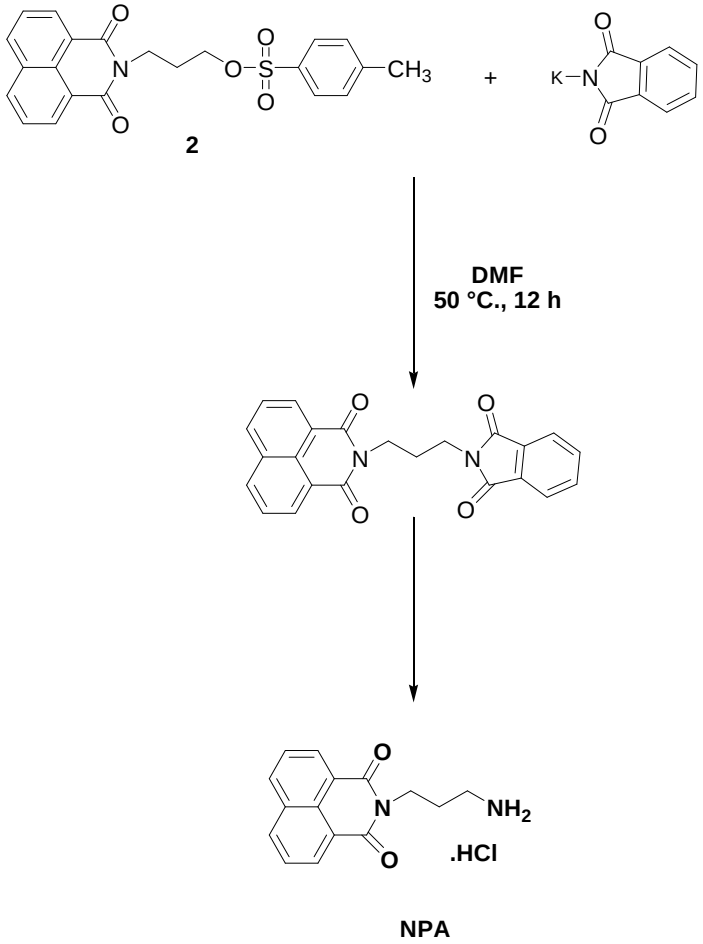

Figure 2.17.: Synthesis of naphthalimidopropylamine (NPA)

To synthesise naphthalimidopropylamine (NPA), nucleophilic substitution of the toluenesulfonyl (tosyl) group from **2** was achieved with potassium phthalimide. Treatment with hydrazine hydrate gave the corresponding amine, **6** (65 %), which was converted to its hydrochloric salt, NPA (26 %) (Scheme A, Reactions **iv** and **v**) (Figure 2.17). **6** was characterised by TLC and NMR. The final product, NPA was characterised by TLC, NMR and MS analyses. For NPA (Figure 2.18), the ^{1}H NMR showed methylene (-CH_2-) groups between 2.0 – 4.1 ppm, in particular, the CH_2-N was observed at 4.1 ppm. The aromatic protons from the naphthalene group were observed between 7.9 – 8.5 ppm, with the amine (-NH_2-) group present at 3.3 ppm. The ^{13}C NMR, for NPA showed aliphatic hydrocarbons (-CH_2-) between 26 - 38 and aromatic carbons from the naphthalene group, between 125 - 165 ppm. The amide group (N-C=O) group was observed at 164 ppm. The DEPT-135 spectra confirmed the -CH_2- groups, which were again inverted (26 – 38 ppm). The quaternary carbons had also disappeared. The ^{1}H, ^{13}C and DEPT-135 spectra of NPA are shown in Figure 2.18.

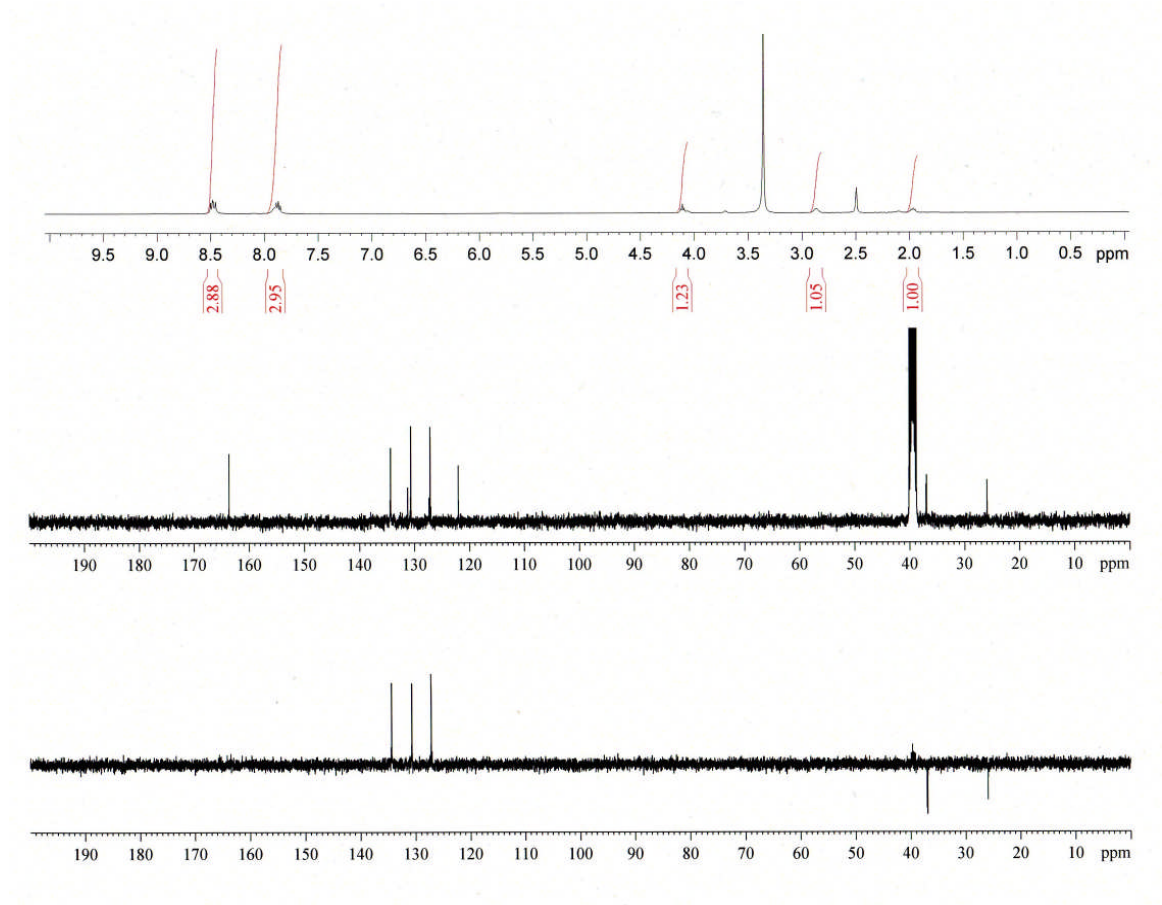

Figure 2.18.: ^{1}H, ^{13}C and DEPT-135 NMR spectra of NPA

BNIPDaoxaoct, BNIPDaCHM, BPHPDadec and NPA were all synthesised by modification of the *N*-alkylation reaction previously used to synthesise the parent BNIPP derivatives (Kong Thoo Lin and Pavlov 2000, Oliveira *et al.* 2007). All of the new BNIPP derivatives exhibited good solubility, at a 10 mM concentration (50 % DMSO/water) and were stored as stock solutions at 0-5 °C. The *N*-alkylation reaction has been further developed by other groups, for example, Filosa and colleagues (2009), who have recently reported the synthesis and biological activity of a series of bisnaphthalimides containing heterocyclic and other cyclic moieties. These alterations include insertion of piperazine, cis-dimethylpiperazine, diazabicyclo [3.2.1] octane and cyclopropane groups into the aminoalkyl linker chain. Filosa *et al*. (2009) adapted and modified the three step reaction described, to suit their specific requirements. It is important to note, that during the tosylation reaction, the best condition in which to synthesise these novel BNIPP derivatives, at a maximum yield, was to use four times excess Ts-Cl (Filosa *et al*. 2009). This was in contrast to the two times excess Ts-Cl used in the successful synthesis of BNIPP derivatives (Kong Thoo Lin and Pavlov 2000, Dance *et al.* 2005, Oliveira *et al.* 2007).

Therefore, the syntheses of many future potential bisnaphthalimido and bisphthalimido derivatives can be achieved by amendment of the highly convenient three step procedure shown in Scheme A and B.

2.5. Conclusions

Two protected bisnaphthalimidopropyl diamino analogues (BNIPDaoxoct and BNIPDaCHM) together with bisphthalimidopropyl diaminodecane (BPHPDadec) and mononaphthalimidopropylamine (NPA) were successfully synthesised and all BNIPP derivatives exhibited good solubility properties in 50 % DMSO.

The synthetic route chosen to produce the protected BNIPP and BPHP derivatives was an *N*-alkylation reaction. This reaction has been used in the successful synthesis of previous BNIPP derivatives, and was found to be simple and reproducible, and did not produce by-products. Complete deprotection gave the BNIPP and BPHP derivatives, as their dihydrobromide salts (69, 75 and 96 % yield, respectively). Via a similar synthetic process NPA was produced. Essentially NPA, a mononaphthalimide derivative, was synthesised by a simple two step reaction, producing NPA as a hydrochloric salt (26 % yield). The successful synthetic strategies adopted for BNIPDaoxoct, BNIPDaCHM, BPHPDadec and NPA has led to the subsequent evaluation of (i) their DNA binding affinities (Chapter 3), (ii) biological properties in human breast cancer MDA-MB-231 and human epithelial MCF-10A cells (Chapters 4 – 6), and (iii) their potential to inhibit histone deacetylase (HDAC) activity (Chapter 7).

Chapter 3

DNA Binding Properties of BNIPP Derivatives

3.1. DNA Binding Properties of BNIPP Derivatives

For over forty years, nucleic acids have been extensively studied as potential targets in anticancer drug design. The interaction of an anticancer drug with Deoxyribonucleic Acid (DNA) initially results in changes to the conformation of the DNA double helix, which subsequently leads to an interruption of the processes involved in DNA replication, transcription and repair, leading ultimately to cell death (Brana *et al.* 2001, Seaton *et al*. 2003, Martinez and Chacon-Garcia 2005, Huang *et al.* 2009). Anticancer drugs can interact with DNA by binding to and/or modifying the DNA structure via several mechanisms of action. These mechanisms include (i) DNA intercalation between the base pairs, (ii) DNA groove binding via non-covalent interactions with the major or minor grooves of the DNA, or (iii) DNA alkylation with interstrand or intrastrand cross linking.

The aim of the experimental work presented in this chapter was to investigate the DNA binding properties of the BNIPP derivatives.

3.1.1. DNA Intercalation

DNA intercalating anticancer drugs usually contain planar or heteroaromatic chromophores with an attached side chain, and reversibly bind to DNA by insertion and stacking between the base pairs of the DNA double helix (Martinez and Chacon-Garcia 2005, Kamal *et al*. 2007, Strekowski and Wilson 2007). DNA intercalators are held in place between the base pairs by Van der Waal's interactions, thus creating a stable complex (Anderson *et al.* 2009). As a result, the DNA becomes partially unwound and lengthens, which leads to the inhibition of DNA replication and transcription (Palchaudhari and Hergenrother 2007, Anderson *et al.* 2009). Classic examples of DNA intercalating compounds include acridines (e.g., proflavine) and anthracyclines (e.g., daunorubicin and doxorubicin) (Demeunynck 2004, Martínez and Chacón-García 2005, Ferguson and Denny 2007, Ashley and Poulton 2009) (Figure 3.1). Proflavin is currently used as a topical antiseptic (Chakraborty and Casu 2009), whilst daunorubicin and doxorubicin, although relatively non-selective, are currently in clinical use as anticancer agents in the treatment of acute leukaemias, breast, ovarian and bladder cancers (Cancer Research UK, 2009a, Cancer Research UK, 2009b)

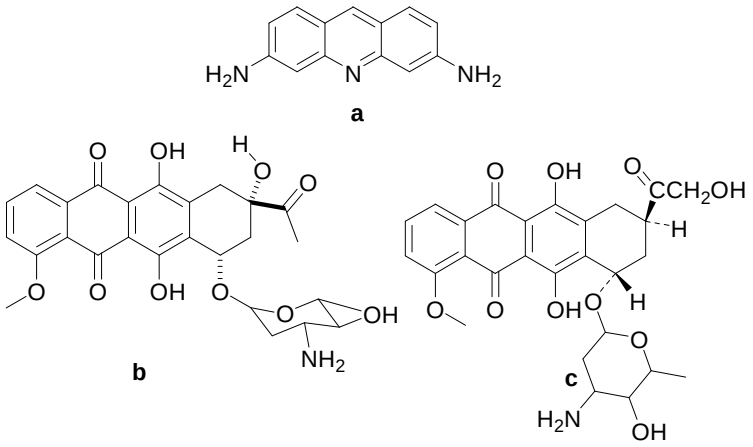

Figure 3.1.: Structures of the DNA intercalating compounds: **a:** Proflavin, **b:** Daunorubicin and **c:** Doxorubicin

In addition to the classic examples of DNA intercalating compounds (Figure 3.1), several structurally uncommon DNA intercalating compounds have been reported in recent years (Palchaudhur and Hergenrother 2007). These compounds do not contain the characteristic features (i.e. fixed planar or heteroaromatic chromophores) usually present in the classic DNA intercalating compounds, but instead have two or three unfused rings (Snyder 2007). Examples include chlorpheniramine, an antihistamine, and prodigiosin, a prospective anticancer agent (Montaner *et al.* 2005, Palchaudhur and Hergenrother 2007, Snyder 2007) (Figure 3.2).

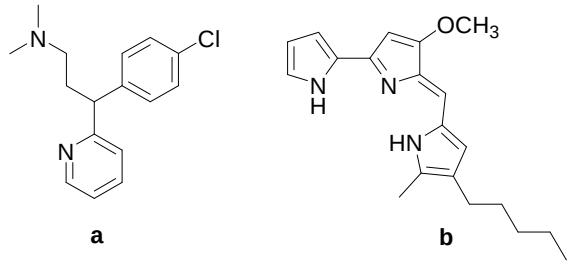

Figure 3.2.: Structures of the structurally uncommon DNA intercalating compounds: **a:** Chlorpheniramine and **b:** Prodigiosin

Several DNA intercalating anticancer compounds have also been shown to prevent the action of the enzyme Topoisomerase (TOPO). There are two key TOPO enzymes, I and II, which are responsible for single-stranded (ss) and double stranded (ds) breaks in DNA, respectively (Palchaudhuri and Hergenrother 2007). The TOPO I enzyme is monomeric, with responsibility of ss DNA cleavage (Forterre *et al.* 2007), whilst the essential ubiquitous TOPO II enzyme found within eukaryotic organisms, catalyses DNA unwinding, and controls the processes required to untangle and unknot ds DNA. Moreover, TOPO II has a fundamental role in DNA replication and transcription, and also aids chromosomal organisation prior to mitosis (Burden and Osheroff 1998, Demeunynck 2004, Denny 2004, Palchaudhuri and Hergenrother 2007, Patrick 2009).

The inhibition of TOPO II enzyme activity can be divided into two classes. The members of the first class are termed TOPO II inhibitors (catalytic inhibitors), whereas the members of the second class are TOPO II poisons. TOPO II inhibitors work by binding the enzyme onto DNA and blocking the overall catalytic activity of the TOPO II enzyme, resulting in cell death (Larsen *et al.* 2003, Montaner *et al.* 2005, Nitiss 2009). TOPO II poisons are aptly named because they do not kill cancer cells by inhibiting the function of the TOPO II enzyme itself, but rather poison DNA by stabilising the levels of TOPO II-DNA complexes irreversibly. Complex stabilisation disables the TOPO II enzyme, thus leading to the formation of 'double strand breaks' (Burden and Osheroff 1998, Demeunynck 2004, Montaner *et* al. 2005, Montecucco and Biamonti 2007, Palchaudhuri and Hergenrother 2007, Nitiss 2009). These ds DNA breaks consequently induce cellular DNA damage, which can again lead to cell death (Nitiss 2009).

Examples of relevant DNA intercalating and DNA non-intercalating compounds that exert their cytotoxic activity as TOPO II poisons are anthracyclines (e.g., daunorubicin and doxorubicin), anthraquinones (e.g., mitoxantrone), and etoposide, respectively (Burden and Osheroff 1998, Kamal *et al*. 2007, Montecucco and Biamonti 2007) (Figures 3.1 and 3.3). These compounds are currently in clinical use as anticancer agents in the treatment of small-cell lung, bladder, stomach and breast cancers (Hande 1998, Minotti *et al.* 2004).

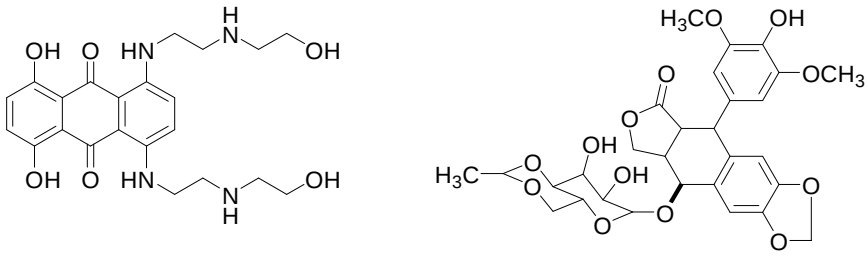

Figure 3.3.: Structures of the DNA intercalating and non-intercalating compounds with TOPO II action: **a:** Mitoxantrone and **b:** Etoposide

The well known cytotoxic DNA intercalating compounds relevant to this project are the naphthalimides (e.g. amonafide) and bisnaphthalimides (e.g. elinafide) as previously stated in Section 1.6 (Figures 1.16 and 1.21) (Brana *et al*. 2001, Brana and Ramos 2001, Martinez and Chacon-Garcia 2005, Yang *et al*. 2005, Filosa *et al.* 2009, González-Bulnes and Gallego 2009). These compounds are structurally similar to the BNIPP derivatives, with the presence of one or two naphthalimido rings respectively, and a flexible aminoalkyl linker chain which contains at least one amine group: an important structural assembly, which has proved to be essential for the attainment of strong DNA binding affinity and cytotoxic activity (Brana *et al*. 1993, 2001). The possible mechanism of action of naphthalimide and bisnaphthalimide derivatives has been shown to be achieved by

intercalation or bis-intercalation of the chromophore unit between the base pairs of the DNA double helix, respectively (Hsiang *et al*. 1989, Brana *et al*. 1993, 2001, Chau *et al.* 2008). Previously investigated BNIPP derivatives also demonstrate DNA binding through bis-intercalation (Pavlov *et al.* 2001, Dance *et al*. 2005). An assessment into the mechanism of action of the newly synthesised (Figure 2.1), and existing BNIPP derivatives (Figure 3.4) will be discussed later in this chapter.

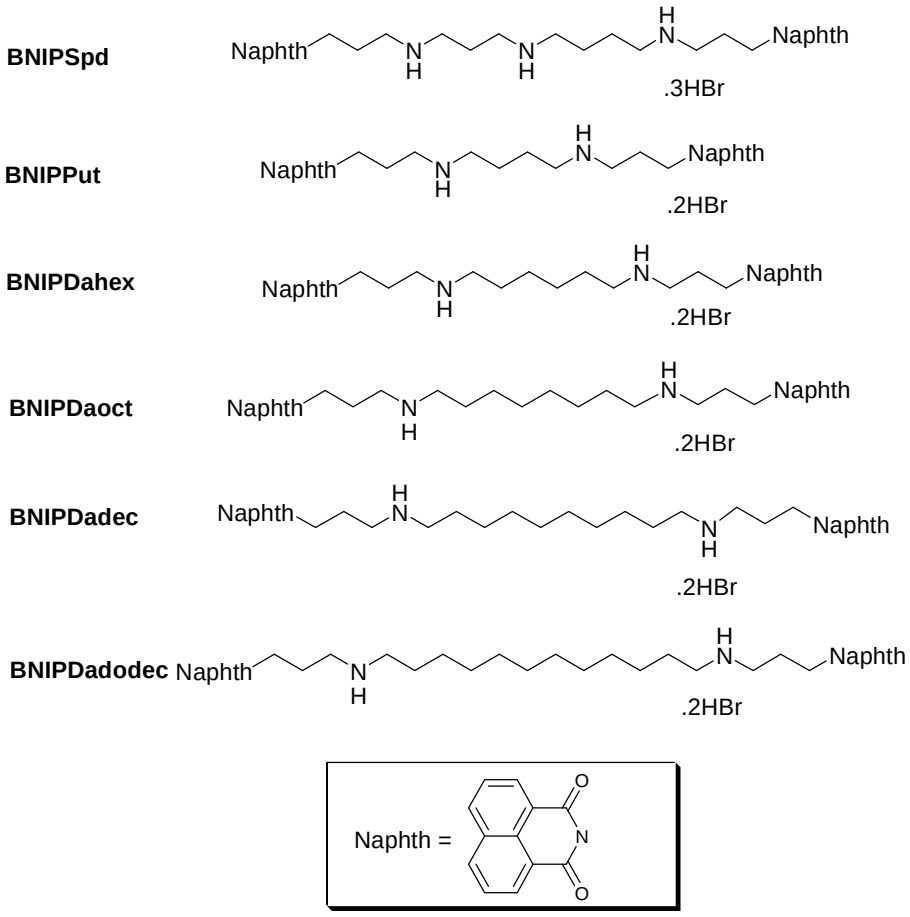

Figure 3.4.: Structures of bisnaphthalimidopropyl polyamine derivatives (BNIPPs): Bisnaphthalimidopropyl Spermidine (BNIPSpd), Bisnaphthalimidopropyl Putrescine (BNIPPut), Bisnaphthalimidopropyl Diaminohexane (BNIPDahex), Bisnaphthalimidopropyl Diaminooctane (BNIPDaoct), Bisnaphthalimidopropyl Diaminodecane (BNIPDadec) and Bisnaphthalimidopropyl Diaminododecane (BNIPDadodec).

3.1.2. DNA Groove Binding

Groove binding compounds are generally crescent-shaped (i.e. rounded or curved) molecules which can interact with either the DNA major or, more often, the DNA minor grooves. DNA groove binders are stabilised by non-covalent (electrostatic) interactions (Lauria *et al.* 2007, Palchaudhuri and Hergenrother 2007). At present, the mechanism of action for the majority of groove binding drugs is relatively unknown. Evidence suggests that these compounds do not dramatically change the structure of DNA, in contrast to DNA intercalating compounds, but rather act in a sequence specific manner by widening the grooves of the DNA, thus directly blocking and/or inhibiting protein-DNA recognition

(Chen *et al*. 1993, Suh and Chaires 1995, Lauria *et al*. 2007, Strekowski and Wilson 2007, Cai *et al.* 2009). The most commonly studied groove binders include mitomycin C, distamycin A and the bisbenzimidazole, Hoechst 33258 (Seaton *et al.* 2003, Strekowski and Wilson 2007, Cai *et al.* 2009) (Figure 3.5). Notably, the anthracyclines (daunorubicin and doxorubicin, Figure 3.1) bind to DNA by both intercalation and groove binding as they possess an aromatic (intercalative) feature and a side (groove binding) chain (Palchaudhuri and Hergenrother 2007).

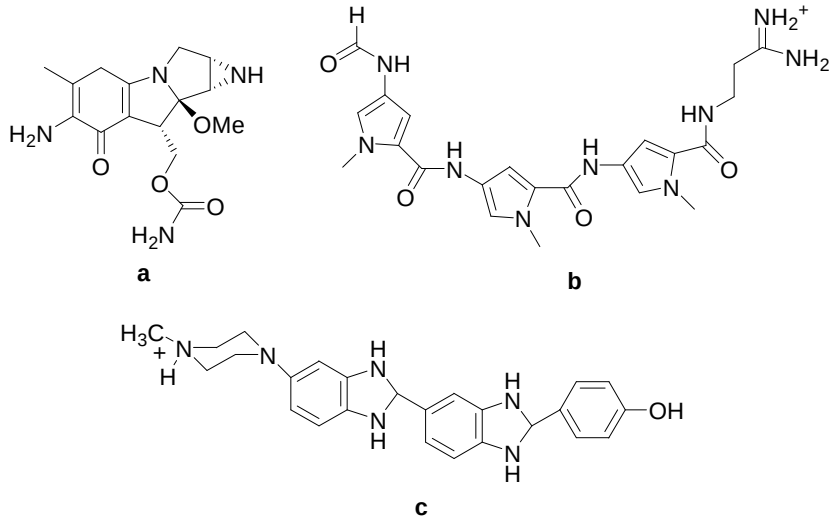

Figure 3.5.: Structures of the DNA groove binding compounds: **a:** Mitomycin C, **b:** Distamycin A and **c:** Bisbenzimide Hoechst 33258

The natural polyamines spermine and spermidine and, to a lesser extent, their precursor putrescine (Figure 1.7) are known to interact and stabilise DNA and RNA duplexes via electrostatic interactions with DNA (Pavlov *et al.* 2001, Peña *et al.* 2007, Winkler *et al.* 2009). Polyamines have also been shown to stabilise double stranded over single stranded structures (Feuerstein *et al.* 1990). Polyamine structures are well adapted to fit into the DNA grooves where they bind strongly with both the major and to a lesser extent the minor grooves (Le Pecq *et al.* 1975, Hou *et al.* 2001, Strekowski and Wilson 2007).

3.1.3. DNA Alkylation

DNA alkylating compounds are electrophilic compounds which react with electron-rich regions on DNA, and are classified as either mono-, bi- or tri-functional. This functionality is reliant upon whether a compound has one, two or three electron-deficient reactive groups (Sanderson and Shield 1996, Patrick 2009). Alkylating agents disrupt DNA by the attachment of alkyl groups to nucleotide bases in particular, the *N*-7 of guanine. This region is particularly susceptible for alkylation, as it is the most nucleophilic site in the DNA (Sanderson and Shield 1996). Alkylating agents can form cross linkages between DNA and proteins **[1]**, or DNA strands, either interstrand **[2]** or intrastrand **[3]**

(Figure 3.6), and are capable of inducing permanent nucleotide mutations (Sanderson and Shield 1996, McHugh *et al.* 2001, Anderson *et al.* 2009, Patrick 2009). Alkylating agents have poor molecular specificity because they can act upon both DNA and proteins. As a result, they can disrupt DNA replication and transcription, and/or alter protein structure and function (Sanderson and Shields 1996, Patrick 2009). Compounds that produce interstrand and intrastrand cross links have been shown to be important effective chemotherapeutic compounds, which are commonly used in the treatment of leukaemias, lymphomas, and solid tumours (i.e. breast, lung and bladder cancers) (McHugh *et al.* 2001, Anderson *et al.* 2009, Cancer Research UK 2009c and 2009d, Patrick 2009). These compounds can be used as both single agents, or as part of a combined chemotherapy regimen (McHugh *et al.* 2001). The mechanism of action of several alkylating agents with regards to interstrand or intrastrand cross links will be discussed further in Sections 3.1.3.1 and 3.1.3.2.

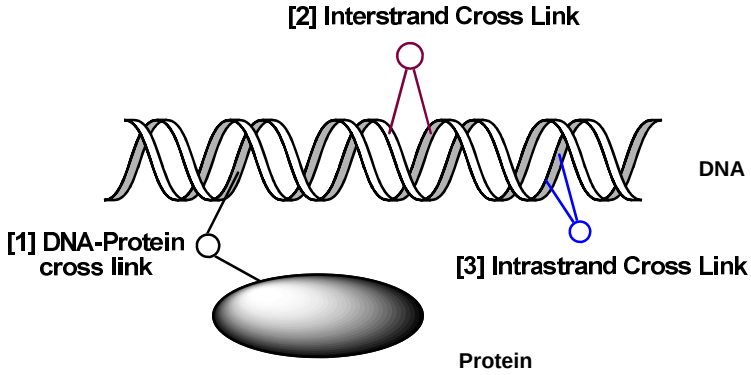

Figure 3.6.: The possible modes of DNA interaction achieved by cross linking compounds (adapted from McHugh *et al.* 2001). **[1]** DNA-Protein cross link, **[2]** Interstrand cross link and **[3]** Intrastrand cross link.

3.1.3.1. Alkylating Agents with Interstrand Cross Linkage

Interstrand cross linking compounds can form cross links between the two complementary strands of DNA which results in the DNA structure becoming distorted. Distortions of the DNA structure, if unrepaired, can cause the inhibition of DNA replication and transcription (McHugh *et al.* 2001). Examples of interstrand cross linking alkylating compounds include the nitrogen mustards (chloromethine and the prodrug, cyclophosphamide) and chloroethylnitrosoureas (carmustine and lomustine) (Figure 3.7).

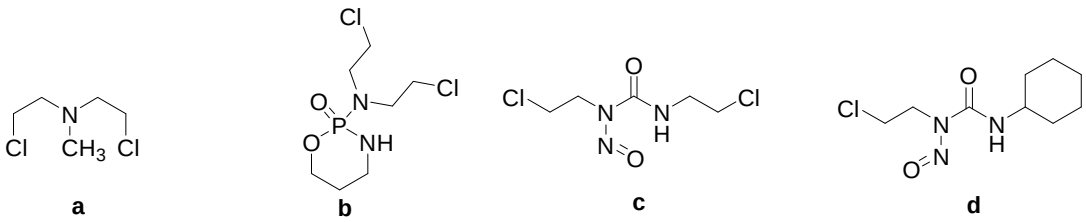

Figure 3.7.: Structures of DNA alkylating compounds with interstrand cross linkage: **a:** Chlormethine, **b:** Cyclophosphamide, **c:** Carmustine and **d:** Lomustine.

It is important to note that the prodrug mitomycin C; an aforementioned groove binder (Figure 3.5) can be converted into monofunctional or bifunctional alkylating agents by bio reductive activation, mediated by flavoenzymes in living cells (Bizanek *et al.* 1992, Rao 1992, Cummings *et al.* 1995). Mitomycin C can form interstrand cross links between guanine groups (Patrick 2009).

3.1.3.2. Alkylating Agents with Intrastrand Cross Linkage

In contrast, intrastrand cross linking compounds can form cross links on the same strand of DNA, which generally occur on the *N*-7 or *O*-6 positions of adjacent guanine molecules (McHugh *et al.* 2001, Patrick 2009). Intrastrand cross linkers are usually platinum (Pt) based agents which are held in place by the formation of covalent Pt-DNA links (Patrick 2009, Pizarro and Sadler 2009). Intrastrand cross links, as with interstrand cross links, can result in distortion and unwinding of DNA, thus inhibiting replication and transcription once more (Malinge *et al.* 1999, McHugh *et al.* 2001). Several critical RNA-dependent activities, such as splicing and translation, can also be inhibited by intrastrand cross links (Hostetter *et al.* 2009). Pt based compounds are also linked to the induction of apoptosis (Hostetter *et al.* 2009, Pizarro and Sadler 2009). The Pt agents cis-diammonia dichloroplatinum (II), known as cisplatin, and carboplatin are the most common examples of intrastrand cross linking compounds (Figure 3.8).

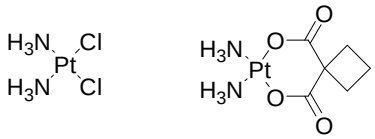

a **b**

Figure 3.8.: Structures of DNA alkylating compounds with intrastrand cross linkage: **a:** Cisplatin and **b:** Carboplatin

3.1.4. Assessment of DNA Binding Interactions

Several *in vitro* experiments have been used to determine the physical interactions of a compound with DNA. These methods include studies into thermal (melting) denaturation, competitive displacement of DNA bound ethidium bromide (EtBr), changes in viscosity, circular dichroism (CD), isothermal titration calorimetry (ITC), NMR spectroscopy (^{31}P NMR spectra), X-ray diffraction, and computer-assisted molecular modelling. All of these methods have been successfully used in the determination of DNA binding interactions (Suh and Chaires 1995, Coury *et al*. 1996, Doyle 1997, Martinez and Chacon-Garcia 2005, Palchaudhuri and Hergenrother 2007, Strekowski and Wilson 2007, Ott *et al*. 2008).

The instrumental techniques of thermal (melting) denaturation (Figure 3.9), competitive displacement of DNA bound EtBr (Figure 3.10) and molecular modelling were

used in this study to investigate DNA binding as a possible mode of action used by BNIPP derivatives.

DNA thermal denaturation is a simple and convenient technique, which is widely used in the identification of derivatives with DNA intercalative properties. In thermal denaturation studies, ds DNA is heated and thermally denatured into ss DNA in the presence and absence of derivatives (Martinez and Chacon-Garcia 2005, Palchaudhuri and Hergenrother 2007) (Figure 3.9). If a derivative stabilises DNA; thermal denaturation is increased (i.e., increase T_m), thus indicating DNA intercalation. The increase in T_m provides an efficient means by which to estimate the extent of DNA intercalation, albeit in a non selective manner. For that reason, the more selective technique of competitive displacement of DNA bound EtBr was employed to verify the mode of action of DNA intercalation (Martinez and Chacon-Garcia 2005, Ott *et al.* 2008).

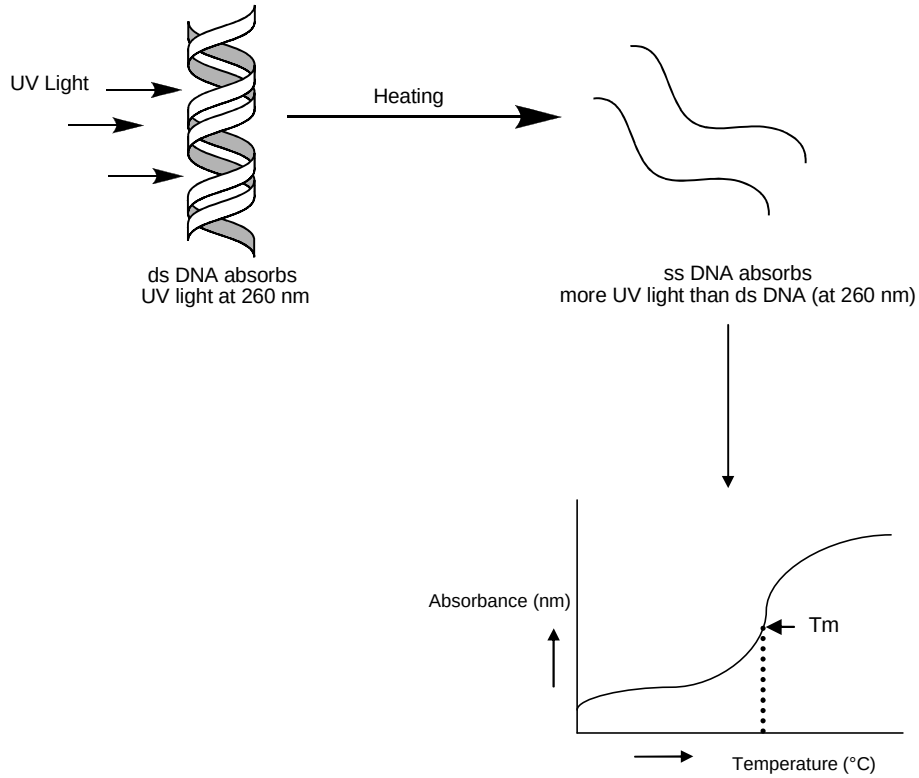

Figure 3.9.: Method of thermal denaturation.

EtBr is a classical DNA intercalator (Figure 3.10A) which results in the substantial enhancement of emitted fluorescence when bound to DNA (McConnaughie and Jenkins 1995, Geall and Blagbrough 2000, Pavlov *et al*. 2001). Intercalating agents exert a higher DNA binding affinity than EtBr will displace DNA-bound EtBr, resulting in fluorescence quenching (Dance *et al*. 2005) (Figure 3.10B). The extent of fluorescence quenching is proportional to the amount of EtBr displaced by a derivative. As a result, the ability of a derivative to competitively displace EtBr bound to DNA can, alongside thermal denaturation, verify the mechanism of binding of selected derivatives (Ott *et al*. 2008).

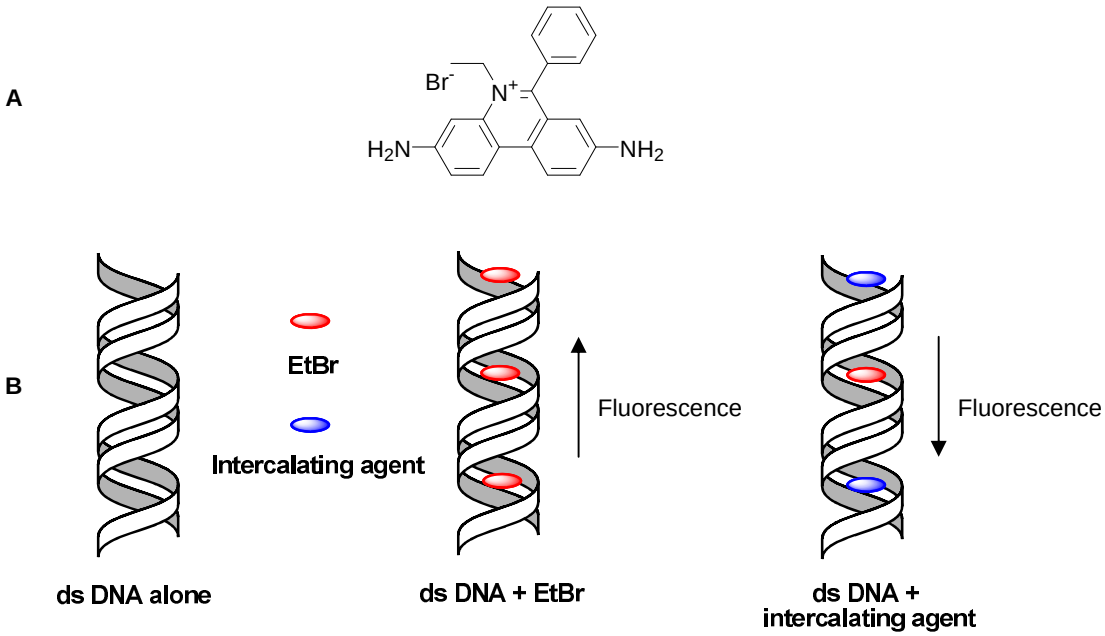

Figure 3.10.: Structure of EtBr (**A**) and method of competitive displacement of DNA bound EtBr (**B**)

3.2. Materials

3.2.1. Materials

All reagents were purchased from Fisher Scientific, UK unless otherwise stated, and were used without purification.

Calf Thymus DNA	Sigma-Aldrich, UK
Dimethyl sulfoxide	Aldrich, UK
Doxorubicin hydrochloride	Sigma-Aldrich, UK
Ethidium Bromide	Sigma-Aldrich, UK
Hoechst 33258	Sigma-Aldrich, UK
Mitoxantrone dihydrochloride	Sigma-Aldrich, UK
Saline Sodium Citrate	Fisons Scientific Apparatus, UK

3.2.2. Instrumentation

Optimal thermal denaturation studies were performed in stoppered quartz cuvettes (1 cm path length) using a Shimadzu UV-1650 PC UV-Vis spectrophotometer fitted with a temperature controller (Shimadzu, Japan), and water supply.

Fluorescent-binding studies were carried out in disposable cuvettes (1 cm path length) using a LS55 Luminescence spectrophotometer (Perkin Elmer, USA), at room temperature (excitation 481 nm; emission 596 nm).

Molecular modelling simulations were performed on a Silicon Graphics Octane R12000 or a Hewlett Packard 1902 workstation. The molecular structures were generated using the Insight-II Version 2005 graphics interface, and Discover 98.0 simulation software (Accelrys, UK).

3.3. Methods

3.3.1. Bisnaphthalimidopropyl (BNIPP) Derivatives

BNIPP derivatives were synthesised as previously described in Section 2.3. Stock solutions of each BNIPP derivative (10 mM for BNIPSpd, BNIPPut, BNIPDahex, BNIPDaoct, BNIPDadec, BNIPDadodec, BNIPDaCHM and BPHPDadec; 90 mM for BNIPDaoxoct and NPA) in 50 % dimethylsulfoxide (DMSO)/water were prepared and stored at 0 – 5 °C until required. Stock solutions of the positive controls: doxorubicin, mitoxantrone and Hoechst 33258 (10 mM), and the natural polyamines: putrescine, spermidine and spermine (10 mM) in 50 % DMSO/water were also prepared, and stored at 0 – 5 °C. Prior to use, all stock solutions were further diluted to the desired final concentration in 0.01 M Saline Sodium Citrate (SSC) buffer.

3.3.2. Thermal Denaturation Studies

A DNA working solution (100 mM) was prepared by dissolving *Calf Thymus* DNA (2.5 mg) in 0.01 M Saline Sodium Citrate (SSC) buffer (100 mL). BNIPP derivatives, positive controls and polyamine working solutions (100 µM) were prepared from their respective stock solutions (10 mM in 50 % DMSO/water), and further diluted to give the final concentration of 10 µM in 0.01 M SSC buffer. DNA-test solutions were prepared by adding 500 µL *Calf Thymus* DNA (100 mM), 400 µL 0.01 M SSC buffer and 100 µL test solution (100 µM) together. The DNA-test solution was mixed and incubated for 12 hours, at room temperature. After 12 hours incubation, the DNA-test solutions were analysed at 260 nm, where the temperature was increased at a rate of 1 °C/minute between 40 – 100 °C, using the UV-Vis spectrophotometer as described in Section 3.2.2. The thermal melting point (T_m (°C)) was computer generated by establishment of the first derivative curve of absorbance against temperature.

3.3.3. Fluorescence-Binding Studies

Calf Thymus DNA solution (100 mM) was prepared as described in Section 3.3.2. EtBr solution (200 µM) was prepared by dissolving 7.886 mg EtBr in distilled water (100 mL). The BNIPP derivative working solutions were prepared as previously described (Section 3.3.2), and were further diluted in 0.01 M SSC to give the final concentrations of 1, 2, 4, 6, 8 and 10 µM. DNA-BNIPP derivative test solutions were prepared by adding varying volumes of the BNIPP derivative solutions in 0.01 M SSC Buffer to *Calf Thymus* DNA (200 µL) and EtBr (20 µL) in 1 mL Eppendorf tubes. DNA-BNIPP derivative solutions were thoroughly mixed, incubated for 15 minutes at room temperature, and analysed using a luminescence spectrophotometer as described in Section 3.2.2. The C_{50}

values are defined as the derivative concentration (μM) required to generate a 50 % decrease in the fluorescence of DNA bound EtBr.

3.3.4. Molecular Modelling

All molecular structures were generated and energy minimised using the Insight II molecular modelling system as described in Section 3.2.2. The cff91 force-field was used for atom potentials and for all energy calculations, minimisations and molecular dynamics simulations. The DNA duplex (PDB ID 108D) used was obtained from the Protein Data Bank, formerly the Brookhaven Protein Database (available from www.pdb.org) (Figure 3.11).

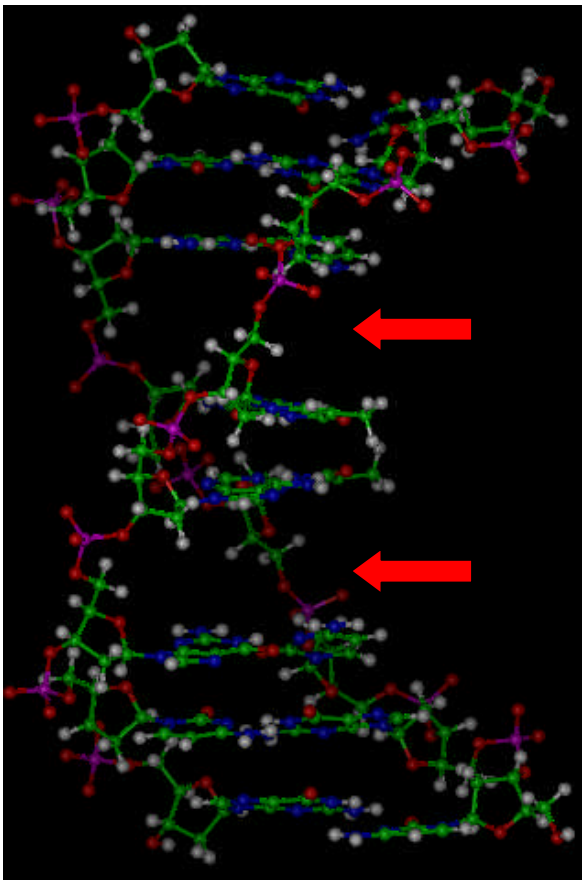

Figure 3.11.: The ball and stick model of the DNA duplex (DUPLEXICI99), looking from a side view. The red arrows indicate the two intercalation sites of the DNA duplex. Carbon atoms are coloured green, nitrogen atoms are blue, oxygen atoms in red and hydrogen atoms in white. Phosphorus counterions are coloured purple.

The intercalation sites of the DNA oligonucleotide d(5'-CGCTAGCG-3')$_2$ were generated by removal of the bis-intercalating dye 1,1'-(4,4,8,8-tetramethyl-4,8-diazaundecamethylene) bis[4-(3-methyl-2,3-dihydrobenzo-1,3-thiazolyl-2-methylidene)quinolinium] tetraiodide (TOTO) (Spielmann *et al*. 1995) (Cairns, Personal Communication). The DNA model with TOTO removed was subsequently used herein to determine the DNA binding affinities of a selection of BNIPP derivatives: BNIPSpd,

BNIPDaoct, BNIPDaoxoct, BNIPDaCHM, BPHPDadec and NPA. Ball and stick images of all the derivatives investigated are shown in Figure 3.12.

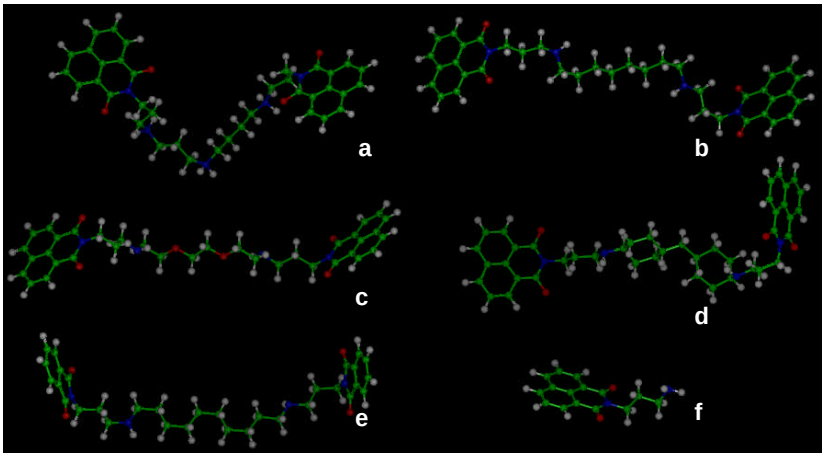

Figure 3.12.: Structures of BNIPP derivatives (a-f) as shown by ball and stick images. The images are **a** BNIPSpd, **b** BNIPDaoct, **c** BNIPDaoxoct, **d** BNIPDaCHM, **e** BPHPDadec and **f** NPA. Carbon atoms are coloured green, nitrogen atoms are blue, oxygen atoms in red and hydrogen atoms in white. Phosphorus counterions are coloured purple.

Manual docking of these BNIPP derivatives was achieved by insertion of the chromophores midway into the two available intercalating sites of the DNA duplex using the program described in Section 3.2.2. All bond and torsion angles were allowed to rotate freely. Two alternative docking conformations were constructed for BNIPSpd, with three docking conformations for BNIPDaoxoct, BPHPDadec and NPA, and four docking conformations for BNIPDaoct and BNIPDaCHM. The DNA-BNIPP derivative complexes were initially submitted for molecular dynamics simulations in the unfixed state. Due to the resultant instability of the unfixed DNA-BNIPP derivative complexes in this environment, especially during dynamic simulations, selected DNA-BNIPP derivative complexes (2 complexes per BNIPP derivative) were resubmitted for molecular dynamic simulations with the bases surrounding the intercalation sites fixed. Each unfixed complex was minimised using a conjugate gradient algorithm (the Polak-Ribiere variant) until an energy convergence criterion of 1 kcal mol^{-1} A^{-1} was reached (steepest descent convergence of 100, and a maximum of 10,000 steps). Fixed complexes were however minimised using the conjugate gradient algorithm until an energy convergence criterion of 0.1 kcal mol^{-1} A^{-1} was reached, with a steepest descent convergence of 100, and a maximum of 50,000 steps. Molecular dynamics (MD) simulations were carried out for 100,000 frequency steps (fs), at 300 K (10 dynamics simulations), with a cut-off distance of 9.5 A. The final average conformations were then minimised as described above.

Binding enthalpies for each BNIPP derivative were determined by calculation of the potential energy of each DNA-BNIPP derivative complex ($E_{COMPLEX}$) and subtracting the sum of the energies of the non intercalated DNA (E_{DNA}) and BNIPP derivatives (E_{BNIPP}) from this value. The enthalpy of binding interactions (E_{BIND}) were calculated using the equation: $E_{BIND} = E_{COMPLEX} - [E_{BNIPP} + E_{DNA}]$, where $E_{COMPLEX}$, E_{BNIPP} and E_{DNA} are the

computed potential energies for the minimised average DNA-BNIPP derivative complex, free BNIPP derivative and free DNA conformations, respectively (Cairns *et al*. 2002), and the more negative the binding energy (E_{BIND}); the stronger the DNA binding interaction.

3.3.5. Data Analysis

Unless otherwise stated, each data set contained a minimum of three independent experiments, in which each experiment comprised of at least three internal replicates, expressed as mean ± Standard Deviation (SD).

3.4. Results

3.4.1. Effect of BNIPP Derivatives on DNA Binding Affinity by Thermal Denaturation

The extent of DNA binding affinity demonstrated by each BNIPP derivative (10 µM) was determined by thermal denaturation (T_m) studies.

The thermal denaturation profile presented in Figure 3.13 displays the thermal denaturation curves obtained in the presence and absence of 10 µM BNIPDaCHM. The curves are a representation of all the thermal denaturation curves obtained for the other BNIPP derivatives, positive controls (data not shown) and polyamines (data not shown).

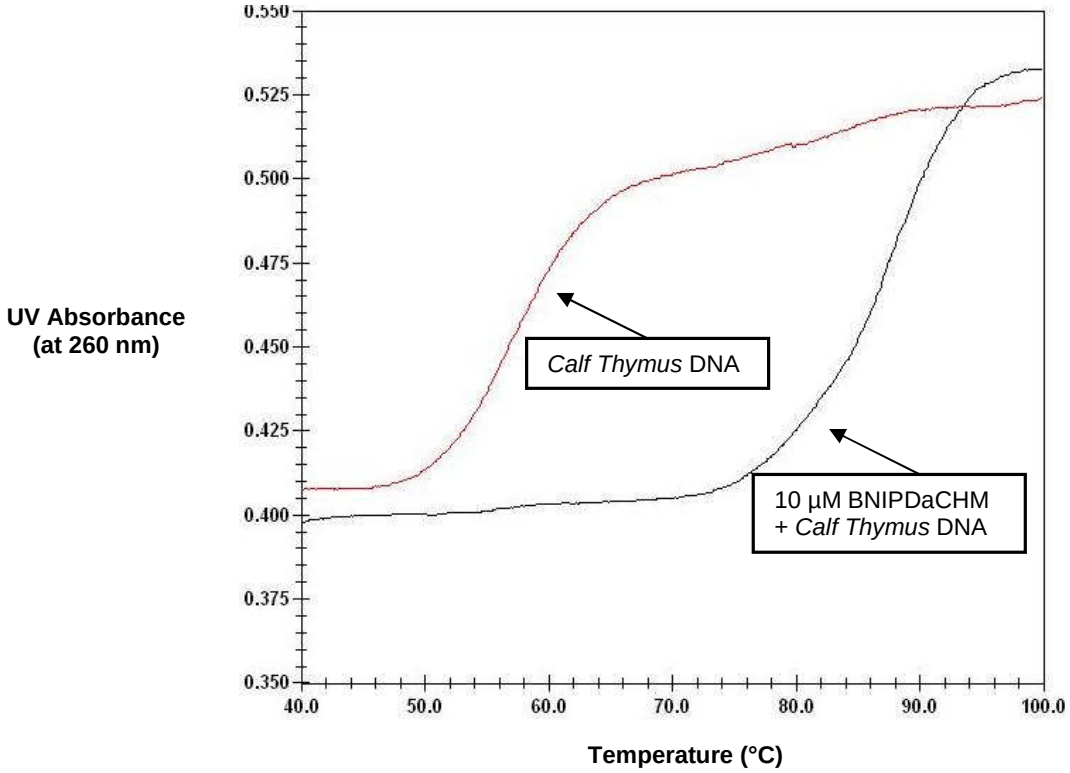

Figure 3.13.: The effect of temperature (°C) on UV absorbance for *Calf Thymus* DNA incubated in the absence and presence of 10 µM BNIPDaCHM. The curves shown in the graph are representative of the thermal denaturation curves obtained for all BNIPP derivatives analysed (data not shown).

Table 3.1 shows the T_m values of each BNIPP derivative, and doxorubicin, mitoxantrone and Hoechst 33258 (10 µM). T_m values for all BNIPP derivatives ranged between 81.2 – 91.9 °C showing melting temperature differences (Δ T_m) of 25.0 – 35.7 °C compared to the melting point of *Calf Thymus* DNA alone (T_m value of 56.2 °C). The increase in T_m from these BNIPP derivatives was in the same range as the extensively studied intercalators, doxorubicin (Δ T_m 30.2 °C) and mitoxantrone (Δ T_m 34.8 °C), suggesting an intercalative DNA binding interaction. The most active DNA binding derivative was identified as BNIPDahex (Δ T_m 35.7 °C).

Table 3.1.: Effect of BNIPP derivative treatment on thermal denaturation

Derivative[a]	T_m (°C)[b]
Calf Thymus DNA alone	56.2 ± 0.4
BNIPSpd	91.5 ± 0.6
BNIPPut	89.2 ± 2.5
BNIPDahex	91.9 ± 0.6
BNIPDaoct	88.7 ± 0.3
BNIPDadec	84.4 ± 0.2
BNIPDadodec	81.2 ± 0.7
BNIPDaoxoct	87.9 ± 0.6
BNIPDaCHM	87.4 ± 1.2
BPHPDadec	72.0 ± 2.4
NPA	66.3 ± 0.9
Doxorubicin	86.4 ± 1.2
Mitoxantrone	91.0 ± 1.5
Hoechst 33258	78.8 ± 0.9

[a] *Calf Thymus* DNA was incubated in the presence or absence of 10 µM BNIPP derivatives, including BPHPDadec, NPA, doxorubicin, mitoxantrone and Hoechst 33258, at room temperature for 12 hours.
[b] T_m is the temperature (°C) when 50% of the DNA is denatured. Data are the mean ± SD of three independent experiments (n = 3).

It is interesting to note that among all of the BNIPP derivatives, the BNIPP derivative with the longest linker chain (i.e., 12 carbons (C12); BNIPDadodec) demonstrated the smallest increase in T_m value (Δ T_m 25.0). In addition, the BNIPP derivative binding strength or the stability of the DNA duplex was marginally affected by the addition of two oxygen atoms (BNIPDaoxoct) or two cyclohexane rings (BNIPDaCHM) in the linker chain, with slightly lower T_m values (Δ T_m 31.7 °C and Δ T_m 31.2 °C, respectively). In contrast, BPHPDadec and NPA induced a relatively small increase in T_m when compared with the other BNIPP derivatives, with Δ T_m values of 15.8 °C and 10.1 °C, respectively. Therefore, these derivatives demonstrated a low intercalative affinity.

3.4.1.1. Effect of Polyamines on DNA Binding Affinity by Thermal Denaturation

Further thermal denaturation studies into the DNA binding interactions of the natural polyamines (putrescine, spermidine and spermine) were investigated and the results are shown in Table 3.2.

Table 3.2.: Effect of natural polyamine treatment on thermal denaturation

***Polyamine*[a]**	***T_m* (°C)[b]**
Calf Thymus DNA alone	56.2 ± 0.4
Putrescine	73.6 ± 0.7
Spermidine	81.4 ± 0.5
Spermine	86.6 ± 1.2

[a] *Calf Thymus* DNA was incubated in the presence or absence of 10 µM polyamine salt, for 12 hours at room temperature.
[b] T_m is the temperature (°C) when 50% of the DNA is denatured. Data are the mean ± SD of three independent experiments (n = 3).

All polyamines resulted in an increase in T_m values ranging between 73.6 – 86.6 °C. Δ T_m values were 17.4, 25.2 and 30.4 °C respectively when compared to the melting point of *Calf Thymus* DNA alone (T_m value of 56.2 °C) (Table 3.2). The order of polyamine thermal denaturation was thus spermine > spermidine > putrescine. This order of binding strength can be explained by the increase in number of secondary amino groups present in the structures of putrescine, spermidine and spermine, respectively. Also, the Δ T_m for spermidine and spermine was greater than that of the extensively studied groove binder, Hoechst 33258 (Δ T_m value of 22.6 °C) (Table 3.1).

3.4.2. *Effect of BNIPP Derivatives on DNA Binding Affinity by Competitive Displacement of EtBr*

The competitive displacement fluorescent assay of DNA bound EtBr was performed to further validate the DNA binding affinity of each BNIPP derivative. The fluorescence quenching of EtBr bound DNA by 1 – 10 µM BNIPDaCHM in 10 µM *Calf Thymus* DNA and 2 µM EtBr is presented in Figure 3.14. The emission spectra are representative of spectra obtained for each BNIPP derivative, except for BPHPDadec and NPA which showed no quenching effects (data not shown).

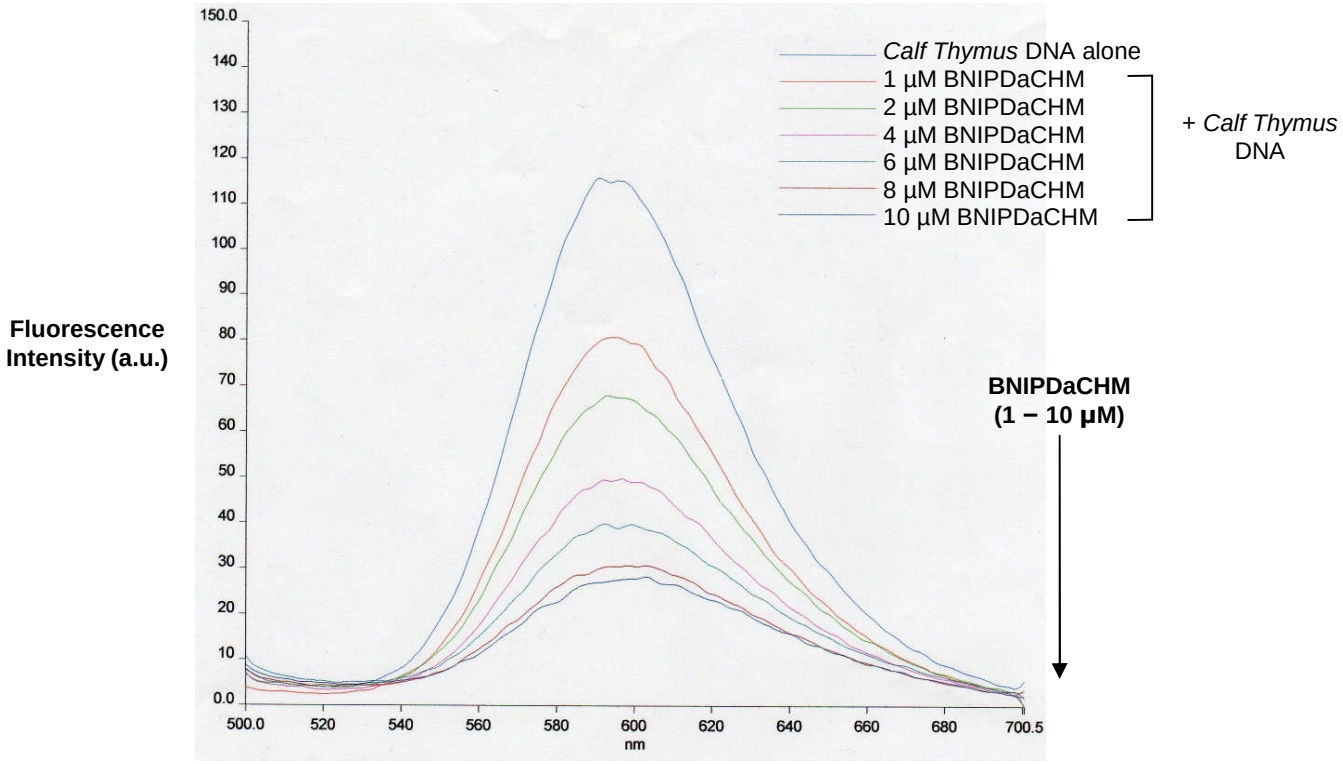

Figure 3.14.: The effect of BNIPDaCHM concentration (1 – 10 µM) on fluorescence intensity for fluorescence quenching of EtBr bound DNA.

Figure 3.15 shows an example of the % fluorescence intensity curve obtained at the excitation/emission maxima (Ex/Em 481/596 nm) plotted against BNIPDaCHM concentration (0 – 10 µM). The curve was representative of the % fluorescence intensity curves obtained for each BNIPP derivative. In contrast, Figure 3.16 shows the % fluorescence intensity curve obtained at the excitation/emission maxima (Ex/Em 481/594 nm) plotted against NPA concentration (0 – 10 µM) where EtBr displacement was not achieved beyond the 50% decrease in fluorescence intensity (i.e., required to achieve a C_{50} value for NPA or BPHPDadec).

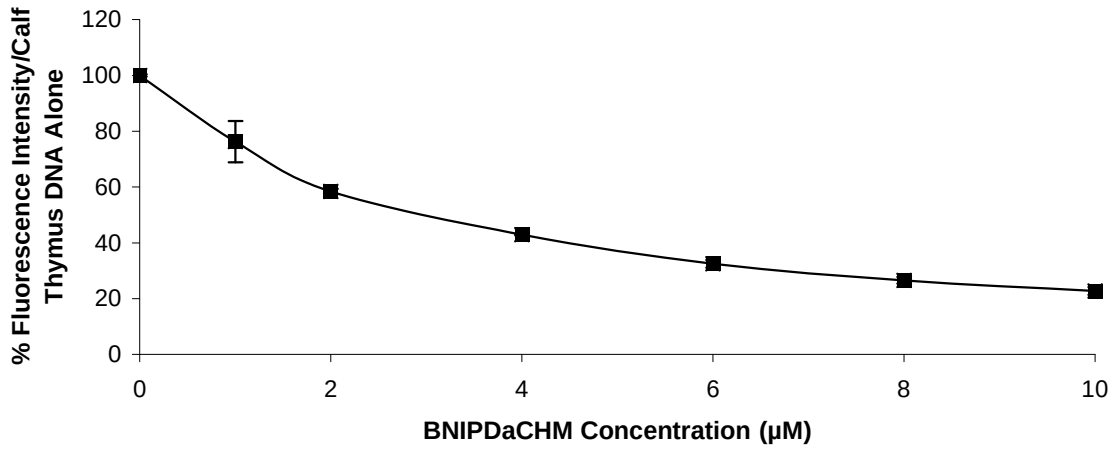

Figure 3.15.: The effect of BNIPDaCHM concentration on % fluorescence intensity. Emissions were recorded at the Ex/Em maxima for the BNIPP derivatives (Ex/Em, BNIPDaCHM, 481/596nm). Date are mean ± SD (n = 3).

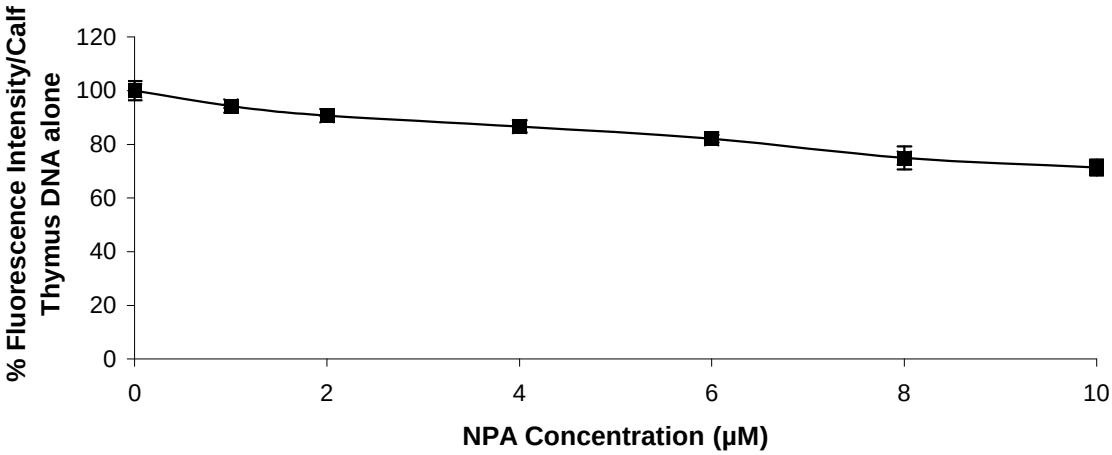

Figure 3.16.: The effect of NPA concentration on % fluorescence intensity. Emissions were recorded at the Ex/Em maxima (Ex/Em, NPA, 481/596nm). Date are mean ± SD (n = 3).

All BNIPP derivatives, except BPHPDadec and NPA (C_{50} > 10 µM) competitively displaced EtBr from DNA, with C_{50} values in the range of 1.4 – 3.8 µM (Table 3.3). The order of BNIPP derivative binding strength to DNA was BNIPSpd > BNIPPut = BNIPDahex > BNIPDaoct > BNIPDadec > BNIPDaoxoct > BNIPDadodec > BNIPDaCHM > BPHPDadec = NPA.

Table 3.3.: The effect of BNIPP derivatives on competitive displacement

Derivative[a]	**C_{50} (μM)**[b]
Calf Thymus DNA alone	ND
BNIPSpd	1.4 ± 0.1
BNIPPut	1.5 ± 0.3
BNIPDahex	1.5 ± 0.1
BNIPDaoct	1.7 ± 0.2
BNIPDadec	1.8 ± 0.1
BNIPDadodec	3.4 ± 0.3
BNIPDaoxoct	1.9 ± 0.4
BNIPDaCHM	3.8 ± 0.1
BPHPDadec	> 10
NPA	> 10

[a] 200 μL *Calf Thymus* DNA, 20 μL EtBr and varying volumes of the BNIPP derivatives were prepared in 1 mL Eppendorf tubes. Solutions were mixed thoroughly and incubated for 15 minutes at room temperature.
[b] C_{50} is the derivative concentration (μM) required to generate a 50 % decrease in the fluorescence of bound EtBr. Data are the mean ± SD of three independent experiments (n = 3).

3.4.3. Molecular Modelling Study

Molecular modelling was carried out as previously described in Section 3.3.4. Figure 3.17 reveals the mode of intercalation, either mono- or bis-intercalation that was simulated by the BNIPP derivatives investigated. The naphthalimido or phthalimido chromophores insert into the DNA duplex and intercalate with the base pairs. The aminoalkyl linker of the bisnaphthalimidopropyl and bisphthalimidopropyl derivatives appear to also bind to the grooves of the DNA duplex, thus also acting as possible groove binders (Figure 3.17).

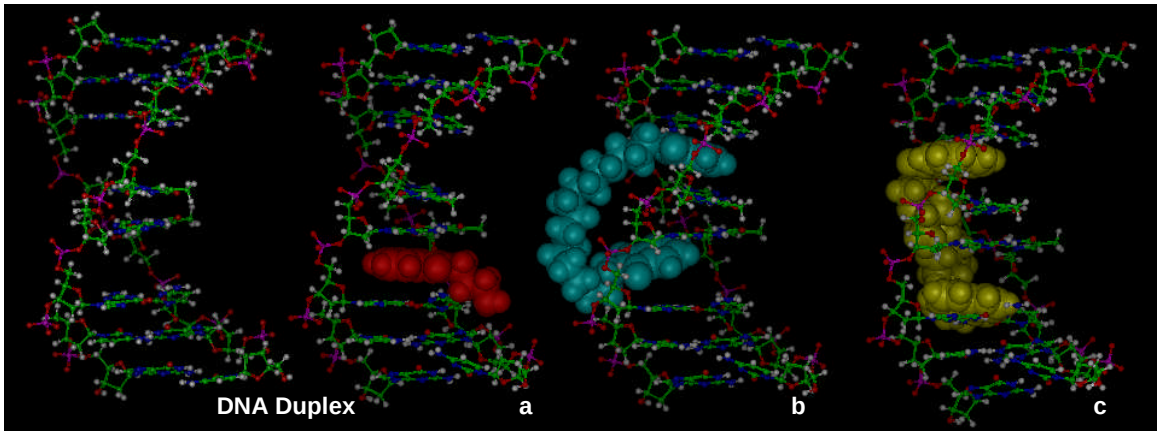

Figure 3.17.: Structures of the DNA Interactions between NPA, BPHPDadec and BNIPDaCHM (a, b and c, respectively) and the DNA Duplex. The DNA is represented as a ball and stick model (carbon atoms are coloured green, nitrogen atoms are blue, oxygen atoms in red, hydrogen atoms in white, and phosphorus counterions are coloured purple). All derivatives are depicted as CPK space-filled models, and are shaded red for NPA, blue for BPHPDadec and yellow for BNIPDaCHM.

Figure 3.18 represents the effects of BNIPDaCHM (a) on the DNA duplex by molecular modelling. Images (b - c) were obtained from the minimised average conformational structure of BNIPDaCHM intercalated into the DNA duplex, when the bases surrounding the intercalation site are either in an unfixed (b) or fixed (c) state. Each image is representative of the minimised average conformations obtained for each derivative when subjected to MD simulations. As shown in Figure 3.18 (a - c), the structure of the DNA duplex was completely distorted and destroyed after MD simulations in both an unfixed or fixed state. In most cases, the DNA duplex appeared to fold in on itself completely during MD simulations.

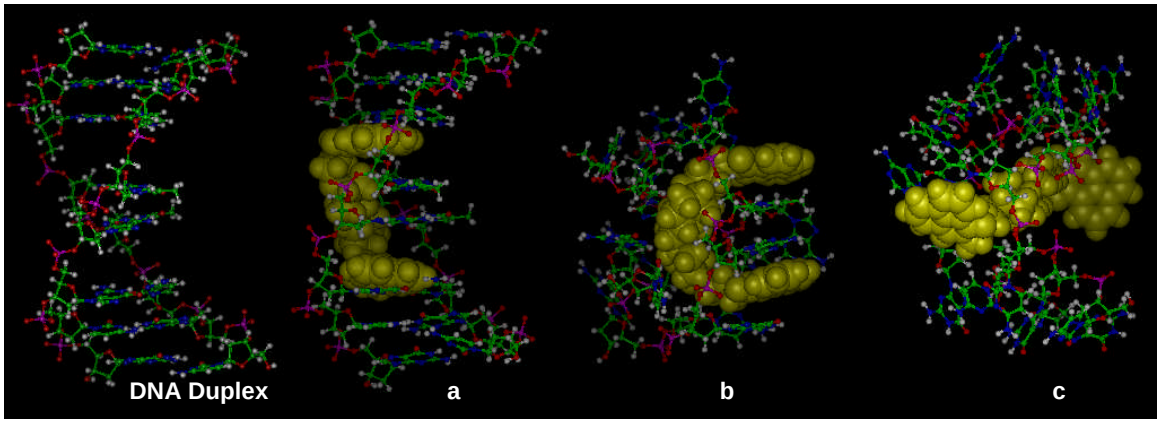

Figure 3.18.: Structures of the DNA Interactions between BNIPDaCHM (a, b and c, respectively) and the DNA Duplex. The DNA is represented as a ball and stick model (carbon atoms are coloured green, nitrogen atoms are blue, oxygen atoms in red, hydrogen atoms in white, and phosphorus counterions are coloured purple). BNIPDaCHM is depicted as a CPK space-filled model, and are shaded yellow, **a** BNIPDaCHM present within the intercalation sites, **b** the final average minimised structure of BNIPDaCHM in the DNA duplex with unfixed intercalation sites, and **c** the final average minimised structure of BNIPDaCHM in the DNA duplex with fixed intercalation sites. These images are representative of the results obtained for each derivative investigated.

Molecular modelling studies were performed on these selected BNIPP derivatives to rationalise the results obtained from the *in vitro* DNA binding studies as shown in Sections 3.4.1 and 3.4.2. The computed energy results associated to each DNA/BNIPP derivative complex with unfixed intercalation sites are presented in Table 3.4.

Table 3.4.: Computed potential energies (kcal mol^{-1}) for the unfixed DNA-BNIPP derivative complexes [a, b]

BNIPP Derivative	*DNA-BNIPP Derivative Complex*	$E_{COMPLEX}$	E_{BIND}
BNIPSpd	i	606.49	-85.65
	ii	627.37	-64.76
BNIPDaoct	i	480.92	-198.19
	ii	536.86	-142.25
	iii	509.34	-169.77
	iv	700.48	21.371
BNIPDaoxoct	i	643.92	224.31
	ii	703.32	283.71
	iii	729.14	309.53
BNIPDaCHM	i	680.50	18.85
	ii	692.18	30.52
	iii	705.93	44.27
	iv	683.522	21.87
BPHPDadec	i	271.65	48.76
	ii	282.55	59.65
	iii	753.57	530.68
NPA	i	294.28	-34.73
	ii	313.21	-15.80
	iii	339.24	10.22

[a] Where E_{DNA} = 227.70 kcal mol^{-1} for the DUPLEXICI99 DNA duplex.
[b] Where E_{BNIPP} is 464.44 kcal mol^{-1} for BNIPSpd, 451.41 kcal mol^{-1} for BNIPDaoct, 191.91 kcal mol^{-1} for BNIPDaoxoct, 433.95 kcal mol^{-1} for BNIPDaCHM, -4.81 kcal mol^{-1} for BPHPDadec and 101.32 kcal mol^{-1} for NPA.

The DNA-BNIPP derivative complexes selected for further MD simulations with fixed intercalation sites were complexes with the most negative E_{BIND} energies. These complexes were i and ii for BNIPSpd, i and iii for BNIPDaoct, i and ii for BNIPDaoxoct, i and iv for BNIPDaCHM, i and ii for BPHPDadec, and i and ii for NPA as shown in Table 3.5.

Table 3.5.: Computed potential energies (kcal mol^{-1}) for the fixed DNA-BNIPP derivative complexes [a, b]

BNIPP Derivative	*DNA-BNIPP Derivative Complex*	$E_{COMPLEX}$	E_{BIND}
BNIPSpd	i	521.97	-170.17
	ii	642.22	-49.92
BNIPDaoct	i	500.53	-178.58
	iii	508.72	-170.39
BNIPDaoxoct	i	644.24	224.63
	ii	661.13	241.53
BNIPDaCHM	i	661.68	0.02
	iv	659.67	-1.98
BPHPDadec	i	462.31	189.42
	ii	255.57	-17.32
NPA	i	304.93	-24.09
	ii	342.52	13.50

[a] Where E_{DNA} = 227.70 kcal mol^{-1} for the DUPLEXICI99 DNA duplex.
[b] Where E_{BNIPP} is 464.44 kcal mol^{-1} for BNIPSpd, 451.41 kcal mol^{-1} for BNIPDaoct, 191.91 kcal mol^{-1} for BNIPDaoxoct, 433.95 kcal mol^{-1} for BNIPDaCHM, -4.81 kcal mol^{-1} for BPHPDadec and 101.32 kcal mol^{-1} for NPA.

The results in Tables 3.4 and 3.5 show that there was little difference observed between the E_{BIND} obtained for the unfixed or fixed bases in the DNA-BNIPP derivatives complexes suggesting that the instability and distortion of the helix (Figure 3.18) played a very small part in the overall interaction. In this study, the more negative the binding energy, the stronger the DNA binding interaction. Due to the presence of negative binding energies, most of the derivatives were identified as active. The order for DNA binding strength, as represented by E_{BIND} (kcal mol^{-1}) was BNIPDaoct > BNIPSpd > NPA > BNIPDaCHM > BPHPDadec > BNIPDaoxoct. These results are in contrast to the rank order obtained from the *in vitro* thermal denaturation and competitive displacement assays (Tables 3.1 and 3.3).

3.5. Discussion

3.5.1. Effect of BNIPP Derivatives on DNA Binding Affinity

In this study, DNA-binding affinities of BNIPP derivatives were achieved via thermal denaturation and competitive EtBr displacement studies (Sections 3.4.1 and 3.4.2). These *in vitro* techniques provided the simplest means by which to study DNA binding mechanisms (Johnson and Thomas 2002, Palchaudhuri and Hergenrother 2007), and were used to evaluate and confirm that DNA was a target utilised by BNIPP derivatives following on from studies by Pavlov *et al*. (2001) and Dance *et al.* (2005).

All BNIPP (10 µM) derivatives were able to stabilise the *Calf Thymus* DNA duplex as demonstrated by increased T_m values (81.2 – 91.9 °C) when compared with *Calf Thymus* DNA alone (T_m value of 56.2 °C) (Table 3.1). As stabilisation of the DNA duplex has been shown to be a common feature of DNA intercalating anti cancer drugs (Martinez and Chacon-Garcia 2005); it was confirmed that BNIPP derivatives interact with DNA through bis-intercalation. These results are also in agreement with the findings of Pavlov *et al.* (2001) and Dance *et al.* (2005).

BNIPDahex was identified to be the most active DNA binding derivative (ΔT_m 35.7 °C), and both BNIPDahex and BNIPSpd (ΔT_m 35.3 °C) had greater DNA binding affinities than the extensively studied intercalator doxorubicin (ΔT_m 30.2 °C) (Table 3.1). Earlier work had identified BNIPSpd to be the most active DNA binding member of the BNIPP derivative series compared to BNIPOSpd and BNIPOSpm (Figures 1.22 and 1.23) (Pavlov *et al.* 2001, Dance *et al.* 2005). Although, a different buffer (i.e., 0.01 M phosphate buffer) was used in previous studies by Pavlov *et al.* (2001) and Dance *et al.* (2005), the DNA binding trends observed in this study are very similar.

The more selective technique of EtBr displacement confirmed the mode of action of BNIPP derivatives relative to DNA intercalation (Section 3.4.2) (Martinez and Chacon-Garcia 2005, Ott *et al.* 2008). BNIPP derivatives induced effective displacement of DNA bound EtBr in a dose dependent manner, thus, effectively competing with EtBr for DNA intercalation sites and, as a result of their higher DNA binding affinities, effectively displaced EtBr. The fluorescent emissions of the DNA bound EtBr were consequently quenched, with C_{50} values in the range of 1.4 – 3.8 µM (Table 3.3). EtBr displacement studies have been used in the literature to investigate many structurally different DNA binding derivatives, for example, combilexines (Hotzel *et al.* 2002) or cation-substituted anthrapyrazoles (Tan *et al.* 2007) (Figure 3.19). Hotzel *et al.* (2002) found weak DNA binding (i.e., C_{50} > 140 µM) with combilexine derivatives, whereas Tan *et al.* (2007) found that cation-substituted anthrapyrazole derivatives were effective DNA binders with C_{50} values ranging between 12 – 21 µM. Therefore, compared with these results, BNIPP

derivatives have higher DNA affinities than the most active cambilexine (**a**) or the most active cation-substituted anthrapyrazoles (**b-c**) (Figure 3.19).

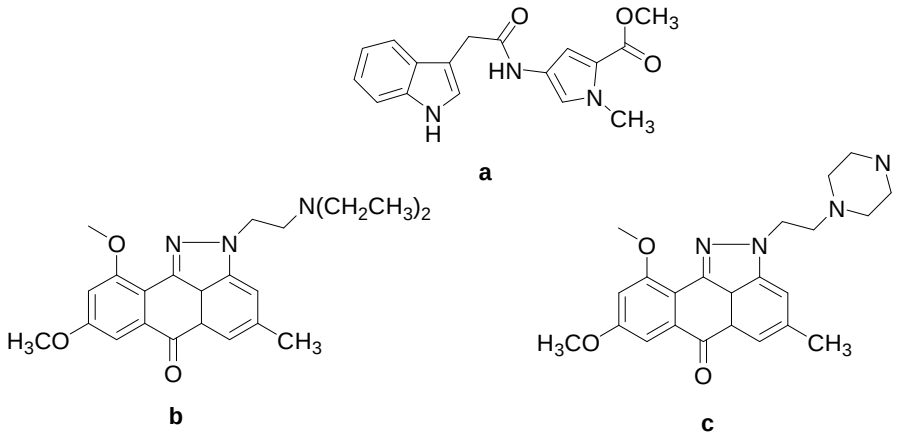

Figure 3.19.: Structures of the most active cambilexine **(a)** and the most active cation-substituted anthrapyrazoles **(b-c)**

DNA binding affinity of BNIPP derivatives can be greatly affected by structural modifications to the central linker chain, including length, rigidity and the number of positive charges. Previous work by Pavlov *et al.* (2001) stated that BNIPP derivatives with spermidine and spermine linker chains showed an influence on the extent of DNA binding affinity. Spermidine (+3 charge) and spermine (+4 charge) linkers exhibited a much higher degree of DNA binding than their linear diaminoalkyl linker counterparts (+2 charge). Therefore, a relationship exists between the number of secondary amines present in the linker chain (i.e., a higher electronegativity) (Feuerstein *et al.* 1990), and an increase in T_m values (i.e., a higher DNA binding affinity), as demonstrated in this study (Table 3.2). In addition, a detailed study carried out by Ouameur and Tajmir-Riahi (2004) calculated the approximate distances between the outer primary amino groups of the all-*trans* conformation (~ 6.23, 11.13 and 16.04 Å, for putrescine, spermidine and spermine, respectively), and showed that the calculated N-N distances were closely related to the length of the major (~ 16.4 Å) and the minor (~ 6.02 Å) grooves of the DNA duplex. Therefore, polyamines have the ideal net charge and size to generate strong DNA groove binding interactions (Le Pecq *et al.* 1975, Hou *et al.* 2001, Strekowski and Wilson 2007), and the results presented in Table 3.2 are in agreement with those findings.

For the BNIPP derivatives, thermal denaturation studies were also used to investigate the effect of further modifications to the central linker chain (Table 3.1). These modifications include an increase in alkyl chain length (i.e., chains with between 4 – 12 methylene groups), and the addition of either two oxygen atoms (i.e., increase charge) or two cyclohexane rings (i.e., to some extent increase linker rigidity). BNIPP derivatives with a chain length of between 4 – 8 methylene groups (BNIPPut, BNIPDahex and BNIPDaoct respectively) exhibited high DNA binding affinities (Δ T_m values 32.5 – 35.7 °C) caused by strong electrostatic and hydrophobic interactions reasoned as groove

binding interactions. The lower DNA binding affinities of BNIPDadec with 10 methylene groups and BNIPDadodec with 12 methylene groups (Δ T_m values of 28.2 and 25.0 °C, respectively) could be explained by an incomplete electrostatic interaction. The increased flexibility in the alkyl linker chain can also contribute to the linker unwinding away from the DNA, and that the two amino groups were not electronegative enough to ensure a stable interaction with the phosphate groups on the DNA duplex. Furthermore, the absence of highly electronegative atoms between the amino groups (e.g., nitrogen or oxygen atoms) would not permit the formation of strong hydrogen bonds which may have stabilised a longer alkyl chain. The derivatives BNIPDaoxoct and BNIPDaCHM exhibited a marginal decrease in DNA binding affinity compared with the more effective BNIPP derivatives (Δ T_m values 31.7 and 31.2 °C, respectively), yet they were more effective than derivatives with linear alkyl chain lengths of > 8 methylene groups. C_{50} values revealed BNIPDaoxoct (C_{50} value of 1.9 μM) to be a more effective DNA binder than BNIPDaCHM (C_{50} value of 3.8 μM) (Table 3.3). The two oxygen atoms are highly electronegative, and can establish strong hydrogen bonds with DNA grooves (major or minor) or with the phosphates of the DNA backbone (Pavlov *et al*. 2001, Filosa *et al.* 2009). However, the differences in C_{50} values were not physiologically different to one another (i.e., a significant physiological difference would be a difference of > 10 μM). These results do suggest that, linker chains, as well as naphthalimido rings are critical in contributing to high DNA binding affinities. The results in this study support the theory that BNIPP derivatives bind to DNA by intercalation (i.e., the naphthalimido rings), and groove binding (i.e., the aminoalkyl linker chain) (Kong Thoo Lin and Pavlov 2000, Pavlov *et al.* 2001).

It is impossible to definitively state whether the BNIPP derivatives bind by both intercalation and groove binding using only thermal denaturation and displacement assays. However, compelling evidence from the structural and *in vitro* data presented in Tables 3.1 and 3.3 do strongly suggest that BNIPP derivatives may utilise both mechanisms. In support of this theory, the symmetrical bisnaphthalimide Elinafide (Figure 1.21) which shares many structural features to that of BNIPP derivatives was found to bis-intercalate into DNA (Bailly *et al.* 1996, Brana *et al.* 2001). In addition, using a combination of DNase I footprinting, chemical probing, NMR and MD simulations, Elinafide was shown to interact in a sequence specific manner with the hexanucleotide $d(ATGCAT)_2$. The linker chain (*N,N*'-bis(ethylene)-1,3-propylenediamine) was positioned within the major groove of the DNA duplex, and its amino groups hydrogen bonded to the guanine bases (Bailly *et al.* 1996, Gallego *et al.* 1999, Brana *et al.* 2001). Using molecular modelling studies Filosa *et al* (2009) reported that several structurally related bisnaphthalimide derivatives, with various aminoalkyl linker substitutions were also bis-intercalators. The planar aromatic moieties were shown to intercalate between the base pairs, and the linker chain was detailed to be the contributory factor in the stability of the

complex, with the formation of Van der Waal's interactions and hydrogen bonds with the minor groove (Filosa *et al.* 2009).

Further studies which verify the groove binding potential, and sequence specificity of BNIPP derivatives should be undertaken to compare with the binding interactions of structurally related derivatives, such as Elinafide. Methods employed to determine these interactions should include viscosity changes, electric linear dichroism, NMR and DNase I footprinting (Palchaudhuri and Hergenrother 2007, Strekowski and Wilson 2007)

It is interesting to note that in comparison with the BNIPP derivatives, BPHPDadec and NPA were not as effective in intercalating with *Calf Thymus* DNA (T_m values of 72.0 and 66.3 °C, thus Δ T_m values of 15.8 and 10.1 °C, respectively), and C_{50} values of > 10 μM (Tables 3.1 and 3.3). The reduced level of DNA intercalation can be related to the structural differences between these derivatives and the BNIPP derivatives. Instead of two naphthalimido rings, BPHPDadec consisted of two phthalimido rings, whilst NPA had only one naphthalimido ring. Taken together, these results have shown that the presence of bisnaphthalimidopropyl functionality and an optimum aminoalkyl linker chain length of 4 – 8 methylene groups are necessary to obtain strong DNA binding interactions.

3.5.2. Molecular Modelling

Molecular modelling studies were undertaken in an attempt to rationalise the *in vitro* DNA binding results obtained for the BNIPP derivatives. Further investigations into the mode of DNA binding were carried out for BNIPSpd, BNIPDaoct, BNIPDaoxoct, BNIPDaCHM, BPHPDadec and NPA through MD simulations using the DNA duplex model described in Section 3.3.4.

The DNA-BNIPP derivative complexes were initially attained by docking the BNIPP derivative midway into the intercalation site on the DNA duplex. The BNIPP derivatives (and BPHPDadec) were docked into both intercalation sites, whilst NPA was docked into only one intercalation site (Figure 3.17). The DNA-BNIPP derivative complexes were initially submitted for MD simulations with all atoms free to move (unfixed state) (Table 3.4). Due to the complete distortion of the DNA complex after MD simulations (Figure 3.18), the DNA-BNIPP derivative complexes were further refined whereby the heavy atoms around the intercalation sites were fixed (Table 3.5). The results produced demonstrated that there were no differences in the images obtained or the rank order of DNA-BNIPP derivative binding energies (Figure 3.18; Tables 3.4 and 3.5). Although, it is important to note that more negative E_{BIND} results were observed when the intercalation sites were fixed (Table 3.5).

The rank order obtained for derivatives after MD simulations were noticeably different to that obtained in the T_m and EtBr displacement studies. There are several reasons for this discrepancy. One of the reasons is the fact that the model used in this study did not have the same base sequence as *Calf Thymus* DNA, thus resulting in

different binding interactions between each system. In order to compare the results of the BNIPP derivatives with that of Elinafide, the DNA hexamer d(ATGCAT)$_2$ should have been utilised (Gallego *et al.* 1999, Brana *et al.* 2004a). Another possible reason is that the DNA-BNIPP derivative complexes were not allowed enough time to relax fully during MD simulations resulting in only a small population of notable trajectories or 'snap shots' per complex. To overcome this issue, the DNA-BNIPP derivative complexes should be heated to 600 K, instead of 300 K, which would increase the number of trajectories and dynamic simulations per DNA-BNIPP derivative complex. A third possibility was that modelling was carried out *in vacuo* using a correction for implicit solvent (Distance Dependent Dielectric of 4, and a Cutoff Distance of 9.5), yet a more realistic model would have been to use an explicit solvent during the MD simulations. However, this would result in more complex and lengthy MD simulations. In all situations, the bases would again be in an unfixed and fixed state to correlate with the results obtained in this study.

Therefore, although the BNIPP derivatives were identified as active DNA binders in the model utilised, it could be stated that the DNA model and MD simulations need to be further refined in order to correlate the results obtained from the *in vitro* DNA binding experiments (Sections 3.4.1 and 3.4.2).

3.6. Conclusions

Thermal denaturation and EtBr displacement studies confirmed that the BNIPP derivatives interact with DNA by the mechanism of bis-intercalation. All BNIPP derivatives, except BPHPDadec and NPA (Δ T_m values of 15.8 and 10.2 °C, and C_{50} values of > 10 μM) exhibited strong DNA binding affinities. High DNA binding affinities were observed in derivatives with an alkyl linker chain length with 4 – 8 methylene groups, and the presence of nitrogen or oxygen atoms were shown to further enhance DNA binding affinity. DNA binding affinity was reduced with longer alkyl linker chains containing more than 10 methylene groups. The DNA binding results confirmed the important structural features required to increase DNA binding affinity. These include (i) bisnaphthalimidopropyl functionality; (ii) an alkyl linker chain of between 4 – 8 methylene groups; and (iii) the presence of at least two amino groups.

MD simulations have also provided evidence that the BNIPP derivatives bind to DNA in an intercalative manner, by exhibiting negative E_{BIND} values for several of the BNIPP derivatives. The MD simulations resulted in the complete distortion of the DNA duplex for all derivatives analysed, although the model used needs to be further refined before additional experiments are undertaken.

In conclusion, the results presented thus far strongly suggest that DNA could be one of the main targets for BNIPP derivatives, and they bind DNA by bis-intercalation. In an attempt to further elucidate the mode of action of selected BNIPP derivatives; their toxicity, mode of cell uptake and their cellular distribution was assessed in breast cancer MDA-MB-231 and breast epithelial MCF-10A cells (Chapter 4).

Chapter 4

Cytotoxicity and Cellular Uptake Studies of BNIPP Derivatives in MDA-MB-231 and MCF-10A Cells

4.1. Cytotoxicity and Cellular Uptake Studies of BNIPP Derivatives in MDA-MB-231 and MCF-10A Cells

The ability of compounds to induce death of cancer cells is one of the first screenings to be carried out in order to elucidate the potential of proposed anti cancer agents.

The aims of the experimental work presented in this chapter were to (i) screen all the BNIPP derivatives for biological activity in breast cancer (MDA-MB-231) and breast epithelial (MCF-10A) cells; (ii) study the cellular uptake and distribution of BNIPSpd, BNIPDaoct, BNIPDaoxoct and BNIPDaCHM in MDA-MB-231 and MCF-10A cells; (iii) investigate a possible mechanism of BNIPP derivative transport into cells, and (iv) determine the effect of BNIPSpd, BNIPDaoct, BNIPDaoxoct and BNIPDaCHM on MDA-MB-231 and MCF-10A intracellular polyamine levels.

4.1.1. Cytotoxicity

Cytotoxic chemotherapy is routinely used in the treatment of early and advanced cancers, including breast cancer (Robson and Verma 2009). Cytotoxic anti cancer agents exert their effect on cancer cells by interfering with the regulatory processes of cell division and proliferation; causing DNA damage, which leads to cell death (Robson and Verma 2009). Thus, the observation of cytotoxic effects provides an initial screen for potential anti cancer agents.

4.1.1.1. Assessment of In Vitro Cytotoxicity

Numerous radioactive and non-radioactive cytotoxicity assays are available to access *in vitro* cell survival and proliferation within mammalian cells. Radioactive assays, including the use of radioisotopes, such as ^{51}Cr, and radiolabelled biochemicals, such as [^{3}H]thymidine, are seldom used nowadays, due to (i) the requirement for highly regulated working environments; (ii) exposure to dangerous radioactive reagents; and (iii) poor radiolabelling of some tumour cells (Nakayama *et al*. 1997, Niu *et al.* 2001). To overcome the problems encountered by radioactive assays, several non-radioactive assays have been developed. Examples include: (i) the reduction of a tetrazolium salt dye, such as MTT, XTT (sodium 2,3-bis(2-methoxy-nitro-5-sulfophenyl)-5-[(phenylamino)-carbonyl]-2H-tetrazolium inner salt), or MTS (3-(4,5-dimethylthiazol-2-yl)-5-(3-carboxymethoxyphenyl)-2-(4-sulfophenyl)-2*H*-tetrazolium inner salt) into their corresponding formazan crystals by intracellular enzymes (Mosmann 1983, Denziot and Lang 1986, Vistica *et al.* 1991, Goodwin *et al.* 1995, Nakayama *et al*. 1997); (ii) the release of intracellular lactate dehydrogenase (LDH) into culture medium by the LDH leakage assay (Fotakis and Timbrell 2006); (iii) the accumulation of neutral red (NR) dye within lysosomes in viable

cells, via the neutral red assay (Valdivieso-Garcia *et al.* 1993, Fotakis and Timbrell 2006); (iv) the reduction of Alamar Blue™ solution which contains resazurin (a fluorescent oxidation-reduction indicator), and is reduced into resurfin by mitochondrial enzymes (Nakayama *et al*. 1997, O'Brien *et al*. 2000, Holst and Oredsson 2005); (v) the incorporation of bromodeoxyuridine (BrdU) into DNA in place of thymidine during DNA replication (Ormerod 1997) or (vi) microscopic staining with Trypan Blue or fluorescent DNA-specific dyes, such as Hoechst 33258 or ethidium bromide (Nakayama *et al*. 1997).

In this study, cytotoxicity was determined using the MTT assay. The MTT assay is one of the most widely used cytotoxicity assays used to investigate a compound's biological activity, due to its simplicity, rapidity, sensitivity and semi-automation, without the use of radioactivity (Mosmann 1983, Denziot and Lang 1986, Twentyman and Luscombe 1987, Pozzolini *et al.* 2003). When added to viable proliferating cells, MTT a yellow, water-soluble, tetrazolium salt dye, is taken up by the cells by endocytosis, and reduced to purple, water-insoluble, formazan crystals, via mitochondrial nicotinamide adenine dinucleotide phosphate (NADH) dependent dehydrogenases (Pozzolini *et al.* 2003, Holst and Oredsson 2005, Fotakis and Timbrel 2006) (Figure 4.1). The reduced insoluble formazan crystals are transported to the cell surface by exocytosis dissolved in a solvent and quantified spectroscopically (Twentyman and Luscombe 1987, Isobe *et al.* 2001). The resultant absorbance value is directly proportional to the number of viable cells (Pozzolini *et al.* 2003, Holst and Oredsson 2005).

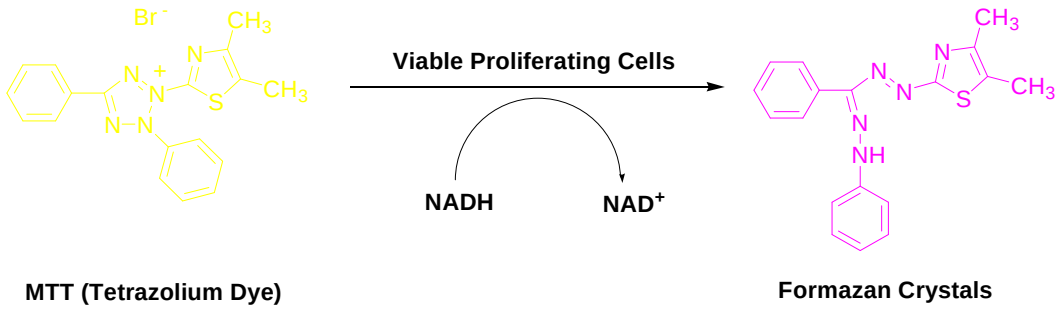

Figure 4.1.: The reduction reaction of yellow MTT tetrazolium salt to purple formazan crystals in viable cells

4.1.2. Cellular Uptake

The uptake of exogenous and endogenous substances into cells can be achieved by several different transport mechanisms. Due to the selectively permeable nature of the plasma membrane; transport of molecules in and out of a cell is achieved in a highly controlled manner. Transport mechanisms include passive diffusion and active transport (Cooper and Hausman 2007). Passive diffusion, the simplest transportation mechanism, allows small polar and non polar molecules (e.g., H_2O, O_2, CO_2 molecules) to diffuse across the membrane down their concentration gradient (Figure 4.2A). In contrast, charged molecules (e.g., H^+, Ca^{2+} or Na^+ ions) or large polar molecules (e.g., glucose)

cannot dissolve across the plasma membrane by passive diffusion and must utilise the mechanism of active transport (Figure 4.2B and 4.2C). Active transport involves the transportation of these latter molecules against their concentration gradient, with the use of an energy source (i.e., from the hydrolysis of Adenosine triphosphate (ATP) (Cooper and Hausman 2007). To further facilitate the uptake of these molecules, specific plasma membrane proteins, which act as transporter systems are utilised. A diverse range of transporter systems are known to exist, and each system transports a molecule across the plasma membrane (Ganapathy *et al.* 2009, Patrick 2009). Examples of these transporter systems include channel proteins or carrier proteins which are responsible for the uptake of ions (e.g., the H^+, Ca^{2+} or Na^+ ions), amino acids (e.g., glutamine or leucine, nucleic acids or polyamines (e.g., putrescine, spermidine or spermine) (Figure 4.2B and C) (Seiler *et al.* 1996, Fuchs and Bode 2005, Cooper and Hausman 2007, Hu *et al.* 2008, Ganapathy *et al.* 2009, Patrick 2009). As a consequence, specific transporter systems have been identified as potential drug targets in the treatment of cancer. Interference with the entry and availability of certain essential nutrients could inhibit the proliferation and differentiation of cancer cells (Gardner *et al.* 2004, Ganapathy *et al.* 2009).

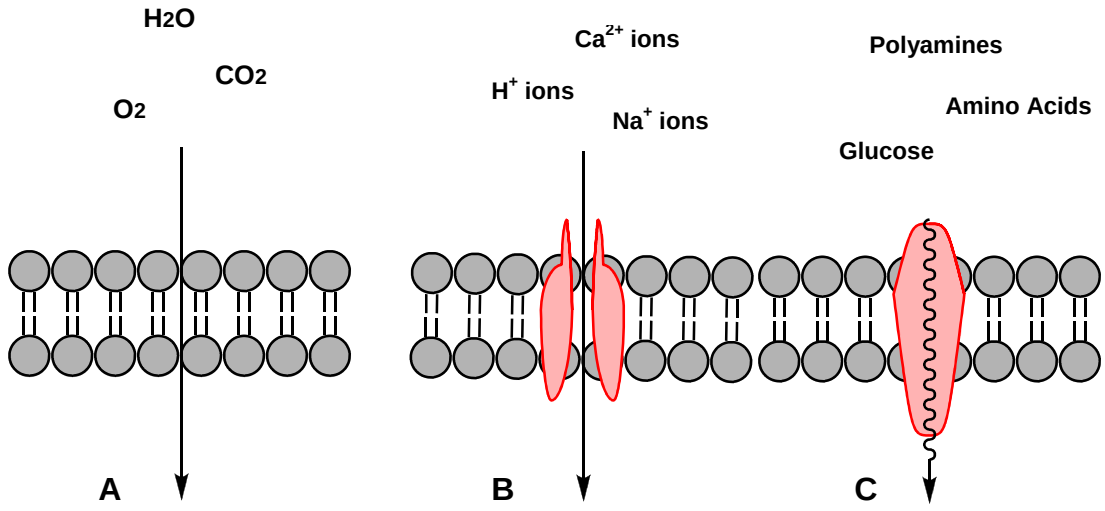

Figure 4.2.: The selective permeability of the plasma membrane. **A** represents passive diffusion, **B** (an ion channel protein) and **C** (a carrier protein) both represent active transport (adapted from Cooper and Hausman 2007, pp. 65)

4.1.2.1. Polyamine Transporter

One example of active transport and of particular interest for this study is the polyamine transporter. Polyamines (Putrescine, Spermidine and Spermine) are present within all prokaryotic and eukaryotic cells, and are essential for normal growth, proliferation, and protein synthesis (Thomas and Thomas 2001, Ah Byun *et al.* 2009) (Section 1.4). These charged nitrogen bearing polycation chains can be sourced endogenously through the highly regulated biosynthetic pathway, or sourced exogenously by active gut uptake from diet (from cheese, fruit or vegetables), and/or adsorption by

intestinal flora (Seiler *et al.* 1990, Milovic *et al.* 2001, Thomas and Thomas 2001, Larqué *et al.* 2007). Exogenous polyamines are taken up by specific cells using a highly regulated, energy-dependent polyamine transporter (PAT) system, as mentioned previously in Section 4.1.2 (Seiler *et al.* 1996, Graminski *et al*. 2002, Mitchell *et al.* 2007). It has been shown that rapidly dividing cells, for example colon, lung and breast cancer cells, contain an activated PAT system, and higher levels of polyamines compared to that of the corresponding non-cancerous cells (Seiler *et al.* 1996, Cullis *et al.* 1999, Wallace *et al*. 2000, Gardner *et al.* 2004, Kaur *et al.* 2005, Tsen *et al.* 2008, Ah Byun *et al.* 2009).

Due to the structural tolerances of the PAT, various synthetic polyamine-like derivatives and analogues, such as anthracen-9-ylmethyl-4,4-triamine trihydrochloride or anthracen-9-ylmethyl-4,4-tetraamine tetrahydrochloride (Figure 4.3), can be imported into cells, via the PAT system (Wang *et al.* 2003a, Gaboriau *et al.* 2004, Gardner *et al*. 2004). For that reason, the BNIPP derivatives studied in this work may utilise the PAT system for their cellular uptake in a similar way to that of other polyamine-like derivatives (Gardner *et al*. 2004, Kaur *et al.* 2008a). In support of the BNIPP derivatives potential use of the energy-dependent PAT system, it was found that incubation at 4 °C notably reduced the uptake of BNIPP derivatives in breast cancer (MCF-7) cells, as determined by reduced fluorescence (Seiler *et al.* 1996, Dance *et al*. 2005, Ralton 2006, Kimura *et al.* 2009). Hence, the PAT represents a potential target for the enhanced uptake of anti cancer drugs (Gardner *et al.* 2004, Tsen *et al*. 2008).

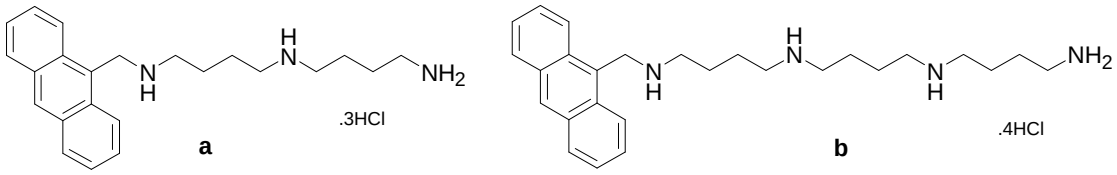

Figure 4.3.: Structures of **a:** Anthracen-9-ylmethyl-4, 4-triamine, trihydrochloride and **b:** Anthracen-9-ylmethyl-4, 4-tetraamine, tetrahydrochloride

Wang and colleagues (2003a, 2003b, 2003c) have identified a useful cellular model, which can be used to determine the selective delivery and entry of non-native polyamine-like derivatives, via the PAT (Mandel and Flintoff 1978, Heaton and Flintoff 1988). This model relies upon the comparative cytotoxicity of polyamine-like derivatives in two Chinese Hamster Ovary (CHO) cell lines. The parental CHO cells have an active PAT (PAT-active), and the CHO-MG cells; isolated after single-step selection for growth resistance to Methylglyoxalbis (guanylhydrazone) (MGBG) (Figure 4.4), represent cells with a mutant PAT, and are thus classified as PAT-inactive (Mandel and Flintoff 1978, Heaton and Flintoff 1988). MGBG growth resistance in the CHO-MG cells was exploited given that MGBG is a known substrate for the PAT system, and an inhibitor of polyamine biosynthesis (e.g., SAMDC inhibition) and mitochondrial function (Mandel and Flintoff

1978, Von Hoff 1994, Ekelund *et al.* 2001, Wang *et al.* 2003c, Casero and Marton 2007). The CHO-MG cells can also provide a delivery system which is independent of the MGBG-specific PAT (Wang *et al.* 2003a, Wang *et al*. 2003b, Wang *et al*. 2003c, Gardner *et al.* 2004, Tsen *et al.* 2008).

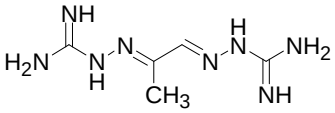

Figure 4.4.: Structure of Methylglyoxalbis (guanylhydrazone) (MGBG)

4.1.3. Intracellular Polyamine Levels

Intracellular polyamine levels have been shown to regulate the rate of cell growth and proliferation (Khuhawar and Qureshi 2001, Thomas and Thomas 2001). Excessive cell growth has been related to high levels of intracellular polyamines, and associated with diseases of uncontrolled cell proliferation, such as cancer, including breast and colon cancers (Pegg 1988, Seiler *et al.* 1996, Wallace *et al.* 2000, Gardner *et al.* 2004, Kaur *et al.* 2005, Tsen *et al.* 2008, Ah Byun *et al.* 2009). In contrast, an inhibition of cell growth has been linked to a decrease in intracellular polyamine levels (Russell 1983, Pegg 1988, Davidson *et al*. 1999). For that reason, depletion of intracellular polyamine levels by cytotoxic derivatives represents a potential target for the inhibition of cancerous cell growth (Graminski *et al.* 2002).

4.1.3.1. Assessment of Intracellular Polyamine Levels

Several biological and chemical methods have been utilised for the detection of intracellular levels of polyamines within plant or animal tissues and, body fluids (Seiler 1977). Biological methods, including enzymatic and immunological methods are seldom used in polyamine detection because they (i) cannot discriminate between spermidine and spermine, and (ii) cannot be automated (Seiler 1977). Chemical methods, including paper chromatography, thin layer chromatography (TLC), paper electrophoresis and high performance liquid chromatography (HPLC) can all be successfully utilised for polyamine determination (Seiler 1977, Marcé *et al.* 1995, Khuhawar and Qureshi 2001). Gas chromatography (GC) has also been used to analyse polyamines, though mainly within foodstuffs (Rogers *et al.* 2003). However, GC is not routinely used for the analysis of body fluids or cancer cells, due to difficulties regularly encountered during sample derivatisation, purification, and separation (Larqué *et al.* 2007). In addition to the above techniques, capillary zone electrophoresis (CZE) and flow injection analysis (FIA) coupled with mass spectrometry (MS) have also gained some importance in the analysis of polyamine levels within serum samples. Although these techniques showed increased detection sensitivity, the overall practicalities of their use for routine polyamine analysis

require further investigation (Khuhawar and Qureshi 2001, Gaboriau *et al.* 2003, Gugliucci 2004).

HPLC, a simple, sensitive and rapid analytical technique, remains the technique of choice for polyamine detection (Smith and Davies 1985, Marcé *et al.* 1995, Teti *et al.* 2002, Gugliucci 2004). Polyamines are positively charged molecules, which must undergo either pre- or post-column derivatisation before they can be sensitively separated and detected by UV absorbance or fluorescence (Marcé *et al* 1995). Pre-column derivatisation with dansyl chloride (5-(dimethylamino) naphthalene-1-sulfonyl chloride) (Figure 4.5) has been successfully utilised to separate and quantify the intracellular levels of putrescine, spermidine and spermine. Dansyl chloride reacts with primary and secondary amines, resulting in the formation of fluorescent di-, tri- and tetra- dansylated polyamine derivatives from putrescine, spermidine and spermine, respectively (Khuhawar and Qureshi 2001). These dansylated derivatives are highly fluorescent and can be separated by reverse-phase HPLC (Kabra *et al* 1986).

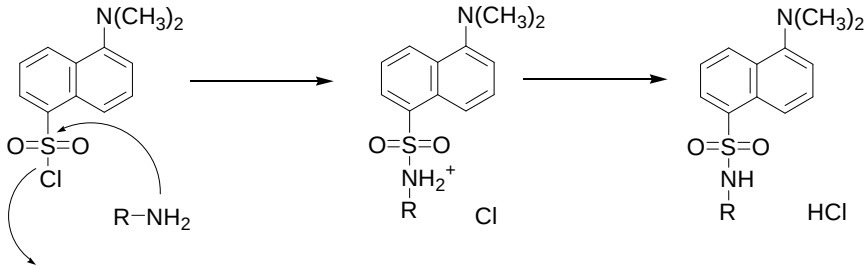

Figure 4.5.: Derivatisation reaction of polyamines (R) with dansyl chloride

4.2. Materials

4.2.1. Materials

All reagents were purchased from Fisher Scientific, UK, unless otherwise stated, and were used without purification.

Choleratoxin	List Biological Laboratories. Inc, USA
Dansyl Chloride	Fluka, UK
Difluoromethylornithine	Sigma-Aldrich, UK
Dimethyl Sulfoxide	Aldrich, UK
DMEM/F12 medium	Lonza, Belgium
Doxorubicin	Sigma-Aldrich, UK
Epidermal Growth Factor	Invitrogen, UK
Etoposide	Sigma-Aldrich, UK
Foetal Calf Serum	Biosera, UK
Horse Serum	Sigma-Aldrich, UK
Human Insulin	Sigma-Aldrich, UK
Hydrocortisone	Sigma-Aldrich, UK
Methylthiazolyldiphenyl-tetrazolium bromide	Sigma-Aldrich, UK
Penicillin/Streptomycin	Invitrogen, UK
Phosphate Buffered Saline	Sigma-Aldrich, UK
RPMI-1640 medium	Gibco, UK
Trypsin-EDTA	Sigma-Aldrich, UK

4.2.2. Instrumentation

Aseptic cell culture techniques were undertaken within a HERASafe Class II Safety Cabinet (Thermo Electron Corporation, Germany). All cell culture plastics were sterile certified and tips were sterilised before use in a Boxer Autoclave (Boxer Lab Equipment, UK). Cells were incubated at 37 °C, in a humidified 5% CO_2 atmosphere within a HERACell Incubator (Heraeus, Germany), and were counted using an improved Neubauer Haemocytometer (Assitent, Germany).

Light and fluorescence microscopy experiments were visualised using a Leica DMIL inverted light microscope (Leica Microsystems, UK) or a Leica DMIL inverted fluorescence microscope (Leica Microsystems, UK) using a UV filter (excitation bandpass (ultraviolet); 340 – 380 nm, emission longpass (blue); 425 nm). Microscopy images were captured using a Leica DC 200 camera (Leica Microsystems, UK) and, viewed using Infranview 3.91 software (Leica Microsystems, UK).

For MTT Assay analysis, a 96 well plate reader (MRX II, Dynex Technologies, USA) was utilised.

Pre-column derivatisation was undertaken using an activated Solid Phase Extraction (SPE) column (Strata C18-E, 100 mg/mL, Phenomenex, UK), attached to a VacMaster-10 (Sopachem, Belgium). HPLC was performed using an Adsorbosphere HS C18 5U, 250 mm x 4.6 mm HPLC column (Adsorbosphere, UK) on a Spectra-Physics SP8700 solvent delivery system with a SP8750 HPLC pump. A Shimadzu RF-535 Fluorescence HPLC monitor was used to detect dansyl fluorescence with excitation and emission filters set at 340 nm and 514 nm, respectively. Results were visualised using a Spectra Physics SP4270 integrator.

4.3. Methods

4.3.1. Cell Lines

4.3.1.1. MDA-MB-231 Cells

Human breast epithelial cancer MDA-MB-231 cells were purchased from the European Collection of Cell Cultures (ECACC) (ECACC; 92020424). MDA-MB-231 cells are metastatic cells, isolated from a pleural effusion of a breast cancer patient (Belkacemi *et al*. 2006). These cells are estrogen receptor-negative, and with a mutant p53 tumour suppressor protein (Koutsilieris *et al*. 1999, Belkacemi *et al*. 2006). MDA-MB-231 cells were maintained in Roswell Park Memorial Institute 1640 medium (RPMI-1640) (containing GlutaMAX™-1 with 25 mM HEPES) (Langdon. 2004) supplemented with 10 % (v/v) Foetal Calf Serum (FCS) and, 1 % Penicillin (100 U/mL)/Streptomycin (100 µg/mL).

4.3.1.2. MCF-10A Cells

Human breast epithelial MCF-10A cells were purchased from the American Tissue Culture Collection (ATCC) (ATCC; CRL-10317). MCF-10A cells are non-tumourigenic cells, derived from the mammary tissue of a fibrocystic disease patient, and were used as the normal cell control in breast cancer studies (Soule *et al.* 1990, Zientek-Targosz *et al.* 2008). These cells are also estrogen receptor-negative (Debnath *et al.* 2003). MCF-10A cells were maintained in Dulbecco's Modified Eagle/Nutrient Mixture F-12 (DMEM/F12) medium supplemented with 5 % (v/v) Horse Serum (HS), Human Insulin (10 µg/mL), Hydrocortisone (0.5 µg/mL), Epidermal Growth Factor (EGF) (20 ng/mL), Choleratoxin (100 ng/mL) and, Penicillin (100 U/mL) / Streptomycin (100 µg/mL). MCF-10A cells were cultured from passage number 103 to 123, due to the increased instability and short lifespan of epithelial cells.

4.3.1.3. CHO and CHO-MG Cells

Two Chinese Hamster Ovary (CHO) cell lines: the parental CHO cells with an active polyamine transporter, and the polyamine-transport deficient mutant cell line, CHO-MG, were kindly donated by Professor Wayne Flintoff, from the University of Western Ontario, Canada (Mandel and Flintoff 1978). CHO and CHO-MG cells were maintained in RPMI 1640 medium (containing L-Glutamine with no Phenol Red) supplemented with 10 % (v/v) FCS and, 0.5 % (v/v) Penicillin (100 U/mL) / Streptomycin (100 µg/mL).

4.3.2. Maintenance of Cell Lines

Cells were incubated at 37 °C, in a humidified 5% CO_2 atmosphere. MDA-MB-231, MCF-10A, CHO and CHO-MG cells were grown in 75 cm^2 tissue culture flasks and sub cultured once 80% confluence was reached. Cells were washed twice with Phosphate Buffered Saline (PBS) and detached with Trypsin-EDTA (1 x in PBS) solution. All cells were counted using an improved Neubauer Haemocytometer.

For experimental analysis, exponentially growing MDA-MB-231 and MCF-10A cells were plated at a density of 1 x 10^4 cells (96 well plate), 8 x 10^4 cells (24 well plate), 4 x 10^5 cells (6 well plate) or 1 x 10^6 cells (25 cm^2 culture flask). CHO and CHO-MG cells were plated at a density of 1 x 10^4 cells (96 well plate). Cells were cultured for 24 hours before incubation with the BNIPP derivatives.

4.3.3. Preparation of BNIPP Derivatives

BNIPP derivatives were synthesised as previously described in Section 2.3, and stored in stock (10 mM or 90 mM) solutions, at 0 – 5 °C until required (refer to Section 3.3.1). Stock solutions of the positive controls: etoposide and doxorubicin (10 mM) in 50 % DMSO were also prepared, and stored at 0 – 5 °C. Prior to use, all stock solutions were diluted to the desired final concentrations with serum free medium (either RPMI 1640 or DMEM/F12).

4.3.4 . Light Microscopy

MDA-MB-231 and MCF-10A (8 x 10^4 cell/well) cells were incubated with BNIPSpd, BNIPDaoct, BNIPDaoxoct or BNIPDaCHM (5 – 10 µM; 500 µL/well; 0.5 – 24 hours, at 37 °C) within 24 well plates and visualised using a Leica DMIL inverted light microscope, as described in Section 4.2.2.

4.3.5. Fluorescence Microscopy

MDA-MB-231 and MCF-10A (8 x 10^4 cells/well) cells were incubated with BNIPSpd, BNIPDaoct, BNIPDaoxoct or BNIPDaCHM (5 - 10 µM; 500 µL/well; 0.5 – 24 hours, at 37 °C) within 24 well plates. After the desired incubation time, the cell culture medium containing the excess BNIPP derivatives was removed, and the cells washed twice with PBS. 1 mL PBS was then added to each well. Cells were visualised using a Leica DMIL inverted fluorescence microscope, as described in Section 4.2.2.

4.3.6. Cytotoxicity

4.3.6.1. Colorimetric 3-(4, 5-dimethylthiazol-2-yl)-2, 5-diphenyl tetrazolium bromide (MTT) Assay

MDA-MB-231 and MCF-10A (1 x 10^4 cells/well) cells were seeded in 96 well plates. After 24 hours, the BNIPP derivatives, etoposide or doxorubicin (100 µL/well; 24 – 72 hours) were added to each well to give a final concentration of 0.01, 0.1, 1, 5, 10, 15, 20 and 40 µM. The latter two compounds were used as positive controls (0.01 – 40 µM). After the desired incubation time (24 – 72 hours), the cell culture medium was removed and 100 µL of sterile-filtered (0.22 µM filter) MTT solution (1 mg/mL in serum free medium) was added to each well (Rollino *et al.* 1995). The plates were incubated for 4 hours, at 37 °C. The MTT solution was carefully removed and DMSO (200 µL) was added to each well. The addition of DMSO allows the dissolution of the metabolised MTT product. The plates were shaken for 20 minutes, at room temperature and the absorbance results quantified by measuring at 560 nm on a 96 well plate reader, as described in Section 4.2.2.

The mean absorbance values for cells treated with different concentrations (0 – 40 µM) of BNIPP derivatives was expressed as % absorbance of cells treated with distilled water (0.025% dH_2O control cells). Control cells were equal to 100%, as no growth inhibition was present. IC_{50} (Inhibitory Concentration) was defined as the derivative concentration that causes 50% growth inhibition of the cell population compared to that of control cells.

4.3.6.2. Polyamine Transporter Studies

CHO and CHO-MG (1 x 10^4 cells/well) cells were incubated with BNIPSpd, BNIPDaoct, BNIPDaoxoct, BNIPDaCHM or MGBG (0-100 µM; for 48 hours) in 96-well plates. The latter was used as a positive control. After 48 hours incubation, at 37 °C, cell viability was determined using the MTT assay, as described in Section 4.3.6.1.

4.3.7. Polyamine Extraction

MDA-MB-231 and MCF-10A (1 x 10^6/25 cm^2 flask) cells were incubated with BNIPSpd, BNIPDaoct, BNIPDaoxoct, BNIPDaCHM (0-5 µM) or α-(Difluoromethyl) ornithine (DFMO) (5 mM). The latter was used as a positive control as it is a selective enzyme-activated inhibitor of Ornithine Decarboxylase (ODC); the first rate limiting enzyme in the polyamine biosynthetic pathway.

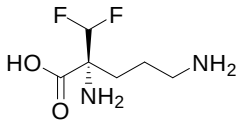

Figure 4.6.: Structure of DFMO

After 24 hours incubation, cells were harvested as described previously (Section 4.3.2) and centrifuged at 2500 rpm (Centaur 2, UK), for 5 minutes, at room temperature. Cells were resuspended in PBS (10 mL) before counting, using an improved Neubauer haemocytometer. Cells were centrifuged again at 2500 rpm (Centaur 2, UK) for 5 minutes and, resuspended in 1 mL PBS. The cell suspension was transferred to a sterile eppendorf and centrifuged at 8500 rpm (ALC Multispeed Refrigerated Centrifuge, Thomson Scientific, UK), for 5 minutes, at 4 °C. The cell pellet was resuspended in 250 µL 10% Perchloric Acid and incubated on ice for 60 minutes, mixing once after 30 minutes. Cells were centrifuged at 12000 rpm (ALC Multispeed Refrigerated Centrifuge, Thomson Scientific, UK), for 20 minutes, at 4 °C. The supernatant containing the polyamine extract was transferred to a fresh sterile Eppendorf tube and stored at -20 °C until required.

4.3.8. HPLC of Polyamines

4.3.8.1. Quantification of Polyamines as Dansyl Derivatives

The pre-column derivatisation method of dansyl derivatives was based on the methods of Kabra *et al* (1986) and Marcé *et al* (1995).

4.3.8.2. Pre-column Derivatisation

In a sterile Eppendorf tube, 200 µL saturated sodium carbonate (7 g/100 mL distilled water), 200 µL dansyl chloride (0.03 g/10 mL acetone, made fresh each day and protected from light) and 50 µL polyamine extract or polyamine standard (in 0.1 M Hydrochloric Acid) were added together. The solution was vortexed for 15 seconds and incubated in the dark for 10 minutes, at 70 °C. The solution was allowed to cool to room temperature before transferring to an activated SPE column (refer to Section 4.2.2). During sample incubation, the SPE column was attached to a VacMaster-10 which was activated with 2 column volumes of methanol (HPLC grade) followed by 2 column volumes of deionised water. Once cooled, the polyamine solution was transferred to the activated SPE column where the liquid was allowed to run through. The column was washed with 2 column volumes of deionised water and the dansylated polyamines eluted with 450 µL methanol.

4.3.8.3. HPLC Analysis

A 20 µL aliquot of the elutant was injected onto the HPLC system, as described in Section 4.2.2. The gradient used is shown in Table 4.1.

Table 4.1.: The HPLC mobile-phase gradient used in dansylated polyamine analysis [a]

Time (mins)	Acetonitrile (%)	H_2O (%)
0	70	30
4	70	30
5	100	0
9	100	0
10	70	30
15	70	30

[a]Acetonitrile (HPLC grade) and water concentration in the mobile phase, expressed as a percent (%) and time, expressed in minutes (mins). The flow rate was 1.5 mL/minute (based on Marce *et al* 1995) (Attenuation 512; PT 2000).

Polyamines were separated and analysed in the order of Putrescine (Put), Spermidine (Spd) and Spermine (Spm) with retention times of 6.1, 8.8 and 9.7 minutes respectively. Figure 4.7 shows a typical chromatogram obtained from the HPLC separation of polyamine standards, Figure 4.8 shows a typical chromatogram of untreated MDA-MB-231 cell extract, whilst Figure 4.9 shows a typical chromatogram of BNIPSpd (5 µM; 24 hours) treated MDA-MB-231 cell extract.

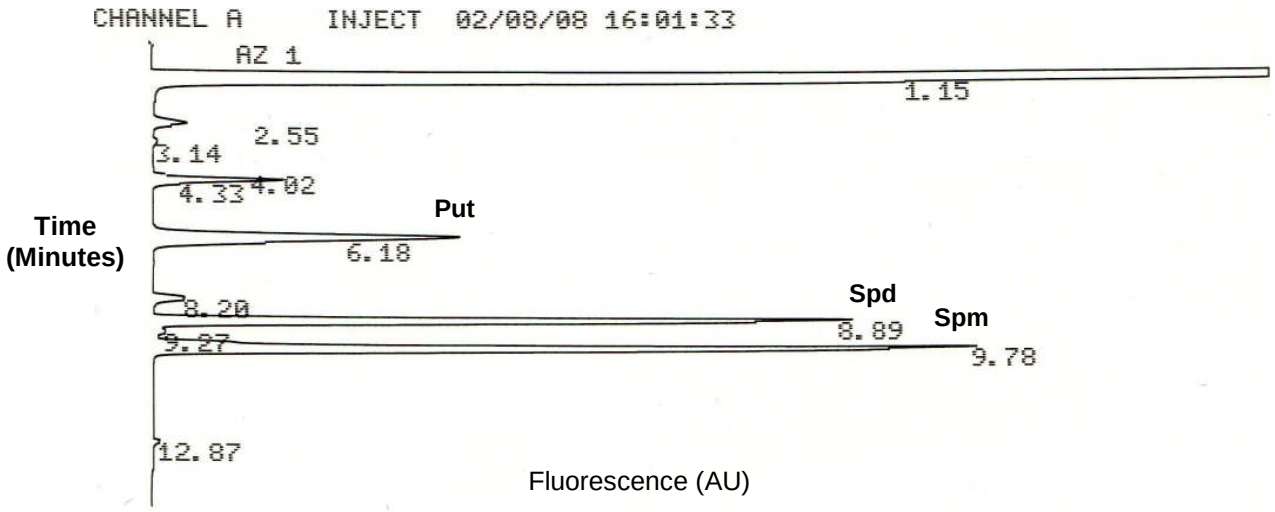

Figure 4.7.: HPLC chromatogram of polyamines standards (Putrescine; Put, Spermidine; Spd and Spermine; Spm). Polyamine standards (in 0.1 M Hydrochloric Acid) were derivatised using dansyl chloride then separated and detected (Ex 340 nm; Em 514 nm) using reverse-phase HPLC (Sections 4.37 and 4.38).

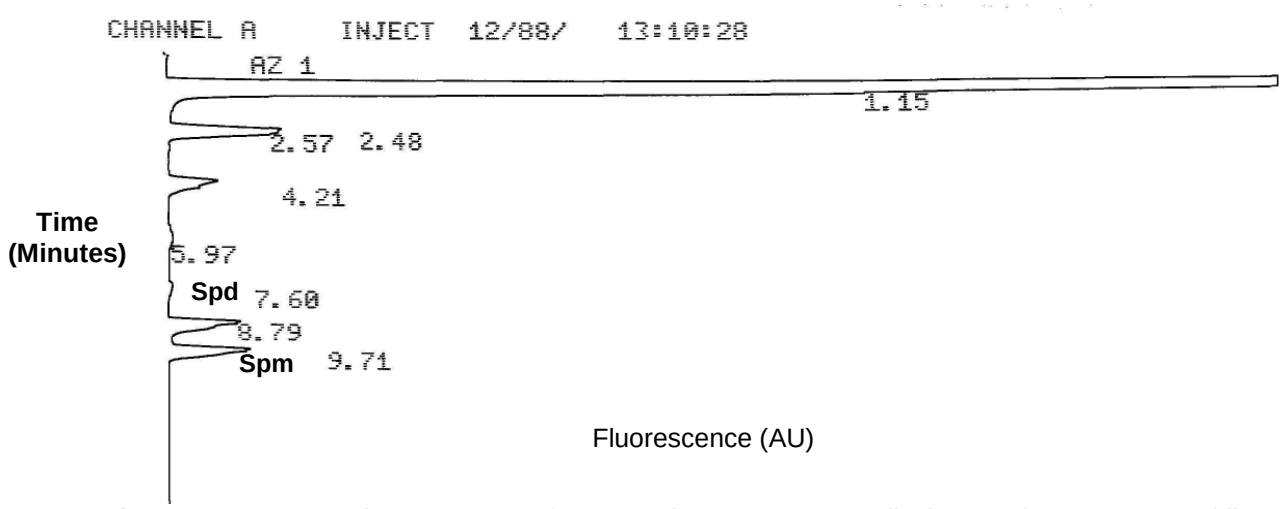

Figure 4.8.: HPLC chromatogram of untreated MDA-MB-231 cells (Putrescine; Put, Spermidine; Spd and Spermine; Spm). Polyamine standards (in 0.1 M Hydrochloric Acid) were derivatised using dansyl chloride then separated and detected (Ex 340 nm; Em 514 nm) using reverse-phase HPLC (Sections 4.37 and 4.38).

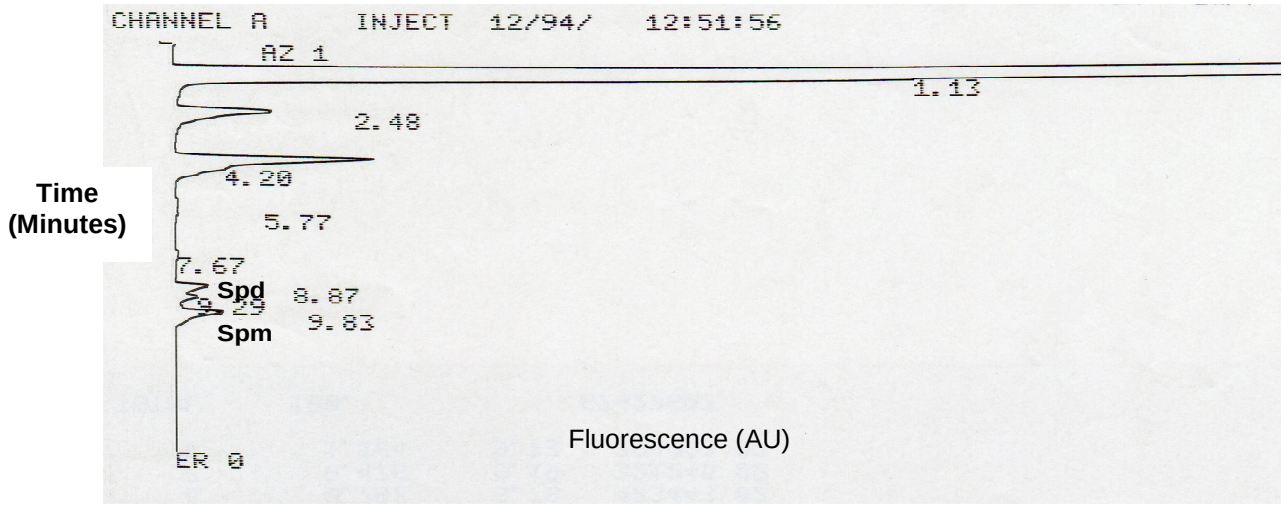

Figure 4.9.: HPLC chromatogram of BNIPP derivative (BNIPSpd; 5 µM) treated MDA-MB-231 cells (Putrescine; Put, Spermidine; Spd and Spermine; Spm). Polyamine standards (in 0.1 M Hydrochloric Acid) were derivatised using dansyl chloride then separated and detected (Ex 340 nm; Em 514 nm) using reverse-phase HPLC (Sections 4.37 and 4.38).

Intracellular polyamine levels in treated MDA-MB-231 and MCF-10A cells were determined using equations from standard curves of polyamine concentration (1 – 50 µM in 0.1 M Hydrochloric Acid) against peak area, as found in Appendix 5 (Figure A.7 – A.9). Appendix 5 shows that the calibration was useable up to 1 µM, however, a limit of detection was not detected as it was not necessary in this study. Intracellular polyamine levels in treated MDA-MB-231 and MCF-10A cells are expressed as µM/1 x 10^6 cells.

4.3.9. Data Analysis

Unless otherwise stated, each data set expressed as mean ± SD was the average of a minimum of three independent experiments. Each experiment comprised at least three internal replicates. Statistical analysis was conducted using the Student's *t*-test. Data were considered significantly different when *P*-value < 0.05 (*P < 0.05, **P < 0.01 and ***P < 0.001).

4.4. Results

4.4.1. Effect of BNIPP Derivatives on Cell Morphology

A qualitative assessment of the changes in cell morphology was assessed in MDA-MB-231 and MCF-10A cells treated with BNIPSpd, BNIPDaoct, BNIPDaoxoct and BNIPDaCHM, at 0.1 - 10 µM, for 24 hours using light microscopy.

4.4.1.1. Cell Morphology Changes in MDA-MB-231 Cells

Changes were observed in BNIPP derivative treated MDA-MB-231 cells after 24 hours compared to untreated cells (Figures 4.10 and 4.11). Cell shape altered in a dose dependent manner in MDA-MB-231 cells treated with 0.1 – 10 µM BNIPDaCHM (Figure 4.10). BNIPSpd, BNIPDaoct and BNIPDaoxoct (0.1 – 10 µM) produced similar results to BNIPDaCHM after 24 hours (data not shown). Figure 4.11 shows untreated MDA-MB-231 cells and MDA-MB-231 cells treated with 10 µM BNIPSpd, BNIPDaoct or BNIPDaoxoct for 24 hours. After 24 hours, cell shape of BNIPP derivative treated MDA-MB-231 cells had notably changed in comparison to untreated MDA-MB-231 cells, as treated MDA-MB-231 cells appeared smaller and rounder and had become detached from the culture plate (Figure 4.11).

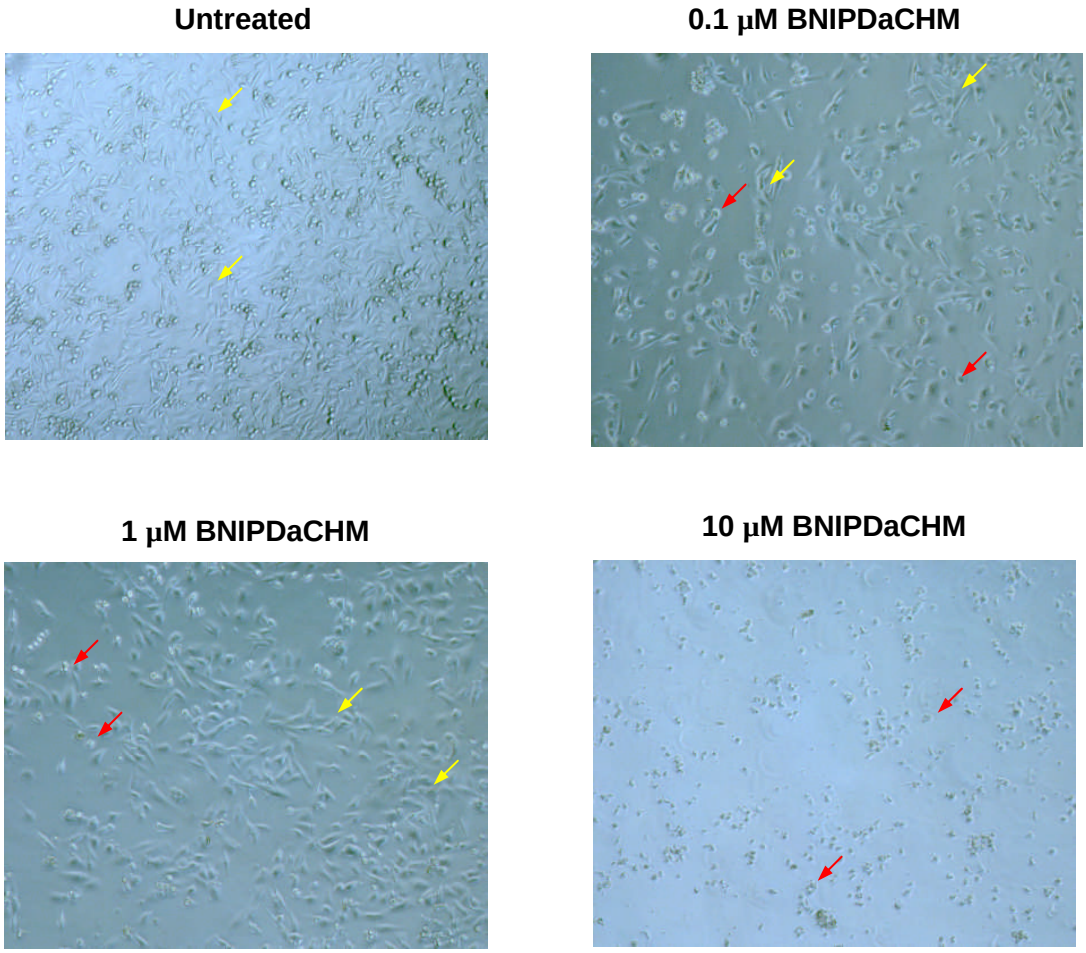

Figure 4.10.: Cell morphology of MDA-MB-231 cells treated with 0 – 10 µM BNIPDaCHM for 24 hours. Cells were visualised using a Leica DMIL inverted light microscope. Images are representative of 3 independent experiments, each comprising of 3 replicates (n =3). Key: viable cells, yellow arrow; rounded cells, red arrow. Magnification x 100.

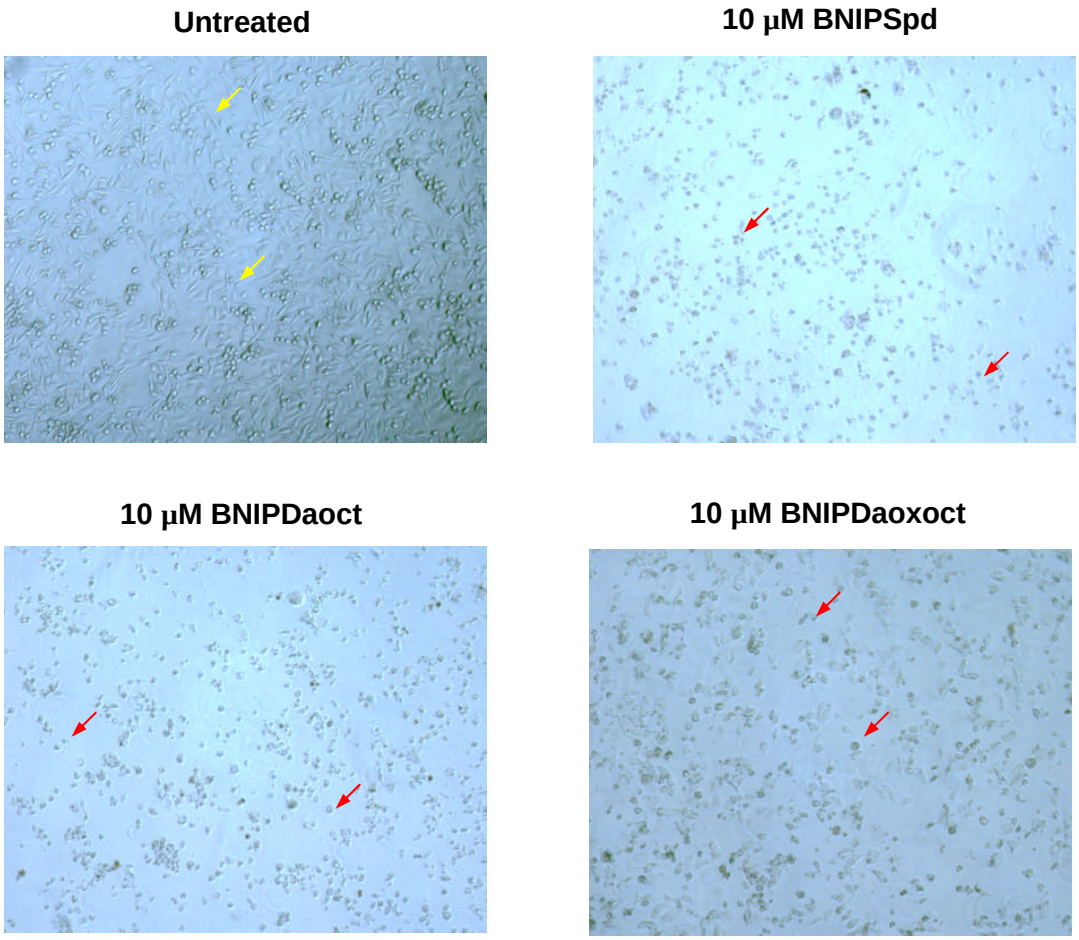

Figure 4.11.: Cell morphology of untreated MDA-MB-231 and BNIPP derivative treated MDA-MB-231 cells (10 μM BNIPSpd, BNIPDaoct and BNIPDaoxoct) for 24 hours. Cells were visualised using a Leica DMIL inverted light microscope. Images are representative of 3 independent experiments, each comprising of 3 replicates (n = 3). Key: viable cells, yellow arrow; rounded cells, red arrow. Magnification x 100.

4.4.1.2. Cell Morphology Changes in MCF-10A Cells

Changes were also observed in BNIPP derivative treated MCF-10A cells after 24 hours compared to untreated cells (Figure 4.12). Changes in MCF-10A cells treated with 10 µM of BNIPSpd, BNIPDaoct, BNIPDaoxoct or BNIPDaCHM included a change to cell shape, in comparison to untreated MCF-10A cells, in particular, after treatment with BNIPDaoct (10 µM; 24 hours).

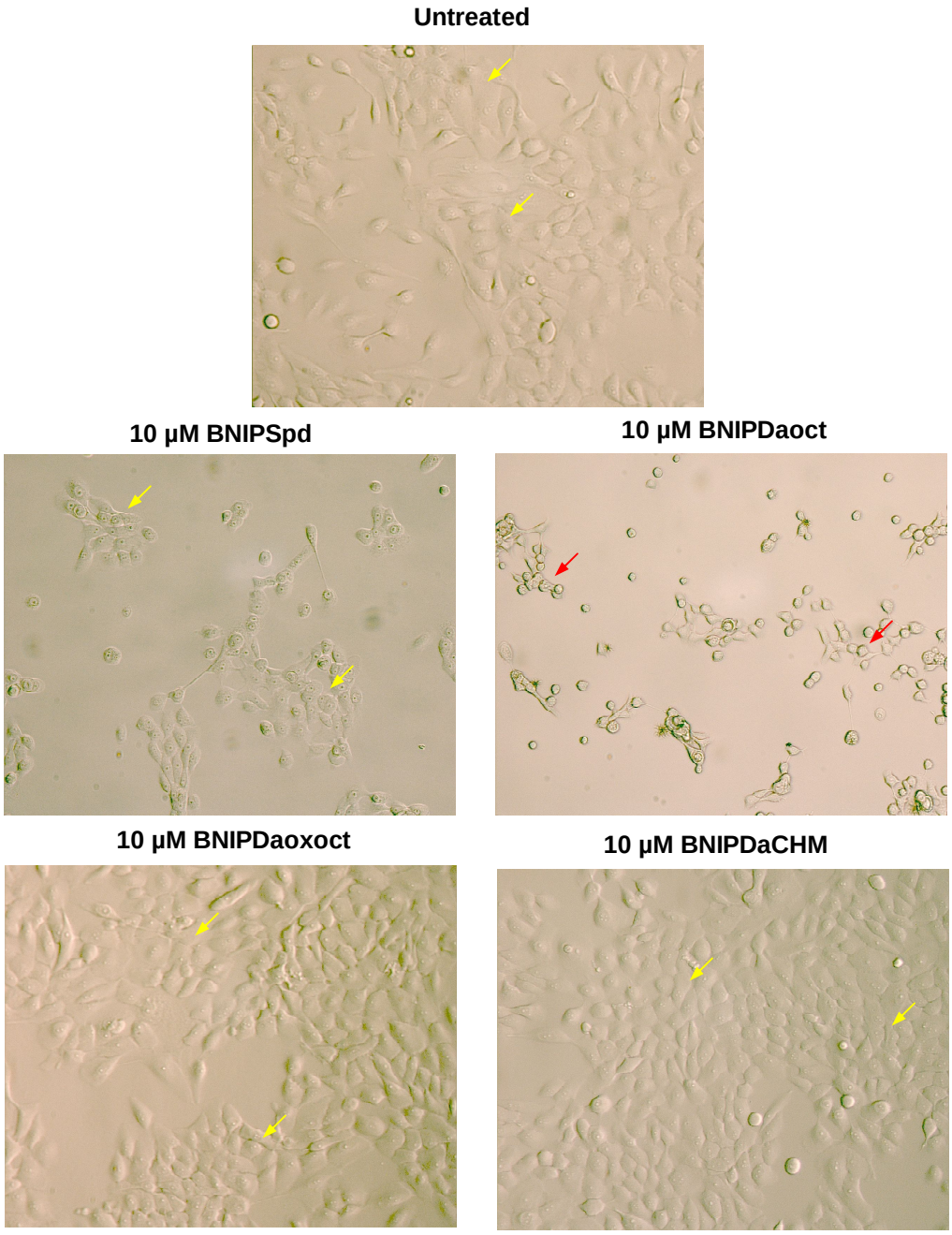

Figure 4.12.: Cell Morphology of untreated MCF-10A and BNIPP derivative treated MCF-10A cells (10 µM BNIPDaCHM, BNIPSpd, BNIPDaoct and BNIPDaoxoct) for 24 hours. Cells were visualised using a Leica DMIL inverted light microscope. Images are representative of 3 independent experiments, each comprising of 3 replicates (n = 3). Key: viable cells, yellow arrow; rounded cells, red arrow. Magnification x 200.

4.4.2. Cytotoxicity in MDA-MB-231 and MCF-10A Cells

Cell viability of MDA-MB-231 and MCF-10A cells treated with different concentrations (0 – 40 µM) of each BNIPP derivative for 24, 48 or 72 hours were assessed by MTT assay.

The curves presented in Figures 4.13 and 4.14 are a representation of the percentage of growth inhibition in MDA-MB-231 cells treated with BNIPSpd (Figure 4.12) or BPHPDadec (Figure 4.13) (0 – 40 µM) after 24 and 48 hours obtained by measuring reduction of MTT tetrazolium dye.

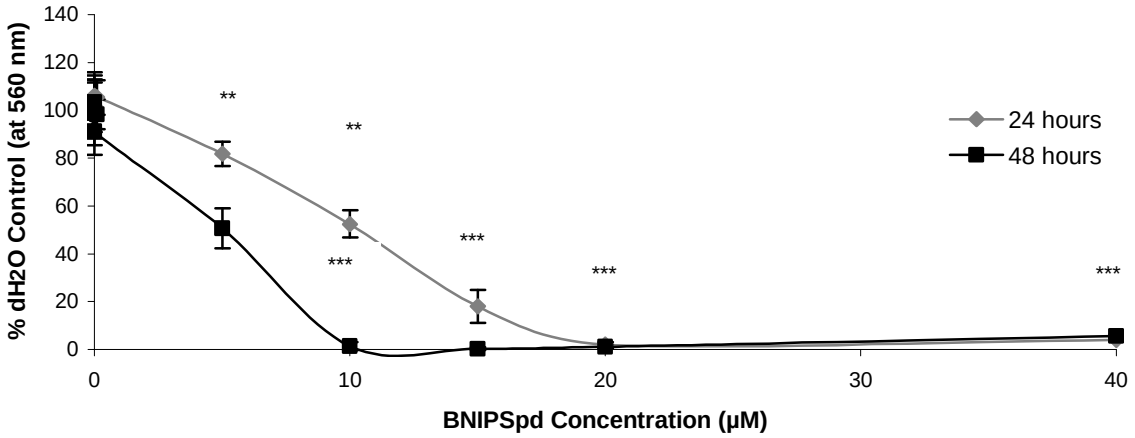

Figure 4.13.: The growth inhibition curve of BNIPSpd in MDA-MB-231 cells after 24 and 48 hours. Cytotoxicity was determined by MTT Assay. Data are mean ± SD of 3 independent experiments (n = 3) each experiment consisted of 6 repeats. The curves are representative of all BNIPP derivatives analysed within MDA-MB-231 and MCF-10A cells. **P < 0.01 and ***P < 0.001 vs. untreated (H_2O control) cells.

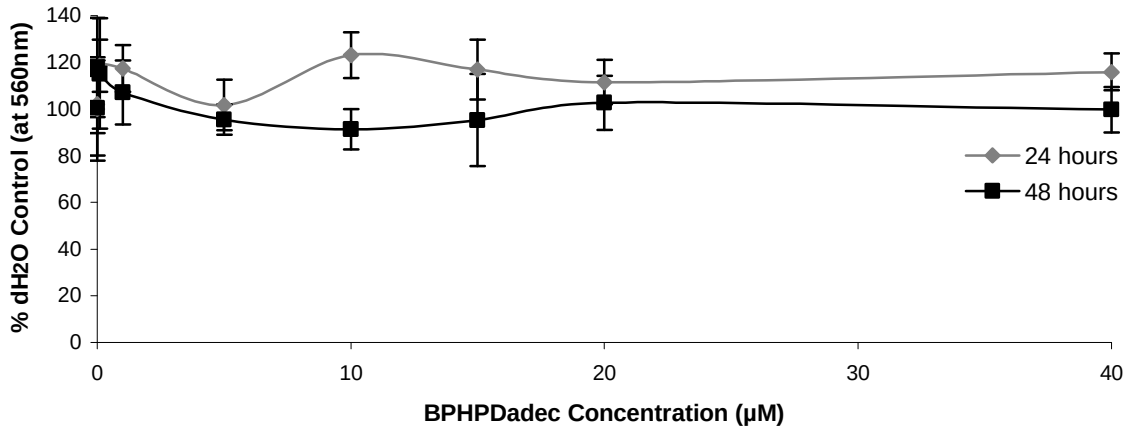

Figure 4.14.: The growth inhibition curve of BPHPDadec in MDA-MB-231 cells after 24 and 48 hours. Cytotoxicity was determined by MTT Assay. Data are mean ± SD of 3 independent experiments (n = 3) each experiment consisted of 6 repeats. The curves are representative of all BNIPP derivatives analysed within MDA-MB-231 and MCF-10A cells.

After 24 hours, BNIPSpd significantly inhibited cell viability (P < 0.01; 47.5% decrease) at 10 µM when compared to the control; with complete MDA-MB-231 cell death at ≥ 20 µM (Figure 4.13). After 48 hours, BNIPSpd significantly inhibited cell viability (P <

0.01; 49.3% decrease) at 5 µM compared to the control; with complete death of MDA-MB-231 cells observed at ≥ 10 µM (Figure 4.13). In contrast, treatment with BPHPDadec (Figure 4.14) resulted in no growth inhibition in MDA-MB-231 cells after 24 or 48 hours (IC_{50} values > 40 µM in both cell lines).

The cytotoxicities of the newly synthesised BNIPP derivatives: BNIPDaoxoct, BNIPDaCHM, BPHPDadec and NPA (Figure 2.1) were compared with the previously synthesised BNIPP derivatives: BNIPSpd, BNIPPut, BNIPDahex, BNIPDaoct, BNIPDadec and BNIPDadodec (Figure 3.4) in MDA-MB-231 and MCF-10A cells. Cytotoxicity results are shown in Tables 4.2 and 4.3.

Table 4.2.: Cytotoxicity of BNIPP derivatives in MDA-MB-231 cells

	IC_{50}[b] (µM)		
Derivative[a]	**24 hrs**	**48 hrs**	**72 hrs**
BNIPSpd	12.7 ± 0.5	4.6 ± 1.5	ND
BNIPPut	7.8 ± 3.6	5.1 ± 0.8	ND
BNIPDahex	7.2 ± 1.4	4.5 ± 0.6	ND
BNIPDaoct	5.0 ± 1.3	2.7 ± 0.3	ND
BNIPDadec	4.8 ± 0.2	3.3 ± 0.7	ND
BNIPDadodec	5.1 ± 0.5	6.9 ± 0.1	ND
BNIPDaoxoct	12.4 ± 5.8	6.1 ± 1.5	6.1 ± 0.1
BNIPDaCHM	6.8 ± 0.3	6.1 ± 0.7	4.2 ± 0.1
BPHPDadec	> 40	> 40	ND
NPA	> 40	> 40	ND
Etoposide	> 40	17.2 ± 0.8	ND
Doxorubicin	14.3 ± 5.9	3.6 ± 0.6	ND

[a] Toxicity was determined by MTT Assay. The results were obtained after treating MDA-MB-231 cells with different BNIPP derivative concentrations (0 – 40 µM) for 24, 48 and 72 hours, at 37°C. Data are mean ± SD of three independent experiments (n=3); each experiment consisted of 6 repeats.

[b] The IC_{50} value was defined as the derivative concentration that causes 50 % growth inhibition of a cell population, compared to that of untreated cells. ND – Not Determined.

Table 4.3.: Cytotoxicity of BNIPP derivatives in MCF-10A cells

	IC_{50}[b] (μM)		
Derivative[a]	**24 hrs**	**48 hrs**	**72 hrs**
BNIPSpd	4.2 ± 0.6	3.9 ± 0.9	ND
BNIPPut	8.1 ± 2.7	5.6 ± 2.3	ND
BNIPDahex	0.8 ± 0.1	0.8 ± 0.1	ND
BNIPDaoct	2.8 ± 0.1	0.8 ± 0.1	ND
BNIPDadec	2.8 ± 0.1	2.8 ± 0.1	ND
BNIPDadodec	4.2 ± 0.3	6.8 ± 0.8	ND
BNIPDaoxoct	6.1 ± 1.6	2.3 ± 0.0	2.4 ± 0.5
BNIPDaCHM	6.1 ± 0.1	5.7 ± 0.8	6.8 ± 0.3
BPHPDadec	> 40	> 40	ND
NPA	> 40	> 40	ND
Etoposide	14.2 ± 1.3	1.2 ± 0.7	ND
Doxorubicin	0.7 ± 0.0	0.2 ± 0.0	ND

[a] Toxicity was determined by MTT Assay. The results were obtained after treating MCF-10A cells with different BNIPP derivative concentrations (0 – 40 μM) for 24, 48 and 72 hours, at 37°C. Data are mean ± SD of three independent experiments (n=3); each experiment consisted of 6 repeats.
[b] The IC_{50} value was defined as the derivative concentration that causes 50 % growth inhibition of a cell population, compared to that of untreated cells. ND – Not Determined.

In both cell lines, all BNIPP derivatives, except for BPHPDadec and NPA (IC_{50} values > 40 μM) exhibited cytotoxicity after 24 hours (with IC_{50} values in the range of 4.8 – 12.7 μM in MDA-MB-231 cells, and 0.8 – 8.0 μM in MCF-10A cells; Tables 4.2 – 4.3). After 48 hours, the cytotoxicity of BNIPP derivatives was enhanced in MDA-MB-231 cells, except after treatment with BNIPDadodec or BNIPDaCHM (i.e., IC_{50} value of BNIPDadodec decreased from 5.1 μM to 6.9 μM after 24 and 48 hours, respectively, whilst the IC_{50} value of BNIPDaCHM was similar after 24 and 48 hours at 6.8 and 6.1 μM, respectively: Table 4.2). However, after 48 hours BNIPP treatment in MCF-10A cells, cytotoxicity was enhanced for all BNIPP derivatives, except after treatment with BNIPDahex or BNIPDadodec (i.e., IC_{50} value of BNIPDahex remained the same after 24 and 48 hours at 0.8 μM, whilst the IC_{50} value of BNIPDadodec decreased from 4.2 μM to 6.8 μM after 24 and 48 hours, respectively; Table 4.3).

Overall, the BNIPP derivatives were more cytotoxic than Etoposide or Doxorubicin treated cells (IC_{50} values of > 40 and 14.3 μM, after 24 hours, and 17.2 and 3.6 μM, after 48 hours, respectively, in MDA-MB-231 cells) (Tables 4.2). Doxorubicin (Adriamycin) and Etoposide (VP-16) were used as positive controls (Figures 3.1 and 3.3). These compounds are both examples of Topoisomerase II (TOPO II) targeting antineoplastic agents, as described in Section 1.6, and are used in the treatment of solid tumours

Cytotoxicity of BNIPP derivatives appears to be cell line dependent as the most cytotoxic derivatives in MDA-MB-231 cells were BNIPDadec (IC_{50} value 4.8 μM, after 24

hours) and BNIPDaoct (IC_{50} value 2.7 µM, after 48 hours). BNIPDahex (IC_{50} value 0.8 µM, after 24 and 48 hours) and BNIPDaoct (IC_{50} value 0.8 µM, after 48 hours) were the most cytotoxic in MCF-10A cells.

4.4.3. Cellular Uptake of BNIPP Derivatives

BNIPP derivatives display inherent fluorescent properties when taken up into cells. These properties were exploited in this study to assess cellular uptake and distribution of BNIPSpd, BNIPDaoct, BNIPDaoxoct and BNIPDaCHM in MDA-MB-231 (Figure 4.15a-c) and MCF-10A cells (Figure 4.16a-c). The degree of fluorescence in cells treated with BNIPP derivatives (10 µM) was assessed by fluorescence microscopy.

4.4.3.1. Cellular Uptake of BNIPP Derivatives in MDA-MB-231 Cells

MDA-MB-231 cells were treated with 10 µM of BNIPSpd, BNIPDaoct, BNIPDaoxoct or BNIPDaCHM and visualised under the fluorescent microscope after 0.5, 1, 2, 4, 6, and 24 hours (Figure 4.15a, b and c shows only images at 0.5, 2 and 6 hours).

After 0.5 hours, only MDA-MB-231 cells treated with BNIPDaoct or BNIPDaCHM showed fluorescence (Figure 4.15a). After 2 hours, fluorescence remained in MDA-MB-231 cells treated with BNIPDaoct or BNIPDaCHM (Figure 4.15b). However, fluorescence observed in BNIPDaoct treated cells after 2 hours was reduced when compared to the fluorescence observed at 0.5 hours. After 6 hours, fluorescence was observed in MDA-MB-231 cells treated with all BNIPP derivatives except BNIPDaoct treated cells (Figure 4.15c). Fluorescence in BNIPSpd or BNIPDaoxoct treated cells was only observed after 6 hours treatment indicating a slower uptake in MDA-MB-231 cells.

Within individual cells, fluorescence appears to be present in difference areas of the cell: nucleus or around it. Using fluorescence microscopy alone it is difficult to clearly locate the fluorescent BNIPP derivatives

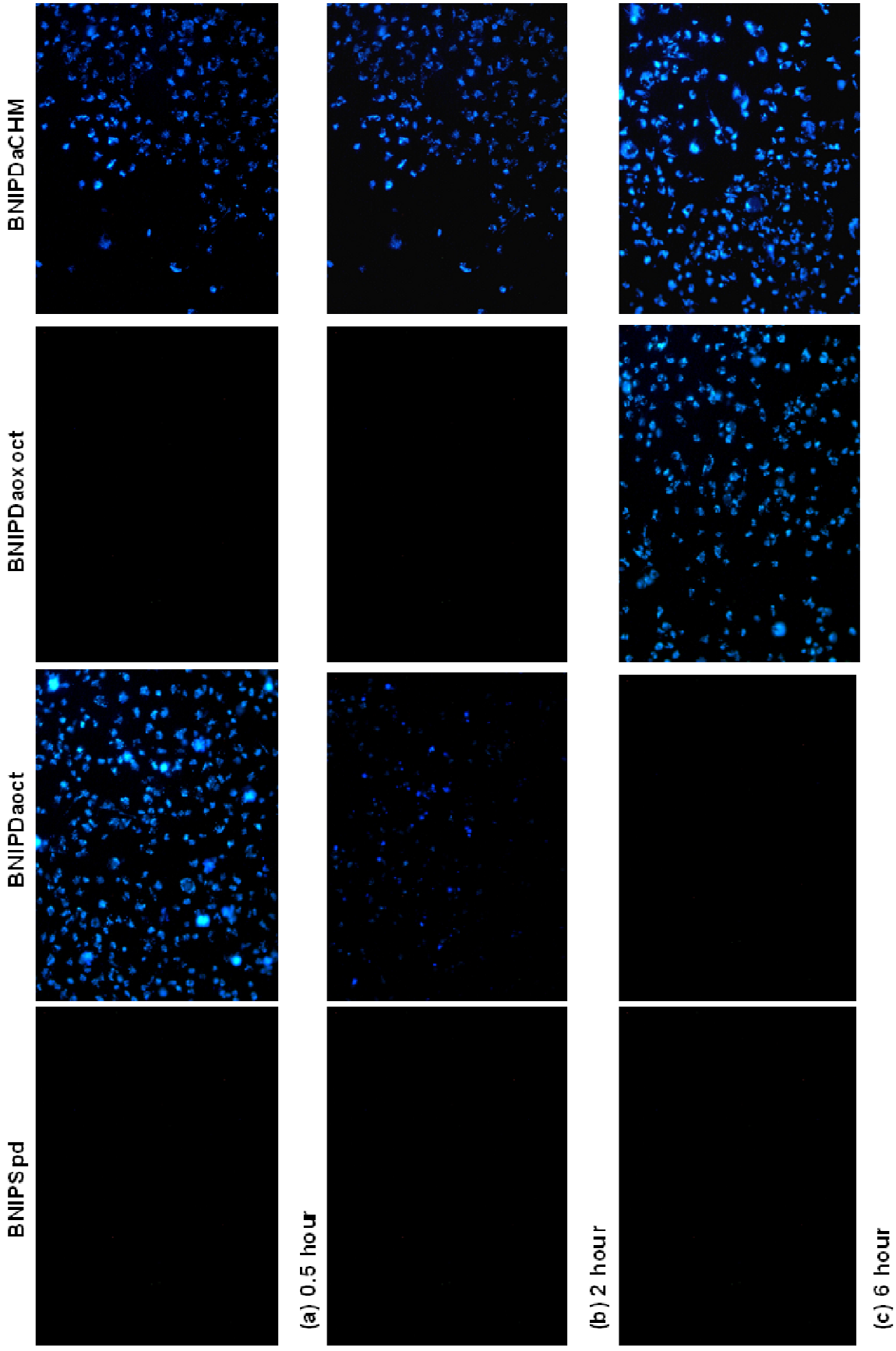

Figure 4.15.: Fluorescence microscopy images of MDA-MB-231 cells treated with 10 µM of BNIPSpd, BNIPDaoct, BNIPDaoxoct or BNIPDaCHM for (a) 0.5, (b) 2 and (c) 6 hours. Cells were visualised using a Leica DMIL inverted fluorescence microscope using a UV filter (ex bandpass (blue); 340 – 380 nm; em longpass (red); 425 nm). Images are representative of 3 independent experiments, each comprising of 3 replicates (n = 3). Magnification x 100.

4.4.3.2. Cellular Uptake of BNIPP Derivatives in MCF-10A Cells

MCF-10A cells were treated with 10 µM of BNIPSpd, BNIPDaoct, BNIPDaoxoct or BNIPDaCHM and visualised under the fluorescent microscope after 0.5, 1, 2, 4, 6, and 24 hours (Figure 4.16a, b and c shows only images at 0.5, 2 and 6 hours).

After 0.5 hours, only MCF-10A cells treated with BNIPDaoct and BNIPDaCHM showed fluorescence (Figure 4.16a). After 2 hours, fluorescence was observed in MCF-10A cells treated with BNIPDaoct, BNIPDaoxoct and BNIPDaCHM (Figure 4.16b). After 6 hours, fluorescence was observed in MCF-10A cells treated with all BNIPP derivatives (Figure 4.16c).

Confirmation of cellular localisation in MCF-10A cells was not possible, for the same reason as for MDA-MB-231 cells (Section 4.4.3.1).

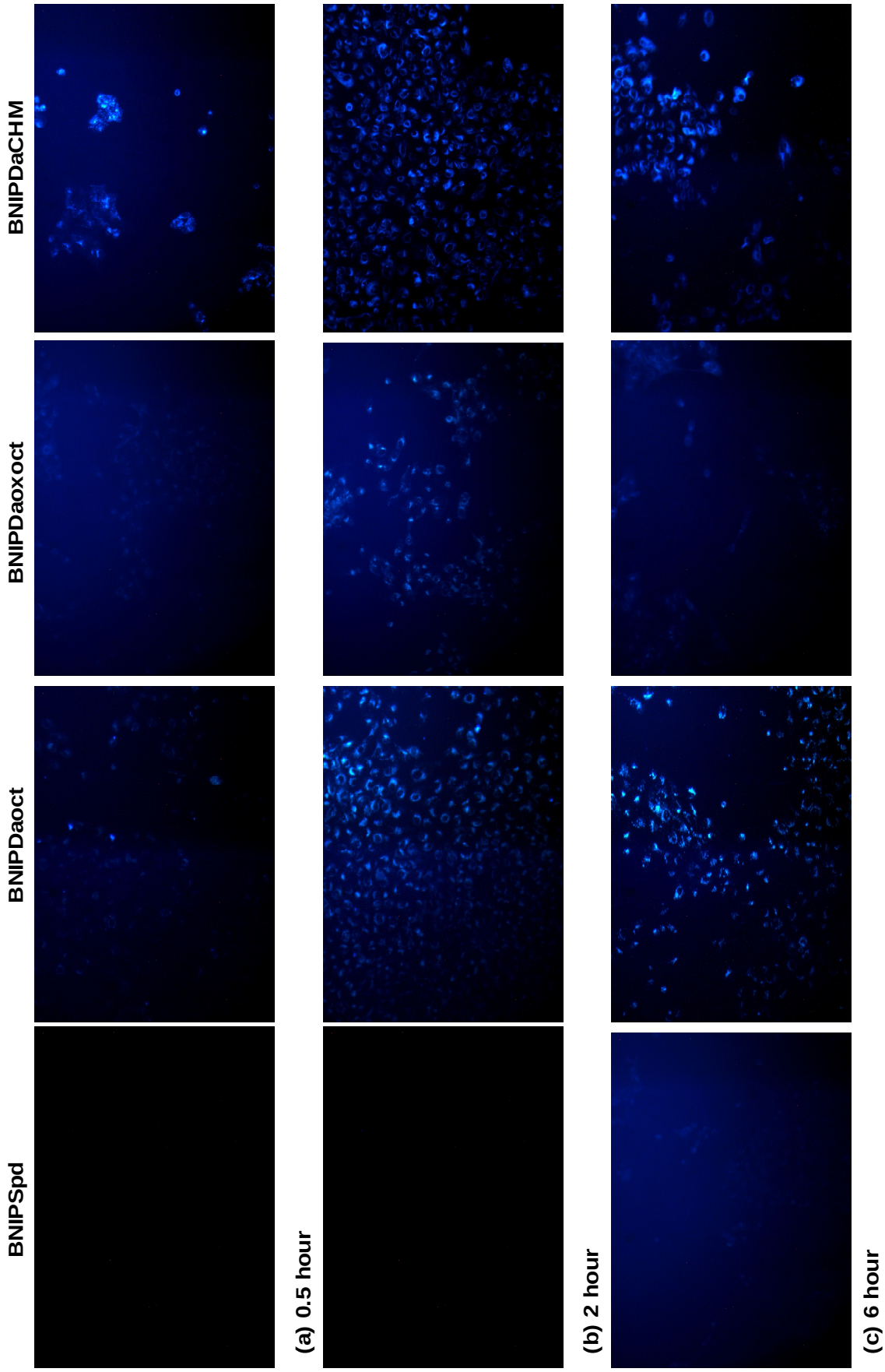

Figure 4.16.: Fluorescence microscopy images of MCF-10A cells treated with 10 µM of BNIPSpd, BNIPDaoct, BNIPDaoxoct or BNIPDaCHM for (a) 0.5, (b) 2 and (c) 6 hours. Cells were visualised using a Leica DMIL inverted fluorescence microscope using a UV filter (ex bandpass (blue); 340 – 380 nm; em longpass (red); 425 nm). Images are representative of 3 independent experiments, each comprising of 3 replicates (n = 3). Magnification x 100.

4.4.4. Polyamine Transporter Studies with BNIPP Derivatives

Cellular entry of BNIPP derivatives via the polyamine transporter (PAT) was studied in CHO-MG and CHO cells treated with different concentrations (0 – 100 µM) of BNIPP derivatives (BNIPSpd, BNIPDaoct, BNIPDaoxoct or BNIPDaCHM) or MGBG for 48 hours and assessed by MTT assay.

The parental CHO cells contain an active polyamine transporter (PAT-active), whilst the mutant CHO-MG cells contain a MGBG-deficient polyamine transporter (PAT-inactive). Comparison of the toxicities of BNIPP derivatives in both cell lines, measured by MTT assay, provides an important indication for delivery via the PAT of the BNIPP derivatives. Data was expressed as a CHO-MG/CHO IC_{50} ratio. Therefore, a derivative that uses the PAT would be highly toxic to CHO cells, but less toxic to CHO-MG cells. Hence, a highly selective PAT derivative would have a high (CHO-MG/CHO) IC_{50} ratio (i.e., > 100).

Table 4.4.: Biological evaluation of BNIPP derivatives in CHO-MG and CHO cells

Derivative[a]	CHO-MG Cells IC_{50}[b] (µM)	CHO Cells IC_{50}[b] (µM)	IC_{50} Ratio[c]
BNIPSpd	74.6 ± 3.1	76.5 ± 5.7	1.0
BNIPDaoct	5.1 ± 0.5	5.8 ± 0.9	0.9
BNIPDaoxoct	26.9 ± 5.9	76.1 ± 2.1	0.4
BNIPDaCHM	6.3 ± 0.4	6.2 ± 0.7	1.0
MGBG[d]	>100	3.3 ± 0.5	>30.2

[a] Toxicity was determined by the MTT Assay. The results were obtained after treating CHO-MG and CHO cells with different BNIPP derivative concentrations (0 – 100 µM) for 48 hours at 37°C. Data are mean ± SD of three independent experiments (n=3); each experiment consisted of 6 repeats.
[b] The IC_{50} value was defined as the derivative concentration that causes 50 % growth inhibition of a cell population, compared to that of untreated (control) cells.
[c] Ratio indicates the (CHO-MG/CHO) IC_{50} ratio; a measure of PAT selectivity.
[d] MGBG, a known substrate for the PAT system was used as a positive control.

BNIPSpd and BNIPDaoxoct displayed low toxicity (i.e., > 10 µM; 74.6 and 26.9 µM, respectively); whilst BNIPDaoct and BNIPDaCHM exhibited high toxicity (5.1 and 6.3 µM, respectively) in CHO-MG cells (Table 4.4). In CHO cells, a similar toxicity trend was observed (BNIPSpd and BNIPDaoxoct showed low toxicity; 76.5 and 76.1 µM, respectively, whilst BNIPDaoct and BNIPDaCHM showed high toxicity; 5.8 and 6.2 µM, respectively).

BNIPSpd, BNIPDaoct nor BNIPDaCHM were not specific to either cell line and produced similar IC_{50} values in both cell line, with CHO-MG/CHO IC_{50} ratios of 1.0, 0.9 and 1.0, respectively. In contrast, BNIPDaoxoct demonstrated a higher toxicity in CHO-MG cells (IC_{50} 26.9 µM compared to 76.1 µM in CHO cells), giving a CHO-MG/CHO IC_{50}

ratio of 0.4. This indicates that BNIPDaoxoct could enter cells by a different mechanism to that of the other BNIPP derivatives investigated. The positive control MGBG showed a lack of toxicity in CHO-MG cells (IC_{50} value of > 100 μM). This was because the CHO-MG cells were isolated for growth resistance to MGBG and are thus defective to MGBG uptake.

CHO-MG/CHO IC_{50} ratios for all BNIPP derivatives ranged from 0.4 – 1.0, indicating that none of the BNIPP derivatives utilise the MGBG-specific PAT system to gain access into cells. This suggests that another mode of cellular entry other than that of the MGBG-specific PAT system is being utilised to transport BNIPP derivatives into cells.

4.4.5. *Changes in Intracellular Polyamine Levels in BNIPP Derivative Treated MDA-MB-231 and MCF-10A Cells*

Changes in intracellular polyamine levels in MDA-MB-231 and MCF-10A cells treated with BNIPP derivatives (BNIPSpd, BNIPDaoct, BNIPDaoxoct or BNIPDaCHM; 0.1 – 5 µM) or DFMO (5 mM) after 24 hours were assessed by pre column derivatisation with dansyl chloride followed by reverse-phase HPLC using fluorescent detection. Intracellular polyamine levels are expressed as putrescine (Put), spermidine (Spd) and spermine (Spm) levels (µM/1x10^6 cells) and are depicted in Figures 4.17 – 4.24. Those polyamines were chosen as they are essential for normal mammalian cell growth and development, for example, cell proliferation stops in polyamine-deficient cells, whilst cell proliferation is initiated in polyamine-rich cells (Pegg 1988).

4.4.5.1. *Intracellular Polyamine Levels in MDA-MB-231 Cells*

MDA-MB-231 cells treated with DFMO (5 mM) mirrored that of the control cells, as all intracellular polyamine levels were not altered (Figures 4.17 – 4.20).

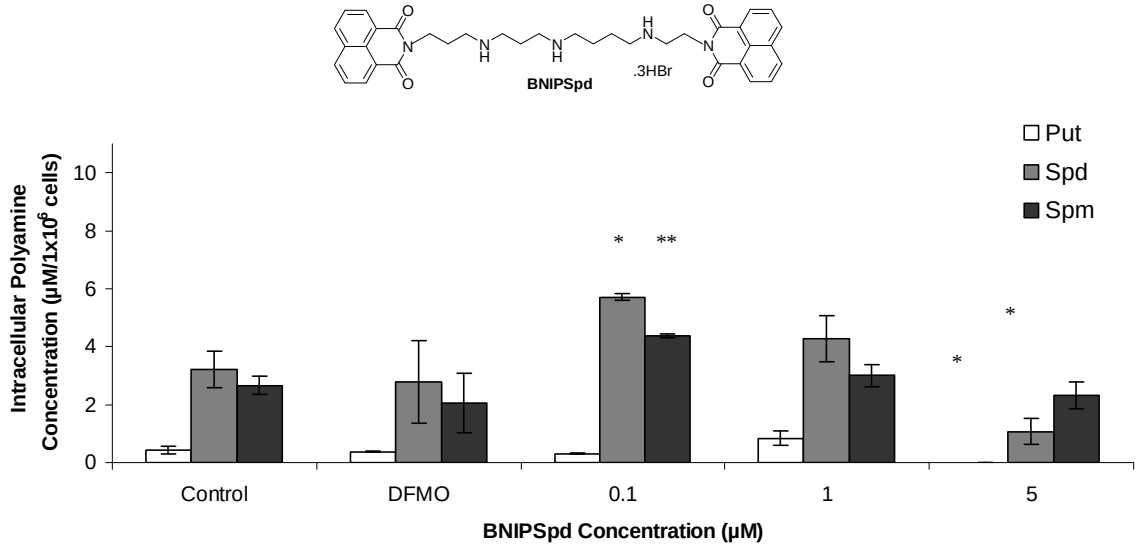

Figure 4.17: Intracellular polyamine levels determined by pre-column derivatisation and HPLC. Data obtained after treating MDA-MB-231 cells with BNIPSpd (0.1–5 µM) for 24 hours. DFMO (5mM) was used as a positive control. Data are mean ± SEM of 3 independent experiments (n = 3). *P<0.05, **P<0.01 vs. untreated (control) cells.

After 24 hours, treatment with 0.1 µM BNIPSpd produced no change in putrescine levels, but spermidine and spermine levels were significantly increased (P < 0.05, increased by 2.5 µM/1x10^6 cells; P < 0.01, increased by 1.7 µM/1x10^6 cells, respectively) compared to control (Figure 4.17). No significant change in putrescine, spermidine or spermine levels were observed with 1 µM BNIPSpd compared to control (Figure 4.17). However, 5 µM BNIPSpd induced a significant decrease (P < 0.05) in putrescine (decreased by 0.43 µM/1x10^6 cells) and spermidine (decreased by 2.2 µM/1x10^6 cells)

levels, whilst no change in spermine levels was observed when compared to the control, after 24 hours (Figure 4.17).

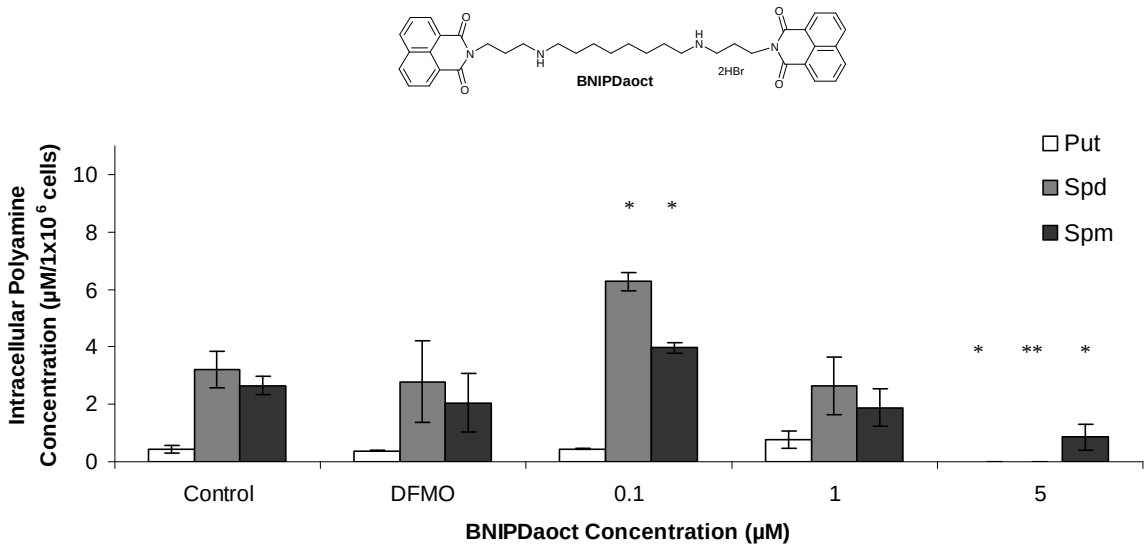

Figure 4.18.: Intracellular polyamine levels determined by pre-column derivatisation and HPLC. Data obtained after treating MDA-MB-231 cells with BNIPDaoct (0.1–5 μM) for 24 hours. DFMO (5mM) was used as a positive control. Data are mean ± SEM of 3 independent experiments (n = 3). *P<0.05, **P<0.01 vs. untreated (control) cells.

After 24 hours, treatment with 0.1 μM BNIPDaoct produced no change in putrescine levels, but spermidine and spermine levels were significantly (P < 0.05) increased (increased by 3.1 and 1.3 μM/1x10^6 cells, respectively) compared to control (Figure 4.18). No significant change in putrescine, spermidine or spermine levels were observed with 1 μM BNIPDaoct compared to the control (Figure 4.18). However, at a concentration of 5 μM, BNIPDaoct significantly reduced putrescine, spermidine and spermine levels (P < 0.05, decreased by 0.4 μM/1x10^6 cells; P < 0.01, decrease by 3.2 μM/1x10^6 cells; P < 0.05, decrease by 1.8 μM/1x10^6 cells) compared to the control, respectively (Figure 4.18).

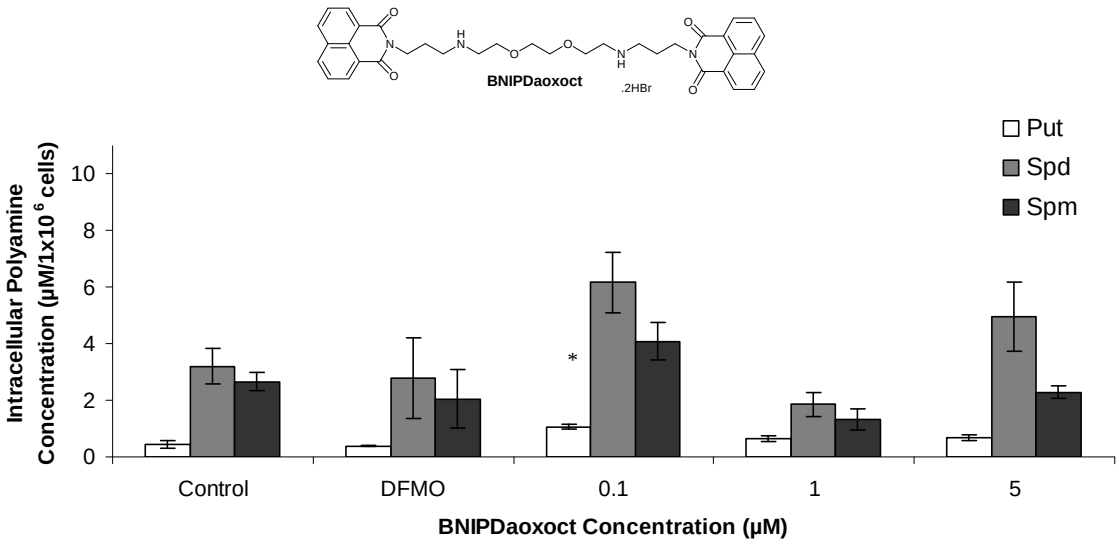

Figure 4.19.: Intracellular polyamine levels determined by pre-column derivatisation and HPLC. Data obtained after treating MDA-MB-231 cells with BNIPDaoxoct (0.1–5 µM) for 24 hours. DFMO (5mM) was used as a positive control. Data are mean ± SEM of 3 independent experiments (n = 3). *P<0.05 vs. untreated (control) cells.

After 24 hours, treatment with 0.1 µM BNIPDaoxoct significantly (P < 0.05) increased (increased by 0.64 µM/1x10^6 cells) putrescine levels, however, no significant changes in spermidine or spermine levels were observed when compared to the control (Figure 4.19). Putrescine, spermidine and spermine levels were not significantly changed following treatment with 1 and 5 µM BNIPDaoxoct compared to that of the control (Figure 4.19).

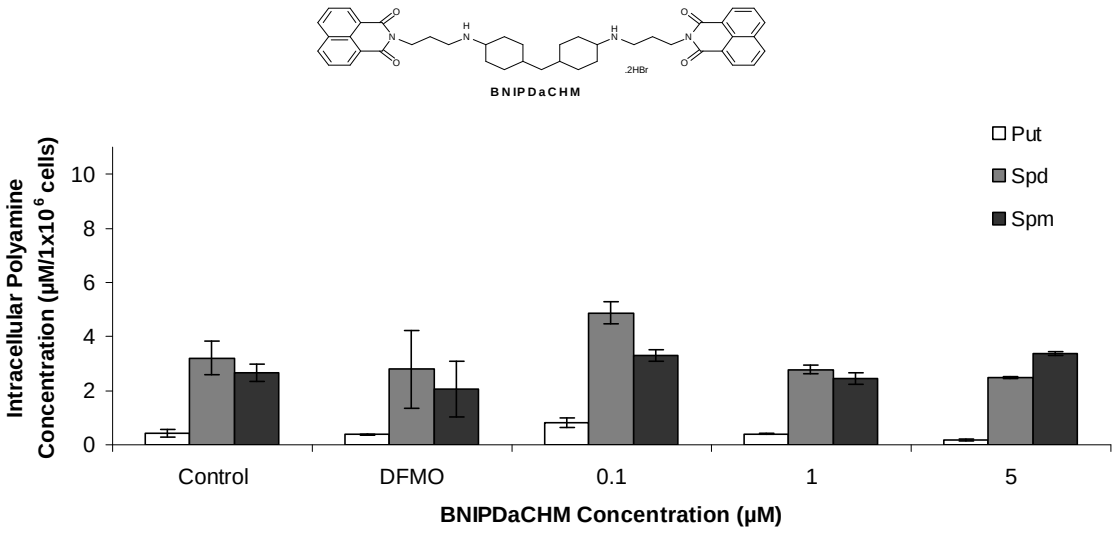

Figure 4.20.: Intracellular polyamine levels determined by pre-column derivatisation and HPLC. Data obtained after treating MDA-MB-231 cells with BNIPDaCHM (0.1–5 µM) for 24 hours. DFMO (5mM) was used as a positive control. Data are mean ± SEM of 3 independent experiments (n = 3).

After 24 hours, BNIPDaCHM (0.1 – 5 µM) treatment resulted in no significant changes to putrescine, spermidine or spermine levels when compared to the control (Figure 4.20).

4.4.5.2. Intracellular Polyamine Levels in MCF-10A Cells

Treatment with DFMO (5 mM) mirrored that of the control MCF-10A cells, as all intracellular polyamine levels were not altered (Figures 4.21 – 4.24).

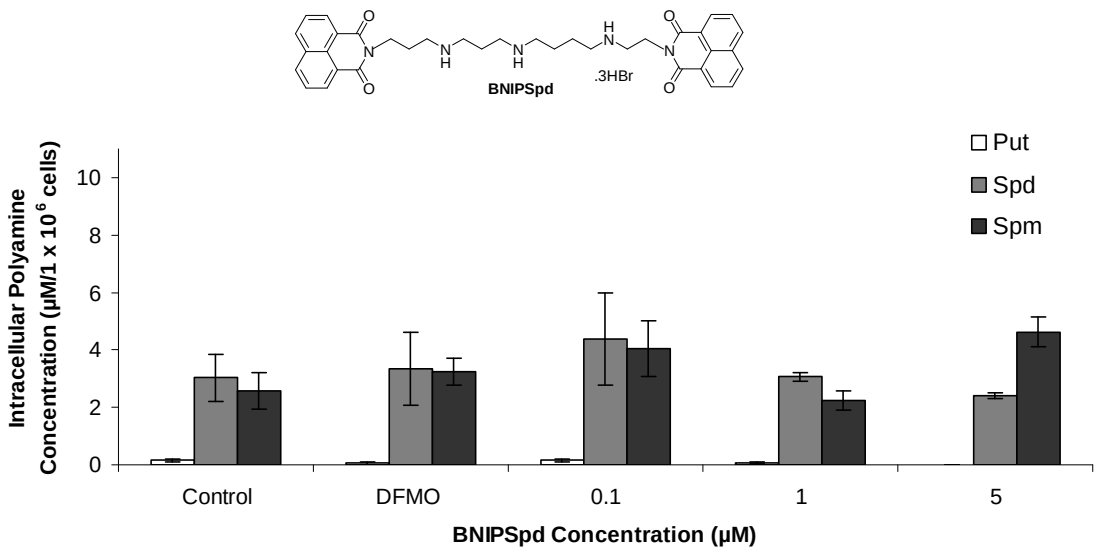

Figure 4.21.: Intracellular polyamine levels determined by pre-column derivatisation and HPLC. Data obtained after treating MCF-10A cells with BNIPSpd (0.1–5 µM) for 24 hours. DFMO (5mM) was used as a positive control. Data are mean ± SEM of 3 independent experiments (n = 3).

After 24 hours, BNIPSpd (0.1 – 5 µM) treatment resulted in no significant changes to putrescine, spermidine or spermine levels when compared to the control (Figure 4.21).

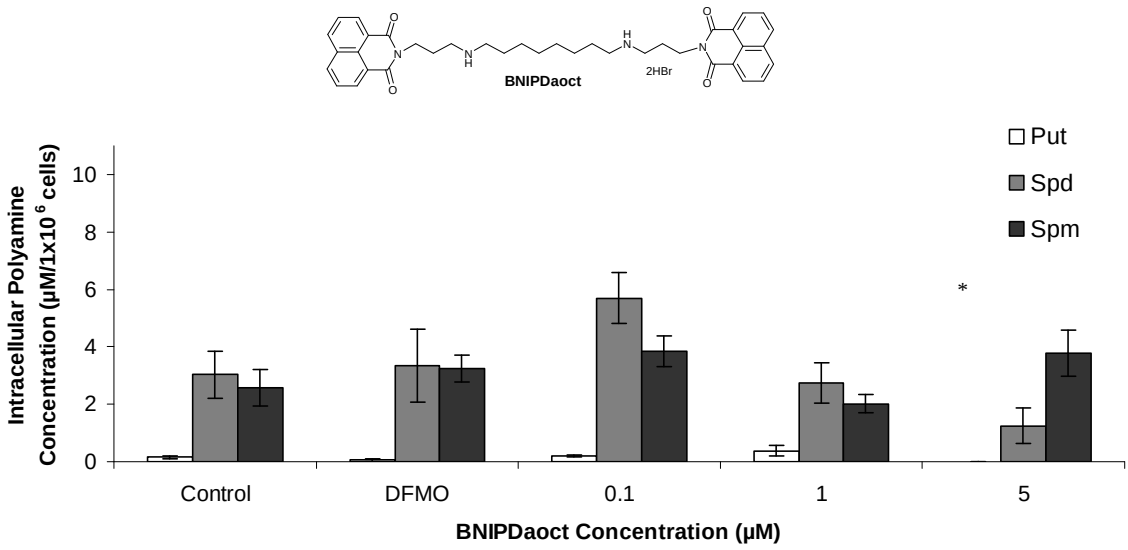

Figure 4.22.: Intracellular polyamine levels determined by pre-column derivatisation and HPLC. Data obtained after treating MCF-10A cells with BNIPDaoct (0.1–5 µM) for 24 hours. DFMO (5mM) was used as a positive control. Data are mean ± SEM of 3 independent experiments (n = 3). *P<0.05 vs. untreated (control) cells.

After 24 hours, treatment of MCF-10A cells with BNIPDaoct (0.1 – 1 µM) did not induce any change in putrescine, spermidine or spermine levels compared to control (Figure 4.22). However, at a concentration of 5 µM, BNIPDaoct significantly (P < 0.05) reduced putrescine levels (decreased by 0.2 µM/1x10^6 cells), whilst spermidine and spermine level were not changed compared to that of the control (Figure 4.22).

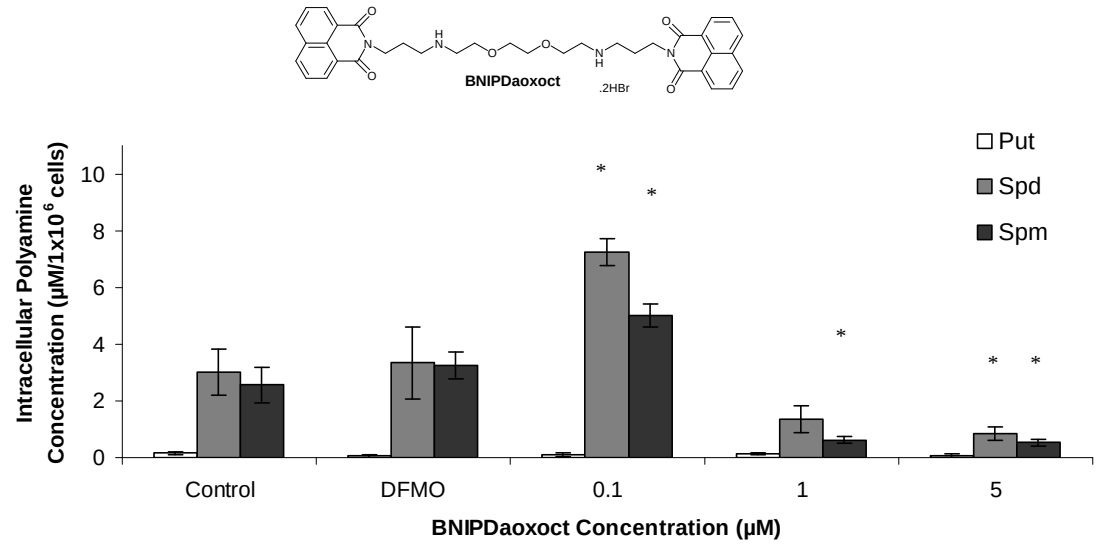

Figure 4.23.: Intracellular polyamine levels determined by pre-column derivatisation and HPLC. Data obtained after treating MCF-10A cells with BNIPDaoxoct (0.1–5 µM) for 24 hours. DFMO (5mM) was used as a positive control. Data are mean ± SEM of 3 independent experiments (n = 3). *P<0.05 vs. untreated (control) cells.

After 24 hours, treatment with 0.1 µM BNIPDaoxoct produced no change in putrescine levels, but spermidine and spermine levels were significantly (P < 0.05) increased (increased by 4.2 and 2.4 µM/1x10^6 cells, respectively) compared to control

(Figure 4.23). With 1 µM BNIPDaoxoct, putrescine and spermidine levels were not changed, but spermine levels were significantly decreased ($P < 0.05$, decreased by 1.9 µM/1x10^6 cells) compared to the control (Figure 4.23). At 5 µM, BNIPDaoxoct did not alter the level of putrescine, but significantly ($P < 0.05$) reduced spermidine and spermine levels (decreased by 2.2 and 2.0 µM/1x10^6 cells, respectively) compared to the control (Figure 4.23).

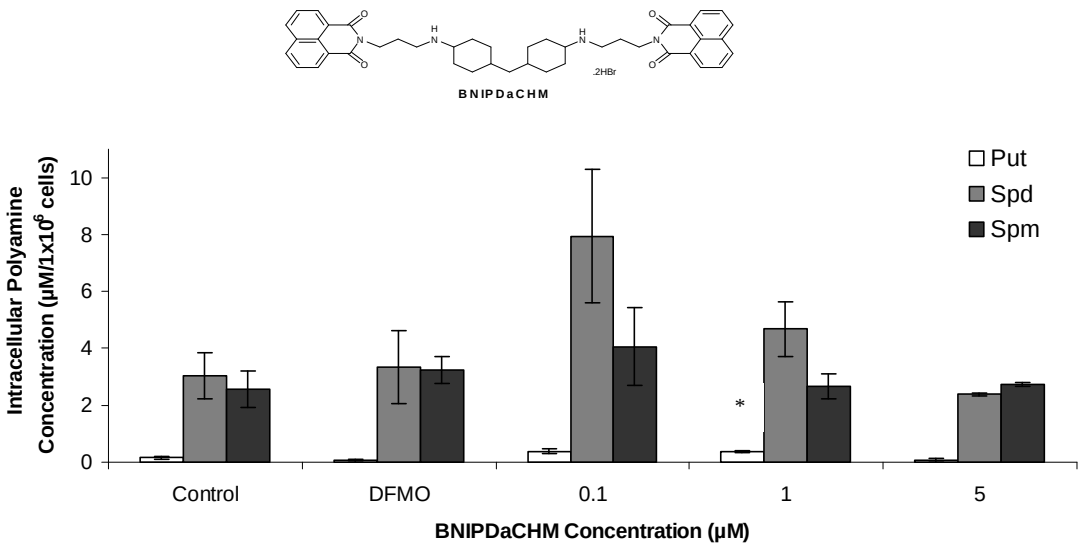

Figure 4.24.: Intracellular polyamine levels determined by pre-column derivatisation and HPLC. Data obtained after treating MCF-10A cells with BNIPDaCHM (0.1–5 µM) for 24 hours. DFMO (5mM) was used as a positive control. Data are mean ± SEM of 3 independent experiments (n = 3). *P<0.05 vs. untreated (control) cells.

After 24 hours, treatment with 0.1 µM BNIPDaCHM produced no significant changes in putrescine, spermidine or spermine levels compared to the control (Figure 4.24). With 1 µM, BNIPDaCHM significantly increased putrescine levels ($P < 0.05$, increased by 0.2 µM/1x10^6 cells), whilst spermidine and spermine levels were not changed when compared with the control (Figure 4.24). No significant change in putrescine, spermidine or spermine levels were observed with 5 µM BNIPDaCHM compared to the control (Figure 4.24).

4.5. Discussion

4.5.1. Effect of BNIPP Derivatives on Cell Morphology

Treatment with BNIPSpd, BNIPDaoct, BNIPDaoxoct or BNIPDaCHM resulted in morphological changes in both MDA-MB-231 (Figures 4.10 – 4.11) and MCF-10A cells (Figure 4.12), as examined by light microscopy. The change in cell morphology and loss of cell adherence, combined with cytotoxicity at µM levels (refer to Section 4.4.2) may suggest that the mode of cell death initiated through BNIPP derivative treatment could be that of apoptosis (Huschtscha *et al*. 1996, Cummings *et al.* 2004, Holdenrieder and Stieber 2004, Lee *et al*. 2008). The mode of cell death will be further discussed in Chapter 6.

4.5.2. Cytotoxicity in MDA-MB-231 and MCF-10A Cells

The results from the *in vitro* cytotoxicity study demonstrate that all BNIPP derivatives, except BPHPDadec and NPA (IC_{50} values > 40 µM) were cytotoxic in MDA-MB-231 and MCF-10A cells (Tables 4.2 and 4.3). These cytotoxicity results are supported by the results obtained with the DNA binding studies, as discussed in Section 3.5.1. None of the BNIPP derivatives were selectively cytotoxic in either cell line studied. BNIPDadec with an IC_{50} value of 4.8 µM, and BNIPDaoct with an IC_{50} value of 2.7 µM were the most cytotoxic derivatives in MDA-MB-231 cells, after 24 and 48 hours, respectively (Table 4.2), whereas in MCF-10A cells, BNIPDahex and BNIPDaoct with IC_{50} values of 0.8 µM were the most cytotoxic, after 24 and 48 hours (Table 4.3).

Earlier work on some BNIPP derivatives had identified the essential structural features responsible for enhanced aqueous solubility and biological activity (Pavlov *et al*. 2001, Oliveira *et al*. 2007). These features include the bisnaphthalimidopropyl functionality, an alkyl linker chain length ideally between 8 – 10 carbons, and the presence of heteroatoms (2 or 3 nitrogen atoms) (Pavlov *et al*. 2001, Dance *et al*. 2005, Oliveira *et al*. 2007).

The majority of research into naphthalimido and bisnaphthalimido derivatives has been focused on the modification of the naphthalimido rings, as described in Sections 1.6.1 and 1.6.2 (Brana *et al.* 1995, Brana and Ramos 2001). In this study, a further expansion of the work of Kong Thoo Lin *et al.* (2000) and Oliveira *et al.* (2007) has been undertaken via modification to only the central linker chain. Two new BNIPP derivatives have been synthesised (described in Section 2.4), with additional modifications to the central linker chain achieved at a point of diversity (Figure 4.25).

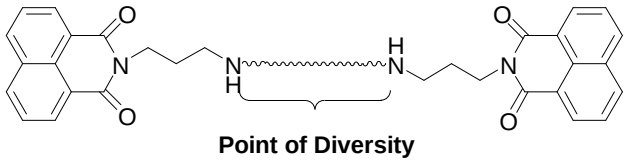

Figure 4.25.: The basic structure of a BNIPP Derivative, including the point of modification (i.e., the point of diversity)

Modifications included the introduction of oxygen atoms (BNIPDaoxoct) and two cyclohexane rings (BNIPDaCHM), and these modifications do not appear to affect either aqueous solubility (results not shown) or cytotoxicity in MDA-MB-231 or MCF-10A cells (IC_{50} values of 12.4 and 6.8 µM, and 6.1 and 6.1 µM, respectively, after 24 hours) (Tables 4.2 and 4.3). However, BNIPOSpm (Ralton 2006, Oliveira *et al*. 2007) (Figure 1.23) which has oxygen atoms in the α-position of the naphthalimido ring was observed to be the least active member of the BNIPP derivative series. Ralton (2006) and Oliveira *et al.* (2007) studied BNIPOSpm in MCF-7, CaCO-2 and HT-29 cells and found IC_{50} values > 50 µM. This observation has further verified that bisnaphthalimidopropyl functionality is an essential structural feature required for enhanced solubility whilst maintaining a good level of biological activity. The exact position of an oxygen atom in the linker chain is also extremely important in maintaining a level of cytotoxicity (Kuksa *et al.* 2002).

Further investigations into bisnaphthalimido functionality were undertaken by replacing the naphthalimido rings with phthalimido rings (BPHPDadec), or by removing a naphthalimido ring entirely (NPA). The result of these modifications was the complete loss of cytotoxicity in BPHPDadec and NPA treated MDA-MB-231 and MCF-10A cells, with IC_{50} values > 40 µM (Tables 4.2 and 4.3). Again it can be stated from the results presented, that cytotoxicity appears to be vitally dependent upon the presence of bisnaphthalimidopropyl groups and a linker chain of < C12 in length.

Interestingly, in recent years several naphthalimide and bisnaphthalimide derivatives have entered Phase I and II clinical trials. The naphthalimide derivative, Amonafide was selected for Phase I and II clinical trials (Saez *et al.* 1989, Brana and Ramos 2001, Brana *et al.* 2003). Amonafide, a mononaphthalimide had demonstrated biological activity against metastatic breast cancer (MBC) (Alami *et al.* 2007) (Figure 1.16). However, amonafide was removed from clinical trials as its metabolite; *N*-acetyl amonafide was responsible for severe myelosuppression (Alami *et al*. 2007)

Several other mononaphthalimide derivatives which are structurally similar to amonafide have been synthesised. Among these, Azonafide (Figure 1.17) and Xanafide (Amonafide L-malate) (Figure 4.26) were the most potent. Azonafide was highly potent against human colon cancer cells, whereas xanafide showed comparable and significant activity *in vitro* against human breast cancer (MCF-7 and MDA-MB-231), prostrate (PC-3) and colon (COLO205) cancer cells (Mayr *et* al. 1998, Ajami and Barlow 2006, Alami *et al*. 2007, Chau *et al*. 2008). Xanafide has recently received FDA Orphan Drug Designation

for the treatment of acute myeloid leukaemia (AML), and is currently undergoing Phase II clinical trials into the treatment of secondary AML (Alami *et al*. 2007, Allen *et al*. 2009).

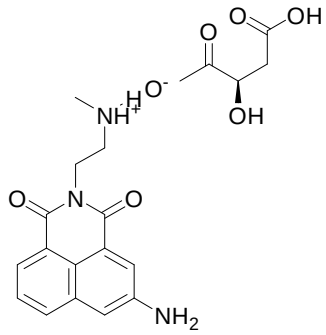

Figure 4.26.: Structure of Xanafide (Amonafide L-malate)

The symmetrical bisnaphthalimide, Elinafide (Figure 1.21), is the most cytotoxic bisnaphthalimide to date, with IC_{50} values of 0.02, 0.07 and 0.32 μM, after 72 hours treatment in HT-29, cervical (HeLa) cancer and PC-3 cells, respectively (Villalona-Calero *et al.* 2001, Brana *et al.* 2003, Denny 2004). Several years ago, elinafide was selected for Phase I and II clinical trials, but due to its dose-limiting toxicity (DLT), being that of a cumulative nature, its future development has been delayed (Denny 2004).

In recent years, modifications to the structure of naphthalimides and bisnaphthalimides have resulted in the synthesis of several new analogues to improve their therapeutic potential. These include the synthesis of naphthalimides (i) with chiral amino acid side chains, (ii) with both natural and synthetic polyamine moieties, (iii) with sulphur substitutions, (iv) with π-excedent furan or thiophene rings fused to the naphthalimide moiety, or (v) with a series of 5-alkylamino substitutions (Brana *et al.* 2004b, Ott *et al.* 2008, Yang *et al*. 2008, Tian *et al*. 2009, Xie *et al*. 2009). Bisnaphthalimides have also been modified with (i) natural and synthetic polyamine moieties, or (ii) heterocyclic and other cyclic moieties (Kong Thoo Lin and Pavlov 2000, Dance *et al.* 2005, Oliveira *et al*. 2007, Filosa *et al*. 2009). These structural modifications have produced derivatives with effective cytotoxicities against various cell lines (e.g., in HT-29, MCF-7 and CaCO-2 cancer cells). Hence, the synthesis of the BNIPP derivatives has addressed the adverse side effects observed in previous members of this family (Amonafide and Elinafide), due to the omission of the primary amine at the 5-position of the naphthalimido ring (Kong Thoo Lin and Pavlov 2000, Dance *et al*. 2005, Oliveira *et al*. 2007, Xie *et al*. 2009).

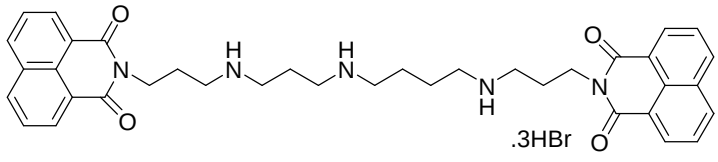

Figure 4.27.: Structure of BNIPSpd

BNIPSpd (spermidine derivative) was identified as the most active member of the BNIPP derivative series (Pavlov *et al*. 2001, Dance *et al*. 2005, Oliveira *et al*. 2007, Ralton *et al*. 2009) (Figure 4.27), against MCF-7, CaCO-2 and HT-29 cancer cells with IC_{50} values of 1.5, 0.47 and 2.4 μM, respectively, after 24 hours treatment. However, in MDA-MB-231 and MCF-10A cells, BNIPSpd was not the most active BNIPP derivative (IC_{50} values of 12.7 and 4.2 μM, respectively, after 24 hours treatment). These results have revealed that MDA-MB-231 cells, a reliable model for estrogen receptor-negative (ER-ve) breast cancer, are more resistant to BNIPSpd treatment than MCF-7 cells (estrogen receptor-positive (ER+ve)/p53 wild type breast cancer cells) (Dance *et al.* 2005). This is possibly because MDA-MB-231 cells are estrogen receptor-independent (ER-ve), do not express wild-type p53 (mutated), and are highly metastatic in nature, in contrast to MCF-7 and MCF-10A cells (Belkacemi *et al*. 2006). MDA-MB-231 cells, in comparison to MCF-7 cells are known to be highly aggressive and thus resistant to current chemotherapy treatments. As a result, a patient diagnosed with estrogen receptor-positive breast cancer will generally have a better prognosis than a patient diagnosed with estrogen receptor-negative breast cancer (Koutsilieris *et al*. 1999, Rochefort *et al.* 2003, Richert *et al.* 2005). It could be suggested that all the BNIPP derivatives will follow a similar trend, due to the different levels in cytotoxicity observed after BNIPSpd treatment in MDA-MB-231 and MCF-7 cells. The increased responsiveness of MCF-7 cells to BNIPSpd treatment could be related to several factors, for example the role of estrogen levels, ER or p53 mutations (Alami *et al.* 2007). Further comparative studies would need to be undertaken to determine the specific and selective cytotoxicity of all the BNIPP derivatives against MDA-MB-231 (ER-ve) and MCF-7 (ER+ve) breast cancer cell lines.

It is interesting to note that all BNIPP derivatives appeared to be more active against MCF-10A cells rather than MDA-MB-231 cells. This may be due to the observation that MCF-10A cells replicate at a faster rate than the MDA-MB-231 cells, as determined by cell count measurements[1] (results not shown).

BNIPP derivatives, due to their structural similarities to the natural polyamines were initially thought to be transported into cells by the use of an active transport system, such as the polyamine transporter (Dance *et al*. 2005). Several BNIPP derivatives were selected for further investigations into their mode of action within a breast cancer cell system. The selected derivatives were BNIPSpd, BNIPDaoct, BNIPDaoxoct and BNIPDaCHM (Figures 4.27 and 4.28). These derivatives all possess distinct structural variations at the point of diversity (Figure 4.25), and have exhibited varying degrees of cytotoxicity (Section 4.4.2).

In MDA-MB-231 cells, alterations to the spermidine linker, such as removal of a nitrogen atom (BNIPDaoct), and replacement of the spermidine linker with two cyclohexane rings (BNIPDaCHM) resulted in an increase in cytotoxicity compared with

[1] Cell count measurements were conducted following cell collection, as described in Section 4.3.1

BNIPSpd (IC_{50} values decreased from 12.7 µM with BNIPSpd, to 5.0 and 6.8 µM, for BNIPDaoct and BNIPDaCHM, Table 4.2). However, when the spermidine linker was replaced by a dioxoctane linker (BNIPDaoxoct); a similar level of cytotoxicity was observed with both BNIPP derivatives (IC_{50} values of 12.4 and 12.7 µM, respectively) (Figure 4.28).

In MCF-10A cells, BNIPSpd had an IC_{50} value of 4.2 µM, after 24 hours (Table 4.3). Changes to the central linker chain as indicated above resulted in an increase in cytotoxicity for BNIPDaoct (IC_{50} value of 2.8 µM), but a decrease in cytotoxicity for BNIPDaoxoct and BNIPDaCHM (IC_{50} values increased from 4.2 µM with BNIPSpd, to 6.0 and 6.1 µM, for BNIPDaoxoct and BNIPaCHM) (Figure 4.28).

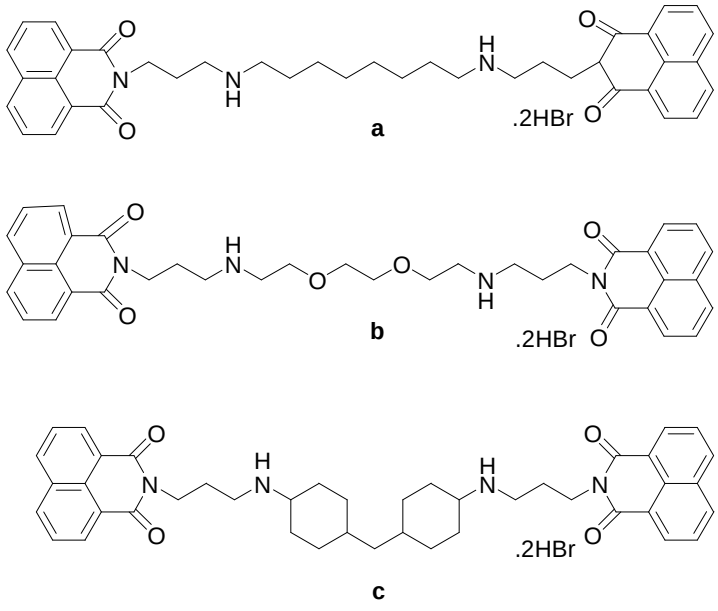

Figure 4.28.: Structures of BNIPDaoct **(a)**, BNIPDaoxoct **(b)** and BNIPDaCHM **(c)**

The modifications to the central linker chain within the selected BNIPP derivatives have resulted in differences in their observed cytotoxicity levels against both MDA-MB-231 and MCF-10A cells. These distinct structural differences might indicate that each derivative may possess an entirely different mechanism for cellular uptake and entry. This was further supported by the differing trends observed for each BNIPP derivative by fluorescence microscopy studies (Figures 4.15a-c – 4.16a-c) (Section 4.4.3), and polyamine transporter studies (Table 4.4) (Section 4.4.4).

4.5.3. Cellular Uptake of BNIPP Derivatives

The inherent fluorescence properties of the BNIPP derivatives allowed the studies of cellular uptake and distribution of BNIPSpd, BNIPDaoct, BNIPDaoxoct or BNIPDaCHM (10 µM) to be monitored by fluorescence microscopy (Figures 4.15a-c – 4.16a-c).

After 0.5 hours, only MDA-MB-231 cells treated with BNIPDaoct or BNIPDaCHM showed fluorescence (Figure 4.15a, b and c). Fluorescence was detectable over time in MDA-MB-231 cells treated with BNIPDaCHM whereas in BNIPDaoct treated MDA-MB-231 cells, fluorescence had disappeared after 6 hours (Figure 4.15a, b and c). This observation is in agreement with the higher toxicity of BNIPDaoct (IC_{50} value 5.0 µM, after 24 hours; Table 4.2), in comparison to BNIPDaCHM (IC_{50} value 6.8 µM, after 24 hours; Table 4.2) and the other BNIPP derivatives examined (BNIPSpd, IC_{50} value 12.7 µM; BNIPDaoxoct, IC_{50} value 12.4 µM, after 24 hours; Table 4.2). The apparent loss in fluorescence within BNIPDaoct treated MDA-MB-231 cells could be the result of BNIPDaoct being transported into the cells faster than the other BNIPP derivatives and metabolised very quickly. Interestingly, the fluorescence of BNIPSpd and BNIPDaoxoct in MDA-MB-231 cells was not observed until after 6 hours incubation. This may be due to the slower cellular uptake of BNIPSpd and BNIPDaoxoct into MDA-MB-231 cells, and hence could explain their lower toxicities (IC_{50} 12.7 and 12.4 µM, after 24 hours, respectively; Table 4.2) when compared with BNIPDaoct and BNIPDaCHM (IC_{50} 5.0 and 6.8 µM, after 24 hours, respectively; Table 4.2) (described in Section 4.5.2).

In MCF-10A cells treated with BNIPDaoct and BNIPDaCHM, fluorescence was observed after 0.5 hours incubation (Figure 4.16a-c). In contrast to treated MDA-MB-231 cells, fluorescence in BNIPDaoct treated MCF-10A cells remained with time (Figure 4.16a-c). BNIPDaoxoct treated cells showed fluorescence after 2 hours, whereas, BNIPSpd treated cells showed fluorescence after 6 hours. It would appear that BNIPP derivatives in MCF-10A cells utilise a mode of cellular uptake that is independent of cytotoxicity. This was a reasonable assumption because the uptake of BNIPSpd, BNIPDaoct, BNIPDaoxoct and BNIPDaCHM (IC_{50} values: 4.2, 2.8, 6.0 and 6.1 µM, after 24 hours, respectively, Table 4.3) into the MCF-10A cells was observed in the order of BNIPDaoct and BNIPDaCHM (0.5 hours), BNIPDaoxoct (2 hours) and BNIPSpd (6 hours). Therefore, the order of cellular uptake and cytotoxicity levels did not correlate with one another in MCF-10A treated cells.

Taken together, the results in this study suggest that each BNIPP derivative is taken up into MDA-MB-231 and MCF-10A cells by different mechanisms (i.e., cytotoxicity in MDA-MB-231 cells is related to uptake, whilst cytotoxicity in MCF-10A cells is not related to uptake), and that BNIPP derivative uptake is cell line dependent. The polyamine transporter studies further support this observation (Section 4.4.4).

In this study, it was difficult to confirm the cellular location of the BNIPP derivatives in MDA-MB-231 and MCF-10A cells. Earlier work by Pavlov *et al.* (2001), however,

showed that 5, 10 and 25 µM of BNIPSpd, BNIPSpm and BNIPOSpm was localised within the cell nuclei of breast cancer (MCF-7) cells, after 8 hours incubation. Further fluorescence microscopy studies with BNIPSpd, BNIPSpm and BNIPOSpm by Dance *et al.* (2005), revealed nuclear localisation in MCF-7 and colon cancer (CaCO-2) cells, after 2, 3 and 12 hours, respectively. Although, in this study, the exact cellular location of the BNIPP derivatives could not be determined in either cell line; it should be noted that future studies would be undertaken using a confocal microscope to allow the greater resolution of specific cell organelles (Cullis *et al.* 1999).

4.5.4. Polyamine Transporter Studies with BNIPP Derivatives

The simple, reliable and sensitive model identified for derivative and conjugate delivery via the MGBG-specific polyamine transporter (Gardner *et al.* 2004, Tsen *et al.* 2008) has been successfully utilised in this study to investigate BNIPP derivative transport for the first time. The PAT model which uses CHO-MG and CHO cell lines (Gardner *et al.* 2004, Tsen *et al.* 2008) was used to identify a possible mechanism of cellular entry employed by the BNIPP derivatives: BNIPSpd, BNIPDaoct, BNIPDaoxoct and BNIPDaCHM.

In this study, none of the BNIPP derivatives enter the cells by the MGBG-specific PAT. This was determined by CHO-MG/CHO IC_{50} ratios which ranged from 0.4 – 1.0 (Table 4.4). Therefore, BNIPP derivatives must enter cells by other mechanisms that are independent of the MGBG-specific PAT. These alternative mechanisms may include passive diffusion and/or utilisation of another transporter or other membrane receptor interactions (Gardner *et al.* 2004).

The MGBG-specific PAT has been thoroughly investigated, and the naturally occurring polyamines (putrescine, spermidine and spermine) are all transported via this transport system (Heaton and Flintoff 1988, Wang *et al.* 2003a, Wang *et al.* 2003b, Wang *et al.* 2003c, Gardner *et al.* 2004, Kaur *et al.* 2005, Tsen *et al.* 2008). The structural tolerances of the PAT system allow transport of non-native polyamine-like derivatives, which contain linear polyamine motifs into different cellular systems (Wang *et al.* 2003a, Wang *et al.* 2003b, Wang *et al.* 2003c). The affinity of a derivative to utilise the PAT has been shown to increase with the increasing number of positive charges, therefore affinity increases from putrescine through to spermine (Seiler *et al.* 1996). However, recent studies into the anthracene-polyamine conjugates have suggested that there are several limitations to the structural tolerances of the PAT system (Wang *et al*. 2001, Wang *et al.* 2003a, Wang *et al.* 2003b, Wang *et al.* 2003c, Kaur *et al.* 2008a).

While BNIPP derivatives do not use the MGBG-specific PAT, many other polyamine-like derivatives and conjugates have been shown to successfully exploit it. These include several anthracene-polyamine conjugates, in particular, anthracen-9-ylmethyl-4,4-triamine trihydrochloride and anthracen-9-ylmethyl-4,4-tetraamine

tetrahydrochloride (Figure 4.3), which are highly selective PAT substrates (CHO-MG/CHO ratios are 148 and 3.1, respectively) (Wang *et al.* 2003a, Gardner *et al.* 2004). The uptake of these anthracene-polyamine conjugates and their analogues has been shown to be dependent upon the number of methylene (-CH_2-) groups, in which, the naphthylmethyl and naphthylethyl conjugates were highly selective PAT substrates (CHO-MG/CHO IC_{50} ratios were > 164), but the naphthylpropyl conjugate had no PAT selectivity (IC_{50} values were > 500, in both cell lines) (Figure 4.29). The addition of an extra methylene group appears to be sufficient to reduce cytotoxicity within CHO-MG and CHO cells. It was demonstrated that increasing tether length, reduced PAT-selectivity (Gardner *et al.* 2004). This trend was also apparent in the anthracenyl series of conjugates, where the most PAT-selective conjugate was anthracen-9-ylmethyl-4, 4-tetraamine tetrahydrochloride (CHO-MG/CHO ratio was 148) (Figure 4.3) (Wang *et al.* 2003a, Gardner *et al.* 2004).

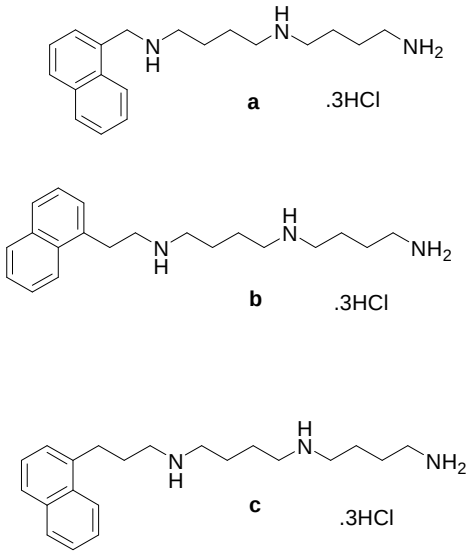

Figure 4.29.: Structures of anthracene-polyamine conjugates (*N*-(4-Aminobutyl)-*N*'-(2-naphthalen-1-yl-methyl)butane-1,4-diamine trihydrochloride **(a)**, *N*-(4-Aminobutyl)-*N*'-(2-naphthalen-1-yl-ethyl)butane-1,4-diamine trihydrochloride **(b)**, and *N*-(4-Aminobutyl)-*N*'-(2-naphthalen-1-yl-propyl)butane-1,4-diamine trihydrochloride) **(c)**

Other anthracenyl conjugates that contain structural similarities to the BNIPP derivatives have been investigated. These include the bis-anthracenyl conjugates, *N*-Anthracen-9-ylmethyl-N^1-{4-[(anthracen-9-ylmethyl)-amino]butyl}butane-1,4-diamine tetrahydrochloride (with two bulky hydrophobic groups, secondary amines and a linker similar to BNIPSpd); N^1-Anthracen-9-ylmethyl-octane-1,8-diamine dihydrochloride (with one bulky hydrophobic group, a primary amine and a eight methylene linker chain similar to BNIPDaoct); 2-(2-{2-[(Anthracen-9-ylmethyl)-amino]-ethoxy}-ethoxy)-ethylamine dihydrochloride (with one bulky hydrophobic group, a primary amine and a linker similar to BNIPDaoxoct), and *N*-{4-[(Anthracen-9-ylmethyl)-amino]butyl}-cyclohexane-1,4-diamine trihydrochloride (with one bulky hydrophobic group and a primary amine) (Figure 4.30a-d) (Wang *et al.* 2003a, Gardner *et al*. 2004). These conjugates were shown to have no preference for either CHO cell line, and therefore do not exploit the polyamine transporter

(CHO-MG/CHO ratios of 1 - 7). The CHO-MG/CHO ratios were comparable to those produced by the BNIPP derivatives (CHO-MG/CHO ratios of 0.4 – 1; Table 4.4).

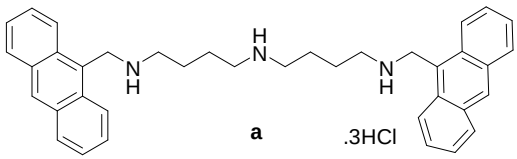

a .3HCl

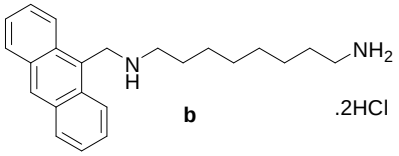

b .2HCl

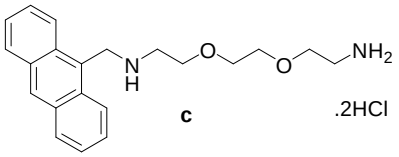

c .2HCl

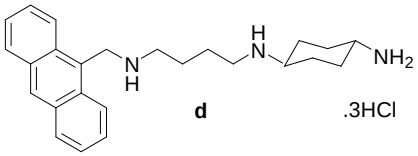

d .3HCl

Figure 4.30.: Structure of bis-anthracenyl conjugates: *N*-Anthracen-9-ylmethyl-N^1-{4-[(anthracen-9-ylmethyl)-amino]butyl}butane-1,4-diamine tetrahydrochloride **(a-d)**

In summary, the polyamine sequence (putrescine, spermidine or spermine), size, N^1-substituents, presence of primary amine, and conjugate length (i.e., the number of methylene groups) are all important structural features required to obtain optimum PAT-selectivity (Seiler 2005, Kaur *et al*. 2008a Kaur *et al*. 2008b, Tsen *et al.* 2008). The *N*-naphthylmethyl 4, 4-triamine conjugate provided the best PAT-selectivity profile (150-fold higher cytotoxicity in CHO cells than in CHO-MG cells), and hence shorter linker groups appear to be essential to impart PAT affinity (Kaur *et al*. 2008a). As a result, the BNIPP derivatives which contain two naphthalimidopropyl groups are too large to be imported into cells via the MGBG-specific polyamine transporter (Kaur *et al.* 2008b). Due to the complexity of the polyamine transport system and its lack of characterisation at a molecular level, it is difficult to state whether the BNIPP derivatives may utilise a currently unknown polyamine transporter, or may due to their structure, inhibit their own cell uptake (Cullis *et al.* 1999, Graminski *et al*. 2002, Mitchell *et al.* 2007, Ralton *et al*. 2007). Further investigations into the mechanism of BNIPP derivative transport into cells would provide a better understanding of the mode of action of BNIPP derivatives within cellular systems.

4.5.5. Intracellular Polyamine Levels

In MDA-MB-231 cells, 24 hours treatment with BNIPSpd or BNIPDaoct, at 0.1 μM, significantly increased spermidine and spermine levels ($P < 0.01$; BNIPSpd; Figure 4.17 and $P < 0.05$; BNIPDaoct; Figure 4.18), whilst BNIPDaoxoct (0.1 μM), significantly increased putrescine levels ($P < 0.05$; BNIPDaoxoct; Figure 4.19) when compared to that of the control. However, at 0.1 μM, BNIPDaCHM did not alter putrescine, spermidine or spermine levels when compared with the control (Figure 4.19). No change to putrescine, spermidine or spermine levels was observed after 24 hours treatment with BNIPSpd, BNIPDaoct, BNIPDaoxoct or BNIPDaCHM, at 1 μM, when compared with the control (Figures 4.17 – 4.19). At 5 μM, BNIPSpd significantly decreased putrescine and spermidine levels ($P < 0.05$), whilst a significant decrease in putrescine ($P < 0.05$), spermidine ($P < 0.01$) and spermine ($P < 0.05$) levels was observed following treatment with BNIPDaoct (5 μM), compared to the control (Figures 4.17 – 4.18). No change in putrescine, spermidine or spermine levels was observed after 24 hours treatment with either BNIPDaoxoct or BNIPDaCHM (5 μM) when compared to the control (Figures 4.19 – 4.20).

In MCF-10A cells, treatment with 0.1 μM BNIPDaoxoct significantly increased spermidine and spermine levels ($P < 0.05$; Figure 4.23), whilst treatment with 1 μM BNIPDaCHM significantly increased putrescine levels ($P < 0.05$; Figure 4.24). Treatment with BNIPDaoct (5 μM) or BNIPDaoxoct (1 – 5 μM) significantly decreased putrescine (BNIPDaoct; $P < 0.05$; Figure 4.22), spermidine and spermine (BNIPDaoxoct; $P < 0.05$; Figures 4.23) levels in MCF-10A cells. No change in polyamine levels (putrescine, spermidine or spermine) were observed after treatment with BNIPSpd (0.1 – 5 μM) in MCF-10A cells (Figure 4.21).

In both cell lines, it was not possible to establish trends in the levels of polyamines after treatment with each BNIPP derivative. This conclusion was supported by inconsistent up- and down- regulation effects reported on intracellular polyamine levels in both MDA-MB-231 and MCF-10A cells (Figures 4.17 – 4.24). The specific effect of BNIPP derivatives on intracellular polyamine levels appears to be related to their different mechanisms of action which could be of a direct or an indirect nature (Holst *et al.* 2006). The influence of BNIPP derivatives on intracellular polyamine levels may be related to their cytotoxicities, and their differing trends in cellular uptake and transport (as described in Sections 4.5.2, 4.5.3 and 4.5.4). Importantly, treatment with 0.1 μM of BNIPSpd, BNIPDaoct or BNIPDaoxoct significantly increased intracellular polyamine levels, as cells react and adapt to the presence of BNIPP derivatives (at a non toxic concentration), hence an increase to cell proliferation should also be observed at this concentration.

In this study, putrescine, spermidine and spermine were all successfully detected using the method of pre-column derivatisation with dansyl chloride followed by HPLC separation and fluorescence detection (Marcé *et al.* 1995, Weeks *et al.* 2000, Huang *et al.*

2003, Burns *et al.* 2009). Putrescine, the precursor of polyamine biosynthesis is rapidly converted into the tri- and tetra-amines, spermidine and spermine, therefore low levels of putrescine can normally be detected in eukaryotic cells (Wallace 1996, Khuhawar and Qureshi 2001). Low levels of putrescine were detected in both MDA-MB-231 and MCF-10A cells, in comparison to the levels of spermidine and spermine. Low or undetectable levels of putrescine have been previously reported in several studies (Bergeron *et al.* 1997, Manni *et al.* 2002, Huang *et al.* 2003, Richert *et al.* 2005, Ralton 2006).

Polyamines are essential in cell proliferation and differentiation, and are important in the progression of the aggressive and resistant features of metastatic breast cancer (Pegg 1988, Glikman *et al.* 1989, Manni *et al*. 2002) (Section 1.4). Rapidly dividing cells, (i.e., cancer cells) have higher levels of ODC activity, thus higher levels of intracellular polyamines (Lindsay and Wallace 1999, Manni *et al*. 2002). These observations were in contrast to the levels determined in the surrounding non-cancerous cells, where lower levels of intracellular polyamines were detected (Khuhawar and Qureshi 2001). It was observed in this study that putrescine levels were higher in untreated MDA-MB-231 cells (0.43 µM/1x10^6 cells) than in untreated MCF-10A cells (0.16 µM/1x10^6 cells), but spermidine and spermine levels were approximately the same in both cell lines (ranging between 3.03 – 3.21 µM/1x10^6 cells and 2.56 – 2.66 µM/1x10^6 cells, respectively) (Figures 4.17 - 4.24). The similarity in the spermidine and spermine levels in MDA-MB-231 and MCF-10A cells may possibly be explained by the observation that MCF-10A cells replicate at a faster rate that the MDA-MB-231 cells (as discussed in Section 4.5.2).

Colon cancer (CaCO-2 and HT-29) cells previously investigated by Ralton (2006) and Ralton *et al.* (2009) had higher concentrations of polyamines than MDA-MB-231 and MCF-10A breast cells (Ralton 2006). The polyamine content of serum and urine in individuals diagnosed with colon cancer have also been found to be highly elevated when compared with breast and prostrate cancer cells, or non-cancerous cells (Levêque *et al.* 2000, Milovic 2001, Wallace and Caslake 2001). This was noted to be due to the readily available uptake of exogenous polyamines from the diet, and/or from the production of polyamines from intestinal flora (as described in Section 4.1.3) (Seiler *et al.* 1990, Milovic *et al.* 2001, Thomas and Thomas 2001, Larqué *et al.* 2007).

Previous studies conducted by Ralton (2006) and Ralton *et al.* (2009) found that the concentration of DFMO that significantly reduced intracellular polyamine levels after treatment for 12 hours (HL60 cells) or 24 hours (CaCO-2 and HT-29 cells) was 5 mM, whereas in MDA-MB-231 and MCF-10A cells, treatment with DFMO (5 mM) for 24 hours did not significantly reduce intracellular polyamine levels. Treatment with 5 µM BNIPSpd, BNIPDaoct, BNIPDaoxoct or BNIPDaCHM induced instead a similar or greater effect on intracellular polyamine levels than DFMO in MDA-MB-231 and MCF-10A cells (Figures 4.17 – 4.24). It should be noted that the effect of DFMO on cancer cells is usually cytostatic, not cytotoxic in nature. Thus, DFMO causes a decrease in cell proliferation,

with a lack of cell death (Meyskens and Gerner 1999). The lack of an effect after DFMO treatment observed in this study could be supported by previous studies (Glikman *et al.* 1989, O'Shaughnessy *et al.* 1999, Manni *et al.* 2002), which showed that DFMO may induce cell-type specificity in metastatic breast cancer cells. Therefore, the effect of DFMO treatment can differ depending on the breast cell line used in an investigation. Another interesting finding was that significant suppression in MDA-MB-231 intracellular polyamine levels was observed only after 6 days of DFMO treatment (> 0.1 mM), as assessed by Glikman and colleagues (1989). However, in this study, DFMO treatment (5 mM) was undertaken for only 24 hours. Further investigations into the effect of DFMO treatment in MDA-MB-231 cells after longer treatment periods would provide a true comparison with published data.

In this study, the reduction in intracellular polyamine levels after BNIPSpd treatment in MDA-MB-231 and MCF-10A cells was different to that observed in CaCO-2 and HT-29 cells (Ralton *et al*. 2009). After 24 hours, BNIPSpd induced a significant decrease in putrescine and spermidine levels in MDA-MB-231 cells (at 5 µM) and no change in intracellular polyamine levels in MCF-10A cells (Figures 4.17 and 4.21), whereas BNIPSpd induced a significant reduction in spermidine and spermine levels in CaCO-2 and HT-29 cells, from ≥ 0.01 µM (Ralton *et al*. 2009). This indicates the potential for each BNIPP derivative to have a cell-specific selectivity in the reduction of intracellular polyamine levels (Huang *et al*. 2003, Holst *et al.* 2006). Interestingly, previous reports into BNIPSpd have proposed that the reduction of intracellular polyamine levels were a direct effect of BNIPSpd treatment, thus contributing to its high cytotoxicity levels in CaCO-2 and HT-29 cells (i.e., IC_{50} values of 0.47 and 2.4 µM, after 24 hours) (Ralton *et al*. 2009). However, the lack of a significant reduction in intracellular polyamine levels in MDA-MB-231 and MCF-10A cells, after BNIPSpd, BNIPDaoct, BNIPDaoxoct or BNIPDaCHM treatment showed that the modulation of polyamine levels in these cells do not appear to be linked directly to cytotoxicity levels. Consequently, the effect of polyamine levels on BNIPP derivative cytotoxicity may again be cell line specific (Huang *et al*. 2003). It should be noted that further investigations into the mechanistic link between the reduction of intracellular polyamine levels and cytotoxicity would provide a better understanding into the mode of action of BNIPP derivatives within different cellular systems.

4.6. Conclusion

The BNIPP derivatives were shown to significantly affect cell morphology and cell viability of MDA-MB-231 and MCF-10A cells treated for 24 hours. Cell morphology was visually altered, with an apparent loss of cell adherence. All BNIPP derivatives, except BPHPDadec and NPA (IC_{50} values of > 40 μM), exhibited cytotoxic properties in both cell lines. With cytotoxicity results confirming the importance of (i) bisnaphthalimidopropyl functionality; (ii) an alkyl chain length of between 8 – 10 alkyl groups; and (iii) two nitrogen atoms in the linker by which to increase aqueous solubility, and maintain biological activity. Cellular uptake studies have revealed that each BNIPP derivative is taken up by a different mode of action as uptake and cytotoxicity results are in agreement in MDA-MB-231 treated cells, but not in MCF-10A treated cells. Thus, the extent of BNIPP derivative uptake appears to be cell line dependent. None of the selected BNIPP derivatives were found to utilise the MGBG-specific PAT system. Due to the size of the BNIPP derivatives (i.e., the naphthalimido groups), it appears that these derivatives are too large to exploit the MGBG-specific PAT system, thus, they may employ another currently unknown mode of cellular entry. Intracellular polyamine levels were up-and down- regulated with different concentrations of BNIPP derivatives in MDA-MB-231 and MCF-10A cells, and as a result, it was not possible to establish trends between polyamine levels and BNIPP derivative induced cytotoxicity.

Due to variations in their central linker chain, BNIPSpd and BNIPDaCHM were selected for further analysis. These derivatives were investigated in order to assess their ability to (i) induce DNA damage (Chapter 5), (ii) initiate cell death (Chapter 6) and (iii) inhibit histone deacetylase activity (Chapter 7).

Chapter 5

DNA Damage and Repair Studies of BNIPP Derivatives in MDA-MB-231 and MCF-10A Cells

5.1. DNA Damage and Repair Studies of BNIPP Derivatives in MDA-MB-231 and MCF0-10A Cells

One of the current therapeutic strategies involves the ability of anti cancer agents to inflict DNA damage and induce cancer cell death (Liao *et al.* 2009). For example, many intercalating anti cancer agents, such as diacridines (Roos *et al.* 1985) and anthracyclines (Swift *et al.* 2006), have been shown to produce DNA strand breaks (e.g., single and double strand breaks). Their therapeutic use relies upon their ability to target DNA by intercalation, and their resultant cytotoxicities are related to the extent of DNA damage induced. This mode of action is considered to be the most effective in the current treatment of cancer (e.g., in acute leukaemias, and breast, ovarian and bladder cancers) (Cancer Research UK, 2009a, Cancer Research UK, 2009b). DNA damaging agents are continually being discovered and developed, supporting the need to investigate the influence of BNIPP derivatives on intracellular DNA stability.

The aims of the experimental work reported in this chapter were to (i) study the extent of DNA damage inflicted in MDA-MB-231 and MCF-10A cells treated with BNIPSpd or BNIPDaCHM, and (ii) determine the ability of these derivatives to interfere with the repair of oxidative or methylation-induced DNA strand breaks in MDA-MB-231 cells.

5.1.1. Significance of DNA Damage within a Cell System

DNA damage can occur within all eukaryotic cells, and is induced by different endogenous or exogenous DNA damaging agents. These agents include (i) products of normal cellular metabolism and proliferation (e.g., free radical attack, reactive oxygen species (ROS) or spontaneous reactions, i.e., mutations), (ii) environmental agents (e.g., ultraviolet (UV) light or ionising (X and γ rays) radiation), or (iii) chemical agents (e.g., alkylating anti cancer agents) (Collins 1996, Hoeijmakers 2001) (Figure 5.1). These agents cause structural changes to the DNA structure with alterations to nucleotides and/or by breakage of the sugar-phosphate backbone, which can lead to a non functional DNA structure (Vijg 2007). Structural changes are responsible for the presence of permanent DNA damage, and if DNA damage cannot be repaired before replication begins, disruption to DNA metabolism and cell cycle arrest can occur; causing cellular ageing, neurodegenerative disorders, tumourigenesis or cancer in somatic cells (Figure 5.1) (Collins 1996, Hoeijmakers 2001, Kastan 2008).

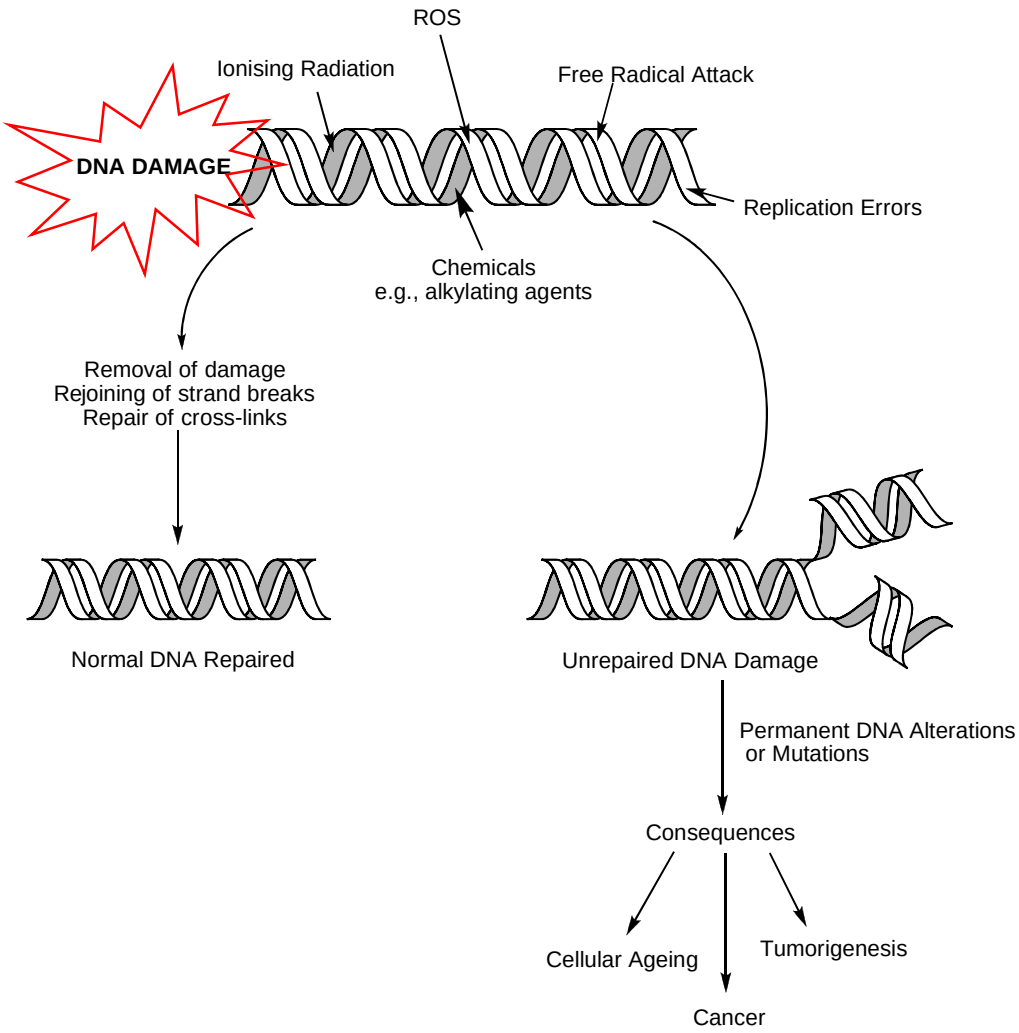

Figure 5.1.: Schematic representation of the causes and consequences of DNA damage in somatic cells [adapted from Collins 1996, pp. 231].

DNA damage is also linked to many heritable cancers which are caused by the inheritance of mutations to genes responsible for DNA damage responses (Kastan 2008). For example, mutations in BRCA1/BRCA2 genes result in the predisposition of breast and ovarian cancers or the inheritance of mutated genes involved in mismatch repair results in the high incidence of hereditary nonpolyposis colon cancer (HNPCC) (Hoeijmakers 2001, Kastan 2008). DNA damage responses are also relevant, as current cancer treatments (i.e., radiotherapy or chemotherapy) target DNA, causing DNA damage and killing cancer cells. As DNA damage can cause cancer and is used in cancer treatment; all cells, therefore, require specific mechanisms that can detect and repair both endogenously and exogenously induced DNA damage.

5.1.2. Mechanisms of DNA Repair within a Cell System

DNA repair mechanisms are utilised to protect cells from DNA damage in response to DNA damaging agents. Cells have an inherent ability to repair DNA damage, and in most cases, DNA damage is “simply reversed” (Collins 1996, pp. 237). The fate of

a cell is dependent upon the extent of DNA damage induced. If minimal DNA damage has been induced; repair mechanisms will cause cell cycle arrest, allowing DNA repair by removal of damage and rejoining of strand breaks, but maximal or too much DNA damage can lead to cells being unable to be repaired thus leading to apoptotic cell death (Figure 5.1) (Collins 1996, Damia and D'Incalci 2007). The former leads to cell survival, whilst the latter leads to cell death (Damia and D'Incalci 2007).

The most important DNA repair mechanisms that can detect and repair DNA damage are shown in Figure 5.2. These repair mechanisms include (i) repair of damaged bases induced by oxidative or methylating agents, by base excision repair (BER), (ii) repair of UV-induced DNA-distorting damage via nucleotide excision repair (NER), (iii) repair of single- (SSBs) or DSBs induced by ionising radiation, free radical attack or methylating anti cancer agents repaired by both homologous recombination (HR) repair or non homologous end joining (NHEJ) repair, and (iv) repair of mispairings and insertion/deletion of nucleotides in newly synthesised DNA by mismatch repair (MMR) (Figure 5.2) (Collins 1996, Damia and D'Incalci 2007, Ljungman 2009). The aforementioned DNA repair mechanisms are generally defective in cancer cells. Thus, the manipulation of DNA repair mechanisms which induce cell death can provide potential targets for anti cancer therapies.

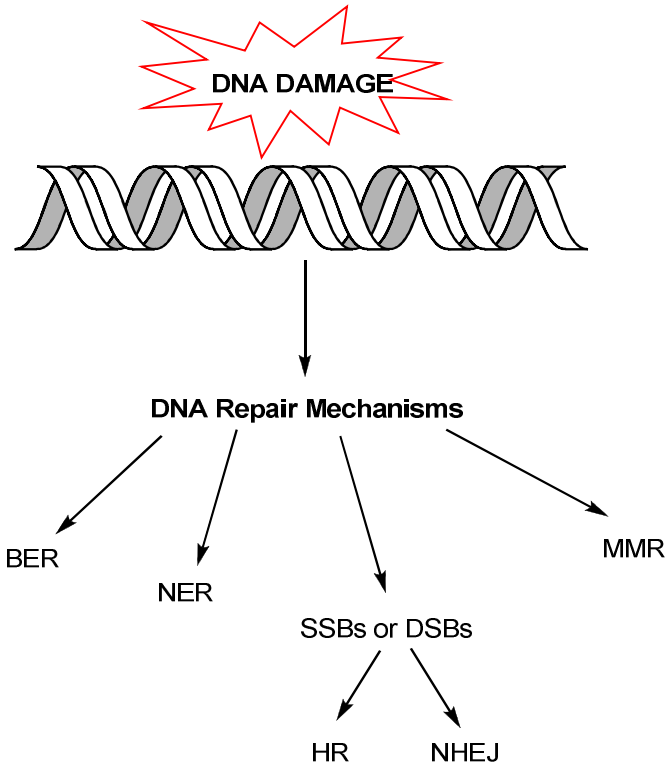

Figure 5.2.: Schematic representation of the main DNA repair mechanisms. BER: Base Excision Repair; NER: Nucleotide Excision Repair; SSBs: Single Strand Breaks; DSBs: Double Strand Breaks; HR: Homologous Recombination; NHEJ: Non Homologous End Joining; MMR: Mismatch Repair [Adapted from Damia and D'Incalci 2007, pp 1792].

5.1.3. Assessment of DNA Strand Breaks

Numerous methods are available to access DNA damage within mammalian cells (Poulsen *et al.* 1999, Kumari *et al.* 2008). Examples include (i) the detection of DNA damage in individual cells by either the neutral or alkali comet assays (Singh *et al.* 1988); (ii) the detection of oxidative DNA damage, via gas chromatography-mass spectrometry (GC-MS) (Nyaga *et al.* 2007), ^{32}P post-labelling combined with high performance liquid chromatography (HPLC) (Munnia *et al.* 2007) or an immunological assay (Leuratti *et al.* 1998), and (iii) detection of multiple DNA modifications, by liquid chromatography tandem MS (Nyaga *et al.* 2007). In this study, DNA strand breaks were assessed using the Single Cell Gel Electrophoresis (SCGE or Comet assay). The alkaline comet assay (pH > 13) was developed by Singh *et al.* in 1988, and due to its high sensitivity (50 – 15,000 breaks/cell), rapidity and reproducibility, is the most widely used technique in the quantification of DNA damage within individual mammalian cells (Fairburn et al. 1995, Piperakis 2009). It can not only detect SSBs and alkali-liable sites (ALS), but has also been adapted to evaluate DNA repair in response to oxidative (Hydrogen peroxide, H_2O_2) or methylation (Methyl methanesulfonate, MMS) induced DNA damage (Duthie *et al*. 2000, Sekihashi *et al*. 2003, Ralton. 2006). Figure 5.3 illustrates the general method of the alkaline comet assay.

For the comet assay, cells were embedded in low melting point (LMP) agarose on a frosted microscope slide (Figure 5.3) and placed in lysis solution consisting of high salts and detergents, to remove cellular proteins (Tice et al. 2000). Prior to electrophoresis, the slides were incubated in an alkaline (pH > 13) electrophoresis buffer to allow alkaline DNA unwinding. Alkaline DNA unwinding produces single stranded DNA and allows the maximum expression of ALSs as SSBs (Tice et al. 2000, Liao *et al.* 2009). After alkaline unwinding, relaxed single stranded DNA was electrophoresised (alkaline conditions, pH > 13) where DNA loops are pulled towards the anode, to form ‘comets’ (Duthie et al. 2000). After electrophoresis, the gels were neutralised and stained with a DNA-binding dye. Comets were visualised with fluorescence microscopy analysis (Gedik et al. 1992, Tice et al. 2000).

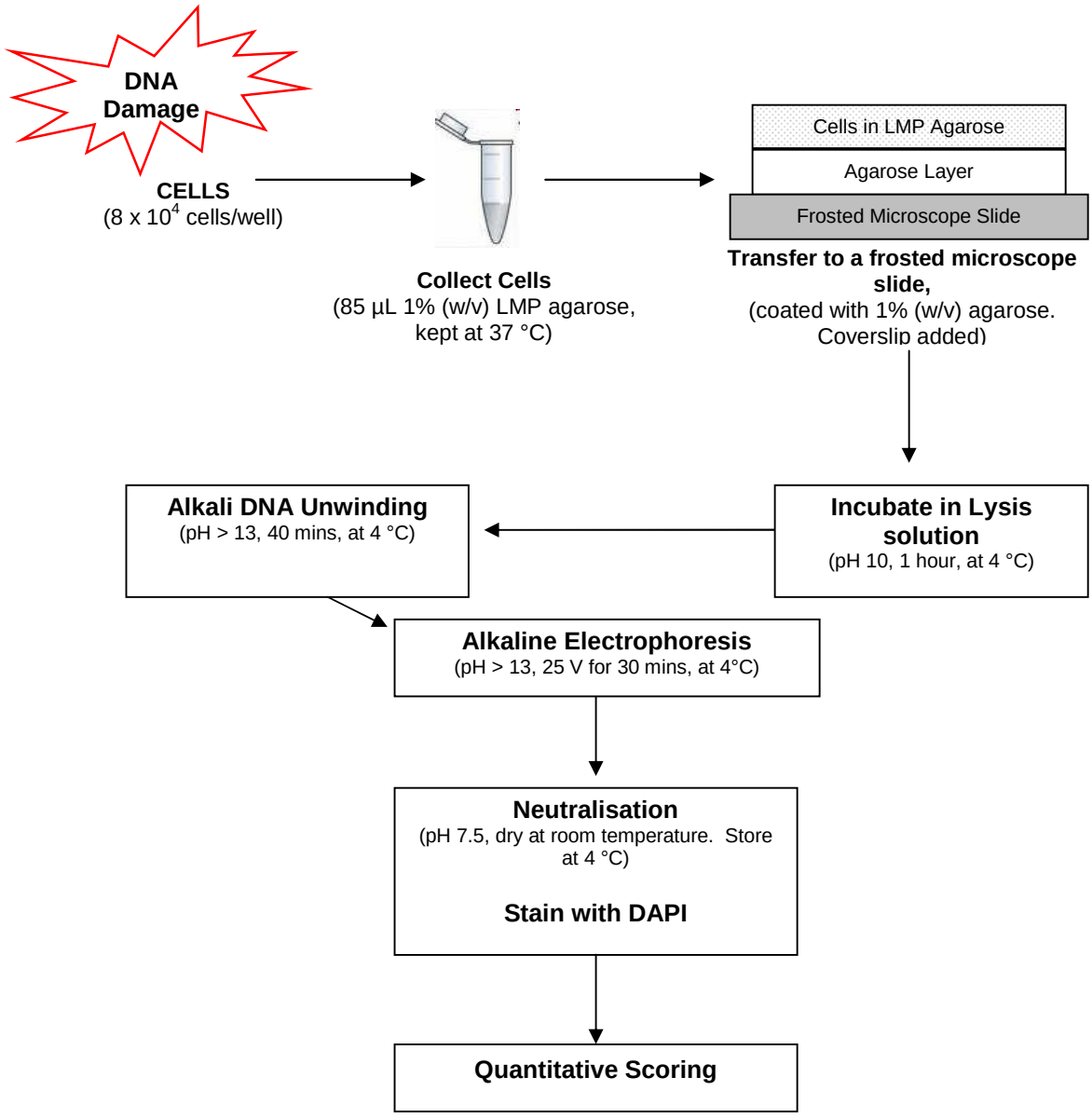

Figure 5.3.: General schematic representation of the alkaline comet assay (The Eppendorf tube image was obtained from www.freeclipartnow.com/science/flasks-tubes).

Figure 5.4 illustrates examples of the visual scoring classifications. An undamaged nucleotid appears with an intact 'head' and no 'tail' (Score 0), whilst a damaged nucleotid appears as a comet with a bright fluorescent 'head' and a 'tail' (Score 4) (Figure 5.4). The relative fluorescence intensity of the 'head' and the length of the 'tail' are directly proportional to the extent of DNA strand breaks (Duthie and Collins 1997). This visualisation method has been previously validated by Duthie and Hawdon (1998), and has been successfully used in the analysis of DNA damage exerted by BNIPSpd, BNIPSpm and BNIPOSpm as described by Dance *et al.* (2005) and Ralton *et al.* (2009).

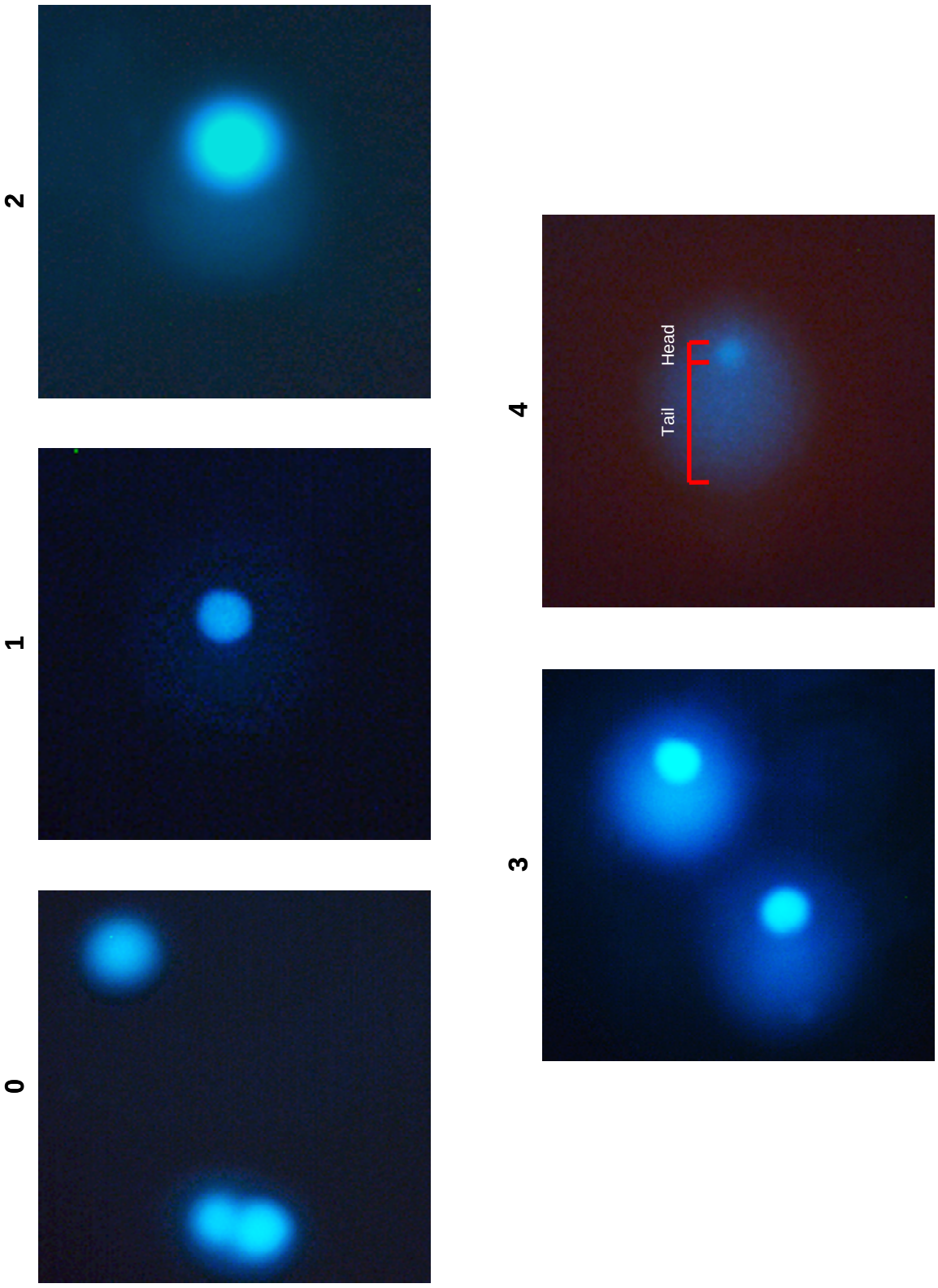

Figure 5.4.: DNA damage in MDA-MB-231 cells as determined by comet assay. Cells were visulised using a Leica DMRB fluorescence microscope with D filter (ex bandpass (violet); 355 – 425 nm; em longpass (green); 470 nm) following staining with DAPI. Images are representative for the comet images obtained for nucleotides with scores 0 – 4 (undamaged – damaged). Magnification x200.

5.2 Materials

5.2.1. Materials

All reagents were purchased from Fisher Scientific, UK unless otherwise stated, and were used without purification.

Agarose	Bioline, UK
Ethylenediaminetetraacetic acid	Sigma-Aldrich, UK
Hydrogen Peroxide	Aldrich, UK
4'6-diamidine-2-phenylindol dihydrochloride	Fluka, UK
Low Melting Point Agarose	Sigma-Aldrich, UK
Methyl Methanesulfonate	Aldrich, UK
Triton-X 100	Sigma-Aldrich, UK

5.2.2. Instrumentation

Aseptic cell culture techniques were undertaken as described in Section 4.2.2.

For Comet assay analysis, a Horizon 20.25 horizontal gel electrophoresis tank (Gibco, UK) was used. The comets were visualised using a Leica DMRB fluorescence microscope (Leica Microsystems, UK) with a D filter (excitation bandpass (violet); 355 – 425 nm, emission longpass (green); 470 nm). Microscopy images were captured using a Leica DFC 300 FX camera (Leica Microsystems, UK), and viewed with a Leica Application Suite (Version 2.71 RI, 2003 – 2007) (Leica Microsystems, Switzerland).

5.3. Methods

5.3.1. Maintenance of Cells

MDA-MB-231 and MCF-10A cells were sub cultured and counted, as described in Sections 4.2.2 and 4.3.1 - 4.3.2. For both DNA damage and repair studies (in response to H_2O_2 or MMS treatment), MDA-MB-231 and MCF-10A cells were seeded in 24 well plates (8 x 10^4 cells/well) and allowed to grow for 24 hours before treatment. The cells were incubated with BNIPSpd or BNIPDaCHM (0 – 10 µM) for up to 24 hours, at 37 °C in 24 well plates, as shown in Figure 5.5.

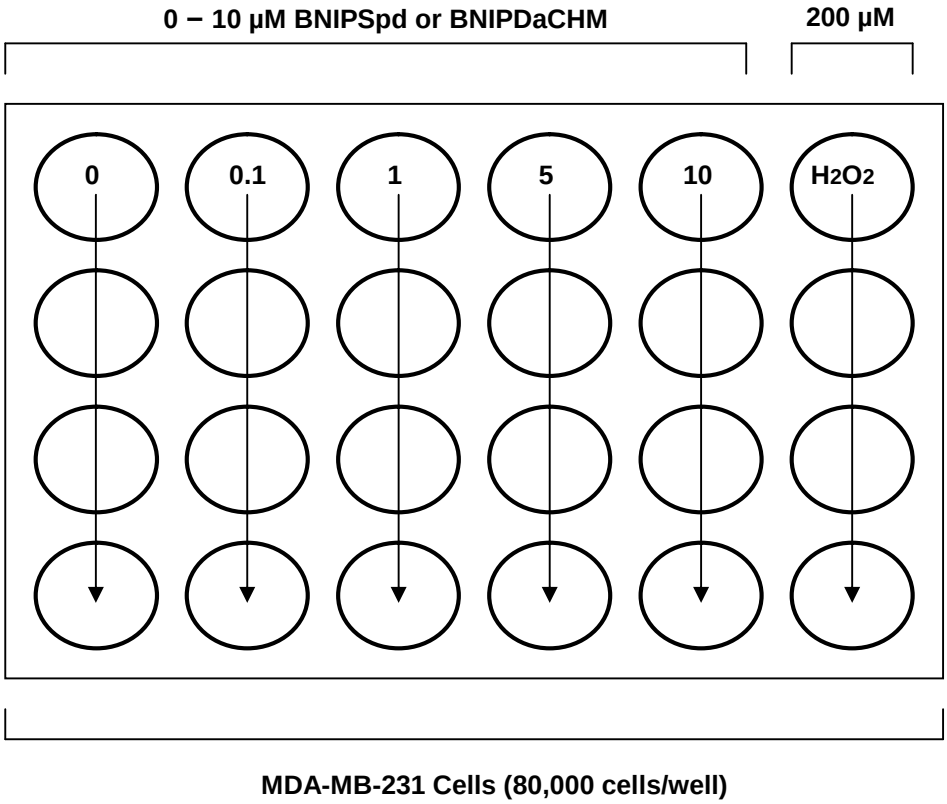

Figure 5.5.: An example of the set up for a 24 well plate used for the DNA damage and repair studies

5.3.2. Preparation of BNIPP Derivatives

The BNIPP derivatives: BNIPSpd and BNIPDaCHM were synthesised as previously described in Section 2.3. BNIPSpd and BNIPDaCHM were diluted to the desired concentrations of 0.1, 1, 5 and 10 µM, as described in Section 4.3.3.

5.3.3. Preparation of H_2O_2 and Methyl Methane Sulfonate (MMS) Solutions

The H_2O_2 stock solution (10 M) was diluted to the desired final concentrations of 50 – 800 µM in PBS. The MMS stock solution (45 mM) was diluted to the desired final concentrations of 0.25 – 5 mM in serum free media. Both control solutions were prepared immediately prior to use.

5.3.4. Slide Preparation

The slides were prepared immediately before use, following the method first described by Singh *et al.* (1988), and further adapted by Dance *et al.* (2005). 85 µL of 1% (w/v) agarose in PBS (at 60 °C) was quickly layered onto a fully frosted microscope slide (Richardson Supply Co., UK) and covered with an 18 x 18 mm cover slip (No. 1 glass). The slides were kept at 4°C until required.

5.3.5. Alkaline Single Cell Gel Electrophoresis (the Comet Assay)

MDA-MB-231 and MCF-10A cells were treated with BNIPSpd and BNIPDaCHM (0.1 – 10 µM) for 24 hours (refer to Figure 5.7). After 24 hours, the MDA-MB-231 and MCF-10A cells were washed with 800 µL of medium containing either 10 % (v/v) FCS or 5 % (v/v) HS, respectively, and the cell solution collected in sterile Eppendorf tubes as described in Section 4.3.1. The cells were centrifuged at 2000 rpm (ALC Multispeed Refrigerated Centrifuge, Thomson Scientific, UK) for 5 minutes, at 4 °C. The supernatant was removed and 85 µL of 1 % (w/v) LMP agarose in PBS (at 37 °C) added quickly to the cell pellet. The cell suspension was transferred onto a pre coated microscope slide; prepared as described in Section 5.3.4. The gel was covered with an 18 x 18 mm cover slip (No. 1 glass) and allowed to harden for 10 minutes, at 4 °C (Figure 5.3). Slides were placed into cooled black staining jars with 200 mL lysis solution (2.5 M NaCl, 0.1 M EDTA, 10 mM Tris, NaOH to pH 10, and 1% (v/v) Triton X-100, pH 10), and incubated for at least 1 hour, at 4 °C. Slides were arranged horizontally in an electrophoresis tank with 1500 mL of cooled electrophoresis buffer (0.3 M NaOH and 1 mM EDTA, pH >13), and incubated for 40 minutes, at 4 °C. Electrophoresis was carried out at 25V for 30 minutes, at 4 °C. The slides were placed into cooled black staining jars with 200 mL neutralising buffer (0.4 M Tris-HCl, pH 7.5), and washed three times for 5 minutes each wash, at 4 °C. Slides were left to dry at room temperature before comet scoring.

5.3.6. Quantification of the Comet Assay

For comet scoring, 20 µL of 4',6-diamidine-2-phenylindol dihydrochloride (DAPI) (1 µg/mL) dye was added to each gel, and covered with a 22 x 22 mm cover slip (No 1 glass). The cells were examined visually and scored using the fluorescence microscope described in Section 5.2.2. One hundred nucleoids were scored per gel, and given a score of 0, 1, 2, 3, or 4 (from undamaged, 0 to maximum damage, 4) (Figure 5.4). The total score of each sample can range from 0 (all undamaged) to 400 (all maximally damaged).

5.3.7. DNA Repair of Oxidative (H_2O_2)-Induced DNA Damage

MDA-MB-231 (8 x 10^4 cells/well) cells were treated with BNIPSpd (non toxic concentrations, 5 and 0.05 µM) or BNIPDaCHM (non toxic concentrations, 0.1 and 1 µM) for 4 and 24 hours, respectively. MDA-MB-231 cells were washed twice with PBS before treatment with H_2O_2 (200 µM) for 5 minutes on ice, to induce oxidative DNA damage. After 5 minutes, the H_2O_2 was removed, and cells washed twice with PBS (500 µL). Fresh RPMI 1640 medium containing 10% (v/v) FCS (1 mL) was added to each well, and cells incubated at 37 °C for up to 24 hours. Cells were collected as previously described in Section 4.3.1 after 0, 2, 4, 8, and 24 hours, and DNA repair of oxidative damage was detected by the Comet assay (Section 5.3.5).

5.3.8. DNA Repair of Methylative (MMS)-Induced DNA Damage

DNA repair of MMS damage was detected in MDA-MB-231 (8 x 10^4 cells/well) cells treated with BNIPDaCHM (non toxic concentration, 1 µM) for 24 hours. MDA-MB-231 cells were washed twice with PBS, and the washes collected. The cells were incubated with MMS (1 mM) for 30 minutes at 37 °C, to induce methylative DNA damage. After 30 minutes, the MMS solution was removed, and collected. Cells were washed twice with PBS (500 µL) and all washes collected. The washes and MMS solution were centrifuged at 4000 rpm for 5 minutes, at room temperature. Fresh RPMI 1640 medium containing 10% (v/v) FCS (1 mL) was added to each well, and cells incubated at 37 °C for up to 24 hours. The cells were collected as previously described (Section 4.3.1) after 0, 2, 4, 8 and 24 hours and were analysed by the Comet assay (Section 5.3.5.).

5.3.9. Data Analysis

Unless otherwise stated, each data set contained a minimum of two independent experiments, in which each experiment was comprised of at least four internal replicates, expressed as mean ± Standard Error of the Mean (SEM). Statistical analysis was

conducted using the unpaired Student's *t*-test. Data were considered significantly different when *P*-value < 0.05 (*$P < 0.05$, **$P < 0.01$ and ***$P < 0.001$).

5.4. Results

5.4.1. Optimisation of H_2O_2-induced DNA Strand Breaks

H_2O_2 was used as a positive control for DNA damage and its concentration was optimised in MDA-MB-231 and MCF-10A cells. Cells were treated with different concentrations of H_2O_2 (0 – 800 µM) for 5 minutes on ice, and DNA strand breaks assessed by Comet assay.

The diagram in Figure 5.6 presents the number of DNA strand breaks induced by different concentrations of H_2O_2 (0 – 800 µM) in MDA-MB-231 cells. Data are not shown for H_2O_2 treatment in MCF-10A cells, as a similar result to H_2O_2 treated MDA-MB-231 cells was found. H_2O_2 (> 50 µM) induced significant DNA strand breaks ($P < 0.05$), above endogenous levels (Figure 5.6). 200 µM H_2O_2 was selected for the DNA damage and repair studies (Sections 5.4.2 and 5.4.3).

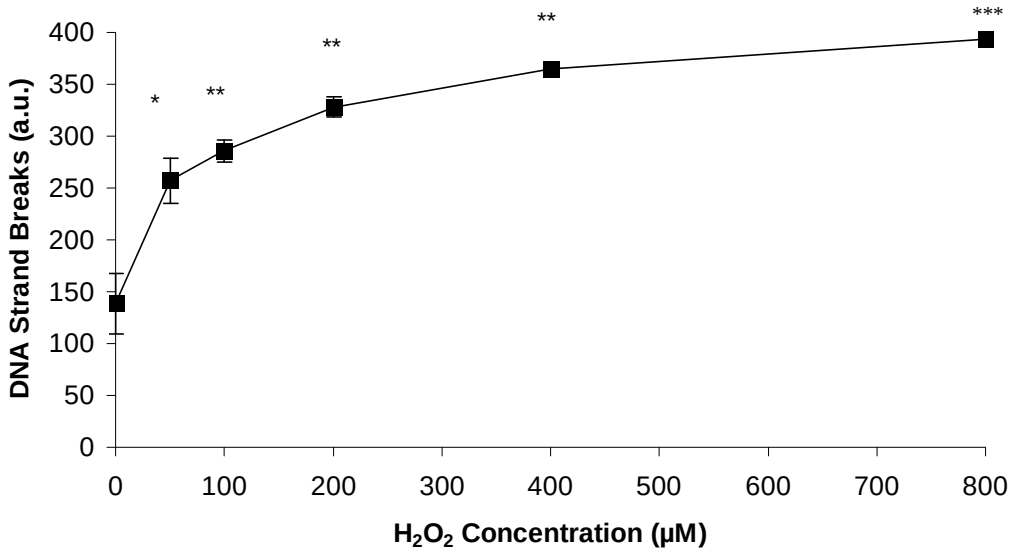

Figure 5.6.: DNA strand breaks in MDA-MB-231 cells as determined by comet assay. Data obtained after treating MDA-MB-231 cells with H_2O_2 (0 – 800 µM) for 5 minutes, on ice. Data are mean ± SEM of 2 independent experiments; with 4 replicates (n = 2). **P*<0.05, ***P*<0.01, ****P*<0.001 vs. untreated cells.

In summary, the total number of DNA strand breaks induced by H_2O_2 (200 µM) in MDA-MB-231 and MCF-10A cells are shown in Table 5.1.

Table 5.1.: Total DNA strand breaks induced by 200 µM H_2O_2 (for 5 minutes on ice)

Cell Line	*Concentration of H_2O_2 (µM)*	*DNA Strand Breaks (a.u.)*
MDA-MB-231	200	327
MCF-10A	200	300

5.4.2. Effect of BNIPP Derivatives on DNA Strand Breaks

The extent of DNA strand breaks induced in BNIPSpd or BNIPDaCHM (0.1 – 10 µM) treated MDA-MB-231 (Section 5.4.2.1) and MCF-10A (Section 5.4.2.2) was determined by Comet assay.

5.4.2.1. Effect of BNIPP Derivatives on the Levels of DNA Strand Breaks in MDA-MB-231 Cells

Both BNIPSpd and BNIPDaCHM (0.1 – 10 µM) induced a significant increase (P < 0.05) in DNA strand breaks compared to endogenous levels, and the increase was dose dependent, after 4 and 24 hours (Figures 5.7 – 5.8) in MDA-MB-231 cells.

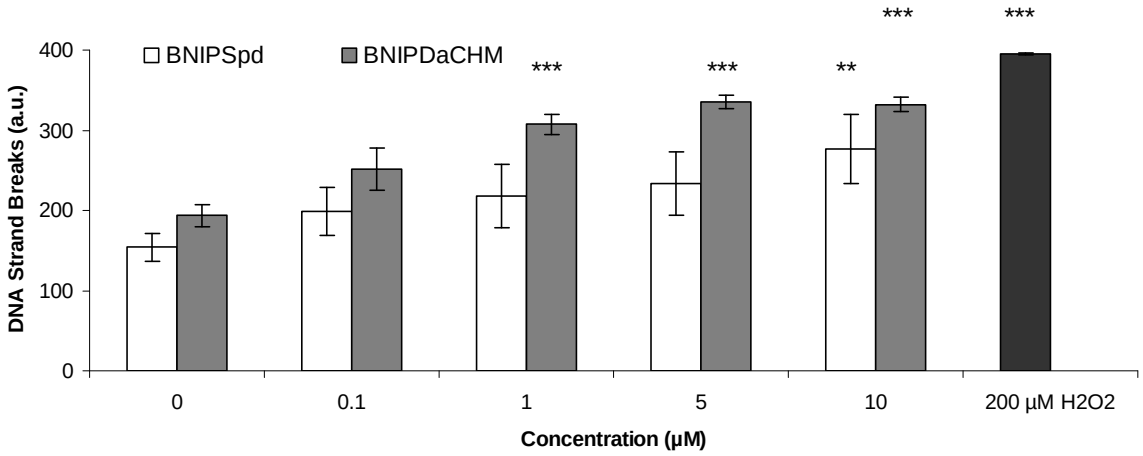

Figure 5.7.: DNA strand breaks in MDA-MB-231 cells after 4 hours treatment determined by comet assay. Data obtained after treating MDA-MB-231 cells with BNIPSpd or BNIPDaCHM (0 – 10 µM) for 4 hours. DNA damage in H_2O_2 (200 µM) treated cells were used as a positive control. Data are mean ± SEM of 8 replicates; 2 independent experiments (n = 2). *P<0.05, **P<0.01, ***P<0.001 vs. untreated (0 µM) cells.

In general, BNIPDaCHM (≥ 1 µM) induced a greater level of DNA strand breaks than BNIPSpd in MDA-MB-231 cells, after 4 hours (Figure 5.7). No significant change in the number of DNA strand breaks was observed with 0.1 µM BNIPSpd or BNIPDaCHM compared to endogenous levels (Figure 5.7). At a concentration of 1 µM, BNIPSpd did not significantly change the number of DNA strand breaks compared to endogenous levels, however, 1 µM BNIPDaCHM significantly increased the number of DNA strand breaks (P < 0.001, an increase of 113.7 strand breaks), compared to endogenous levels (Figure 5.7). At a concentration of 5 µM, BNIPSpd did not significantly change the number of DNA strand breaks compared to endogenous levels; yet, 5 µM BNIPDaCHM significantly increased the number of DNA strand breaks (P < 0.001, an increase of 141.5 strand breaks), compared to endogenous levels (Figure 5.7). At 10 µM, both BNIPSpd and BNIPDaCHM significantly increased the number of DNA strand breaks (P < 0.01, an increase of 122.3 strand breaks; P < 0.001, an increase of 138.5 strand breaks, respectively), compared to endogenous levels (Figure 5.7). At 200 µM, H_2O_2 significantly

increased the number of DNA strand breaks (P < 0.001, an increase of 241.0 strand breaks), compared to endogenous levels (Figure 5.7).

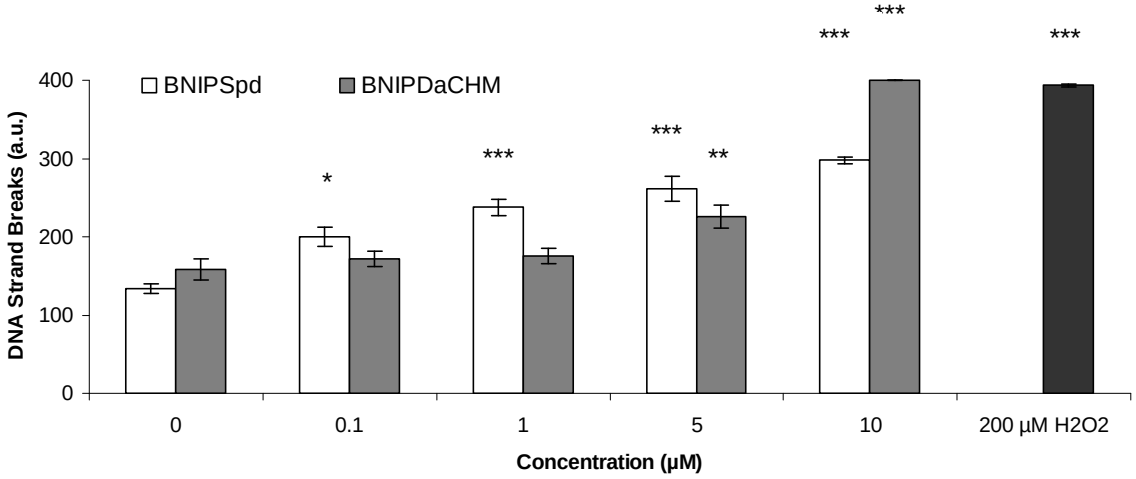

Figure 5.8.: DNA strand breaks in MDA-MB-231 cells after 24 hours treatment determined by comet assay. Data obtained after treating MDA-MB-231 cells with BNIPSpd and BNIPDaCHM (0 – 10 µM) for 24 hours. DNA damage in H_2O_2 (200 µM) treated cells were used as a positive control. Data are mean ± SEM of 8 replicates; 2 independent experiment (n = 2). *P<0.05, **P<0.01, ***P<0.001 vs. untreated (0 µM) cells.

However, in general after 24 hours, BNIPSpd (≥ 0.1 µM) induced a greater level of DNA strand breaks than BNIPDaCHM in MDA-MB-231 cells (Figure 5.8). At a concentration of 0.1 µM, BNIPSpd significantly increased the number of DNA strand breaks (P < 0.05, an increase of 66.3 strand breaks), whilst BNIPDaCHM (0.1 µM) did not significantly change the number of DNA strand breaks, compared to endogenous levels (Figure 5.8). At 1 µM, BNIPSpd significantly increased the number of DNA strand breaks (P < 0.001, an increase of 103.5 strand breaks), but 1 µM BNIPDaCHM did not change the number of DNA strand breaks, compared to endogenous levels (Figure 5.8). At 5 µM, both BNIPSpd and BNIPDaCHM significantly increased the number of DNA strand breaks (P < 0.001, an increase of 127.8 strand breaks; P < 0.01, an increase of 67.4 strand breaks, respectively), compared to endogenous levels (Figure 5.8). The number of DNA strand breaks were also significantly increased (P < 0.001) following treatment with 10 µM of BNIPSpd or BNIPDaCHM (an increase of 163.8 and 241.6 strand breaks, respectively), compared to endogenous levels (Figure 5.8). At 200 µM, H_2O_2 significantly increased the number of DNA strand breaks (P < 0.001, an increase of 235.2 strand breaks), compared to endogenous levels (Figure 5.8).

5.4.2.2. Effect of BNIPP Derivatives on the Levels of DNA Strand Breaks in MCF-10A Cells

Both BNIPSpd and BNIPDaCHM (0.1 – 10 µM) induced a dose and time dependent significant increase (P < 0.05) in DNA strand breaks compared to endogenous levels, after 4 and 24 hours (Figures 5.9 – 5.10), in MCF-10A cells.

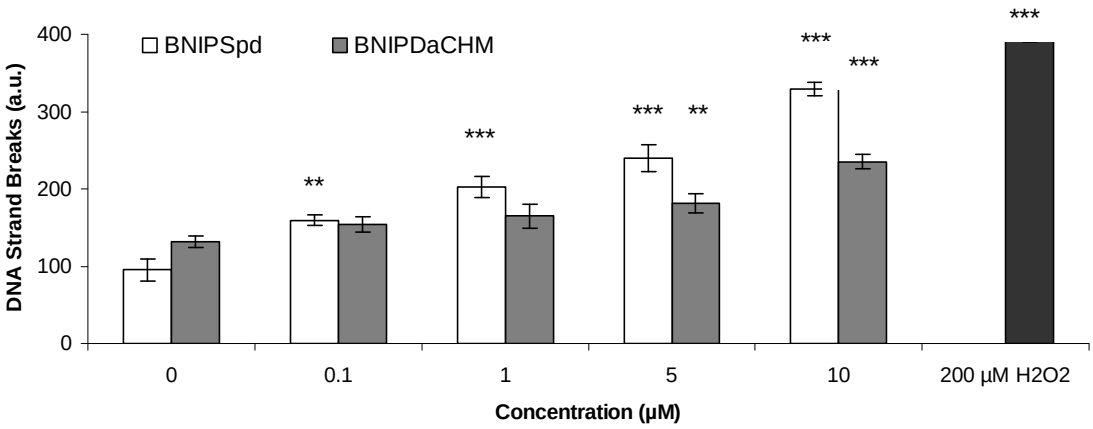

Figure 5.9.: DNA strand breaks in MCF-10A cells after 4 hours treatment determined by comet assay. Data obtained after treating MCF-10A cells with BNIPSpd and BNIPDaCHM (0 – 10 µM) for 4 hours. DNA damage in H_2O_2 (200 µM) treated cells were used as a positive control. Data are mean ± SEM of 8 replicates; 2 independent experiment (n = 2). **P*<0.05, ***P*<0.01, ****P*<0.001 vs. untreated (0 µM) cells.

In general, BNIPSpd (≥ 0.1 µM) induced a greater level of DNA strand breaks than BNIPDaCHM in MCF-10A cells, after 4 hours (Figure 5.9). At a concentration of 0.1 µM, BNIPSpd significantly increased the number of DNA strand breaks ($P < 0.01$, an increase of 64.2 strand breaks), whilst no change in the number of DNA strand breaks was observed with 0.1 µM BNIPDaCHM, compared to endogenous levels (Figure 5.9). At 1 µM, BNIPSpd significantly increased the number of DNA strand breaks ($P < 0.001$, an increase of 106.9 strand breaks), but BNIPDaCHM (1 µM) did not significantly change the number of DNA strand breaks, compared to endogenous levels (Figure 5.9). However, at a concentration of 5 µM, both BNIPSpd and BNIPDaCHM significantly increased the number of DNA strand breaks ($P < 0.001$, an increase of 144.2 strand breaks; $P < 0.01$, an increase of 49.9 strand breaks, respectively), compared to endogenous levels (Figure 5.9). At 10 µM, both BNIPSpd and BNIPDaCHM also significantly increased the number of DNA strand breaks ($P < 0.001$, an increase of 234.1 and 104.0 strand breaks, respectively), compared to endogenous levels (Figure 5.9). At 200 µM, H_2O_2 significantly increased the number of DNA strand breaks ($P < 0.001$, an increase of 260.4 strand breaks), compared to endogenous levels (Figure 5.9).

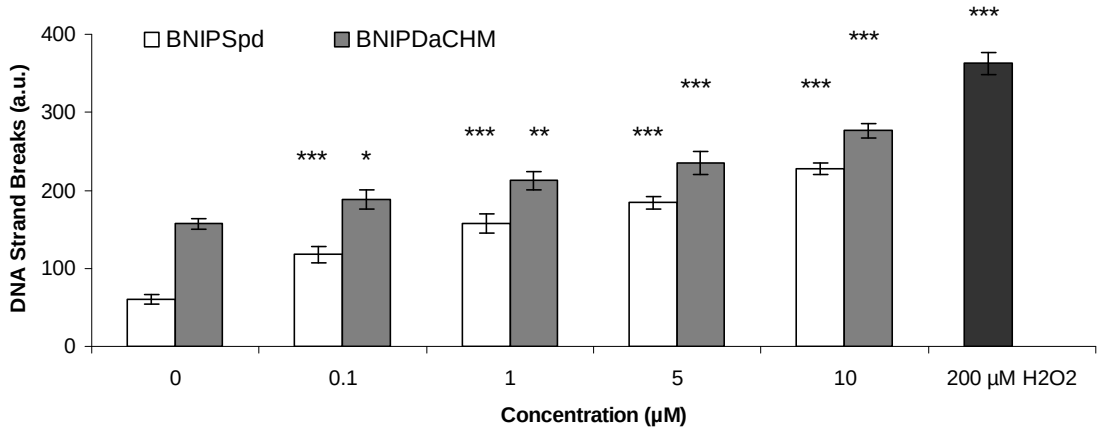

Figure 5.10.: DNA strand breaks in MCF-10A cells after 24 hours treatment determined by comet assay. Data obtained after treating MCF-10A cells with BNIPSpd and BNIPDaCHM (0 – 10 µM) for 24 hours. DNA damage in H_2O_2 (200 µM) treated cells were used as a positive control. Data are mean ± SEM of 8 replicates; 2 independent experiment (n = 2). **P*<0.05, **P<0.01, ****P*<0.001 vs. untreated (0 µM) cells.

In general, both BNIPSpd and BNIPDaCHM were able to significantly increase DNA strand breaks in MCF-10A cells at ≥ 0.1 µM, after 24 hours (Figure 5.10). At 0.1 µM, both BNIPSpd and BNIPDaCHM significantly increased the number of DNA strand breaks (*P* < 0.001, an increase of 57.3 strand breaks; *P* < 0.05, an increase of 30.9 strand breaks), compared to endogenous levels (Figure 5.10). At 1 µM, both BNIPSpd and BNIPDaCHM significantly increased the number of DNA strand breaks (*P* < 0.001, an increase of 97.3 strand breaks; *P* < 0.01, an increase of 55.7 strand breaks compared to endogenous levels (Figure 5.10), with similar findings at 5 µM BNIPSpd and BNIPDaCHM (*P* < 0.001, 123.7 and 77.6 strand breaks, respectively) and 10 µM BNIPSpd and BNIPDaCHM (*P* < 0.001, 167.2 and 119.8 strand breaks, respectively), when compared to endogenous levels (Figure 5.10). At 200 µM, H_2O_2 significantly increased the number of DNA strand breaks (*P* < 0.001, an increase of 302.1 strand breaks), compared to endogenous levels (Figure 5.10).

MCF-10A cells were observed to be more susceptible to the action of BNIPSpd or BNIPDaCHM with respect to DNA strand breaks than MDA-MB-231 cells (Figures 5.7 – 5.10). Lower concentrations of BNIPSpd and BNIPDaCHM (≥ 0.1 µM) induced a significant increase in the number of DNA strand breaks (*P* < 0.05) in MCF-10A cells, after 4 and 24 hours (Figures 5.9 – 5.10), compared to 10 µM BNIPSpd or 1 µM BNIPDaCHM, after 4 hours (Figure 5.7), or 0.1 µM BNIPSpd or 5 µM BNIPDaCHM, after 24 hours (Figure 5.8) in MDA-MB-231 cells.

5.4.3. Effect of BNIPP Derivatives on DNA Repair Mechanisms

The ability of BNIPSpd or BNIPDaCHM to interfere with DNA repair mechanisms was determined by Comet assay in MDA-MB-231 cells damaged with H_2O_2 (200 µM for 5 minutes, on ice) and MMS (1 mM for 30 minutes, at 37°C).

5.4.3.1. Repair of H_2O_2-Induced DNA Strand Breaks in MDA-MB-231 Cells

MDA-MB-231 cells were pre incubated in the presence or absence of non toxic concentrations of BNIPSpd (5 and 0.05 µM) or BNIPDaCHM (0.1 and 1 µM) for 4 and 24 hours, respectively. These concentrations were chosen from the DNA strand break studies as shown in Figures 5.7 – 5.8. Repair was measured as described in Section 5.3.7.

H_2O_2-induced DNA strand breaks were slowly repaired in MDA-MB-231 control (cells incubated in the absence of either BNIPP derivative) cells. This was clearly evident, as DNA strand breaks had decreased, and had almost returned to endogenous levels, after 24 hours (Figures 5.11 – 5.12).

After a 4 hour pre-incubation with BNIPSpd (5 µM), MDA-MB-231 cells were unable to effectively repair H_2O_2-induced DNA damage. As DNA strand breaks were significantly different ($P < 0.01$) between BNIPSpd treated and untreated MDA-MB-231 cells, after 8 hours (Figure 5.11A), and although, the difference between BNIPSpd treated and untreated MDA-MB-231 cells was not significant after 24 hours; BNIPSpd treated cells were unable to completely repair DNA strand breaks, as endogenous levels were not reached (i.e., the number of DNA strand breaks were 36.6 strand breaks higher than endogenous levels) (Figure 5.11A). After a 4 hour pre-incubation with BNIPDaCHM (0.1 µM), MDA-MB-231 cells were unable to effectively repair H_2O_2-induced DNA damage. As, DNA strand breaks were significantly different ($P < 0.05$) between BNIPDaCHM treated and untreated MDA-MB-231 cells, after 24 hours, and DNA strand breaks had not returned to endogenous levels (i.e., the number of DNA strand breaks were 39.4 strand breaks higher than endogenous levels, respectively) (Figure 5.11B).

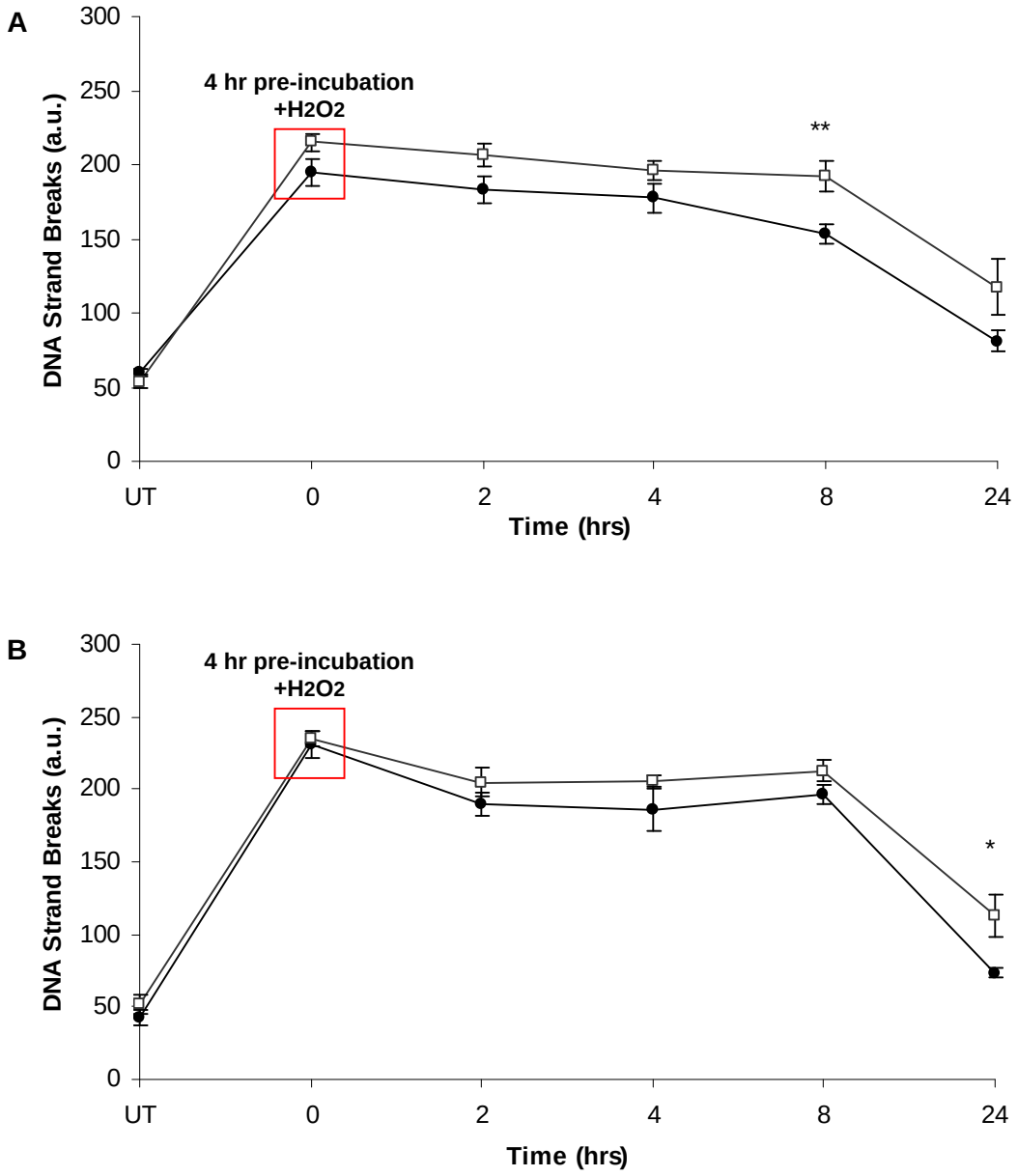

Figure 5.11.: Repair of DNA strand breaks in MDA-MB-231 cells. Cells were pre incubated in the presence (□) and absence (●) of non toxic concentrations of either BNIPSpd (5 µM) (**A**) or BNIPDaCHM (0.1 µM) (**B**) for 4 hours. Cells were incubated with 200 µM H_2O_2 for 5 minutes on ice, and then incubated at 37 °C for up to 24 hours. At intervals during this 24 hour incubation, DNA strand breaks were analysed immediately (0 hour) or after 2, 4, 8 and 24 hours by Comet assay. UT represents cells which were not incubated with H_2O_2 (200 µM). Data are mean ± SEM of 8 replicates; 2 independent experiments (n = 2). **P*<0.05, ***P*<0.01, ****P*<0.001 vs. absence of BNIPP derivative at each corresponding time point.

After a 24 hour pre-incubation with BNIPSpd (0.05 µM), MDA-MB-231 cells were unable to effectively repair H_2O_2-induced DNA damage. As DNA strand breaks were significantly different ($P < 0.05$) between BNIPSpd treated and untreated MDA-MB-231 cells, after 2, 4 and 24 hours, and DNA strand breaks had not returned to endogenous levels (i.e., the number of DNA strand breaks were 29.7 strand breaks higher than endogenous levels) (Figure 5.12A). After a 24 hour pre-incubation with BNIPDaCHM (1 µM), MDA-MB-231 cell repair mechanisms were significantly delayed ($P < 0.01$). As MDA-MB-231 cells were unable to repair H_2O_2-induced DNA damage after 4 ($P < 0.01$), 8

($P < 0.001$) and 24 ($P < 0.001$) hours, and since DNA strand breaks were not returned to endogenous levels (i.e., the number of DNA strand breaks were 46.3 strand breaks higher than endogenous levels) (Figure 5.12B). Therefore, BNIPDaCHM (1 µM) was more effective than BNIPSpd (0.05 µM) in the inhibition of MDA-MB-231 cell repair mechanisms (Figure 5.12).

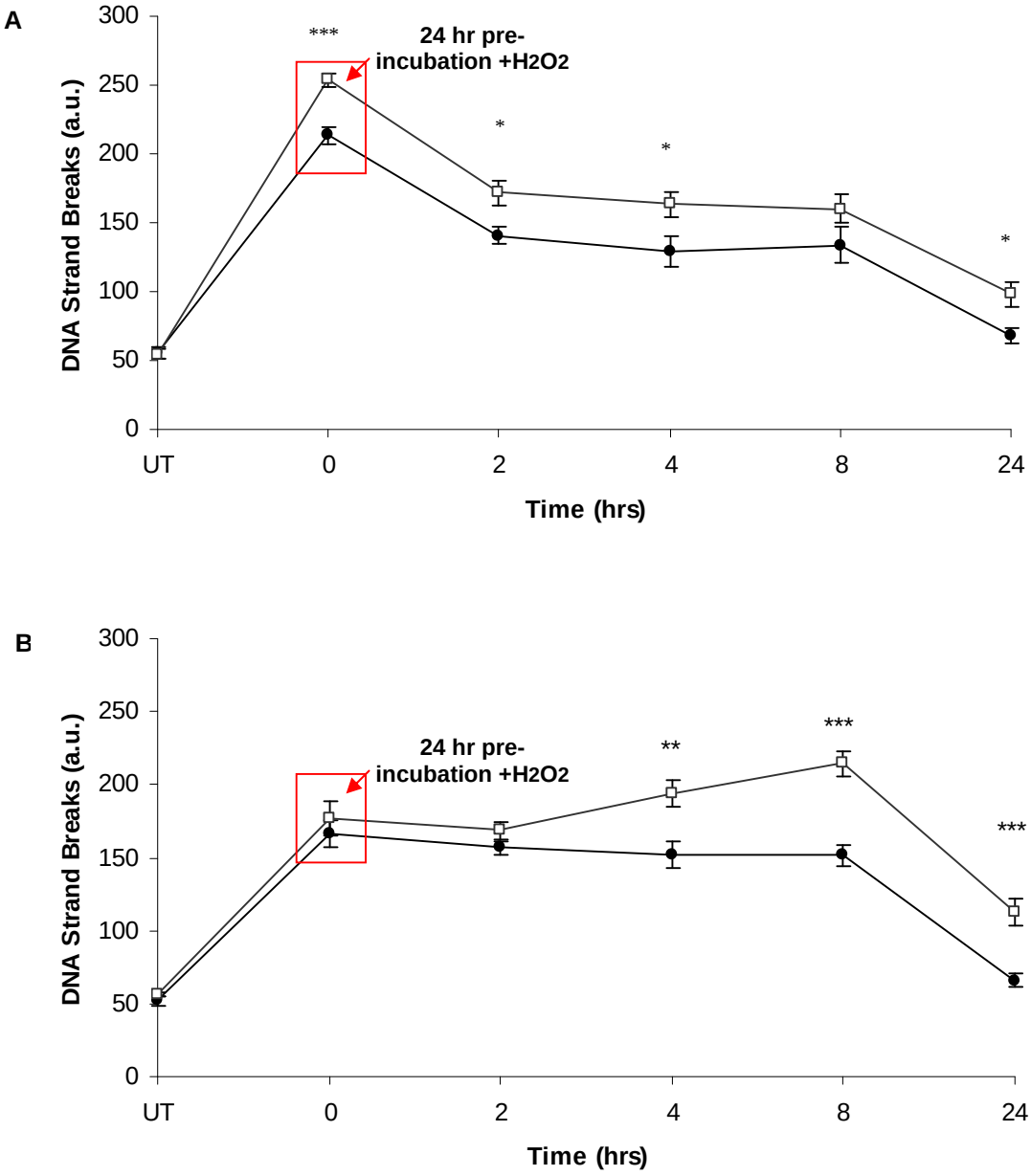

Figure 5.12.: Repair of DNA strand breaks in MDA-MB-231 cells. Cells were pre incubated in the presence (□) and absence (●) of non toxic concentrations of either BNIPSpd (0.05 µM) (**A**) or BNIPDaCHM (1 µM) (**B**) for 24 hours. Cells were incubated with 200 µM H_2O_2 for 5 minutes on ice, and then incubated at 37 °C for up to 24 hours. At intervals during this 24 hour incubation, DNA strand breaks were analysed immediately (0 hour) or after 2, 4, 8 and 24 hours by Comet assay. UT represents cells which were not incubated with H_2O_2 (200 µM). Data are mean ± SEM of 8 replicates; 2 independent experiment.s (n = 2) **P*<0.05, ***P*<0.01, ****P*<0.001 vs. absence of BNIPP derivative at each corresponding time point.

5.4.3.2. Repair of BNIPDaCHM-induced DNA Strand Breaks in MDA-MB-231 Cells

The ability of BNIPDaCHM to induce DNA strand breaks at a higher concentration (1 µM) after 24 hours, than at 4 hours (0.1 µM) was investigated further by Comet assay (Figure 5.13).

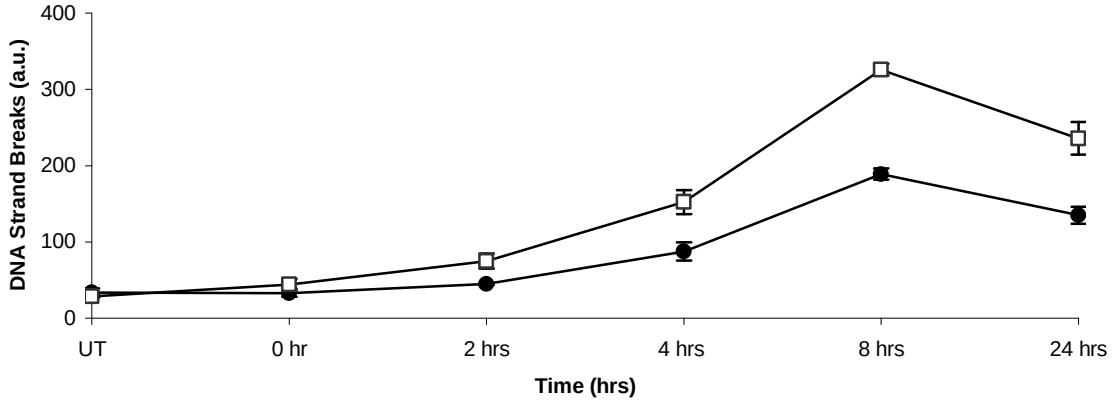

Figure 5.13.: Repair of DNA strand breaks in MDA-MB-231 cells. Cells were pre incubated in the presence (□) and absence (●) of BNIPDaCHM (1 µM) for 24 hours. At intervals during this 24 hour incubation, DNA strand breaks were analysed immediately (0 hour) or after 2, 4, 8 and 24 hours by Comet assay. UT represents cells which were not incubated with BNIPDaCHM. Data are mean ± SEM of 4 replicates (n = 1).

DNA strand breaks in both untreated and BNIPDaCHM treated MDA-MB-231 cells (1 µM) were affected in a similar manner. The number of DNA strand breaks increased up to 8 hours, but appeared to repair between 8 and 24 hours (Figure 5.13), as DNA strand breaks were returned to endogenous levels. However, MDA-MB-231 cells were unable to completely repair the induced DNA strand breaks, as DNA strand breaks were not returned to endogenous levels (Figure 5.13). Thus, at the non toxic concentration of 1 µM, BNIPDaCHM induced DNA repair, following DNA damage in MDA-MB-231 cells.

5.4.3.3. Optimisation of MMS-induced DNA Strand Breaks in MDA-MB-231 Cells

As MMS was used to induce methylative DNA damage, its concentration was optimised in MDA-MB-231 cells. Cells were treated with different concentrations of MMS (0 – 5 mM) for 30 minutes at 37 °C, and DNA strand breaks assessed by Comet assay.

The diagram in Figure 5.14 presents the number of DNA strand breaks induced by different concentrations of MMS (0 – 5 mM) after 30 minutes in MDA-MB-231 cells. MMS (≥ 0.25 mM) induced significant DNA strand breaks ($P < 0.05$) compared to endogenous levels (Figure 5.14). Therefore, 1 mM MMS was selected for the DNA repair studies (Section 5.4.3.4).

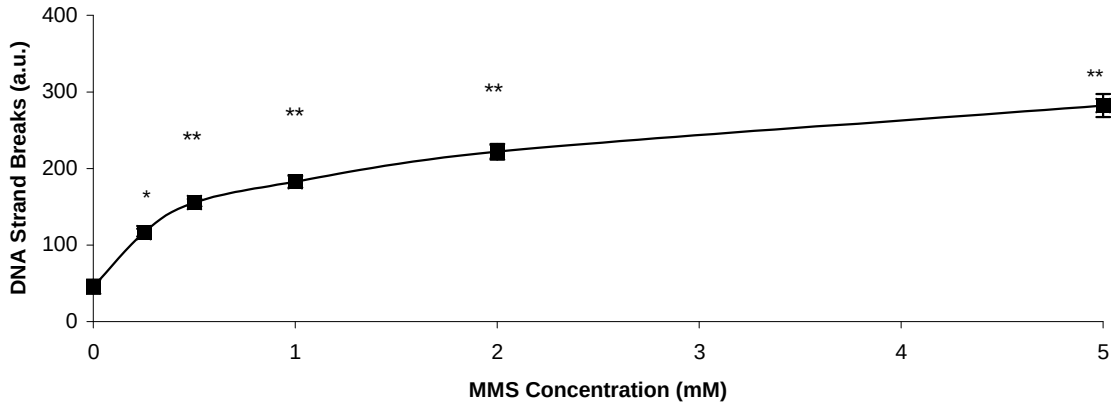

Figure 5.14.: DNA strand breaks in MDA-MB-231 cells determined by comet assay. Data obtained after treating MDA-MB-231 cells with MMS (0 – 5 mM) for 30 minutes, at 37°C. Data are mean ± SEM of 2 independent experiments (n = 2). **P*<0.05, ***P*<0.01 vs. untreated cells.

5.4.3.4. Repair of MMS-Induced DNA Strand Breaks in MDA-MB-231 Cells

The ability of BNIPDaCHM (1 µM, for 24 hours) to compromise the repair of MMS-induced DNA strand breaks in MDA-MB-231 cells was further investigated. Both untreated and BNIPDaCHM treated MDA-MB-231 cells were unable to effectively repair MMS-induced DNA damage, as after 24 hours, the number of DNA strand breaks were 91.5 and 77.5 strand breaks higher than endogenous levels, respectively (Figure 5.15).

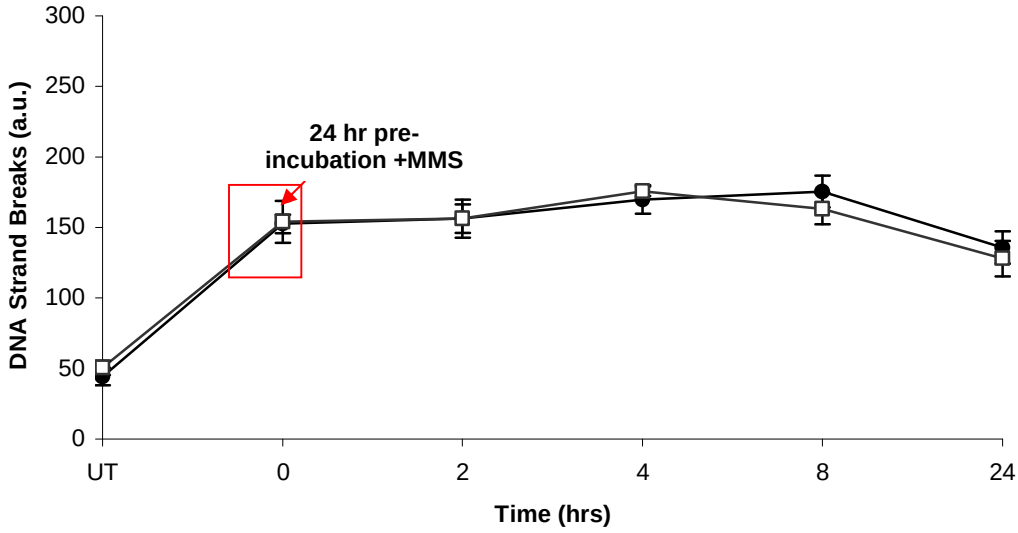

Figure 5.15.: Repair of DNA strand breaks in MDA-MB-231 cells. Cells were pre incubated in the presence (□) and absence (●) of non toxic concentrations of BNIPDaCHM (1 µM) for 24 hours. Cells were incubated with 1 mM MMS for 30 minutes at 37 °C, and then incubated at 37 °C for up to 24 hours. At intervals during this 24 hour incubation, DNA strand breaks were analysed immediately (0 hour) or after 2, 4, 8 and 24 hours by Comet assay. UT represents cells which were not incubated with MMS (1 mM). Data are mean ± SEM of 4 replicates only (n = 1).

5.5. Discussion

5.5.1. Effect of BNIPP Derivatives on DNA Strand Breaks in MDA-MB-231 and MCF-10A Cells

Treatment with BNIPSpd and BNIPDaCHM induced DNA instability in MDA-MB-231 (Figures 5.7 – 5.8) and MCF-10A cells (Figures 5.9 – 5.10). BNIPSpd and BNIPDaCHM significantly induced ($P < 0.05$) a dose dependent increase in DNA strand breaks above endogenous levels within both cell lines.

In MDA-MB-231 cells, BNIPDaCHM induced significant strand breaks ($P < 0.001$) with ≥ 1 µM after 4 hours; whereas BNIPSpd required 24 hours to induce the same level of strand breaks (Figures 5.7 – 5.8). These results were in agreement with the cellular uptake studies (Section 4.4.3.1 and Figure 4.16), where BNIPDaCHM was observed within MDA-MB-231 cells after 0.5 hours whilst BNIPSpd was not observed until 6 hours. It is important to note that these results were also consistent with the cytotoxicity studies (Table 4.2), where after 24 hours in MDA-MB-231 cells, BNIPDaCHM was more cytotoxic (IC_{50} 6.8 µM) than BNIPSpd (IC_{50} 12.7 µM).

In contrast, BNIPSpd induced significant strand breaks ($P < 0.01$) in MCF-10A cells with ≥ 0.1 µM after 4 hours, and both derivatives (at ≥ 0.1 µM) were equally as effective in the inducement of significant strand breaks ($P < 0.05$) after 24 hours (Figures 5.9 – 5.10). These results are in agreement with the cytotoxicity studies (Table 4.3) in MCF-10A cells (24 hours) where BNIPSpd was shown to be more cytotoxic (IC_{50} 4.2 µM) than BNIPDaCHM (IC_{50} 6.1 µM). Although the results are in contradiction to the cellular uptake studies (Section 4.4.3.2 and Figure 4.17), where BNIPDaCHM and BNIPSpd were observed within MCF-10A cells after 0.5 and 6 hours, respectively, these results suggest that DNA damage may be responsible for BNIPP toxicity.

MCF-10A treated cells were more susceptible to DNA strand breaks than MDA-MB-231 treated cells (Figures 5.7 – 5.10). This result was similar to the findings of Starcevic *et al*. (2003), where sensitivity to oxidative DNA damage induced by H_2O_2 (1 – 100 µM for 5 minutes) decreased with progression towards tumorigenicity (i.e., the parental nontumorigenic MCF-10A cells were more susceptible to DNA strand breaks than the tumorgenic MCF-10AT or MCF-10ATG3B cells[1]).

The DNA strand breaks observed in MDA-MB-231 and MCF-10A cells may also be attributed to the ability of BNIPP derivatives to strongly bind to DNA via bis intercalation (ΔT_m 35.3 and 31.2 °C, respectively) (Chapter 3, in particular Table 3.1). Results are consistent with the findings of Roos *et al.* (1985), who studied intracellular DNA damage produced by a series of diacridines. Roos *et al.* (1985) found that a large

[1] MCF-10AT cells are T_{24} *Ha-ras*-transformed MCF-10A cells, and MCF-10ATG3B cells are a third generation MCF-10AT descendant.

increase in DNA strand breaks was strongly related to their increased DNA binding affinity.

The results presented in this chapter are complementary to the work carried out by Dance *et al.* (2005) and Ralton *et al.* (2009), who investigated the extent of DNA damage induced by BNIPSpd, BNIPSpm and BNIPOSpm within HL60, MCF-7 CaCO-2, and HT-29 cells. Both Dance *et al.* (2005) and Ralton *et al.* (2009) found that BNIPSpd was the most effective at inducing DNA strand breaks when compared with BNIPSpm or BNIPOSpm. After 4 hours, the extent of DNA strand breaks induced by 100 µM BNIPSpd in MCF-7, CaCO-2 and HT29 cells (Dance *et al.* 2005, Ralton *et al.* 2009) was in the same range as DNA strand breaks induced by 10 µM BNIPSpd in MDA-MB-231 and MCF-10A cells (i.e., between 250 – 300 DNA strand breaks) (Figures 5.7 and 5.9). Therefore, BNIPSpd and BNIPDaCHM can induce greater DNA strand breaks in MDA-MB-231 and MCF-10A cells than BNIPSpd, BNIPSpm or BNIPOSpm could in MCF-7, CaCO-2 or HT29 cells (Dance *et al.* 2005, Ralton *et al.* 2009). This finding may suggest that within the former cell lines, DNA damage has a greater contribution towards BNIPP toxicity.

Only two other polyamine analogues have been investigated with regards to their effects on DNA integrity. The spermine analogue, N^1, N^{11}-diethylnorspermine (BENSpm) (10 µM) (Figure 1.11) and the polyamine biosynthesis inhibitor, 4-amidinoindan-1-one 2'-amidinohydrazone (CGP 48664) (20 µM) (Figure 5.16) were found to significantly induce DNA damage in breast cancer (MCF-7, L56Br-C1 and HCC1937) cells.

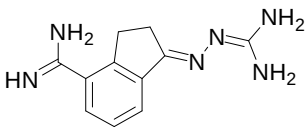

Figure 5.16.: Structure of 4-amidinoindan-1-one 2'-amidinohydrazone (CGP 48664)

Johansson *et al.* (2008) found that more DNA damage was detected in L56Br-C1 treated cells than in the other breast cancer cell lines investigated. BENSpm-treated MCF-10A cells (10 µM, for 48 hours) were found to induce less DNA damage when compared with untreated MCF-10A cells (Johansson *et al.* 2008). Johansson *et al.* theorised that DNA damage induced by BENSpm or CGP 48664 was related to polyamine depletion, but not apoptosis (Johansson *et al.* 2008). In contrast, BNIPSpd and BNIPDaCHM do not appear to induce DNA strand breaks as a result of polyamine depletion (Section 4.4.5 and Figures 4.16 – 4.23).

The ability of BNIPSpd and BNIPDaCHM to induce DNA damage in MDA-MB-231 and MCF-10A cells is supported by previous qualitative studies by Brana *et al.* (2003, 2004a, 2004b). In their studies they showed that naphthalimide derivatives did not affect the level of DNA damage in colon HT-29 cancer cells, whereas bisnaphthalimide derivatives induced an increase in DNA damage in colon HT-29 cancer cells, and that their subsequent cytotoxicities were related to their ability to induce DNA damage.

5.5.2. Effect of BNIPP Derivatives on DNA Repair Mechanisms in MDA-MB-231 Cells

All cells have an inherent ability to effectively remove and repair DNA damage induced by both endogenous and exogenous DNA damaging agents. BNIPP derivatives have been shown to induce DNA damage in MDA-MB-231 and MCF-10A cells (Figure 5.7 – 5.10), and also inhibit DNA repair mechanisms. The repair of H_2O_2-induced DNA damage was investigated since H_2O_2 can generate SSBs and DSBs as a result of oxidative stress, and can induce carcinogenesis (Halliwell and Aruoma 1991, Lindahl 1993).

In this study, MDA-MB-231 cells treated with BNIPSpd (5 and 0.05 µM) or BNIPDaCHM (0.1 and 1 µM) for 4 and 24 hours were unable to effectively repair oxidative-induced DNA damage (Figures 5.11 and 5.12). After 24 hours, the ability of MDA-MB-231 cells to repair oxidative DNA damage was significantly inhibited ($P < 0.05$) by both BNIPP derivatives at non toxic concentrations (i.e., concentrations that did not induce significant changes in DNA strand breaks after 24 hours treatment), and at concentrations which were 6 times less toxic than the IC_{50} values (12.7 µM and 6.8 µM for BNIPSpd and BNIPDaCHM, respectively). These results are in agreement to those obtained by Ralton (2006), where DNA repair of oxidative-induced DNA damage in CaCO-2 cells was inhibited by non toxic concentrations of BNIPSpd, BNIPSpm and BNIPOSpm (0.1 µM).

The repair of MMS-induced DNA damage was investigated since MMS has been shown to induce DNA methylation which causes mispairing and DSBs, and mutagenesis (Lundin *et al.* 2005). DSBs occur by conversion of guanine to 7-methylguanine or adenine to 3-methyladenine (Lundin *et al.* 2005). In this study, MDA-MB-231 cells treated with BNIPDaCHM (1 µM, for 24 hours) were unable to effectively repair MMS-induced DNA strand breaks (Figure 5.15). The type of damage induced by MMS is considerably greater and more dramatic than that induced by H_2O_2 (Lundin *et al.* 2005, Duthie. personal communication). The repair results in MDA-MB-231 cells are consistent with this observation.

It is difficult to compare the BNIPP derivative results with other anti cancer agents since their abilities to effectively repair oxidative- or alkylation-induced DNA damage remain to be extensively investigated.

5.6. Conclusion

BNIPSpd and BNIPDaCHM induced DNA instability in MDA-MB-231 and MCF-10A cells. Results show that BNIPSpd and BNIPDaCHM significantly induced a dose dependent increase in the number of DNA strand breaks compared to endogenous levels, after 4 and 24 hours treatment. In MDA-MB-231 cells, BNIPSpd required a longer treatment time (24 hours) to induce the same level of strand breaks as BNIPDaCHM. However, in MCF-10A cells, BNIPSpd was able to induce more DNA strand breaks than BNIPDaCHM suggesting that MCF-10A cells are more sensitive to the BNIPP derivatives in relation to DNA strand breaks than MDA-MB-231 cells. Also, MDA-MB-231 cells treated with BNIPSpd or BNIPDaCHM were unable to effectively repair oxidative-induced DNA damage. BNIPDaCHM, however, did not inhibit the ability of MDA-MB-231 cells to repair alkylation-induced DNA damage.

In conclusion, the results presented thus far show that the derivatives, BNIPSpd and BNIPDaCHM, (i) bind to DNA by bis-intercalation, (ii) are cytotoxic, (iii) can induce significant DNA strand breaks in MDA-MB-231 and MCF-10A cells, and (iv) can retard DNA repair of oxidative- and alkylation-induced DNA damage in MDA-MB-231 cells. The BNIPP derivatives BNIPSpd and BNIPDaCHM were further studied in order to assess their role in inducing cell death within MDA-MB-231 cells (Chapter 6).

Chapter 6

Cell Cycle Studies of BNIPP Derivatives in MDA-MB-231 Cells

6.1. Cell Cycle Studies of BNIPP Derivatives in MDA-MB-231 Cells

Alterations to cell proliferation and suppression of cell death are important regulatory mechanisms that are central in cancer development (Evan and Vousden 2001). As a result, important therapeutic strategies involve the ability of anti cancer agents to inflict cell cycle arrest and selectively trigger cancer cell death. Many cytotoxic and DNA damaging agents, such as doxorubicin (Aroui *et al.* 2009) (Figure 3.1) and etoposide (Montecucco and Biamonti 2007) (Figure 3.3) have been shown to induce cell cycle (G1 or G2/M) arrest and apoptotic cell death (Lin *et al.* 2010). Therefore, it is important to investigate the potential of BNIPP derivatives to induce cell cycle arrest and apoptotic cell death, as a consequence of their ability to intercalate with DNA (Sections 3.4.1 and 3.4.2), and induce significant DNA strand breaks in MDA-MB-231 cells (Section 5.4.2.1).

The aims of the experimental work reported in this chapter were to study (i) the mode of cell death, (ii) cell cycle analysis, and (iii) p53 and $p21^{Waf1/Cip1}$ mRNA levels in MDA-MB-231 cells treated with BNIPSpd or BNIPDaCHM.

6.1.1. Induction of Apoptotic Cell Death

Apoptosis is a highly controlled process that is paramount in normal cell development and is responsible for the removal of damaged or dysfunctional cells from a cell population, for example, during embryonic development or cell turnover (Schultz and Harrington 2003). Apoptotic pathways are thus complex and tightly controlled by multiple biochemical mediators, such as the B-cell lymphoma 2 (Bcl-2) family (Gross *et al.* 1999, Schultz and Harrington 2003). The characteristics of apoptosis involve cell shrinkage, cytoplasmic and plasma membrane blebbing, chromatin condensation, DNA fragmentation and the formation of apoptotic bodies which are removed by the process of phagocytosis (Kerr et al 1994, Jin and El-Deiry 2005, Scovassi 2006, Burz et al 2009) (Figure 1.3).

6.1.1.1. Assessment of Apoptosis

Apoptotic cell death *in vitro* can be assessed using numerous methods (Tables 6.1 and 6.2). Classic morphological detection methods involve the use of light or electron microscopic-based techniques which are, although rather non-specific, unquantifiable and operator specific, remain in use today due to their simplicity, rapidity and/or overall low cost (Chamond *et al.* 1999, Galluzzi *et al.* 2009) (Table 6.1). In addition, the use of vital dyes (i.e. can distinguish between viable and dead cells) (Salami and Karami-Tehrani 2003, Baskić *et al.* 2006) or exclusion dyes (i.e., cannot enter healthy cells but can enter

cells with a compromised plasma membrane) have been incorporated into light microscopy methods to visually distinguish between viable and dead cells in a cell population (Galluzzi *et al.* 2009). Besides light microscopic-based techniques, fluorescent microscopy can provide a method with greater experimental sensitivity due to a higher signal-to-noise ratio (Galluzzi *et al.* 2009) (Table 6.1). This technique can, for example, identify viable, apoptotic and necrotic cells via acridine orange/ethidium bromide (AO/EB) staining (Park *et al.* 2004, Baskić *et al.* 2006), or visualise nuclear condensation by staining with Hoechst 33258/33342 or 4',6-diamidino-2-phenylindole (DAPI) (Salami and Karami-Tehrani 2003, Galluzzi *et al.* 2007).

Table 6.1.: Methods used in the morphological identification of apoptotic cell death

Method	***Morphological Detection***	***Distinguishes between Apoptosis and Necrosis***	***Reference***
Light Microscope	Chromatin condensation; plasma membrane disruption	Yes	Salami and Karami-Tehrani 2003
- Annexin V			Galluzzi *et al*. 2009
- TUNEL			
Electron Microscope	Subtle organelle change (i.e., at an ultrastructural level)	Yes	Krysko *et al.* 2008
- SEM/TEM			Wahab *et al.* 2009
Fluorescence Microscope	Discrimination between viable, apoptotic and necrotic cells, nuclear identification and confirmation of DNA fragmentation	Yes	Park *et al.* 2004, Baskić *et al.* 2006, Galluzzi *et al.* 2007
- AO/EB staining			
- Hoechst 33342			
- DAPI			
- TUNEL			

Abbreviations: TUNEL, terminal deoxynucleotidyl transferase-mediated dUTP nick-end labelling; SEM, scanning electron microscope; TEM, transmission electron microscope; AO/EB, acridine orange/ethidium bromide; DAPI, 4',6-diamidino-2-phenylindole

Biochemical detection methods are also used for the determination of apoptosis by studying cell death on a single cell basis via flow cytometry (Galluzzi *et al*. 2009) (Figure 6.1). Cells stained with fluorescent dyes are injected into sheath fluid and passed through a light source (e.g., a laser). Each cell scatters light differently, with the fluorescent dye becoming excited to a higher energy state. Energy released can be measured

simultaneously with the use of various parameters (or detectors, e.g., forward scattered light (FSC; equating to cell size, distinguishing between cellular debris and viable cells), side scattered light (SSC; equating to granular content) or fluorescence detection channels FL-1 to -4), and results indicate the physical and chemical events (characteristics) of each cell (Rahman *et al.* 2006).

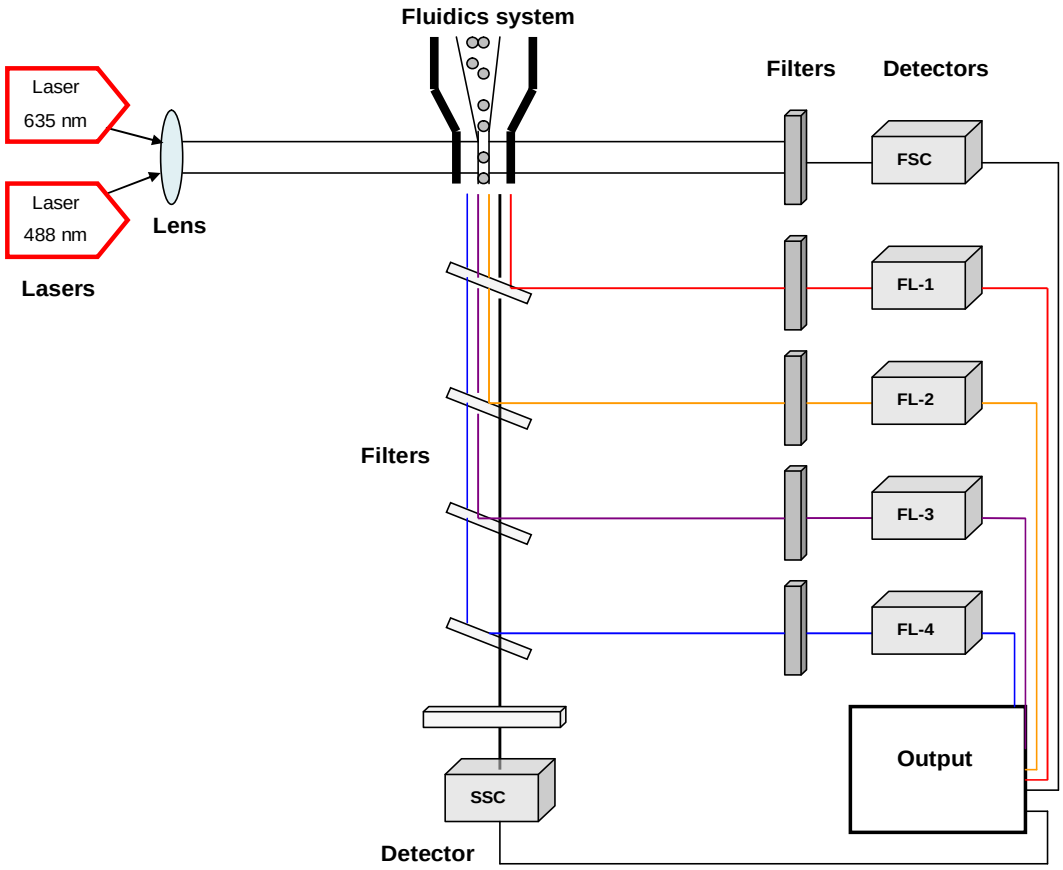

Figure 6.1.: Schematic diagram of a typical flow cytometer (adapted from Rahman *et al.* 2006) (FSC, Forward Scattered Light; FL-1 to -4, Fluorescent detection channels; SSC, Side Scattered Light)

In contrast to microscopy-based (light and fluorescence) methods (Table 6.1), flow cytometric methods rapidly produce specific, quantifiable and unbiased results with high throughput screening available (Galluzzi *et al.* 2009). Flow cytometry can, for example, quantify cells with a sub-G1 DNA content via DAPI or propidium iodide (PI) staining (Shu *et al.* 1997, Wang *et al.* 2008); detect phosphatidylserine (PS) exposure on the outer layer of the plasma membrane (Vermes *et al.* 1995, Van Engeland *et al.* 1996, Krysko *et al.* 2008) and also determine caspase activation (Belloc *et al.* 2000, Vermes *et al.* 2000, Galluzzi *et al.* 2009) (Table 6.2).

Table 6.2.: Methods used in the biochemical identification of apoptotic cell death

Method	***Biochemical Detection***	***Distinguishes between Apoptosis and Necrosis***	***Reference***
Flow Cytometry - Annexin V - Caspase activation - DAPI - PI - TUNEL	Determination of early apoptosis before DNA fragmentation or nuclear breakdown, identification of active caspases, analysis of cell cycle distribution and apoptosis (i.e., sub-G1 population), detection of free 3' ends in DNA	Yes	Vermes *et al.* 1995, Van Engeland *et al.* 1996, Shu *et al.* 1997, Belloc *et al.* 2000, Vermes *et al.* 2000, Krysko *et al.* 2008, Wang *et al.* 2008, Galluzzi *et al.* 2009

Abbreviations: DAPI, 4', 6-diamidino-2-phenylindole; PI, propidium iodide; TUNEL, terminal deoxynucleotidyl transferase-mediated dUTP nick-end labelling

Additional methods to detect apoptotic cell death include DNA agarose gel electrophoresis with ethidium bromide staining, that can determine apoptotic, internucleosomal DNA fragmentation to produce a 'DNA ladder' (200 – 5000bp DNA fragments) whilst necrotic, non-specific DNA degradation produces a 'smear' of randomly fragmented DNA (Park *et al.* 2004, Baskić *et al.* 2006), nuclear magnetic resonance (NMR) (i.e., detection of mobile lipid domains) (Mikhailenko *et al.* 2005), high performance liquid chromatography (HPLC) (i.e., the detection of cytochrome c from rat liver mitochondria) (Crouser *et al.* 2003) and mass spectrometry (MS) (i.e., the identification of proteins released by mitochondria) (Patterson *et al.* 2000, Galluzzi *et al.* 2009).

In this chapter, loss of plasma membrane integrity was detected using fluorescence microscopy and flow cytometry techniques described below (Section 6.1.1.2a and 6.1.1.2b).

6.1.1.2. Assessment of Membrane Integrity

The plasma membrane in animal cells acts as a selectively permeable barrier that protects the cellular contents from stress or damage induced by external sources, such as that caused by anti cancer agents (Figure 4.2). As an animal cell does not have a cell wall for additional protection; the plasma membrane is highly vulnerable to disruption which can ultimately lead to cell death (McNeil and Steinhardt 1997). Hence, cell

membrane leakage has been used in the detection of apoptotic cell death (Vermes *et al.* 1995, Vermes *et al.* 2000, Krysko *et al.* 2008).

6.1.1.2.a. Acridine Orange/Ethidium Bromide Staining

A common, rapid and simple method for the detection of chromatin changes relative to plasma membrane integrity is the morphological identification of viable (early and late) apoptotic and necrotic cells by fluorescence microscopy following AO/EB staining (Galluzzi *et al.* 2009). Both AO dye and EB dye intercalate with DNA; AO fluoresces green in viable cells, whilst EB fluoresces orange in non-viable (i.e., necrotic) cells (Park *et al.* 2004). AO can stain both viable and non-viable cells as it can pass through the plasma membrane but EB can only be taken up in cells when the plasma membrane integrity has been compromised, thus, can only be observed in late apoptotic or necrotic cells. Therefore, dependent on the stage of membrane integrity loss (i.e., apoptosis or necrosis), cells can be stained in one of 4 different ways (Table 6.3).

Table 6.3.: Classification of cell viability by AO/EB staining

Cell Viability	***Incorporated Dye***	***Visual Appearance of Cells after AO/EB Staining[a]***
Viable	AO	Uniformly green with intact structure
Early Apoptosis	AO	Green with bright green dots in nuclei showing chromatin condensation and nuclear fragmentation
Late Apoptosis	EB	Orange with bright orange dots showing chromatin condensation and nuclear fragmentation
Necrosis	EB	Uniformly orange with intact structure

[a] Ralton (2006) and Cao *et al.* (2009).

6.1.1.2.b. Annexin V-FITC/7-AAD Staining

The simple, rapid and powerful biochemical method in the detection of exposed PS residues on the outer layer of the plasma membrane can identify between apoptotic and necrotic cells. In normal cells, PS is located in the inner layer of the plasma membrane, but during apoptotic cell death, PS is externalised to the outer layer of the plasma membrane (e.g., by a 'flip-flop' action; an inward movement of PS refers to flip, whilst an external movement of PS refers to flop), as its presence is required for removal of apoptotic cells by phagocytosis (Krysko *et al.* 2008) (Figure 6.2).

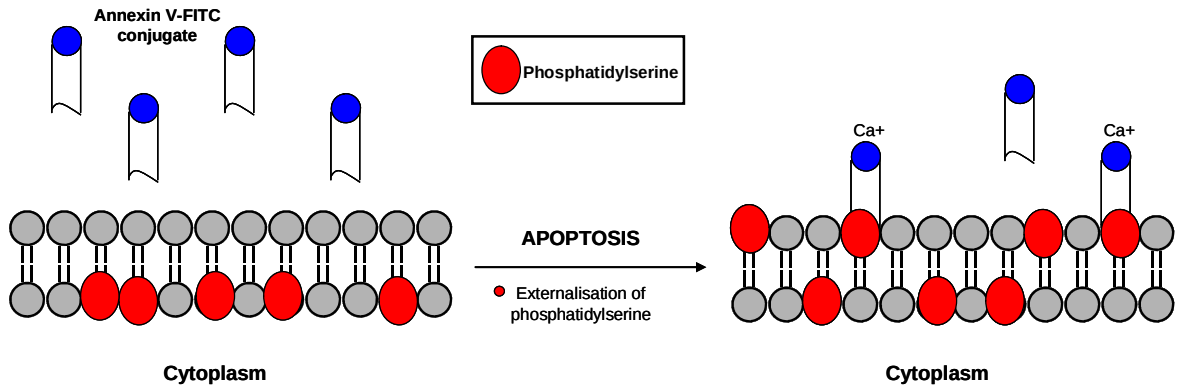

Figure 6.2.: Schematic representation of the annexin V-FITC assay (adapted from American Basic Gene Associate Bioscience Inc. 2006)

As PS movement has been identified as an early marker in apoptotic cell death (Van Engeland *et al.* 1996, Vermes *et al.* 2000, Krysko *et al.* 2008) detection can be achieved through flow cytometry, following staining with an annexin V conjugate labelled with fluorescein isothiocyanate (annexin V-FITC), in conjunction with an 7-amino-actinomycin D (7-AAD) viability dye. Annexin V is a Ca^{2+}-dependent phospholipid-binding protein that can bind reversibly to PS, with high affinity (Van Engeland *et al.* 1996), whilst 7-AAD is fluorescent DNA-binding agent that binds specifically between the guanine and cytosine bases (Gaforio *et al.* 2002). Thus, annexin V-FITC stains apoptotic cells before morphological changes have occurred (Van Engeland *et al.* 1996), whereas 7-AAD labels cells where plasma membrane integrity has been lost thus necrotic cells.

6.1.2. Cell Cycle Distribution

The regulation of the cell cycle is a highly controlled process that involves the duplication of cell contents and is important in cell division (Deep and Agarwal 2008, Meeran and Katiyar 2008). Alterations to, and/or arrest of cell cycle progression at any phase can result in uncontrolled cell growth, hence, the development of cancer (Deep and Agarwal 2008).

Cell cycle progression involves four phases: Gap phase 1 (G1); DNA synthesis (S); Gap phase 2 (G2) collectively known as interphase, and Mitosis (M) (Figure 6.3). During the gap (G1 and G2) phases, cells are prepared for DNA synthesis and mitosis, respectively. DNA synthesis (i.e., replication of DNA) and mitosis (i.e., separation of the chromosomes and division of the cell achieved via the key stages of prophase, metaphase, anaphase and telophase) occur during the S and M phases, respectively (Griffiths *et al.* 2008, Meeran and Katiyar 2008) (Figure 6.3). Also during cell division and development, cells may exit the cell cycle and enter a non-dividing, quiescent phase (G0) before returning to the G1 phase (Park and Lee 2003, Swanton 2004) (Figure 6.3). The cell cycle is tightly regulated by cyclin/cyclin dependent kinase complexes (CDKs), and multiple cell cycle "checkpoints" (Pietenpol and Stewart 2002, Meeran and Katiyar 2008).

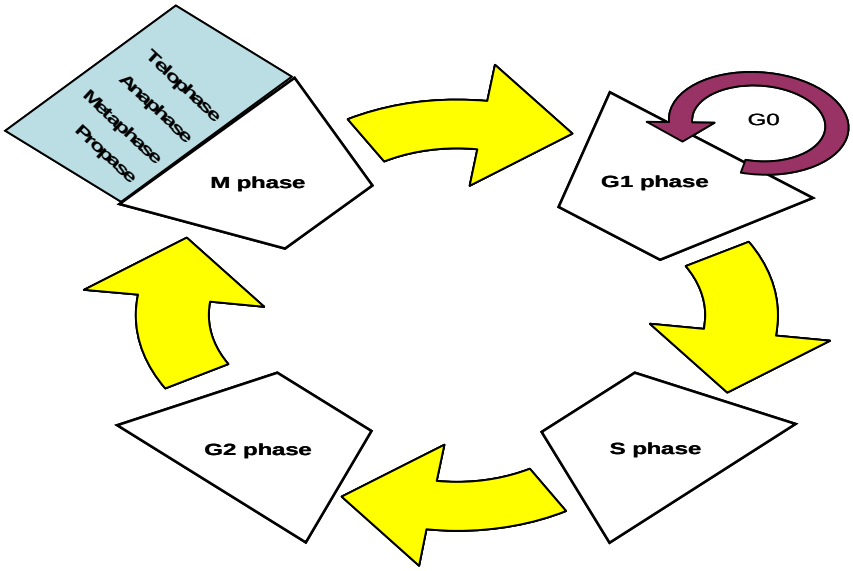

Figure 6.3.: Schematic representation of the cell cycle [Abbreviations: Go, quiescent phase; G1 phase, Gap phase 1; S phase, DNA synthesis; G2 phase, Gap phase 2; M phase, Mitosis]

Cell cycle checkpoints allow (i) repair of cell damage; (ii) depletion of exogenous cell stress and/or (iii) the supply of growth factors including hormones and nutrients (Pietenpol and Stewart 2002). If DNA repair cannot be achieved then apoptotic cell death will be induced. Therefore, defects in cell cycle checkpoints can lead to permanent DNA damage, thus the development of cancer (Meeran and Katiyar 2008).

Briefly, CDKs are activated when bound to regulatory proteins (cyclins), thus forming heterodimeric complexes that control progression from one phase to the next via cell cycle checkpoints (i.e., at G1/S phase and G2/M phase) (Swanton 2004, Deep and Agarwal 2008, Meeran and Katiyar 2008). For example, the cyclin D family (D1, D2 and D3; bind and activate CDK4 and CDK6), and the cyclin E family (E1 and E2; interact and activate CDK2) are responsible for cell progression through the restriction point from G1 to S phase by phosphorylation of the retinoblastoma protein (Rb) (Swanton 2004, Deep and Agarwal 2008). Hence, cyclin/CDK complexes play a key role in the positive regulation and coordination of numerous cell cycle checkpoints.

Furthermore, CDK activity can be negatively regulated by CDK inhibitors (CDKIs) which induce cell cycle arrest in response to cell cycle checkpoint signals, in particular, the CDK-interacting protein/kinase-inhibitor protein (Cip/Kip) family: $p21^{Waf1/Cip1*}$, $p27^{Kip1}$ and $p57^{Kip2}$ (Park and Lee 2003). $P21^{Waf1/Cip1}$ has a prominent role in cell growth arrest via DNA damage and has been identified as an important downstream effector of the tumour suppressor gene p53 (Park and Lee 2003, Ocker and Schneider-Stock 2007). Alongside $p21^{Waf1/Cip1}$, p53 gene has been implicated as an essential component in cell cycle arrest and apoptotic cell death (Figure 6.4) but in a majority of cancers, the p53 gene is mutated, for example, in the case of breast cancer MDA-MB-231 cells (Koutsilieris *et al*. 1999,

* $p21^{Waf1/Cip1}$ known as a CDK inhibitor 1A (CDK-N1A), alternatively known as a CDK-interacting protein 1 (Cip1) or wild-type p53-activated fragment 1 (Waf1) (Ocker and Schneider-Stock 2007).

Pietenpol and Stewart 2002, Belkacemi *et al*. 2006). For example, DNA damage can activate cell cycle arrest and apoptosis via p53-dependent apoptosis or p53-dependent activation of $p21^{Waf1/Cip1}$, thus protecting cells from apoptotic cell death (Gasco *et al.* 2002, Park *et al.* 2008). Although $p21^{Waf1/Cip1}$ has also been implicated in apoptotic cell death as it possesses proapoptotic functions under certain conditions (Gartel and Tyner 2002, Ghanem and Steinman 2005) yet these mechanisms are not fully understood. Thus targeting $p21^{Waf1/Cip1}$ may have therapeutic benefits and, as a consequence, several small molecules have recently been identified to interact with $p21^{Waf1/Cip1}$ (Park *et al.* 2008, Ljungman 2009).

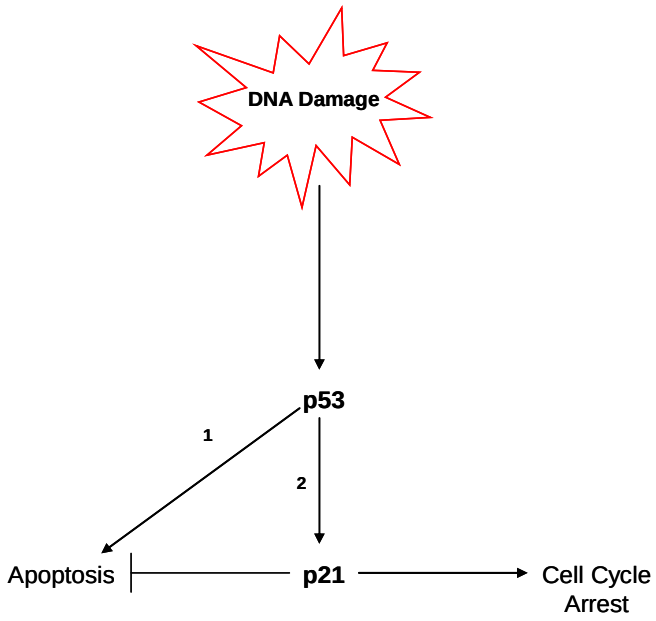

Figure 6.4.: Simplistic scheme for p53-dependent apoptosis. DNA damage can activate two pathways: **1**, p53-dependent apoptosis and **2**, p53-dependent activation of $p21^{Waf1/Cip1}$ that can protect cells from apoptosis (adapted from Gartel and Tyner 2002).

6.1.2.1. Assessment of Cell Cycle Distribution

In this study, cell cycle distribution was detected using flow cytometry following PI staining. PI is a DNA intercalator that can bind to DNA specifically following the loss of plasma membrane integrity (Bertho *et al.* 2000). The amount of PI is proportional to DNA content and thus indicates the distribution of cells within the cell cycle (Cancer Research UK 2008) (Figure 6.5). Cells in the G1 phase have a DNA content of 2n (i.e., diploid), the DNA content of cells in S phase doubles from 2n to 4n and remains at 4n during the G2 phase (Figure 6.5). At M phase DNA content rapidly returns to 2n with the formation of two daughter nuclei. In addition, cells that have DNA content of < 2n represent apoptotic cells with a low DNA content (i.e., a sub-G1 cell population).

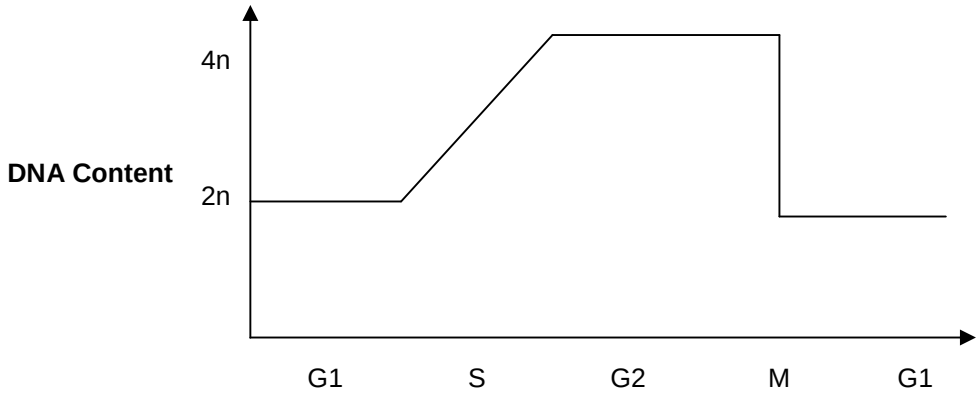

Figure 6.5.: DNA distribution at each phase of the cell cycle [Abbreviations: G1, Gap phase 1; S, DNA synthesis; G2, Gap phase 2; M, Mitosis]

6.1.2.2. Assessment of p53 and p21$^{Waf1/Cip1}$ Gene Expression

P53 and p21$^{Waf1/Cip1}$ messenger ribonucleic acid (mRNA) levels were detected using reverse transcription polymerase chain reaction (RT-PCR). RT-PCR provides a sensitive method to quantify expression of individual genes (Freeman *et al.* 1999, Felton *et al.* 2004). Briefly, RT produces a single-stranded copy of complementary DNA (cDNA) from the isolated RNA, via the action of the retroviral enzyme, reverse transcriptase (Freeman *et al.* 1999). The cDNA is then amplified by PCR. PCR is traditionally a three step reaction, involving denaturation (i.e., of cDNA template), annealing (i.e., binding of primers to template) and elongation (i.e., extension from primers using *Taq* polymerase to produce complementary strands) (Dale and Von Schantz 2002).

6.2. Materials

6.2.1. Materials

All reagents were purchased from Fisher Scientific, UK unless otherwise stated, and were used without purification.

Acridine Orange	Sigma-Aldrich, UK
Bovine Serum Albumin	New England Biolabs Inc, UK
Citric Acid	Sigma-Aldrich, UK
Chloroform	Sigma-Aldrich, UK
Coulter Clenz™ Cleaning Agent	Beckman Coulter, France
Ethylenediaminetetraacetic Acid	Sigma-Aldrich, UK
DEPC-Treated Water	Ambion Inc, UK
Deoxynucleotide Triphosphates	Promega, USA
Ethidium Bromide	Sigma-Aldrich, UK
Formaldehyde	Sigma-Aldrich, UK
IsoFlow™ Sheath Fluid	Beckman Coulter, France
Isopropanol	BDH Chemicals Inc, UK
Propidium Iodide	Sigma-Aldrich, UK
Random Primers	Promega, USA
Ribonuclease A	Sigma-Aldrich, UK
RNaseOUT	Invitrogen, UK
Sodium dihydrogen orthophosphate	BDH Chemicals Inc, UK
Superscript™ III Reverse Transcriptase	Invitrogen, UK
Taq DNA Polymerase	Sigma-Aldrich, UK
TRIzol	Invitrogen, UK
100bp Ladder	Promega, USA

The Annexin V-FITC/7-AAD kit (PN IM3614) was purchased from Beckman Coulter (France). The Superscript™ III RT product (Invitrogen) contains SuperScript™ III RT, 5x first strand buffer and dithiothreitol (DTT). The Taq DNA Polymerase product (Sigma-Aldrich) contains *Taq* DNA polymerase, PCR buffer and magnesium chloride ($MgCl_2$) solution, whilst the 100bp ladder product (Promega) contains a 100bp ladder and loading dye. p53, $p21^{Waf1/Cip1}$ and β-actin primers (i.e., forward and reverse) were supplied by Invitrogen, UK.

6.2.2. Instrumentation

Aseptic cell culture techniques were undertaken as described in Section 4.2.2.

Acridine orange/ethidium bromide (AO/EB) stained MDA-MB-231 cells were visualised using a Leica DMIL inverted fluorescence microscope (Leica Microsystems, UK) with a UV filter (excitation bandpass (blue); 450 – 490 nm, emission longpass (yellow); 515 nm) and Leica DC200 camera (Leica Microsystems, UK).

Flow cytometric analysis of MDA-MB-231 cells stained with reagents from the Annexin V-FITC/7-AAD kit or propidium iodide were analysed on an Coulter Epics XL-MCL flow cytometer (Beckman Coulter, UK) using EXPO32 ADC XL 4 color and EXPO32 ADC analysis software (Beckman Coulter, UK). For apoptosis analysis, 10,000 single events were recorded and analysed using the FL-1 channel for annexin V-FITC detection and the FL-4 channel for detection of 7-AAD fluorescence. The percentage of apoptotic and necrotic cells were calculated from histograms of LOG FL-1 (525 nm) and LOG FL-4 (675 nm) plots, respectively. For cell cycle analysis, 10,000 single events were recorded. The percentage of cells with DNA content of sub-G1 and in cell cycles phases (G1, S and G2/M) were calculated from histograms of linear FL-2 plots (575 nm) in the ungated region.

MDA-MB-231 cells were counted using an improved Neubauer Haemocytometer (Assistent, Germany) and a Leica DMIL microscope (Leica Microsystems, UK) for loss of cell number experiments.

Total RNA was quantified using a Heλios γ UV spectrophotometer (Thermo Spectronic, USA). Samples for RT-PCR were prepared within a Microflow Laminar Flow Cabinet (MHD Limited, UK), and all plastics were RNase free; eppendorf tubes and tips were Molecular BioProducts and Maxymum Recovery™ products, respectively (Thermo Fisher Scientific, UK). RT-PCR was conducted in an *i*Cycler Thermal Cycler (Bio-Rad Laboratories, USA), and for gel electrophoresis analysis a Bio-Rad Wide Mini-Sub Cell gel electrophoresis tank with PowerPac Basic power pack (Bio-Rad Laboratories, USA) was used. Bands were visualised with a ChemiDoc EQ system (Bio-Rad Laboratories, USA) and quantified using Quantity One (Version 4.5.0) software (Bio-Rad Laboratories, USA).

6.3. Methods

6.3.1. Maintenance of Cells

Exponentially growing MDA-MB-231 cells were sub cultured and counted, as described in Sections 4.2.2 and 4.3.1. The individual experimental conditions for each method are described in subsequent sections (Sections 6.3.3 – 6.3.7).

6.3.2. Preparation of BNIPP Derivatives

The BNIPP derivatives: BNIPSpd and BNIPDaCHM were synthesised as previously described in Section 2.3. BNIPSpd and BNIPDaCHM were diluted from stock solutions (10 mM) to the desired concentrations of 1, 5 and 10 µM, as described in Section 4.3.2.

6.3.3. Acridine Orange/Ethidium Bromide Staining

MDA-MB-231 cells (8 x 10^4 cells/mL) were treated with BNIPSpd or BNIPDaCHM (1, 5 and 10 µM; 0.5 – 24 hours at 37°C), or etoposide (10 µM; 24 hours at 37°C) within 24 well plates. After the desired incubation time (0.5, 1, 2, 4, 6 or 24 hours), medium containing BNIPSpd or BNIPDaCHM and non-adherent cells was removed, and adherent cells washed twice with PBS. 40 µL of acridine orange/ethidium bromide (100 µg/mL each in PBS) was added to 1 mL PBS and incubated with adherent cells for 2 minutes at room temperature. The AO/EB solution was removed, cells washed twice with PBS and 1 mL PBS added. AO/EB stained cells were visualised by fluorescence microscopy, as described in Section 6.2.2.

6.3.4. Annexin V-FITC / 7-AAD Staining

MDA-MB-231 cells (4 x 10^5 cells) were treated with BNIPSpd or BNIPDaCHM (1 and 5 µM) for 0.5 – 6 hours at 37°C within 6 well plates. After the desired incubation time (0.5, 4 or 6 hours), medium containing BNIPSpd or BNIPDaCHM was removed and discarded. Adherent cells were washed twice with ice-cold PBS. Cells were collected as described in Section 4.3.1 and centrifuged at 2,250 rpm (ALC Multispeed Refrigerated Centrifuge, Thomson Scientific, UK) for 5 minutes at 4°C. The supernatant was discarded, pellet resuspended in 100 µL of ice-cold Binding Buffer (1x in dH_2O), 10 µL Annexin V-FITC solution, 20 µL 7-AAD viability dye, mixed gently and incubated on ice for 15 minutes in the dark. After 15 minutes, 400 µL of ice-cold Binding Buffer (1x in dH_2O) was added and mixed gently. Annexin V-FITC and 7-AAD stained cell preparations were analysed within 30 minutes by flow cytometry as described in Section 6.2.2.

Formaldehyde (3%) was used as an experimental control due to its ability to induce maximal apoptotic cell death after 30 minutes, and was used to configure the gate settings for subsequent flow cytometry experiments. Briefly, MDA-MB-231 cells were treated with 500 µL formaldehyde for 30 minutes on ice and centrifuged at 2250 rpm (ALC Multispeed Refrigerated Centrifuge, Thomson Scientific, UK) for 5 minutes at 4°C. The supernatant was removed and from this point on, cells were treated in the same manner as samples treated with BNIPSpd and BNIPDaCHM (refer above in Section 6.3.4).

6.3.5. MDA-MB-231 Cell Number

MDA-MB-231 cells (8 x 10^4 cells/mL) were treated with BNIPDaCHM (1, 5 and 10 µM; 0.5 – 24 hours at 37°C) or etoposide (10 µM; 24 hours at 37°C) within 24 well plates. After the desired incubations (0.5, 4, 6 or 24 hours), cells were collected and counted as previously described (Section 4.3.1 and 6.2.2).

6.3.6. Cell Cycle Analysis

MDA-MB-231 cells (1 x 10^6 cells) were treated with BNIPSpd or BNIPDaCHM (5 µM), or etoposide (10 µM) for 24 hours at 37°C within 25 cm^2 culture flasks. After 24 hours, BNIPSpd, BNIPDaCHM or etoposide solutions were removed and collected. Cells were washed twice with PBS (2 mL) and washes collected. Cells were removed from culture flasks as described in Section 4.3.1, combined to the collected washes, and centrifuged at 2,500 rpm (ALC Multispeed Refrigerated Centrifuge, Thomson Scientific, UK) for 5 minutes at 4 °C. The supernatant was discarded, pellet resuspended in 1 mL PBS and transferred to an Eppendorf tube. Cells were centrifuged again at 2,500 rpm for 5 minutes at 4 °C, the supernatant discarded and the pellet resuspended in 100 µL PBS. 70% (v/v) ice-cold ethanol (900 µL) was added and incubated for 2 hours at -20°C. Cells were then centrifuged 5,000 rpm for 5 minutes at 4 °C, the pellet was resuspended in 1 mL PBS followed by re-centrifugation at 5,000 rpm for 5 minutes at 4 °C. The pellet was resuspended in 500 µL PBS and 500 µL DNA extraction buffer (0.2 M Na_2HPO_4, 4 mM citric acid, pH 7.8), and incubated for 5 minutes at room temperature. The extract was centrifuged at 5,000 rpm for 5 minutes at 4 °C, the supernatant removed, the pellet resuspended in 500 µL of DNA staining solution (0.2 mg/mL Ribonuclease A (DNAse-free) and 20 µg/mL propidium iodide (PI) in PBS) and incubated for 30 minutes at 4 °C in the dark. PI stained nuclei were analysed by flow cytometry as described in Section 6.2.2.

6.3.7. RNA Extraction from MDA-MB-231 Cells

MDA-MB-231 cells (1 x 10^6 cells) were treated with BNIPDaCHM (5 µM; 1 – 24 hours at 37 °C) within 25 cm^2 culture flasks. After the desired incubations (1, 4 or 6 hours), cells were washed twice with PBS and total RNA extracted using TRIzol reagent

according to manufacturer's instructions. Briefly, 1 mL TRIzol was added to cells and incubated for 3 minutes at room temperature. The cell lysate was transferred to an RNase free Eppendorf tube and incubated for 5 minutes at RT. Chloroform (200 µL) was quickly added, the tube was shaken by hand for 15 seconds, incubated for 3 minutes at room temperature, and then centrifuged at 13,000 rpm for 5 minutes at 4°C. The colourless aqueous layer containing RNA was removed and transferred to a fresh RNase free Eppendorf tube. Isopropanol (500 µL) was added to the aqueous layer, mixed gently and incubated for 10 minutes at room tempertaure. Samples were then centrifuged at 13,000 rpm for 10 minutes at 4 °C. The supernatant was removed, RNA pellet washed with 500 µL 75% ethanol/DEPC-Treated water ($DEPC_{H2O}$), mixed and centrifuged at 8,000 rpm for 5 minutes at 4 °C. The supernatant was removed and the RNA pellet air dried for 5 – 10 minutes. The RNA pellet was stored in $DEPC_{H2O}$ (15 – 20 µL) and incubated for 2 hours at -20 °C.

6.3.7.1. RNA Quantification

Total RNA purity and concentration were quantified by UV spectrophotometry (Section 6.2.2). RNA samples were heated for 5 minutes at 65 °C for complete dissolution then incubated for 5 minutes on ice prior to spectrophotometric measurements. Samples were diluted (1:200 in $DEPC_{H2O}$), mixed and the optical density (OD) read at 260 nm and 280 nm. The OD_{260} and OD_{280} readings correlate with RNA and protein concentrations, respectively. RNA purity was calculated by a ratio of readings taken at 260 nm and 280 nm wavelengths (i.e., OD_{260}:OD_{280}). Total RNA concentration (RNA_{CONC}) was determined by the following equation:

$$\mathbf{RNA_{CONC}\ (\mu g/\mu L)} = OD_{260} \times 40 \times \text{Dilution Factor} / 1000$$

6.3.8. RT-PCR Analysis

6.3.8.1. Reverse Transcriptase

Reverse transcription (RT) was performed using 100 ng (1 µL) of total RNA. First strand synthesis of complementary DNA (cDNA) was carried out with 5x first strand buffer, DTT (100 mM), deoxynucleotide triphosphate (dNTP's (dATP, dCTP, dGTP and dTTP); 10 mM), recombinant ribonuclease inhibitor RNaseOUT™, bovine serum albumin (BSA; 1 mg/mL), random hexadeoxynucleotides (250 ng/µL) and Superscript™ III RT in a 20 µL RT reaction mixture. RT reaction conditions were 10 minutes at 25 °C, 52 minutes at 42 °C and 15 minutes at 72 °C.

6.3.8.2. Polymerase Chain Reaction

A 3 µL aliquot of the RT reaction mixture was subsequently used for polymerase chain reaction (PCR). PCR was carried out with the gene specific primers (p53 and $p21^{Waf1/Cip1}$) and β-actin as an internal control (Table 6.4). The expected amplicon size for the DNA fragments were 205bp for p53, 130bp for $p21^{Waf1/Cip1}$ and 250bp for β-actin. PCR was carried out with 1 x PCR buffer, $MgCl_2$ (25 mM), forward primer (10 µM), reverse primer (10 µM) and *Taq* DNA polymerase in a 15 µL reaction mixture. PCR reaction conditions were started with a 'hot-start' of 4 minutes at 94 °C, 25 cycles of 1 minute denaturation at 94 °C, annealing for 2 minutes at 59 °C (2 minutes at 68 °C for β-actin), 2 minutes extension at 72 °C and 1 cycle of 8 minutes at 72 °C.

Table 6.4.: Forward and reverse primer sequences

Primer	***Forward Primer Sequence (5' – 3')***	***Reverse Primer Sequence (5' – 3')***
p53	cca ggg cag cta cgg ttt c	ctc cgt cat gtg ctg tga ctg
$p21^{Waf1/Cip1}$	cct gtc act gtc ttg tac cct	gcg ttt gga gtg gta gaa atc t
β-actin	cat gta cgt tgc tat cca ggc	ctc ctt aat gtc acg cac gat

6.3.9. Agarose Gel Electrophoresis

Amplified PCR products were separated on a 1.5% (w/v) agarose gel in 1x TRIS-borate ethylenediaminetetraacetic acid (EDTA) buffer and stained with ethidium bromide (10 mg/mL). PCR products (10 µL) were loaded into the gel with 2 µL 6x loading dye. A 100bp DNA ladder (7.5 µL) was added with 1.5 µL 6x loading dye as a reference indicator. The PCR products were ran for 25 minutes at 80V, visualised, and quantified using software as described in Section 6.2.2.

6.3.10. Optimisation of PCR Primers by Amplification Number

PCR conditions were optimised by varying the number of PCR amplification cycles in order to be in the linear phase of the PCR reaction. Several different PCR amplification cycles (i.e., 25, 28 and 30) were investigated (Figure 6.4.5), and RT-PCR was carried out as described in Sections 6.3.8.1 and 6.3.8.2. 25 cycles were selected as the optimum number of amplification cycles and used in subsequent PCR experiments (Figure 6.6).

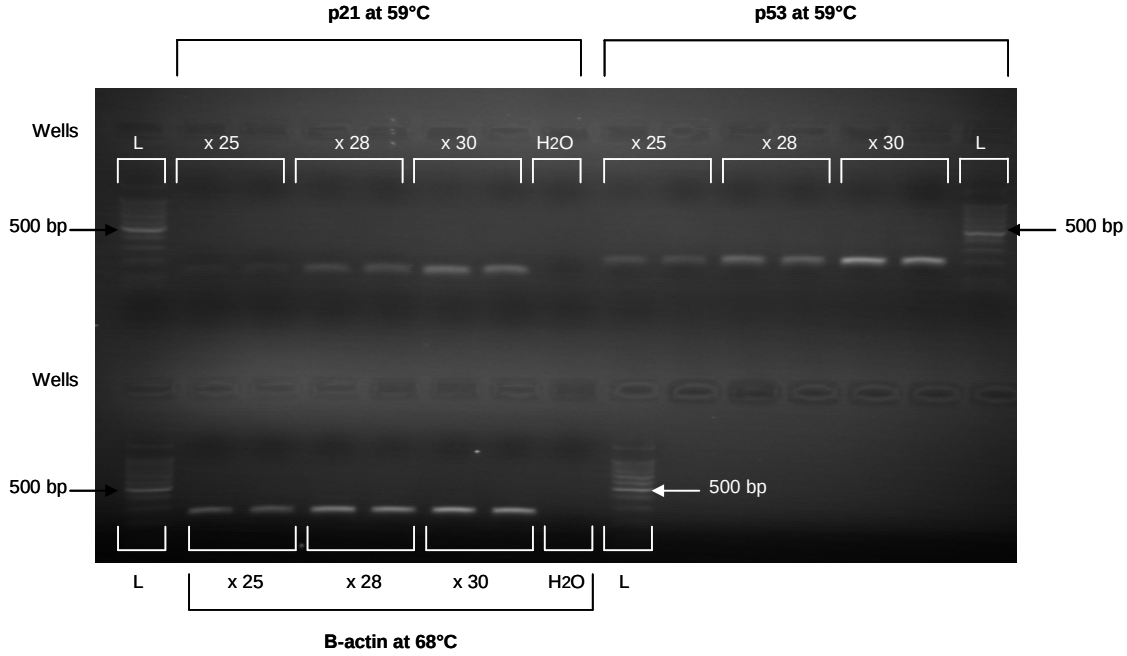

Figure 6.6.: Optimisation of amplification cycle number. Optimisation of $p21^{Waf1/Cip1}$, p53 and β-actin expression was carried out in MDA-MB-231 cells after 24 hours [PCR conditions described in Section 6.3.8.2]. Image is representative of one of 2 optimisation experiments. L denotes the position of 100bp ladder.

6.3.11. Data Analysis

Unless otherwise stated, each data set contained a minimum of three independent experiments, in which, each experiment was comprised of at least three internal replicates expressed as mean ± Standard Error of the Mean (SEM). Statistical analysis was conducted using an unpaired student's *t*-test. Data were considered significantly different when *P*-value < 0.05.

6.4. Results

6.4.1. Membrane Integrity of BNIPP Derivative Treated MDA-MB-231 Cells

The effect of BNIPSpd (1 - 5 µM; 0.5 – 24 hours; Figure 6.7), BNIPDaCHM (1 - 5 µM; 0.5 – 24 hours; Figure 6.8) and the positive control etoposide (10 µM; 24 hours; Figure 6.9) on chromatin changes in MDA-MB-231 cells relative to membrane integrity was determined by fluorescence microscopy following AO/EB staining. AO fluoresces green in viable cells with intact membranes, whilst EB fluoresces orange in non-viable (i.e., necrotic) cells (refer to Section 6.1.1.2.a and Table 6.3).

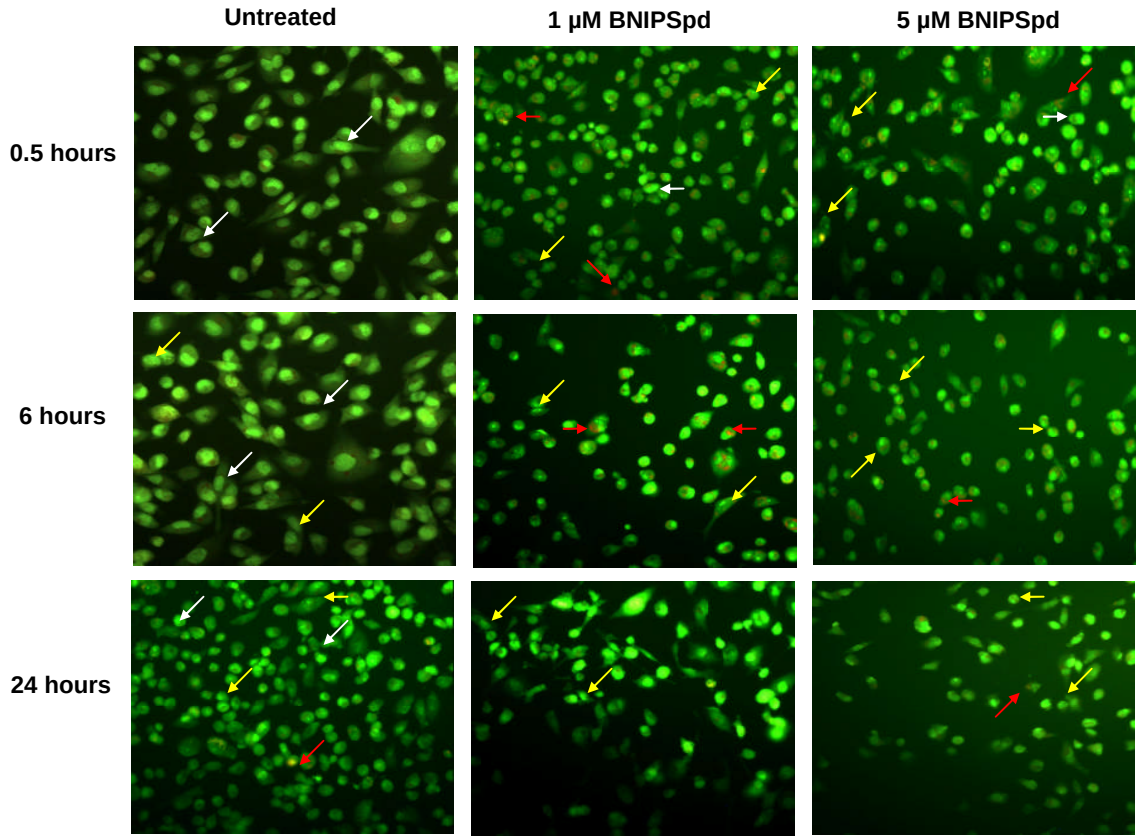

Figure 6.7.: Changes in cell morphology in adherent MDA-MB-231 cells treated with 1 – 5 µM BNIPSpd for 0.5, 6 and 24 hours. Cells were visualised using a Leica DMIL inverted fluorescence microscope using a UV filter (excitation bandpass (blue); 450 - 490 nm, emission longpass (yellow); 515 nm. Images are representative of 3 independent experiments undertaken in triplicate (n = 3). Key: viable cells, white arrow; early apoptotic cells, yellow arrow; late apoptotic cells, red arrow. Magnification x 200.

After 0.5 hours treatment, MDA-MB-231 membrane integrity was compromised by 1 and 5 µM BNIPSpd with the presence of early and late apoptotic cells compared to untreated cells (Figure 6.7). However, it was apparent that not all MDA-MB-231 cells had been compromised after 0.5 hours as viable cells were still evident within the treated MDA-MB-231 cell population (Figure 6.7). After 6 hours treatment, late apoptotic cells were evident in 1 and 5 µM BNIPSpd treated MDA-MB-231 cells, in comparison to

untreated cells (Figure 6.7). After 24 hours, MDA-MB-231 cells treated with 1 and 5 μM BNIPSpd confirmed the presence of apoptotic cells, in comparison to untreated cells (Figure 6.7). However, early and late apoptotic cells were also present in untreated cells.

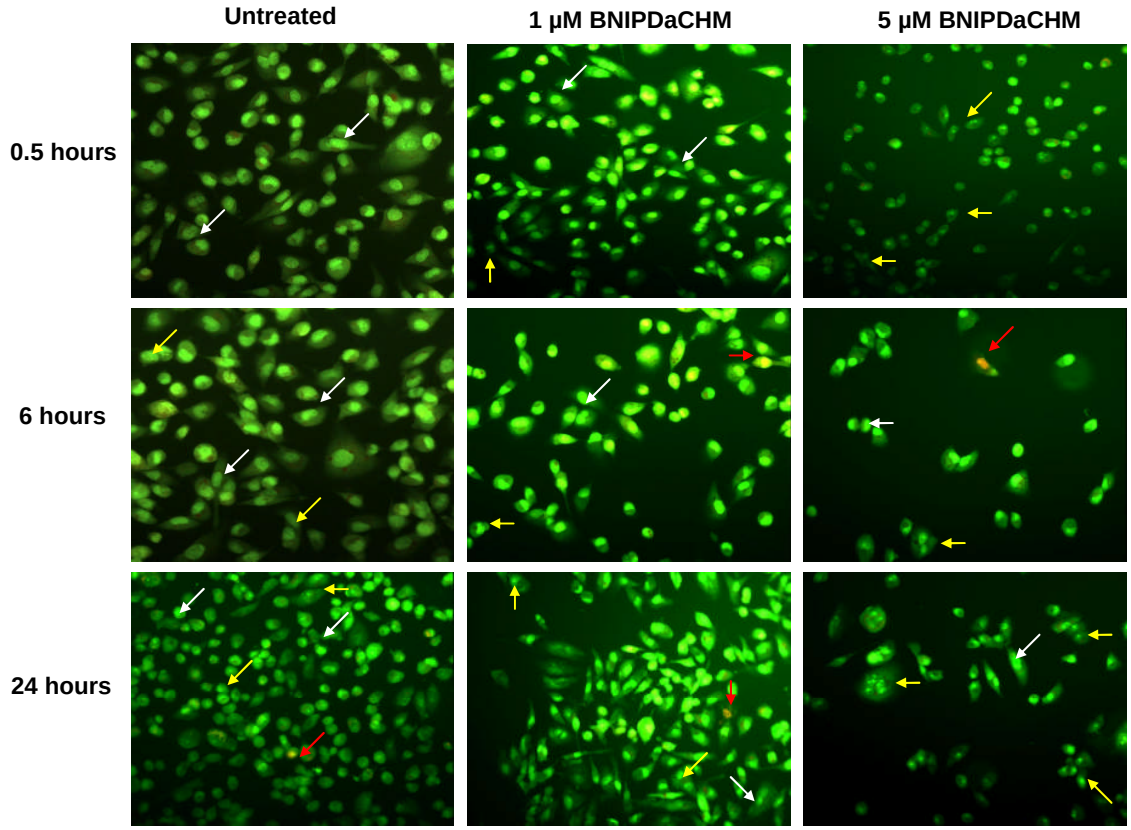

Figure 6.8.: Changes in cell morphology in adherent MDA-MB-231 cells treated with 1 – 5 μM BNIPDaCHM for 0.5, 6 and 24 hours. Cells were visualised using a Leica DMIL inverted fluorescence microscope using a UV filter (excitation bandpass (blue); 450 - 490 nm, emission longpass (yellow); 515 nm. Images are representative of 3 independent experiments undertaken in triplicate (n = 3). Key: viable cells, white arrow; early apoptotic cells, yellow arrow; late apoptotic cells, red arrow. Magnification x 200.

Membrane integrity was compromised by ≥ 1 μM BNIPDaCHM (Figure 6.8). After 0.5 hours, MDA-MB-231 cells treated with 1 and 5 μM BNIPDaCHM produced early apoptotic cells in a dose dependent manner compared with untreated cells (Figure 6.8). After 6 hours, late apoptotic cells were evident in 1 and 5 μM BNIPDaCHM treated MDA-MB-231 cells, in comparison to untreated cells (Figure 6.8). However, viable and early apoptotic cells were present in both untreated, and BNIPDaCHM treated MDA-MB-231 cells after 6 hours treatment (Figure 6.8). After 24 hours, viable, early and late apoptotic cells were evident in untreated and treated (1 and 5 μM) MDA-MB-231 cells (Figure 6.8). Treatment with 5 μM BNIPDaCHM (0.5 – 24 hours) was extremely toxic to MDA-MB-231 cells with the visible loss of cell number compared with untreated cells (Figure 6.8).

The results presented in Figure 6.9 demonstrate that a higher loss of membrane integrity (i.e., late apoptotic cells) was observed in etoposide (10 μM) rather than BNIPP derivative (5 μM) treated MDA-MB-231 cells after 24 hours (Figure 6.9). However, MDA-

MB-231 cells treated with BNIPSpd or BNIPDaCHM (5 µM) were found to exhibit a greater level of cell shrinkage than etoposide (10 µM) treated MDA-MB-231 cells (Figure 6.9).

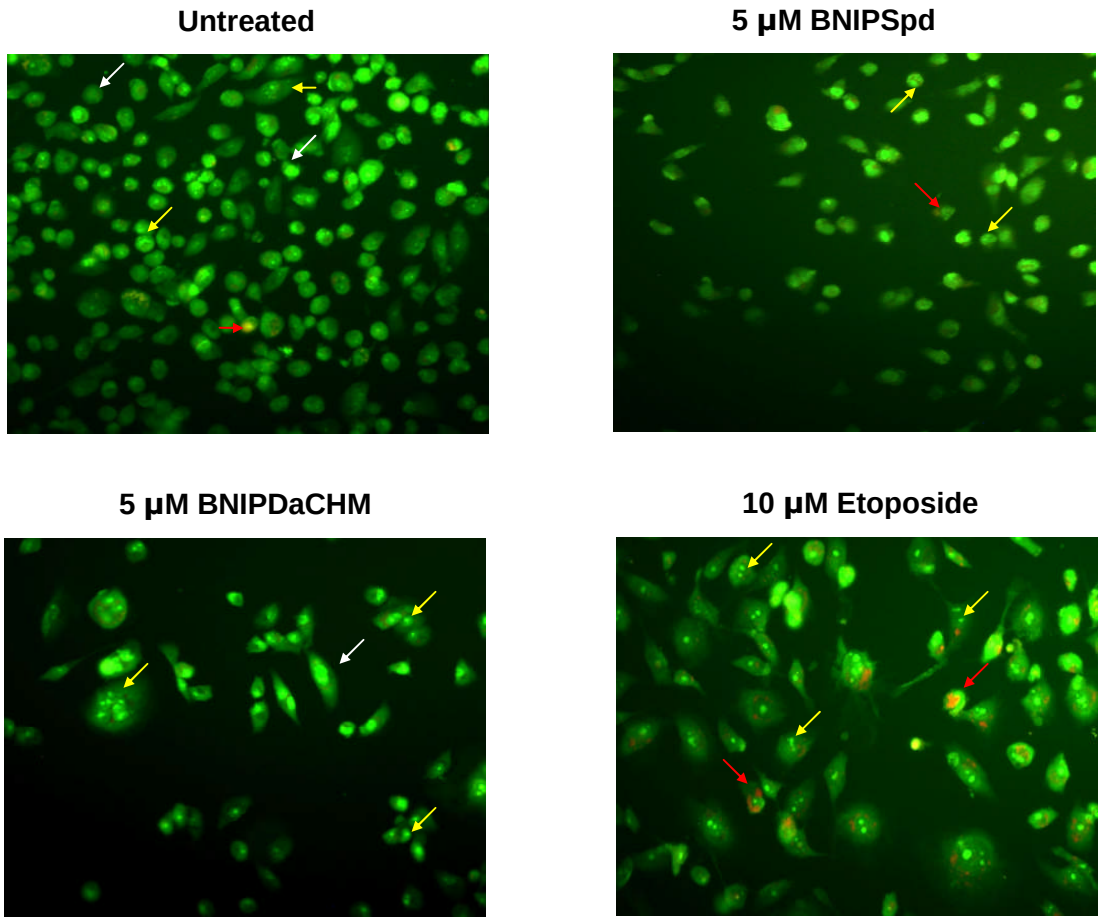

Figure 6.9.: Changes in cell morphology in adherent MDA-MB-231 cells treated with 5 µM BNIPSpd, 5 µM BNIPDaCHM or 10 µM etoposide for 24 hours. Cells were visualised using a Leica DMIL inverted fluorescence microscope using a UV filter (excitation bandpass (blue); 450 - 490 nm, emission longpass (yellow); 515 nm. Images are representative of 3 independent experiments undertaken in triplicate (n = 3). Key: viable cells, white arrow; early apoptotic cells, yellow arrow; late apoptotic cells, red arrow. Magnification x 200.

6.4.2. Phosphatidylserine Exposure and Membrane Integrity in MDA-MB-231 Cells Treated with BNIPP Derivatives

The effects of BNIPSpd or BNIPDaCHM (1 – 5 µM; 0.5, 4 and 6 hours) on PS exposure and plasma membrane integrity in adherent MDA-MB-231 cells were quantified using flow cytometry following annexin V-FITC staining and 7-AAD labelling (Figure 6.10 – 6.13). The diagram in Figure 6.10 presents the apoptotic and necrotic histograms obtained after 0.5 hours treatment with DMSO (0.025%), BNIPDaCHM (5 µM) or formaldehyde (3% v/v) in MDA-MB-231 cells.

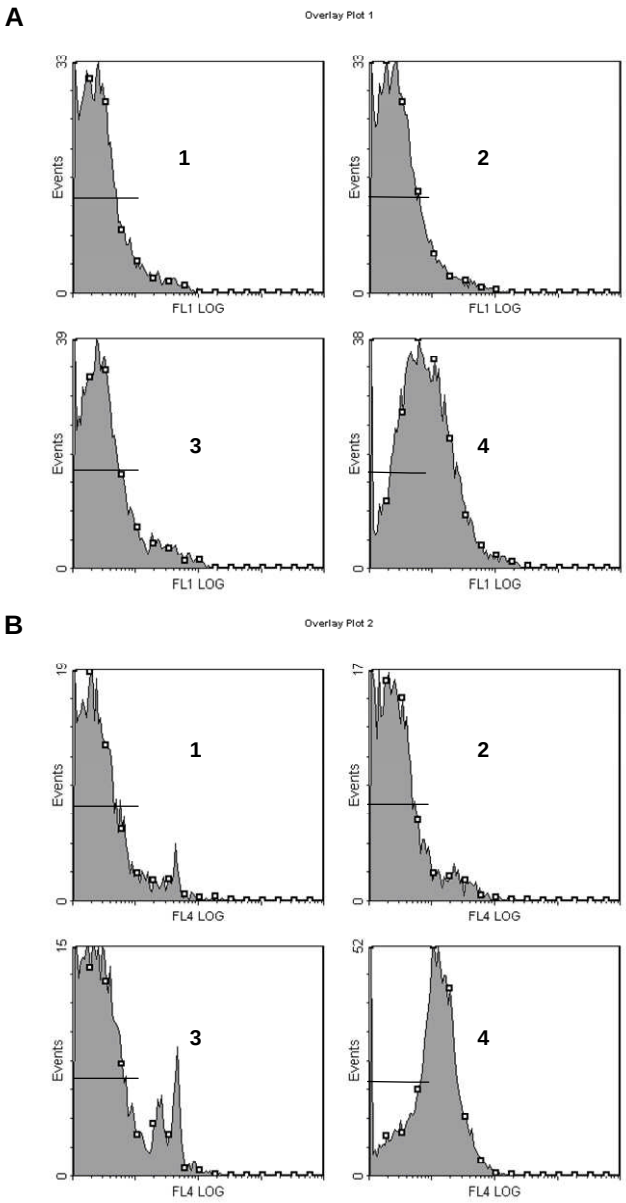

Figure 6.10.: Apoptotic (A) and necrotic (B) distribution of MDA-MB-231 cells (A1-4 and B1-4). MDA-MB-231 cells (untreated; 1) were treated for 0.5 hours with DMSO (2), 5 µM BNIPDaCHM (3) and 3% (v/v) formaldehyde (4) and stained with annexin V-FITC/7-AAD before flow cytometric analysis (10,000 events were recorded). Line markers indicate the gates used to detect apoptotic (annexin V-FITC stained cells) and necrotic (7-AAD labelling) cells. Images are representative of one of three independent experiments and were obtained using EXPO32 ADC analysis software.

The results for PS exposure relative to increased damage of the plasma membrane, as shown as a ratio to the control (i.e., untreated MDA-MB-231 cells), since barely any apoptotic or necrotic cells were present in the control cells after cells were detached by trypsinisation using Trypsin-EDTA (1x in PBS) solution (refer to Section 4.3.1). Annexin V-FITC stains apoptotic cells as it specifically binds to exposed PS residues on the outer layer of the plasma membrane, whilst 7-AAD viability dye can only label cells where the plasma membrane integrity has been lost. Thus, 7-AAD uptake can occur in only necrotic cells (refer to Section 6.1.1.2.b).

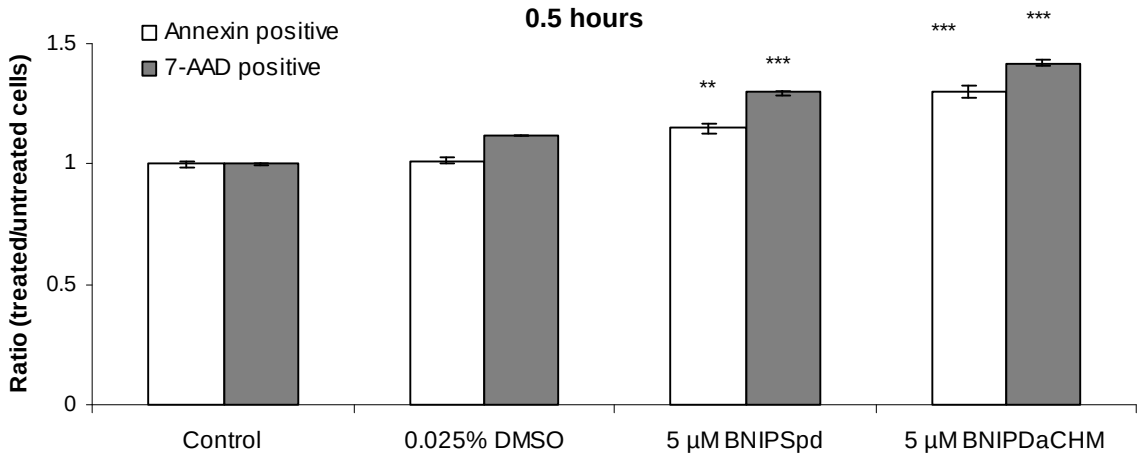

Figure 6.11.: PS exposure and membrane integrity profiles. Profiles were determined by flow cytometry following annexin V-FITC staining and 7-AAD labelling after 0.5 hours treatment with BNIPSpd or BNIPDaCHM (5 µM). 10,000 single events were recorded, and cells labelled with annexin V but not 7-AAD were annexin positive. Cells labelled with 7-AAD denoted as 7-AAD positive. Data are presented as a ratio to the untreated cells and represent mean ± SEM of 3 independent experiments conducted in duplicate (n = 3). ***P*<0.01, ****P*<0.001 compared with untreated MDA-MB-231 control.

After 0.5 hours, no significant difference in annexin V-FITC staining or 7-AAD labelling was observed following DMSO (0.025%) treatment when compared to the control (Figure 6.11). Interestingly, BNIPSpd and BNIPDaCHM (5 µM) both significantly increased annexin V-FITC staining ($P < 0.01$; a 15% increase and $P < 0.001$; a 30% increase, respectively) and 7-AAD labelling ($P < 0.001$; a 30% increase and $P < 0.001$; a 42% increase, respectively) when compared to the control (Figure 6.11). Plasma membrane integrity was thus compromised following treatment with BNIPSpd or BNIPDaCHM (5 µM; 0.5 hours) as a higher proportion of MDA-MB-231 cells were labelled with 7-AAD rather than annexin V-FITC.

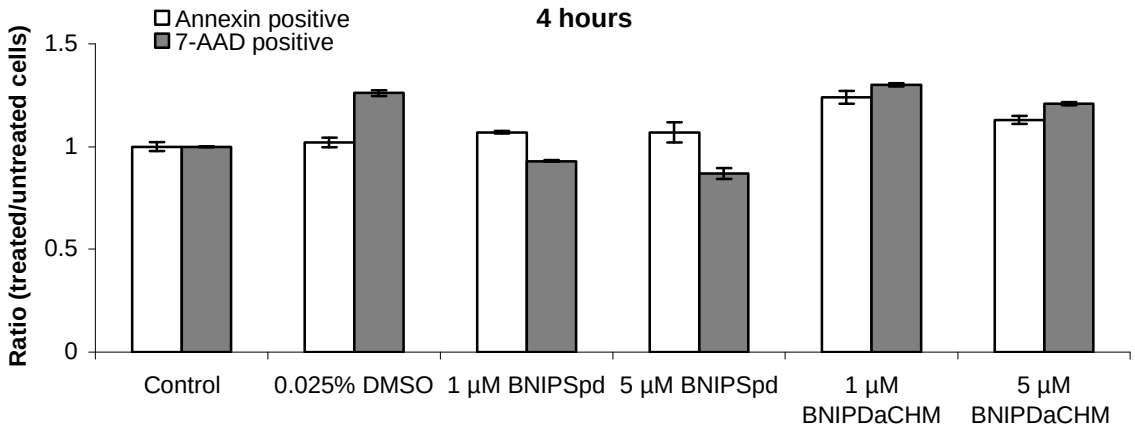

Figure 6.12.: PS exposure and membrane integrity profiles. Preliminary profiles were determined by flow cytometry following annexin V-FITC staining and 7-AAD labelling after 4 hours treatment with BNIPSpd or BNIPDaCHM (1 and 5 µM). 10,000 single events were recorded, and cells labelled with annexin V but not 7-AAD were annexin positive. Cells labelled with 7-AAD were denoted as 7-AAD positive. Data are presented as ratio to the untreated cells and represent mean ± SD of 2 independent experiments conducted in triplicate (n = 2).

Results from two experiments for PS exposure and membrane integrity in MDA-MB-231 cells treated with BNIPSpd or BNIPDaCHM (1 – 5 µM) were obtained after 4 (Figure 6.12) and 6 hours (Figure 6.13). After 4 hours, DMSO (0.025%) treatment produced no difference in annexin V-FITC staining but an increase in 7-AAD labelling was evident when compared to the control (Figure 6.12). MDA-MB-231 cells treated with 1 – 5 µM BNIPSpd showed a similar trend with an increase in annexin V-FITC staining and a decrease in 7-AAD staining compared to the control, thus indicating a higher proportion of MDA-MB-231 cells without plasma membrane damage (Figure 6.12). However, treatment with BNIPDaCHM (1 – 5 µM) resulted in an increase in both annexin V-FITC staining and 7-AAD labelling relative to the control indicating a loss of plasma membrane integrity (Figure 6.12).

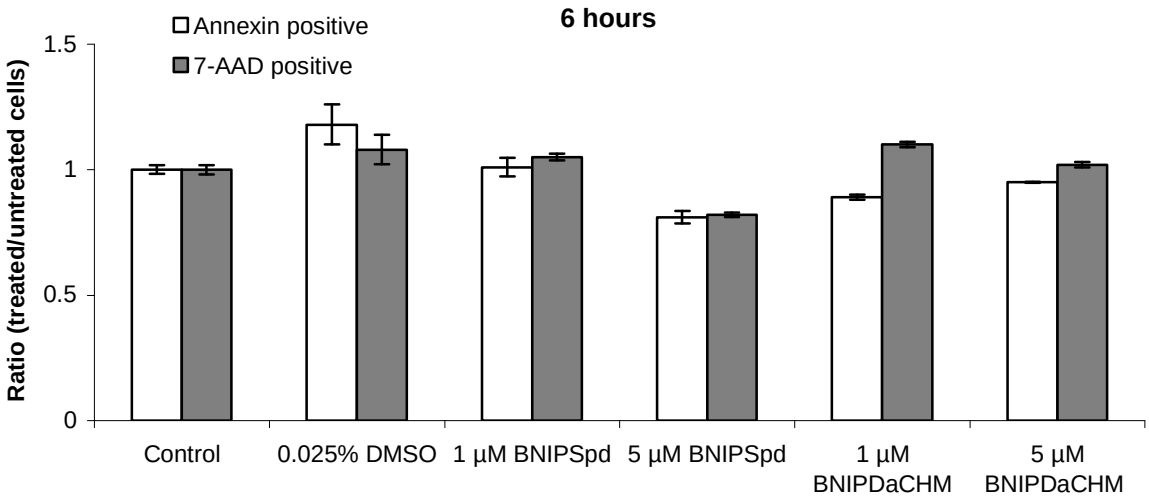

Figure 6.13.: PS exposure and membrane integrity profiles. Preliminary profiles were determined by flow cytometry following annexin V-FITC staining and 7-AAD labelling after 6 hours treatment with BNIPSpd or BNIPDaCHM (1 and 5 µM). 10,000 single events were recorded, and cells labelled with annexin V but not 7-AAD were annexin positive. Cells labelled with 7-AAD were denoted as 7-AAD positive. Data are presented as ratio to the untreated cells and represent mean ± SD of 2 independent experiments conducted in triplicate (n = 2).

After 6 hours, DMSO (0.025%) treatment produced an increase in both annexin V-FITC staining and 7-AAD labelling relative to the control (Figure 6.13). Following BNIPSpd (1 µM) treatment, annexin V-FITC staining mirrored that of the control whilst 7-AAD labelling increased relative to the control (Figure 6.13). BNIPSpd (5 µM) treatment resulted in a decrease in both annexin V-FITC staining and 7-AAD labelling relative to the control (Figure 6.13). A similar trend was found after treatment with 1 BNIPDaCHM and 5 µM BNIPDaCHM as annexin V-FITC staining and 7-AAD labelling were decreased and increased, respectively indicating a loss of plasma membrane integrity (Figure 6.13).

6.4.3. Cell Growth in MDA-MB-231 Cells Treated with BNIPDaCHM

The effect of BNIPDaCHM (1 - 10 µM) treatment on adherent MDA-MB-231 cell numbers (i.e., cell proliferation) after 0.5, 4, 6 and 24 hours treatment was determined by microscopical cell count experiments, as shown in Figure 6.14.

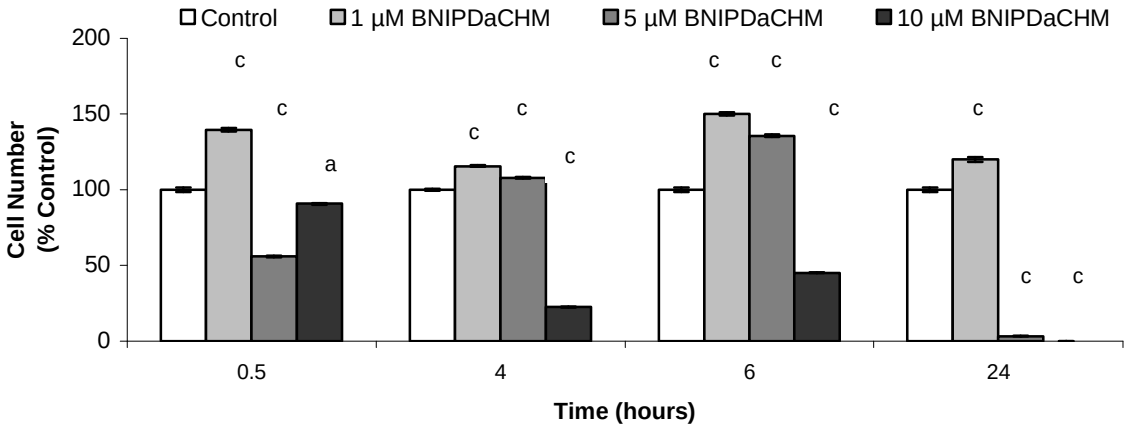

Figure 6.14.: MDA-MB-231 cell number after treatment with BNIPDaCHM. MDA-MB-231 cells were treated for 0.5, 4, 6 and 24 hours with 0 – 10 µM BNIPDaCHM. Cell number was determined by direct microscopical cell counting of adherent cells using a Neubauer haemocytometer. Data are mean ± SEM of 2 independent experiments conducted in quadruplicate (n = 2). $^{a}P<0.05$, $^{b}P<0.01$, $^{c}P<0.001$ compared with respective untreated MDA-MB-231 control.

After 0.5 hours treatment, MDA-MB-231 cell growth was significantly activated by 1 µM BNIPDaCHM ($P < 0.001$; a 39.5% increase) when compared to the control. MDA-MB-231 cell growth was significantly inhibited by 5 µM ($P < 0.001$; a 44.2% decrease) and 10 µM ($P < 0.05$; a 9.3% decrease) BNIPDaCHM when compared to the control (Figure 6.14).

After 4 hours treatment, MDA-MB-231 cell growth was significantly activated by 1 µM ($P < 0.001$; a 15.5% increase) and 5 µM ($P < 0.001$; a 7.9% increase) BNIPDaCHM when compared to the control. MDA-MB-231 cell growth was significantly inhibited by 10 µM BNIPDaCHM ($P < 0.001$; a 77.4% decrease) when compared to the control (Figure 6.14).

After 6 hours treatment, MDA-MB-231 cell growth was significantly activated by 1 µM ($P < 0.001$; a 50% increase) and 5 µM ($P < 0.001$; a 35.7% increase) when compared to the control. MDA-MB-231 cell growth was significantly inhibited by 10 µM BNIPDaCHM ($P < 0.001$; a 54.8% decrease) when compared to the control (Figure 6.14).

After 24 hours treatment, MDA-MB-231 cell growth was significantly activated by 1 µM ($P < 0.001$; a 20% increase) when compared to the control. MDA-MB-231 cell growth was significantly inhibited by 5 µM ($P < 0.001$; a 96.7% decrease) and 10 µM ($P < 0.001$; a 100% decrease) when compared to the control (Figure 6.14).

In summary, BNIPDaCHM (1 μM) activated MDA-MB-231 cell growth over a 24 hour time-course. After 0.5 and 24 hours, BNIPDaCHM (5 μM) inhibited MDA-MB-231 cell growth, but after 4 and 6 hours MDA-MB-231 cell growth was activated with 5 μM BNIPDaCHM. BNIPDaCHM (10 μM) inhibited MDA-MB-231 cell growth over a 24 hour time-course (Figure 6.14).

6.4.4. *Cell Cycle Effects by BNIPP Derivatives in MDA-MB-231 Cells*

The effect of BNIPSpd, BNIPDaCHM (5 µM) or the positive control etoposide (10 µM) on MDA-MB-231 cell cycle was determined by flow cytometry following PI staining after 24 hours of treatment. The diagram in Figure 6.15, presents the cell cycle distribution histograms obtained after 24 hours treatment of DMSO (0.025%), BNIPSpd (5 µM), BNIPDaCHM (5 µM) and etoposide (10 µM) in MDA-MB-231 cells. The results of DNA distribution are arranged as gap phase 1 (G1), DNA synthesis (S) phase and gap phase 2/mitosis (G2/M) populations in Figure 6.16. The sub-G1 population which represents apoptotic cells with a low DNA content are shown in Figure 6.17.

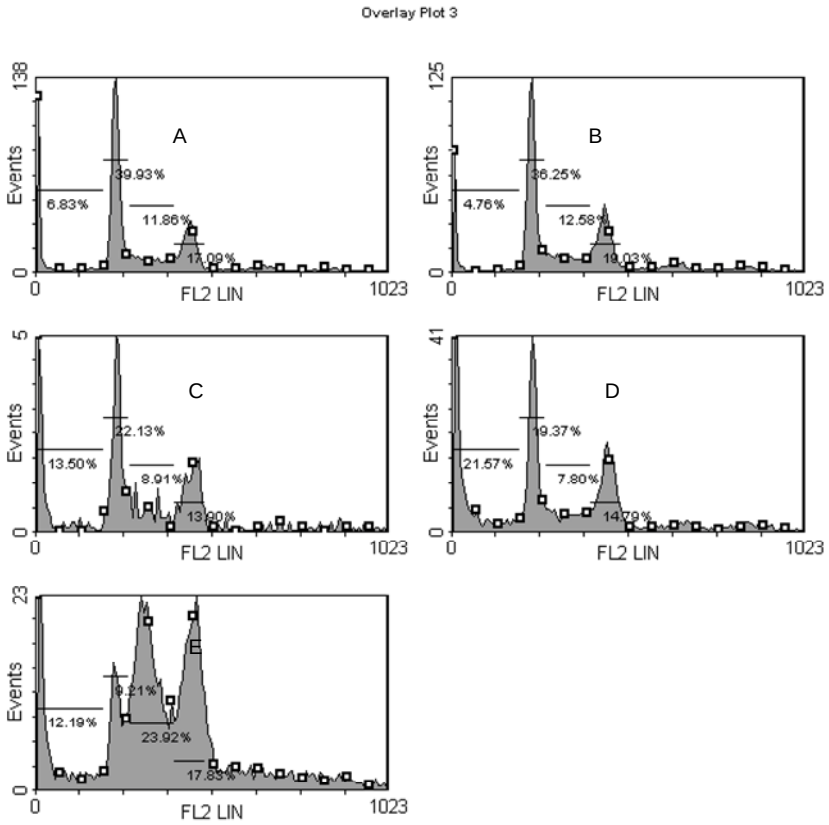

Figure 6.15.: Cell cycle distribution of MDA-MB-231 cells (A-E). MDA-MB-231 cells were untreated (A) and treated for 24 hours with DMSO (B), 5 µM BNIPSpd (C), 5 µM BNIPDaCHM (D) and 10 µM Etoposide (E) and stained with PI before flow cytometric analysis (10,000 events were recorded). Line markers (left – right) indicate the approximate regions of the cell cycle; sub-G1 phase; G1 phase; S phase; G2/M phase. Images are representative of one of four independent experiments and were obtained using EXPO32 ADC analysis software.

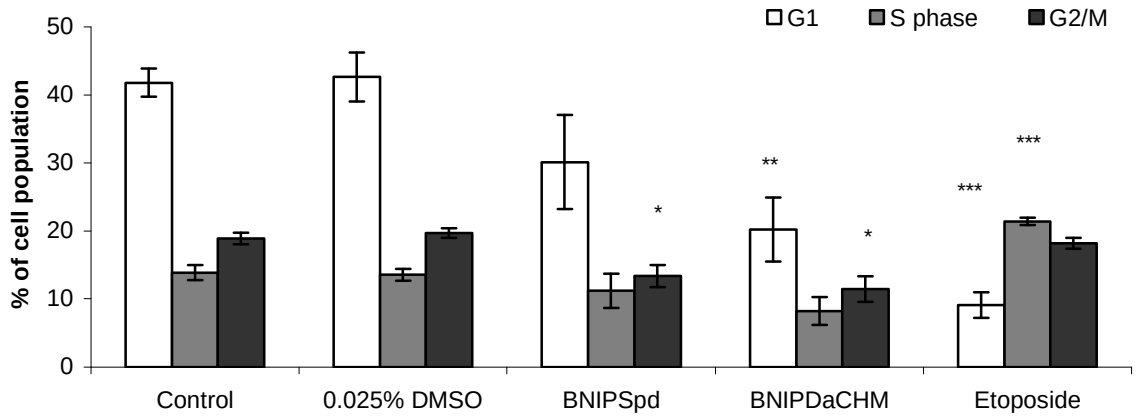

Figure 6.16.: Quantification of cell cycle profiles. Profiles were determined by flow cytometry following PI staining after 24 hours treatment with BNIPSpd or BNIPDaCHM (5 µM). Etoposide (10 µM) and DMSO (0.025%) were used as positive and negative controls respectively. 10,000 single events were recorded, and the percentage of cells with DNA content in cell cycles phases (G1, S and G2/M) were calculated from histograms of linear FL-2 plots in the ungated region. Data are mean ± SEM of 4 independent experiments conducted in duplicate (n = 4). **P*<0.05, ***P*<0.01, ****P*<0.001 compared with respective untreated MDA-MB-231 control.

After 24 hours, control cells had accumulated in the G1 phase (Figure 6.16). MDA-MB-231 cells exposed to DMSO (0.025%) mirrored those of control cells (Figure 6.16). Therefore, 0.025% DMSO did not have an effect on MDA-MB-231 cells. Treatment with BNIPSpd (5 µM) exhibited a decrease in the proportion of MDA-MB-231 cells in all cell cycle phases relative to the control, in particular the G2/M phase ($P < 0.05$; a 5.5% decrease) (Figure 6.16). Treatment with BNIPDaCHM (5 µM) also exhibited a decrease in the proportion of MDA-MB-231 cells in all cell cycle phases relative to the control, in particular the G1 ($P < 0.01$; a 21.6% decrease) and G2/M phases ($P < 0.05$; a 7.4% decrease) (Figure 6.16). Treatment with etoposide (10 µM) exhibited a pronounced decrease in the proportion of MDA-MB-231 cells in G1 phase ($P < 0.001$; a 32.7% decrease) and an increase in S-phase ($P < 0.001$; a 7.5% increase) relative to the control. Whereas cells present in the G2/M phase mirrored that of control cells (Figure 6.16).

Since MDA-MB-231 cell number was found to be significantly decreased with ≥ 5 µM BNIPDaCHM (Section 6.4.3 and Figure 6.13), it was important to determine the proportion of MDA-MB-231 cells with a sub-G1 DNA content and results are presented in Figure 6.17.

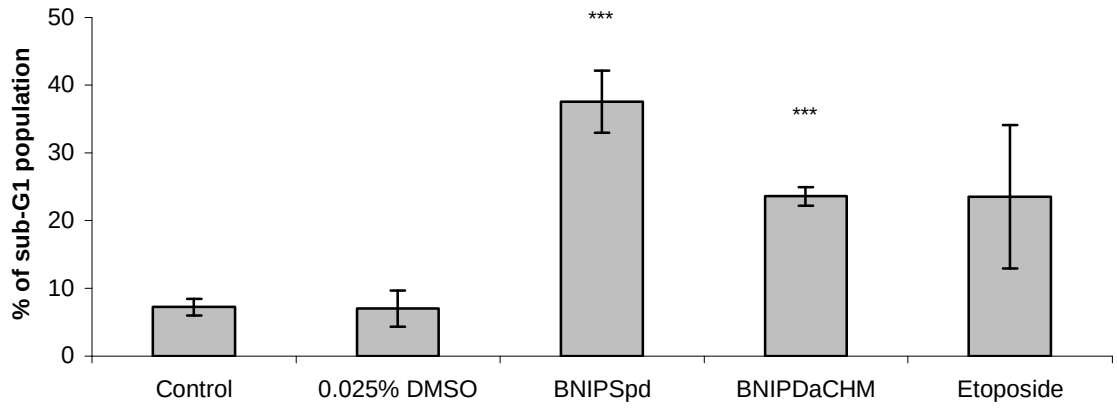

Figure 6.17.: Quantification of sub-G1 cell cycle profile. Profiles were determined by flow cytometry following PI staining after 24 hours treatment with BNIPSpd or BNIPDaCHM (5 µM). Etoposide (10 µM) and DMSO (0.025%) were used as positive and negative controls, respectively. 10,000 single events were recorded, and the percentage of cells with DNA content in sub-G1 was calculated from histograms of linear FL-2 plots in the ungated region. Data are mean ± SEM of 4 independent experiments conducted in duplicate (n = 4). ***P<0.001 compared with respective untreated MDA-MB-231 control.

After 24 hours, treatment with DMSO (0.025%) produced cells with a sub-G1 DNA content which mirrored that of control cells (Figure 6.17). Treatment with BNIPSpd (5 µM) exhibited a significant increase in the proportion of cells with sub-G1 content (P < 0.001; a 30.4% increase) relative to the control (Figure 6.17). BNIPDaCHM (5 µM) treatment also produced a significant increase in the sub-G1 population (P < 0.001; a 16.4% increase) relative to the control, whilst 10 µM etoposide did not significantly increase the sub-G1 population to the same extent as BNIPSpd or BNIPDaCHM in relation to the control (Figure 6.17).

6.4.5. *Effect of BNIPDaCHM on p53 and p21$^{Waf1/Cip1}$ mRNA Expression Levels in MDA-MB-231 Cells*

The effect of BNIPDaCHM (5 µM) on p53 (Section 6.4.5.1) and p21$^{Waf1/Cip1}$ (Section 6.4.5.2) mRNA expression levels was determined in MDA-MB-231 cells by RT-PCR studies.

6.4.5.1. *Effect on p53 mRNA Expression Levels*

Treatment with BNIPDaCHM (5 µM) does not significantly alter p53 mRNA levels after 1, 4 or 24 hours of treatment as shown in Figure 6.18.

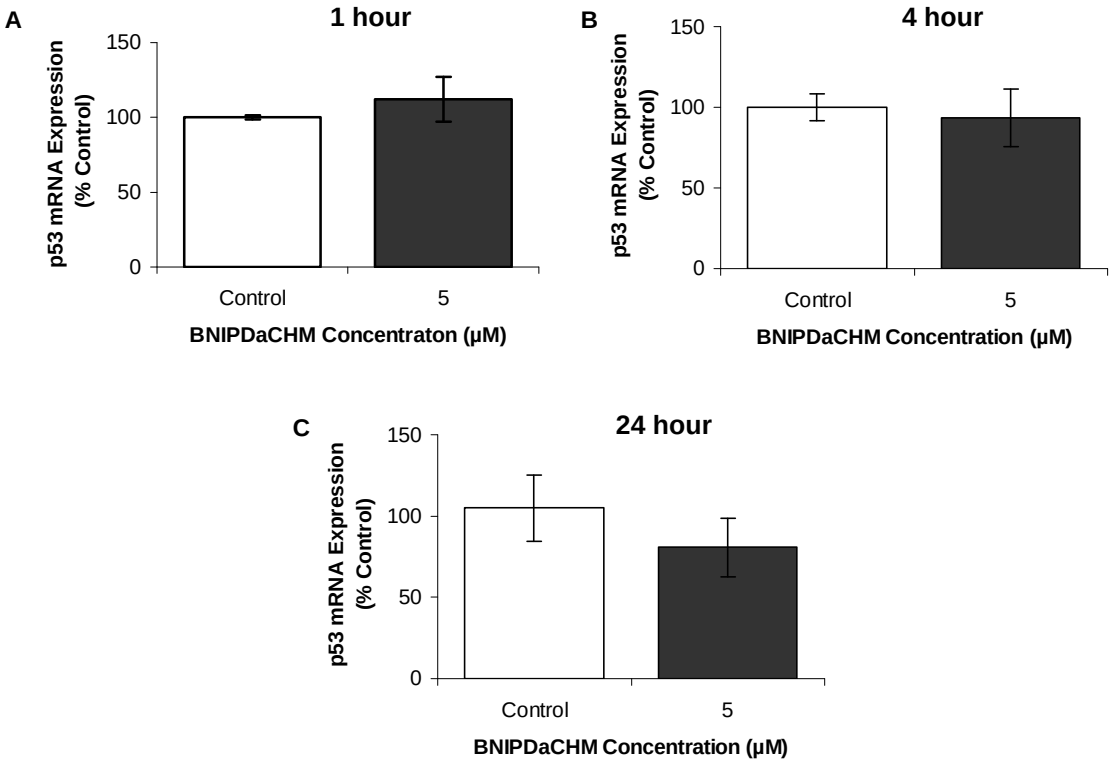

Figure 6.18.: Expression levels of p53 mRNA in BNIPDaCM treated MDA-MB-231 cells by RT-PCR. MDA-MB-231 cells were treated with 5 µM BNIPDaCHM for 1 (**A**), 4 (**B**) and 24 (**C**) hours. Total RNA was extracted and RT-PCR carried out using p53 specific primers and β-actin as an internal control. Data are mean ± SEM of 3 independent experiments conducted in duplicate (n = 3).

6.4.5.2. Effect on p21$^{Waf1/Cip1}$ mRNA Expression Levels

Treatment with BNIPDaCHM (5 µM) increased p21$^{Waf1/Cip1}$ mRNA levels in a time-dependent manner with a significant increase observed after 4 hours treatment ($P < 0.01$; a 24.7% increase) rather than after 1 hour treatment (Figure 6.19).

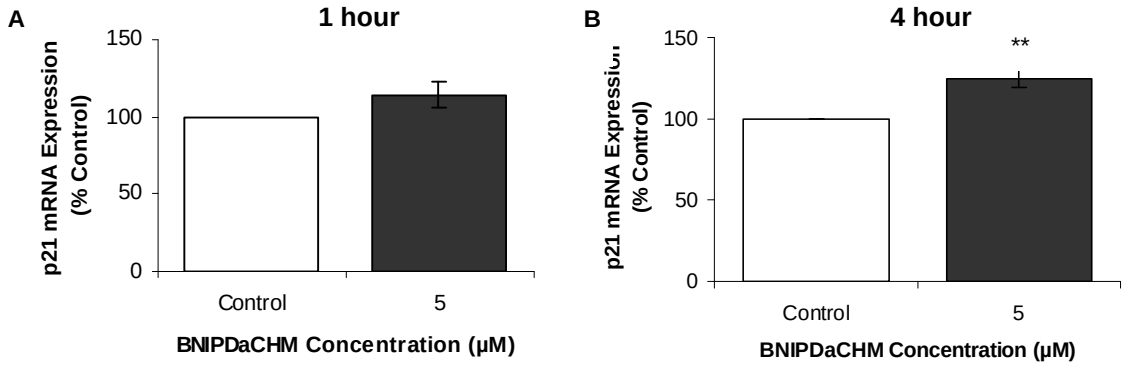

Figure 6.19.: Expression levels of p21$^{Waf1/Cip1}$ mRNA in BNIPDaCM treated MDA-MB-231 cells by RT-PCR. MDA-MB-231 cells were treated with 5 µM BNIPDaCHM for 1 (**A**) and 4 (**B**) hours. Total RNA was extracted and RT-PCR carried out using p21$^{Waf1/Cip1}$ specific primers and β-actin as an internal control. Data are mean ± SEM of 3 independent experiments conducted in duplicate (n = 3). ***P*<0.01 compared with untreated MDA-MB-231 control values.

6.4.6. Effect of BNIPSpd on p53 and p21$^{Waf1/Cip1}$ mRNA Expression Levels in MDA-MB-231 Cells

The effect of BNIPSpd (5 µM) on p53 and p21$^{Waf1/Cip1}$ mRNA levels was determined in MDA-MB-231 cells by RT-PCR studies (Figure 6.20).

After 4 hours, treatment with BNIPSpd (5 µM) did not alter the levels of p53 or p21$^{Waf1/Cip1}$ mRNA in MDA-MB-231 cells (Figure 6.20).

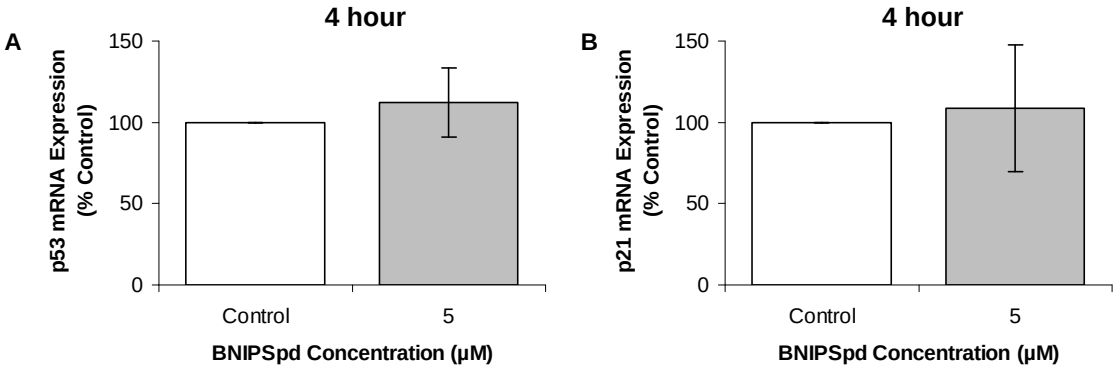

Figure 6.20.: Expression levels of p53 and p21$^{Waf1/Cip1}$ mRNA in BNIPSpd treated MDA-MB-231 cells by RT-PCR. p53 (**A**) and p21$^{Waf1/Cip1}$ (**B**) mRNA levels were determined after 4 hours treatment with 5 µM BNIPSpd. Total RNA was extracted and RT-PCR carried out using p53 and p21$^{Waf1/Cip1}$ specific primers with β-actin as an internal control. Data are mean ± SEM of 3 independent experiments conducted in duplicate (n = 3).

6.5. Discussion

6.5.1. Membrane Integrity of BNIPP Derivative Treated MDA-MB-231 Cells

Treatment with ≥ 1 μM BNIPSpd or BNIPDaCHM resulted in changes to membrane integrity in MDA-MB-231 cells (Figure 6.7 and 6.8), as examined by fluorescence microscopy following AO/EB staining. The visible staining of AO/EB in adherent MDA-MB-231 cells indicated the presence of viable, early and late apoptotic cells identified by colour and appearance; however, it was difficult to identify necrotic cells. This observation is supported by cell morphology changes (Section 4.4.1.1; Figure 4.11 and Section 6.4.1; Figures 6.7 and 6.8), combined with an apparent loss of cells (Section 6.4.3 and Figure 6.14) after BNIPP derivative treatment.

These results are an extension of studies carried out by Ralton *et al.* (2009), where apoptotic cell death was investigated in BNIPSpd treated colon cancer CaCO-2 and HT-29 cells. BNIPSpd (≥ 0.5 μM) was found to induce a loss of plasma membrane integrity, chromatin condensation, nuclear and apoptotic-like cell fragmentation in CaCO-2 and HT-29 cells after 24 hours (Ralton *et al.* 2009). Therefore, these results together suggest that BNIPP derivatives can induce apoptotic cell death in breast (MDA-MB-231) and colon (CaCO-2 and HT-29) cancer cells (Ralton *et al.* 2009).

6.5.2. Phosphatidylserine Exposure and Membrane Integrity in MDA-MB-231 Cells Treated with BNIPP Derivatives

A quantitative assessment into the effect of BNIPP derivatives on the induction of early apoptosis in adherent MDA-MB-231 cells was conducted. PS exposure and plasma membrane integrity were measured by flow cytometry following annexin V-FITC staining and 7-AAD labelling (Section 6.4.2 and Figures 6.11 – 6.13).

BNIPSpd and BNIPDaCHM (1 – 5 μM; 0.5, 4 and 6 hours) increased annexin V-FITC staining, and 7-AAD labelling in MDA-MB-231 cells (Figures 6.11 – 6.13), with the exception of BNIPSpd, where 7-AAD labelling was reduced, when compared to control, following treatment with 1 and 5 μM BNIPSpd after 4 hours (Figure 6.12) and 5 μM BNIPSpd after 6 hours (Figure 6.13). These results indicate that BNIPP derivatives are able to elicit externalisation of PS residues and early plasma membrane damage in MDA-MB-231 cells after ≥ 0.5 hours treatment (Figure 6.11). Results are supported as treatment with DMSO (0.025%) did not induce a significant difference in annexin V-FITC staining or 7-AAD labelling when compared to control (Figure 6.11). This result strongly supports the conclusion that BNIPP derivatives induce early apoptosis, and that the results are not a stress response of the cells or an experimental artefact. The

observations of membrane integrity changes detected by AO/EB staining (Section 6.4.1 and Figures 6.7 – 6.9) also support these results.

The results presented suggest that damage to the plasma membrane could be an important mechanism in BNIPDaCHM-induced cytotoxicity within MDA-MB-231 cells. Given that an increase in 7-AAD labelling was observed after 0.5 hours with 5 µM, 4 hours with 1 and 5 µM and 6 hours with 1 and 5 µM BNIPDaCHM indicating a loss in plasma membrane integrity in a time-dependent manner. Apoptosis was also found to be significantly induced to a greater degree in cells treated with BNIPDaCHM ($P < 0.001$; a 30% increase) rather than BNIPSpd ($P < 0.01$; a 15% increase) after 0.5 hours (Figure 6.11). This result was supported by the cellular uptake studies (Section 4.4.3.1 and Figure 4.15), as BNIPDaCHM was observed within MDA-MB-231 cells after 0.5 hours, whilst BNIPSpd was not observed until after 6 hours.

It is difficult to directly compare the results for early apoptotic cell death obtained in this study with that of other apoptosis inducing anti cancer agents, as there does not appear to be any previous information available which details apoptotic cell death after only 0.5 hours treatment. However, one study did attempt to investigate early apoptotic cell death following exposure to cisplatin (5 and 10 mg/L) (Figure 3.8) in human malignant pleural mesothelioma (P31) cells after 0.5, 2 and 24 hours (Janson *et al.* 2008). In that work, Janson *et al.* (2008) found that annexin V staining was not increased following exposure to 5 and 10 mg/L cisplatin after 0.5 hours. This study supports the use of annexin V-FITC staining as a reliable technique to detect early apoptotic cell death, as it aimed to use it to detect apoptosis after 0.5 hours. Thus, the induction of early apoptosis following 0.5 hours treatment with BNIPP derivatives is an interesting and novel observation.

It is important to note that experiments conducted in Section 6.4.2 need to be repeated at least one more time, particularly the annexin V-FITC / 7-AAD staining after 4 and 6 hours.

6.5.3. Cell Growth in MDA-MB-231 Cells Treated with BNIPDaCHM

Treatment with BNIPDaCHM (0 – 10 µM) resulted in changes to cell proliferation in MDA-MB-231 cells (Figure 6.14), as examined by microscopical cell counts. Apoptosis can be identified by a loss of cell number or growth with the formation of floating (apoptotic) cells (Soldatenkov *et al.* 1998, Holdenrieder and Stieber 2004). MDA-MB-231 cell number was found to be significantly reduced with ≥ 5 µM BNIPDaCHM ($P < 0.001$; a 96.7% decrease; Figure 6.14) over a 24 hour time-course. These results are in agreement with the cell morphology studies (Section 4.4.1.1 and Figure 4.11); where BNIPDaCHM treatment resulted in changes to the morphology of MDA-MB-231 cells and

cytotoxicity studies (Table 4.2); where an IC_{50} value of 6.8 µM was determined after 24 hours treatment with BNIPDaCHM.

The decreased number of adherent MDA-MB-231 cells with ≥ 5 µM BNIPDaCHM after 4, 6 and 24 hours treatment may imply that BNIPDaCHM could be more cytotoxic than initially determined in Section 4.4.2. This can be proposed since only adherent, not floating cells were investigated in the cytotoxicity study (Section 4.4.2). Therefore, for that reason, cell cycle (Section 6.4.4) studies were undertaken using both adherent and non-adherent MDA-MB-231 cells. The use of the whole cell population can thus provide a more accurate assessment of the potential of BNIPP derivatives to induce cell cycle arrest and apoptotic cell death in breast cancer cells.

6.5.4. Cell Cycle Effects by BNIPP Derivatives in MDA-MB-231 Cells

The experimental work presented in Section 6.4.4 was the first quantitative study of cell cycle effects to be undertaken with the BNIPP derivatives. Cell cycle analysis was carried out using the technique of flow cytometry following PI staining reported by Bestwick *et al.* (2007).

Treatment with BNIPSpd or BNIPDaCHM (5 µM) induced cell cycle instability in MDA-MB-231 cells after 24 hours with the increased appearance of a sub-G1 population ($P < 0.001$; a 30.4% and 16.4% increase, respectively) (Figure 6.17). Sub-G1 population has been linked to cells with fragmented DNA, and is indicative of apoptotic cells (Shu *et al.* 1997, Bestwick and Milne 2006, Wang *et al.* 2008). This result was supported by the findings from the Annexin V-FITC/7-AAD viability assay (Section 6.4.2 and Figures 6.11 - 13) and MDA-MB-231 cell counts (Section 6.4.3 and Figure 6.14). In addition, the significant increase in the number of DNA strand breaks induced by BNIPSpd after 24 hours (Section 5.4.2.1 and Figure 5.8) could be responsible for the high level of cells present in the sub-G1 population (Figure 6.17).

The effect of structurally related bisnaphthalimide derivatives were studied by Bailly *et al.* (2003) and Filosa *et al.* (2009). Bailly *et al.* (2003) found that MCI3335 (2 µM; 24 hours) (Figure 6.21) exhibited little effect on cell cycle progression in CEM leukaemia cells, whilst Filosa *et al.* (2009) found that *N*, *N*'-bis[2-(5-nitro-1,3-dioxo-2,3-dihydro-1H-benz[*de*]-iso-quinolin-2-yl)] propane-2-ethanediamine (Figure 1.25) was unable to block cell cycle progression in HT-29 colon cancer cells. These findings are similar to those found for BNIPSpd and BNIPDaCHM with regards to their effect on the G1, S and G2/M phases. Bailly *et al.* (2003) and Filosa *et al.* (2009) did not document the sub-G1 populations of treated CEM or HT-29 cells; therefore it is difficult to fully compare these bisnaphthalimide derivatives with the BNIPP derivatives used in this study.

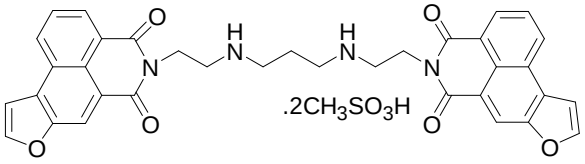

Figure 6.21.: Structure of MCI3335

To elucidate the mode of action utilised by BNIPP derivatives, it is important to refer to the spermine analogues discussed in Section 5.5.1, BENSpm (Figure 1.11) and CGP 48664 (Figure 5.16). These derivatives were investigated with regards to their effects on cell cycle progression by Alm *et al.* (2000) and Johansson *et al.* (2008). Alm *et al.* (2000) found that BENSpm (7.5 µM; 24 - 48 hours treatment) initially prolonged S phase progression in Chinese Hamster Ovary (CHO) cells before affecting the other cell cycle phases. In breast cancer (MCF-7 and L54Br-C1) cells, Johansson *et al.* (2008) found that BENSpm (10 µM; 24, 48 and 72 hours) exhibited an increase in G1 phase and a decrease in S phase. CGP 48664 (20 µM; 24 - 72 hours) induced an increase in G1 phase and decrease in S phase, similar to that of BENSpm, in MCF-7 and L54Br-C1 cells after 24 hours treatment, but after 48 hours, CGP 48664 (20 µM) decreased G1 phase and increased S phase when compared with control L54Br-C1 cells (Johansson *et al.* 2008). Johansson *et al.* (2008) also found that neither treatment induced any major effects in G2/M phase in either cell line. It was suggested by Johansson *et al.* (2008) that cell cycle arrest induced by BENSpm and CGP 48664 was cell line dependent and related to polyamine depletion, not apoptosis. In contrast, BNIPSpd and BNIPDaCHM do not appear to induce their effects on cell cycle progression through polyamine depletion (Section 4.4.5 and Figures 4.16 – 4.23) but rather by apoptotic induction (Section 6.4.2 and Figure 6.11). In support, Holst *et al.* (2006) found that the conformationally restricted polyamine analogue CGC-11047 (*cis*-**iii** analogue) (Figure 1.13) exhibited a significant sub-G1 population ($P < 0.05$) in breast cancer L56Br-C1 cells, and it was concluded that the effects of CGC-11047 were not related to polyamine depletion but rather another mechanism of action, such as apoptosis (Holst *et al.* 2006). Confirmation that BNIPP derivatives disrupt cell cycle progression by apoptosis induction will, however, require further investigation.

6.5.5. Effect of BNIPP Derivatives on p53 and p21$^{Waf1/Cip1}$ mRNA Expression Levels in MDA-MB-231 Cells

The experimental work presented in Sections 6.4.5 and 6.4.6 was the first quantitative study to be carried out into the effect of BNIPP derivatives on p53 and p21$^{Waf1/Cip1}$ mRNA expression levels in MDA-MB-231 cells using RT-PCR.

The results reveal that expression levels of p53 mRNA were not altered by BNIPDaCHM (5 µM) after 1, 4 or 24 hours treatment (Figure 6.18). Similarly expression

levels of $p21^{Waf1/Cip1}$ mRNA was not altered by BNIPDaCHM (5 µM) after 1 hour treatment; although after 4 hours treatment with BNIPDaCHM (5 µM), $p21^{Waf1/Cip1}$ mRNA levels were significantly increased ($P < 0.01$; a 24.7% increase) (Figure 6.19). BNIPSpd (5 µM) did not alter p53 or $p21^{Waf1/Cip1}$ mRNA expression levels in MDA-MB-231 cells after 4 hours (Figure 6.20).

P53 and $p21^{Waf1/Cip1}$ have both been implicated in cell cycle arrest and apoptotic cell death (Belkacemi *et al*. 2006, Park *et al.* 2008). Functional p53 can activate $p21^{Waf1/Cip1}$ which in turn results in cell cycle arrest (refer to Figure 6.4). It is evident that functional p53 is extremely important in the induction of p53-dependent apoptosis as a result of DNA damage. However, in this study the breast cancer MDA-MB-231 cells used throughout express a mutant, non functional p53. Therefore, the results suggest that DNA damage induced following treatment with BNIPDaCHM can affect $p21^{Waf1/Cip1}$ expression and apoptotic cell death through a p53-independent pathway. Thus, the induction of $p21^{Waf1/Cip1}$ could be a possible mode of action through which BNIPDaCHM inhibits MDA-MB-231 cell growth and provokes apoptotic cell death. However, it is difficult to compare this result with other cytotoxic anti cancer agents as their ability to induce $p21^{Waf1/Cip1}$ mRNA levels remains to be extensively investigated.

$P21^{Waf1/Cip1}$ over expression after 4 hours (Figure 6.19) does not correspond with its ability to induce cell cycle arrest since neither BNIPSpd nor BNIPDaCHM were able to induce cell cycle arrest after 24 hours (Section 6.4.4 and Figure 6.16). These preliminary results are inconclusive and it is, therefore, important to carry out further studies in order to determine the mode of action utilised by the BNIPP derivatives. More extensive investigations into the relationship between $p21^{Waf1/Cip1}$ and cell cycle arrest will need to be undertaken especially in relation to time frame and concentration.

6.6. Conclusions

The BNIPP derivatives, BNIPSpd and BNIPDaCHM, were assessed for their effect on the mode of cell death and cell cycle distribution within MDA-MB-231 cells. Results presented suggest that treatment with either BNIPSpd or BNIPDaCHM can significantly induce apoptotic cell death in MDA-MB-231 cells after only 0.5 hours treatment and that plasma membrane integrity was lost in a time-dependent manner (1 – 5 µM; 0.5 – 24 hours). Cell cycle arrest was not evident during any phase of the cell cycle (BNIPSpd or BNIPDaCHM; 5 µM; 24 hours), even though $p21^{Waf1/Cip1}$ mRNA was over expressed after BNIPDaCHM treatment (4 hours). Also the sub-G1 population was significantly increased following treatment with either BNIPP derivative. This result was indicative of an apoptotic cell population, but further investigations into the mode of cell death induced in a p53-independent manner by the BNIPP derivatives will be required.

In conclusion, although the mode of action utilised to inhibit the proliferation of MDA-MB-231 cells is not yet fully understood; the cytotoxic, DNA damaging and suggested apoptotic properties of BNIPSpd and BNIPDaCHM have potential implications on their clinical use as an anti cancer agents. To further elucidate the mode of action of several BNIPP derivatives, histone deacetylase (HDAC) activity were studied (Chapter 7).

Chapter 7

Histone Deacetylase Activity Studies of BNIPP Derivatives

7.1. Histone Deacetylase Activity Studies of BNIPP Derivatives

One of the most recently identified therapeutic targets involves the ability of potential anti cancer agents to inhibit histone deacetylase (HDAC) activity (Ropero and Esteller 2007, Paris *et al.* 2008). Many structurally different natural and synthetic derivatives have been shown to inhibit class I, II, III and IV HDAC activity, such as, trichostatin A (TSA) (Yoshida *et al.* 1990) or splitomicin (Hirao *et al.* 2003) (Figure 7.1). HDAC enzyme inhibitors are continually being discovered and developed, and in 2006 the U.S. Food and Drug Administration (FDA) approved the first HDAC inhibitor suberoyl hydroxamic acid (SAHA; Vorinostat; Figure 7.1), for the treatment of cutaneous T-cell lymphoma (CTCL) (Mann *et al.* 2007, Richon *et al.* 2009). Therefore, it is important to investigate the potential influence of BNIPP derivatives, as a consequence of their ability to induce p21 mRNA expression levels (Section 6.4.5.2) on class I, II and III HDAC inhibition.

The aim of the experimental work reported in this chapter was to study the effect of BNIPP derivatives on class I, II and III HDAC activity.

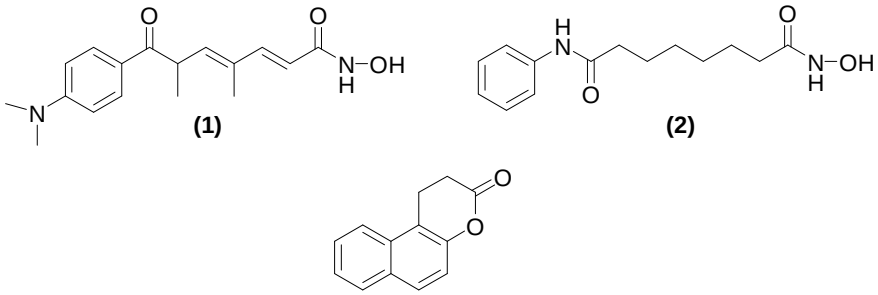

Figure 7.1.: Structures of TSA (**1**), SAHA (**2**) and splitomicin (**3**)

7.1.1. The HDAC Family

The control of gene expression, and thus, DNA repair, cell proliferation and differentiation are highly regulated by the enzymes histone acetyltransferases (HATs) and HDACs (Ropero and Esteller 2007). HATs are responsible for acetylation, whilst HDACs control deacetylation of specific lysine residues (i.e., addition/removal of ε-amino groups, respectively; Figure 7.2) in the *N*-terminal extension of core histones (i.e., H2A, H2B, H3 and H4) (Figure 1.6), and non-histone proteins (e.g., p53, forkhead box O transcription factor (FOXO) or tubulin) (Carey and La Thangue 2006, Schemies *et al.* 2009, Witt *et al.* 2009).

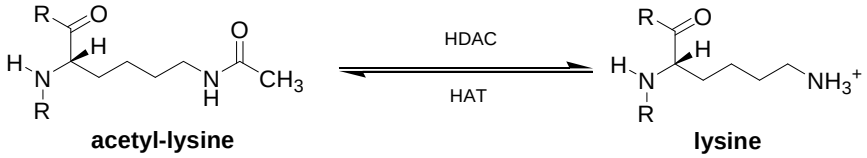

Figure 7.2.: Reversible deacetylation of specific lysine residues

Generally, histone hyperacetylation is associated with an open, unfolded chromatin structure with transcriptional activation, whilst histone hypoacetylation correlates with a closed, folded chromatin structure with transcriptional silencing. HDACs are appealing therapeutic targets for the development of potential anti cancer agents (Stimson and La Thangue 2009), since altered HDAC activity is linked to cancer development, and its inhibition (i.e., histone hyperacetylation) can cause growth arrest, induce cell differentiation, upregulate critical genes (e.g., p53) and induce apoptosis (Glaser 2007, Bieliauskas and Pflum 2008).

HDACs belong to four structurally and functionally distinct classes (i.e., class I – IV), which are subdivided according to their homology with yeast HDAC proteins, and cellular location (Ropero and Esteller 2007). Class I (i.e., HDAC-1, -2, -3, and -8) are homologous to the transcriptional regulatory protein Rpd3 in yeast and are located in the nucleus; class II (i.e., class IIA; HDAC-4, -5, -7 and -9 with a single active site, or class IIB; HDAC-6 and -10 with two active sites) are homologous to histone deacetylase Hda1 in yeast and are located in both the nucleus and cytoplasm; and class IV consists of only one member (i.e., HDAC-11), which is homologous to the class I and II HDACs, and is also found in the nucleus (Ropero and Esteller 2007). Very little information can be found for the expression and function of HDAC-11; therefore it will not be discussed further in this chapter. Class III HDAC enzymes, or sirtuins (i.e., SIRT1 – 7) are homologous to the yeast Silent information regulator 2 (Sir2) protein family and can be found in various cellular locations (e.g., SIRT1, SIRT2 and SIRT3 are present in the nucleus, cytoplasm and mitochondria, respectively) (Paris *et al.* 2008).

Class I and II HDACs are named “classical” HDACs and are zinc (Zn^{2+})-dependent proteases that are grouped together because of their sequence similarities (Paris *et al.* 2008), and sensitivity to TSA (**1**). In contrast, sirtuins are insensitive to TSA (**1**) and are dependent on nicotinamide adenine dinucleotide (NAD^{+}) (Ropero and Esteller 2007).

7.1.2. Classical HDACs

The classical HDACs consist of 10 Zn^{2+}-dependent proteases, each with various cellular functions. In summary, class I HDACs, HDAC-1, -2, -3 and -8, are responsible for cell proliferation and gene regulation, including apoptosis, mitosis (Li *et al.* 2006), contractile capacity (Waltregny *et al.* 2005, Paris *et al.* 2008) and cardiac morphogenesis (Montgomery *et al.* 2007). Class II HDACs, HDAC-4, -5, -6, -7, -9 and -10, are

responsible for hypoxia-inducible factor 1 (HIF-1) stability (Qian *et al.* 2006), cardiac development (Chang *et al.* 2004), deacetylation of tubulin and microtubules (Zhang *et al.* 2003), and can also regulate apoptosis, while very little is known about the function of HDAC-10 (Paris *et al.* 2008). Additionally, HDACs were found to be overexpressed in several cancer cell types, for example, Jin *et al* (2008) found that HDAC-1, -2 and -3 were overexpressed in 18 ovarian cancer tissues (i.e., serous, mucinous or endometrioid ovarian cancer tissues), Saji *et al.* (2005) found that HDAC-6 was overexpressed in breast cancer MCF-7 cells, and Ouaissi *et al.* (2008) found HDAC-7 to be increased in pancreatic adenocarcinomas. For that reason HDACs appear to play a significant role in carcinogenesis, and have a potential therapeutic role in cancer treatment.

Besides the treatment of cancer, HDAC inhibitors may also have a potential role in the treatment of asthma or allergic diseases (e.g., by suppression of tumor necrosis factor alpha (TNFα) and interleukin-1 (IL-1) (Glaser 2007, Bhavsar *et al.* 2008), or in the treatment of neurodegenerative disorders (e.g., Huntington's, Parkinson's or Alzheimer's disease) (Chuang *et al.* 2009).

7.1.2.1. Classical HDAC Inhibitors

HDAC inhibitors fall into four structural distinct groups. These include (i) hydroxamic acids such as, TSA (**1**) and SAHA (**2**) (Figure 7.1), PXD101 (belinostat; **4**) and scriptaid (**5**; has structural features similar to the BNIPP derivatives), (ii) cyclic tetrapeptides such as, depsipeptide (FK - 228; **6**), (iii) benzamides such as, pyridylmethyl-N-{4-[2-aminophenyl)-carbamoyl]-benzyl}-carbamate (MS-275; **7**) and MGCD-0103 (**8**) and (iv) short chain fatty acids such as, valproic acid (**9**) (Figure 7.3).

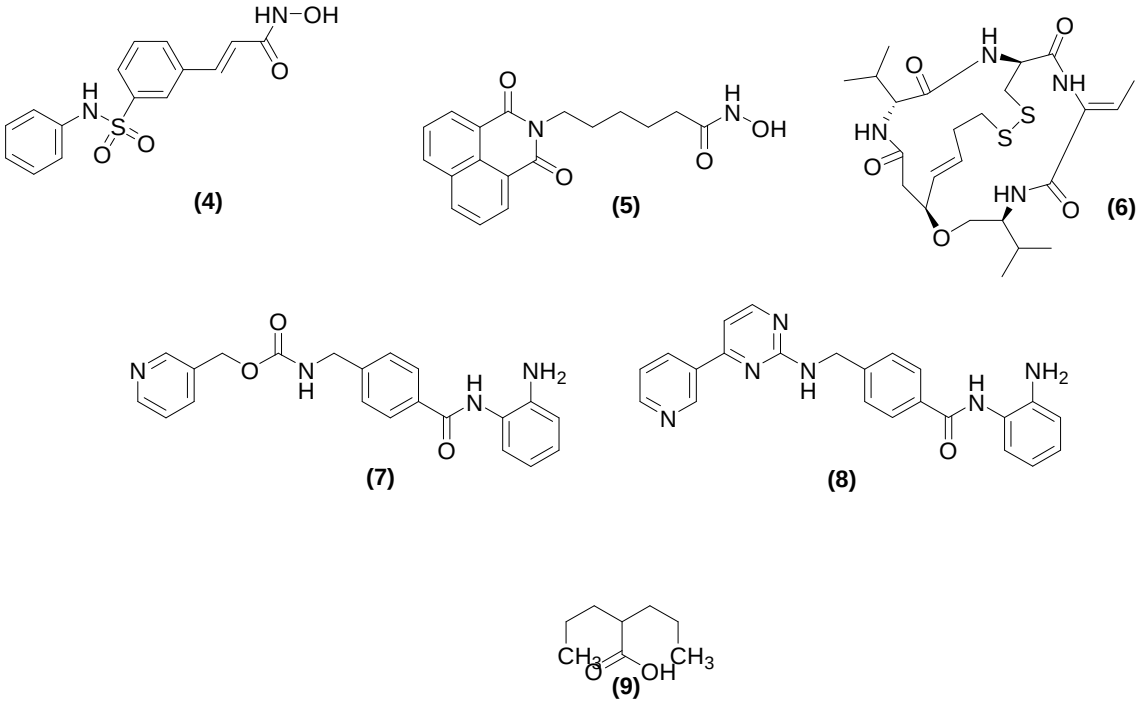

Figure 7.3.: Structures of PXD101 (**4**), scriptaid (**5**), depsipeptide (**6**), MS-275 (**7**), MGCD-0103 (**8**) and valproic acid (**9**).

The most extensively studied HDAC inhibitors are hydroxamic acid based derivatives, which are highly potent (i.e., inhibition achieved at nM concentrations) with a well-defined mechanism of action (Stimson and La Thangue 2009).

Classical HDAC inhibitors have a standard modular structure consisting of a surface recognition cap, a linker chain and a zinc-binding group (Figure 7.4). This structure allows extensive inhibitor recognition through several means. These include (i) the surface recognition cap interacting with residues on the entrance of the active site, (ii) the zinc-binding group interacting with the catalytic metal atom within the active site and (iii) the linker chain which is generally hydrophobic allowing the cap and zinc-binding group to position and thus interact effectively with the active site (Vannini *et al.* 2004, Bieliauskas and Pflum 2009).

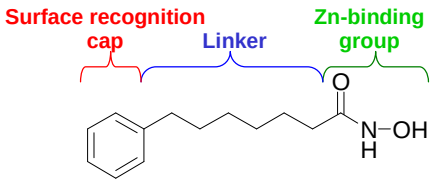

Figure 7.4.: General structure of class I and II HDAC inhibitors

Several HDAC inhibitors within clinical development were found to be generally non selective towards individual HDACs, and were found to either inhibit all or several HDAC enzymes simultaneously (Cang *et al.* 2009, Witt *et al.* 2009). Nevertheless, as an example, hydroxamic acid based derivatives such as, TSA (**1**) or SAHA (**2**) are highly potent non selective HDAC inhibitors (i.e., inhibition achieved at nM concentrations), and the non-hydroxamic acid based derivatives such as, depsipeptide (**6**) or MS-275 (**7**) are selective class I HDAC inhibitors. Details of HDAC inhibitor selectivity and clinical development has been summarised in Table 7.1.

Table 7.1.: Summary of classical HDAC inhibitor classification and specificity [adapted from Stimson and La Thangue (2009) and Witt *et al.* 2009]

Inhibitor	***Inhibition***	***Potency***	***Clinical Status***	***Reference***
TSA (**1**)	Unselective	nM	nd	Yoshida *et al.* 1990
SAHA (**2**)	Unselective	nM	Approved, Phase I, II and III	Mann *et al.* 2007
PXD101 (**4**)	Unselective	nM	Phase I and II	Steele *et al.* 2008, Ramalingham *et al.* 2009
Scriptaid (**5**)	Unselective	µM	nd	Su *et al.* 2000, Tong *et al.* 2006
Depsipeptide (**6**)	Class I	nM	Phase I and II	Schrump *et al.* 2008
MS-275 (**7**)	Class I	µM	Phase II	Hauschild *et al.* 2008
MGCD-0103 (**8**)	Class I	µM	Phase II	Blum *et al.* 2009
Valproic acid (**9**)	Class II	mM	Phase I and II	Rocca *et al.* 2009

Abbreviations: nd, no data

Although not included in Table 7.1, several selective class II HDAC inhibitors exist. These include tubacin (**10**) and mercaptoacetamide (**11**) (Figure 7.5) which exhibit selective inhibition of HDAC-6 and thus a decrease in α-tubulin acetylation (Haggarty *et al.* 2003, Kozikowski *et al.* 2007, Schemies *et al.* 2009).

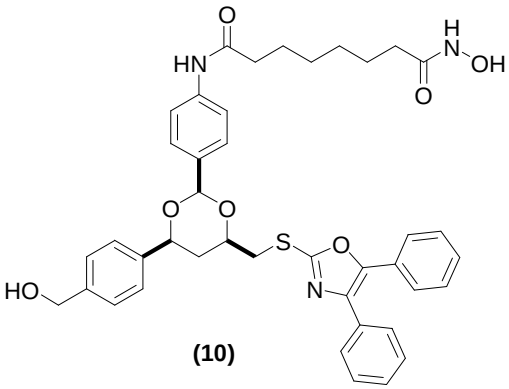

(10)

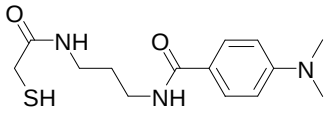

(11)

Figure 7.5.: Structures of tubacin (**10**) and mercaptoacetamide (**11**)

Extensive modifications have been made to each region of the standard modular structure of HDAC inhibitors (Figure 7.4). These involve the addition of cyclic peptide moieties at the cap region (e.g., depsipeptide; **6**) which produced class I selectivity; removal of the hydroxamic acid group for benzamide groups (e.g., MS-275; **7**) displayed HDAC-1 and -3 selectivity compared to HDAC-6 and -8; or the introduction of an amide bond in the linker, in contrast to TSA (**1**), resulted in class I selectivity (Bieliauskas and Pflum 2009).

The synthesis of more selective HDAC inhibitors could provide a better understanding of the different functions of each HDAC enzyme, and may also generate HDAC inhibitors with greater efficacy and lower toxicities (Carew *et al.* 2008).

7.1.3. Class III HDACs

Class III HDACs, or sirtuins are not classified as Zn^{2+}-dependent, but rather, NAD^{+}-dependent that produce nicotinamide and the unique by-product *O*-acetyl adenosine diphosphate (ADP) ribose (Tanner *et al.* 2000, Jiang 2008). Sirtuins consist of seven protein deacetylase members and they either catalyse NAD^{+}-dependent acetylation (i.e., SIRT-1 – 3, and -5) or mediate mono-ADP-ribose-ribosyltransferase (SIRT-4 and -6) activity (Zhang *et al.* 2009). SIRT1 has been the most extensively investigated sirtuin, but interest is gathering for the other sirtuin proteins. Each sirtuin has various cellular functions which are summarised in Table 7.2.

Table 7.2.: Summary of the biological functions of sirtuins

Sirtuin	***Cellular Location***	***Biological Function***	***Reference***
SIRT1	nucleus	target p53, FOXO, Ku70, NF-κB, p300 by deacetylation target p53-dependent apoptosis	Vaziri *et al.* 2001, Cheng *et al.* 2003, Alcaín and Villalba 2009a
SIRT2	cytoplasm	target α tubulin and deacetylate histone H4	North *et al.* 2003
SIRT3	mitochondria	deacetylate acetyl co-A synthase 2	Schlicker *et al.* 2008
SIRT4	mitochondria	ADP-ribosylation of glutamate dehydrogenase	Haigis *et al.* 2006
SIRT5	mitochondria	deacetylate cytochrome c	Schlicker *et al.* 2008
SIRT6	nucleus	deacetylate histone H3 lysine 9 (H3K9), regulate chromatin	Michishita *et al.* 2008
SIRT7	nucleolus	nd	-

Abbreviations: nd, no data

The biological function of SIRT7 is currently unknown and remains to be elucidated, but Ashraf *et al.* (2006) observed that levels of SIRT7 expression were significantly increased in breast cancer MCF-7 cells (Alcaín and Villalba 2009a). This observation has shown that sirtuins appear to play a significant role in carcinogenesis and have, thus, the potential to aid cancer diagnosis and treatment (Ashraf *et al.* 2006).

Beyond cancer treatment, sirtuins have also been suggested through calorie restriction (CR) studies, to have a role in the treatment of diseases of ageing such as, neurodegenerative diseases (e.g., Parkinson's or Alzheimer's disease), type 2 diabetes and cardiovascular diseases (Milne *et al.* 2007, Westphal *et al.* 2007, Milne and Denu 2008).

7.1.3.1. Class III Inhibitors

Inhibitors of Class III HDACs tend to inhibit SIRT1 and SIRT2, and include suramin (**12**), cambinol (**13**), 6-chloro-2, 3, 4, 9-tetrahydro-1H-carbazole-1-carboxamide (EX-527; **14**), splitomicin (**15**), sirtinol (**16**), salermide (**17**) and nicotinamide (**18**) (Figure 7.6).

In summary, **12** and **14** have been found to be highly potent (nM) non selective and selective (i.e., SIRT1 enzyme) inhibitors, respectively (Solomon *et al.* 2006, Schuetz *et al.* 2007). **13**, **16**, **17** and **18** are potent SIRT1 and SIRT2 inhibitors at µM concentrations (Schmidt *et al.* 2004, Mai *et al.* 2005, Heltweg *et al.* 2006, Lara *et al.* 2009), and **15** at µM levels was selective for Sir2 (Hirao *et al.* 2003).

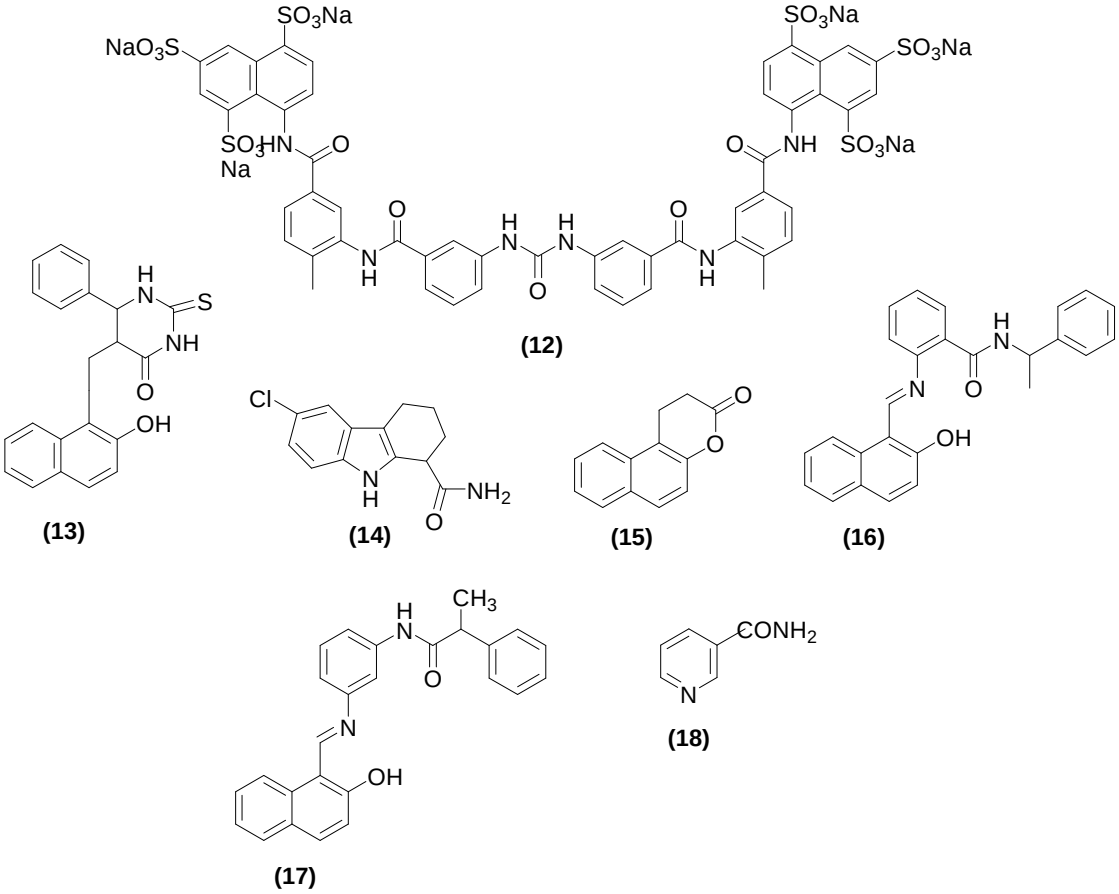

Figure 7.6.: Structures of suramin (**12**), cambinol (**13**), EX-527 (**14**), splitomicin (**15**), sirtinol (**16**), salermide (**17**) and nicotinamide (**18**)

7.1.3.2. Class III Activators

Sirtuin enzymes can be activated by natural and synthetic derivatives such as resveratrol (3,4',5-trihydroxy-*trans*-stilbene, **19**) (Howitz *et al*. 2003), and *N*-[2-[3-(piperazin-1-ylmethyl)imidazo [2,1-b][1,3]thiazol-6-yl]phenyl] quinoxaline-2-carboxamide (SRT1720, **20**) (Milne *et al.* 2007) (Figure 7.7). SIRT activation has predominantly focused on the SIRT1 enzyme and since sirtuins are dependent upon NAD^+; activation could result in the overconsumption or depletion of NAD^+, thus provoking cell death (Alcaín and Villalba 2009b).

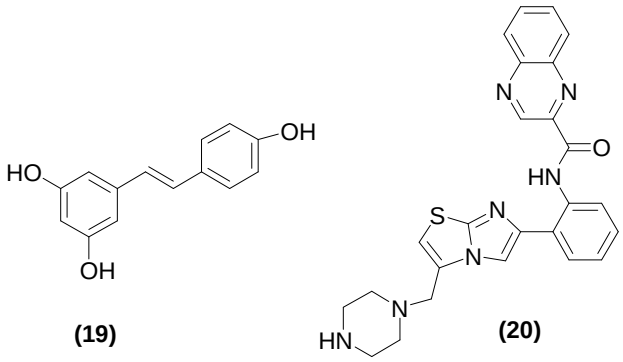

Figure 7.7.: Structures of resveratrol (**19**) and SRT1720 (**20**).

7.1.4. Assessment of HDAC Activity

Several methods have been utilised for the *in vitro* assessment of cellular HDAC activity. Traditional detection methods involved the use of acetate-radiolabelled histones from chicken reticulocytes (Wegener *et al.* 2003) or histone peptide substrates, e.g., [^{3}H] acetyl-histone, [^{3}H] acetyl-histone peptides or oligopeptides (Hoffmann *et al.* 1999, Engleka 2003, Heltweg and Jung 2003, Wegener *et al.* 2003, Heltweg *et al.* 2005). Unfortunately, these labelling methods are rarely used in the detection of HDAC activity because they (i) require radioactivity, thus the use of expensive laboratory equipment and waste management procedures, (ii) are difficult to standardise, (iii) are time consuming, and (iv) are not suitable for high throughput screening (Wegener *et al.* 2003, Heltweg *et al.* 2005). Unlabelled histone peptide substrates have also been used, but detection requires resolution by HPLC and UV detection, and thus the method has a low sample throughput (Heltweg *et al.* 2005). Non isotopic substrates, e.g., fluorescence-labelled histone peptides or acetylated lysine derivatives (e.g., *N*-(4-methyl-7-coumarinyl)-*N*-α-(*tert*-butyloxycarbonyl)-*N*-ε-acetyllysinamide; MAL) can provide a commercially available alternative to the radiolabelled or unlabelled histone peptide substrates (Hoffmann *et al.* 1999, Heltweg *et al.* 2005).

7.1.4.1. HDAC Colourimetric Assay

The easy to use, rapid, homogenous and non-isotope assays provided by BIOMOL International (Plymouth Meeting, USA) can detect HDAC enzyme activity. The BIOMOL International HDAC colourimetric assay can determine the activity of HDAC1 and 2 enzymes. The assay uses the unique *Color de Lys*™ (Colorimetric histone deAcetylase Lysyl) substrate/developer system which works by a two step reaction (Figure 7.8). In the first step, the *Color de Lys*™ substrate which contains an acetylated lysine side chain was added to a sample containing HDAC activity (e.g., HeLa nuclear extract). Deacetylation of the substrate (i.e., removal of an acetyl group from the *N*-acetyl lysine side chain), results in substrate sensitisation, so that, in the second step, addition of the *Color de Lys*™ developer produces a chromophore.

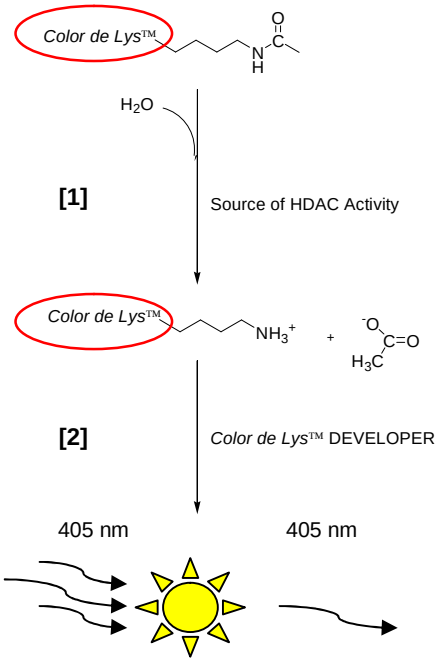

Figure 7.8.: Two step reaction (**[1]** and **[2]**) of the HDAC colorimetric activity assay [adapted from the manufacturer instructions for the HDAC Colorimetric Assay/Drug Discovery Kit – AK-501]

7.1.4.2. HDAC Fluorimetric Assay

In a similar two step reaction method, the BIOMOL International HDAC fluorimetric assay (Figure 7.9) can detect the HDAC activity of class I HDACs (HDAC-1- 3 and HDAC-8) and class II HDACs (HDAC-4 - 7, HDAC- 9 - 10). The assay works by the same principle as the abovementioned assay system but in this case uses a *Fluor de Lys*™ (Fluorogenic histone deAcetylase Lysyl) substrate/developer system as an alternative to the *Color de Lys*™ substrate/developer. The result is the formation of a fluorophore, produced after *Fluor de Lys*™ substrate sensitisation.

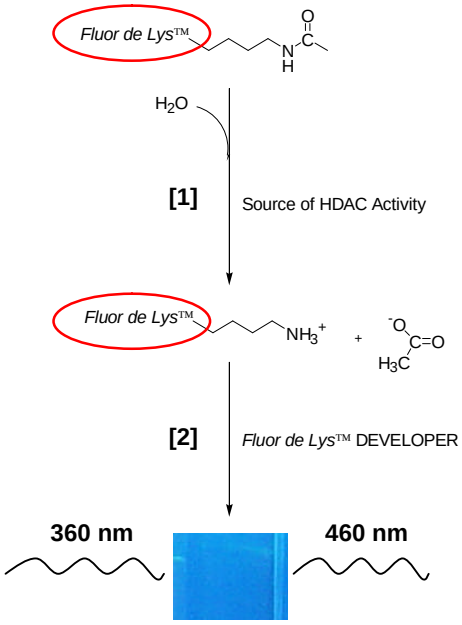

Figure 7.9.: Two step reaction (**[1]** and **[2]**) of the HDAC fluorimetric activity assay [adapted from the manufacturer's instructions for the HDAC Fluorimetric Assay/Drug Discovery Kit – AK-500]

7.1.4.3. SIRT Fluorimetric Assays

In addition, the BIOMOL International SIRT2 and SIRT1 fluorimetric assays (Figure 7.10) can detect SIRT2 and SIRT1 enzyme activity, respectively. These assays work by a similar principle to that of the previous HDAC fluorimetric assay (Figure 7.9), but in this case, the cosubstrate NAD^+ is required. Each assay works by a two step reaction (Figure 7.10), so, for example, in the first step of the SIRT2 fluorimetric assay, the *Fluor de Lys*™-SIRT2 substrate which contains the p53 sequence Gln-Pro-Lys-Lys(ε-acetyl) is incubated with human recombinant SIRT2 ($hSir^{SIRT2}$) and the cosubstrate NAD^+. Deacetylation of the substrate results in substrate sensitisation, so that in the second step, addition of the *Fluor de Lys*™ developer II produces a fluorophore. In the SIRT1 fluorimetric assay, the same two step reaction is followed except the *Fluor de Lys*™-SIRT1 substrate contains the p53 sequence Arg-His-Lys-Lys (ε-acetyl).

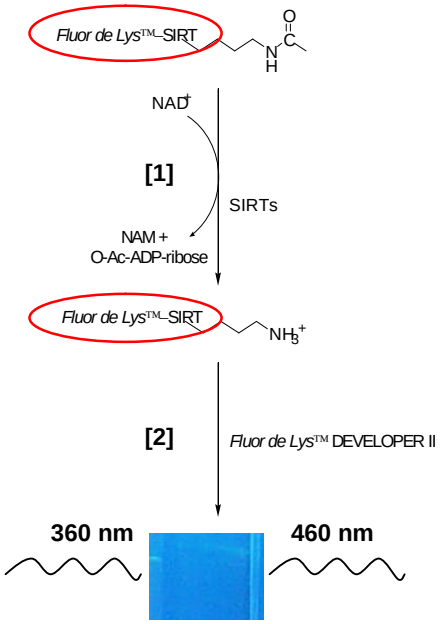

Figure 7.10.: Two step reaction (**[1]** and **[2]**) of the SIRT (SIRT2 and SIRT1) fluorimetric activity assay [adapted from the manufacturer's instructions for the SIRT2 Fluorimetric Drug Discovery Kit (AK-556) and SIRT1 Fluorimetric Drug Discovery Kit (AK-555)]. Nicotinamide Adenine Dinucleotide (NAD^+), a cosubstrate is consumed in the reaction to produce nicotinamide (NAM) and O-acetyl-ADP-ribose (O-ac-ADP-ribose).

7.1.4.4. Molecular Modelling

Besides the commercially available assay kits above, molecular modelling methods were used to characterise the binding potential and inhibitory action of BNIPP derivatives on protein models. Little is currently known about the inhibitory action of sirtuin inhibitors as there is only the crystal structure of SIRT2 available (Finnin *et al.* 2001) (Figure 7.11).

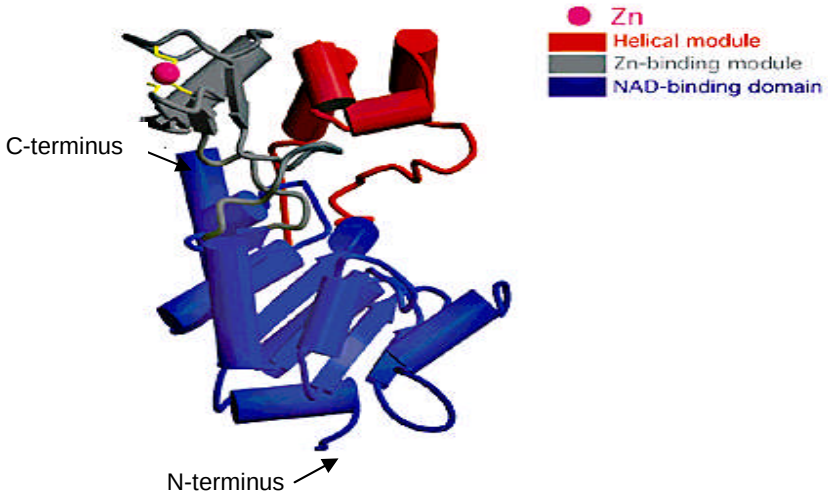

Figure 7.11.: Structure of SIRT2 (adapted from Finnin *et al.* 2001). The structure consists of two binding domains that are connected by four crossovers of the polypeptide chain. The larger (NAD-binding) domain consists of a Rossman fold (in blue), whilst the smaller domain consists of a helical module (in red) and a Zn-binding module (in grey).

SIRT2 has a 304-amino acid catalytic core, which consists of two domains: a larger (NAD-binding) domain and a smaller (helical and zinc (Zn)-binding) domain (Finnin *et al.* 2001). The assessments of BNIPP derivative interactions were undertaken in the NAD^+ binding pocket of the larger domain. Interestingly, the NAD^+ binding pocket is divided into three distinct regions: the A site (i.e., for binding of adenine-ribose, via residues Asn286 and Glu288), the B site (i.e., for binding of nicotinamide-ribose, via His187 and Gln167), and the C site (i.e., completely hidden, deep within the NAD-binding pocket) (Finnin *et al.* 2001, North and Verdin 2004). Finnin *et al.* (2001) found that mutations in His187 and Gln167 resulted in a loss in SIRT2 enzyme activity, thus, strongly suggesting that these residues, in the B site, have a particularly important role in human SIRT2 catalysis (North and Verdin 2004).

7.2. Materials

7.2.1. Materials

All reagents were purchased from Fisher Scientific, UK unless otherwise stated, and were used without purification.

The *Color de Lys*™ colorimetric assay/drug discovery kit (AK-501) and *Fluor de Lys*™ fluorimetric assay/drug discovery kits (AK-500, AK-555 and AK-556) were from BIOMOL International (Plymouth Meeting, USA).

7.2.2 . Instrumentation

Colourimetric readings were obtained using a µQuant MQX200 universal microplate spectrophotometer (Biotek International. Inc, USA), with absorbance measured at 405 nm.

Fluorescence readings were recorded using a LS55 Luminescence spectrophotometer with plate reader (Perkin Elmer, USA) with excitation and emission wavelengths, 360 nm and 460 nm, respectively. Samples were analysed by FLWinLab software operated from a DELL Optiplex GX110 computer.

All modelling and docking simulations were carried out on a Silicon Graphics Fuel workstation with IRIX 6.5 operating system using the comparative protein structure modelling program MODELLER, and Sybyl 6.9 molecular modelling packages (i.e., the Biopolymer, MOLCAD and FlexX modules) (Tripos., USA).

7.3. Methods

7.3.1. Preparation of BNIPP Derivatives

The BNIPP derivatives: BNIPSpd, BNIPDaoct, BNIPDaoxoct and BNIPDaCHM were synthesised as previously described in Section 2.3. The BNIPP derivatives were diluted from stock solutions (10 mM) to the desired concentration of 10 µM in assay buffer, either KI-143 (HDAC assay buffer) or KI-286 (Sirtuin assay buffer), prior to use.

7.3.2. In Vitro Colourimetric Assay for Class I HDAC Activity

The assay of HDAC1 and HDAC2-inhibitory activity was performed using the *Color de Lys*™ colourimetric assay/drug discovery kit (AK-501) according to manufacturer's instructions. Briefly, the assay was carried out in a ½ volume clear microplate (KI-101) using 0.2 mM *Color de Lys*™ substrate (KI-138), nuclear extract from HeLa cells (KI-137) and HDAC assay buffer (KI-143; 25 mM Tris/Cl, pH 8.0, 137 mM NaCl, 2.7 mM KCl and 1 mM $MgCl_2$). The buffer, TSA (0.05 µM from BIOMOL International, GR309-9090) or BNIPP derivative (10 µM) in assay buffer (10 µL in 50 µL total volume of reaction mixture) and HeLa extract were equilibrated for 5 minutes, at 37 °C. The reaction was started by addition of the *Color de Lys*™-substrate (25 µL). Solutions were mixed thoroughly, and incubated for 30 minutes, at 37 °C. Subsequently, the reaction was stopped by the addition of 50 µL of the *Color de Lys*™-developer (KI-139; 1x) plus 1 µM TSA, and left for an additional 30 minutes, at 37 °C. Results were then obtained by measuring the absorbance at 405 nm, as described in Section 7.2.2. The mean absorbance value for HeLa extract treated with different BNIPP derivatives was expressed as a % of untreated HeLa extract (control). The mean absorbance value for the control was equal to 100% as no HDAC inhibition was present. The results are shown as % activity of the control versus each BNIPP derivative (BNIPSpd, BNIPDaoct, BNIPDaoxoct or BNIPDaCHM, at 10 µM).

7.3.3. In Vitro Fluorimetric Assay for Class I and II HDAC Activity

The assay for the inhibitory activity of the class I HDACs (HDAC1-3 and HDAC8) and class II HDACs (HDAC4-7, HDAC9-10) was performed using the *Fluor de Lys*™ fluorimetric assay/drug discovery kit (AK-500) according to manufacturer's instructions. Briefly, the assay was carried out in a ½ volume white microplate (KI-110) using 116 µM *Fluor de Lys*™ substrate (KI-104), nuclear extract from HeLa cells (KI-140) and HDAC assay buffer (KI-143; see section 7.3.1 for buffer contents). The buffer, TSA (0.05 µM) or BNIPP derivative (10 µM) in buffer (10 µL in 50 µL total volume of reaction mixture) and HeLa extract were equilibrated for 5 minutes, at room temperature. The reaction was

started by the addition of the *Fluor de Lys*™-substrate (25 µL). Solutions were mixed thoroughly, and incubated for 10 minutes, at room temperature. Subsequently, the reaction was stopped by the addition of 50 µL of the *Fluor de Lys*™-developer (KI-105; 1x) plus 1 µM TSA, and left for an additional 10 minutes, at room temperature. Results were then obtained by fluorescence emission and reading the samples in a luminescence spectrophotometer, as described in Section 7.2.2. The results were expressed as % activity of the control versus each concentration of BNIPP derivative (BNIPSpd, BNIPDaoct, BNIPDaoxoct and BNIPDaCHM, at 10 and 50 µM), as described in Section 7.3.2.

7.3.4. In Vitro Assay for SIRT2 Enzyme Activity

The assay of SIRT2-inhibitory activity was performed using the *Fluor de Lys*™ fluorimetric drug discovery kit (AK-556) according to manufacturer's instructions. Briefly, the assay was carried out in a ½ volume white microplate (KI-110) using 186 µM *Fluor de Lys*™-SIRT2 deacetylase peptide substrate (KI- 179), 547 µM NAD^+ (KI-282), recombinant $hSir2^{SIRT2}$ enzyme (SIRT2; SE-251; 0.2U/µL) and sirtuin-assay buffer (KI-286; HDAC assay buffer, KI-143, supplemented with 1 mg/mL BSA). The buffer, SIRT2-enzyme, and suramin or BNIPP derivative in buffer (10 µM; 10 µL in 50 µL total volume of reaction mixture) were equilibrated for 5 minutes, at 37 °C. The reaction was started by the addition of the *Fluor de Lys*™-substrate with NAD^+ (25 µL). Solutions were mixed thoroughly, and incubated for 30 minutes, at 37 °C. Subsequently, the reaction was stopped by the addition of 50 µL of the *Fluor de Lys*™-developer II (KI-176; 1x) plus 2 mM Nicotinamide (KI-283), and left for an additional 45 minutes, at room temperature. After a further 10 minutes, the results were obtained by reading the samples in a luminescence spectrophotometer, as described in Section 7.2.2. The mean absorbance value for SIRT2 enzyme treated with different BNIPP derivatives were expressed as a % of untreated SIRT2 enzyme (control). The mean absorbance value for the control was equal to 100% as no SIRT2 enzyme inhibition was present. The results are shown as % activity of the control versus each BNIPP derivative (BNIPSpd, BNIPDaoct, BNIPDanon, BNIPDaoxoct and BNIPDaCHM, at 10 µM).

The SIRT2 enzyme (SE-251) is a 389 amino acid protein with a molecular weight of 43 kDa; produced from human cDNA (Genbank accession no: #NM_012237) expressed in *Escherichia coli* (*E.coli*). The SIRT2 enzyme is stored in 25 mM Tris, pH 7.5, 100 mM NaCl, 5mM dithiothreitol (DTT), and 10% glycerol, at -70 °C.

7.3.5. *In Vitro Assay for SIRT1 Enzyme Activity*

The assay of SIRT1-inhibitory activity was performed using the *Fluor de Lys*™ fluorimetric drug discovery kit (AK-555) according to manufacturer's instructions. Briefly, the assay was carried out in a ½ volume white microplate (KI-110) using 64 µM *Fluor de Lys*™-SIRT1 deacetylase peptide substrate (KI- 177), 558 µM NAD^+ (KI-282), recombinant $hSir2^{SIRT1}$ enzyme (SE-239) and sirtuin-assay buffer (KI-286; HDAC assay buffer, KI-143, see Section 7.3.4). The buffer, SIRT1-enzyme, and suramin, resveratrol or BNIPP derivative in buffer (10 µM; 10 µL in 50 µL total volume of reaction mixture) were equilibrated for 5 minutes, at 37 °C. The reaction was started by the addition of the *Fluor de Lys*™-substrate with NAD^+ (25 µL). Solutions were mixed thoroughly, and incubated for 30 minutes, at 37 °C. Subsequently, the reaction was stopped by addition of 50 µL of the *Fluor de Lys*™-developer II (KI-176; 1x) followed by 2 mM Nicotinamide (KI-283), and left for an additional 45 minutes, at room temperature. After a further 10 minutes, the results were obtained by reading the samples in a luminescence spectrophotometer as described in Section 7.2.2. SIRT1 enzyme activity was expressed as % activity of the control (untreated $hSir^{SIRT1}$) versus each BNIPP derivative (BNIPSpd, BNIPDaoct, BNIPDanon, BNIPDadec, BNIPDaoxaoct or BNIPDaCHM, at 10 µM), as described in Section 7.3.4.

The SIRT1 enzyme (SE-239) is a 747 amino acid protein with a molecular weight of 82 kDa; produced from human cDNA (Genbank accession no: #NM012238) expressed in *E.coli*. The SIRT1 enzyme is stored in 25 mM Tris, pH 7.5, 100 mM NaCl, 5mM DTT, and 10% glycerol, at -70 °C.

7.3.6. *Molecular Modelling and Docking of BNIPP Derivatives*

The molecular modelling and docking experiments of BNIPDanon, BNIPDaCHM, BNIP(4,4)Dapm and BNIP(3,4)Dapm in hSIRT2 and hSIRT1 were conducted by Mr Simranjeet Kaur and Dr. Nilanjan Roy (National Institute of Pharmaceutical Education and Research, India) according to the method of Kadam *et al.* (2006) and Tavares *et al.* (2010).

All molecular structures were generated and energy minimised with the MODELLER and Sybyl molecular modelling systems (Section 7.2.2). The structure of human SIRT2 (PDB ID 1J8F) was used as a template for both hSIRT2 and hSIRT1, and was obtained from the Protein Data Bank, formerly the Brookhaven Protein Database (available from www.pdb.org).

7.3.7. *Data Analysis*

Unless otherwise stated, each data set contained a minimum of three independent experiments, in which each experiment was comprised of at least two internal replicates,

expressed as mean ± Standard Error of the Mean (SEM). Statistical analysis was conducted using a Student's *t*-test. Data were considered significantly different when *P*-value < 0.05.

7.4. Results

The experimental work presented in this chapter is the first quantitative study of HDAC activity to be undertaken with the bisnaphthalimidopropyl derivatives BNIPDaoxoct and BNIPDaCHM.

7.4.1. Effect of BNIPP Derivatives on Class I HDAC Activity

The effect of BNIPSpd, BNIPDaoct, BNIPDaoxoct and BNIPDaCHM (10 µM) on Class I HDAC activity (HDAC1 and HDAC2) was determined by the *Color de Lys*™ assay system. HeLa nuclear extract, rich in HDAC activity was tested as the control, whilst TSA (0.05 µM) was used as a positive control. The results are shown in Figure 7.12.

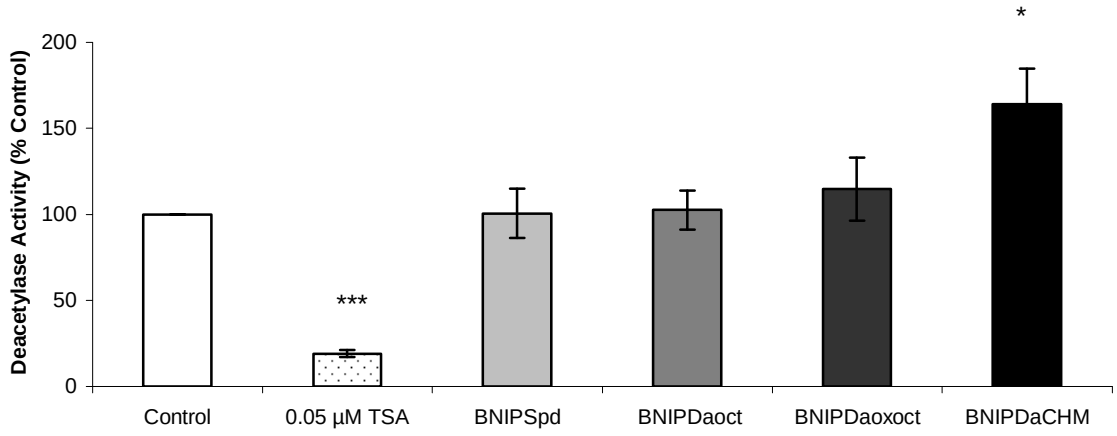

Figure 7.12.: Class I HDAC activity was determined using the HDAC colorimetric assay/drug discovery kit. HeLa nuclear extract was incubated (37 °C) with 0.2 mM *Color de Lys*-substrate and TSA (0.05 µM; positive control) or BNIPSpd, BNIPDaoct, BNIPDaoxoct and BNIPDaCHM (10 µM). Reactions were stopped after 30 minutes with *Color de Lys*-developer, and the absorbance measured at 405 nm. Data are expressed as mean ± SEM of 3 independent experiments (n = 3). **P*<0.05, ****P*<0.001 compared with control values.

TSA (0.05 µM) treatment induced a significant decrease ($P < 0.001$) in HDAC activity (81% decrease) when compared to the control (i.e., untreated HeLa extract) (Figure 7.12). However, no significant differences in HDAC activity were observed with 10 µM BNIPSpd, BNIPDaoct or BNIPDaoxoct when compared to the control (Figure 7.12). Interestingly, BNIPDaCHM (10 µM) did induce a significant increase ($P < 0.05$) in HDAC activity (64% increase) when compared to the control (Figure 7.12).

7.4.2. *Effect of BNIPP Derivatives on Class I and II HDAC Activity*

The effect of BNIPSpd, BNIPDaoct, BNIPDaoxoct and BNIPDaCHM (10 µM) on class I (HDAC1-3 and HDAC8) and class II (HDAC4-7 and HDAC9-10) HDAC activity was determined by the *Fluor de Lys*™ assay system. HeLa nuclear extract was tested as the control, and TSA (0.05 µM) was used as a positive control. The results are shown in Figure 7.13.

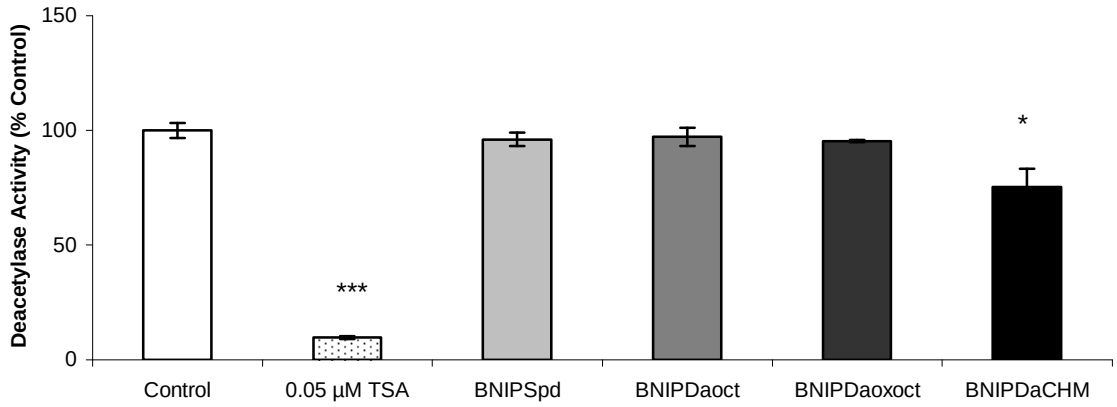

Figure 7.13.: Class I and II HDAC activity was determined using the HDAC fluorimetric assay/drug discovery kit. HeLa nuclear extract was incubated (room temperature) with 116 µM *Fluor de Lys*-substrate and TSA (0.05 µM; positive control) or BNIPSpd, BNIPDaoct, BNIPDaoxoct and BNIPDaCHM (10 µM). Reactions were stopped after 10 minutes with *Fluor de Lys*-developer, and the fluorescence measured (excitation 360 nm, emission 460 nm). Data are expressed as mean ± SEM of 3 independent experiments (n = 3). **P*<0.05, ****P*<0.001 compared with control values.

A significant decrease ($P < 0.001$) in HDAC activity (90% decrease) was induced by 0.05 µM TSA, when compared to the control (i.e., untreated HeLa extract) (Figure 7.13). HDAC activity was not affected with BNIPSpd, BNIPDaoct or BNIPDaoxoct (10 µM) but with BNIPDaCHM (10 µM) a significant decrease ($P < 0.05$) in HDAC activity (25% decrease) was observed, when compared with the control (Figure 7.13).

7.4.3. Effect of BNIPP Derivatives on SIRT2 Enzyme Activity

The ability of BNIPSpd, BNIPDaoct, BNIPDanon, BNIPDadec, BNIPDaoxoct and BNIPDaCHM (10 µM) to influence SIRT2 enzyme activity was determined by the *Fluor de Lys*™-SIRT2 fluorescent assay system. Bisnaphthalimidopropyl diaminononane (BNIPDanon) and Bisnaphthalimidopropyl diaminodecane (BNIPDadec) were also investigated to determine what influence increasing the length of the central alkyl linker chain (i.e., from 8 methylene groups to 9 - 10 methylene groups) would have on SIRT2 enzyme activity. Suramin (10 µM) was tested as a positive control. The results are shown in Figure 7.14.

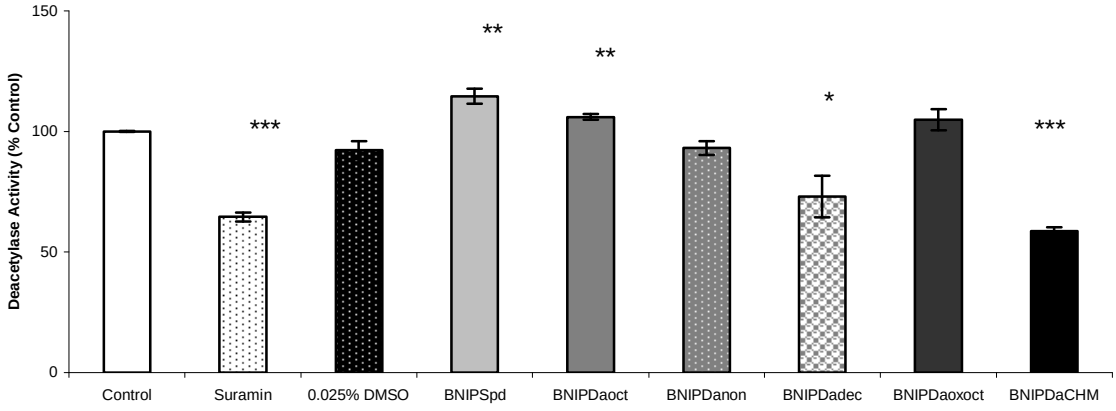

Figure 7.14.: SIRT2 enzyme activity was determined using the SIRT2 fluorimetric drug discovery kit. Recombinant hSir2^{SIRT2} enzyme was incubated (37 °C) with 186 µM *Fluor de Lys*™-SIRT2 substrate with 547 µM NAD^+ and suramin, or BNIPP derivatives (10 µM). Reactions were stopped after 30 minutes with *Fluor de Lys*™ developer II, and the fluorescence measured (excitation 360 nm, emission 460 nm). Data are expressed as mean ± SEM of 3 independent experiments (n = 3). **P*<0.05, ***P*<0.01, ****P*<0.001 compared with control values.

Suramin (10 µM) treatment induced a significant decrease ($P < 0.001$) in SIRT2 enzyme activity (36% decrease) when compared to the control (Figure 7.14). Since high concentrations of DMSO can affect SIRT2 enzyme activity; a 0.025% DMSO control (i.e., solvent control) was analysed, as shown in Figure 7.13. DMSO (0.025%) was found to be a suitable solvent vehicle for the dilution of BNIPP derivatives prior to analysis in this assay, because SIRT2 enzyme activity was not affected when compared to the control.

Two of the 6 BNIPP derivatives tested showed significant SIRT2 enzyme activation ($P < 0.01$), at 10 µM (BNIPSpd, 15% increase, and BNIPDaoct, 6% increase) when compared to the control (Figure 7.14). BNIPDanon and BNIPDaoxoct were considered to be inactive, since SIRT2 enzyme activity was not affected by treatment at 10 µM (Figure 7.14). The remaining BNIPP derivatives, BNIPDadec ($P < 0.05$; 27% decrease) and BNIPDaCHM ($P < 0.001$; a 41% decrease) showed significant SIRT2 enzyme inhibition, at 10 µM (Figure 7.14).

Given that BNIPDaCHM was the most active BNIPP derivative tested at 10 µM (i.e., 41% decrease in SIRT2 enzyme activity compared to a 36% decrease with suramin) (Figure 7.14), further analysis at various concentrations was carried out using the *Fluor de Lys*™-SIRT2 fluorescent assay system. The results obtained are presented in Figure 7.15.

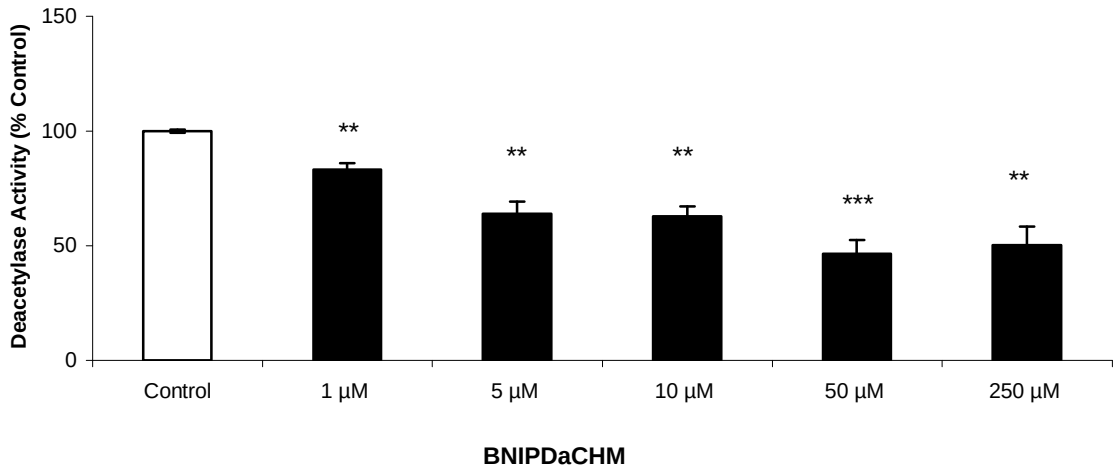

Figure 7.15.: SIRT2 enzyme activity was determined using the SIRT2 fluorimetric drug discovery kit. Recombinant hSir2^{SIRT2} enzyme was incubated (37 °C) with 186 µM *Fluor de Lys*™-SIRT2 substrate with 547 µM NAD^+ and BNIPDaCHM. Reactions were stopped after 30 minutes with *Fluor de Lys*™ developer, and the fluorescence measured (excitation 360 nm, emission 460 nm). Data are expressed as mean ± SEM of 3 independent experiments (n = 3). ***P*<0.01, ****P*<0.001 compared with control values.

From the results presented for BNIPDaCHM (Figure 7.15), all concentrations tested (1 – 250 µM) induced a significant decrease ($P < 0.01$; at 1, 5, 10 and 250 µM; $P < 0.001$; at 50 µM) in SIRT2 enzyme activity, when compared to the control (Figure 7.15). Interestingly, the most significant inhibition ($P < 0.001$) was observed at 50 µM, with a 54% decrease in activity. A saturation point appeared to have been reached at 50 µM, since treatment with 250 µM BNIPDaCHM (50% decrease) was not able to further decrease SIRT2 enzyme activity.

7.4.4. Effect of BNIPP Derivatives on SIRT1 Enzyme Activity

The ability of BNIPSpd, BNIPDaoct, BNIPDanon, BNIPDadec, BNIPDaoxct and BNIPDaCHM (10 µM) to influence SIRT1 enzyme activity was determined by the *Fluor de Lys*™-SIRT1 fluorescent assay system. Suramin (10 µM) and resveratrol (10 µM) were tested as positive controls for SIRT1 enzyme inhibition and activation, respectively. Results are shown in Figure 7.16.

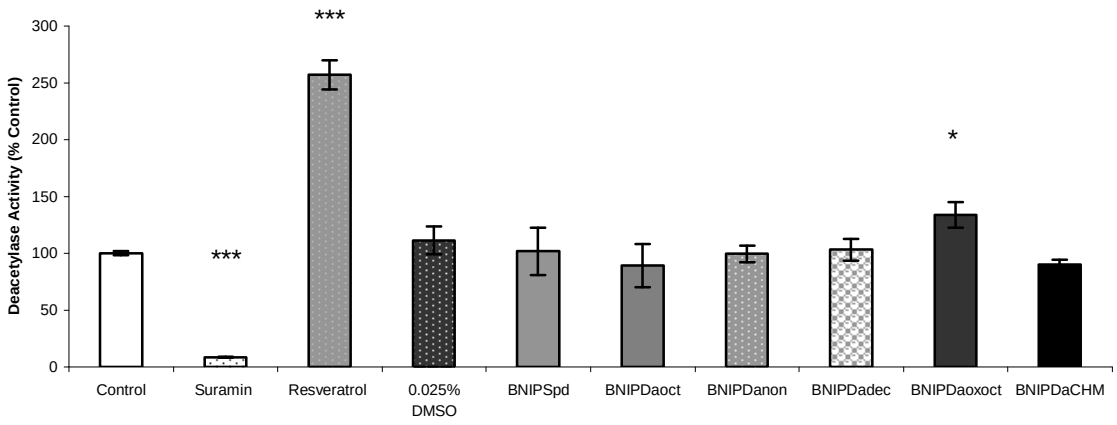

Figure 7.16.: SIRT1 enzyme activity was determined using the SIRT1 fluorimetric drug discovery kit. Recombinant hSir2^{SIRT1} enzyme was incubated (37 °C) with 64 µM *Fluor de Lys*™-SIRT1 substrate with 558 µM NAD^+ and suramin, resveratrol or BNIPP derivatives (10 µM). Reactions were stopped after 30 minutes with *Fluor de Lys*™ developer II, and the fluorescence measured (excitation 360 nm, emission 460 nm). Data are expressed as mean ± SEM of 3 independent experiments (n = 3). **P*<0.05, ****P*<0.001 compared with control values.

Suramin (10 µM) treatment induced a significant decrease ($P < 0.001$) in SIRT1 enzyme activity (91% decrease), whilst resveratrol (10 µM) treatment induced a significant increase ($P < 0.001$) in SIRT1 enzyme activity (157% increase) when each was compared to the control (Figure 7.16). SIRT1 enzyme activity was not affected by the solvent control (i.e., 0.025% DMSO). Thus, DMSO (0.025%) was also a suitable solvent for the dilution of BNIPP derivative in this fluorescent assay (refer to Section 7.4.3).

BNIPSpd, BNIPDaoct, BNIPDanon, BNIPDadec and BNIPDaCHM (10 µM) were considered to be inactive since SIRT1 activity was not affected when compared with the control (Figure 7.16). Therefore, only one among the 6 BNIPP derivatives tested showed a significant effect ($P < 0.01$; 34% increase) on SIRT1 enzyme activity; BNIPDaoxoct (10 µM), when compared to the control (Figure 7.16).

7.4.5. Examination of hSIRT2 and hSIRT1 Inhibitor Binding Sites

BNIPDaCHM, the BNIPP derivative with the greatest observed inhibitory action towards SIRT2 enzyme activity (refer to Section 7.4.3) was selected for docking studies to determine its binding potential and validate its inhibitory action on hSIRT2 and hSIRT1 protein models. The results for BNIPDaCHM binding on hSIRT2 and hSIRT1 can be found in Figures 7.17a and b, and 7.18a and b, respectively.

Figures 7.17a and 7.18a represent the results of docking BNIPDaCHM into the NAD^+ binding pocket (A, B and C pockets) of hSIRT2 or hSIRT1, respectively, with the competitive binding of BNIPDaCHM with NAD^+ on hSIRT2 and hSIRT1, respectively shown in Figures 7.17b and 7.18b. BNIPDaCHM was found to bind within the NAD^+ binding pocket, hence showing competition with NAD^+, as shown in Figures 7.17 - 7.18a and b. The docking scores for BNIPDaCHM binding on hSIRT2 and hSIRT1 were -13.648 and -21.240 kcal/mol^{-1}, respectively (i.e., the more negative the docking score, the stronger the interaction), and the numbers of hydrogen bonds formed were five and four bonds, respectively (Tables 7.3 and 7.4). In hSIRT2, BNIPDaCHM interacts with the residues Ser263 and Thr262 in the A pocket, and with His187 and Gln167 in the B pocket; it is directed away from the C pocket, as shown in Figure 7.17. BNIPDaCHM shows an interaction with the A and C pockets in hSIRT1, but not with the B pocket (Figure 7.17). The residues involved in hydrogen bonding with BNIPDaCHM in hSIRT1 include Ser201 and Asn224 present in the A pocket, with Asn105 and Arg33 in the C pocket. Thus, based on these docking studies, subtle differences in the docking mode of BNIPDaCHM on hSIRT2 and hSIRT1 can be observed.

a

b

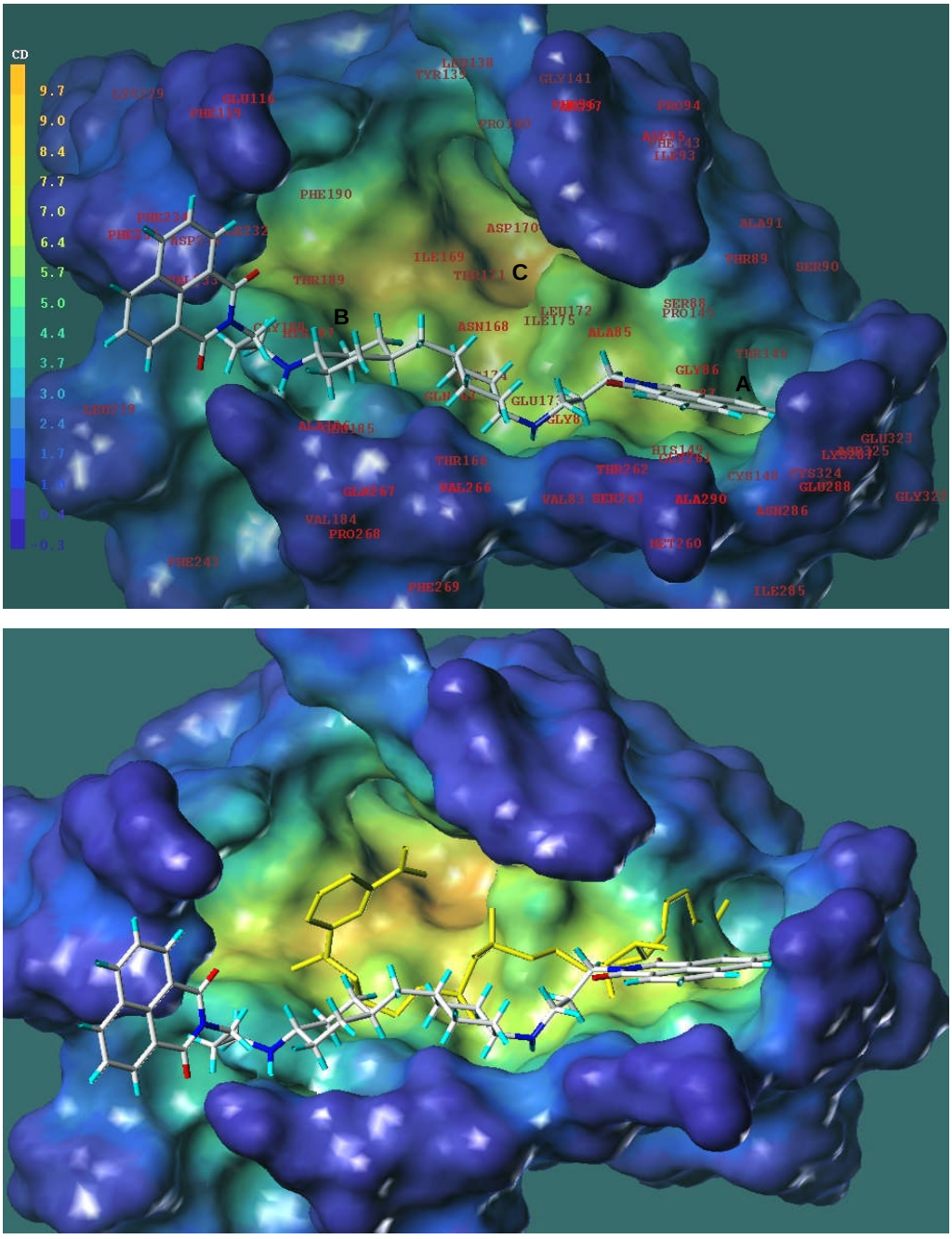

Figure 7.17.: Docking studies of BNIPDaCHM (**a**) and competitive binding of BNIPDaCHM and NAD^+ (**b**) in the NAD^+ binding pocket of hSIRT2. BNIPDaCHM is depicted as a ball and stick model (carbon atoms are coloured white, nitrogen atoms in blue, oxygen atoms in red and hydrogen atoms in turquoise), and the NAD^+ molecule is shown in yellow. The A, B and C pockets of the NAD^+ binding site are indicated (**a**) (black letters).

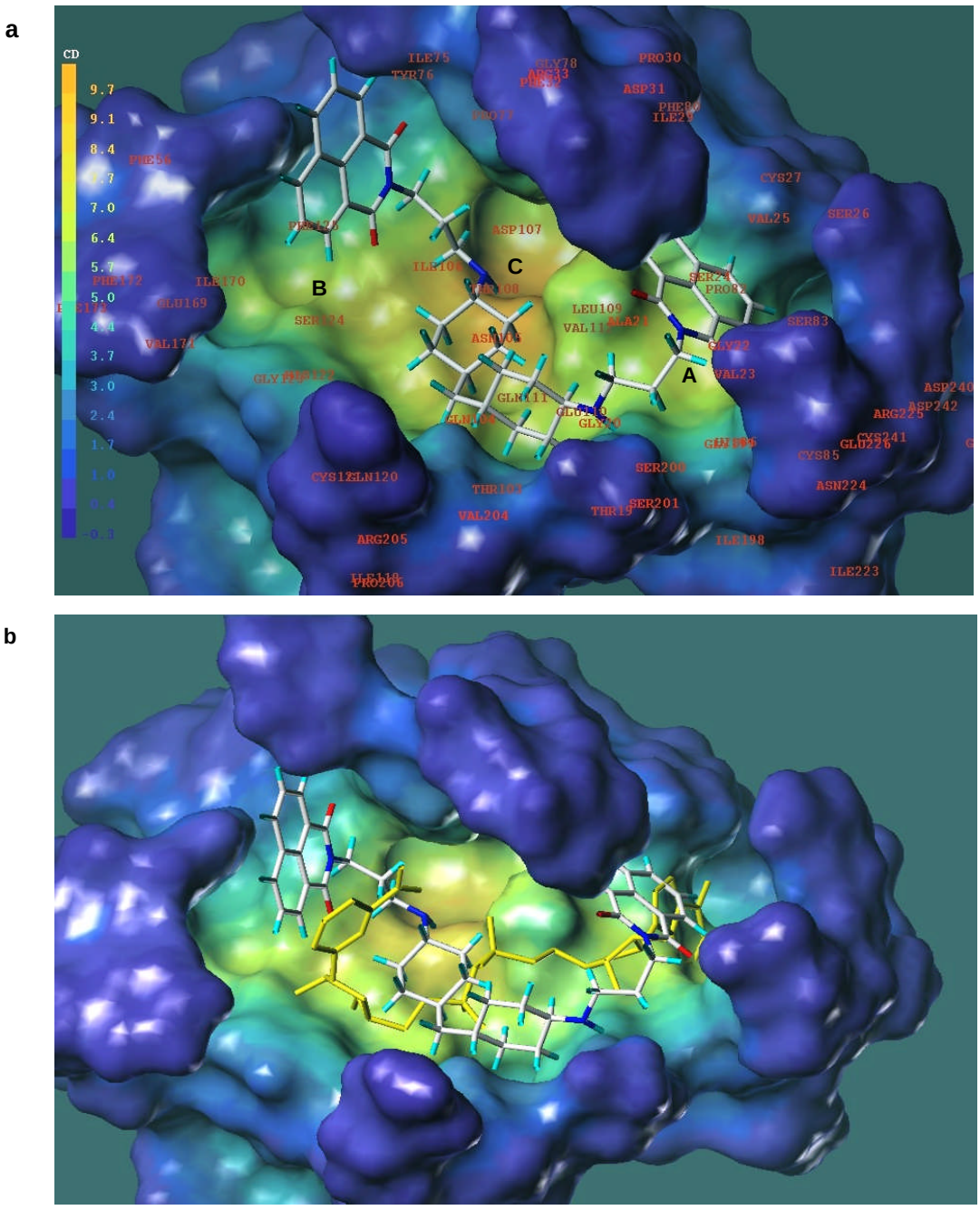

Figure 7.18.: Docking studies of BNIPDaCHM (**a**) and competitive binding of BNIPDaCHM and NAD^+ (**b**) in the NAD^+ binding pocket of hSIRT1. BNIPDaCHM is depicted as a ball and stick model (carbon atoms are coloured white, nitrogen atoms in blue, oxygen atoms in red and hydrogen atoms in turquoise), and the NAD^+ molecule is shown in yellow. The A, B and C pockets of the NAD^+ binding site are indicated (**a**) (black letters).

Based on the results obtained for BNIPDaCHM, additional docking studies on hSIRT2 and hSIRT1 were carried out for the structurally similar BNIPP derivatives BNIPDanon, BNIP(4,4)Dapm and BNIP(3,4)Dapm (Figure 7.19). The results obtained on each protein model are shown in Tables 7.3 and 7.4.

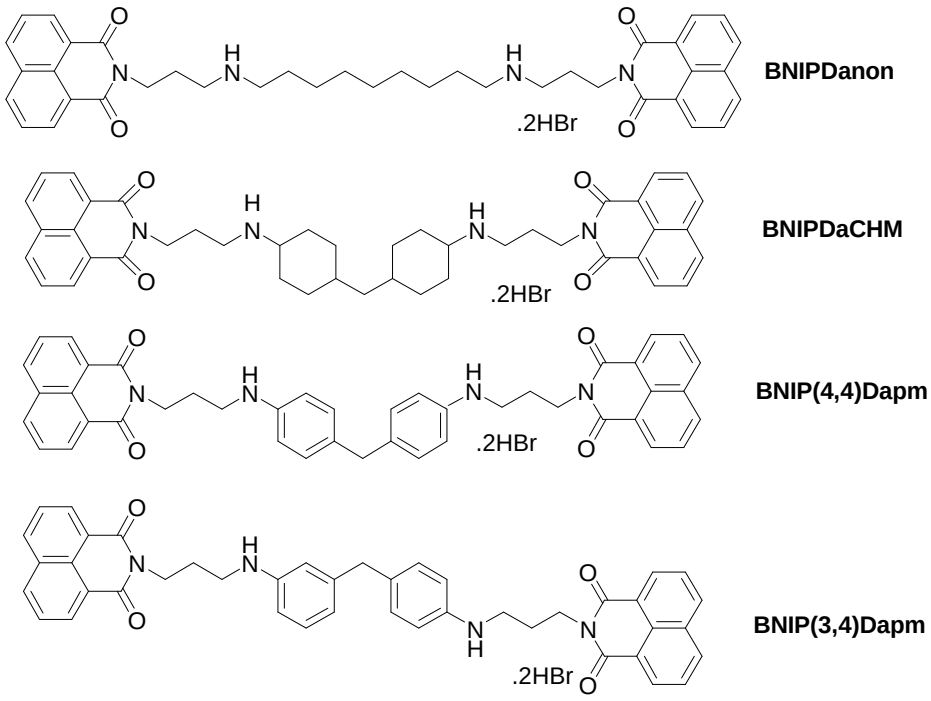

Figure 7.19.: Structures of bisnaphthalimidopropyl diaminononane (BNIPDanon), BNIPDaCHM, bisnaphthalimidopropyl-4,4-diaminophenylmethane (BNIP(4,4)Dapm) and bisnaphthalimidopropyl-3,4-diaminophenylmethane (BNIP(3,4)Dapm)

Table 7.3.: Docking studies for BNIPP derivatives in hSIRT2

BNIPP Derivative	***Docking Score (kcal/mol^{-1})***	***H Bond Residues***	***Total No. of H Bonds***
BNIPDanon	-14.639	**His187**[a], Gln267, Ala85, Gly261, Ser263	6
BNIPDaCHM	-13.648	**His187**[a], **Gln167**[a], Ser263, Thr262	5
BNIP(4,4)Dapm	-21.626	Gln267, **Gln167**[a]	3
BNIP(3,4)Dapm	-21.023	Phe234, **Gln167**[a], Ala85	3

[a] Residues in bold, i.e., **His187** (**His122** in hSIRT1) and **Gln167** (**Gln104** in hSIRT1) are reported to have a role in SIRT2 enzyme catalysis (Finnin *et al.* 2001).

Table 7.4.: Docking studies of BNIPP derivatives in hSIRT1

BNIPP Derivative	***Docking Score (kcal/mol^{-1})***	***H Bond Residues***	***Total No. of H Bonds***
BNIPDanon	-14.770	**Gln104**[a], Ser201, Arg33, Asn224	5
BNIPDaCHM	-21.240	Asn105, Ser01, Arg33, Asn24	4
BNIP(4,4)Dapm	-25.208	Arg33, Asp31, Asn224	5
BNIP(3,4)Dapm	-26.704	**Gln104**[a], **His122**[a], Phe172	3

[a] Refer to footnote of Table 7.1.

The results presented in Tables 7.3 and 7.4 show that alterations to the central alkyl linker chain increased interactions in the NAD^+ binding pocket, since more negative docking scores were observed with BNIP(4,4)Dapm and BNIP(3,4)Dapm, when compared to BNIPDaCHM (Figures 7.17 and 7.18). The order of docking, as represented by docking score (kcal/mol^{-1}) in hSIRT2 was BNIP(4,4)Dapm > BNIP(3,4)Dapm > BNIPDanon > BNIPDaCHM, whilst in hSIRT1, the order was BNIP(3,4)Dapm > BNIP(4,4)Dapm > BNIPDaCHM > BNIPDanon. All BNIPP derivatives were found to bond to hSIRT2 and hSIRT1 with at least one of the essential residues (i.e., His187 and Gln167 in hSIRT2, or His122 and Gln104 in hSIRT1), which are available to make hydrogen bonds. Therefore, BNIP(4,4)Dapm and BNIP(3,4)Dapm could be the most potent SIRT2 and -1 inhibitors of the BNIPP derivative series, respectively.

7.5. Discussion

Previous studies into the BNIPP derivatives has been focused on their effects on (i) cell cytotoxicity, (ii) intracellular polyamine levels, (iii) cellular localisation and DNA damage, (iv) their interaction with DNA, and (v) their mode of cell death (Pavlov *et al*. 2001, Dance *et al.* 2005, Ralton *et al.* 2009). The effect of BNIPP derivatives on the regulation of HDAC activity, had not, thus far, been assessed.

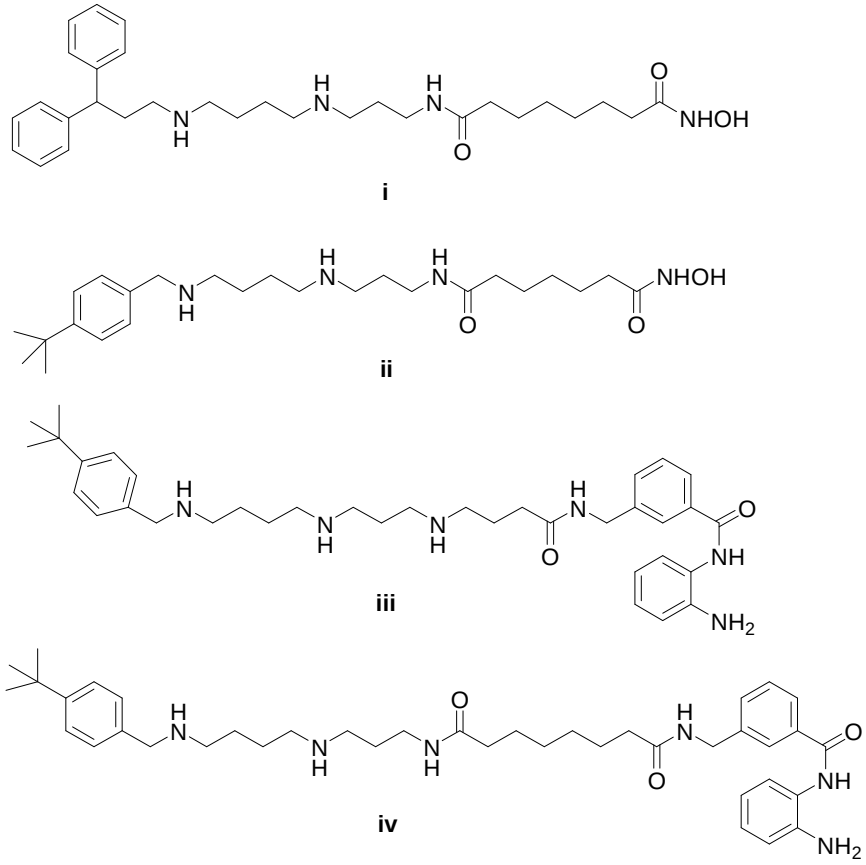

Figure 7.20.: Structures of the polyaminohydroxamic acids SV-63-41 (**i**) and SV-65-38C (**ii**), and polyaminobenzamides SV-65-50C (**iii**) and SV-68-3 (**iv**).

Polyamine-based analogue induced HDAC inhibition has not been widely reported, with research predominantly focused on Class I and II HDAC inhibition. A small number of polyamine-based analogues, for example, polyaminohydroxamic acids (PAHAs; e.g., SV-63-41 and SV-65-38C) and polyaminobenzamides (PABAs; e.g., SV-65-50C and SV-68-3) (Figure 7.20) have been found to inhibit HDAC activity by Boncher *et al.* (2007) and Varghese *et al.* (2008) (Casero and Woster 2009). PAHA's and PABA's inhibition of Class I and II HDACs was detected by the *Fluor de Lys*™ assay system (Boncher *et al.* 2007, Varghese *et al.* 2008). Varghese *et al.* (2008) found that the PAHA analogues SV-63-41 and SV-65-38C produced 46.3 and 51.5 % inhibition of HDAC activity at 1 µM, respectively, whilst the PABA analogues SV-65-50C and SV-68-3 produced 37.4 and 51.2% inhibition of HDAC activity, at 5 µM, respectively. It was also highlighted by

Varghese *et al.* (2008) that HDAC inhibition with PAHAs and PABAs was increased as the length of the linker chain was increased.

7.5.1. Effect of BNIPP Derivatives on Class I Activity

Class I (HDAC1 and -2) activity levels were measured by the *Color de Lys*™ assay system (Huang *et al.* 2002) (Figure 7.8). Data showed that 10 µM of BNIPSpd, BNIPDaoct or BNIPDaoxoct did not affect HDAC1 and -2 activity; however HDAC activity was significantly increased ($P < 0.05$; a 64% increase) when the HeLa nuclear extract was treated with 10 µM BNIPDaCHM (Figure 7.12). These results were similar to the findings of Do *et al.* (2009), who studied HDAC activity in murine S91 and B16 melanoma cells treated with sulforaphane microspheres[2] (Figure 7.21) using the same colorimetric *Color de Lys*™ assay system. HDAC activity was increased when compared to that of the positive control (HeLa nuclear extract), when S91 and B16 cells were treated with 20 and 30 µM sulforaphane microspheres (Do *et al.* 2009). However, a decrease in HDAC activity was observed in S91 and B16 cells treated with 50 µM of sulforaphane microspheres when compared with control (Do *et al.* 2009). These findings may suggest that a higher concentration of each BNIPP derivative (i.e., > 10 µM) may be required to significantly decrease HDAC1 and -2 activities, in particular, decrease HDAC activation observed after treatment with 10 µM of BNIPDaCHM.

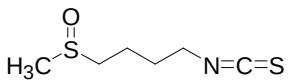

Figure 7.21.: Structure of sulforaphane.

In contrast, Ohtsuki *et al.* (2009), who also studied HDAC activity using the same colorimetric *Color de Lys*™ assay system found that for the first time, the *N*-methylpyrrole (P) and *N*-methyllimidazole (I) polyamide (PI polyamide) SAHA conjugates, **i** and **ii** (Figure 7.22) were able to significantly decrease ($P < 0.05$) HDAC activity at 1 µM.

[2] Sulforaphane is an effective anticancer agent which acts by HDAC inhibition (Clarke *et al.* 2008, Do *et al.* 2009). However, sulforaphane has a short half-life (i.e., < 2 hours) and is very unstable in normal conditions due to its rapid metabolism and excretion. Therefore, to overcome these problems, sulforaphane was encapsulated in albumin microspheres (Do *et al.* 2009).

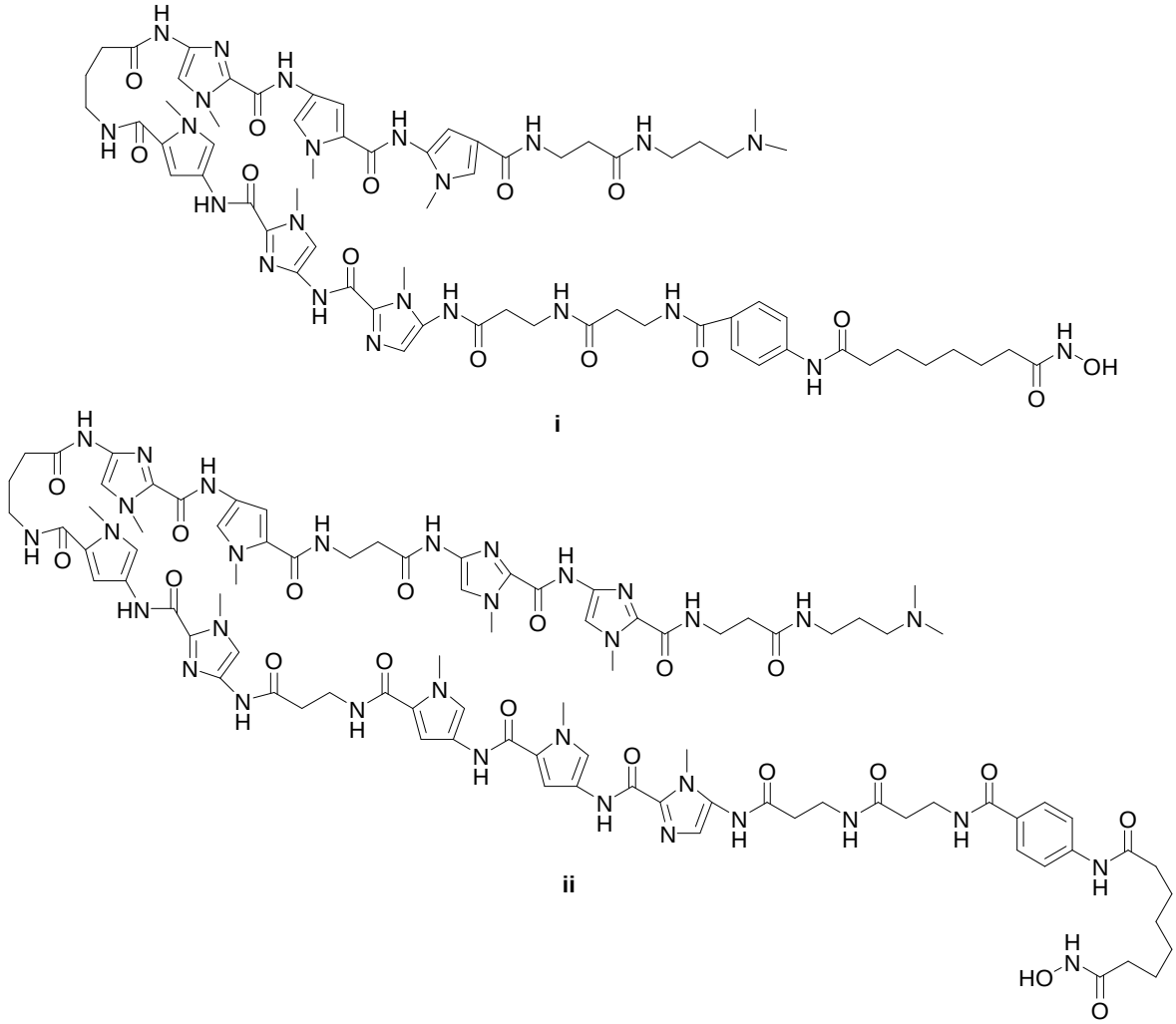

i

ii

Figure 7.22.: Structures of the PI polyamine-SAHA conjugates, **i** and **ii**.

PI polyamide-SAHA conjugates, **i** and **ii** (Figure 7.22) contain, as their names indicate, SAHA: the most potent hydroxamic acid-based inhibitor of class I, II and IV HDACs (Ohtsuki *et al.* 2009, Smith and Workman 2009). The structure of SAHA is very important to its overall HDAC inhibitory activity, in particular, the presence of a hydroxamic acid group (i.e., a zinc binding functional group). The BNIPP derivatives were found to be inactive as class I HDAC inhibitors (Section 7.4.1; Figure 7.12), and this could be due to the absence of a hydroxamic acid group, rather than the naphthalimide groups. Scriptaid (Figure 7.3), a HDAC inhibitor which possesses a naphthalimide group, a five methylene linker chain and a hydroxamic acid group was observed to be an effective HDAC inhibitor (i.e., > 100-fold increase in histone acetylation in cultured human pancreatic carcinoma (PANC-1) cells) with low toxicity as reported by Su *et al.* (2000). Scriptaid does contain a hydroxamic acid group, and therefore, supports the importance of hydroxamic acid-based derivatives as potent (nM) class I HDAC inhibitors (Marks *et al.* 2000, Stimson *et al.* 2009).

7.5.2. Effect of BNIPP Derivatives on Class I and Class II HDAC Activity

A further assessment into the effect of BNIPP derivatives on HDAC activity levels was conducted, where class I and II HDAC activity was measured by the *Fluor de Lys*™ assay system (Figure 7.9). HDAC enzyme activity was not altered by treatment with BNIPSpd, BNIPDaoct or BNIPDaoxoct at 10 µM, but was significantly decreased ($P < 0.05$; a 25% decrease) when HeLa nuclear extract was treated with 10 µM BNIPDaCHM (Figure 7.13). This finding suggests that BNIPDaCHM may inhibit class I and II HDAC enzymes.

Caution should be employed when comparing the % inhibition results of the BNIPP derivatives directly with other potential HDAC inhibitors investigated using the *Fluor de Lys*™ assay system, since other groups, such as Son *et al.* (2007), Oyelere *et al.* (2009) and Patil *et al.* (2010) tend to note HDAC enzyme activity as only an IC_{50} value (i.e., the concentration that inhibits 50% of HDAC activity), which was not determined for the BNIPP derivatives in this study.

Chen *et al.* (2008), who studied HDAC inhibition by a series of SAHA-like hydroxamates incorporating a 1, 2, 3-triazole ring as a surface recognition cap discovered that derivatives with cap groups consisting of naphthalenes and quinolines were potent HDAC inhibitors (IC_{50} values ranged between 1.8 – 15.3 nM for naphthalenes; 2.1 – 151.5 nM for quinolines). However, Andrianov *et al.* (2009) reported that if a derivative consisted of two aromatic groups linked together to form a tricyclic system; HDAC inhibitory activity was lost (IC_{50} value 338 nM). Therefore, the lack of potent class I and II HDAC inhibition observed after treatment with BNIPP derivatives could be due to the lack of a hydroxamic acid group as discussed in Section 7.5.1, together with the presence of two large aromatic caps (i.e., the naphthalimidopropyl groups). However, the replacement of the naphthalimido groups with phthalimido groups could provide a suitable alternative. Remiszewski *et al.* (2002) found two phthalimide derivatives with 5 and 6 carbon linker chains were potent HDAC enzyme inhibitors with IC_{50} values of 0.515 and 0.357 µM, respectively. Furthermore, Shinji *et al.* (2005) found that additional phthalimide-based derivatives (Figure 7.23) could inhibit HDAC enzyme activity at nM levels (i.e., IC_{50} values of 572, 358 and 709 nM on HDAC1, -4 and -6, respectively). Thus, the bisphthalimidopropyl derivative BPHPDadec should be investigated to determine its potential effects on class I and II HDAC inhibition.

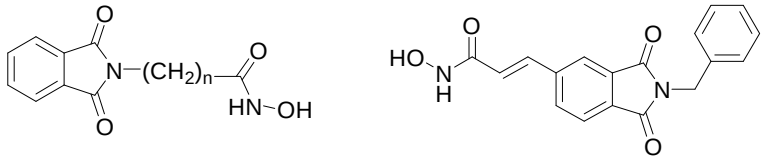

i ii

Figure 7.23.: Structures of **(i)** the phthalimido-based derivatives from Remiszewski *et al.* (2002), and **(ii)** the most potent phthalimido-based derivative from Shinji *et al.* (2005).

In addition to the importance of cap size, it is also important to consider the length of the linker chain. Chen *et al.* (2008) found that an increase in HDAC inhibition was related to the presence of more methylene groups in the linker chain[3]. The observation that linker chain length was an important structural feature required in achieving optimum HDAC inhibition was also highlighted by Varghese *et al.* (2008) and Andrianov *et al.* (2009). For that reason, the activity of SIRT1 and SIRT2 enzymes were monitored with the inclusion of BNIPDanon and BNIPDadec to give an indication as to whether increasing the length of the linker chain in BNIPP derivatives could increase their potential to inhibit HDAC enzymes.

To date, no other symmetrical derivatives have been found to inhibit Class I and II HDAC enzyme activity. Therefore, the BNIPP derivatives may provide a novel structural backbone, unlike SAHA-based derivatives for potential Class I and II HDAC inhibition.

7.5.3. Effect of BNIPP Derivatives on SIRT2 Enzyme Activity

The effect of BNIPSpd, BNIPDaoct, BNIPDanon, BNIPDadec, BNIPDaoxoct and BNIPDaCHM (10 µM) on SIRT2 enzyme activity was also determined by the *Fluor de Lys*™ fluorescent assay system (Figure 7.10). As mentioned above, BNIPDanon and BNIPDadec were investigated to determine their effect on SIRT2 enzyme activity with the length of the central alkyl linker chain of the BNIPP derivatives being increased (> 8 methylene groups). Data showed that 10 µM of BNIPDanon or BNIPDaoxoct did not affect SIRT2 enzyme activity and were considered to be inactive (Figure 7.14). However, 10 µM of BNIPSpd or BNIPDaoct significantly activated SIRT2 enzyme activity ($P < 0.01$; a 15 and 6% increase, respectively), whereas, 10 µM of BNIPDadec and BNIPDaCHM significantly inhibited SIRT2 enzyme activity ($P < 0.05$; a 27% decrease, and $P < 0.001$; a 41% decrease, respectively) (Figure 7.14). These results show that alkyl linker chain length appears to contribute in some way in the activity of BNIPP derivatives against the SIRT2 enzyme. For example, SIRT2 enzyme inhibition increases from BNIPDanon to BNIPDadec; as the length of the alkyl linker chain increases from nine to ten methylene

[3] IC_{50} values for derivatives with 5 – 6 methylene groups in the linker chain were 14.2 and 9.6 µM, respectively whereas, derivatives with 3 – 4 methylene groups in the linker chain were not determinable and 110.0 µM, respectively as determined by the *Fluor de Lys*™ assay system (Chen *et al.* 2008).

groups. The most effective and selective SIRT2 enzyme inhibitor in this series has two cyclohexane rings in its linker chain (i.e., nine carbons), and was more potent than suramin (10 μM; $P < 0.001$; a 36% decrease) (Figure 7.14). Inhibitory activity of suramin (10 μM) towards SIRT2 was in agreement with the previously published results presented in the BIOMOL International manufacturer's instructions and Zhang *et al.* (2009) (i.e., an IC_{50} value of 20.5 μM). Additional BNIPP derivatives will need to be examined to provide a full assessment of the optimum alkyl linker chain length required for SIRT2 enzyme inhibition.

It is important to note that a series of symmetrical SIRT2 enzyme inhibitors have been synthesised by Kiviranta *et al.* (2006). In this series of derivatives, the backbone contains a central aromatic group which is either a 1, 4-disubstituted benzene or naphthalene group connected by a nitrogen atom with an amine or imine function (Kiviranta *et al.* 2006) (Figure 7.23). These derivatives (Figure 7.24) contain similar structural features to that of the BNIPP derivatives, especially BNIPDaCHM. Both sets of derivatives contain a central aromatic group, which is disubstituted, and connected by a nitrogen atom with amine functionality. This is very interesting since BNIPDaCHM was found to be the most active and selective member of the BNIPP derivative series.

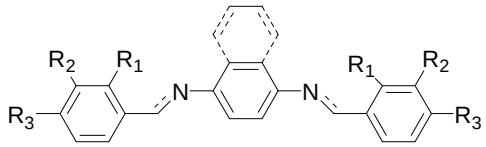

R = H, OH OR OCH_3

Figure 7.24.: General structures of *N*, *N*'-Bisbenzylidenebenzene-1,4-diamines and *N*, *N*'-Bisbenzylidenenaphthalene-1,4-diamines [Dashed bonds show the various structures for these derivatives].

Surprisingly, the BNIPP derivatives bearing either a spermidine linker or eight methylene groups within their linker chain (BNIPSpd and BNIPDaoct, respectively), did not inhibit SIRT2 enzyme activity, but rather behaved as modest selective SIRT2 enzyme activators at 10 μM (Figure 7.14). This is the first time that BNIPP derivatives have been reported as SIRT2 enzyme activators, and is also a very important finding given that SIRT2 enzyme activation has not been widely reported, with most research focused on SIRT1 enzyme activation (Borra *et al.* 2005, Mai *et al.* 2009). Results are in agreement with the findings of Mai *et al*. (2009), who studied activation and inhibition of SIRT1, SIRT2 and SIRT3 enzyme activities with a series of 1, 4-Dihydropyridine (DHP) derivatives at 50 μM by using the same *Fluor de Lys*™ assay system. Mai *et al.* (2009) found that the insertion of a benzyl group in the *N*1 position of the DHP ring led to a dose-dependent activation of all SIRT enzymes (i.e., by derivatives **i** (MC2562), **ii** (MC2563) and **iii** (MC2566); Figure 7.25). However, if a cyclopropyl, phenyl or phenethyl group was

inserted at the same *N*1 position; SIRT1 and -2 enzyme inhibition, not activation, was evident (Mai *et al.* 2009).

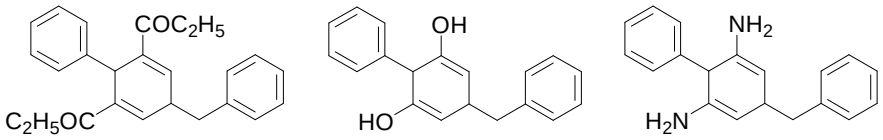

i **ii** **iii**

Figure 7.25.: Structures of the 1,4-Dihydropyridine derivatives, **i** (MC2562), **ii** (MC2563) and **iii** (MC2566).

It is unclear at this stage the mode of action utilised by BNIPSpd and BNIPDaoct for SIRT2 enzyme activation, but it appears that enzyme activation with these BNIPP derivatives is specific for the SIRT2 enzyme, as shown by comparison with the results obtained in the SIRT1 enzyme activity studies (Section 7.4.4; Figure 7.16).

7.5.4. Effect of BNIPP Derivatives on SIRT1 Enzyme Activity

The effect of BNIPSpd, BNIPDaoct, BNIPDanon, BNIPDadec, BNIPDaoxoct and BNIPDaCHM (10 µM) on SIRT1 enzyme activity was determined by the *Fluor de Lys*™ fluorescent assay system (Figure 7.10). BNIPDanon and BNIPDadec were again investigated to determine the effect of increasing the length of the alkyl linker chain (> 8 methylene.groups). The results show that 10 µM of BNIPDaoxoct significantly activated SIRT1 enzyme activity ($P < 0.01$; a 34% increase); whilst the remaining BNIPP derivatives did not affect SIRT1 enzyme activity, and were thus considered to be inactive (Figure 7.16). The significant inhibitory activity ($P < 0.001$; a 91% decrease) of suramin (10 µM) towards SIRT1 was in agreement with results presented in the BIOMOL International manufacturer's instructions. However, it was found that in this *Fluor de Lys*™ assay, suramin exerted a greater level of SIRT1 inhibition than has been previously reported by Schuetz *et al.* (2007), Zhang *et al.* (2009) and Tavares *et al.* (2010).

The results towards the SIRT1 enzyme were in contrast to the SIRT2 enzyme activity results (Figure 7.14), since alkyl chain length does not appear to contribute to an increase in activity of the BNIPP derivatives. For example, the activity of the SIRT1 enzyme was not altered as the length of the alkyl linker chain was increased from eight to ten methylene groups (i.e., from BNIPDaoct to BNIPDadec). This result was not surprising as Tavares *et al.* (2010) had found that a greater level of SIRT1 inhibition was observed by BNIPP derivatives with ≤ 6 methylene groups (e.g., BNIPDabut; IC_{50} 73.1 µM or BNIPDahex; IC_{50} 93.5 µM).

The lack of SIRT1 enzyme inhibitory activity observed after treatment with the BNIPP derivatives at 10 µM could be explained by the findings of Tavares *et al*. (2010). Tavares *et al.* (2010) studied 12 BNIPP derivatives with regard to their activity against the

human SIRT1 enzyme using a commercially available Cyclex SIRT1/Sir2 deacetylase fluorimetric kit (Cyclex Co. Ltd, Japan), and found that all BNIPP derivatives were less potent against SIRT1 than the *Leishmania infantum* SIR2-related protein 1 (LiSIR2RP1). Four out of the 12 BNIPP derivatives tested by Tavares *et al.* (2010) (i.e., BNIPSpd, BNIPDaoct, BNIPDanon and BNIPDadec) were also tested against the SIRT1 enzyme in Section 7.4.4. These derivatives exhibited IC_{50} values of 94.8, 116.5, 97.4 and 113.8 µM, respectively. Therefore, these findings suggest that a higher concentration of each BNIPP derivative (i.e., > 10 µM) may be required to significantly inhibit the activity of the SIRT1 enzyme.

The selective activation of SIRT1 enzyme activity by BNIPDaoxoct was an interesting and novel discovery. This result has identified a synthetic SIRT1 activator, with a structural backbone that is unrelated to resveratrol or other recognized small-molecule SIRT1 activators including SRT1720 (Figure 7.7).

The natural and synthetic SIRT1 activators resveratrol and SRT1720, respectively, are structurally unrelated to one another (Figure 7.7); however they are both potent and selective SIRT1 activators (Milne *et al.* 2007, Alcaín and Villalba 2009b, Baur 2009). SRT1720 can bind to the same site on the SIRT1-acetylated peptide complex and can mimic the same anti-ageing effects of calorie restriction, but is 1000 times more effective than resveratrol (Milne *et al.* 2007, Alcaín and Villalba 2009b). Milne *et al.* (2007) found that the potency of SRT1720 (i.e., the concentration of derivative required to increase enzyme activity by 50%; $EC_{1.5}$) was 0.16 µM with a maximum activation of 781% (compared with an $EC_{1.5}$ of 46.2 µM and maximum activation of 201% for resveratrol).

BNIPDaoxoct was not able to induce SIRT1 activation to the same extent as resveratrol, as was evident in Figure 7.16. However, the results presented in Section 7.4.4 are in partial agreement with results revealed by Howitz *et al.* (2003) as to the level of resveratrol activation achieved. Howitz *et al.* (2003) found that resveratrol could induce a 2-fold increase at 11 µM, but in this study, it was found that resveratrol had induced a 2.5-fold increase in SIRT1 activation at 10 µM ($P < 0.001$; 157.2% increase). The results also show that BNIPDaoxoct ($P < 0.01$; a 33.9% increase) was almost two times less effective than resveratrol ($P < 0.001$; 157.2% increase) (Figure 7.16).

Borra *et al.* (2005) and Pacholec *et al.* (2010) have observed that the activation of SIRT1 by resveratrol and SRT1720 is dependent upon an acetyl-peptide substrate covalently attached to a non-physiological fluorophore, like that of the substrate available in the *Fluor de Lys*™ assay system. No SIRT1 enzyme activation by either activator was observed when the same acetylated peptide, lacking a fluorophore, was used (Denu 2005, Alcaín and Villalba 2009b). Given this information, the use of resveratrol or SRT1720 to activate the SIRT1 enzyme has to be carefully interpreted (Denu 2005). Therefore, further experiments will need to be conducted to confirm the direct or indirect activation of the SIRT1 enzyme with BNIPDaoxoct.

7.5.5. Examination of hSIRT2 and hSIRT1 Inhibitor Binding Sites

The binding potential and inhibitory action of BNIPDaCHM were determined by docking on to the crystal structures of hSIRT2 and hSIRT1 (Finnin *et al.* 2001). BNIPDaCHM was found to be best suited as a SIRT2 inhibitor rather than a SIRT1 inhibitor, owing to its (i) low docking score (i.e., -13.648 kcal/mol^{-1}), (ii) high number of hydrogen bonds (i.e., five hydrogen bonds), (iii) greater interaction with the SIRT2 target (i.e., hydrogen bonding with the residues His187, Gln167, Ser263 and Thr262), and (iv) snug fit into the NAD^+ binding pocket (Figure 7.17). These results can be related to the *in vitro* SIRT2 activity studies (Section 7.4.4 and Figure 7.14), which show BNIPDaCHM to be a potent SIRT2 inhibitor ($P < 0.001$; a 41.4% decrease).

In addition to BNIPDaCHM, three other BNIPP derivatives BNIPDanon, BNIPDa(4,4)Dapm and BNIPDa(3,4)Dapm were investigated for their binding potentials and inhibitory action on hSIRT2 and hSIRT1 (Tables 7.3 and 7.4). Data revealed that alterations to the central alkyl linker chain such as, replacement of the two cyclohexane rings (BNIPDaCHM) with (i) 9 methylene groups (BNIPDanon), (ii) para substituted diphenylmethane groups (BNIP(4,4)Dapm), or (iii) meta substituted diphenylmethane groups (BNIP(3,4)Dapm) resulted in an increase in docking score compared with BNIPDaCHM (e.g., docking scores obtained with hSIRT2 were decreased from -13.648 kcal/mol^{-1} with BNIPDaCHM, to – 14.639, -21.023 and -21.626 kcal/mol^{-1} for BNIPDanon, BNIP(3,4)Dapm and BNIP(4,4)Dapm, respectively; Table 7.3). In contrast to hSIRT2 results, the docking scores obtained with hSIRT1 revealed that BNIP(3,4)Dapm was the most potent SIRT1 inhibitor (Table 7.4). It is important to note that docking scores can be misleading, and are not absolute. Therefore, the docking score, position docked in the NAD^+ binding pocket, number of hydrogen bonds, and number of hydrogen bonds made with important residues (i.e., His167 and Gln167 in hSIRT2, and Gln104 and His122 in hSIRT1) of each BNIPP derivative needs to be considered before the most active BNIPP derivative can be identified. As a result of these considerations, BNIPDaCHM and BNIP(3,4)Dapm were identified as the most potent SIRT2 and SIRT1 inhibitors, respectively.

The results presented for BNIPDanon on hSIRT1 were in agreement with those of Tavares *et al.* (2010), who studied BNIPDanon in a similar hSIRT1 protein model. BNIPDanon was found to be a good SIRT1 inhibitor with a low docking score (i.e., -15.8 kcal/mol^{-1}), high interaction with the SIRT1 target (i.e., five hydrogen bonds), and was shown to competitively bind to the NAD^+ binding pocket.

7.6. Conclusion

The BNIPP derivatives, BNIPSpd, BNIPDaoct, BNIPDaoxoct and BNIPDaCHM, including BNIPDanon and BNIPDadec were tested *in vitro* for their effect on HDAC activity. The most effective HDAC inhibitor was BNIPDaCHM with a 24.8 and 41.4% decrease in Class I – II and SIRT2 enzyme activities at 10 µM, respectively, while the most effective SIRT2 and SIRT1 enzyme activators were BNIPSpd (a 14.5% increase in SIRT2 enzyme activity, at 10 µM) and BNIPDaoxoct (a 33.9% increase in SIRT1 enzyme activity, at 10 µM), respectively. Furthermore, BNIPDaCHM exhibited potent and selective SIRT2 enzyme inhibitor properties, with the ability to bind strongly to the NAD^+ binding pocket by the formation of hydrogen bonds with the residues His187 and Gln167.

In conclusion, symmetrical BNIPP derivatives with a novel structural backbone have, for the first time, been identified as potential effective and selective HDAC inhibitors, and activators.

Chapter 8

Final Summary, Conclusion and Future Work

8.1. Final Summary and Conclusion

The aim of this study was to synthesise new bisnaphthalimidopropyl polyamine (BNIPP) derivatives and evaluate their effect and mode of action in a breast cancer cell system. The work presented in this study is complementary to the work previously undertaken by Kong Thoo Lin and Pavlov (2000), Pavlov *et al.* (2001), Kong Thoo Lin *et al.* (2003), Dance *et al.* (2005), Oliveira *et al.* (2007) and Ralton *et al.* (2009).

It was essential to determine the influence of BNIPP derivatives on their DNA binding ability, as DNA is an important and valuable target in anti cancer drug design. The strong DNA binding affinities observed in this study may account for the subsequent changes to cell morphology, cytotoxicity and DNA instability (i.e., through DNA strand breaks and repair mechanisms) detected after BNIPP derivative treatment in MDA-MB-231 and MCF-10A cells. Apoptotic cell death was determined in breast cancer MDA-MB-231 cells to identify the mode of cell death attained by BNIPP derivatives. Interestingly, apoptosis had been previously observed in HL-60 promyelocytic leukaemia cells (Kong Thoo Lin *et al.* 2003) and colon cancer (CaCO-2 and HT-29) cells (Ralton *et al.* 2009). In addition, effects of BNIPP derivative treatment on cell cycle distribution and p53 and $p21^{Waf1/Cip1}$ mRNA expression levels were determined to further evaluate the mode of cell death. Finally, it was important to investigate the potential role of the BNIPP derivatives on HDAC inhibition, since HDAC inhibitors have shown promise as anti cancer agents.

Four new BNIPP derivatives (BNIPDaoxoct, BNIPDaCHM, BPHPDadec and NPA) were successfully synthesised by modification of the *N*-alkylation reaction previously used to synthesise the parent BNIPP derivatives (Kong Thoo Lin and Pavlov 2000, Oliveira *et al.* 2007). The simple and reproducible three step procedure (Scheme A and B; Chapter 2) utilised in this study was highly convenient, adaptable and could easily be used for the synthesis of future BNIPP and related derivatives (as it has been employed by Filosa *et al.* 2009).

The BNIPP derivatives interact with DNA by bis-intercalation (i.e., via the naphthalimido groups) and groove binding (i.e., via the aminoalkyl linker chain). The results presented in this study are in agreement with those previously obtained by Pavlov *et al.* (2001) and Dance *et al.* (2005). BNIPDahex was the most active BNIPP derivative (ΔT_m 35.7 °C) closely followed by BNIPSpd (ΔT_m 35.3 °C); both of which had a greater DNA affinity than the extensively studied intercalator, doxorubicin (ΔT_m 30.2 °C) (Table 3.1). It was observed that modifications to the central linker chain resulted in changes to DNA binding affinity. BNIPP derivatives whose central linker chain resembled that of the natural polyamines (i.e., spermidine or spermine) (Pavlov *et al.* 2001, Dance *et al.* 2005)

exhibited a higher degree of DNA binding affinity than their linear alkyl linker counterparts (Tables 3.1 and 3.3). BNIPPut, BNIPDahex and BNIPDaoct with 4, 6 and 8 methylene groups respectively exhibited high DNA binding affinities (ΔT_m values ranging between 32.5 - 35.7 °C) whereas DNA binding affinity was reduced with BNIPDadec and BNIPDadodec with 10 and 12 methylene groups respectively (ΔT_m values of 28.2 and 25.0 °C). The new BNIPP derivatives, BNIPDaoxoct and BNIPDaCHM exhibited a marginal decrease in DNA binding affinity compared with the more active BNIPP derivatives (i.e., BNIPPut, BNIPDahex or BNIPDaoct), with ΔT_m values of 31.7 and 31.2 °C, respectively; but were more effective than BNIPP derivatives with a linker chain of > 8 methylene groups (Tables 3.1 and 3.3). It was found that BPHPDadec and NPA were not effective DNA intercalators (ΔT_m values of 15.8 and 10.1 °C, respectively and C_{50} values of > 10 µM; Tables 3.1 and 3.3). This emphasises the importance of bisnaphthalimidopropyl functionality and an optimum alkyl linker chain length of between 4 – 8 methylene groups.

BNIPP derivatives (except BPHPDadec and NPA; IC_{50} values > 40 µM) were cytotoxic in both cell lines (MDA-MB-231 (Table 4.2) and MCF-10A (Table 4.3) cells). Cytotoxicity was also affected by modifications to the central linker chain, for example, in MDA-MB-231 cells, alterations to the spermidine linker chain (BNIPSpd) with removal of a nitrogen atom (BNIPDaoct) or replacement with two cyclohexane rings resulted in an increase in cytotoxicity (IC_{50} values decreased from 12.7 µM with BNIPSpd to 5.0 and 6.8 µM for BNIPDaoct and BNIPDaCHM, respectively (Table 4.2).

In MDA-MB-231 and MCF-10A cells, the BNIPP derivatives BNIPSpd, BNIPDaoct, BNIPDaoxoct and BNIPDaCHM resulted in alterations to cell morphology (Figures 4.9 – 4.11). Furthermore, MDA-MB-231 cells treated with BNIPDaoct and BNIPDaCHM exhibited fluorescence after 0.5 hours. BNIPSpd and BNIPDaoxoct, however, required a longer incubation time to enter the cell, as fluorescence was not observed until after 6 hours (Figure 4.15), suggesting that uptake time might be related to cytotoxicity in MDA-MB-231 cells as BNIPDaoct and BNIPDaCHM were observed to have a higher toxicity (IC_{50} values 5.0 and 6.8 µM after 24 hours, respectively; Table 4.2) and faster uptake (0.5 hours) than BNIPSpd and BNIPDaoxoct (IC_{50} values 12.7 and 12.4 µM after 24 hours, respectively; Table 4.2; observed after 6 hours). A different mechanism of cellular uptake and entry unrelated to cytotoxicity was observed in MCF-10A cells treated with BNIPSpd, BNIPDaoct, BNIPDaoxoct or BNIPDaCHM. Fluorescence was observed after 0.5 hours in MCF-10A cells treated with BNIPDaoct and BNIPDaCHM; BNIPDaoxoct treated MCF-10A cells showed fluorescence after 2 hours, whereas MCF-10A cells treated with BNIPSpd showed fluorescence after 6 hours (Figure 4.16). The results suggest that BNIPP derivative uptake is cell line dependent.

Four BNIPP derivatives (i.e., BNIPSpd, BNIPDaoct, BNIPDaoxoct and BNIPDaCHM with different modifications to the central linker chain) were chosen to determine whether these BNIPP derivatives entered cells via the MGBG-specific PAT and reduced intracellular polyamine levels. None of the BNIPP derivatives chosen entered cells by use of the MGBG-specific PAT, as CHO-MG/CHO IC_{50} ratios ranged from 0.4 – 1.0 (Table 4.4). The BNIPP derivatives must, therefore, utilise alternative entry mechanisms that are independent of the MGBG-specific PAT, such as, passive diffusion or through another transporter, as suggested by Gardner *et al.* (2004) for N^1-arylalkylpolyamines. It is possible that BNIPP derivatives are too large to be imported into cells via the MGBG-specific PAT system, as suggested by Kaur *et al.* (2008b) for large N^1-cargoes (e.g., *N*-[4-(4-amino-butylamino)-butyl]-*N*'-(4,6-dihydro-pyren-1-ylmethyl)-butane-1,4-diamine). The BNIPP derivatives were able to induce different responses in intracellular polyamine levels in MDA-MB-231 and MCF-10A cells. Responses included:

(i) no change (i.e., BNIPDaCHM and BNIPSpd (0.1 – 5 μM) in MDA-MB-231 and MCF-10A cells, respectively; Figures 4.19 and 4.20)

(ii) an increase (i.e., BNIPSpd, BNIPDaoct and BNIPDaoxoct (0.1 μM) in MDA-MB-231 cells (Figures 4.16 – 4.18), and BNIPDaoxoct and BNIPDaCHM (0.1 μM) in MCF-10A cells (Figures 4.22 and 4.23)

(iii) a decrease (i.e., BNIPSpd and BNIPDaoct (5 μM) significantly reduced intracellular polyamine levels in MDA-MB-231 cells ($P < 0.05$ and $P < 0.01$, respectively; Figures 4.16 and 4.17), whilst BNIPDaoct (5 μM) and BNIPDaoxoct (≥ 1 μM) significantly reduced intracellular polyamine levels in MCF-10A cells ($P < 0.05$; Figures 4.21 and 4.22) in intracellular polyamine levels.

The reduction of intracellular polyamine levels could be responsible for the toxicity of BNIPSpd or BNIPDaoct, but not in the case of BNIPDaCHM within MDA-MB-231 cells.

Intracellular DNA stability was assessed to support BNIPP derivative induced cytotoxicity and, in the case of BNIPSpd treated cells, to support the significant reduction ($P < 0.05$) of intracellular polyamine levels. BNIPSpd and BNIPDaCHM significantly induced ($P < 0.05$) DNA strand breaks above endogenous levels in a dose dependent manner in both cell lines (MDA-MB-231 and MCF-10A cells). However, BNIPSpd required a longer treatment time to induce the same level of DNA strand breaks as BNIPDaCHM in MDA-MB-231 cells (Figures 5.7 and 5.8). These results suggest that DNA strand breaks may be related to:

(i) cellular uptake studies, as BNIPDaCHM was observed after 0.5 hours, whilst BNIPSpd was not observed until after 6 hours (Figure 4.15)

(i) cytotoxicity, as BNIPDaCHM was more cytotoxic (IC_{50} 6.8 µM) than BNIPSpd (IC_{50} 12.7 µM) after 24 hours (Table 4.2)

(ii) DNA binding affinity via bis-intercalation (Δ T_m 35.3 and 31.2 °C, for BNIPSpd and BNIPDaCHM, respectively).

However, MCF-10A cells were more sensitive to the effect of BNIPSpd than BNIPDaCHM (Figures 5.19 and 5.10). These results indicate that DNA damage is a principal mode of action for BNIPSpd and BNIPDaCHM in MDA-MB-231 and MCF-10A cells

It was important to determine the effect of BNIPP derivatives on DNA repair mechanisms, as cells have an inherent ability to effectively remove and repair DNA damage. BNIPSpd and BNIPDaCHM were found to significantly inhibit the ability of MDA-MB-231 cells to repair oxidative-induced DNA damage at non toxic concentrations (i.e., concentrations that did not induce significant changes to DNA strand breaks nor induced cytotoxicity in MDA-MB-231 cells), even after 24 hours. However, following MMS-induced DNA damage, BNIPDaCHM did not inhibit the ability of MDA-MB-231 cells to repair DNA damage. Thus, BNIPDaCHM induces contrasting effects on the repair of DNA strand breaks. The results, however, confirm that DNA damage induced by MMS was greater and more dramatic than oxidative-induced DNA damage (Lundin *et al.* 2005, Duthie. personal communication). Therefore, the inability to repair DNA damage following treatment with either BNIPSpd or BNIPDaCHM could be exploited to increase DNA strand breaks, and induce apoptotic cell death.

Apoptotic cell death was preliminarily investigated in this study in BNIPSpd or BNIPDaCHM treated MDA-MB-231 cells. BNIPSpd and BNIPDaCHM induced apoptosis (i.e., by loss of plasma membrane integrity, PS externalisation and increase in the proportion in sub-G1 population) and, BNIPDaCHM resulted in a decrease of cell number, in a time dependent manner (0.5 – 24 hours). Interestingly, apoptotic cell death was observed after only 0.5 hours treatment; a remarkable and novel discovery for derivatives belonging to the BNIPP family. 7-AAD labelling was also prominent after 0.5 hours, thus indicating the strong presence of necrotic cells ($P < 0.001$; a 0.30 increase with BNIPSpd, and $P < 0.001$; a 0.42 increase with BNIPDaCHM; Figure 6.10). Cell cycle arrest was not evident after 24 hours, although $p21^{Waf1/Cip1}$ mRNA expression was significantly over expressed ($P < 0.01$; a 24.7% increase; Figure 6.20) in a p53-independent manner after 4 hours treatment with BNIPDaCHM (5 µM). BNIPSpd did not alter p53 or $p21^{Waf1/Cip1}$ mRNA expression levels after 4 hours in MDA-MB-231 cells. It can be hypothesised that BNIPSpd and BNIPDaCHM initiate cell death by different mechanisms (Figures 8.1 and

8.2), and modifications to the central linker chain have resulted in dramatic changes to the individual response produced.

As HDACs are responsible for the control of gene expression including the activation of DNA damage and induction of $p21^{Waf1/Cip1}$ mRNA expression levels; it was important to determine the effect of BNIPP derivatives with modifications to their central linker chain on HDAC inhibition. BNIPDaCHM (10 µM) was the most effective HDAC inhibitor as demonstrated by a 24.8% ($P < 0.05$) decrease in Class I-II activity (Figure 7.12) and a 41.4% ($P < 0.001$) decrease in SIRT2 enzyme activity (Figure 7.13). In addition, BNIPDaCHM was also found to be a potent and selective SIRT2 enzyme inhibitor as demonstrated by strong binding to the NAD^+ binding pocket (i.e., formation of hydrogen bonds with His187 and Gln167 residues). BNIPSpd (10 µM), however, was an effective SIRT2 activator (a 14.5% ($P < 0.01$) increase). Once more modifications to the central linker chain appeared to contribute to the activity of BNIPP derivatives against HDAC inhibition, in particular, SIRT2 enzyme activity (e.g., alterations to the central linker chain with an increase in alkyl length from nine to ten methylene groups (BNIPDanon to BNIPDadec) or replacement with two cyclohexane rings (BNIPDaCHM) resulted in an increase in HDAC inhibition; Figure 7.13).

The results discussed in this study indicate that BNIPSpd and BNIPDaCHM have different modes of action in treated MDA-MB-231 cells. The proposed modes of actions are presented in Figures 8.1 and 8.2.

Finally, the BNIPP derivative that would be offered to a manufacturer for further development would be BNIPDaCHM. This is due to its ability to induce a cytotoxic effect (at a µM level), fast cellular uptake (0.5 hours), induction of significant DNA strand breaks (> 1 µM), and early apoptotic cell death (0.5 hours) and, the potent and selective inhibition of the SIRT2 enzyme. Thus, providing a potential anti cancer agent.

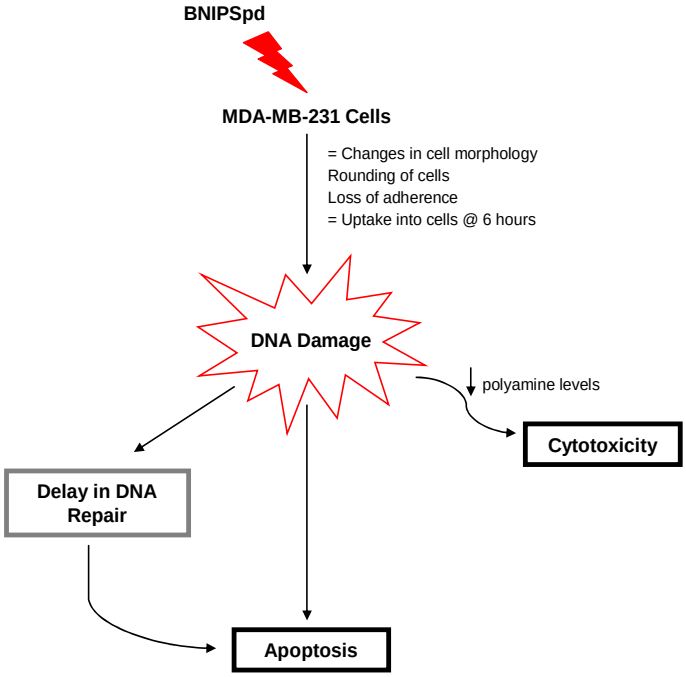

Figure 8.1.: Schematic representation of the mode of action of BNIPSpd in MDA-MB-231 cells

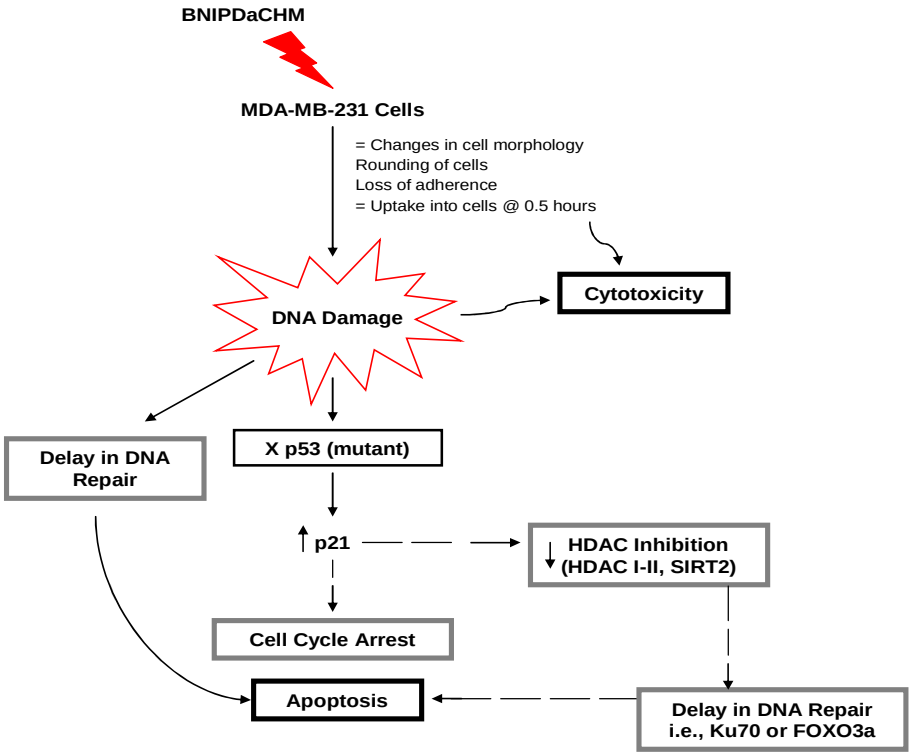

Figure 8.2.: Schematic representation of the mode of action of BNIPDaCHM in MDA-MB-231 cells [Key: - - - denotes possible mode of action]

8.2. Future Work

8.2.1. DNA Binding Affinity

All BNIPP derivatives were found to interact with DNA through bis-intercalation and it was proposed that the mechanism of groove binding may be utilised. Therefore, to further determine the DNA binding affinity of these derivatives; it is important to verify their groove binding potential and sequence specificity, allowing a complete study and comparison with structurally related derivatives, via NMR spectroscopy (Strekowski and Wilson 2007). Furthermore, repeating the molecular modelling with a more suitable DNA duplex model (with various spacers between the DNA intercalation sites) could provide a better computational model for high throughput screening of future BNIPP and related derivatives.

8.2.2. Cellular Uptake and Localisation

Although experiments into the exact cellular location of BNIPP derivatives could not be conducted in this study; it would be of benefit to explore this area further as an indication of BNIPP derivative action. Analysis of specific cell organelles after BNIPP treatment would further elucidate their mode of action in a breast cancer cell system, for example, use of nuclear specific Picogreen quenching by flow cytometry to analyse mitochondrial DNA, as carried out by Ashley and Poulton (2009), or real time fluorescence microscopy to analyse cell distribution undertaken by Peixoto *et al.* (2009).

8.2.3. DNA Damage and Repair

Both BNIPP derivatives were able to induce DNA strand breaks and hinder DNA repair suggesting a principal mode of action for BNIPSpd and BNIPDaCHM in MDA-MB-231 cells. To further elucidate their mode of action, with regards to DNA repair mechanisms; it is important to investigate the main DNA repair pathways (Section 5.1.2; Figure 5.2) by, for example, microarray analysis of gene expression (Collins 1996, Damia and D'Incalci 2007, Ljungman 2009). This would offer a valuable insight into the potential these derivatives have as anti cancer agents. In addition, analysis into the regulation of specific DNA repair enzymes, for example, O^6-alkylguanine-DNA-alkyltransferase (AGT) or poly (ADP-ribose) polymerase (PARP) could provide opportunities by which to identify novel targets for, or increase the known DNA damaging abilities of BNIPSpd or BNIPDaCHM (Damia and D'Incalci 2007).

As the accumulation of DNA damage and defects in DNA repair mechanisms have been linked to HDAC inhibition (Gaymes *et al.* 2006); it would be encouraging to analyse

and confirm that DNA damage was caused by HDAC inhibition after BNIPP derivative treatment.

8.2.4. Mode of Cell Death

Apoptosis induced in MDA-MB-231 cells by BNIPSpd and BNIPDaCHM was investigated in this study using morphological (i.e., AO/EB staining observed via fluorescence microscopy) and biochemical detection methods (i.e., PS externalisation by annexin V-FITC staining and 7-AAD labelling, and detection of a sub-G1 population through PI staining). The observation that apoptotic cell death was induced by BNIPSpd and BNIPDaCHM should be confirmed by further investigations including, caspase activation (i.e., caspase-3, 7 and 8), DNA fragmentation, and also a detailed analysis into the principal biochemical mediators of apoptosis, in particular, the pro- (Bax, Bak, etc.) and antiapoptotic families (Bcl-2, Bcl-X_L, etc.) (Carew *et al.* 2008).

Apoptotic cell death was observed in BNIPSpd and BNIPDaCHM (5 µM) treated cells after only 0.5 hours; however, necrotic cells were also evident (Figure 6.10). This implies that BNIPSpd and BNIPDaCHM could activate other forms of cell death, rather than apoptosis, for example, mitotic catastrophe, necrosis, autophagy or senescence (Cohen-Jonathan *et al.* 1999, Mansilla *et al.* 2006, Portugal *et al.* 2009). These forms of cell death (in particular, mitotic catastrophe explained by abnormal mitosis caused by a p53 mutation) (Bertheau *et al.* 2008) can be determined, for example, by characterising the main DNA repair pathways (refer to Section 8.2.3) and investigating protein levels during mitosis (Cahuzac *et al.* 2010).

8.2.5. Cell Cycle Regulation

Cell cycle arrest in MDA-MB-231 cells treated with BNIPSpd and BNIPDaCHM was not evident after 24 hours following PI staining, even though $p21^{Waf1/Cip1}$ mRNA expression was induced in a p53-independent manner: a classical mechanism in HDAC inhibitor-induced cell cycle arrest (Carew *et al.* 2008). Further research into the CDK-Cip/Kip family, including $p27^{Kip1}$ (Park and Lee 2003) would be required (Rao *et al.* 1998). Supplementary studies into the cyclin D and E families should also be investigated to determine the role that BNIPP derivatives have on cell cycle regulation (Rao *et al.* 1998).

8.2.6. HDAC Inhibition

The preliminary investigation into HDAC inhibition by BNIPP derivatives found that BNIPDaCHM was a more potent and selective SIRT2 enzyme inhibitor than suramin (a known SIRT2 inhibitor) (Zhang *et al.* 2009). Thus, determining the further potential of BNIPDaCHM as a selective SIRT2 inhibitor would establish a novel mode of action for

BNIPP derivatives. For that reason, all BNIPP derivatives will need to be examined, thus, providing a full assessment into what effect modifications to the central linker chain have on HDAC inhibition.

As SIRT2 inhibitors have been shown to target α tubulin, and deacetylate histone H4 (North *et al.* 2003, Schemies *et al.* 2009); it would be important to determine the ability of BNIPDaCHM to elicit an effect on each of these SIRT2 targets *in vitro*.

As ERs play an important role in cell proliferation, and since they are positively or negatively regulated by HATs or HDACs, respectively (Im *et al.* 2008); further investigations could provide an important link between BNIPP derivatives, ERs and HDAC activity. Additionally, to determine cell-specific mechanisms; it would be beneficial to evaluate cell cycle arrest and induction of apoptotic cell death within ER positive breast cancer cells (previously investigated by Dance *et al.* 2005).

References

AH BYUN, J, HO CHOI, M, HEE MOON, M, KONG, G, and CHUL CHUNG, B., 2009. Serum Polyamines in Pre- and Post-Operative Patients with Breast Cancer Corrected by Menopausal Status. *Cancer Letters*, 273, pp. 300 – 304

AJAMI, A.M, and BARLOW, D.O., 2004. *Amonafide Salts*. United States Patent 6693198 2004-17-02

AJAMI, A.M, and BARLOW, D.O., 2006. *Amonafide Salts*. United States Patent 6989390 B2 2006-24-01

ALAMI, N, PATERSON, J, BELANGER, S, JUSTE, S, GRIESHABER, C.K, and LEYLAND-JONES, B., 2007. Comparative Analysis of Xanafide Cytotoxicity in Breast Cancer Cell Lines. *British Journal of Cancer*, 97, pp. 58 – 64

ALCAÍN, F.J, and VILLALBA, J.M., 2009a. Sirtuin Inhibitors. *Expert Opinion on Therapeutic Patents*, 19 (3), pp. 283 - 294

ALCAÍN, F.J, and VILLALBA, J.M., 2009b. Sirtuin Activators. *Expert Opinion on Therapeutic Patents*, 19 (4), pp. 403 - 414

ALLEN, S.L, KOLITZ, J.E, LUNDBERG, A.S, BENNETT, J.M, CAPIZZI, R.L, and BUDMAN, D.R., 2009. Phase I Trials of Amonafide as Monotherapy and In Combination with Cytarabine in Patients with Poor-Risk Acute Myeloid Leukemia. *Leukemia Research*, doi: 10.1016/j.leukres.2009.07.038

ALM, K, BERNTSSON, S.H, KRAMER, D.L, PORTER, C.W, and OREDSSON, S.M., 2000. Treatment of Cells with the Polyamine Analogue N^1, N^{11}-diethylnorspermine Retards S Phase Progression within One Cell Cycle. *European Journal of Biochemistry*, 267, pp. 4157 – 4164

AMERICAN BASIC GENE ASSOCIATE BIOSCIENCE INC, 2006. *Annexin V-FITC/PI Apoptosis Detection Kits*. [online] ABGAB Corporation. Available from: http://www.abgab.com/KA1001.asp [Accessed 16 February 2010]

ANDERSON, R.J, GROUNDWATER, P.W, TODD, A, and MOORE, A., 2009. An Overview of Cancer Treatments. *The Pharmaceutical Journal*, 283, pp. 511 - 512

ANDRIANOV, V, GAILITE, V, LOLA, D, LOZA, E, SEMENIKHINA, V, KALVINSH, I, FINN, P, PETERSEN, K.D, RITCHIE, J.W.A, KHAN, N, TUMBER, A, COLLINS, L.S, VADLAMUDI, S.M, BJÖRKLING, F, and SEHESTED, M., 2009. Novel Amide Derivatives as Inhibitors of Histone Deactylase: Design, Synthesis and SAR. *European Journal of Medicinal Chemistry*, 44, pp. 1067 – 1085

ARCAMORE, F.M., 1992. The development of new anticancer drugs. *World Journal of Microbiology and Biotechnology*, 8 (Supplement 1), pp. 74 – 76

AROUI, S, BRAHIM, S, De WAARD, M, BRÉARD, J, and KENANI, A., 2009. Efficient Induction of Apoptosis by Doxorubicin Coupled to Cell-Penetrating Peptides Compared to Unconjugated Doxorubicin in the Human Breast Cancer Cell Line MDA-MB-231. *Cancer Letters*, 285, pp. 28 – 38

ASBURY, R, BLESSING, J.A, LOOK, K.Y, BULLER, R, and LUCCI, J.A., 1997. A Phase II Trial of Amonafide in Patients with Nonsquamous Cell Carcinoma of the Cervix: A Gynecologic Oncology Group Study. *American Journal of Clinical Oncology*, 20 (6), Abstract, pp. 626 – 627

ASHLEY, N, and POULTON, J., 2009. Mitochondrial DNA is a Direct Target of Anti-Cancer Anthracycline Drugs. *Biochemical and Biophysical Research Communications*, 378, pp. 450 – 455

ASHRAF, N, ZINO, S, MACINTYRE, A, KINGSMORE, D, PAYNE, A.P, GEORGE, W.D, and SHIELS, P.G., 2006. Altered Sirtuin Expression is Associated with Node-Positive Breast Cancer. *British Journal of Cancer*, 95, pp. 1056 - 1061

BAILLY, C, BRANA, M, and WARING, M.J., 1996. Sequence-Selective Intercalation of Antitumour Bisnaphthalimides into DNA, Evidence for an Approach via the Major Groove. *European Journal of Biochemistry*, 240, pp. 195 – 208

BAILLY, C, CARRASCO, C, JOUBERT, A, BAL, C, WATTEZ, N, HILDEBRAND, M-P, LANSIAUX, A, COLSON, P, HOUSSIER, C, CACHO, M, RAMOS, A, and BRANA, M.F., 2003. Chromophore-Modified Bisnaphthalimides: DNA Recognition Topoisomerase Inhibition, and Cytotoxic Properties of Two Mono- and Bisfuronaphthalimides. *Biochemistry*, 42 (14), pp. 4136 – 4150

BALDUCCI, L., 2007. Molecular insight in cancer treatment and prevention. *The International Journal of Biochemistry and Cell Biology*, 39, pp. 1329 – 1336

BASKIĆ, D, POPOVIĆ, S, RISTIĆ, P, and ARSENIJEVIĆ, N.N., 2006. Analysis of Cycloheximide-induced Apoptosis in Human Leukocytes: Fluorescence Microscopy using Annexin V/Propidium Iodide Versus Acridin Orange/Ethidium Bromide. *Cell Biology International*, 30, pp. 924 – 932

BAUR, J.A., 2009. Biochemical Effects of SIRT1 Activators. *Biochimica et Biophysica Acta*, doi: 10.1016/j.bbapap.2009.10.025

BELKACEMI, L, LAM, E, CALDWELL, J.D, SIEMENS, D.R, and GRAHAM, C.H., 2006. Stimulation of Human Breast Carcinoma Cell Invasiveness and Urokinase Plasminogen Activator Activity by Glucose Deprivation. *Experimental Cell Research*, 312, pp. 1685 – 1692

BELLOC, F, BELAUD-ROTUREAU, M.A, LAVIGNOLLE, V, BASCANS, E, BRAZ-PEREIRA, E, DURRIEU, F, and LACOMBE, F., 2000. Flow Cytometry Detection of Caspase 3 Activation in Preapoptotic Leukemic Cells. *Cytometry*, 40, pp. 151 - 160

BERGERON, R.J, FENG, Y, WEIMAR, W.R, MCMANIS, J.S, DIMOVA, H, PORTER, C, RAISLER, B, and PHANSTIEL, O., 1997. A Comparison of Structure-Activity Relationships between Spermidine and Spermine Analogue Antineoplastics. *Journal of Medicinal Chemistry*, 40, pp. 1475 – 1494

BERGERON, R.J., 1986. Methods for the Selective Modification of Spermidine and its Homologues. *Accounts of Chemical Research*, 19, pp. 105 - 113

BERGERON, R.J, McMANIS, J.S, LIU, C.Z, FENG, Y, WEIMAR, W.R, LUCHETTA, G.R, WU, Q, ORTIZ-OCASIO, J, VINSON, J.R.T, KRAMER, D, and PORTER, C., 1994. Antiproliferative Properties of Polyamine Analogues: A Structure-Activity Study. *Journal of Medicinal Chemistry*, 37, pp. 3464 – 3476

BERGERON, R.J, NEIMS, A.H, McMANIS, J.S, HAWTHORNE, T.R, VINSON, J.R.T, BORTELL, R, and INGENO, M.J., 1988. Synthetic Polyamine Analogues as Antineoplastics. *Journal of Medicinal Chemistry*, 31, pp. 1183 – 1190

BERTHEAU, P, ESPIÉ, M, TURPIN, E, LEHMANN, J, PLASSA, L-F, VARNA, M, JANIN, A and DE THÉ, H., 2008. *TP53* Status and Response to Chemotherapy in Breast Cancer. *Pathobiology*, 75, pp. 132 – 139

BERTHO, A.L, SANTIAGO, M.A, and COUTINHO, S.G., 2000. Flow Cytometry in the Study of Cell Death. *Memórias do Instituto Oswaldo Cruz*, 95 (3), pp. 429 – 433

BESTWICK, C.S, and MILNE, L., 2006. Influence of Galangin on HL-60 Cell Proliferation and Survival. *Cancer Letters*, 243, pp. 80 - 89

BESTWICK, C.S, MILNE, L, and DUTHIE, S.J., 2007. Kaempferol Induced Inhibition of HL-60 Cell Growth Results from a Heterogeneous Response, Dominated by Cell Cycle Alterations. *Chemico-Biological Interactions*, 170, pp. 76 – 85

BHAVSAR, P, ADMED, T, and ADCOCK, I.M., 2008. The Role of Histone Deacetylases in Asthma and Allergic Diseases. *Journal of Allergy and Clinical Immunology*, 121 (3), pp. 580 – 584

BIELIAUSKAS, A.V, and PFLUM, M.K.H., 2008. Isoform-selective Histone Deacetylase Inhibitors. *Chemical Society Reviews*, 37 (7), pp. 1402 – 1413

BIZANEK, R, McGUINNESS, B.F, NAKANISHI, K, and TOMASZ, M., 1992. Isolation and Structure of an Intrastrand Cross-Link Adduct of Mitomycin C and DNA. *Biochemistry*, 31, pp. 3084 - 3091

BLOWS, W.T., 2005. *The Biological Basis of Nursing: Cancer*. Abingdon: Routledge.

BLUM, K.A, ADVANI, A, FERNANDEZ, L, VAN DER JAGT, R, BRANDWEIN, J, KAMBHAMPATI, S, *et al.*, 2009. Phase II Study of the Histone Deacetylase Inhibitor MGCD0103 in Patients with Previously Treated Chronic Lymphocytic Leukemia. *British Journal of Haematology*, 147 (4), pp. 507 – 514

BONCHER, T, BI, X, VARGHESE, S, CASERO Jr, R.A, and WOSTER, P.M., 2007. Polyamine-based Analogues as Biochemical Probes and Potential Therapeutics. *Biochemical Society Transactions*, 35 (2), pp. 356 – 363

BORRA, M.T, SMITH, B.C, DENU, J.M., 2005. Mechanism of Human SIRT1 Activation by Resveratrol. *The Journal of Biological Chemistry*, 280 (17), pp 17187 – 17195

BOUSQUET, P.F, BRANA, M.F, CONLON, D, FITZGERALD, K.M, PERRON, D, COCCHIARO, C, *et al.*, 1995. Preclinical Evaluation of LU79553: A Novel Bis-naphthalimide with Potent Antitumour Activity. *Cancer Research*, 55, pp. 1176 – 1180

BRAITHWAITE, A, and SMITH, F.J., 1994. Plane Chromatography. In: A . BRAITHWAITE and F.J. SMITH. *Chromatographic Methods*. 4th Edition. London: Chapman and Hall. pp. 24 – 45

BRANA, M.F, CASTELLANO, J.M, ROLDAN, C.M, SANTOS, A, VAZQUEZ, D, and JIMENEZ, A., 1980. Synthesis and Mode(s) of Action of a New Series of Imide Derivatives of 3-nitro-1,8 naphthalic Acid. *Cancer Chemotherapy and Pharmacology*, 4 (1), pp. 61 – 66

BRANA, M.F, CASTELLANO, J.M, MORAN, M, PEREZ de VEGA, M.J, ROMERDAHL, C.R, QIAN, X-D, *et al.,* 1993. Bis-naphthalimides: A New Class of Antitumour Agents. *Anti-Cancer Drug Design*, 8, pp. 257 – 268

BRANA, M.F, CASTELLANO, J.M MORAN, M, PEREA de VEGA, M.J, QIAN, X-D, ROMERDAHL, C.A, and KEILHAUER, G., 1995. Bisnaphthalimides. 2. Synthesis and Biological Activity of 5, 6-acenaphthalimidoalkyl-1, 8-naphthalimidoalkyl amines. *European Journal of Medicinal Chemistry*, 30, pp. 235 – 239

BRANA, M.F, CASTELLANO, J.M, PERRON, D, MAHER, C, CONLON, D, BOUQUET, P.F, *et al.*, 1997. Chromophore-Modified Bis-naphthalimides: Synthesis and Antitumour Activity of Bis-Dibenz [de, h] isoquinoloine-1, 3-diones. *Journal of Medicinal Chemistry*, 40, pp. 449 – 454

BRANA, M.F, CACHO, M, GRADILLAS, A, de PASCUAL-TERESA, B, and RAMOS, A., 2001. Intercalators as Anti-Cancer Drugs. *Current Pharmaceutical Design*, 7, pp. 1745 – 1780

BRANA, M.F, and RAMOS, A., 2001. Naphthalimides as Anticancer Agents: Synthesis and Biological Activity. *Current Medicinal Chemistry – Anti-Cancer Agents*, 1, pp. 237 – 255

BRANA, M.F, CACHO, M, RAMOS, A, DOMÍNGUEZ, M.T, POZUELO, J.M, ABRADELO, C, *et al.*, 2003. Synthesis, Biological Evaluation and DNA Binding Properties of Novel Mono and Bisnaphthalimides. *Organic and Biomolecular Chemistry*, 1, pp. 648 - 654

BRANA, M.F, CACHO, M, GARCIA, M.A, de PASCUAL-TERESA, B, RAMOS, A, DOMINGUEZ, M.T, *et al.*, 2004a. New Analogues of Amonafide and Elinafide, Containing Aromatic Heterocycles: Synthesis, Antitumour Activity, Molecular Modeling, and DNA Binding Properties. *Journal of Medicinal Chemistry*, 47, pp. 1391 – 1399

BRANA, M.F, GRADILLAS, A, GOMEZ, A, ACERO, N, LLINARES, F, MUNOZ-MINGARRO, D, *et al.*, 2004b. Synthesis, Biological Activity, and Quantitative Structure-Activity Relationship Study of Azanaphthalimide and Arylnaphthalimide Derivatives. *Journal of Medicinal Chemistry*, 47 (9), pp. 2236 - 2242

BROWN, D.M., 2005. *Naphthalimide synthesis including Amonafide synthesis and pharmaceutical preparations thereof*. United States patent 20050113579 2005-26-0

BURDEN, D.A, and OSHEROFF, N., 1998. Mechanism of Action of Eukaryotic Topoisomerase II and Drugs Targeted to the Enzyme. *Biochimica et Biophysica Acta*, 1400, pp. 139 – 154

BURNS, M.R, GRAMINSKI, G.F, WEEKS, R.S, CHEN, Y, and O'BRIEN, T.G., 2009. Lipophilic Lysine-Spermine Conjugates are Potent Polyamine Transport Inhibitors for Use in Combination with a Polyamine Biosynthesis Inhibitor. *Journal of Medicinal Chemistry*, 52, pp 1983 – 1993

BURZ, C, BERINDAN-NEAGOE, I, BELACESCU, O, and IRIMIE, A., 2009. Apoptosis in Cancer: Key Molecular Signaling Pathways and Therapy Targets. *Acta Oncologica*, 48, pp. 811 – 821

CAHUZAC, N, STUDÉNY, A, MARSHALL, K, VERSTEEGE, I, WETENHALL, K, PFEIFFER, B, *et al.*, 2010. An Unusual DNA Binding Compound, S23906, Induces Mitotic Catastrophe in Cultured Human Cells. *Cancer Letters*, 289, pp. 178 - 187

CAI, X, GRAY Jr, P.J, and Von HOFF, D.D., 2009. DNA Minor Groove Binders: Back in the Groove. *Cancer Treatment Reviews*, 35, pp. 437 - 450

CAIRNS, D, MICHALITSI, E, JENKINS, T.C, and MACKAY, S.P., 2002. Molecular Modelling and Cytotoxicity of Substituted Anthraquinones as Inhibitors of Human Telomerase. *Bioorganic and Medicinal Chemistry*, 10, pp. 803 – 807

CANCERBACKUP, 2008. *Risk Factors and Causes of Breast Cancer*. [online] Cancerbackup: Macmillan Cancer Support. Available from: http://www.cancerbackup.org.uk/Cancertype/Breast/Causesdiagnosis/Causes [Accessed 7 July 2009]

CANCER RESEARCH UK, 2004. *How Do Cells Become Cancerous?* [Online] London: Cancer Research UK. Available from: http://info.cancerresearchuk.org/cancerandresearch/learnaboutcancer/whatiscancer/howdocellsbecome/ [Accessed 29 March 2006]

CANCER RESEARCH UK, 2008. *Cell Cycle Analysis – Propidium Iodide*. [online] London: Cancer Research UK. Available from: http://science.cancerresearchuk.org/sci/facs/facs_major_apps/cell_cycle_analysis/propidium_iodide/?version=1 [Accessed 17 February 2010]

CANCER RESEARCH UK, 2009a. *UK Cancer Incidence Statistics for Common Cancers*. [online] London: Cancer Research UK. Available from: http://info.cancerresearchuk.org/cancerstats/incidence/commoncancers/ [Accessed 26 June 2009]

CANCER RESEARCH UK, 2009b. *CancerStats Key Facts on Cancer*. [online] London: Cancer Research UK. Available from: http://info.cancerresearchuk.org/cancerstats/keyfacts/?a=5441 [Accessed 26 June 2009]

CANCER RESEARCH UK, 2009c. *CancerStats Key Facts on Breast Cancer*. [online] London: Cancer Research UK. Available from: http://info.cancerresearchuk.org/cancerstats [Accessed 26 June 2009]

CANCER RESEARCH UK, 2009d. *UK Cancer Mortality Statistics for Common Cancers*. [online] London: Cancer Research UK. Available from: http://info.cancerresearchuk.org/cancerstats/mortality/cancerdeaths/ [Accessed 26 June 2009]

CANCER RESEARCH UK, 2009e. *Paget's Disease*. [online] London: Cancer Research UK. Available from: http://www.cancerhelp.org.uk/help/default.asp?page=5074 [Accessed 30 June 2009]

CANG, S, MA, Y, and LIU, D., 2009. New Clinical Developments in Histone Deacetylase Inhibitors for Epigenetic Therapy of Cancer. *Journal of Hematology and Oncology*, 2, pp. 22 – 33

CAO, X, WANG, A.H, JIAO, R.Z, WANG, C.L, MAO, D.Z, YAN, L, and ZENG, B., 2009. Surfactin Induces Apoptosis and G_2/M Arrest in Human Breast Cancer MCF-7 Cells Through Cell Cycle Factor Regulation. *Cell Biochemistry and Biophysics*, 55, pp. 163 – 171

CAREW, J.S, GILES, F.J, and NAWROCKI, S.T., 2008. Histone Deactylase Inhibitors: Mechanism of Cell Death and Promise in Combination Cancer Therapy. *Cancer Letters*, 269, pp. 7 - 17

CAREY, N, and LA THANGUE, N.B., 2006. Histone Deacteylase Inhibitors: Gathering Pace. *Current Opinion in Pharmacology*, 6, pp. 369 – 375

CASADO, A, ROSELL, R, GARCIA-GOMEZ, R, DIAZ-RUBIO, E, PEREZ-MANGA, G, FONT, A, BENEVIDAS, A, and MARTIN, M., 1996. Phase II Study of Mitonafide in Non-small Cell Lung Cancer (NSCLC). *Investigational New Drugs*, 14 (4), pp. 415 – 417

CASERO Jr, R.A, and MARTON, L.J., 2007. Targeting Polyamine Metabolism and Function in Cancer and Other Hyperproliferative Diseases. *Nature Reviews*, 6, pp. 373 - 390

CASERO, R.A, and WOSTER, P.M., 2001. Terminally Alkylated Polyamine Analogues as Chemotherapeutic Agents. *Journal of Medicinal Chemistry*, 44 (1), pp. 1 – 26

CASERO, R.A, and WOSTER, P.M., 2009. Recent Advances in the Development of Polyamine Analogues as Antitumor Agents. *Journal of Medicinal Chemistry*, 52, pp. 4551 – 4573

CHAKRABORTY, B, and CASU, S., 2009. Interaction of BSA with Proflavin: A Spectroscopic Approach. *Journal of Luminescence*, 129, pp. 34 – 39

CHAMOND, R.R, ANON, J.C, AGUILAR, C.M, and PASADAS, F.G., 1999. Apoptosis and Disease. *Algerol Immunology Clinical*, 14 (6), pp. 367 – 374

CHANG, S, McKINSEY, T.A, ZHANG, C.L, RICHARDSON, J.A, HILL, J.A, and OLSON, E.N., 2004. Histone Deacetylase 5 and 9 Govern responsiveness of the Heart to a Subset of Stress Signals and Play Redundant Roles in Heart Development. *Molecular and Cellular Biology*, 24 (19), pp. 8467 – 8476

CHAU, M, CHRISTENSEN, J.L, AJAMI, A.M, and CAPIZZI, R.L., 2008. Amonafide, a Topoisomerase II Inhibitor, is Unaffected by P-glycoprotein-mediated Efflux. *Leukemia Research*, 32 (2), pp. 465 – 473

CHEN, A.Y, YU, C, GATTO, B, and LIU, L.F., 1993. DNA Minor Groove-Binding Ligands: A Different Class of Mammalian DNA Topoisomerase I Inhibitors. *Proceedings of the National Academy of Sciences. USA*, 90, pp. 8131 – 8135

CHEN, P.C, PATIL, V, GUERRANT, W, GREEN, P, and OYELERE, A.K., 2008. Synthesis and Structure-activity Relationship of Histone Deacetylase (HDAC) Inhibitors with Triazole-linked Cap Group. *Bioorganic and Medicinal Chemistry*, 16, pp. 4839 – 4853

CHENG, H-L, MOSTOSLAVSKY, R, SAITO, S, MANIS, J.P, GU, Y, PATEL, P, BRONSON, R, APPELLA, E, ALT, F.W, and CHUA, K.F., 2003. Developmental Defects and p53 Hyperacetylation in Sir2 Homolog (SIRT1)-Deficient Mice. *Proceedings of the National Academy of Sciences*, 100 (19), pp. 10794 - 10799

CHIANG, A.C, and MASSAGUÉ, J., 2008. Molecular Basis of Metastasis. *The New England Journal of Medicine*, 359 (26), pp. 2814-2823

CHILDS, A.C, MEHTA, D.J, and GERNER, E.W., 2003. Polyamine-Dependent Gene Expression. *Cellular and Molecular Life Sciences*, 60, pp. 1394 - 1406

CHUANG, D-M, LENG, Y, MARINOVA, Z, KIM, H-J, and CHIU, C-T., 2009. Multiple Roles of HDAC Inhibition in Neurodegenerative Conditions. *Trends in Neurosciences*, 32 (11), pp. 591 – 601

CLARKE, J.D, DASHWOOD, R.H, and HO, E., 2008. Multi-targeted Prevention of Cancer by Sulforaphane. *Cancer Letters*, 269, pp. 291 – 304

COHEN-JONATHAN, E, BERNHARD, E.J, and McKENNA, W.G., 1999. How Does Radiation Kill Cells? *Current Opinion in Chemical Biology*, 3, pp. 77 – 83

COLLINS, A.R., 1996. DNA Damage and Repair. In: E.E. BITTAR and N BITTAR, eds. *Principles of Molecular Biology, Volume 5: Molecular and Cellular Genetics.* Greenwich: JAI Press. pp. 229 – 254

COOPER, G.M, and HAUSMAN, R.E., 2007. *The Cell A Molecular Approach*. 4th Edition. Washington D.C.: ASM Press

COURY, J.E, McFAIL-ISOM, L, WILIIAMS, L.D, and BOTTOMLEY, L.A., 1996. A Novel Assay for Drug-DNA Binding Mode, Affinity, and Exclusion Number: Scanning Force Microscopy. *Proceedings of the National Academy of Sciences. USA*, 93, pp. 12283 – 12286

CREAVEN, P.J, PEREZ, R, PENDYALA, L, MEROPOL, N.J, LOEWEN, G, LEVINE, E, BERGHORN, E, and RAGHAVEN, D., 1997. Unusual Central Nervous System Toxicity in

a Phase I Study of N^1, N^{11} diethylnorspermine in Patients with Advanced Malignancy. *Investigational New Drugs*, 15 (3), pp. 227 – 234

CRISS, W.E., 2003. A Review of Polyamines and Cancer. Perspectives in Medical Sciences. *Turkish Journal of Medical Science*, 33, pp. 195 – 205

CROUSER, E.D, GADD, M.E, JULIAN, M.W, HUFF, J.E, BROEKEMEIER, K.M, ROBBINS, K.A, and PFEIFFER, D.R., 2003. Quantitation of Cytochrome *c* Release from Rat Liver Mitochondria. *Analytical Biochemistry*, 317, pp. 67 - 75

CULLIS, P.M, GREEN, R.E, MERSON-DAVIS, L, and TRAVIS, N., 1999. Probing the Mechanism of Transport and Compartmentalisation of Polyamines in Mammalian Cells. *Chemistry and Biology*, 6, pp. 717 – 729

CUMMINGS, J, SPANSWICK, V.J, and SMYTH, J.F., 1995. Re-evaluation of the Molecular Pharmacology of Mitomycin C. *European Journal of Cancer*, 31A (12), pp. 1928 - 1933

CUMMINGS, J, WARD, T.H, RANSON, M, and DIVE, C., 2004. Apoptosis Pathway-Targeted Drugs – From the Bench to the Clinic. *Biochimica et Biophysica Acta*, 1705, pp. 53 – 66

D'AGOSTINI, F, IZZOTTI, A, BALANSKY, R.M, BENNICELLI, C, and De FLORA, S., 2005. Modulation of Apoptosis by Cancer Chemopreventive Agents. *Mutation Research*, 591, pp 173 – 186

DALE, J, and VON SCHANTZ, M., 2002. *From Genes to Genomes: Concepts and Applications of DNA Technology*. Chichester: John Wiley and Sons Ltd, pp. 144 - 148

DAMIA, G, and D'INCALCI, M., 2007. Targeting DNA Repair as a Promising Approach in Cancer Therapy. *European Journal of Cancer*, 43, pp. 1791 - 1801

DANCE, A-M, RALTON, L, FULLER, Z, MILNE, L, DUTHIE, S, BESTWICK, C.S and KONG THOO LIN., 2005. Synthesis and biological activities of bisnaphthalimido polyamines derivatives: cytotoxicity, DNA binding, DNA damage and drug localization in breast cancer MCF 7 cells. *Biochemical Pharmology*, 69, pp. 19 – 27

DAVIDSON, N.E, HAHM, H.A, McCLOSKEY, D.E, WOSTER, P.M, and CASERO, R.A. Jr., 1999. Clinical Aspects of Cell Death in Breast Cancer: The Polyamine Pathway as a New Target for Treatment. *Endocrine-Related Cancer*, 6, pp.69 – 73

DEBNATH, J, MUTHUSWAMY, S.K, and BRUGGE, J.S., 2003. Morphogenesis and Oncogenesis of MCF-10A Mammary Epithelial Acini Grown in Three-Dimensional Basement Membrane Cultures. *Methods*, 30, pp. 256 – 268

DEBRUIN, L.S, and JOSEPHY, P.D., 2002. Perspectives of the Chemical Etiology of Breast Cancer. *Environmental Health Perspectives*, 110 (1), pp. 119 - 128

DEEP, G, and AGARWAL, R., 2008. New Combination Therapies with Cell Cycle Agents. *Current Opinion of Investigational Drugs*, 9 (6), pp. 591 – 604

DEMEUNYNCK, M., 2004. Antitumour Acridines. *Expert Opinion on Therapeutic Patents*, 14 (1), pp. 55 – 70

DENNY, W.A., 2004. Emerging DNA Topoisomerase Inhibitors as Anticancer Drugs. *Oncologic, Endocrine and Metabolic*, 9 (1), pp. 105 – 133

DENU, J.M., 2005. The Sir2 Family of Protein Deacetylases. *Current Opinion in Chemical Biology*, 9, pp. 431 - 440

DENZIOT, F, and LANG, R, 1986. Rapid Colorimetric Assay for Cell Growth and Survival. *Journal of Immunological Methods*, 89, pp. 271 – 277

DO, D.P, PAI, S.B, RIZVI, S.A.A, D'SOUZA, M.J., 2009. Development of Sulforaphane-encapsulated Microspheres for Cancer Epigenetic Therapy. *International Journal of Pharmaceutics*, doi:10.1016/j.ijpharm.2009.11.009

DOYLE, M.L., 1997. Characterisation of Binding Interactions by Isothermal Titration Calorimetry. *Current Opinion in Biotechnology*, 8, pp. 31 – 35

DUTHIE, S.J. and COLLINS, A., 1997. The Influence of Cell Growth, Detoxifying Enzymes and DNA Repair on Hydrogen Peroxide-Mediated DNA Damage (measured using the Comet assay) in Human Cells. *Free Radical Biology & Medicine*, 22 (4), pp. 717-724

DUTHIE, S.J, and HAWDON, A., 1998. DNA Instability (Strand Breakage, Uracil Misincorporation, and Defective Repair) is Increased by Folic Acid Depletion in Human Lymphocytes *In Vitro*. *The Federation of American Societies for Experimental Biology Journal*, 12, pp. 1491 - 1497

DUTHIE, S.J., NARAYANAN, S., BLUM, S., PIRIE, L., and BRAND, G.M., 2000. Folate Deficiency *In Vitro* Induces Uracil Misincorporation and DNA Hypomethylation and Inhibits DNA Excision Repair in Immortalized Normal Human Colon Epithelial Cells. *Nutrition and Cancer*, 37 (2), pp. 245-251

EKELUND, S, NYGREN, P, and LARSSON, R., 2001. Guanidino-Containing Drugs in Cancer Chemotherapy: Biochemical and Clinical Pharmacology. *Biochemical Pharmacology*, 61, pp. 1183 – 1193

ENGLEKA, M., 2003. A Two-step Fluorometric Assay for Cellular Histone Deacetylase Activity. Application Note. Plymouth Meeting, PA: BIOMOL Research Laboratories Inc

EPPING, M.T, and BERNARDS, R., 2009. Molecular Basis of the Anti-Cancer Effects of Histone Deacetylase Inhibitors. *The International Journal of Biochemistry and Cell Biology*, 41, pp. 16 – 20

ESTELLER, M., 2008. Epigenetics in Cancer. *The New England Journal of Medicine*, 358, pp. 1148 - 1159

EVAN, G.I, and VOUSDEN, K.H., 2001. Proliferation, Cell Cycle and Apoptosis in Cancer. *Nature*, 411, pp. 342 – 348

FAIRBURN, D.W., OLIVE, P.L., and O'NEILL, K.L., 1995. The Comet Assay: A comprehensive review. *Mutation Research*, 339, pp. 37-59

FELTON, T, HARRIS, G.C, PINDER, S.E, SNEAD, D.R.J, CARTER, G.I, BELL, J.A, HAINES, A, KOLLIAS, J, ROBERTSON, J.F.R, ELSTON, C.W, and ELLIS, I.O., 2004. Identification of Carcinoma Cells in Peripheral Blood Samples of Patients with Advanced Breast Carcinoma using RT-PCR Amplification of CK7 and MUC1. *The Breast*, 13, pp. 35 – 41

FERGUSON, L.R, and DENNY, W.A., 2007. Genotoxicity of Non-Covalent Interactions: DNA Intercalators. *Mutation Research*, 623, pp. 14 – 23

FEUERSTEIN, B.G, PATTABIRAMAN, N, and MARTON, L.J., 1990. Molecular Mechanics of the Interactions of Spermine with DNA: DNA Bending as a Result of Ligand Binding. *Nucleic Acid Research*, 18 (5), pp. 1271 - 1282

FILOSA, R, PEDUTO, A, DI MICCO, S, DE CAPRARIIS, P, FESTA, M, PETRELLA, A, CAPRANICO, G, and BIFULCO, G., 2009. Molecular Modelling Studies, Synthesis and Biological Activity of a Series of Novel Bisnaphthalimides and Their Development as New DNA Topoisomerase II Inhibitors. *Bioorganic and Medicinal Chemistry*, 17, pp. 13 – 24

FINNIN, M.S, DONIGIAN, J.R, and PAVLETICH, N.P., 2001. Structure of the Histone Deacetylase SIRT2. *Nature Structural Biology*, 8 (7), pp. 621 – 625

FORTERRE, P, GRIBALDO, S, GADELLE, D, and SERRE, M-C., 2007. Origin and Evolution of DNA Topoisomerases. *Biochimie*, 89, pp 427 - 446

FORTUNE, J.M, and OSHEROFF, N., 2000. Topoisomerase II as a Target for Anticancer Drug: When Enzymes Stop Being Nice. *Progress in Nucleic Acid Research and Molecular Biology*, 64, pp. 221 -253

FOTAKIS, G, and TIMBRELL, J.A., 2006. In vitro Cytotoxicity Assays: Comparison of LDH, Neutral Red, MTT and Protein Assay in Hepatoma Cell Lines Following Exposure to Cadmium Chloride. *Biochemistry and Cell Biology*, 78, pp. 415 – 426

FREEMAN, W.M, WALKER, S.J, and VRANA, K.E., 1999. Quantitative RT-PCR: Pitfalls and Potential. *BioTechniques*, 26, pp. 112 - 125

FRIEDRICHS, K, HÖLZEL, F, and JÄNICKE, F., 2002. Combination of Taxanes and Anthracyclines in First-Line Chemotherapy of Metastatic Breast Cancer: An Interim Report. *European Journal of Cancer*, 38, pp. 1730 – 1738

FUCHS, B.C, and BODE, B.P., 2005. Amino Acid Transporters ASCT2 and LAT1 in Cancer: Partners in Crime? *Seminars in Cancer Biology*, 15, pp. 254 – 266

GABORIAU, F, HAVOUIS, R, MOULINOUX, J-P, and DELCROS, J-G., 2003. Atmospheric Pressure Chemical Ionization-Mass Spectrometry Method to Improve the Determination of Dansylated Polyamines. *Analytical Biochemistry*, 318, pp. 212 - 220

GABORIAU, F, KREDER, A, CLAVREUL, N, MOULINOUX, J-P, DELCROS, J-G, and LESCOAT, G., 2004. Polyamine Modulation of Iron Uptake in CHO Cells. *Biochemical Pharmacology*, 64, pp. 1629 – 1637

GAFORIO, J.J, SERRANO, M.J, ALGARRA, I, ORTEGA, E, and ALVAREZ De CIENFUEGOS, G., 2002. Phagocytosis of Apoptotic Cells Assessed by Flow Cytometry Using 7-Aminoactinomycin D. *Cytometry*, 49, pp. 8 - 11

GALLEGO, J, and REID, B.R., 1999. Solution Structure and Dynamics of a Complex between DNA and the Antitumor Bisnaphthalimide LU-79553: Intercalated Ring Flipping on the Millisecond Time Scale. *Biochemistry*, 38, pp. 15104 – 15115

GALLUZZI, L, ZAMZAMI, N, De La MOTTE ROUGE, T, LEMAIRE, C, BRENNER, C, and FROEMER, G., 2007. Methods for the Assessment of Mitochondrial Membrane Permeabilization in Apoptosis. *Apoptosis*, 12, pp. 803 – 813

GALLUZZI, L, AARONSON, S.A, ABRAMS, J., *et al.* 2009. Guidelines for the Use and Interpretation of Assays for Monitoring Cell Death in Higher Eukaryotes. *Cell Death and Differentiation*, 16, pp. 1093 – 1107

GANAPATHY, V, THANGARAJU, M, and PRASAD, P.D., 2009. Nutrient Transporters in Cancer: Relevance to Warburg Hypothesis and Beyond. *Pharmacology and Therapeutics*, 121, pp. 29 – 40

GARDNER, R.A, DELCROS, J-G, KONATE, F, BREITBEIL III, F, MARTIN, B, SIGMAN, M, HUANG, M, and PHANSTIEL IV, O., 2004. N^1-substituent effects in the selective

delivery of polyamine conjugates into cells containing active polyamine transporters, *Journal of Medicinal Chemistry*, 47, pp. 6055-6069

GARTEL, A.L, and TYNER, A.L., 2002. The Role of the Cyclin-dependent Kinase Inhibitor p21 in Apoptosis. *Molecular Cancer Therapeutics*, 1, pp. 639 – 649

GASCO, M, SHAMI, S, and CROOK, T., 2002. The p53 Pathway in Breast Cancer. *Breast Cancer Research*, 4, pp. 70 - 76

GAYMES, T.J, PADAU, R.A, PLA, M, ORR, S, OMIDVAR, N, CHOMIENNE, C, MUFTI, G.J, and RASSOOL, F.V., 2006. Histone Deacetylase Inhibitors (HDI) Cause DNA Damage in Leukemia Cells: A Mechanism for Leukemia-Specific HDI-Dependent Apoptosis? *Molecular Cancer Research*, 4 (8), pp. 563 - 573

GEALL, A.J, and BLAGBROUGH, I.S., 2000. Rapid and Sensitive Ethidium Bromide Fluorescence Quenching Assay of Polyamine Conjugate-DNA Interactions for the Analysis of Lipoplex Formation in Gene Therapy. *Journal of Pharmaceutical and Biomedical Analysis*, 22, pp. 849 - 859

GEDIK, C.M., EWEN, S.W.B., and COLLINS, A.R., 1992. Single-cell Gel Electrophoresis Applied to the Analysis of UV-C Damage and Its Repair in Human Cells. *International Journal of Radiation Biology*, 62 (3), pp, 313-320

GHANEM, L and STEINMAN, R., 2005. A Proapoptotic Function of p21 in Differentiating Granulocytes. *Leukemia Research*, 29, pp. 1315 - 1323

GLASER, K.B., 2007. HDAC Inhibitors: Clinical Update and Mechanism-based Potential. *Biochemical Pharmacology*, 74, pp. 659 – 671

GLIKMAN, P, MANNI, A, DEMERS, L, and BARTHOLOMEW, M., 1989. Polyamine Involvement in the Growth of Hormone-Responsive and –Resistant Human Breast Cancer Cells in Culture. *Cancer Research*, 49, pp. 1371 – 1376

GONZÁLEZ-BULNES, L and GALLEGO, J., 2009. Indirect Effects Modulating the Interaction between DNA and a Cytotoxic Bisnaphthalimide Reveal a Two-Step Binding Process. *Journal of American Chemical Society*, 131, pp. 7781 - 7791

GOODWIN, C.J, HOLT, S.J, DOWNES, S, and MARSHALL, N.J., 1995. Microculture Tetrazolium Assays: A Comparison between Two New Tetrazolium Salts, XTT and MTS. *Journal of Immunological Methods*, 179, pp. 95 – 103

GRAMINSKI, G.F, CARLSON, C.L, ZIEMER, J.R, CAI, F, VERMEULEN, N.M.J, VANDERWERF, S.M, and BURNS, M.R., 2002. Synthesis of Bis-Spermine Dimers that are Potent Polyamine Transport Inhibitors. *Bioorganic and Medicinal Chemistry*, 12, pp. 35 – 40

GRIFFITHS, A.J.F, WESSLER, S.R, LEWONTIN, R.C, and CARROLL, S.B., 2008. *Introduction to Genetic Analysis*. 9th Edition. New York: W.H. Freeman and Company

GRITL-LINDE, A, RUCH, J-V, and LINDE, A., 1995. Polyamine Depletion-Mediated Effects on Murine Odontogenesis are Dependent on Tooth Developmental Stage and Culture Conditions. *International Journal of Developmental Biology*, 39, pp. 383 - 393

GROSS, A, McDONNELL, J.M, and KORSMEYER, S.J., 1999. BCL-2 Family Members and the Mitochondria in Apoptosis. *Genes and Development*, 13, pp. 1899 - 1911

GUGLIUCCI, A., 2004. Polyamines as Clinical Laboratory Tools. *Clinica Chimica Acta*, 344, pp. 23 – 35

GUPTA, G.P, and MASSAGUÉ, J., 2006. Cancer Metastasis: Building a Framework. *Cell*, 127, pp. 679 – 695

HACKER, A, MARTON, L.J, SOBOLEWSKI, M, and CASERO, R.A., 2008. In Vitro and In Vivo Effects of the Conformationally Restricted Polyamine Analogue CGC-11047 on Small Cell and Non-Small Cell Lung Cancer Cells. *Cancer Chemotherapy and Pharmocology*, 63, pp. 45 – 53

HAGGARTY, S.J, KOELLER, K.M, WONG, J.C, GROZINGER, C.M, and SCHREIBER, S.L., 2003. Domain-selective Small-Molecule inhibitor of Histone Deacetylase 6 (HDAC6)-mediated Tubulin Deacetylation. *Proceedings of the National Academy of Sciences of the United States of America*, 100 (8), pp. 4389 – 4394

HAHM, H.A, ETTINGER, D.S, BOWLING, K, HOKER, B, LING CHEN, T, ZABELINA, Y, and CASERO, R.A. Jr., 2002. Phase I Study of N^1, N^{11}-Diethylnorspermine in Patients with Non-Small Cell Lung Cancer. *Clinical Cancer Research,* 8, pp. 684 – 690

HAIGIS, M.C, MOSTOSLAVSKY, R, HAIGIS, K.M, FAHIE, K, CHRISTODOULOU, D.C, MURPHY, A.J, *et al.*, 2006. SIRT4 Inhibits Glutamate Dehydrogenase and Opposes the Effects of Calorie Restriction in Pancreatic β Cells. *Cell*, 126, pp. 941 - 954

HALLIWELL, B, and ARUOMA, O.I., 1991. DNA Damage by Oxygen-Derived Species: Its Mechanism and Measurement in Mammalian Systems. *Federation of European Biochemical Societies Letters*, 281, pp 9 – 19

HANAHAN, D, and WEINBURG, R.A., 2000. The Hallmarks of Cancer. *Cell*, 100, pp. 57 – 70

HANDE, K.R., 1998. Etoposide: Four Decades of Development of a Topoisomerase II Inhibitor. *European Journal of Cancer*, 34 (10), pp. 1514 - 1521

HANNUN, Y.A., 1997. Apoptosis and the Dilemma of Cancer Chemotherapy. *Blood*, 89 (6), pp 1845 – 1853

HAUSCHILD, A, TREFZER, U, GARBE, C, KAEHLER, K.C, UGUREL, S, KIECKER, F, *et al.*, 2008. Multicenter Phase II Trial of the Histone Deacetylase Inhibitor Pyridylmethyl-N-{4-[2-aminophenyl)-carbamoyl]-benzyl}-carbamate in Pretreated Metastatic Melanoma. *Melanoma Research*, 18 (4), pp. 274 – 278

HEATON, M.A, and FLINTOFF, W.F., 1988. Methylglyoxal-bis(guanylhydrazone)-Resistant Chinese Hamster Ovary Cells: Genetic Evidence That More Than a Single Locus Controls Uptake. *Journal of Cellular Physiology*, 136, pp. 133 - 139

HECTOR, S, TUMMALA, R, KISIEL, N.D, DIEGELMAN, P, VUJCIC, S, CLARK, K, *et al.*, 2008. Polyamine Catabolism in Colorectal Cancer Cells following Treatment with Oxaliplatin, 5-Fluorouracil and N^1, N^{11} diethylnorspermine. *Cancer Chemotherapy and Pharmacology*, 62, pp. 517 – 527

HELTWEG, B, and JUNG, M., 2003. A Homogeneous Nonisotopic Histone Deacetylase Activity Assay. *Journal of Biomolecular Screening*, 8, pp. 89 - 95

HELTWEG, B, TRAPP, H, and JUNG, M., 2005. In Vitro Assays for the Determination of Histone Deacetylase Activity. *Methods*, 36, pp. 332 – 337

HELTWEG, B, GATBONTON, T, SCHULER, A.D, POSAKONY, J, LI, H, GOEHLE, S, KOLLIPARA, R, *et al.*, 2006. Antitumor Activity of a Small-Molecule Inhibitor of Human Silent Information Regulator 2 Enzymes. *Cancer Research*, 66 (8), pp. 4368 – 4377

HIRAO, M, POSAKONY, J, NELSON, M, HRUBY, H, JUNG, M, SIMON, J.A, and BEDALOV, A., 2003. Identification of Selective Inhibitors of NAD^+-dependent Deacetylases Using Phenotypic Screens in Yeast. *The Journal of Biological Chemistry*, 278 (26), pp. 52773 - 52782

HOBBS, C.A, PAUL, B.A, and GILMOUR, S.K., 2002. Deregulation of Polyamine Biosynthesis Alters Intrinsic Histone Acetyltransferase and Deacetylase Activities in Murine Skin and Tumors. *Cancer Research*, 62, pp. 67 - 74

HOEIJMAKERS, J.H.J., 2001. Genome Maintenance Mechanisms for Preventing Cancer. *Nature*, 411, pp. 366 – 374

HOFFMANN, K, BROSCH, G, LOIDL, P, and JUNG, M., 1999. A Non-isotopic Assay for Histone Deacetylase Activity. *Nucleic Acids Research*, 27 (9), pp. 2057 – 2058

HOLDENRIEDER, S, and STIEBER, P., 2004. Apoptotic Markers in Cancer. *Clinical Biochemistry*, 37 (7), pp. 605 – 617

HOLST, C.M, FRYDMAN, B, MARTON, L.J, and OREDSSON, S.M., 2006. Differential Polyamine Analogue Effects in Four Human Breast Cancer Cell Lines. *Toxicology*, 223, pp. 71 - 81

HOLST, C.M and OREDSSON, S.M., 2005. Comparison of Three Cytotoxicity Tests in the Evaluation of the Cytotoxicity of a Spermine Analogue on Human Breast Cancer Cell Lines. *Toxicology In Vitro*, 19, pp. 379 – 387

HONRADO, E, BENÍTEZ, J, and PALACIOS, J., 2006. Histopathology of BRCA1- and BRCA2-associated Breast Cancer. *Critical Reviews in Oncology/Hematology*, 59, pp. 27 – 39

HOSTETTER, A.A, CHAPMAN, E.G, and DeROSE, V.J., 2009. Rapid Cross-Linking of an RNA Internal Loop by the Anticancer Drug Cisplatin. *Journal of American Chemical Society*, 131, pp. 9250 – 9257

HOTZEL, C, MAROTTO, A, and PINDUR, U., 2002. Design, Synthesis, DNA-binding and Cytotoxicity Evaluation of New Potential Combilexines. *European Journal of Medicinal Chemistry*, 37, pp. 367 - 378

HOU, M-H, LIN, S-B, YUANN, J-M.P, LIN, W-C, WANG, A.H-J, and KAN, L-S., 2001. Effects of Polyamines on the Thermal Stability and Formation Kinetics of DNA Duplexes with Abnormal Structure. *Nucleic Acids Research*, 29 (24), pp. 5121 – 5128

HOWITZ, K.J, BITTERMAN, K.J, COHEN, H.Y, LAMMING, D.W, LAVU, S, WOOD, J.G, *et al.*, 2003. Small Molecule Activators of Sirtuins Extend *Saccharomyces cerevisiae* Lifespan. *Nature*, 425, pp. 191 - 196

HSIANG, Y-H, JIANG, J.B, and LIU, L.F., 1989. Topoisomerase II-Mediated DNA Cleavage by Amonafide and Its Structural Analogs. *Molecular Pharmacology*, 36, pp. 371 – 376

HU, S, FRANKE, R.M, FILIPSKI, K.K, HU, C, ORWICK, S.J, de BRUIJIN, E.A, *et al.*, 2008. Interaction of Imatinib with Human Organic Ion Carriers. *Clinical Cancer Research*, 14 (10), pp. 3141 - 3148

HU, W, and KAVANAUGH, J.J., 2003. Anticancer Therapy Targeting the Apoptotic Pathway. *The Lancet Oncology*, 4, pp 721 – 729

HUANG, Y, TAN, M, GOSINK, M, WANG, K.K.W, and SUN Y., 2002. Histone Deactylase 5 is not a p53 Target Gene, But its Overexpression Inhibits Tumor Cell Growth and Induces Apoptosis. *Cancer Research*, 62, pp. 2913 – 2922

HUANG, Y, HAGER, E.R, PHILLIPS, D.L, DUNN, V.R, HACKER, A, FRYDMAN, B, *et al.*, 2003. A Novel Polyamine Analog Inhibits Growth and Induces Apoptosis in Human Breast Cancer Cells. *Clinical Cancer Research*, 9, pp 2769 – 2777

HUANG, F, ZHAO, M, ZHANG, X, WANG, C, QIAN, K, KUO, R-Y, *et al.*, 2009. Synthesis, DNA Intercalation and 3D QSAR Analysis of *cis*-2,4,5-trisubstituted 1,3-dithiolanes as a Novel Class of Antitumour Agents. *Bioorganic and Medicinal Chemistry*, 17, pp. 6085 – 6095

HUSCHTSCHA, L.I., BARTIER, W.A., ANDERSSON ROSS, C.E., and TATTERSALL, M.H.N., 1996. Characteristics of Cancer Cell Death after Exposure to Cytotoxic Drugs *in vitro*. *British Journal of Cancer*, 73, pp. 54 – 60

IGNEY, F., and KRAMMER, P.H., 2002. Death and Anti-Death: Tumour Resistance to Apoptosis. *Nature Reviews*, 2, pp. 277 - 288

IM, J.Y, PARK, H, KANG, K.W, CHOI, W.S, and KIM, H.S., 2008. Modulation of Cell Cycles and Apoptosis in Apicidin in Estrogen Receptor (ER)-positive and-negative human breast cancer cells. *Chemico-Biological Interactions*, 172, pp. 235 - 244

ISOBE, I, YANAGISAWA, K, and MICHIKAWA, M., 2001. 3-(4, 5-Dimethylthiazol-2-yl)-2, 5-Diphenyltetrazolium Bromide (MTT) Causes Akt Phophorylation and Morphological Changes in Intracellular Organellae in Cultured Rat Astrocytes. *Journal of Neurochemstry*, 77, pp. 274 – 280

JANSON, V, and BEHNAM-MOTLAGH, P., 2008. Phase-Contrast Microscopy Studies of Early Cisplatin-Induced Morphological Changes of Malignant Mesothlioma Cells and the Correspondence to Induced Apoptosis. *Experimental Lung Research*, 34, pp. 49 – 67.

JIANG, W-J., 2008. Sirtuins: Novel Targets for Metabolic Disease in Drug Development. *Biochemical and Biophysical Research Communications*, 373, pp. 341 – 344

JIN, Z, and EL-DEIRY, W.S., 2005. Overview of Cell Death Signalling Pathways. *Cancer Biology and Therapy*, 4 (2), pp. 139 – 163

JIN, K.L, PAK, J.H, PARK, J-Y, CHOI, W.H, LEE, J-Y, KIM, J-H, NAM, J-H., 2008. Expression Profile of Histone Deacetylases 1, 2 and 3 in Ovarian Cancer Tissues. *Journal of Gynaecological Oncology*, 19 (3), pp. 185 - 190

JOHANSSON, V.M, OREDSSON, S.M, and ALM, K., 2008. Polyamine Depletion with Two Different Polyamine Analogues Causes DNA Damage in Human Breast Cancer Cell Lines. *DNA and Cell Biology*, 27 (9), pp. 1 – 9

JOHNSON, H.A, and THOMAS, N.R., 2002. Polyhydroxylated Azepanes as New Motifs for DNA Monor Groove Binding Agents. *Bioorganic and Medicinal Chemistry Letters*, 12, pp. 237 – 241

KABRA, P., LEE, H., LUBICH, W. and MARTON, L.J., 1986. Solid-phase extraction and determination of dansyl derivatives of unconjugated and acetylated polyamines by reverse-phase liquid chromatography: improved separation systems for polyamines in cerebrospinal fluid, urine and tissue. *Journal of Chromatography*, 380(1), pp. 19-32

KADAM, R.U, KIRAN, V.M, and ROY, N., 2006. Comparative Protein Modeling and Surface Analysis of Leishmania Sirtuin: A Potential Target for Antileishmanial Drug Discovery. *Bioorganic and Medicinal Chemistry Letters*, 16, pp. 6013 - 6018

KAMAL, A, RAMU, R, TEKUMALLA, V, RAMESH KHANNA, G.B, BARKUME, M.S, JUVEKAR, A.S, and ZINGDE, S.M., 2007. Synthesis, DNA Binding, and Cytotoxicity Studies of Pyrrolo[2,1-c][1,4]benzodiazepine-anthraquinone Conjugates. *Bioorganic and Medicinal Chemistry*, 15, pp. 6868 – 6875

KASTAN, M.B., 2008. DNA Damage Responses: Mechanisms and Roles in Human Disease. *Molecular Cancer Research*, 6 (4), pp. 517 – 524

KAUFMANN, S., 1989. Induction of Endonucleolytic DNA cleavage in Human Acute Myelogenous Leukemia Cells by Etoposide, Camptothecin, and Other Cytotoxic Anticancer Drugs: A Cautionary Note. *Cancer Research*, 49, pp 5870 - 5878

KAUR, N, DELCROS, J-G, MARTIN, B, and PHANSTIEL, IV, O., 2005. Synthesis and Biological Evaluation of Dihydromotuporamine Derivatives in Cells Containing Active Polyamine Transporters. *Journal of Medicinal Chemistry*, 48, pp 3832 – 3839

KAUR, N, DELCROS, J-G, IMRAN, J, KHALED, A, CHEHTANE, M, TSCHAMMER, N, *et al.*, 2008a. A Comparison of Chloroambucil- and Xylene-Containing Polyamines Leads to Improved Ligands for Accessing the Polyamine Transport System. *Journal of Medicinal Chemistry*, 51, pp. 1393 – 1401

KAUR, N, DELCROS, J-G, ARCHER, J, WEAGRAFF, N.Z, MARTIN, B, and PHANSTIEL IV, O., 2008b. Designing the Polyamine Pharmacophore: Influence of *N*-Substituents on the Transport Behavior of Polyamine Conjugates. *Journal of Medicinal Chemistry*, 51, pp. 2551 – 2560

KERR, J.F.R, WINTERFORD, C.M, and HARMAN, B.V., 1994. Apoptosis. Its Significance in Cancer and Cancer Therapy. *Cancer*, 73 (8), pp. 2013 – 2026

KEY, T.J, VERKASALO, P.K, and BANKS, E., 2001. Epidemiology of Breast Cancer. *The Lancet Oncology*, 2, pp. 133 - 140

KHUHAWAR, M.Y, and QURESHI, G.A., 2001. Polyamines as Cancer Markers: Applicable Separation Methods. Review. *Journal of Chromatography B*, 764, pp. 385 – 407

KIMURA, O, TSUKAGOSHI, K, and ENDO, T., 2009. Uptake of Phenoxyacetic Acid Derivatives into CaCO-2 Cells by the Moncaboxylic Acid Transporters. *Toxicology Letters*, 189, pp. 102 – 109

KIVIRANTA, P.H, LEPPÄNEN, J, KYRYLENKO, S, SALO, H.S, LAHTELA-KAKKONEN, M, TERVO, A.J, *et al.*, 2006. *N*, *N*'-Bisbenzylidenebenzene-1,4-diamines and *N*, *N*'-Bisbenzylidenenaphthalene-1,4-diamines as Sirtuin Type 2 (SIRT2) Inhibitors. *Journal of Medicinal Chemistry*, 49, pp. 7907 – 7911

KONG THOO LIN, P, DANCE, A-M, BESTWICK, C, and MILNE, L., 2003. The Biological Activities of New Polyamine Derivatives as Potential Therapeutic Agents. *Biochemical Society Transactions*, 31 (2), pp. 407 - 410

KONG THOO LIN, P, and PAVLOV, V.A., 2000. The Synthesis and In Vitro Cytotoxic Studies of Novel Bis-naphthalimidopropyl Polyamine Derivatives. *Bioorganic & Medicinal Chemistry Letters*, 10, pp. 1609 – 1612

KOUTSILIERIS, M, REYES-MORENO, C, CHOKI, I, SOURLA, A, DOILLON, C, and PAVLIDIS, N., 1999. Chemotherapy Cytotoxicity of Human MCF-7 and MDA-MB-231 Breast Cancer Cells is Altered by Osteoblast-Derived Growth Factors. *Molecular Medicine*, 5, pp. 86 – 97

KOZIKOWSKI, A.P, CHEN, Y, GAYSIN, A, CHEN, B, D'ANNIBALE, M.A, SUTO, C.M, and LANGLEY, B.C., 2007. Functional Differences in Epigenetics Modulators – Superiority of Mercaptoacetamide-Based Histone Deacetylase Inhibitors Relative to Hydroxamates in Cortical Neuronprotection Studies. *Journal of Medicinal Chemistry*, 50, pp. 3054 – 3061

KRISTENSEN, L.S, NIELSEN, H.M, and HANSEN, L.L., 2009. Epigenetics and Cancer Treatment. *European Journal of Pharmacology*, 625, pp. 131 - 142

KRYSKO, D.V, BERGHE, T.V, D'HERDE, K, and VANDENABEELE, P., 2008. Apoptosis and Necrosis: Detection, Discrimination and Phagocytosis. *Methods*, 44, pp. 205 - 221

KUKSA, V.A, PAVLOV, V.A, and KONG THOO LIN, P., 2002. Novel Oxa-Spermine Homologues: Synthesis and Cytotoxic Properties. *Bioorganic and Medicinal Chemistry*, 10, pp. 691 – 697

KUMARI, S, RASTOGI, R.P, SINGH, K.L, SINGH, S.P, and SINHA, R.P., 2008. DNA Damage: Detection Strategies. *EXCLI Journal*, 7, pp. 44 - 62

LACROIX, M, and LECLERCQ, G., 2004. Relevance of Breast Cancer Cell Lines as Models for Breast Tumours: An Update. *Breast Cancer Research and Development*, 83, pp. 249 - 289

LACROIX, M., 2006. Significance, detection and markers of disseminated breast cancer cells. *Endocrine Related Cancer*, 13, pp. 1033-1067

LANGDON, S.P (edited by)., 2004. Cancer Cell Culture, Methods and Protocols. *Humana Press Inc*, New Jersey

LARA, E, MAI, A, CALVANESE, V, ALTUCCI, L, LOPEZ-NIEVA, P, MARTINEZ-CHANTAR, M.L, *et al.*, 2009. Salermide, A Sirtuin Inhibitor with a Strong Cancer Specific Proapoptotic Effect. *Oncogene*, 28, pp. 781 - 791

LARQUÉ, E, SABATER-MOLINA, M, and ZAMORA, S., 2007. Biological Significance of Dietary Polyamines. *Nutrition*, 23, pp. 87 – 95

LARSEN, A.K, ESCARGUEIL, A.E, and SKLADANOWSKI, A., 2003. Catalytic Topoisomerase II Inhibitors in Cancer Therapy. *Pharmacology and Therapeutics*, 99, pp. 167 – 181

LAURIA, A, MONTALBANO, A, BARRAJA, P, DATTOLO, G, and ALMERICO, A-M., 2007. DNA Minor Groove Binders: An Overview on Molecular Modelling and QSAR Approaches. *Current Medicinal Chemistry*, 14 (20), pp. 2136 – 2160

LEE, S-K, KIM, H-N, KANG, Y-R, WOO LEE, C, KIM, H-M, CHO HAN, D, *et al.*, 2008. Obavatol Inhibits Colorectal Cancer Growth by Inhibiting Tumor Cell Proliferation and Inducing Apoptosis. *Bioorganic and Medicinal Chemistry*, 16, pp. 8397 – 8402

LEGUBE, G, and TROUCHE, D., 2003. Regulating Histone Acetyltransferases and Deacetylases. *EMBO Reports*, 4, pp. 944 - 947

LE PECQ, J-B, LE BRET, M, BARBET, J, and ROQUES, B., 1975. DNA Polyintercalating Drugs: DNA Binding of Diacridine Derivatives. *Proceedings of the Nathional Academy of Sciences of the United States of America*, 72 (8), pp. 2915 - 2919

LERMAN, L.S., 1961. Structural Considerations in the Interaction of DNA and Acridines. *Journal of Molecular Biology*, 3, pp. 18 – 30

LEURATTI, C, SINGH, R, LAGNEAU, C, FARMER, P.B, PLASTARAS, J.P, MARNETT, L.J, and SHUKER, D.E.G., 1998. Determination of Malondialdehyde-Induced DNA Damage in Human Tissues using an Immunoslot Blot Assay. *Carcinogenesis*, 19 (11), pp. 1919 - 1924

LEVÊQUE, J, FOUCHER, F, BANSARD, J-Y, HAVOUIS, R, GRALL, J-Y, and MOULINOUX, J-P., 2000. Polyamine Profiles in Tumor, Normal Tissue of the Homologous Breast, Blood, and Urine of Breast Cancer Sufferers. *Breast Cancer Research and Treatment*, 60, pp. 99 – 105

LI, Y, KAO, G.D, GARCIA, B.A, SHABANOWITZ, J, HUNT, D.F, QUIN, J, *et al.*, 2006. A Novel Histone Deacetylase Pathway Regulates Mitosis by Modulating Aurora B Kinase Activity. *Genes and Development*, 20, pp. 2566 – 2579

LIAO, W, McNUTT, M.A, and ZHU, W-G., 2009. The Comet Assay: A Sensitive Method for Detecting DNA Damage in Individual Cells. *Methods*, 48, pp. 46 – 53

LIN, K-L, SU, J-C, CHIEN, C-M, TSENG, C-H, CHEN, Y-L, CHANG, L-S, and LIN, S-R., 2010. Naphto[1,2-*b*]furan-4,5-dione Induces Apoptosis and S-phase Arrest of MDA-MB-231 Cells Through JNK and ERK Signalling Activation. *Toxicology In Vitro*, 24, pp. 61 – 70

LINDAHL, T., 1993. Instability and Decay of the Primary Structure of DNA. *Nature*, 362, pp. 709 - 715

LINDSAY, G.S, and WALLACE, H.M., 1999. Changes in Polyamine Catabolism in HL-60 Human Promyelogenous Leukaemic Cells in Response to Etoposide-Induced Apoptosis. *Biochemical Journal*, 337, pp. 83 – 87

LJUNGMAN, M., 2009. Targeting the DNA Damage Response in Cancer. *Chemical Reviews*, 109, pp. 2929 - 2950

LLOMBART, M, POVEDA, A, FORNER, E, FERNANDEZ-MARTOS, C, GASPER, C, MUNOZ, M, *et al.*, 1992. Phase I Study of Mitonafide in Solid Tumours. *Investigational New Drugs*, 10 (3), pp. 177 – 181

LOUDON, G.M., 2002a. Introduction to Spectroscopy: Infrared Spectroscopy and Mass Spectroscopy. In: G.M. LOUDON. *Organic Chemistry*. 4th Edition. Oxford: Oxford University Press. pp. 497 – 538

LOUDON, G.M., 2002b. Nuclear Magnetic Resonance Spectroscopy. In: G.M. LOUDON. *Organic Chemistry*. 4th Edition. Oxford: Oxford University Press. pp. 539 – 605

LOWE, S.W, and LIN, A.W., 2000. Apoptosis in Cancer. *Carcinogenesis*, 21 (3), pp 485 – 495

LUNDIN, C, NORTH, M, ERIXON, K, WALTERS, K, JENSSEN, D, GOLDMAN, A.S.H, HELLEDAY, T., 2005. Methyl Methanesulfonate (MMS) Produces Heat-Labile DNA Damage But No Detectable *In Vivo* DNA Double-Strand Breaks. *Nucleic Acids Research*, 33 (12), pp. 3799 – 3811

LUO, J, SOLIMINI, N.L, and ELLEDGE, S.J., 2009. Principles of Cancer Therapy: Oncogene and Non-Oncogene Addiction. *Cell*, 136, pp. 823 - 837

MACFARLANE, M., 2009. Cell Death Pathways – Potential Therapeutic Targets. *Xenobiotica*, 39 (8), 616 - 624

MAI, A, MASSA, S, LAVU, S, PEZZI, R, SIMEONI, S, RAGNO, R, *et al.*, 2005. Design, Synthesis, and Biological Evaluation of Sirtinol Analogies as Class III Histone/Protein Deacetylase (Sirtuin) Inhibitors. *Journal of Medicinal Chemistry*, 48, pp. 7789 - 7795

MAI, A, VALENTE, S, MEADE, S, CARAFA, V, TARDUGNO, M, NEBBIOSO, A, GALMOZZI, *et al.*, 2009. Study if 1,4-Dihydropyridine Structural Scaffold: Discovery of Novel Sirtuin Activators and Inhibitors. *Journal of Medicinal Chemistry*, 52, pp. 5496 - 5504

MALINGE, J-M, GIRUAD-PANIS, M-J, and LENG, M., 1999. Interstrand Cross-Links of Cisplatin Induce Striking Distortions in DNA. *Journal of Inorganic Biochemistry*, 77, pp. 23 - 29

MANDEL, J-L, and FLINTOFF, W.F., 1978. Isolation of Mutant Mammalian Cells Altered in Polyamine Transport. *Journal of Cellular Physiology*, 97 (3), pp. 335 – 344

MANN, B.S, JOHNSON, J.R, COHEN, M.H, JUSTICE, R, and PAZDUR, R., 2007. FDA Approval Summary: Vorinostat for Treatment of Advanced Primary Cutaneous T-Cell Lymphoma. *The Oncologist*, 12, 1247 – 1252

MANNI, A, WASHINGTON, S, GRIFFITH, J.W, VERDERAME, M.F, MAUGER, D, DEMERS, *et al.*, 2002. Influence of Polyamines on *In Vitro* and *In Vivo* Features of Aggressive and Metastatic Behavior by Human Breast Cancer Cells. *Clinical and Experimental Metastasis*, 19, pp. 95 – 105

MANSILLA, S, PRIEBE, W, and PORTUGAL, J., 2006. Mitotic Catastrophe Results in Cell Death by Caspase-Dependent and Caspase-Independent Mechanisms. *Cell Cycle*, 5 (1), pp. 53 - 60

MARCÉ, M., BROWN, D.S., CAPELL, T., FIGUERAS, X. and TIBURICO, A.F., 1995. Rapid high-performance liquid chromatographic method for the quantitation of polyamines as their dansyl derivatives: application to plant and animal tissues. *Journal of Chromatography B, Biomedical Applications*, 666(2), pp. 329-335

MARKS, P.A, RICHON, V.M, and RIFKIND, R.A., 2000. Histone Deacetylase Inhibitors: Inducers of Differentiation or Apoptosis of Transformed Cells. *Journal of the National Cancer Institute*, 92 (15), pp. 1210 – 1216

MARTINEZ, R, and CHACON-GARCIA, L., 2005. The Search of DNA-Intercalators as Antitumoral Drugs: What Worked and What Did Not Work. *Current Medicinal Chemistry*, 12, pp. 127 – 151

MAYR, C.A, SAMI, S.M, REMERS, W.A, and DORR, R.T., 1998. Identification and Characterisation of *In Vitro* Metabolites of 2-[2'-(Dimethylamino)Ethyl]-1,2-Dihydro-3H-Dibenz[De,H]Isoquinoline-1,3-Dione (Azonafide). *Drug Metabolism and Disposition*, 26 (2), pp. 105 – 109

McCONNAUGHIE, A.W, and JENKINS, T.C., 1995. Novel Acridine-Traiazenes as Prototype Combilexins: Synthesis, DNA Binding and Biological Activity. *Journal of Medicinal Chemistry*, 38, pp. 3488 – 3501

McHUGH, P.J, SPANSWICK, V.J, and HARTLEY, J.A., 2001. Repair of DNA Interstrand Crosslinks: Molecular Mechanisms and Clinical Relevance. *The Lancet Oncology*, 2, pp. 483 – 490

McNEIL, P.L, and STEINHARDT, R.A., 1997. Loss, Restoration, and Maintenance of Plasma Membrane Integrity. *The Journal of Cell Biology*, 137 (1), pp. 1 – 4

MEERAN, S.M, and KATIYAR, S.K., 2008. Cell Cycle Control as a Basis for Cancer Chemoprevention through Dietary Agents. *Frontiers in Bioscience*, 13, pp. 2191 – 2202

MEYSKENS, Jr, F.L, and GERNER, E.W., 1999. Developemnt of Difluoromethylornithine (DFMO) as a Chemoprevention Agent. *Clinical Cancer Research*, 5, pp. 945 – 951

MICHISHITA, E, McCORD, R.A, BERBER, E, KIOI, M, PADILLA-NASH, H, DAMIAN, M, *et al.*, 2008. SIRT6 is a Histone H3 Lysine 9 Deacetylase that Modulates Telomeric Chromatin. *Nature*, 452, pp. 492 – 497

MIKHAILENKO, V.M, PHILCHENKOV, A.A, and ZAVELEVICH, M.P., 2005. Analysis of ^{1}H NMR-detectable Mobile Lipid Domains for Assessment of Apoptosis Induced by Inhibitors of DNA Synthesis and Replication. *Cell Biology International*, 29, pp. 33 – 39

MILNE, J.C, LAMBERT, P.D, SCHENK, S, CARNEY, D.P, SMITH, J.J, GAGNE, D.J, *et al.*, 2007. Small Molecule Activators of SIRT1 as Therapeutics for the Treatment of Type 2 Diabetes. *Nature*, 450, pp. 712 – 716

MILNE, J.C, and DENU, J.M., 2008. The Sirtuin Family: Therapeutic Targets to Treat Diseases of Ageing. *Current Opinion in Chemical Biology*, 12, pp. 11 – 17

MILOVIC, V., 2001. Polyamine in the Gut Lumen: Bioavailability and Biodistribution. *European Journal of Gastroenterology and Hepatology*, 13, pp. 1021 - 1025

MILOVIC, V, FAUST, D, TURCHANOWA, L, STEIN, J, and CASPARY, W.F., 2001. Permeability Characteristics of Polyamines across Intestinal Epithelium Using the CaCO-2 Monolayer System: Comparison between Transepithelial Flux and Mitogen-Stimulated Uptake into Epithelial Cells. *Nutrition*, 17, pp.462 – 466

MINOTTI, G, MENNA, P, SALVATORELLI, E, CAIRO, G, and GIANNI, L., 2004. Anthracyclines: Molecular Advances and Pharmacologic Developments in Antitumour Activity and Cardiotoxicity. *Pharmacological Reviews*, 56, pp. 185 – 229

MINUCCI, S, and PELICCI, P.G., 2006. Histone Deacetylase Inhibitors and the Promise of Epigenetic (and more) Treatments for Cancer. *Nature*, 6, pp. 38 - 51

MITCHELL, J.L.A, THANE, T.K, SEQUEIRA, J.M, and THOKALA, R., 2007. Unusual Aspects of the Polyamine Transport System Affect the Design of Strategies for Use if Polyamine Analogues in Chemotherapy. *Biochemical Society Transactions*, 35 (2), pp. 318 – 321

MONTANER, B, CASTILLO-ÁVILA, W, MARTINELL, M, ÖLLINGER, R, AYMAMI, J, GIRALT, E, and PÉREZ-TOMÁS, R., 2005. DNA Interaction and Dual Topoisomerase I and II Inhibition Properties of the Anti-Tumor Drug Prodigiosin. *Toxicological Sciences*, 85, pp. 870 - 879

MONTECUCCO, A, and BIAMONTI, G., 2007. Cellular Response to Etoposide Treatment. *Cancer Letters*, 252, pp. 9 – 18

MONTGOMERY, R.L, DAVIS, C.A, POTTHOFF, M.J, HABERLAND, M, FIELITZ, J, QI, X, *et al.*, 2007. Histone Deacetylases 1 and 2 Redundantly Regulate Cardiac Morphogenesis, Growth and Contractility. *Genes and Development*, 21, pp. 1790 – 1802

MOSMANN, T., 1983. Rapid Colorimetric Assay for Cellular Growth and Survival: Application to Proliferation and Cytotoxicity Assays. *Journal of Immunological Methods*, 65, pp. 55 – 63

MUNNIA, A, SALETTA, F, ALLIONE, A, PIRO, S, CONFORTINI, M, MATULLO, G, and PELUSO, M., 2007. ^{32}P Post-Labelling Method Improvements for Aromatic Compound-Related Molecular Epidemiology Studies. *Mutabenesis*, 22 (6), pp. 381 – 385

NAKAYAMA, G.R, CATON, M.C, NOVA, M.P, and PARANDOOSH, Z., 1997. Assessment of the Alamar Blue Assay for Cellular Growth and Viability In Vitro. *Journal of Immunological Methods*, 204, pp. 205 – 208

NATIONAL CANCER INSTITUTE, 2006. *Inflammatory Breast Cancer: Questions and Answers*. [online] Bethesda, Maryland: U.S. National Institutes of Health. Available from: http://www.cancer.gov/cancertopics/factsheet/sites-types/ibc [Accessed 30 June 2009]

NELSON, H., HUFFMAN, L.H., FU, R., et al., 2005 (Sep 6). Genetic risk assessment and BRCA mutation testing for breast and ovarian cancer susceptibility: systematic evidence review for the U.S. Preventive Services Task Force. *Annals of Internal Medicine*, 143 (5), pp. 362 - 379

NITISS, J.L., 2009. Targeting DNA Topoisomerase II in Cancer Chemotherapy. *Nature Reviews Cancer*, 9 (5), pp. 338 350

NIU, Q-X, ZHAO, C-Y, and Jing, Z-A., 2001. An Evaluation of the Colourimetric Assays Based on Enzymatic Reactions Used in the Measurement of Human Natural Cytotoxicity. *Journal of Immunological Methods*, 251, pp. 11 – 19

NHS CHOICES UK, 2008. *Breast Cancer (female) Overview*. [online] London: NHS UK. Available from: http://www.nhs.uk/Conditions/Cancer-of-the-breast-female/Pages/Introduction.aspx [Accessed 30 June 2009]

NORTH, B.J, MARSHALL, B.L, BORRA, M.T, DENU, J.M, and VERDIN, E., 2003. The Human Sir2 Ortholog, SIRT2, is an NAD^+-Dependent Tubulin Deacetylase. *Molecular Cell*, 11, pp. 437 – 444

NORTH, B.J, and VERDIN, E., 2004. Sirtuins: Sir2-Related NAD-Dependent Protein Deacetylases. *Genome Biology*, 5, pp. 224 - 235

NYAGA, S.G, JARUGA, P, LOHANI, A, DIZDAROGLU, M, and EVANS, M.K., 2007. Accumulation of Oxidatively Induced DNA Damage in Human Breast Cancer Cell Lines Following Treatment with Hydrogen Peroxide. *Cell Cycle*, 6 (12), pp. 1472 - 1478

O'BRIEN, J, WILSON, I, ORTON, T, and POGNAN, F., 2000. Investigation of the Alamar Blue (Resazurin) Fluorescent Dye for the Assessment of Mammalian Cell Cytotoxicity. *European Journal of Biochemistry*, 267, pp 5421 – 5426

OCKER, M, and SCHNEIDER-STOCK, R., 2007. Histone Deacteylase Inhibitors: Signalling Towards $p21^{cip1/waf1}$. *The International Journal of Biochemistry and Cell Biology*, 39, pp. 1367 – 1374

OHTSUKI, A, KIMURA, M.T, MINOSHIMA, M, SUZUKI, T, IKEDA, M, BANDO, T, *et al.*, 2009. Synthesis and Properties of PI Polyamine-SAHA Conjugate. *Tetrahedron Letters*, 50, pp. 7288 – 7292

OLIVEIRA, J, RALTON, L, TAVARES, J, CODEIRO-DA-SILVA, A, BESTWICK, C. S, MACPHERSON, A, and KONG THOO LIN, P., 2007. The Synthesis and the *In Vitro* Cytotoxicity Studies of Bisnaphthalimidopropyl Polyamine Derivatives against Colon Cancer Cells and Parasite *Leishmania infantum*. *Bioorganic and Medicinal Chemistry*, 15 (1), pp. 541 – 545

ORMEROD, M.G., 1997. Analysis of Cell Proliferation Using the Bromodeoxyuridine/Hoechst-Ethidium Bromide Method. In: J.W. POLLARD and J.M. WALKER, eds. *Basic Cell Culture Protocols*. 2nd Edition. Totowa: Humana Press. pp. 357 – 366

O'SHAUGHNESSY, J.A, DEMERS, L.M, JONES, S.E, ARSENEAU, J, KHANDELWAL, P, GEORGE, T, *et al.*, 1999. α-Difluoromethylornithine as Treatment for Metastatic Breast Cancer Patients. *Clinical Cancer Research*, 5, pp. 3438 – 3444

OTT, I, XU, Y, LIU, J, KOKOSCHKA, M, HARLOS, M, SHELDRICK, W.S., and QIAN, X., 2008. Sulfur-Substituted Naphthalimides as Photoactivatable Anticancer Agents: DNA Interaction, Fluorescence Imaging, and Phototoxic Effects in Cultured Tumor Cells. *Bioorganic and Medicinal Chemistry*, 16, pp. 7107 – 7116

OUAISSI, M, SIELEZNEFF, I, SILVESTRE, R, SASTRE, B, BERNARD, J-P, LAFONTAINE, J.S, *et al.*, 2008. High Histone Deacetylase 7 (HDAC7) Expression is Significantly Associated with Adenocarcinomas of the Pancreas. *Annals of Surgical Oncology*, 15 (8), pp. 2318 – 2328

OUAMEUR, A.A, and TAJMIR-RIAHI, H-A., 2004. Structural Analysis of DNA Interactions with Biogenic Polyamine and Cobalt(III)hexamine Studied by Fourier Transform Infrared and Capillary Electrophoresis. *The Journal of Biological Chemistry*, 279 (40), pp. 42041 – 42054

OYELERE, A.K, CHEN, P.C, GUERRANT, W, MWAKWARI, S.C, HOOD, R, ZHANG, Y, and FAN, Y., 2009. Non-peptide Macrocyclic Histone Deacetylase Inhibitors. *Journal of Medicinal Chemistry*, 52, pp. 456 – 468

PACHOLEC, M, CHRUNYK, B, CUNNINGHAM, D, FLYNN, D, GRIFFITH, D, GRIFFOR, M, *et al.*, 2010. SRT1720, SRT2183, SRT1460, and Resveratrol are Not Direct Activators of SIRT1. *The Journal of Biological Chemistry*, doi/10.1074/jbc.M109.088682

PALCHAUDHURI, R, and HERGENROTHER, P.J., 2007. DNA as a Target for Anticancer Compounds: Methods to Determine the Mode of Binding and the Mechanism of Action. *Current Opinion in Biotechnology*, 18, pp. 497 – 503

PARIS, M, PORCELLONI, M, BINASCHI, M, and FATTORI, D., 2008. Histone Deacetylase Inhibitors: From Bench to Clinic. *Journal of Medicinal Chemistry*, 51 (6), pp. 1505 – 1529

PARK, M-T, and LEE, S-J., 2003. Cell Cycle and Cancer. *Journal of Biochemistry and Molecular Biology*, 36 (1), pp. 60 – 65

PARK, L.O, YOON, J.H, KIM, J.D, SEO, J.T, and BAE, S.N., 2004. Necrotic Cell Death of Ovarian Adenocarcinoma Caused by Seminal Plasma. *Gynecologic Oncology*, 93, pp. 671 – 679

PARK, S-H, WANG, X, LIU, R, LAM, K.S, and WEISS, R.H., 2008. High Throughput Screening of a Small Molecule One-bead-one-compound Combinatorial Library to identify Attenuators of p21 as Chemotherapy Sensitizers. *Cancer Biology and Therapy*, 7 (12), pp. 2015 - 2022

PATIL, V, GUERRANT, W, CHEN, P.C, GRYDER, B, BENICEWICZ, D.B, KHAN, S.I, *et al.*, 2010. Antimalarial and Antileishmanial Activities of Histone Deacetylase Inhibitors with Triazole-linked Cap Group. *Bioorganic and Medicinal Chemistry*, 18, pp. 415 – 425

PATRICK, G.L., 2009. *An Introduction to Medicinal Chemistry*. 4th Edition. New York: Oxford University Press

PATTERSON, S.D, SPAHR, C.S, DAUGAS, E, SUSIN, S.A, IRINOPOULOU, T, KOEHLER, C, and KROEMER, G., 2000. Mass Spectrometric Identification of Proteins Released from Mitochondria Undergoing Permeability Transition. *Cell Death and Differentiation*, 7, pp. 137 - 144

PAVLOV, V, KONG THOO LIN, P, and RODILLA, V., 2001. Cytotoxicity, DNA Binding and Localisation of Novel Bis-naphthalimidopropyl Polyamine Derivatives. *Chemico-Biological Interactions*, 137, pp. 15 – 24

PAVLOV, V, RODILLA, V, and KONG THOO LIN, P., 2002. Growth, Morphological and Biochemical Changes in Oxa-Spermine Derivative-Treated MCF-7 Human Breast Cancer Cells. *Life Sciences*, 71, pp. 1161 – 1173

PEGG, A.E, and McCANN, P.P., 1982. Polyamine Metabolism and Function. *AJP- Cell Physiology*, 243, C212 – C221

PEGG, A.E., 1988. Polyamine Metabolism and Its Importance in Neoplastic Growth and a Target for Chemotheraphy. *Cancer Research*, 48 (4), pp. 759 – 774

PEGG, A.E, WECHTER, R, PAKALA, R, and BERGERON, R.J., 1989. Effect of N^1, N^{12}-Bis (ethyl) spermine and Related Compounds on Growth and Polyamine Acetylation, Content, and Excretion in Human Colon Tumour Cells. *Journal of Biological Chemistry*, 264 (20), pp.11744 – 11749

PEIXOTO, P, ZEGHIDA, W, CARREZ, D, WU, D-T, WATTEZ, N, CROISY, A, *et al.*, 2009. Unusual Cellular Uptake of Cytotoxic 4-hydroxymethyl-3-aminoacridine. *European Journal of Medicinal Chemistry*, 44, pp. 4758 - 4763

PEÑA, C, ALFONSO, I, TOOTH, B, VOELCKER, N.H, and GOTOR, V., 2007. Synthesis and Stereoselective DNA Binding Abilities of New Optically Active Open-Chain Polyamines. *Journal of Organic Chemistry*, 72 (6), pp. 1924 – 1930

PIETENPOL, J.A, and STEWART, Z.A., 2002. Cell Cycle Checkpoint Signalling: Cell Cycle Arrest versus Apoptosis. *Toxicology*, 181-182, pp. 475 - 481

PIPERAKIS, S.M., 2009. Comet Assay: A Brief History. *Cell Biology and Toxicology*, 25, pp. 1 – 3

PIZARRO, A.M, and SADLER, P.J., 2009. Unusual DNA Binding Modes for Metal Anticancer Complexes. *Biochimie*, 91, pp. 1198 - 1211

PORTER, C.W, CAVANAUGH, P.F, Jr, STOLOWICH, N, GANIS, B, KELLY, E, and BERGERON, R.J., 1985. Biological Properties of N^4 and N^1, N^8-spermidine Derivatives in Cultured L1210 Leukaemia Cells. *Cancer Research*, 45 (5), pp. 2050 – 2057

PORTER, C.W, and BERGERON, R.J., 1988. Regulation of Polyamine Biosynthetic Activity by Spermidine and Spermine Analogs – A Novel Antiproliferative Strategy. *Advances in Experimental Medicine and Biology*, 250, pp. 677 - 690

PORTER, C.W, McMANIS, L, CASERO, R.A. Jr, and BERGERON, R.J., 1987. Relative Abilities of Bis(ethyl) Derivatives of Putrescine, Spermidine and Spermine to Regulate Polyamine Biosynthesis and Inhibit L1210 Leukaemia Cell Growth. *Cancer Research*, 47 (11), pp. 2821 – 2825

PORTUGAL, J, BATALLER, M, and MANSILLA, S., 2009. Cell Death Pathways in Response to Antitumor Therapy. *Tumori - Journal of Experimental and Clinical Oncology*, 95 (4), pp. 409 – 421

POULSEN, H.E, WEIMANN, A, and LOFT, S., 1999. Methods to Detect DNA Damage by Free Radicals: Relation to Exercise. *Proceedings of the Nutrition Society*, 58, pp. 1007 – 1014

POZZOLINI, M, SCARFI, S, BENATTI, U, and GIOVINE, M., 2003. Interference in MTT Cell Viability Assay in Activated Macrophage Cell Line. *Analytical Biochemistry*, 313, pp. 338 – 341

QIAN, D.Z, KACHHAP, S.K, COLLIS, S.J, VERHEUL, H.M.W, CARDUCCI, M.A, ATADJA, P, and PILI, R., 2006. Class II Histone Deacetylases are Associated with VHL-

Independent Regulation of Hypoxia-Inducible Factor 1α. *Cancer Research*, 66 (17), pp. 8814 – 8821

RAHMAN, M, LANE, A, SWINDELL, A, and BARTRAM, S., 2006. *Introduction to Flow Cytometry*. [online] Oxford: Serotec Ltd. Available from: http://www.abdserotec.com/uploads/Flow-Cytometry.pdf [Accessed 22 March 2010]

RALTON, L.D., 2006. *Novel polyamine based anticancer agents: Evaluation of the mode of action*. Unpublished PhD Thesis, The Robert Gordon University, Aberdeen

RALTON, L, BESTWICK, C.S and KONG THOO LIN, P., 2007. Polyamine Analogues and Derivatives as Potential Anticancer Agents. *Current Bioactive Compounds*. 3 (3), pp. 179 – 191

RALTON, L, BESTWICK, C.S, MILNE, L, DUTHIE, S, and KONG THOO LIN, P., 2009. Bisnaphthalimidopropyl Spermidine induces Apoptosis within Colon Carcinoma Cells. *Chemico-Biological Interactions*, 177, pp. 1 – 6

RAMALINGHAM, S.S, BELANI, C.P, RUEL, C, FRANKEL, P, GITLITZ, B, KOCZYWAS, M, *et al.*, 2009. Phase II Study of Belinostat (PXD101), A Histone Deacetylase Inhibitor, for Second Line Therapy of Advanced Malignant Pleural Mesothelioma. *Journal of Thoracic Oncology*, 4 (1), pp. 97 - 101

RAO, S.N., 1992. Modelling Drug-Nucleic Acid Interactions: An Exercise in Computer Graphics and Computational Chemistry. In: C.L PROPST and T.J PERUN, eds. *Nucleic Acid Targeted Drug Design*. New York: Marcel Dekker Inc

RAO, S, LOWE, M, HERLICZEK, T.W, and KEYOMARSI, K., 1998. Lovastatin Mediated G1 Arrest in Normal and Tumor Breast Cells is Through Inhibition of CDK2 Activity and Redistribution of p21 and p27, Independent of p53. *Oncogene*, 17, pp. 2393 – 2402

REDDY, V.K, VALASINAS, A, SARKAR, A, BASU, H.S, MARTON, L.J, and FRYDMAN, B., 1998. Conformationally Restricted Analogues of N^1, N^{11}-bisethylspermine: Synthesis and Growth Inhibitory Effects on Human Tumor Cell Lines. *Journal of Medicinal Chemistry*, 41, pp. 4723 – 4732

REMISZEWSKI, S.W, SAMBUCETTI, L.C, ATADJA, P, BAIR, K.W, CORNELL, W.D, GREEN, M.A, *et al.*, 2002. Inhibitors of Human Histone Deacetylase: Synthesis and Enzyme and Cellular Activity of Straight Chain Hydroxamates. *Journal of Medicinal Chemistry*, 45 (4), pp. 753 – 757

RICHERT, M.M, PHADKE, P.A, MATTERS, G, DIGIROLAMO, D.J, WASHINGTON, S, DEMERS, L.M, *et al.*, 2005. Metastasis of Hormone-Independent Breast Cancer to Lung and Bone is Decreased by α-Difluoromethylornithine Treatment. *Breast Cancer Research*, 7 (5), pp.819 – 827

RICHON, V.M, GARCIA-VARGAS, J, and HARDWICK, J.S., 2009. Development of Vorinostat: Current Applications and Future Perspectives for Cancer Therapy. *Cancer Letters*, 280, pp. 201 - 210

ROBSON, D, and VERMA, S., 2009. Anthracyclines in early-stage breast cancer: Is it the end of an era? *Oncologist*, [Epub ahead of print]

ROCCA, A, MINUCCI, S, TOSTI, G, CROCI, D, BALLARINI, M, NOLE, F, *et al.*, 2009. A Phase I-II Study of the Histone Deacetylase Inhibitor Valproic Acid Plus Chemoimmunotherapy in Patients with Advanced Melanoma. *British Journal of Cancer*, 100, pp. 28 – 26

ROCHEFORT, H, GLONDU, M, SAHLA, M.E, PLATET, N, and GARCIA, M., 2003. How to Target Estrogen Receptor-Negative Breast Cancer? *Endocrine-Related Cancer*, 10, pp. 261 - 266

ROEMMELE, R.C, and RAPOPORT, H., 1988. Removal of *N*-Arylsulfonyl Groups from Hydroxy α-Amino Acids. *Journal of Organic Chemistry*, 53, pp. 2367 – 2371

ROGERS, P.L, STARUSZKIEWICZ, W.F, and BENNER Jr, R.A., 2003. Gas Chromatographic Method for Putrescine and Cadaverine in Shrimp. *Journal of AOAC International*, 86 (6), pp. 1172 - 1178

ROLLINO, C, BORSA, S, BELLONE, G, PICCOLI, G, and EMANUELLI, G., 1995. False Positive Results with MTT Assay. *Journal of Immunological Methods*, 185, pp. 141 – 143

ROOS, A.A.G, WAKELIN, L.P.G, and HENDRY, S.J., 1985. Intracellular DNA Damage Produced by a Series of Diacridines. *Biochemical Journal*, 226, pp. 175 – 182

ROPERO, S, and ESTELLER, M., 2007. The Role of Histone Deacetylase (HDACs) in Human Cancer. *Molecular Oncology*, 1, pp. 19 – 25

ROSELL, R, CARLES, J, ABAD, A, RIBELLES, N, BARNADAS, A, BENAVIDES, A, and MARTIN, M., 1992. Phase I Study of Mitonafide in 120 Hours Continuous Infusion in Non-Small Cell Lung Cancer. *Investigational New Drugs*, 10 (3), pp. 171 – 175

RUSSELL, D.H, COMBEST, W.L, DUELL, E.A, STANISKI, M.A, ANDERSON, T.F, and VOORHEES, J.J., 1978. Glucocorticoid Inhibits Elevated Polyamine Biosynthesis in Psoriasis. *Journal of Investigative Dermatology*, 71, pp. 177 – 181

RUSSELL, D.H., 1983. Clinical Relevance of Polyamines. *Critical Reviews in Clinical Laboratory Sciences*, 18 (3), pp. 261 – 311

SAEZ, R, CRAIG, J.B, KUHN, J.G, WEISS, G.R, KOELLER, J, PHILLIPS, J, HAVLIN, K, HARMAN, G, HARDY, J, MELINK, T.J, SAROSY, G.A, and VON HOFF, D.D., 1989. Phase I Clinical Investigations of Amonafide. *Journal of Clinical Oncology*, 7 (9), pp. 1351 – 1358

SAJI, S, KAWAKAMI, M, HAYASHI, S-I, YOSHIDA, N, HIROSE, M, HORIGUCHI, S-I, *et al.*, 2005. Significance of HDAC6 Regulation Via Estrogen Signaling for Cell Motility and Prognosis in Estrogen Receptor-Positive Breast Cancer. *Oncogene*, 24, pp. 4531 – 4539

SALAMI, S, and KARAMI-TEHRANI, F., 2003. Biochemical Studies of Apoptosis Induced By Tamoxifen in Estrogen Receptor Positive and Negative Breast Cancer Cell Lines. *Clinical Biochemistry*, 36, pp. 247 - 253

SAMI, S.M, DORR, R.T, ALBERTS, D.S, and REMERS, W.A., 1993. 2-Substituted 1, 2-Dihydro-3H-dibenz [de.h] isoquinoline-1, 3-diones. A New Class of Antitumour Agents. *Journal of Medicinal Chemistry*, 36, pp. 765 – 770

SANDERSON, B.J.S., and SHIELD, A.J., 1996. Mutagenic Damage to Mammalian Cells by Therapeutic Alkylating Agents. *Mutation Research*, 355, pp. 41 – 57

SAUNDERS, L.R, and VERDIN, E., 2006. Ornithine Decarboxylase Activity in Tumor Cell Lines Correlates with Sensitivity to Cell Death Induced by Histone Deacetylase Inhibitors. *Molecular Cancer Therapeutics*, 5 (11), pp. 2777 - 2785

SCHEMIES, J, SIPPL, W, and JUNG, M., 2009. Histone Deacetylase Inhibitors that Target Tubulin. *Cancer Letters*, 280 (2), pp. 222 – 232

SCHLICKER, C, GERTZ, M, PAPATHEODOROU, P, KACHHOLZ, B, BECKER, C.F.W, and STEEGBORN, C., 2008. Substrates and Regulation Mechanisms for the Human Mitochondrial Sirtuins Sirt3 and Sirt5. *Journal of Molecular Biology*, 382, pp. 790 – 801

SCHMIDT, M.T, SMITH, B.C, JACKSON, M.D, and DENU, J.M., 2004. Coenzyme Specificity of Sir2 Protein Deacetylases. *The Journal of Biological Chemistry*, 279 (38), pp. 40122 - 40129

SCHRUMP, D.S, FISCHETTE, M.R, NGUYEN, D.M, ZHAO, M, LI, X, KUNST, T.F, HANCOX, A, *et al.*, 2008. Clinical and Molecular Responses in Lung Cancer Patients Receiving Romidepsin. *Clinical Cancer Research*, 14 (1), pp. 188 – 198

SCHUETZ, A, MIN, J, ANTOSHENKO, T, WANG, C-L, ALLALI-HASSANI, A, DONG, A, LOPPNAU, P, *et al.*, 2007. Structural Basis of Inhibition of the Human NAD^+-Dependent Deacetylase SIRT5 by Suramin. *Structure*, 15, pp. 377 – 389

SCHULTZ, D.R, and HARRINGTON Jr, W.J., 2003. Apoptosis: Programmed Cell Death at a Molecular Level. *Seminars in Arthritis and Rheumatism*, 32 (6), pp. 345 – 369

SCHWARTZMAN, R.A, and CIDLOWSKI, J.A., 1993. Apoptosis: The Biochemistry and Molecular Biology of Programmed Cell Death. *Endocrine Reviews*, 14 (2), pp. 133 – 151

SCOVASSI, A.I., 2006. Apoptosis and Cell Death. In: A. TORRIGLIA, and P. CRISANTI-LASSIAZ, eds. *Apoptosis in the Retina*. Kerala: Transworld Research Network. pp. 1 – 11

SEATON, A, HIGGINS, C, MANN, J, BARON, A, BAILLY, C, NEIDLE, S, van den BERG, H., 2003. Mechanistic and Anti-Proliferative Studies of Two Novel, Biologically Active *Bis*-benzimidazoles. *European Journal of Cancer*, 39, pp. 2548 – 2555

SEILER, N., 1977. Assay Procedures for Polyamines in Urine, Serum, and Cerebrospinal Fluid. *Clinical Chemistry*, 23 (9), pp 1519 – 1528

SEILER, N, SARHAN, S, GRAUFFEL, C, JONES, R, KNÖDGEN, B, and MOULINOUX, J-P., 1990. Endogenous and Exogenous Polyamines in Support of Tumor Growth. *Cancer Research*, 50, pp. 5077 - 5083

SEILER, N, DELCROS, J.-G and MOULINOUX, J., 1996. Polyamine Transport and Cytotoxicity inMammalian Cell. An Update. *International Journal of Biochemistry and Cell Biology*, 28, pp.843 – 861

SEILER, N, ATANASSOV, C.L, and RAUL, F., 1998. Polyamine Metabolism as a Target for Cancer Chemoprevention (Review). *International Journal of Oncology*, 13 (5), pp. 993 – 1006

SEILER, N., 2000. Oxidation of Polyamines and Brain Injury. *Neurochemical Research*, 25 (4), pp. 471 – 490

SEILER, N., 2005. Pharmacological Aspects of Cytotoxic Polyamine Analogs and Derivatives for Cancer Therapy. *Pharmacology and Therapeutics*, 107, pp. 99 – 119

SEKIHASHI, K., SAITOH, H., SAGA, A., HORI, K., NAKAGAWA, M., MIYAGAWA, M. and SASAKI, Y.F., 2003. Effect of In Vitro Exposure Time on Comet Assay Results. *Environmental Mutagen Research*, 25, pp. 83-86

SHU, C-H, YANG, W.K, SHIH, Y-L, KUO, M-L, and HUANG, T-S., 1997. Cell Cycle G2/M Arrest and Activation of Cyclin-dependent Kinases Associated with Low-dose Paclitaxel-induced Sub-G1 Apoptosis. *Apoptosis*, 2, pp. 463 – 470

SHINJI, C, NAKAMURA, T, MAEDA, S, YOSHIDA, M, HASHIMOTO, Y, and MIYACHI, H., 2005. Design and Synthesis of Phthalimide-type Histone Deacetylase Inhibitors. *Bioorganic and Medicinal Chemistry*, 15, pp. 4427 - 4431

SINGH, N, McCOY, M, TICE, R, and SCHNEIDER, E., 1988. A Simple Technique for Quantitation of Low Levels of DNA Damage in Individual Cells. *Experimental Cell Research*, 175 (1), pp. 184-191

SIUZDAK, G., 1996. Ion Sources and Sample Introduction. In: G. SIUZDAK. *Mass Spectrometry for Biotechnology*. La Jolla: Academic Press.

SMITH, M.A, and DAVIES, P.J., 1985. Separation and Quantitation of Polyamines in Plant Tissue by High Performance Liquid Chromatography of Their Dansyl Derivatives. *Plant Physiology*, 78, pp. 89 – 91

SMITH, K.T, and WORKMAN, J.L., 2009. Histone Deacetylase Inhibitors: Anticancer Compounds. *The International Journal of Biochemistry and Cell Biology*, 41, pp. 21 – 25

SOLDATENKOV, V.A, PRASAD, S, VOLOSHIN, Y, and DRITSCHILO, A., 1998. Sodium Butyrate Induces Apoptosis and Accumulation of Ubiquitinated Proteins in Human Breast Carcinoma Cells. *Cell Death and Differentiation*, 5, pp. 307 – 312

SNYDER, R.D., 2007. Assessment of Atypical DNA Intercalating Agents in Biological and *In Silico* Systems. *Mutation Research*, 623, pp. 72 – 82

SOLDATENKOV, V.A, PRASAD, S, VOLOSHIN, Y, and DRITSCHILO, A., 1998. Sodium Butyrate Induces Apoptosis and Accumulation of Ubiquitinated Proteins in Human Breast Carcinoma Cells. *Cell Death and Differentiation*, 5, pp. 307 – 312

SOLOMON, J.M, PASUPULETI, R, XU, L, McDONAGH, T, CURTIS, R, DISTEFANO, P.S, and HUBER, L.J., 2006. Inhibition of SIRT1 Catalytic Activity Increases p53 Acetylation by Does Not Alter Cell Survival Following DNA Damage. *Molecular and Cellular Biology*, 26 (1), pp. 28 - 38

SON, I.H, CHUNG, I-M, LEE, S.I, YANG, H.D, and MOON, H-I., 2007. Pomiferin, Histone Deacetylase Inhibitor Isolated from the Fruits of *Maclura pomifera*. *Bioorganic and Medicinal Chemistry*, 17, pp. 4753 – 4755

SOULE, H.D, MALONEY, T.M, WOLMAN, S.R, PETERSON Jr, W.D, BRENZ, R, McGRATH, C.M, RUSSO, J, PAULEY, R.J, JONES, R.F, and BROOKS, S.C., 1990. Isolation and Characterisation of a Spontaneously Immortilised Human Breast Epithelial Cell Line, MCF-10. *Cancer Research*, 50, pp. 6075 – 6086

SPIELMANN, H.P, WEMMER, D.E, and JACOBSEN, J.P., 1995. Solution Structure of A DNA Complex with the Fluorescent Bis-Intercalator TOTO Determined by NMR Spectroscopy. *Biochemistry*, 34, pp. 8542 – 8553

STARCEVIC, S.L, DIOTTE, N.M, ZUKOWSKI, K.L, CAMERON, M.J, and NOVAK, R.F., 2003. Oxidative DNA Damage and Repair in a Cell Lineage Model of Human Proliferative Breast Disease (PBD). *Toxicological Sciences*, 75, pp. 74 – 81

STAVROS, A.T, THICKMAN, D, RAPP, C.L, DENNIS, M.A, PARKER, S.H, and SISNEY, G.A., 1995. Solid Breast Nodules: Use of Sonography to Distinguish between Benign and Malignant Lesions. *Radiology*, 196, pp. 123 – 134

STEELE, N.L, PLUMB, J.A, VIDAL, L, TJØRNELUND, J, KNOBLAUCH, P, RASMUSSEN, A, *et al.*., 2008. A Phase I Pharmacokinetic and Pharmacodynamic Study of the Histone Deacetylase Inhibitor Belinostat in Patients with Advanced Solid Tumors. *Clinical Cancer Research*, 14 (3), pp. 804 – 810

STIMSON, L, and La THANGUE, N.B., 2009. Biomarkers for Predicting Clinical Responses to HDAC inhibitors. *Cancer Letters*, 280, pp. 177 - 183

STREKOWSKI, L, and WILSON, B., 2007. Noncovalent Interactions with DNA: An Overview. *Mutation Research*, 623, 3 – 13

STREIFF, R.R, and BENDER, J.F., 2001. Phase I Study of N^1, N^{11} Diethylnorspermine (DENSpm) Administered TID for 6 Days in Patients with Advanced Malignancies. *Investigational New Drugs*, 19 (1), pp. 29 – 31

SU, G.H, SOHN, T.A, RYU, B, and KERN, S.E., 2000. A Novel Histone Deacetylase Inhibitor Identified by High-Throughput Transcriptional Screening of a Compound Library. *Cancer Research*, 60, pp. 3137 – 3142

SUH, D, and CHAIRES, J.B., 1995. Criteria for the Mode of Binding of DNA Binding Agents. *Bioorganic and Medicinal Chemistry*, 3 (6), pp. 723 – 728

SWANTON, C., 2004. Cell-cycle Targeted Therapies. *The Lancet Oncology*, 5, pp. 27 - 36

SWIFT, L.P, REPHAELI, A, NIEDELMAN, A, PHILIPS, D.R, and CUTTS, S.M., 2006. Doxorubicin-DNA Adducts Induce a Non-Topoisomerase II-Mediated Form of Cell Death. *Cancer Research*, 66, pp. 4863 - 4871

TABOR, C.W, and TABOR, H., 1985. Polyamines in Microorganisms. *Microbiological Reviews,* 49 (1), pp. 81 – 99

TAN, J-H, LU, Y-J, HUANG, Z-S, GU, L-Q, and WU, J-Y., 2007. Spectroscopic Studies of DNA Binding Modes of Cation-Substituted Anthrapyrazoles Derived from Emodin. *European Journal of Medicinal Chemistry*, 42, pp. 1169 - 1175

TANNER, K.G, LANDRY, J, STERNGLANZ, R, and DENU, J.M., 2000. Silent Information Regulator 2 Family of NAD-dependent Histone/Protein Deacetylases Generates a Unique Product, 1-*O*-acetyl-ADP-ribose. *Proceedings of the National Academy of Sciences*, 97 (26), pp. 14178 - 14182

TAVARES, J, OUAISSI, A, KONG THOO LIN, P, LOUREIRO, I, KAUR, S, ROY, N, and CORDEIRO-DA-SILVA, A., 2010, Bisnaphthalimidopropyl Derivatives as Inhibitors of *Leishmania* SIR2 Related Protein 1. *ChemMedChem*, 5, pp. 140 – 147

TAYLOR, D.M, MAXWELL, M.M, LUTHI-CARTER, R, and KAZANTSEV, A.G., 2008. Biological and Potential Therapeutic Roles of Sirtuin Deacetylases. *Cellular and Molecular Life Sciences*, 65, pp. 4000 – 4018

TETI, D, VISALLI, M, and McNAIR, H., 2002. Analysis of Polyamines as Markers of (Patho)Physiological Conditions. *Journal of Chromatography B*, 781, pp. 107 - 149

THOMAS G., 2000. Medicinal Chemistry. An Introduction. Chicester: John Wiley and Sons, pp. 405

THOMAS, T, and THOMAS, T.J., 2001. Polyamines in Cell Growth and Cell Death: Molecular Mechanisms and Therapeutic Applications. Review. *Cellular and Molecular Life Sciences*, *CMLS*, 58, pp. 244 – 258

TIAN, Z-Y, XIE, S-Q, DU, Y-W, MA, Y-F, ZHAO, J, GAO, W-Y, and WANG, C-J., 2009. Synthesis, Cytotoxicity and Apoptosis of Naphthalimide Polyamine Conjugates as Antitumor Agents. *European Journal of Medicinal Chemistry*, 44, pp. 393 – 399

TICE, R.R, AGURELL, E, ANDERSON, D, BURLINSON, B, HARTMANN, A, KOBAYASHI, H, *et al.*, 2000. Single Cell Gel/Comet Assay: Guidelines for *In Vitro* and *In Vivo* genetic toxicology testing. *Environmental and Molecular Mutagenesis*, 35, pp. 206-221

TONG, M, DING, Y, TAI, H-H., 2006. Histone Deacetylase Inhibitors and Transforming Growth Factor-β Induce 15-hydroxyprostaglandin Dehydrogenase Expression in Human Lung Adenocarcinoma Cells. *Biochemical Pharmacology*, 72, pp.701 – 709

TSEN, C, ILTIS, M, KAUR, N, BAYER, C, DELCROS, J-G, von KALM, L, PHANSTIEL IV, O., 2008. A *Drosophila* Model to Identify Polyamine-Drug Conjugates that Target the Polyamine Transporter in an Intact Epithelium. *Journal of Medicinal Chemistry*, 51, pp. 324 - 330

TWENTYMAN, P.R, and LUSCOMBE, M., 1987. A Study of Some Variables in a Tetrazolium Dye (MTT) Based Assay for Cell Growth and Chemosensitivity. *British Journal of Cancer*, 56 (3), pp. 279 - 285

VALDIVIESO-GARCIA, A, CLARKE, R.C, RAHN, K, DURETTE, A, MacLEOD, D.L, and GYLES, C.L., 1993. Neutral Red Assay for Measurement of Quantitative Vero Cell Cytotoxicity. *Applied and Environmental Microbiology*, 59 (6), pp. 1981 – 1983

VAN ENGELAND, M, RAMAEKERS, F.C.S, SCHUTTE, B, and REUTELINGSPERGER, C.P.M., 1996. A Novel Assay to Measure Loss of Plasma Membrane Asymmetry during Apoptosis of Adherent Cells in Culture. *Cytometry*, 24, pp. 131 – 139

VANNINI, A, VOLPARI, C, FILOCAMO, G, CASAVOLA, E.C, BRUNETTI, M, RENZONI, D, CHAKRAVARTY, P, PAOLINI, C, DE FRANCESCO, R, GALLINARI, P, STEINKÜHLER, C, and DI MARCO, S., 2004. Crystal Structure of a Eukaryotic Zinc-dependent Histone Deacetylase, Human HDAC8, Complexed with a Hydroxamic Acid Inhibitor. *Proceedings of the National Academy of Sciences*, 101 (42), pp. 15064 - 15069

VARGHESE, S, SENANAYAKE, T, MURRAY-STEWART, T, DOERING, K, FRASER, A, CASERO Jr, R.A, and WOSTER, P.M., 2008. Polyaminohydroxamic Acids and Polyaminobenzamides as Isoform Selective Histone Deacetylase Inhibitors. *Journal of Medicinal Chemistry*, 51, pp. 2447 – 2456

VAZIRI, H, DESSAIN, S.K, EATON, E.N, IMAI, S-I, FRYE, R.A, PANDITA, T.K, GUARENTE, L, and WEINBERG, R.A., 2001. *hSIR2*^{SIRT1} Functions as an NAD-Dependent p53 Deacetylase. *Cell*, 107, pp. 149 – 159

VERMES, I, HAANEN, C, STEFFENS-NAKKEN, H, and REUTELINGSPERGER, C., 1995. A Novel Assay for Apoptosis Flow Cytometric Detection of Phosphatidylserine Expression on Early Apoptotic Cells Using Fluorescein Labelled Annexin V. *Journal of Immunological Methods*, 184, pp. 39 - 51

VERMES, I, HAANEN, C, and REUTELINGSPERGER, C., 2000. Flow Cytometry of Apoptotic Cell Death. *Journal of Immunological Methods*, 243, pp. 167 – 190

VIJG, J., 2007. *Ageing of the Genome. The Dual Role of DNA in Life and Death*. Oxford: Oxford University Press

VILLALONA-CALERO, M.A, EDER, J.P, TOPPMEYER, D.L, ALLEN, L.F, FRAM, R, VELAGAPUDI, R, *et al.*, 2001. Phase I and Pharmacokinetic Study of LU79553, a DNA Intercalating Bisnaphthalimide, in Patients with Solid Malignancies. *Journal of Clinical Oncology*, 19 (3), pp. 857 – 869

VISTICA, D.T, SKEHAN, P, SCUDIERO, D, MONKS, A, PITTMAN, A, and BOYD, M.R., 1991. Tetrazolium-based Assays for Cellular Viability: A Critical Examination of Selected Parameters Affecting Formazan Production. *Cancer Research*, 51, pp. 2515 – 2520

VON HOFF, D.D., 1994. MGBG: Teaching an old Drug New Tricks. *Annals of Oncology*, 5, pp. 487 – 493

WAHAB, S.I.A, ABDUL, A.B, ALZUBAIRI, A.S, ELHASSAN, M.M, and MOHAN, S., 2009. In Vitro Ultramorphological Assessment of Apoptosis Induced by Zerumbone on (HeLa). *Hindawi Publishing Corporation*, doi: 10.1155/2009/769568

WALLACE, H.M., 1996. Polyamines in Human Health. *Proceedings of the Nutrition Society*, 55 (1B), pp. 419 – 431

WALLACE, H.M., 2007. Targeting Polyamine Metabolism: A Viable Therapeutic/Preventative Solution for Cancer? *Expert Opinion on Pharmacotherapy. Review*, 8 (13), pp. 2109 - 2116

WALLACE, H.M, and CASLAKE, R., 2001. Polyamines and Colon Cancer. *European Journal of Gastroenterology and Hepatology*, 13 (9), pp. 1033 – 1039

WALLACE, H.M, DUTHIE, J, EVANS, D.M, LAMOND, S, NICOLL, K.M, and HEYS, S.D., 2000. Alterations in Polyamine Catabolic Enzymes in Human Breast Cancer Tissue. *Clinical Cancer Research*, 6, pp. 3657 - 3661

WALLACE, H.M, and FRASER, A.V., 2003. Polyamine Analogues as Anticancer Drugs. *Biochemical Society Transactions*, 31 (2), pp. 393 – 396

WALTREGNY, D, GLÉNISSON, W, TRAN, S.L, NORTH, B.J, VERDIN, E, COLIGE, A, and CASTRONOVO, 2005. HDAC8 Associates with Smooth Muscle Cell Contractility. *FASEB Journal*, 19, pp. 966 - 968

WANG, C, DELCROS, J-G, BIGGERSTAFF, J, PHANSTIEL IV, O., 2003a. Synthesis and Biological Evaluation of N^1-(Anthracen-9-ylmethyl) triamines as Molecular Recognition Elements for the Polyamine Transporter, *Journal of Medicinal Chemistry*, 46, pp. 2663-2671

WANG, C, DELCROS, J-G, BIGGERSTAFF, J, and PHANSTIEL IV, O., 2003b. Molecular Requirements for Targeting the Polyamine Transport System: Synthesis and Biological Evaluation of Polyamine Anthracene Conjugates, *Journal of Medicinal Chemistry*, 46, pp. 2672-2682

WANG, C, DELCROS, J-G, CANNON, L, KONATE, F, CARIAS, H, BIGGERSTAFF, J, GARDNER, R.A, and PHANSTIEL IV, O., 2003c. Defining the Molecular Requirements for the Selective Delivery of Polyamine Conjugates into Cells Containing Active Polyamine Transporters, *Journal of Medicinal Chemistry*, 46, pp. 5129-5138

WANG, Y.A, JOHNSON, S.K, BROWN, B.L, McCARRAGHER, L.M, AL-SAKKAF, K, ROYDS, J.A, and DOBSON, P.R.M., 2008. Enhanced Anti-cancer Effect of a Phosphatidylinositol-3 Kinase Inhibitor and Doxorubicin on Human Breast Epithelial Cell Lines with Different p53 and Oestrogen Receptor Status. *International Journal of Cancer*, 123, pp. 1536 - 1544

WANG, L, PRICE, H.L, JUUSOLA, J, KLINE, M, and PHANSTIEL IV, O., 2001. The Influence of Polyamine Architecture on the Transport and Topoisomerase II Inhibitory Properties of Polyamine DNA-Intercalator Conjugates. *Journal of Medicinal Chemistry*, 44, pp. 3682 - 3691

WARING, M.J, GONZALEZ, A, JIMENEZ, A, and VASQUEZ, D., 1979. Intercalative Binding of DNA derived from 3-nitro-1, 8-naphthalic acid. *Nucleic Acid Research*, 7 (1), pp. 217 – 230

WEEKS, R.S, VANDERWERF, S.M, CARLSON, C.L, BURNS, M.R, O'DAY, C.L, CAI, F, *et al.*, 2000. Novel Lysine-Spermine Conjugate Inhibits Polyamine Transport and Inhibits Cell Growth when given with DFMO. *Experimental Cell Research*, 261, pp. 293 – 302

WEGENER, D, HILDMANN, C, and SCHWIENHORST, A., 2003. Recent Progress in the Development of Assays Suited for Histone Deacetylase Inhibitor Screening. *Molecular Genetics and Metabolism*, 80, pp. 138 – 147

WESTPHAL, C.H, DIPP, M.A, and GUARENTE, L., 2007. A Therapeutic Role for Sirtuins in Diseases of Ageing? *Trends in Biochemical Sciences*, 32 (12), pp. 555 - 560

WIDAKOWICH, C, de AZAMBUJA, E, GIL, T, CARDOSO, F, DINH, P, AWADA, A, and PICCART-GEBHART, M., 2007. Molecular Targeted Therapies in Breast Cancer: Where Are We Now? *The International Journal of Biochemistry & Cell Biology*, 39, pp. 1375 – 1387

WINKLER, J, SAADAT, K, DIAZ-GAVILAN, M, URBAN, E, and NOE, C.R., 2009. Oligonucleotide-Polyamine Conjugates: Influence of Length and Position of 2'-Attached Polyamines on Duplex Stability and Antisense Effect. *European Journal of Medicinal Chemistry*, 44, pp. 670 – 677

WITT, O, DEUBZER, H.E, MILDE, T, OEHME, I., 2009. HDAC Family: What are the Cancer Relevant Targets? *Cancer Letters*, 277, pp. 8 - 21

WOLFF, A.C, ARMSTRONG, D.K, FETTING, J.H, CARDUCCI, M.K, RILEY, C.D, BENDER, J.F, *et al.*, 2003. A Phase II Study of the Polyamine Analog N^1, N^{11}-Diethylnorspermine (DENSpm) Daily for Five Days Every 21 Days in Patients with Previously Treated Metastatic Breast Cancer. *Clinical Cancer Research*, 9, pp. 5922 – 5928

World Cancer Research Fund-UK, 2010. *Reducing Your Risk of Breast Cancer*. [online] London: WCRF-UK. Available from: http://www.wcrf-uk.org/research/types_of_cancer/breast_cancer.php [Accessed 16 March 2010]

XIE, L, XU, Y, WANG, F, LIU, J, QIAN, X, and CUI, J., 2009. Synthesis of New Amonafide Analogues Via Coupling Reaction and Their Cytotoxic Evaluation and DNA-Binding Studies. *Bioorganic and Medicinal Chemistry*, 17, pp. 804 – 810

YAMAGUCHI, Y, and HAYASHI, S-I., 2009. Estrogen-Related Cancer Microenviroment of Breast Carcinoma. *Endocrine Journal*, 56 (1), pp. 1 - 7

YANG, X, and LIPPMAN, M.E., 1999. BRCA1 and BRCA2 in Breast Cancer. *Breast Cancer Research and Treatment*, 54, pp. 1 – 10

YANG, P, YANG, Q, and QIAN, X., 2005. Novel DNA Bis-Intercalators of Isoquinolino[4,5-*bc*]acridines: Design, Synthesis and Evaluation of Cytotoxic Activity. *Tetrahedron*, 61, pp. 11895 - 11901

YANG, Q, YANG, P, QIAN, X, and TONG, L., 2008. Naphthalimide Intercalators with Chiral Amino Side Chains: Effects of Chirality on DNA Binding, Photodamage and Antitumor Cytotoxicity. *Bioorganic and Medicinal Chemistry*, 18, pp. 6210 – 6213

YOSHIDA, M, KIJIMA, M, AKITA, M, and BEPPU, T., 1990. Potent and Specific Inhibition of Mammalian Histone Deacetylase Both *in Vivo* and *in Vitro* by Trichostatin A. *The Journal of Biological Chemistry*, 265 (5), pp. 17174 – 17179

ZHANG, Y, NA, L, CARON, C, MATTHIAS, G, HESS, D, KHOCHBIN, S, and MATTHIAS, P., 2003. HDAC-6 Interacts with and Deacetylates Tubulin and Microtubules *in vivo*. *The EMBO Journal*, 22 (5), pp. 1168 – 1179

ZHANG, Y, AU, Q, ZHANG, M, BARBER, J.R, CHUNG NG, S, and ZHANG, B., 2009. Identification of a Small Molecule SIRT2 Inhibitor with Selective Tumor Cytotoxicity. *Biochemical and Biophysical Research Communications*, 386, pp. 729 -733

ZHIVOTOVSKY, B, and ORRENIUS, S., 2010. Cell Death Mechanisms: Cross-Talk and Role in Disease. *Experimental Cell Research*, doi: 10.1016/j.yexcr.2010.02.037

ZIENTEK-TARGOSZ, H, KUNNEV, D, HAWTHORN, L, VENKOV, M, MATSUI, S-I, CHENEY, R.T, and IONOV, Y., 2008. Transformation of MCF-10A Cells by Random Mutagenesis with Frameshift Mutagen ICR191: A Model for Identifying Candidate Breast-Tumor Suppressors. *Molecular Cancer*, 7, pp. 51 – 63

Public Output

European Journal of Medicinal Chemistry 45 (2010) 1430–1437

Contents lists available at ScienceDirect

European Journal of Medicinal Chemistry

journal homepage: http://www.elsevier.com/locate/ejmech

Original article

Synthesis, cytotoxicity and DNA-binding of novel bisnaphthalimidopropyl derivatives in breast cancer MDA-MB-231 cells

Gemma A Barron [a], Giovanna Bermano [b], Amanda Gordon [a], Paul Kong Thoo Lin [a,*]

[a] School of Pharmacy and Life Sciences, The Robert Gordon University, St. Andrew Street, Aberdeen, AB25 1HG, Scotland, UK
[b] Centre of Obesity Research and Epidemiology (CORE), Faculty of Health and Social Care, The Robert Gordon University, St. Andrew Street, Aberdeen, AB25 1HG, Scotland, UK

ARTICLE INFO

Article history:
Received 2 August 2009
Received in revised form
7 December 2009
Accepted 18 December 2009
Available online 28 December 2009

Keywords:
Bisnaphthalimides
Synthesis
Cytotoxicity
DNA-binding
Uptake
Anticancer[1]

ABSTRACT

New naphthalimidopropyl, bisphthalimidopropyl and bisnaphthalimidopropyl (BNIP) derivatives were synthesised and characterised. Their interactions with *Calf Thymus* DNA were studied by UV spectrophotometric analysis and a competitive Ethidium bromide displacement assay. Cytotoxicity was determined by MTT assay in a breast cell system (MDA-MB-231 and MCF-10A cells). All BNIPs exhibited strong DNA-binding properties and cytotoxic activity with IC_{50} values in the range of 0.83–12.68 μM (24 and 48 h treatment). In addition, the uptake of BNIP derivatives within cancer cells was not via utilisation of the MGBG polyamine transporter. Put together the results confirm that the presence of the bisnaphthalimidopropyl and alkyl linker functionality are crucial for exerting DNA-binding and cytotoxic properties, hence demonstrating promise in their further development as potential anti cancer agents.

1. Introduction

DNA-binding compounds, such as, the cytotoxic DNA-intercalating compounds, naphthalimides and bisnaphthalimides have been shown to exert potential anti cancer activity [1–3]. However these compounds tend to be insoluble in aqueous solutions, thus making their testing difficult [4]. For a number of years, we have been designing and synthesising bisnaphthalimidopropyl derivatives (BNIPs) linked to natural polyamines [5] and to a selection of diamino and triamino alkyl chains, which resulted in enhanced aqueous solubility, without compromising their biological activity against a panel of cancer cell lines [6–8]. Furthermore, Bisnaphthalimidopropyl spermidine (BNIPSpd) (Fig. 1), the most active member of the BNIP series was shown to cause cell death by apoptosis, deplete polyamine pools in drug treated cells, and also induce oxidative DNA damage at a non toxic concentration [8,9]. In addition to our current research, Filosa et al. [10] have recently reported the synthesis and biological activity of a number of bisnaphthalimido derivatives containing heterocycles and other cyclic moieties, such as, piperazine, cis-dimethylpiperazine, diazabicyclo [3.2.1] octane and cyclopropane. These compounds exhibited *in vitro* cytotoxicity with IC_{50} values ranging from 0.04 to 6.1 μM after 72 h treatment in human colon carcinoma HT-29 cells [10].

Here, we report the synthesis of a selection of new derivatives: bisnaphthalimidopropyl diamino alkylamines (BNIPDahex, BNIPDadodec, BNIPDaoxoct, BNIPDaCHM), bisphthalimidopropyl diaminodecane (BPHPDadec) and mononaphthalimidopropylamine (NPA) (Fig. 2). The rationale for synthesising these analogues (Fig. 2) was to demonstrate that the bisnaphthalimido moiety is essential for biological activity. For example, in BPHPdadec, the naphthalimido rings had been replaced by phthalimido rings, and in NPA, only one naphthalimido ring was present. Furthermore oxygen atoms or cyclohexane rings were also introduced into the linker chain to determine whether the biological activity of these derivatives would be affected, bearing in mind that earlier work demonstrated that the length of the linker chain was important for enhanced solubility and effective biological activity [7]. The DNA-binding affinity was studied using UV and fluorescence spectroscopy, and cytotoxicity against human breast MDA-MB-231 and

Abbreviations: BNIPPut, Bisnaphthlimidopropyl putrescine; BNIPDahex, Bisnaphthalimidopropyl diaminohexane; BNIPDaoct, Bisnaphthalimidopropyl diaminooctane; BNIPDadec, Bisnaphthalimidopropyl diaminodecane; BNIPDadodec, Bisnaphthalimidopropyl diaminododecane; BNIPDaoxoct, Bisnaphthalimidopropyl diaminooxaoctane; BNIPDaCHM, Bisnaphthalimidopropyl diaminodicyclohexylmethane; DMF, Dimethylformamide; DMSO, Dimethylsulfoxide; MTT, 3-(4,5-dimethylthiazol-2-yl)-2,5-diphenyltetrazolium bromide; T_m, midpoint of thermal denaturation.

* Corresponding author. Tel.: +44 1224 262818; fax: +44 1224 262828.
E-mail address: p.kong@rgu.ac.uk (P. Kong Thoo Lin).

0223-5234/$ – see front matter © 2009 Elsevier Masson SAS. All rights reserved.
doi:10.1016/j.ejmech.2009.12.047

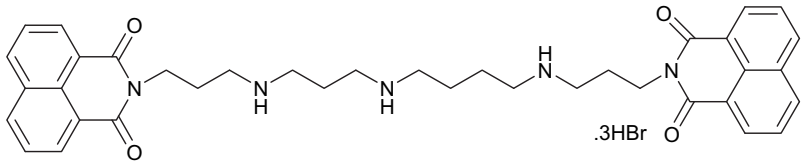

Fig. 1. Structure of bisnaphthalimidopropyl spermidine (BNIPSpd).

MCF-10A cells was evaluated with the MTT assay. The results were compared with previously synthesised analogues: BNIPSpd, BNIPPut, BNIPDaoct and BNIPDadec [5,7,9]. By using fluorescence microscopy and exploiting the inherent fluorescent properties of these derivatives, BNIPSpm and BNIPSpd were found to be located within human breast carcinoma MCF-7 cells after 6 h drug exposure [9]. In this paper, we have extended these studies to assess the relationship between uptake times and cytotoxicity of BNIPSpd, BNIPDaoct, BNIPDaoxoct and BNIPDaCHM (10 μM) in MDA-MB-231 cells. Furthermore, we have also for the first time determined whether these BNIP derivatives enter cells via the polyamine transport system (PAT) [11]. Chinese hamster ovary (CHO) cells and a PAT deficient mutant cell line (CHO-MG) were used to assess the selective transport of these BNIP derivatives via the PAT system [12–16].

2. Results and discussion

2.1. Chemistry

The synthetic strategy (Scheme 1A) adopted to synthesise the bisnapthalimidopropyl diamino analogues; BNIPDahex, BNIPDadodec, BNIPDaoxoct and BNIPDaCHM was based on methods previously developed [5,7,9]. The common starting material in the synthesis of BNIPDahex, BNIPDadodec, BNIPDaoxoct and BNIPDaCHM was toluenesulfonyloxypropylnaphthalimide, **2**, which was prepared from *N*-(3-hydroxypropyl) naphthalimide, **1**. Protection and activation of the alkyldiamines was carried out with mesitylenesulfonyl chloride in pyridine at room temperature to give compounds **3**–**6** in high yield. For the synthesis of the fully protected BNIP derivatives, N-alkylation with toluenesulfonyloxypropylnaphthalimide, **2**, in the presence of caesium carbonate in anhydrous DMF yielded fully protected BNIP derivatives which upon deprotection with hydrobromic acid/glacial acetic acid in CH_2Cl_2 gave BNIPDahex, BNIPDadodec, BNIPDaoxoct and BNIPDaCHM, as their corresponding dihydrobromide salts. To synthesise naphthalimidopropylamine (NPA) (Scheme 1A), nucleophilic substitution of the *O*-tosyl group from **2** was achieved with potassium phthalimide. Treatment with hydrazine hydrate gave the corresponding amine that was converted to its hydrochloric salt, NPA. BPHPDadec was synthesised by treating dimesitylenediaminodecane, **7**, with *N*-(3-bromopropyl) phthalimide in DMF in the presence of caesium carbonate (Scheme 1B). Subsequent deprotection with hydrobromic acid/glacial gave BPHPDadec. All derivatives studied exhibited good solubility (50% DMSO/water) at 10 mM concentration and were stored at 0–5 °C.

2.2. Biological activities

2.2.1. DNA-binding properties

The midpoint of thermal denaturation (T_m) of *Calf Thymus* DNA duplexes in the presence of the synthesised BNIP derivatives was

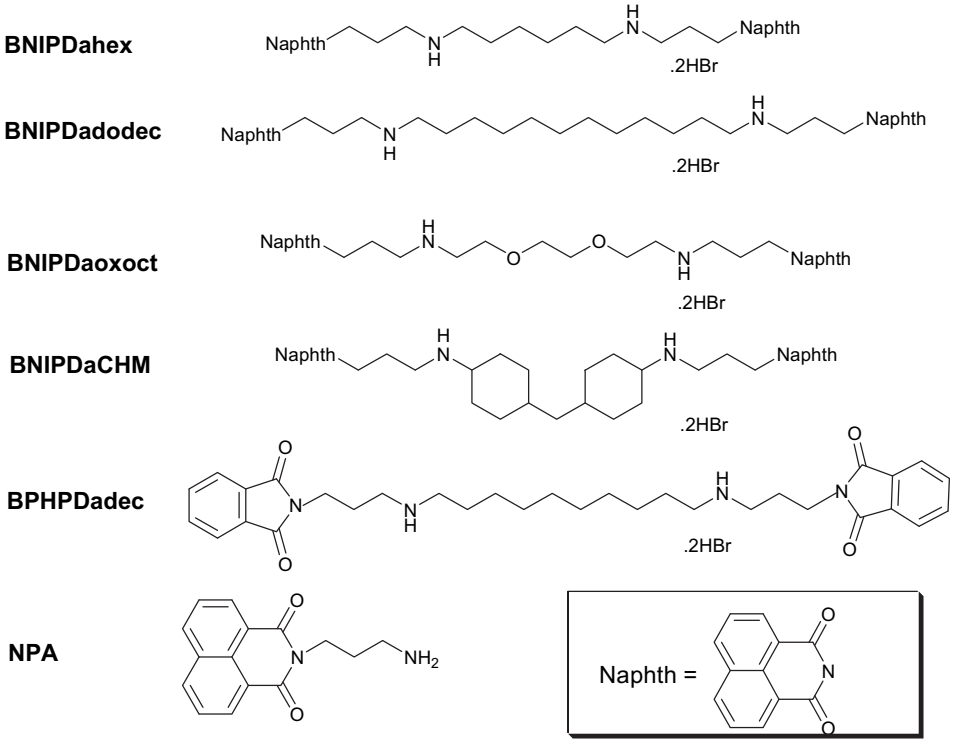

Fig. 2. Structures of the new bisnaphthalimidopropylalkyl-diamine, bisphthalimidopropyl diaminodecane and mononaphthalimidopropylamine derivatives.

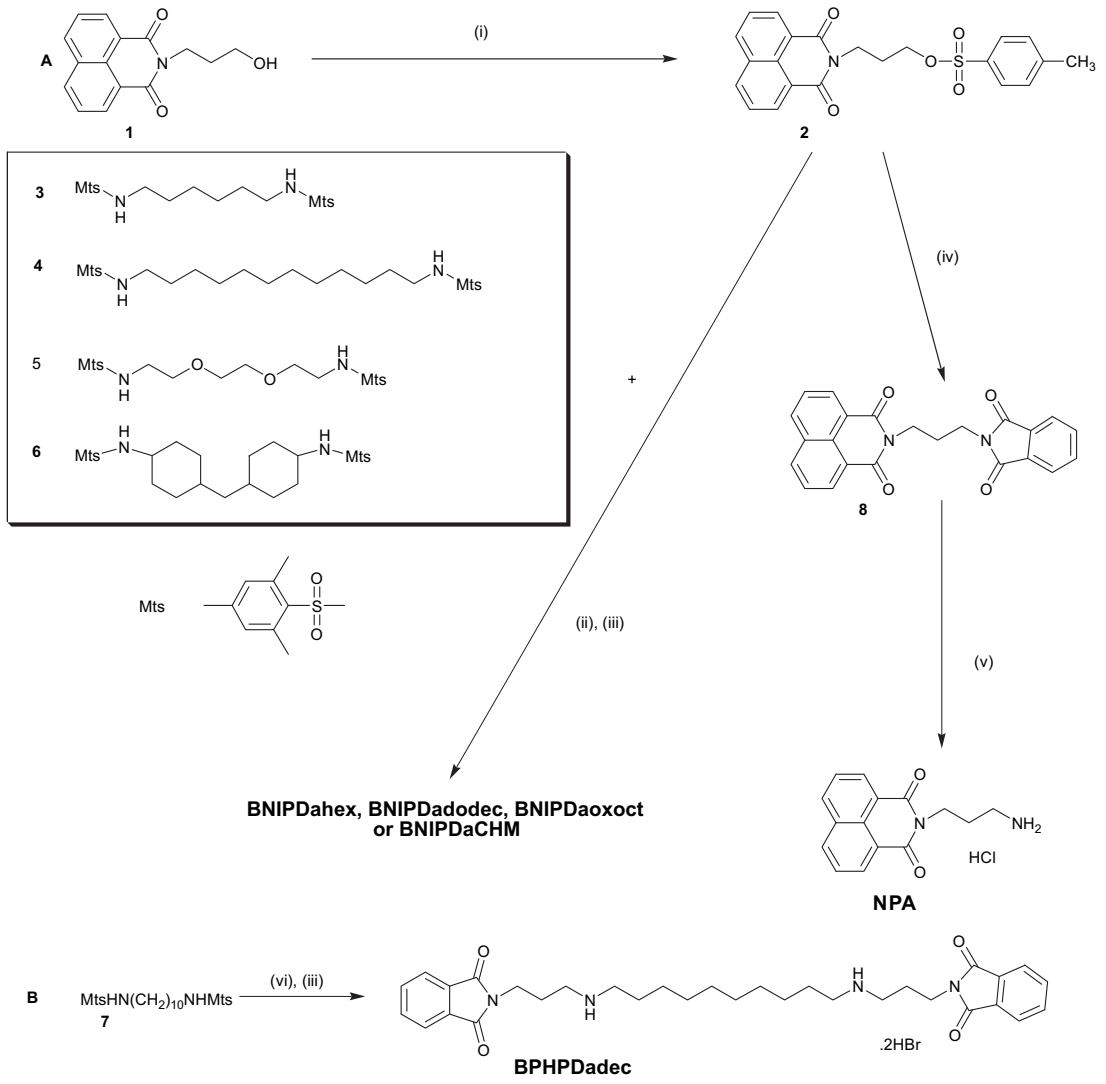

Scheme 1. A: Synthetic strategy for the synthesis of bisnaphthalimidopropylalkyl-diamine derivatives. Reagents and Conditions: (i) tosyl-Cl, Pyridine, 0–5 °C, 12 h (ii) **2**, Mts, Cs_2CO_3, DMF, 85 °C, 12 h for **3** and **4**, 50 °C, 96 h for **5** and **6**. (iii) HBr/glacial CH_3CO_2H, CH_2Cl_2, RT, 24 h (iv) tosyl-Cl, $C_8H_4KNO_2$, DMF, 50 °C, 12 h (v) **8**, C_2H_5OH, hydrazine hydrate, 85 °C, 12 h; Ethanol/conc. HCl. B: (vi) **7**, *N*-(3-(bromopropyl) phthalimide, Cs_2CO_3, DMF, 85 °C, 12 h.

determined. Doxorubicin, Mitoxantrone and Hoesht 33258, known DNA intercalators [17–19] were used as positive controls and the results are presented in Table 1.

All BNIP derivatives (10 μM) showed an increase in T_m ranging between Δ 25.0–35.7 °C when compared to the melting point of a *Calf Thymus* DNA duplex. The increase in T_m from these derivatives is in the same range as the positive controls (doxorubicin (Δ 30.2 °C) and mitoxantrone (Δ 34.8 °C)). Among all the BNIP derivatives, the BNIP derivative with the longest linker chain (BNIPDadodec) resulted in the smallest increase in T_m (Δ 25.0). However, the introduction of oxygen atoms (BNIPDaoxoct) and cyclohexane rings (BNIPDaCHM) in the linker chain did not affect the enhanced stability of the DNA duplex (Δ 31.7 °C and Δ 31.2 °C, respectively). Bisphthalimidopropyl diaminodecane (BPHPDadec) and mononaphthalimidopropylamine (NPA) induced a relatively small increase in the T_m of Δ 15.8 °C and Δ 10.1 °C, respectively compared to the BNIP derivatives. These results confirm that the presence of the bisnaphthalimido functionality is essential to achieve high DNA–BNIP interactions.

Ethidium bromide (EtBr) binds to DNA by intercalation and its fluorescence is enhanced when bound to DNA [6,20]. Compounds which exert a higher DNA-binding affinity than EtBr displace the EtBr, causing fluorescence quenching [9]. The concentration (μM) of BNIP derivative that causes a 50% decrease in the fluorescence of DNA bound EtBr is defined as C_{50} value. A competitive displacement fluorimetric assay of DNA bound EtBr was performed to evaluate the DNA-binding affinity of all of the following BNIP derivatives: BNIPSpd, BNIPPut, BNIPDahex, BNIPDaoct, BNIPDaoct, BNIPDadec, BNIPDadodec, BNIPDaCHM, BNIPDaoxoct, BPHPDadec and NPA (Table 1). All BNIP derivatives, except BPHPDadec and NPA displaced ethidium bromide from DNA with C_{50} values in the range of 1.4–3.8 μM (Table 1). The order of binding strength to DNA is BNIPSpd > BNIPPut = BNIPDahex > BNIPDaoct > BNIPDadec > BNIPD aoxoct > BNIPDadodec > BNIPDaCHM > BPHPDadec = NPA (C_{50} > 10 μM) (Table 1). These results confirmed that bisnapthalimido functionality is paramount in achieving strong DNA–BNIP interactions.

2.2.2. Cytotoxic studies

In our previous work, the natural polyamines, spermidine (BNIPSpd) and spermine (BNIPSpm) were linked to bisnaphthalimidopropyl moieties to enhance solubility, whilst retaining

Table 1
Effect of derivative treatment on the thermal denaturation (T_m) of *Calf thymus* DNA and ethidium bromide displacement bound to *Calf thymus* DNA (C_{50}).

Compound[a]	T_m (°C)[b]	C_{50} (μM)[c]
	10 μM	
Calf Thymus DNA alone	56.2 ± 0.4	ND
BNIPSpd	91.5 ± 0.6	1.4 ± 0.1
BNIPPut	89.2 ± 2.5	1.5 ± 0.3
BNIPDahex	91.9 ± 0.6	1.5 ± 0.1
BNIPDaoct	88.7 ± 0.3	1.7 ± 0.2
BNIPDadec	84.4 ± 0.2	1.8 ± 0.1
BNIPDadodec	81.2 ± 0.7	3.4 ± 0.3
BNIPDaCHM	87.4 ± 1.2	3.8 ± 0.1
BNIPDaoxoct	87.9 ± 0.6	1.9 ± 0.4
BPHPDadec	72.0 ± 2.4	> 10
NPA	66.3 ± 0.9	> 10
Doxorubicin	86.4 ± 1.2	ND
Mitoxantrone	91.0 ± 1.5	ND
Hoesht 33258	78.8 ± 0.9	ND

[a] *Calf Thymus* DNA was incubated in the presence or absence of the BNIP derivatives overnight.
[b] T_m is the temperature (°C) when 50% of the DNA is denatured. Data are the means ± SD of three independent experiments.
[c] C_{50} is the drug concentration (μM) required to generate a 50% decrease in the fluorescence of bound Ethidium Bromide. Data are the mean ± SD of three independent experiments.

Table 2
Cytotoxicity of BNIP derivatives against MDA-MB-231 and MCF-10A cells.

Compound[a]	MDA-MB-231 Cells		MCF-10A Cells	
	IC_{50} (μM)[b]		IC_{50} (μM)[b]	
	24 h	48 h	24 h	48 h
BNIPSpd	12.68 ± 0.47	4.59 ± 1.35	4.19 ± 0.55	3.97 ± 0.97
BNIPPut	7.86 ± 3.59	5.12 ± 0.83	8.1 ± 2.68	5.67 ± 2.31
BNIPDahex	7.22 ± 1.43	4.54 ± 0.57	0.84 ± 0.09	0.83 ± 0.11
BNIPDaoct	4.99 ± 1.34	2.68 ± 0.29	2.77 ± 0.09	0.87 ± 0.12
BNIPDadec	4.85 ± 0.22	3.32 ± 0.69	2.77 ± 0.11	2.82 ± 0.05
BNIPDadodec	5.11 ± 0.51	6.88 ± 0.06	4.17 ± 0.25	6.83 ± 0.82
BNIPDaCHM	6.84 ± 0.26	6.06 ± 0.68	6.06 ± 0.13	5.71 ± 0.83
BNIPDaoxoct	12.39 ± 5.78	6.15 ± 1.49	6.1 ± 1.56	2.27 ± 0.01
BPHPDadec	>40	>40	>40	>40
NPA	>40	>40	>40	>40
Doxorubicin[c]	14.35 ± 5.92	3.61 ± 0.61	0.75 ± 0.01	0.18 ± 0.01

[a] Cytotoxicity was determined by MTT Assay. The results were obtained after treating MDA-MB-231 and MCF-10A cells with different BNIP derivative concentrations (0–40 μM) for 24 and 48 h at 37 °C. Data are mean ± SD of 3 independent experiments ($n = 3$).
[b] IC_{50} is defined as the drug concentration required to reduce the absorbance to 50% of the control values [9].
[c] Doxorubicin, an important DNA intercalator was used as a control.

good *in vitro* cytotoxicity against human breast cancer MCF-7 cells, with IC_{50} values in the region of 1.38–2.91 μM after 48 h treatment [6]. Our second generation of BNIP derivatives showed that modulating the length of the alkyl linker chain had an effect on both solubility and *in vitro* cytotoxicity against human colon cancer Caco-2 cells [7]. In the latter work [7], we showed that longer alkyl chains (C7–C10) provided a moderate increase in solubility, although cytotoxicity was not affected, with IC_{50} values in the range of 0.47–6.2 μM after 24 h treatment. *In vitro* cytotoxicity of the novel BNIP derivatives with linker chains containing the longest alkyl chain to date (C12), oxygen (BNIPDaoxoct) and cyclohexane rings (BNIPDaCHM) together with BPHPDadec and NPA were assessed against the human breast adenocarcinoma cell line (MDA-MB-231) and the non-tumorigenic epithelial cell line (MCF-10A). Both cell lines (1×10^4cells/100 μL) were incubated in growth media (FCS free media) containing each BNIP derivative at various concentrations (0–40 μM, for 24 or 48 h) (Tables 2 and 3) and their cytotoxicities determined by MTT assay [21].

In both cell lines, all the BNIP derivatives tested, except for BPHPDadec and NPA (IC_{50} values > 40 μM) exhibited good cytotoxicity with IC_{50} values in the range of 4.85–12.68 μM in MDA-MB-231 cells, and 0.84–8.1 μM in MCF-10A cells after 24 h treatment. Treatment after 48 h resulted in an approximately two fold increase in cytotoxicity for most of the BNIP derivatives tested. The presence of oxygen atoms and cyclohexane rings within the linker chain do not appear to affect cytotoxicity. It is interesting to note that all the derivatives appeared to be more active against MCF-10A cells rather than MDA-MB-231 cells. This may be due to the observation that MCF-10A cells replicate at a faster rate than the MDA-MB-231 cells, determined by cell count measurements (results not shown). From the above results, it can clearly be shown that the presence of the bisnaphthalimidopropyl moieties is vital for maximum *in vitro* cytotoxicity.

2.2.3. Drug uptake

In order to relate cytotoxicity of BNIP derivatives to the speed of uptake into cells, the property of BNIP derivatives to fluorescence once taken up into cells was exploited [22]. MDA-MB-231 cells (8×10^4 cells/well) were treated with 10 μM of BNIPSpd, BNIPDaoct, BNIPDaoxoct or BNIPDaCHM and they were visualised using a fluorescence microscope after 0.5, 1, 2, 4, 6 and 24 h.

After 0.5 h incubation, only cells incubated with BNIPDaoct and BNIPDaCHM showed fluorescence. The fluorescence remained with time, except for BNIPDaoct, which after 2 h the fluorescence had almost completely disappeared. This observation may explain the higher toxicity of BNIPDaoct (IC_{50} 4.99 μM), whereby it is being taken up and metabolised resulting in the quick lost of fluorescence by the cells compared with the other derivatives examined. Interestingly, fluorescence in cells incubated with BNIPSpd and BNIPDaoxoct was noted after only 6 h incubation, indicating slower uptake into the cells. This may reflect the lower toxicity of these BNIP derivatives (IC_{50} 12.68 and 12.39 μM, respectively) when compared with BNIPDaoct and BNIPDaCHM (IC_{50} 4.99 and 6.84 μM, respectively).

2.2.4. Polyamine transporter

The drug uptake experiments discussed above, demonstrate that each BNIP derivative has a different rate of uptake in MDA-MB-231 cells. Many polyamine analogues and derivatives have been shown to use a polyamine transporter (PAT) system to enter cells. It has been reported that methylglyoxalbis(guanylhydrazone) (MGBG) uses a distinct polyamine transporter, which is also used by several anthracene-polyamine conjugates [12–15,23–26]. We assessed whether the BNIP derivatives reported in this paper

Table 3
Cytotoxicity of BNIP derivatives against CHO and CHO-MG cells.

Compound[a]	CHO	CHO-MG	IC_{50} Ratio[c]
	IC_{50}[b] (μM)	IC_{50}[b] (μM)	
BNIPSpd	76.5 ± 5.7	74.6 ± 3.1	1.0
BNIPDaoct	5.8 ± 0.9	5.1 ± 0.5	0.9
BNIPDaoxoct	76.1 ± 2.1	26.9 ± 5.9	0.4
BNIPDaCHM	6.2 ± 0.7	6.3 ± 0.4	1.0
MGBG[d]	3.3 ± 0.5	>100	>30.2

[a] Toxicity was determined by MTT Assay. The results were obtained after treating CHO-MG and CHO cells with different BNIP derivative concentrations (0–100 μM) for 48 h at 37 °C. Data are mean ± SD of 3 independent experiments.
[b] IC_{50} is defined as the drug concentration required to reduce the absorbance to 50% of the control values [9].
[c] The ratio indicates the (CHO-MG/CHO) IC_{50} ratio, a measure of PAT selectivity. Highly selective polyamine transporter ligands will have high (CHO-MG/CHO) IC_{50} ratios [15].
[d] MGBG, a known substrate for the PAT system was used as a control.

utilised the MGBG polyamine transporter to enter cancerous cells. Two Chinese Hamster Ovary (CHO) cell lines were used: the parental CHO cells with an active polyamine transporter and the polyamine-transport deficient mutant cell line, CHO-MG. The latter represents cells with no polyamine transporter activity. This provides a delivery system model which is independent of the polyamine transporter [12,23,27]. CHO-MG cells were isolated for growth resistance to MGBG, which is a known substrate for PAT [12,15,23,28]. The comparison between the toxicity of the BNIP derivatives in both cell lines provided an important indication of BNIP delivery via the polyamine transporter system. A derivative which uses the polyamine transporter would be highly toxic to CHO cells, yet less toxic to CHO-MG cells [12–14,29]. Therefore, highly selective polyamine transporter ligands will have high (CHO-MG/CHO) IC_{50} ratios [15].

The toxicity of the BNIP derivatives, BNIPSpd, BNIPDaoct, BNIPDaoxoct and BNIPDaCHM was determined in CHO and CHO-MG cells using the MTT assay [21].

BNIPSpd and BNIPDaoxoct exhibited weak activity in CHO cells with IC_{50} values of 76.5 and 76.1 μM, respectively (Table 3). This may be due to the slow uptake of these compounds as demonstrated in MDA-MB-231 cells. However, BNIPDaoct, BNIP-DaCHM and MGBG showed high activity with IC_{50} ranging from 3.3 to 6.2 μM. All BNIP derivatives except for MGBG produced similar results in CHO-MG cells. The lack of activity from MGBG was due to its inability to enter the cells. Based on the IC_{50} ratio values of CHO-MG/CHO, it would appear that none of the BNIP derivatives (CHO-MG/CHO ratios ranging from 0.4 to 1.0) utilised the PAT system, in contrast to MGBG (ratio $>$ 30.2) to gain access to CHO-MG and CHO cells. Therefore, the uptake of BNIPs into cells may involve different mechanisms of entry, such as passive diffusion, utilisation of another transporter, interactions on the outer surface of the plasma membrane and other membrane receptor interactions [15].

3. Conclusions

All BNIP derivatives, except BPHPDadec and NPA exhibited good cytotoxic activity in both MDA-MB-231 and MCF-10A cells. Furthermore all BNIP derivatives intercalate effectively to *Calf Thymus* DNA, as demonstrated by the increased T_m values and effective competitive displacement of EtBr from EtBr bound to DNA. The BNIP derivative with the longest alkyl chain (BNIPDadodec) resulted in a decrease in DNA-binding, while the introduction of oxygen atoms (BNIPDaoxoct) and cyclohexane rings (BNIPDaCHM) in the linker chain did not significantly affect DNA-binding. BPHPDadec and NPA demonstrated much lower DNA-binding affinities than the other BNIP derivatives, resulting in a loss of toxicity. These results confirm that the presence of bisnaphthalimidopropyl functionality and a linker chain of $<$C12 are essential in achieving high DNA-binding interactions and cytotoxic properties. Fluorescence microscopy analysis showed BNIPDaoct and BNIPDaCHM are being taken up by cells much quicker than BNIPSpd and BNIPDaoxoct. None of the BNIP derivatives studied used the MGBG specific PAT system suggesting that another mode of cellular entry other than this PAT is being utilised by the BNIP derivatives.

In conclusion modifications to the linker chain in the BNIP derivatives, by the introduction of oxygen atoms and cyclohexane rings enhanced cellular uptake and biological activity in breast cancer cells. It is suggested that DNA may be a potential target for the cytotoxic activity of these BNIP derivatives. The biological properties of these BNIP derivatives indicate their potential as future cancer therapeutic agents.

4. Experimental

4.1. Materials

Human breast cancer MDA-MB-231 (ECACC, 92020424) and human breast epithelial MCF-10A cells (ATCC, CRL-10317) were purchased from the European Collection of Cell Cultures and the American Tissue Culture Collection respectively. Chinese Hamster Ovary (CHO) cells and polyamine-transport deficient mutant (CHO-MG) cells were kindly provided by Dr. Wayne Flintoff, from the University of Western Ontario, Canada. All reagents were purchased from Acros Organics, Fisher Scientific, Lancaster and Sigma–Aldrich, unless otherwise stated and were used without purification. Thin Layer Chromatography (TLC) was performed on silica gel 60 F_{254} aluminium plates (Merck) in chloroform/methanol (99:1 or 97:3). ^{1}H NMR was recorded on a Bruker 400 Ultrashield spectrometer operating at 400.1 MHz for ^{1}H and 100.6 MHz for ^{13}C. Accurate mass spectra were obtained by ESI on a ZQ4000 (low resolution) or MAT95XP (accurate mass) analytical instrument (EPSRC National Mass Spectrometry Service Centre at Swansea University, Swansea). BNIPSpd, BNIPPut, BNIPDaoct and BNIPDadec were synthesised and characterised according to our methods previously described [5,7].

4.2. Chemical synthesis

The synthetic strategy (Scheme 1A) adopted to synthesise the bisnapthalimidopropylalkyl-diamine analogues; BNIPDahex, BNIP-Dadodec, BNIPDaoxoct and BNIPDaCHM was based on methods previously developed in our laboratory [5,7,9].

4.2.1. General method for the synthesis of dimesityalkyl diamines (**3**–**7**) (Schemes 1A–B)

Corresponding diamines were dissolved in anhydrous pyridine followed by the addition of mesitylenesulphonyl chloride (2.1 M excess). The resulting solution was stirred at room temperature for 4 h. Removal of the pyridine followed by the addition of icy water (200 mL), resulted in the formation of a precipitate. The latter was filtered off, washed thoroughly with water and dried under *vacuo*. All the dimesitylalkyldiamines synthesised, showed only one spot on TLC and they were used in the next step without further purification.

4.2.1.1. N^1,N^8-Dimesitylhexane ***3***. (58%), ^{1}H NMR ($CDCl_3$): δ 7.0 (s, aromatic protons), 4.8 (t, NH), 2.8 (q, $-CH_2-$N), 2.6 (s, CH_3.Mts), 2.3 (s, CH_3.Mts), 1.4 (t, $-CH_2-$), 1.1 (s, $-CH_2-$). ^{13}C NMR ($CDCl_3$): δ 140–127 (aromatic carbons), 42.3 (2 $\times$ CH_2–NH), 29.3 (2 $\times$ CH_2), 25.9 (2 $\times$ CH_2), 22. (CH_3.Mts), 20.9 (CH_3.Mts).

4.2.1.2. N^1,N^{12}-Dimesityldodecane ***4***. (74%) ^{1}H NMR ($CDCl_3$): δ 7.0 (s, aromatic protons), 4.4 (t, NH), 2.9 (q, $-CH_2-$N), 2.6 (s, CH_3.Mts), 2.3 (s, CH_3.Mts), 1.5 (t, $-CH_2-$), 1.2 (s, $-CH_2-$). ^{13}C NMR ($CDCl_3$): δ 140–127 (aromatic carbons), 41.6 (2 $\times$ CH_2–NH), 28.5 (2 $\times$ CH_2), 26.9 (2 $\times$ CH_2), 25.8 (2 $\times$ CH_2), 22.7 (2 $\times$ CH_2), 22.5 (2 $\times$ CH_2), 21.5 (CH_3.Mts), 13.6 (CH_3.Mts).

4.2.1.3. N^1,N^8-Dimesityl-3,6-dioxaoctane ***5***. (66%), ^{1}H NMR ($CDCl_3$): δ 6.9 (s, aromatic protons), 5.5 (t, $-CH_2-$O), 3.4 (t, $-CH_2-$O), 3.0 (q, $-CH_2-$N), 2.5 (s, CH_3.Mts), 2.2 (s, CH_3.Mts). ^{13}C NMR ($CDCl_3$): δ 140–127 (aromatic carbons), 70.7 (4 $\times$ CH_2–O), 40.7 (2 $\times$ CH_2–NH), 21.5 (CH_3.Mts), 13.6 (CH_3.Mts).

4.2.1.4. N^4,N^4-Dimesityldicyclohexylmethane ***6***. (61%), ^{1}H NMR ($CDCl_3$): δ 8.6 (s, NH), 7.7–7.0 (m, aromatic protons), 4.6 (t, $-CH_2-$N), 2.6 (q, CH_3.Mts), 2.3 (q, CH_3.Mts), 1.8–0.8 (m, $-CH_2-$ and

cyclohexane protons). ^{13}C NMR ($CDCl_3$): δ 140–127 (aromatic carbons), 43 (2 × CH–N), 39 (CH_2), 30.1–27.0 (cyclohexane carbons), 21.5 (CH_3.Mts), 13.6 (CH_3.Mts).

4.2.1.5. N^1,N^{10}-Dimesityldecane **7**. (75%), ^1H NMR ($CDCl_3$): δ 6.9 (s, aromatic protons), 4.6 (t, NH), 2.9 (q, –CH_2–N), 2.7 (s, CH_3.Mts), 2.3 (s, CH_3.Mts), 1.5 (t, –CH_2–), 1.2 (s, –CH_2–). ^{13}C NMR ($CDCl_3$): δ 140.0–127.0 (aromatic carbons), 40.7 (2 × CH_2–NH), 30.0–26.0 (8 × CH_2), 21.5 (CH_3.Mts), 13.6 (CH_3.Mts) (Scheme 1B).

*4.2.2. Synthesis of toluenesulfonyloxypropylnaphthalimide (**2**) (Scheme 1A)*

Naphthalic anhydride (6.46 g, 32.58 mmol) was dissolved in DMF (70 mL), followed by the addition of aminopropanol (2.45 g, 32.58 mmol) and DBU (7.45 mL). The solution was stirred at 85 °C for 4 h. The resulting residue was poured into icy water (200 mL) to form a precipitate. The latter was filtered off and washed with water. This compound, *N*-(3-hydroxypropyl) naphthalimide **1** (82.9%), was pure enough to be taken to the next step without further purification. ^1H NMR ($CDCl_3$): δ 8.5–7.5 (m, aromatic protons), 4.3 (t, CH_2–O), 3.6 (t, N–CH_2), 3.2 (broad, s, OH), 2.1 (m, CH_2). ^{13}C NMR ($CDCl_3$): δ 161 (C═O), 136–122 (aromatic carbons), 58, 38, 31 (3 × CH_2).

1 (5.10 g, 20 mmol) was dissolved in anhydrous pyridine (80 mL). The solution was stirred for 15 min at 0 °C. Tosyl chloride (5.72 g, 30 mmol) was added, slowly, over 30 min. The solution was left overnight at 4 °C. The solution was poured into icy water (200 mL) to form a precipitate. The latter was filtered off and washed thoroughly with water. The crude product was recrystallised with ethanol to form Toluenesulfonyloxypropylnaphthalimide **2** (75%). ^1H NMR ($CDCl_3$): δ 8.6–7.6 (m, aromatic protons), 7.2 (m, O-Tos aromatic protons), 4.2 (m, CH_2–O, CH_2), 2.3 (s, CH_3), 2.0 (m, CH_2). ^{13}C NMR ($CDCl_3$): δ 161 (C═O), 138–125 (aromatic carbons), 129–144 (O-Tos aromatic carbons), 70, 38, 29 (3 × CH_2), 20 (CH_3).

4.2.3. General N-alkylation reaction (Scheme 1A)

Dimesitylated polyamines (**3**–**6**) (0.5 g) were dissolved in DMF (7 mL) followed by the addition of **2** (2.1 M excess) and caesium carbonate (6 M excess). The solution was left stirring overnight at 85 °C (**3**-**4**). For **5** and **6**, the solution was left for 96 h at 50 °C. Reaction completion was monitored by thin layer chromatography. The solution was poured into icy water (200 mL) to form a precipitate. HCl (20 mL, 2 M) was added to neutralise the solution, the precipitate was collected by filtration and washed thoroughly with water.

4.2.4. General deprotection reaction (Scheme 1A–B)

The fully protected polyamine derivatives were dissolved in anhydrous dichloromethane followed by the addition of hydrobromic acid/glacial acetic acid. The solution was left stirring for 24 h at room temperature. The precipitate formed was filtered off and washed with dichloromethane (20 mL) and, ether (5 mL) (BNIP-Dahex, BNIPDadodec and BNIPDaCHM). For BNIPDaoxoct, the dichloromethane/hydrobromic acid/glacial acetic acid was removed under *vacuo* and the residue was washed with dichloromethane (5 mL). The crude product recrystallised with absolute ethanol.

4.2.4.1. BNIPDahex. (91%) ^{13}C NMR (DMSO-d_6): 24.5 (CH_2), 25.2 (CH_2), 25.4 (CH_2), 36.7 (CH_2), 44.8 (N–CH_2), 46.5 (N–CH_2), 122.0, 127.1, 130.6, 131.2, 134.3 (Aromatic Carbons), 163.6 (C═O). HRMS (FAB): Calcd. for $C_{36}H_{40}N_4O_4$ Br_2, 671.2227 $[M - Br]^+$, found: 671.2221 $[M - Br]^+$.

4.2.4.2. BNIPDadodec. (80%) ^{13}C NMR (DMSO-d_6): δ 163.6 (C═O), 134.3, 131.2, 130.6, 127.1, 122.0 (aromatic carbons), 46.6 (N–CH_2), 44.7 (N–CH_2), 36.7–24.5 (–CH_2–). HRMS (FAB): Calcd. for $C_{42}H_{52}N_4O_4$ Br_2, 755.3166 $[M - Br]^+$, found: 755.3168 $[M - Br]^+$.

4.2.4.3. BNIPDaoxoct. (69%) ^{13}C NMR (DMSO-d_6): δ 161 (C═O), 138–125 (aromatic carbons), 72 (O–CH_2), 70 (O–CH_2), 50–30 (–CH_2–). HRMS (FAB): Calcd. for $C_{36}H_{40}N_4O_6Br_2$, 702.6134 $[M - 2H - Br]^+$, found: 702.2589 $[M - 2H - Br]^+$.

4.2.4.4. BNIPDaCHM. (75%) ^{13}C NMR (DMSO-d_6): δ 161.0 (C═O), 136.0–122.0 (aromatic carbons), 51.0–27.0 (–CH_2– and cyclohexane carbons). HRMS (FAB): Calcd. for $C_{43}H_{50}N_4O_4Br_2$, 685.3753 $[M - H - 2Br]^+$, found: 685.3748 $[M - H - 2Br]^+$.

4.2.5. Synthesis of naphthalimidopropylamine, NPA (Scheme 1A)

4.2.5.1. Step 1 (Scheme 1A). **2** (0.5 g, 1.22 mmol) was dissolved in DMF (7 mL) followed by the addition of Potassium phthalimide (1.95 M excess) (0.44 g, 2.37 mmol). The solution was left stirring for 12 h at 50 °C. Reaction completion was monitored by thin layer chromatography. The solution was poured into icy water (200 mL) to form a precipitate. The precipitate was collected by filtration, washed thoroughly with water and recrystallised with absolute ethanol. **8** (65%) ^1H NMR ($CDCl_3$): δ 8.2–7.5 (m, aromatic protons), 4.3 (t, CH_2–N), 3.8 (t, N–CH_2, naphthalimido), 2.1 (m, –CH_2). ^{13}C NMR ($CDCl_3$): δ 161.0 (C═O), 140.0–123.0 (aromatic carbons), 39.0 (CH_2–N), 38.0 (N–CH_2), 27.0 (–CH_2–).

4.2.5.2. Step 2 (Scheme 1A). **8** (0.5 g, 1.3 mmol) was dissolved in Ethanol (25 mL) followed by the addition of Hydrazine hydrate (10 M excess) (650 μL, 13 mmol). The solution was left stirring for 12 h at 85 °C. Reaction completion was monitored by thin layer chromatography. The ethanol was evaporated followed by the addition of dichloromethane (10 mL) giving rise to a precipitate. The latter was filtered off and the filtrate was evaporated to dryness to give a thick oil as naphthalimidopropylamine in quantitative yield. The latter was immediately converted to its corresponding hydrochloride salt by dissolving the amine in ethanol (2 mL), followed by the addition of conc. HCl (3 mL) and ether (10 mL). The white precipitate formed was filtered off, recrystallised (95% ethanol) and dried under *vacuo* to give *NPA* (26%) as the hydrochloride salt. ^{13}C (DMSO-d_6): δ 165 (C═O), 140–125 (aromatic carbons), 39 (CH_2–NH_2), 38 (N–CH_2), 30 (–CH_2–). HRMS (FAB): Calcd. For $C_{15}H_{14}N_2O_2$ 255.1131 $[M + H]^+$, found: 255.1128 $[M + H]^+$.

4.2.6. Synthesis of bisphthalimidopropyldiaminodecane (BPHPDadec)

4.2.6.1. N^1,N^{10}-Dimesityldecane **7**. (0.5 g, 0.931 mmol) was dissolved in DMF (7 mL) followed by the addition of *N*-(3-bromopropyl) phthalimide (2.1 M excess) (0.52 g, 19.56 mmol) and caesium carbonate (6 M excess) (1.81 g, 5.586 mmol). The solution was left stirring overnight at 85 °C. Reaction completion was monitored by thin layer chromatography. The solution was poured into icy water (200 mL) to form a precipitate followed by the addition of HCl (20 mL, 2 M) The precipitate was collected by filtration, washed thoroughly with water and dried under *vacuo*.

The fully protected polyamine derivative (0.2 g, 2.19 mmol) was dissolved in anhydrous dichloromethane (5 mL) followed by the addition of hydrobromic acid/glacial acetic acid (0.8 mL). The solution was left stirring for 24 h at room temperature. The precipitate formed was filtered off and washed with dichloromethane (20 mL), ether (5 mL) and dried under *vacuo* (BPHPDadec) as its dihydrobromide salt.

4.2.6.2. BPHPDadec. (96%) ^{13}C NMR (DMSO-d_6): δ 168 (C═O), 142–122 (aromatic carbons), 46 (NH–CH_2), 39 (N–CH_2), 32–27 (–CH_2–).

HRMS (FAB): Calcd. for $C_{32}H_{44}N_4O_4Br_2$, 547.3279 $[M - 2HBr + H]^+$, found: 547.3281 $[M - 2HBr + H]^+$

4.3. Biological activities

4.3.1. Thermal denaturation studies

Thermal denaturation (melting) experiments were performed in a stoppered quartz cuvettes (1 cm path length) using a Shimadzu UV-1650 PC UV–vis spectrophotometer fitted with a temperature controller (Shimadzu, Japan) and water supply. The temperature was increased at a rate of 1 °C/min over a range of 40–100 °C. *Calf Thymus* DNA working solutions were prepared by dissolving DNA (2.5 mg) in 0.01 M Saline Sodium Citrate (SSC) Buffer (100 mL). The DNA–BNIP solutions were prepared from BNIP stock solutions (10 mM in 50% DMSO), which were further diluted from a working solution (100 μM) to give the final concentration of 10 μM. The thermal melting point, T_m (°C) was measured by determining the change in midpoint of the thermal denaturation curves of DNA.

4.3.2. Fluorescence-binding studies

Fluorescent-binding experiments were carried out by the competitive displacement fluorometric assay of DNA bound Ethidium Bromide (EtBr)-BNIP solutions. *Calf Thymus* DNA solution was prepared by dissolving DNA (2.5 mg) in 0.01 M SSC Buffer (100 mL). EtBr solution (200 μM) was prepared by dissolving EtBr (7.886 mg) in distilled water (100 mL). The BNIP solutions were prepared from BNIP stock solutions (10 mM in 50% DMSO) and were further diluted from a working solution (100 μM), to give the final concentrations of 1, 2, 4, 6, 8 and 10 μM in 0.01 M SSC buffer. DNA–BNIP test solutions were prepared by adding varying volumes of BNIP solutions in 0.01 M SSC Buffer, dependent upon drug concentration (μM) to a fixed volume of *Calf Thymus* DNA (200 μL) and EtBr (20 μL) in 1 mL Eppendorfs. All measurements were determined in disposable cuvettes (1 cm path length) using an LS55 Luminescence spectrophotometer (Perkin Elmer, USA), at room temperature (excitation 481 nm and emission 596 nm). The C_{50} values are defined as the drug concentration (μM) required to generate a 50% decrease in the fluorescence of bound EtBr.

4.3.3. Cell culture and drug treatment

MDA-MB-231 cells were maintained in RPMI 1640 medium (containing GlutaMAX™-1 with 25 mM HEPES) (Gibco, UK) supplemented with 10% (v/v) foetal calf serum (FCS) (Biosera, UK) and 1% penicillin (100 U/mL)/streptomycin (100 μg/mL) (Gibco, UK). MCF-10A cells were maintained in DMEM/F12 medium (Lonza, Belgium) supplemented with 5% (v/v) horse serum, human insulin (10 μg/mL), hydrocortisone (0.5 μg/mL), epidermal growth factor (20 ng/mL) (Invitrogen, UK), chloratoxin (100 ng/mL), penicillin (100 U/mL)/streptomycin (100 μg/mL) (Invitrogen, UK). CHO and CHO-MG cells were maintained in RPMI 1640 medium (containing L-Glutamine, no Phenol Red) (Gibco, UK) supplemented with 10% (v/v) FCS (Biosera, UK) and 0.5% (v/v) penicillin (100 U/mL)/streptomycin (100 μg/mL) (Invitrogen, UK). All cells were incubated at 37 °C in a humidified 5% CO_2 atmosphere. Exponentially growing cells were plated at 8×10^4/mL into 24 well plates or 1×10^4cells/100 μL into 96-well plates and incubated for 24 h, before incubation with BNIP derivatives. Stock solutions (10 mM) of the BNIP derivatives in 50% (v/v) dimethylsulfoxide (DMSO) were stored at 4 °C and were further diluted in fresh FCS free medium immediately prior to use.

4.3.4. Cytotoxic studies

The growth inhibitory effect of the BNIP derivatives were determined using the standard colourimetric 3-(4,5-dimethylthiazol-2-yl)-2, 5-diphenyltetrazolium bromide (MTT) assay. MDA-MB-231 and MCF-10A (1×10^4cells/100 μL) cells were incubated with BNIPSpd, BNIPPut, BNIPDahex, BNIPDaoct, BNIPDadec, BNIPDadodec, BNIPDaoxoct, BNIPDaCHM, BPHPDadec and NPA (0–40 μM; 24 and 48 h) in 96-well plates (Nunc, UK). After the desired incubation time with BNIP derivatives, at 37 °C, the culture medium was removed and 100 μL of MTT solution (1 mg/mL) in FCS free medium was added to each well. The plates were incubated at 37 °C for 4 h. At the end of incubation period, the MTT solution was removed and pure DMSO (200 μL) added to each well. The plates were shaken for 20 min. The metabolised MTT product, dissolved in DMSO was quantified by reading the absorbance at 560 nm from a plate reader (MRX II, Dynex Technologies, USA). IC_{50} values are defined as the drug concentrations required to reduce the absorbance to 50% of the control values.

4.3.5. Drug uptake

BNIP derivative localisation within exponentially growing MDA-MB-231 cells plated at a density of 8×10^4/mL into 24 well plates (Nunc, UK) was observed using fluorescence microscopy. After 24 h, 10 μM BNIPSpd (data not shown), BNIPDaoct, BNIPDaoxoct or BNIPDaCHM were added to the cells. After the desired incubation time, the cell culture medium was removed, and the cells washed twice with Phosphate Buffer Saline (PBS) (Oxoid Ltd, UK). 1 mL PBS was added to each well, and the cells observed under an inverted fluorescence microscope (Leica DMIL) with a high pressure mercury burner (Leica Microsystems, UK), using a UV filter (excitation bandpass (blue); 340–380 nm, emission longpass (red); 425 nm). Images were captured using a Leica DC 200 camera (Leica Microsystems, UK) and viewed using Irfanview 3.91 software (Leica Microsystems, UK).

4.3.6. Polyamine transporter

CHO and CHO-MG cells were used to assess the selective transport of BNIP derivatives via the polyamine transporter (PAT). CHO and CHO-MG (1×10^4cells/100 μL) cells were incubated with BNIPSpd, BNIPDaoct, BNIPDaoxoct or BNIPDaCHM (0–100 μM; for 48 h) in 96-well plates (Nunc, UK). After 48 h incubation, at 37 °C, cell viability was determined using the MTT assay, as described above.

4.4. Statistics

A minimum of three independent experiments were conducted for each set of analyses, where all experiments comprised of at least three internal replicates. Data is presented as mean ± SD.

Acknowledgements

The authors would like to thank The Robert Gordon University (RDI Funding) and the Royal Society of Chemistry for financial support, and the EPSRC National Mass Spectrometry Service Centre at Swansea University, Swansea for mass spectral analysis. Special thanks to Professor Wayne Flintoff from the University of Western Ontario, Canada for kindly donating the CHO and CHO-MG cell lines, and Dr Graeme Kay from The Robert Gordon University, UK for providing Doxorubicin, Mitoxantrone and Hoechst 33258.

References

[1] M.F. Brana, M. Cacho, A. Gradillas, B. de Pascual-Teresa, A. Ramos, Intercalators as anticancer drugs. Curr. Pharm. Des. 7 (2001) 1745–1780.
[2] M.F. Brana, A. Ramos, Naphthalimides as anti-cancer agents: synthesis and biological activity. Curr. Med. Chem. Anti-Cancer Agents 1 (2001) 237–255.
[3] L. Ralton, C.S. Bestwick, P. Kong Thoo Lin, Polyamine analogues and derivatives as potential anticancer agents. Curr. Bioact. Comp. 3 (2007) 179–191.

[4] M.F. Brana, J.M. Castellano, M. Moran, M.J. Perez de Vega, X.D. Qian, C.R. Romerdahl, G. Keihauer, Bis-naphthalimides. 2. synthesis and biological activity of 5,6-acenaphthalimidoalkyl-1,8-naphthalimidoalkyl amines. Eur. J. Med. Chem. 30 (1995) 235–239.
[5] P. Kong Thoo Lin, V. Pavlov, The synthesis and in vitro cytotoxic studies of novel bis-naphthalimidopropyl polyamine derivatives. Bioorg. Med. Chem. Lett. 10 (2000) 1609–1612.
[6] V. Pavlov, P. Kong Thoo Lin, V. Rodilla, Cytotoxicity, DNA binding and localisation of novel bis-napthalimidopropyl polyamine derivatives. Chem. Biol. Interact. 137 (2001) 15–24.
[7] J. Oliveira, L. Ralton, J. Tavares, A. Codeiro-da-Silva, C.S. Bestwick, A. McPherson, P. Kong Thoo Lin, The synthesis and the in vitro cytotoxicity studies of bisnapththalimidopropyl derivatives against colon cancer cell and parasite *Leishmania infantum*. Bioorg. Med. Chem. 15 (2007) 541–545.
[8] L. Ralton, C.S. Bestwick, L. Milne, S. Duthie, P. Kong Thoo Lin, Bisnaphthalimidopropyl spermidine induces apoptosis within colon carcinoma cells. Chemico-Biolog. Interact. 177 (2009) 1–6.
[9] A.-M. Dance, L. Ralton, Z. Fuller, L. Milne, S. Duthie, C.S. Bestwick, P. Kong Thoo Lin, Synthesis and biological activities of bisnaphthalimido polyamine derivatives: cytotoxicity, DNA binding, DNA damage and drug localization in breast cancer MCF-7 cells. Biochem. Pharmacol. 69 (2005) 19–27.
[10] R. Filosa, A. Peduto, S. Di Micco, P. de Caprariis, M. Festa, A. Petrella, G. Capranico, G. Bifulco, Molecular modelling studies, synthesis and biological activity of a series of novel bisnaphthalimides and their development as new DNA topoisomerase II inhibitors. Bioorg. Med. Chem. 17 (2009) 13–24.
[11] N. Seiler, J.-G. Delcros, J.P. Moulinoux, Polyamine transport and cytotoxicity in mammalian cells. An update. Int. J. Biochem. Cell. Biol. 28 (1996) 843–861.
[12] C. Wang, J.-G. Delcros, L. Cannon, F. Konate, H. Carias, J. Biggerstaff, R.A. Gardner, O. Phanstiel IV, Defining the molecular requirements for the selective delivery of polyamine conjugates into cells containing active polyamine transporters. J. Med. Chem. 46 (2003) 5129–5138.
[13] C. Wang, J.-G. Delcros, J. Biggerstaff, O. Phanstiel IV, Synthesis and biological evaluation of N^1-(anthracen-9-ylmethyl) triamines as molecular recognition elements for the polyamine transporter. J. Med. Chem. 46 (2003) 2663–2671.
[14] C. Wang, J.-G. Delcros, J. Biggerstaff, O. Phanstiel IV, Molecular requirements for targeting the polyamine transport system: synthesis and biological evaluation of polyamine anthracene conjugates. J. Med. Chem. 46 (2003) 2672–2682.
[15] R.A. Gardner, J.-G. Delcros, F. Konate, F. Breitbeil III, B. Martin, M. Sigman, M. Huang, O. Phanstiel IV, N^1-substituent effects in the selective delivery of polyamine conjugates into cells containing active polyamine transporters. J. Med. Chem. 47 (2004) 6055–6069.
[16] N. Kaur, J.-G. Delcros, J. Imran, A. Khaled, M. Chehtane, N. Tschammer, B. Martin, O. Phanstiel IV, A comparison of chloroambucil- and xylene-containing polyamines leads to improved ligands for accessing the polyamine transport system. J. Med. Chem. 51 (2008) 1393–1401.
[17] F. Arcamone, Doxorubicin, Anticancer Antibiotics, Medicinal Chemistry Series, Vol. 17, Academic Press, New York, 1981.
[18] F.E. Durr, R.E. Wallace, R.V. Citarella, Molecular and biochemical pharmacology of mitaxantrone. Cancer Treat. Rev. 10 (1983) 3–11.
[19] D.E. Comings, Mechanisms of chromosome banding. VIII Hoechst 33258-DNA interaction. Chromosoma 52 (1975) 229–243.
[20] A.W. McConnaughie, T.C. Jenkins, Novel acridine-triazenes as prototype combilexins: synthesis, DNA binding and biological activity. J. Med. Chem. 38 (1995) 3488–3501.
[21] T. Mosmann, Rapid colorimetric assay for cellular growth and survival: application to proliferation and cytotoxicity assays. J. Immuno. Methods 65 (1983) 55–63.
[22] J.C. Stockert, M. Canete, A. Villanueva, A. Juarranz, C.I. Trigoso, M.F. Brana, Fluorescence of chromatin DNA induces by antitumoral naphthalimides. Z. Naturforsch. 38 (1997) 3488–3501.
[23] J.L. Mandel, W.F. Flintoff, Isolation of mutant mammalian cells altered in polyamine transport. J. Cellular Physiol. 97 (1978) 335–344.
[24] O. Phanstiel IV, H.L. Price, L. Wang, J. Juusola, M. Kilne, S.M. Shah, The effect of polyamine homologation on the transport and cytotoxicity properties of polyamine-(DNA-intercalator) conjugates. J. Org. Chem. 65 (2000) 5590–5599.
[25] C. Wang, H.L. Price, J. Juusola, M. Kilne, O. Phanstiel IV, The influence of polyamine architecture on the transport and topoisomerase II inhibitory properties of polyamine DNA-intercalator conjugates. J. Med. Chem. 44 (2001) 3682–3691.
[26] C. Tsen, M. Iltis, N. Kaur, C. Bayer, J.-G. Delcros, L. von Kalm, O. Phanstiel IV, A *drosophila* model to identify polyamine-drug conjugates that target the polyamine transporter in an intact epithelium. J. Med. Chem. 51 (2008) 324–330.
[27] T.L. Byers, R. Wechter, M.E. Nuttall, A.E. Pegg, Expression of a human gene for polyamine transport in Chinese hamster ovary cells. Biochem. J. 263 (1989) 745–752.
[28] S. Xie, P. Cheng, G. Liu, Y. Ma, J. Zhao, M. Chehtane, A.R. Khaled, O. Phanstiel IV, C. Wang, Synthesis and bioevaluation of N-(arylalkyl)-homospermidine conjugates. Bioorg. Med. Chem. Lett. 17 (2007) 4471–4475.
[29] J.-G. Delcros, S. Tomasi, S. Carrington, B. Martin, J. Renault, I.S. Blagbrough, P. Uriac, Effect of spermine conjugation on the cytotoxicity and cellular transport of acridine. J. Med. Chem. 45 (2002) 5098–5111.

Poster Presentation at Health Implications of Dietary Amines – A Joint COST Action 922 and Biochemical Society Focused Meeting (Biochemistry Society meeting), Aberdeen, UK, 19 - 21 October 2006

The *In Vitro* Studies of Novel Bisnaphthalimidopropyl Polyamine Derivatives against CaCO-2 Cells

Gemma A Barron [*a], Giovanna Bermano[b], Lynda Ralton[a], Amanda Gordon[a] and Paul Kong Thoo Lin[a]

[a]School of Pharmacy and Life Sciences, The Robert Gordon University, St. Andrew Street, Aberdeen, AB25 1HG, Scotland, UK

[b]Centre of Obesity Research and Epidemiology (CORE), Faculty of Health and Social Care, The Robert Gordon University, St. Andrew Street, Aberdeen, AB25 1HG, Scotland, UK

The in vitro studies of novel polyamine derivatives; Bisnaphthalimidopropyl Spermidine (BNIPSpd), Decane (BNIPDadec) and Diaminononane (BNIPDanon), were investigated to establish their therapeutic anti-cancer potential against human colon cancer cells (CaCo-2). These novel compounds demonstrated good in vitro cytotoxicity with CaCo-2 cells exhibiting IC50 values ranging between 0.5 μM – 19.9 μM and 1.3 μM – 11.2 μM after 24 and 48 hours drugs exposure respectively. Strong evidence of apoptotic cell death from these novel compounds was determined through Acridine Orange/Ethidium Bromide uptake and cell morphology experiments. The effect of BNIPSpd, BNIPDadec and BNIPDanon (1 μM – 10 μM drug concentrations) on the level of polyamines on CaCo-2 cells were studied. The results showed significant changes in polyamine levels after 24 hour drug exposure. Furthermore, the modulation of HO-1 (Heme-Oxygenase) and Bcl-xL (Anti-apoptotic) genes was also studied after drug treatment and these results will be presented and discussed. In conclusion, the results obtained from this work demonstrate that the novel Bis-naphthalimidopropyl polyamine derivatives exhibit very good potency against CaCo-2 cells while initiating cell death by apoptosis and hence have the potential in the future to become therapeutic anti-cancer agents.

The *In Vitro* Studies of Novel Bis-naphthalimidopropyl Polyamine Derivatives Against CaCO-2 Cells

Barron G *., Bermano G., Gordon A., Ralton L., and Kong Thoo Lin P.

School of Life Sciences, The Robert Gordon University, St Andrew St, Aberdeen, UK, AB25 1HG

Background

- Colorectal cancer is the third most common cancer within the UK and percentage survival rates remain limited.
- The discovery of new therapeutic targets and hence the design and synthesis of novel compounds are active cancer research areas.
- In 2000, novel Bisnaphthalimidopropyl polyamine compounds were synthesised in our laboratories. These compounds consist of two naphthalimido rings linked by natural polyamines, such as spermidine and spermine. They exhibit cytotoxic activity in a variety of cancer cell lines cultured *in vitro*.[1,2,3]

Aims

- To determine the cytotoxicity of the recently synthesised novel bis-naphthalimidopropyl polyamine compounds, BNIPSpd, BNIPDadec and BNIPDanon against CaCO-2 cells.
- To determine whether these bis-naphthalimidopropyl compounds cause cell death by apoptosis.
- To investigate the effect of these compounds on polyamine levels in drug treated CaCO-2 cells.

Results

Cytotoxicity Studies Using MTT Assay

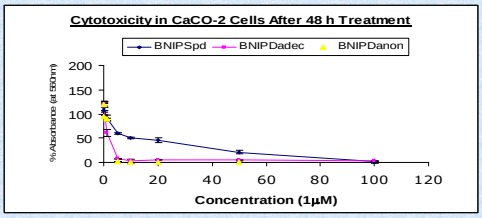

Dose-response curve obtained after treating CaCO-2 cells with varying drug concentrations (0.01 – 100µM) for 48 h.

Drug	24 h Exposure IC_{50} (µM)	48 h Exposure IC_{50} (µM)
BNIPSpd	19.9	11.2
BNIPDadec	4.0	1.5
BNIPDanon	0.5	1.3

IC50 Values of BNIPSpd, BNIPDanon, and BNIPDadec measured on CaCO-2 Cells after 24 and 48 h Drug Treatment. Data are mean ± SD for 6 replicates. 5-Fluorouracil was used as a positive control and gave IC_{50} values of 184.1µM and 115.3µM for 24 h and 48 h respectively.

- All three compounds demonstrate significant *in vitro* cytotoxicty with IC_{50} values of 0.5µM – 19.9µM (24h) and 1.3µM – 11.2µM (48h).

References

1. Kong Thoo Lin P, Pavlov V.A., *Bioorg. Med. Chem. Lett.* 10 (**2000**) 1609 – 1611
2. Pavlov V.A., Kong Thoo Lin P, Rodilla V., *Chem Biol Interact* 137 (**2001**) 15 – 24
3. Dance A.M., Ralton L, Fuller Z, Milne L, Duthie S, Bestwick C.S., Kong Thoo Lin P., *Biochem. Pharmacol.* 69 (**2005**) 19 - 27

Corresponding Author. Tel: +44-1224-262831 *Email Address: prs.barron@rgu.ac.uk

Acridine Orange/Ethidium Bromide Staining in Drug Treated Cells (24 h)

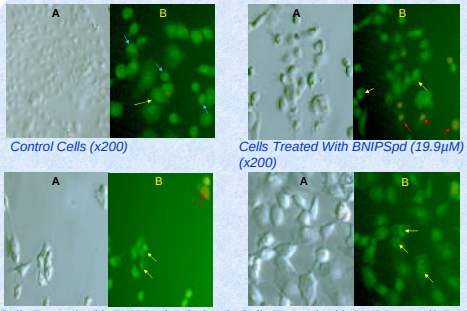

Control Cells (x200)

Cells Treated With BNIPSpd (19.9µM) (x200)

Cells Treated With BNIPDadec (4.0µM) (x200)

Cells Treated With BNIPDanon (0.5µM) (x200)

(A) Light Microscope (B) Acridine Orange/Ethidium Bromide Staining

Polyamine Levels in Drug Treated Cells

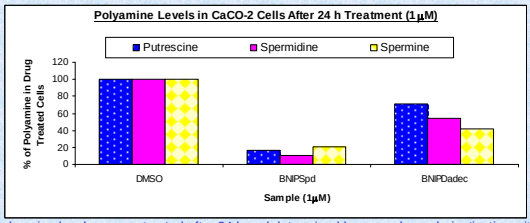

Polyamine levels were extracted after 24 h and determined by pre-column derivatisation with dansyl chloride followed by HPLC analysis.

- Polyamine levels exhibited a significant decrease after 24 h treatment with BNIPSpd and BNIPDadec at 1µM (presented result) and 10µM. Similar observations were obtained after 48 and 72 h drug exposure.

HO-1 and Bcl-x_L Gene Expression

- No change in the expression of HO-1 (Heme-Oxygenase - stress gene) and Bcl-x_L (Anti-apoptotic gene) genes was observed following exposure to BNIPSpd (19.9µM), BNIPDadec (4.0µM) and BNIPDanon (0.5µM) for 24 h.

Conclusion

- All of the novel polyamine derivatives inhibit the growth of CaCO-2 cells. The order of cytotoxicity was BNIPDanon > BNIPDadec > BNIPSpd.
- All compounds tested induced morphological changes and initiated early apoptosis. Late apoptosis was observed in BNIPSpd and BNIPDadec treated cells.
- Polyamine levels were decreased after 24, 48 and 72 h treatment with either BNIPSpd or BNIPDadec (1µM & 10µM).
- Bis-naphthalimidopropyl polyamine derivatives may have the potential in the future to become therapeutic cancer agents. Further work is ongoing to elucidate the mode of action of these drugs.

Acknowledgement

This work was supported by The Robert Gordon University, Aberdeen.

Poster Presentation at Industry Tours for Postgraduates (Royal Society of Chemistry), Edinburgh/Glasgow, UK, 16 – 18th March 2008 and 9th Tetrahedron Symposium Challenges in Organic and Bioorganic Chemistry (Elsevier meeting), Berkeley, USA, 22 -25th July 2008

Synthesis, Cytotoxicity and DNA Binding Studies of Novel Bisnaphthalimidopropyl Polyamine Derivatives (BNIPPs)

Gemma A Barron [*a], **Giovanna Bermano**[b], **Amanda Gordon**[a] **and Paul Kong Thoo Lin**[a]

[a]School of Pharmacy and Life Sciences, The Robert Gordon University, St. Andrew Street, Aberdeen, AB25 1HG, Scotland, UK

[b]Centre of Obesity Research and Epidemiology (CORE), Faculty of Health and Social Care, The Robert Gordon University, St. Andrew Street, Aberdeen, AB25 1HG, Scotland, UK

DNA binding compounds exhibit the potential to exert anti cancer activities, such as, the cytotoxic DNA-intercalating compounds; naphthalimides and bisnaphthalimides[1,2]. These compounds, however, tend to be very insoluble in aqueous solutions, which subsequently makes their testing difficult. In our laboratory, we have designed and synthesised bisnaphthalimidopropyl fragments linked to the natural polyamines; putrescine, spermidine and spermine[3], resulting in enhanced aqueous solubility, without compromisation of biological activity[4]. More recent work has shown that these derivatives are observed within the cell nuclei (after 6 and 12 hours treatment), produce significant DNA damage, DNA fragmentation, elevated caspase-3 activity and form 'condensed bodies' strongly suggesting that the mechanism of cell death is apoptosis[5,6].

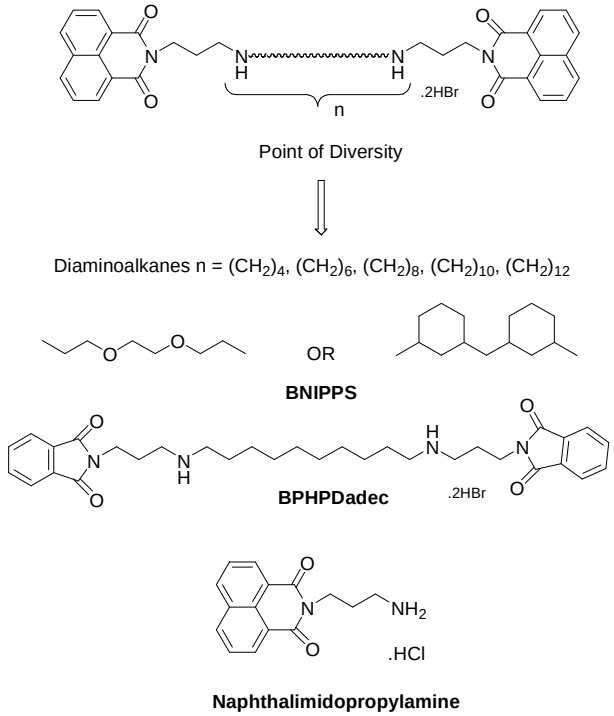

Figure 1.: BNIPP derivatives, BPHPDadec and Naphthalimidopropylamine

Here we report the synthesis of a number of derivatives including the Bisnaphthalimidopropyl diaminoalkanes, Bisnaphthalimidopropyl diaminodecane (BPHPDadec) and Naphthalimidopropylamine (Figure 1). We also study the structure activity relationship of these newly synthesised derivatives compared with the derivatives previously reported by our group[6], determined by MTT assay[7], in a breast cancer cell system (MDA-MB-231 and MCF-10A cells). The DNA binding properties were studied using UV spectrophotometric analysis and competitive ethidium bromide displacement experiments. All the BNIPPs exerted cytotoxic activity with IC_{50} values in the range of 0.83 – 12.68 μM (24 and 48 hour treatment) and, an increase of T_m by Δ 26.85 – 37.2°C with C_{50} values between 1.46 – 3.8. μM. The C_{50} values are defined as the drug

concentration required to reduce the fluorescence of initially DNA-bound ethidium bromide by 50%. These results signifiy the importance of Bisnaphthalimidopropyl functionality in exerting significant cytotoxic and DNA binding properties, consequently demonstrating promise in their further development as potential anti cancer agents. Their mode of action is currently under investigation.

Keywords: Bisnaphthalimidopropyl; Synthesis; Cytotoxicity; DNA Binding

[1] Brana, M.F, Cacho, M, Gradillas, A, de Pascual-Teresa, B and Ramos, A., (2001) Curr. Pharm. Des. **7**, 1745-1780
[2] Brana, M.F and Ramos, A., (2001) Curr. Med. Chem. Anti-Canc. Agents **1**, 237-255
[3] Kong Thoo Lin, P and Pavlov, V., (2000) Bioorg. Med. Chem. Lett **10**, 1609-1612
[4] Pavlov, V, Kong Thoo Lin, P and Rodilla, V., (2001) Chem. Biol. Interact **137**, 15-24
[5] Dance, A-M, Ralton, L, Fuller, Z, Milne, L, Duthie, S, Bestwick, C.S and Kong Thoo Lin, P., (2005) Biochem. Pharmacol **69**, 19-27
[6] Oliveira, J, Ralton, L, Tavares, J, Codeiro-da-Silva, A, Bestwick, C.S, McPherson, A and Kong Thoo Lin, P., (2007) Bioorg. Med. Chem. **15 (1)**, 541-545
[7] Mosmann, T., (1983) J. Immunol. Methods **65**, 55-63

Synthesis, Cytotoxicity and DNA Binding Studies of Novel Bisnaphthalimidopropyl Polyamine Derivatives (BNIPPs)

G.A Barron, G Bermano*, A Gordon and P Kong Thoo Lin

School of Pharmacy and Life Sciences, The Robert Gordon University, St Andrew St, Aberdeen, AB25 1HG, UK

* Centre of Obesity Research and Epidemiology (CORE), Faculty of Health and Social Care, The Robert Gordon University, St Andrew St, Aberdeen, AB25 1HG, UK

Introduction

❑DNA binding compounds exhibit the potential to exert anti cancer activities, such as, the cytotoxic DNA-intercalating compounds; naphthtalimides and bisnaphthalimides. [1,2] However, these compounds tend to be very insoluble in aqueous solutions, thus making their testing difficult.

❑In 2000, our laboratory designed and synthesised bisnaphthalimidopropyl fragments linked to the natural polyamines, putrescine, spermidine and spermine, [3] resulting in enhanced aqueous solubility, without compromising biological activity. [4]

Aims

❑To design, synthesise and characterise new BNIPPs with a number of alkyl diamines and, to establish structure activity relationships (SARs) in a breast cell system (MDA-MB-231 and MCF-10A Cells), determined using the MTT Assay

❑To determine the effects of the BNIPPs on DNA binding capacity, determined by midpoint of thermal denaturation (Tm) and ethidium bromide displacement experiments.

Results

Organic Synthesis

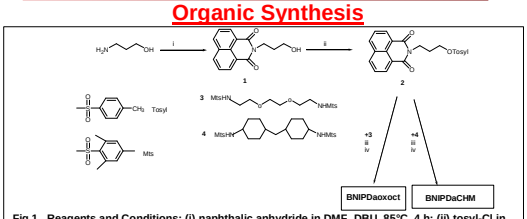

Fig 1. Reagents and Conditions: (i) naphthalic anhydride in DMF, DBU, 85°C, 4 h; (ii) tosyl-Cl in pyridine, 0-5°C, overnight; (iii) mesitylated polyamines, DMF, 85°C, overnight; (iv) HBr/glacial CH_3CO_2H in CH_2Cl_2, RT , 24 h.

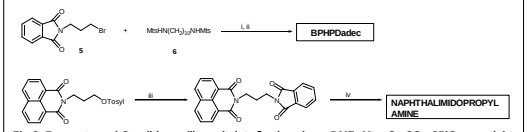

Fig 2. Reagents and Conditions: (i) mesitylated polyamines, DMF, Mts, Cs_2CO_3, 85°C, overnight; (ii) HBr/glacial CH_3CO_2H in CH_2Cl_2, RT , 24 h; (iii) tosyl-Cl, DMF, $C_6H_4KNO_2$, 50°C, overnight; (iv) C_2H_5OH, hydrazine hydrate, 85°C, overnight.

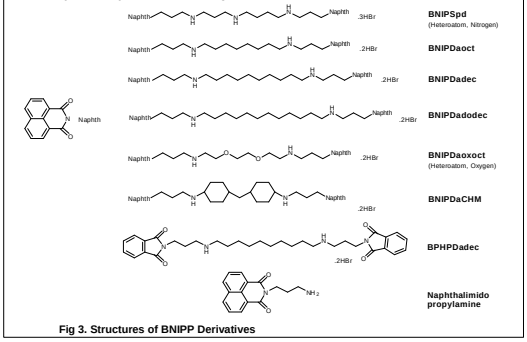

Fig 3. Structures of BNIPP Derivatives

References

1. Brana, M.F, Cacho, M, Gradillas, A, de Pascual-Teresa, B and Ramos, A., (2001) Curr. Pharm. Des. **7**, 1745-1780
2. Brana, M.F, and Ramos, A., (2001) Curr. Med. Chem. Anti-Canc. Agents, **1**, 237-255
3. Kong Thoo Lin, P and Pavlov, V., (2000) Bioorg. Med. Chem. Lett, **10**, 1609-1612
4. Pavlov, V, Kong Thoo Lin, P and Rodilla, V., (2001) Chem Biol Interact **137**, 15-24

Corresponding Author. Tel: +44-1224-262831 *Email Address: prs.barron@rgu.ac.uk*

Cytotoxicity

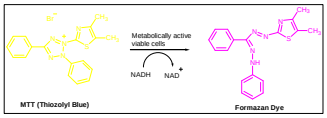

Fig 4. The Reduction Reaction of MTT Solution

Compound (a)	24 hrs (*μM*)	48 hrs (*μM*)
BNIPSpd	12.7 ± 0.5	4.6 ± 1.4
BNIPDaoct	5.0 ± 1.3	2.7 ± 0.3
BNIPDadec	4.9 ± 0.2	3.3 ± 0.7
BNIPDadodec	5.1 ± 0.5	6.9 ± 0.1
BNIPDaoxoct	12.4 ± 5.8	6.2 ± 1.5
BNIPDaCHM	6.8 ± 0.3	6.1 ± 0.7
BPHPDadec	> 40	> 40
Naphthalimidopropylamine	> 40	> 40
Etoposide	> 40	17.2 ± 0.7

Fig 5. IC_{50} values of BNIPP derivatives against MDA-MB-231 Cells

Compound (a)	24 hrs (*μM*)	48 hrs (*μM*)
BNIPSpd	*4.2 ± 0.5*	*3.9 ± 0.9*
BNIPDaoct	*2.7 ± 0.1*	*0.8 ± 0.1*
BNIPDadec	*2.7 ± 0.1*	*2.8 ± 0.1*
BNIPDadodec	*4.2 ± 0.3*	*6.8 ± 0.8*
BNIPDaoxoct	*6.1 ± 0.5*	*2.3 ± 0.0*
BNIPDaCHM	*6.1 ± 0.1*	*5.7 ± 0.8*
BPHPDadec	> 40	> 40
Naphthalimidopropylamine	> 40	> 40
Etoposide	14.2 ± 1.3	1.2 ± 0.7

Fig 6. IC_{50} values of BNIPP derivatives against MCF-10A Cells

(a) Cytotoxicity was determined by MTT Assay. The results were obtained after treating MDA-MB-231 and MCF-10A cells with different derivative concentrations (0-40 μM) after 24 and 48 hours incubation at 37°C. Data are mean ± SD of 6 replicates of three independent experiments

(IC_{50} is defined as the concentration of the BNIPPs requires to inhibit cell growth by 50%, compared to the control values)

DNA Binding

Thermal Denaturation

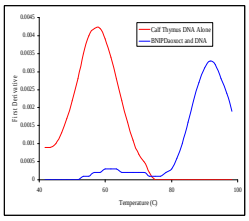

Fig 7. An example of the 1st Derivative curve of temperature vs absorbance for Calf Thymus DNA and BNIPDaoxoct (10μM)

	Tm (°C) (b)	
Compound (a)	*5 μM*	*10 μM*
Calf Thymus DNA alone		*57.7 ± 0.9*
BNIPSpd	*93.2± 0.2*	*93.5 ± 0.7*
BNIPDaoct	*92.2 ± 0.2*	*91.7 ± 0.5*
BNIPDadec	*88.0 ± 0.0*	*88.6 ± 0.5*
BNIPDadodec	*85.5 ± 0.2*	*84.5 ± 0.7*
BNIPDaoxoct	*89.5 ± 0.3*	*92.1 ± 0.7*
BNIPDaCHM	88.4 ± 0.5	89.6 ± 0.0
BPHPDadec	69.5 ± 3.0	70.2 ± 2.4
Naphthalimido propylamine	78.3 ± 0.0	79.8 ± 1.5

Fig 8. Effect of BNIPP treatment on the Thermal Denaturation (Tm) of Calf Thymus DNA

(a) Calf Thymus DNA was incubated in the presence or absence of the BNIPP derivatives for 5 minutes. The temperature was increased at the rate of 2°C/minute over a range of 40°C to 100°C. Data are means ± SD of three independent experiments. Tm was determined from the maxima peak of the first derivative, when 50% of the DNA is denatured.

Fluorescence – Binding Studies

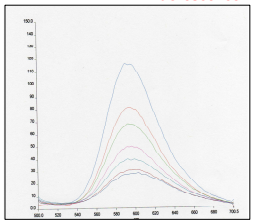

Fig. 9. An example of the fluorescence reduction for BNIPDaCHM

Compound (a)	C_{50} (*μM*)
BNIPSpd	*1.5 ± 0.1*
BNIPDaoct	*1.7 ± 0.2*
BNIPDadec	*1.8 ± 0.1*
BNIPDadodec	*3.4 ± 0.3*
BNIPDaoxoct	*1.9 ± 0.4*
BNIPDaCHM	3.8 ± 0.1
BPHPDadec	> 10
Naphthalimido propylamine	> 10

Fig. 10. Effect pf BNIPP treatment on Ethidium Bromide displacement

(a) Calf Thymus DNA was incubated in the presence and absence of BNIPP derivatives for 5 minutes. Concentration range 0-10μM. Data are means ± SD of three independent experiments. C_{50} was determined as the concentration required to reduce the fluorescence of initially DNA-bound Ethidium Bromide by 50%.

Conclusion

❑The SAR results reveal that two naphthalimido rings are required, the alkyl chain improves biological activity, although is not dependent upon length and, a decrease in activity was observed with the presence of heteroatoms within the chain (BNIPSpd and BNIPDaoxoct).

❑The results confirm the importance of naphthalimido functionality, in exerting significant cytotoxic and DNA binding properties, consequently demonstrating promise in their further development as potential anti cancer agents.

❑The mode of action of selected compounds is currently under investigation

Acknowledgement

This work was supported by The Robert Gordon University, Aberdeen.

Conference Presentation at the 42nd IUPAC Congress, The Chemistry-Biology Interface: Drug Targets and Diagnostics (Royal Society of Chemistry meeting), Glasgow, UK, 2 – 7 th August 2009

S210_017 Synthesis and Biological Activity of Novel Bisnaphthalimidopropyl Polyamine Derivatives against Breast Cancer MDA-MB-231 Cells

Gemma A Barron [*a], Giovanna Bermano[b], Amanda Gordon[a] and Paul Kong Thoo Lin[a]

[a]School of Pharmacy and Life Sciences, The Robert Gordon University, St. Andrew Street, Aberdeen, AB25 1HG, Scotland, UK

[b]Centre of Obesity Research and Epidemiology (CORE), Faculty of Health and Social Care, The Robert Gordon University, St. Andrew Street, Aberdeen, AB25 1HG, Scotland, UK

Naphthalimides and bisnaphthalimides are cytotoxic DNA-intercalating compounds which exert potential as anti-cancer agents [1, 2] . However, these compounds generally tend to be insoluble in aqueous solutions, thus making biological testing difficult. For several years, our group have been synthesising and characterising bisnaphthalimidopropyl derivatives linked by natural polyamines [3], diamino and, triamino alkyl linker chains, which resulted in enhanced aqueous solubility, without significantly affecting their biological activity [4, 5, 6]. Recent work has shown that bisnaphthalimidopropyl spermidine (BNIPSpd) induces oxidative DNA damage, depletes polyamine levels and causes cell death, by apoptosis, within HT-29 and CaCO-2 cells [7]. Here we report upon a number of new phthalimide and naphthalimidopropyl polyamine derivatives, including the bisnaphthalimidopropyl diaminoalkanes (BNIPPs), bisphthalimidopropyl diaminodecane (BPHPDadec) and mononaphthalimidopropylamine (NPA). Their cytotoxic properties were determined by MTT assay, in breast cancer MDA-MB-231 cells and compared with derivatives previously reported by our group [6]. All the BNIPPs exhibited significant cytotoxic activity, after 24 and 48 hours, with IC_{50} values in the range of 2.68 – 12.68 µM. The fluorescent properties of BNIPSpd, bisnaphthalimidopropyl diaminooctane (BNIPDaoct), bisnaphthalimidopropyl diaminooxaoctane (BNIPDaoxoct) and bisnaphthalimidopropyl diaminodicyclohexylmethane (BNIPDaCHM), in relation to cellular localisation, were determined by fluorescence microscopic analysis. It was revealed that a 10 µM derivative concentration and after a 6-h drug incubation, showed BNIPDaoct, BNIPDaoxoct and BNIPDaCHM were all located within the cell, while the presence of BNIPSpd was not observed until after 24-h drug incubation. Using the single cell gel electrophoresis (COMET) assay, it was found that BNIPSpd and BNIPDaoxoct, showed significant DNA damage to MDA-MB-231 treated cells, in a dose dependent manner, after 4 and 24-h drug incubations. The mode of cell death, in relation to apoptosis, shall also be discussed. Therefore, it is concluded that these derivatives exert cytotoxic effects, DNA damage and apoptosis, which have been shown to be related to the rate of derivative uptake into the cells, consequently demonstrating promise in their further development as potential anti cancer agents. The study of BNIPPs as potential Histone Deacetylases (HDAC) inhibitors will also be discussed.

References:

[1] Brana, M.F, Cacho, M, Gradillas, A, de Pascual-Teresa, B and Ramos, A., *Curr. Pharm. Des.* 2001, **7**, 1745-1780

[2] Brana, M.F and Ramos, A., *Curr. Med. Chem. Anti-Canc. Agents*, 2001, **1**, 237-255

[3] Kong Thoo Lin, P and Pavlov, V., *Bioorg Med Chem Lett*, 2000, **10**, 1609-1612

[4] Pavlov, V, Kong Thoo Lin, P and Rodilla, V., *Chem Biol Interact*, 2001, **137**, 15-24

[5] Dance, A-M. et al., *Biochem Pharmacol*, 2005, **69**, 19-27

[6] Oliveira, J. et al., *Bioorg Med Chem*, 2007, **15 (1)**, 541-545

[7] Ralton, L.D et al., *Chem Biol Interact*, 2009, **177**, 1-6

Appendices

Appendix 1

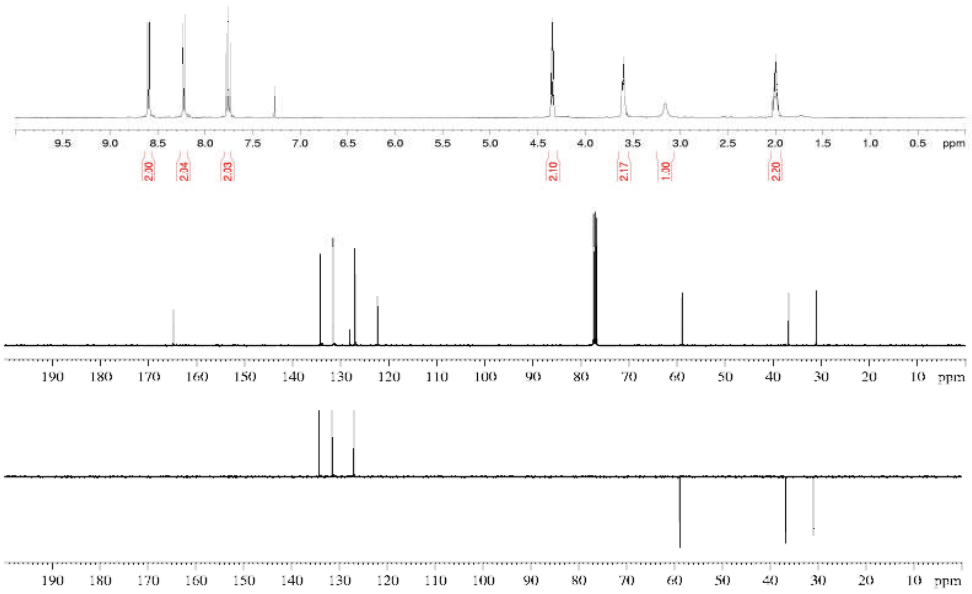

Figure A.1.: ^{1}H, ^{13}C and DEPT spectra of N-(3-hydroxypropyl) naphthalimide, **1** (^{1}H, top, ^{13}C, middle and DEPT, bottom).

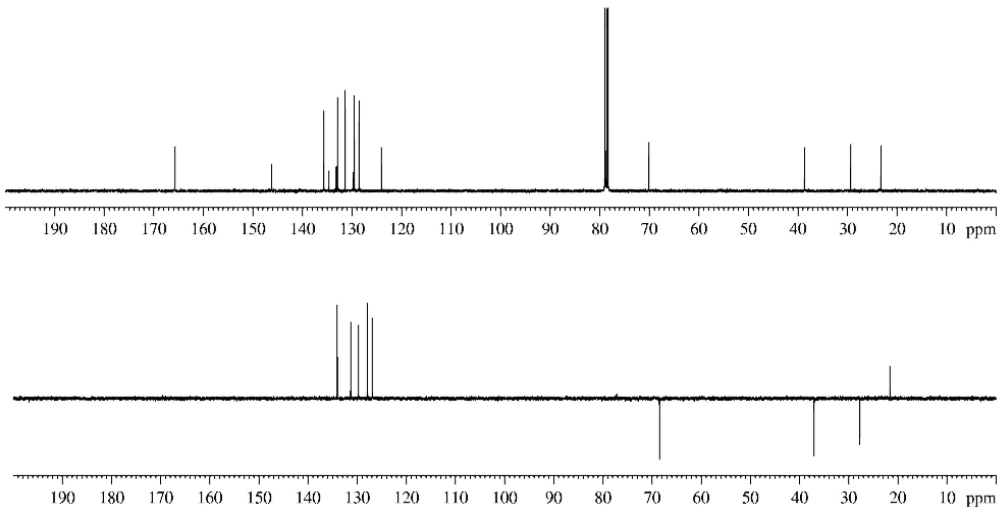

Figure A.2.: ^{13}C and DEPT spectra of toluensulfonyloxypropylnaphthalimide, **2** (^{13}C, top and DEPT, bottom).

Appendix 2

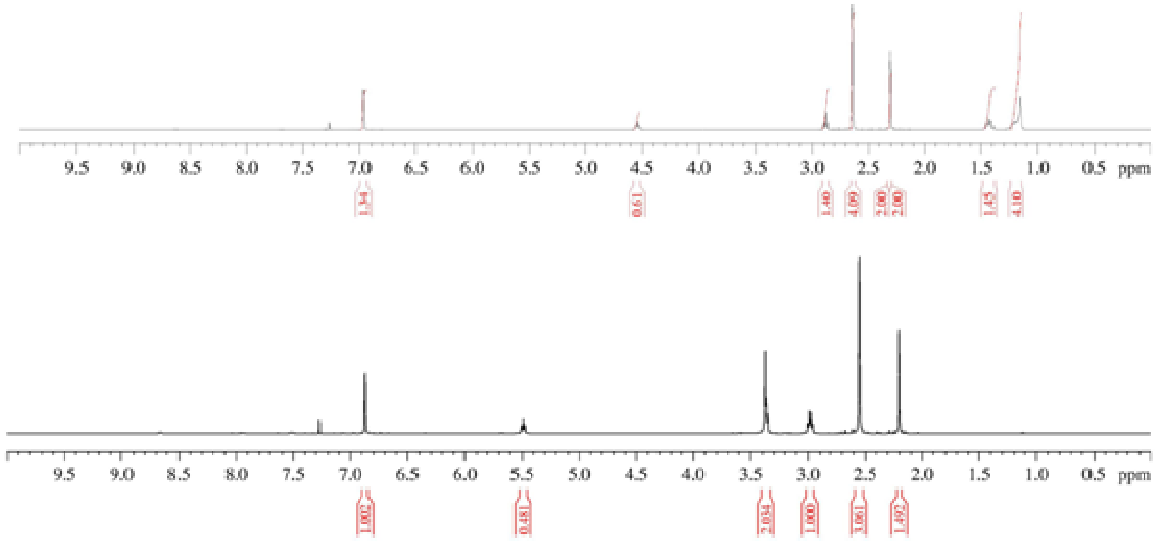

Figure A.3.: ^{1}H spectra of the dimesitylalkyldiamines, **3** and **5**. (**5**, top and **3**, bottom).

Appendix 3

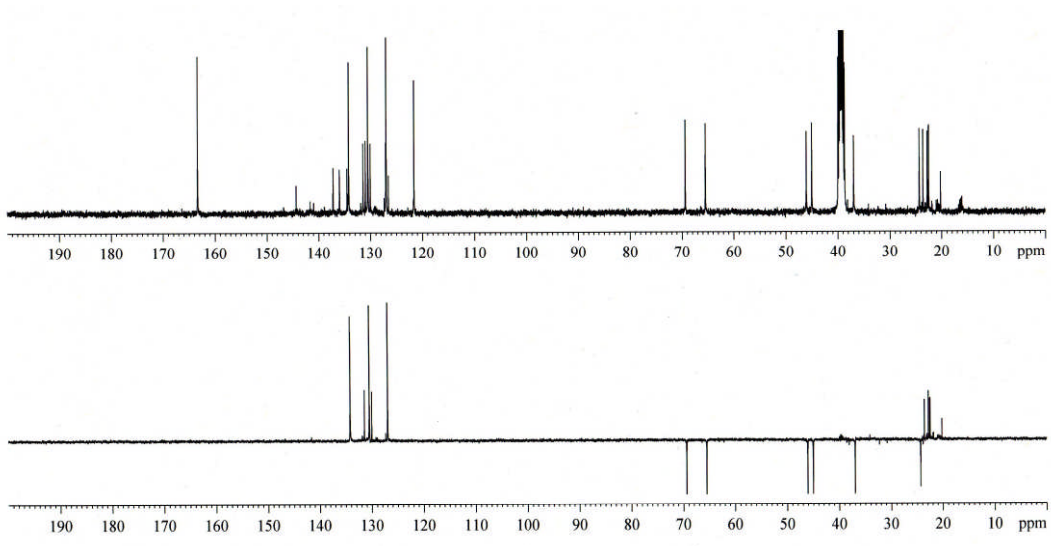

Figure A.4.: ^{13}C and DEPT spectra of BNIPDaoxaoct. (^{13}C, top and DEPT, bottom).

Appendix 4

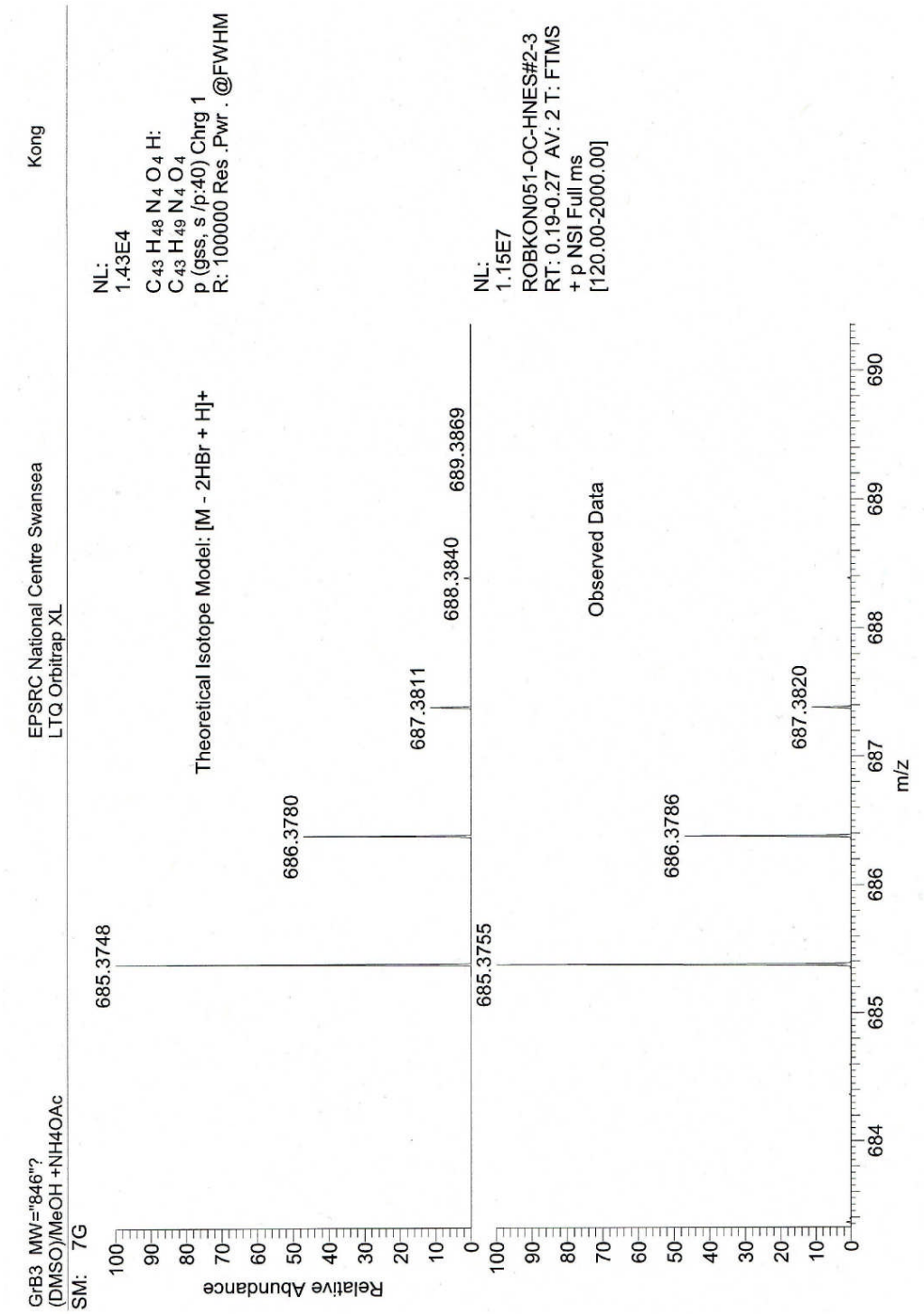

Figure A.5.: MS for BNIPDaCHM

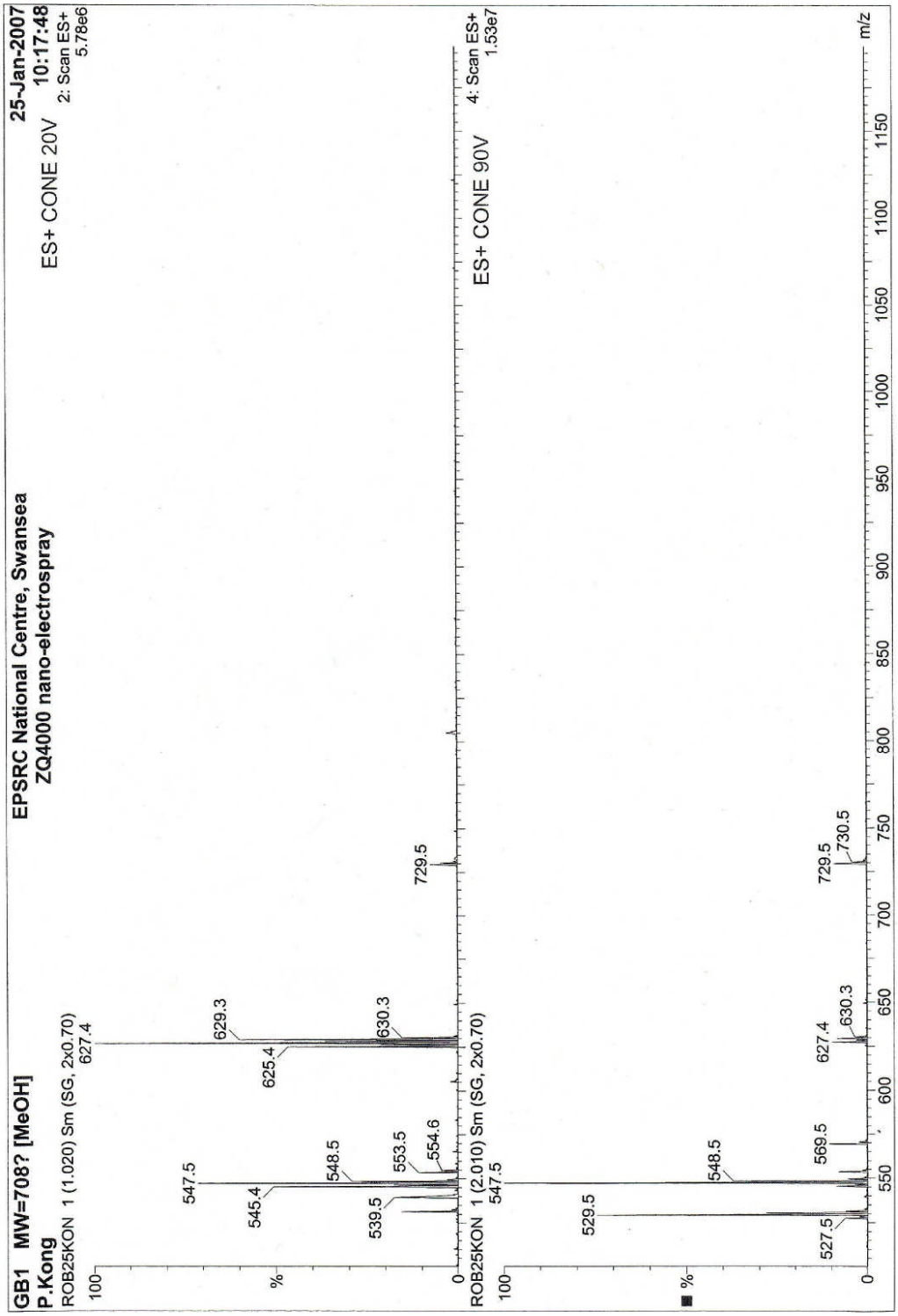

Figure A.6.: MS for BPHPDadec

Appendix 5

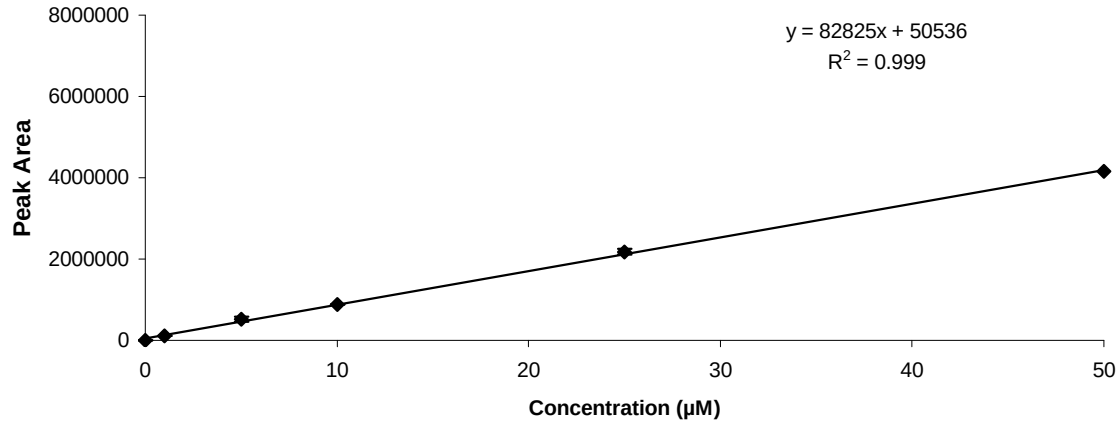

Figure A 7.: Standard curve for putrescine

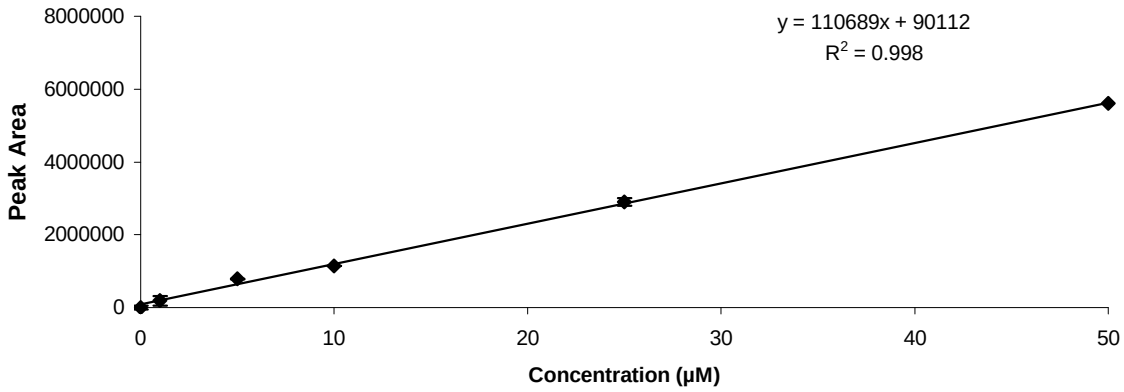

Figure A 8.: Standard curve for spermidine

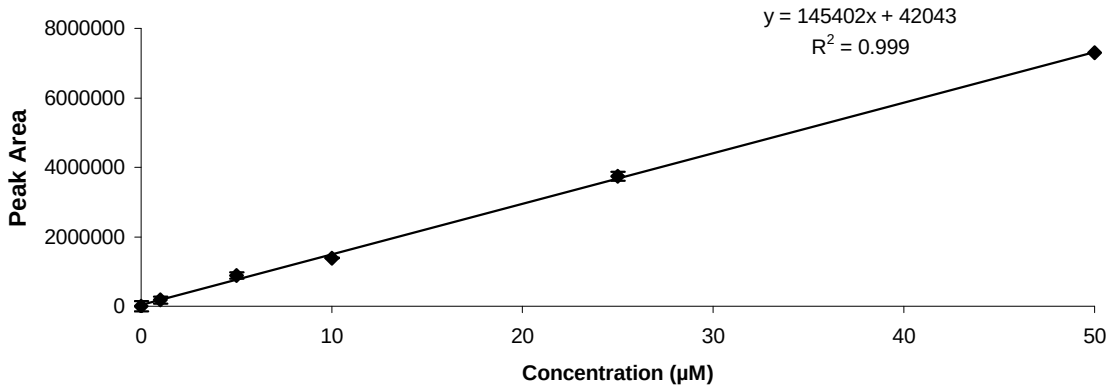

Figure A 9.: Standard Curve for Spermine